Vol. 153, October 1, 1983
Complete in one issue

ISSN 0003-2670

ANALYTICA CHIMICA ACTA

International journal devoted to all branches of analytical chemistry

ELSEVIER

ANALYTICA CHIMICA ACTA

International journal devoted to all branches of analytical chemistry
Revue internationale consacrée à tous les domaines de la chimie analytique
Internationale Zeitschrift für alle Gebiete der analytischen Chemie

PUBLICATION SCHEDULE FOR 1983

	J	F	M	A	M	J	J	A	S	O	N	D
Analytica Chimica Acta	145	146	147	148	149	150/1 150/2	151/1	151/2	152	153	154	155

Scope. *Analytica Chimica Acta* publishes original papers, short communications, and reviews dealing with eve aspect of modern chemical analysis, both fundamental and applied.

Submission of Papers. Manuscripts (three copies) should be submitted as designated below for rapid and efficie handling:

Papers from the Americas to: Professor Harry L. Pardue, Department of Chemistry, Purdue University, West Lafayett IN 47907, U.S.A.

Papers from all other countries to: Dr. A. M. G. Macdonald, Department of Chemistry, The University, P.O. Box 36 Birmingham B15 2TT, England. Papers dealing particularly with computer techniques to: Professor J. T. Cler Universität Bern, Pharmazeutisches Institut, Baltzerstrasse 5, CH-3012 Bern, Switzerland.

Submission of an article is understood to imply that the article is original and unpublished and is not being considere for publication elsewhere. Upon acceptance of an article by the journal, authors will be asked to transfer the copyrigl of the article to the publisher. This transfer will ensure the widest dissemination of information.

Information for Authors. Papers in English, French and German are published. There are no page charge Manuscripts should conform in layout and style to the papers published in this Volume. Authors should consu Vol. 132, p. 239 for detailed information. Reprints of this information are available from the Editors or from: Elsevi Editorial Services Ltd., Mayfield House, 256 Banbury Road, Oxford OX2 7DH (Great Britain).

Reprints. Fifty reprints will be supplied free of charge. Additional reprints (minimum 100) can be ordered. An ord form containing price quotations will be sent to the authors together with the proofs of their article.

Advertisements. Advertisement rates are available from the publisher.

Subscriptions. Subscriptions should be sent to: Elsevier Science Publishers B.V., Journals Department, P.O. Bc 211, 1000 AE Amsterdam, The Netherlands. Tel: 5803 911, Telex: 18582.

Publication. *Analytica Chimica Acta* appears in 11 volumes in 1983. The subscription for 1983 (Vols. 145–155) Dfl. 1980.00 plus Dfl. 220.00 (p.p.h.) (total approx. U.S. $880.00). All earlier volumes (Vols. 1–144) except Vols. 2 and 28 are available at Dfl. 200.00 (U.S. $80.00), plus Dfl. 15.00 (U.S. $6.00) p.p.h., per volume.

Our p.p.h. (postage, packing and handling) charge includes surface delivery of all issues, except to subscribers in th U.S.A., Canada and India who receive all issues by air delivery (S.A.L. — Surface Air Lifted) at no extra cost. For th rest of the world, airmail and S.A.L. charges are available upon request.

Claims for issues not received should be made within three months of publication of the issues. If not they cannot b honoured free of charge.

For further information, or a free sample copy of this or any other Elsevier Science Publishers journal, readers in th U.S.A. and Canada can contact the following address: Elsevier Science Publishing Co., Inc., Journal Informatio Center, 52 Vanderbilt Avenue, New York, NY 10017, U.S.A., Tel: (212) 867-9040.

FORENSIC SCIENCE INTERNATIONAL

An International Journal
Dedicated to the Applications of Science
to the Administration of Justice

Forensic Science International is an international journal for the publication of original contributions in the many different scientific disciplines pertaining to the forensic sciences.
Such fields would include, for example, forensic pathology and histochemistry, chemistry, biochemistry and toxicology (including drugs, alcohol, etc.) biology (including the identification of hairs and fibres), serology, odontology, psychiatry, etc., as well as investigations of value to public health in its broadest sense, and the important marginal area where medicine and the law overlap.

Forensic Science International publishes:

- Original Papers
- Review Articles
- Letters to the Editor
- Book Reviews
- Case Reports

This journal covers all legal aspects of the general disciplines listed above, as well as specialist topics of forensic interest that are included in, or are related to, these disciplines, e.g.:

- Biochemical and chemical analyses, and the forensic application of advanced analytical, physical, chemical and instrumental techniques
- Bite mark evidence – Battered-child syndrome
- Questioned documents
- Ballistics, projectiles and wounds
- Fingerprints and identification
- Tool marks
- Contact traces
- Poisoning
- Breathalysers
- Accident investigation and mass disasters

1983: Vols. 21 & 22
(2 volumes in 6 issues)
Subscription Price: US $ 142.00 including postage and handling.
ISSN 0379-0738

The **SCIENCE AND TECHNOLOGY DIVISION** of
Elsevier Science Publishers B.V.
publisher of scientific books and journals
has an immediate opening for a FULL-TIME

EDITOR

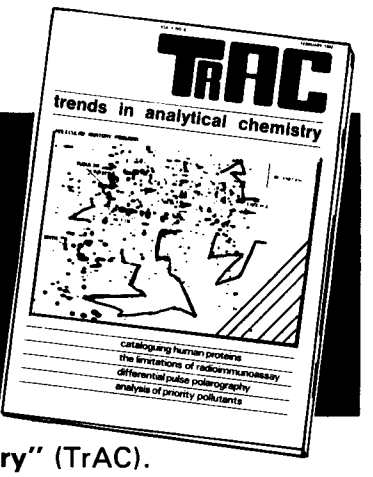

for our journal **"Trends in Analytical Chemistry"** (TrAC).

TrAC is a monthly current-awareness publication covering the latest developments over the whole field of analytical chemistry. As well as editing and supervising the production of each monthly issue, the editor is involved in the marketing of the journal.

The responsibilities comprise

- establishing the necessary contacts with, and networks of, editorial advisors and contributors to obtain a continuing flow of material for publication.
- sub-editing or rewriting editorial input received from out-of-house.
- reporting on major conferences, seminars, meetings and case situations.

Candidates should be experienced in reporting and have organizational skills and an eye for detail. An educational background in analytical chemistry or related fields is essential.

The successful candidate will also be involved in other aspects of the Elsevier chemistry publishing programme and will be given an opportunity to develop other Elsevier projects. The position will be based either in South-East England or in Amsterdam.

Applications with full curriculum vitae and passport photograph should be sent to ELSEVIER SCIENCE PUBLISHERS B.V., P.O. Box 2400, 1000 CK Amsterdam, The Netherlands, attn. Mrs. J. Monker.

ELSEVIER

2283

ANNOUNCEMENT

ANALYTICAL METHODS AND PROBLEMS IN BIOTECHNOLOGY

An International Symposium, Noordwijkerhout, The Netherlands, 17-19 April 1984

(Organized under the auspices of the Section on Analytical Chemistry of the Royal Netherlands Chemical Society and the Netherlands Biotechnological Society)

Scope of the Symposium

The development of analytical methods for biotechnological applications is an area of growing importance. Analytical methods currently available are now being adapted for practical use in biotechnological research, development and industrial production. But a large gap remains to be bridged between experts in analytical methodology and experts in biotechnology.
The purpose of the Symposium is to outline the problems faced in this field and to describe the rapid developments taking place. It is aimed at an interdisciplinary audience of those involved in industrial and academic biotechnology, as well as at analytical chemists themselves.

Scientific Programme

The Symposium is expected to cover a wide and representative range of current research activity on all aspects of analytical chemistry related to biotechnology. Analytical tools will be presented for process control in industrial biotechnology, for environmental biotechnology, and for fundamental research. The Programme will consist of invited plenary lectures, invited and submitted research papers and discussion sessions. The official language will be English and the following sessions are planned: Analytical Strategies, Analytical Techniques, Process Control.

Further Information

Those wishing to receive the first circular, which will include the topics of the Symposium, should contact: W.A. Scheffers, Symposium Analytical Methods and Problems in Biotechnology, Delft University of Technology, Laboratory of Microbiology, Julianalaan 67A, NL-2628 BC Delft, The Netherlands. Tel: (015)-78 24 11.

ANALYTICA CHIMICA ACTA
VOL. 153 (1983)

ANALYTICA CHIMICA ACTA

International journal devoted to all branches of analytical chemistry

ELSEVIER Amsterdam–Oxford–New York–Tokyo

Anal. Chim. Acta, Vol. 153 (1983)

0003-2670/83/$03.00

Printed in The Netherlands

Analytica Chimica Acta, 153 (1983) 1—13
Elsevier Science Publishers B.V., Amsterdam — Printed in The Netherlands

REPLACEMENT ION CHROMATOGRAPHY WITH FLAME PHOTOMETRIC DETECTION

S. W. DOWNEY and G. M. HIEFTJE*
Department of Chemistry, Indiana University, Bloomington, IN 47405 (U.S.A.)
(Received 31st January 1983)

SUMMARY

Replacement ion chromatography (r.i.c.) is a new detection scheme for ion chromatography with the potential of very low detection limits and universal application. In this first example of r.i.c., a counter-cation associated with an eluting anion is stoichiometrically replaced in a cation-exchange column by a flame-photometrically-active cation (e.g., Li^+) which is then directed into a total-consumption burner. Measured atomic emission from the replacement ion (Li^+) in the flame thus provides an indirect but quantitative measurement of eluting anion concentration. It is demonstrated that the reduction of the concentration of free ions in the eluting solvent is crucial to r.i.c.; otherwise detection limits and precision are degraded. Cation concentrations can be similarly quantified when separated sample cations are replaced by Li^+. The conditions for useful operation of the new r.i.c. instrument are presented and examples are provided of sensitive and efficient ion replacement. Detection limits for monovalent ions (e.g., chloride) are at the low micromolar level. The limitations and capabilities of the technique are critically appraised and possible extensions are considered.

The separation of ions in aqueous solutions by ion-exchange chromatography is straightforward and can be done routinely. Unfortunately, the sensitive detection of the separated ions, specifically inorganic ions, is not as simple as their separation. Recently, suitable detection schemes to measure the conductivity of flowing chromatographic eluents have been developed [1—5]. These detectors allow convenient monitoring of ions with low pK_d values, that cannot be measured by optical absorption or electrochemical means. The technique, termed ion chromatography, has adequate sensitivity for many applications [6] and is currently a rapidly growing area of research.

One problem associated with the use of conductivity detectors for ion chromatography is the high conductance of solvents needed to achieve separation of the sample ions. Two approaches have been successfully used to cope with this difficulty [7]; the background conductance of the solvent can be suppressed chemically or suitable column—eluent combinations can be used to reduce solvent conductance.

Chemical suppression of conductance was developed first [1]. In this approach, a column is placed in series with the separator column. This suppressor column contains an ion-exchange resin capable of reducing (usually by acid—base neutralization) the conductance of the solvent.

0003-2670/83/$03.00

Sample ion conductivity is then measured against a much lower background. The use of two columns in this approach has several minor drawbacks: separation is slowed, chromatographic resolution is reduced, and suppressor column regeneration can interrupt determinations. However, these problems can be overcome or tolerated and conveniently used systems are now commercially available.

Ion chromatography without suppressor columns, in contrast, offers high-speed separation and better chromatographic resolution than the two-column systems. It is also inherently simpler and more reliable, but requires the measurement of small conductance changes in the presence of slightly higher solvent conductances. Appropriately, the emphasis in this area of single-column technology is in the development of low-capacity ion-exchange resins for use with low-conductance solvents [2—5]. Ion separation units based on this latter scheme are also commercially available.

Conductivity measurements themselves have several drawbacks, the most important of which are limited sensitivity and an intolerance to temperature changes. Conductivity values can vary by as much as 0.5—3%/°C [8]. Accordingly, conductivity detectors must be carefully thermostated or require reference cells for temperature compensation [9].

Another type of single-column ion-chromatographic technology has recently been reported [10, 11]. Indirect photometric chromatography measures a transparent sample ion concentration by monitoring the changes in absorbance that the solute causes in a photometrically absorbing solvent. This alternative technique offers high-speed separations and good resolution. Under carefully selected conditions, sensitive measurement of ions is possible; however, determinations done in this manner are restricted to solvent systems that have adequate absorbances at chromatographically useful concentrations. Importantly, weakly conducting but separable ions can be determined with this detector and its temperature dependence is negligible.

Other types of spectroscopic detectors have been introduced for ion chromatography. A non-specific flame photometer has been coupled to a liquid chromatograph for divalent cation measurement [12]. Recently, post-column reactors were developed to form colored metal complexes to be measured by absorption spectrophotometry [13].

Post-column reactors have been used to improve conductometric measurements as well. For example, Nordmeyer, Lamb and co-workers [14, 15] have replaced divalent sample cations with H^+ to improve conductivity measurements in systems using Ba^{2+} and Pb^{2+} eluents with precipitation suppressors. Instabilities caused by pH effects were also minimized.

The purpose of the present paper is to describe and evaluate a new detector for ion chromatography which exhibits higher sensitivity than the designs described above, yet is applicable to all ions separable by ion chromatography. Significantly, the scheme is useful for the detection of both conducting and relatively non-conducting anions or cations and is

almost completely insensitive to temperature. This new technique, which is called replacement ion chromatography (r.i.c.), is introduced here as a method for ion measurement and uses flame photometric detection. However, alternative applications and experimental arrangements are possible and will be suggested.

Replacement ion chromatography is conceptually an approach whereby sample ions are first separated chromatographically, but are then stoichiometrically replaced in the eluent by an ion that can be detected more sensitively than the sample ion itself. In the example of r.i.c. presented here, lithium ions are used to replace the counter-cations associated with sample anions. Charge neutrality makes the measurement of counter-ion concentration a quantitatively reliable method of indirectly measuring sample anion concentration. Alternatively, sample cations can be directly replaced with lithium ions. Again, charge balance ensures quantitative replacement. Once replacement is complete, the eluent is directed to a flame photometer dedicated to lithium measurement. Chromatograms are therefore simply a plot of lithium concentration as a function of time. Individual ions are identified by means of their retention times, the same procedure used with conductivity (or other nonspecific) detectors. Either peak height or peak area can be used to quantify the response.

A detector dedicated to the measurement of a single ionic species can be optimized for that function and should be an inherently sensitive device, especially when the detector is mass-sensitive, as is the flame photometer. Moreover, only a single ionic species is needed for calibration, assuming unity replacement efficiency. Of course, peak areas would be utilized in single-ion calibration.

With flame photometric detection, several distinct advantages are realized. First, lithium (and therefore sample ions) can be measured with very low detection limits; detection limits for lithium in flame emission photometers are well below the micromolar level [16]. The reasons for this low detection limit are the very low spectral background from flames at the lithium 670-nm spectral line and the small spin—orbit splitting in the $2^2P_{3/2}$—$2^2S_{1/2}$ transitions in lithium [17, 18]. Second, calibration curves are linear over several orders of magnitude of concentration. Third, the detector is relatively insensitive to fluctuations in ambient temperature. Finally, it is suitable for quantifying non-conducting or weakly conducting ions.

In this first example of r.i.c., it is demonstrated that the concentration of the replacement ion is a reliable, indirect measurement of sample-ion concentration. Moreover, r.i.c. efficiency is shown to be unaffected even when one uses a replacement ion of higher relative affinity for the replacement-ion-exchange resin than the replaced ion. Improved sensitivity is achieved compared to conventional detectors. For example, the detection limit for chloride is 1 μM with r.i.c. A generalized scheme of ion measurement by r.i.c. is described for both anions and cations.

EXPERIMENTAL

In its present embodiment, r.i.c. is implemented by installing an ion-exchange column between the separator column and the flame-photometric detector (cf. Fig. 1). This "replacement" column contains a pretreated cation-exchange resin in a specific ionic form (Li^+). As cations enter the replacement column, their flow through the column is severely retarded. Meanwhile, co-eluting anions quickly pass through the replacement column. As these anions exit the column to the flame, they are accompanied by the replacement ion (Li^+), to maintain charge neutrality in the replacement column.

Because the replacement process must be quantitative for all cations entering the replacement column, the ionic strength of the eluent must be reduced before it enters the replacement column. A suppressor column is used for this purpose.

The components of the r.i.c. instrument shown in Fig. 1 are listed in Table 1. Importantly, only solvent composition and the polarities of separation and suppressor columns must be changed to enable r.i.c. to be used alternatively for cation or anion separation modes.

The chromatograph of Fig. 1 incorporates a high-pressure pump (Milton Roy Co. mini-pump, Riviera Beach, FL), a four-port injector valve (Altex model 210, Berkeley, CA) and a 0.25-ml sample loop. A commercial 25-cm cation column (Wescan Instruments, Santa Clara, CA) was used to separate sample cations. Cation suppressor and replacement columns were constructed from 6-mm o.d., 4.6 mm i.d. stainless steel tubing. Bio-Rad AG1-X8 anion-exchange resin was used to pack the suppressor columns whereas Dowex 5OW-X8 cation exchanger was used in the replacement columns. Columns of different lengths and internal diameters and containing resin of different particle sizes were constructed for testing. Dry-resin packing procedures produced columns that were superior to those which were slurry-packed. Modular flexibility was provided by appropriate low-dead-volume chromatographic fittings (Swagelok models SS-400-6-1LV, Crawford Fitting Co., Niagara Falls, Ontario).

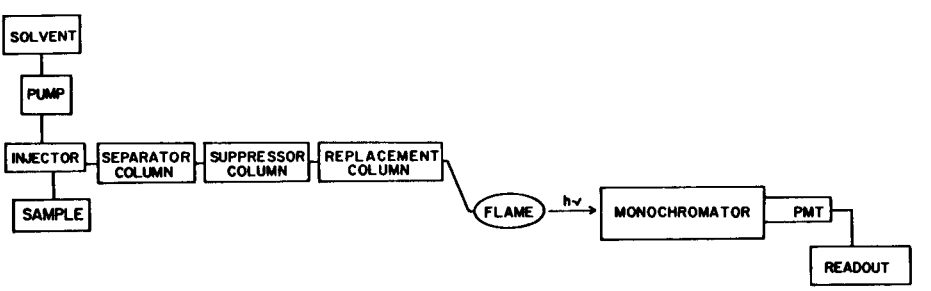

Fig. 1. Block diagram of experimental apparatus used for replacement ion chromatography. Here, alkali-metal replacement is used in conjunction with flame photometric detection.

TABLE 1

Equipment used in replacement ion chromatography for cations and anions with alkali-metal replacement and flame photometric detection

Equipment	Kind of separation	
	Cation chromatography	Anion chromatography
Analytical column	Cation separator	Anion separator
Solvent	Acidic	Basic
Suppressor column type	Basic	Acidic
Replacement mode	Sample-ion replacement	Counter-ion replacement
Replacement column	High capacity cation-exchange column; Li^+ form	
Pump and injector	Standard h.p.l.c. equipment	
Replacement-ion detection; flame emission spectrometer	Total consumption burner, focusing lens, monochromator, photomultiplier, readout device	

Initial measurement of anions by r.i.c. was completed at an eluent pH of 8.7 using a 25-cm silica-solid-support anion column (Universal Scientific, Atlanta, GA) followed in series by a 20-cm acidic suppressor column (6-mm o.d., 4.6 mm i.d.) containing Dowex 50W-X8 cation-exchange resin (50—100 mesh). The third column was a 5-cm replacement cation column (same diameters and packing material as the suppressor column) in the Li^+ form.

Most of the anion r.i.c. experiments were done at high eluent pH with Dionex-brand (Sunnyvale, CA) polymer separator and suppressor columns. In these experiments, an anion suppressor column was treated with the appropriate alkali-metal salt and used as the replacement column. The columns were conveniently coupled with Omnifit (Atlantic Beach, NY) 1/4-28 threaded fittings with 1.6 mm o.d., 0.3 mm i.d. tubing. A Rheodyne 7010 injector (Berkeley, CA) with a 0.100-ml sample loop was used for sample introduction.

The flame photometer consisted of a total-consumption air—hydrogen burner (Beckman Instruments, Fullerton, CA), a 50-cm focal-length, 40-mm diameter lens (Ealing Optics, South Natick, MA), a small monochromator, operated with a spectral bandpass of 0.67 nm (JY H-20; Instruments SA, Metuchen, NJ) and a red-sensitive photomultiplier tube (model R446, Hamamatsu Corp., Middlesex, NJ). The output photocurrent was amplified by an electrometer (model 610A, Keithley Instruments, Cleveland, OH), filtered by a passive RC filter with a one-second time constant and recorded on a strip-chart recorder (model SR-204, Heath Co., Benton Harbor, MI).

In anion r.i.c., the acidic suppressor column was regenerated with 1 M nitric acid whereas the replacement column was regenerated with 1 M lithium hydroxide. The replacement column required regeneration far less frequently than did the suppressor column. Conveniently, in cation r.i.c., the basic suppressor column and cation replacement column could be simultaneously regenerated with 1 M lithium hydroxide. After any regeneration, each column was rinsed with deionized water.

RESULTS AND DISCUSSION

Figure 2 is a replacement-ion chromatogram of monovalent anions obtained using lithium ions to replace the counter-cations associated with each eluting anion. In this case, the eluent after the suppressor column is in the carbonic-acid form whereas sample anions are in the form of strong acids. The replacement column simply converts each acid to the corresponding lithium salt which is detected by flame-emission spectrometry.

Detection limits of r.i.c.

Unfortunately, in the foregoing scheme the suppressor-column reaction product, carbonic acid, has a relatively large acidity constant (4.5×10^{-7}) [19]; the hydrogen ion concentration of the 25 mM carbonic acid solution entering the replacement-ion column was calculated and measured to be 10^{-4} M. This hydrogen ion, when replaced by an equivalent amount of lithium ion, results in a background bleed of 0.1 mM lithium. The emission in the flame from this amount of lithium was quite intense and produced a rather substantial continuous baseline signal. The turbulence of the total-consumption burner produced the resulting noise evident in Fig. 2. Despite this rather large background noise, detection limits for chloride and nitrate were found to be 0.02 mM (0.7 and 1.2 mg l^{-1}, respectively).

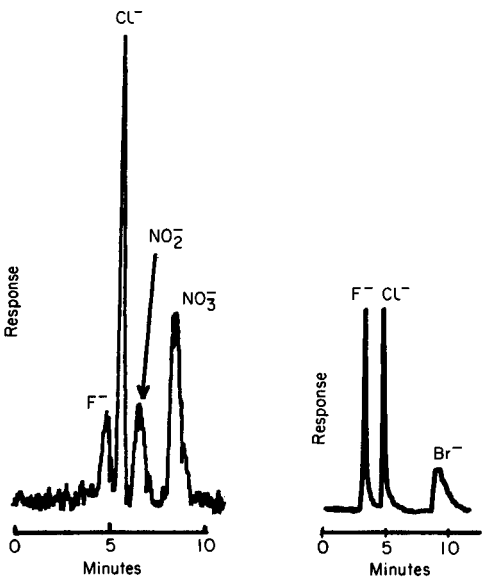

Fig. 2. Detection of monovalent anions by flame-photometric r.i.c. with a silica solid-support separator column. Concentrations: 0.25 mM F^-; 1 mM Cl^-; 0.5 mM NO_2^-; 1 mM NO_3^-. Injection volume 0.25 ml; eluent 1 mM Na_2CO_3, 24 mM $NaHCO_3$, pH 8.7; flow rate 1.5 ml min^{-1}.

Fig. 3. Detection of halides (1 mM each) by r.i.c. with Dionex ion chromatography columns. Eluent 2.0 mM Na_2CO_3, pH 10.5; flow rate 1.8 ml min^{-1}; injection volume 0.100 ml. Lithium emission measured at 670 nm.

The background replacement-ion bleed in Fig. 3 is only slightly lower than that exhibited in Fig. 2, even though the total salt concentration in the eluent was lower by more than a factor of ten. This fact verifies the importance of free ions in the eluent to detection limits in r.i.c. In Fig. 3 as in Fig. 2, the suppressor-column reaction product is carbonic acid; the 2 mM carbonate eluent leaving the suppressor column in Fig. 3 can be calculated and measured to be at pH 4.5 ± 0.2 ($[H^+]$ = 0.03 mM). The measured lithium bleed from the replacement column was 0.05 mM, indicating that nearly all hydrogen ion entering the replacement column results from dissociation of carbonic acid and represents an unavoidable background bleed when carbonic acid is the suppressor-column product. The detection limits for the halides with the carbonate eluent are accordingly not statistically different from those obtained with the HCO_3^-/CO_3^{2-} eluent, i.e., 0.02 mM for fluoride and chloride (0.4 and 0.7 mg l^{-1} respectively) and 0.05 mM (4 mg l^{-1}) for bromide.

Clearly, if r.i.c. with flame photometric detection is to yield dramatically improved limits relative to conductometric detection, an eluent must be used that has a suppressor-column reaction product with a very low acidity constant or which operates with very low concentrations of eluent ions. To illustrate this point, hydroxide was used as an eluent to obtain a simple separation of fluoride and chloride. As this eluent passes through the acidic suppressor column, the hydroxide is effectively neutralized and produces a very low ionic-strength effluent. Consequently, the replacement-ion bleed is substantially reduced. Figure 4 shows a replacement-ion chromatogram of fluoride and chloride obtained near their detection limit with the hydroxide eluent. The detection limit for these ions was calculated to be 0.8 μM (15 μg l^{-1}) for fluoride and 1.1 μM (35 μg l^{-1}) for chloride at a signal-to-noise ratio of 2.

The background bleed observed in Fig. 4 corresponds to 3 μM lithium, a value which is 30-fold higher than predicted from the dissociation constant of pure water. Moreover, the measured pH of the eluent leaving the suppressor column was 5.6. The source of this unexpectedly high background bleed was ultimately traced to the purity of the "deionized" water used in the preparation of the eluent solution and ion standards. Micromolar levels of ionic impurities (sodium, calcium and magnesium salts) were identified by inductively-coupled plasma emission spectroscopy. Evident in Fig. 4 is the "water dip" [1] also suggesting that slightly higher levels of impurities exist in the eluent than in the ion standards; the additional contaminants come from either trace levels ($\approx 10^{-5}$ M) of other salts in the 1 M sodium hydroxide (Baker Ultrex) used to make the eluent or from a separate, unintentional contamination. The use of purer solvents and reagents would minimize these background ion artifacts. Of course, preparing the standards in the eluent eliminates this dip. The retention time of the dip was noticed to change in the usual fashion [1, 20].

Apparently, noise and therefore the precision and detection limits in the present r.i.c. system are governed by replacement-ion bleed and the noise

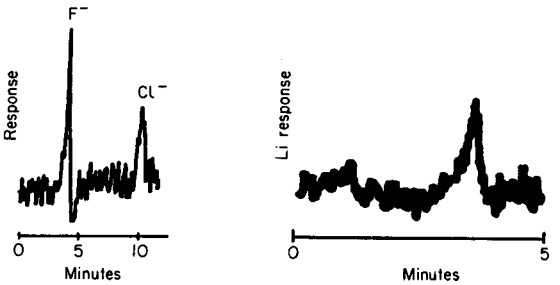

Fig. 4. Fluoride and chloride (10 μM each) detected with replacement ion chromatography. Eluent 0.01 M NaOH; flow rate 1.7 ml min^{-1}; injection volume 0.100 ml. Lithium emission measured at 670 nm.

Fig. 5. Flame photometric detection of a 0.1 ml injection of 10^{-7} M lithium hydroxide. Flame coupled directly to anion separation column. Eluent: deionized water at 1.5 ml min^{-1}. Detection limit calculated as 14 nM at a signal-to-noise ratio of 2.

this bleed generates in the emission signal from the turbulent flame. In turn, ion bleed is limited by the fundamental dissociation of suppressor-column reaction products. In the absence of any lithium ion background bleed, the absolute detection limit achievable with this flame photometric detector for lithium was found to be 14 nM (0.1 $\mu g\ l^{-1}$). To determine this value, 0.100-ml aliquots of lithium solutions were injected onto the anion separation column, deionized water served as eluent and the flame photometer was placed immediately after the column. Under these conditions, no significant degradation of chromatographic resolution occurs and no background bleed should exist. Figure 5 shows a trace of a 10^{-7} M lithium ion injection through the single column.

The 70-fold discrepancy between detection limits obtained for lithium ion in the presence (1 μM) and absence (14 nM) of replacement-ion bleed can be explained from the relationship between signal-to-noise ratio (S/N) and detected photocurrent in a flicker-noise-limited emission measurement [21]: $S/N = i_s/k\bar{i}_b$. For r.i.c., i_s is the signal current (net peak height), i_b is the average background current (with or without Li^+ bleed), and k is the "flicker factor". The flicker factor is a measure of the amount of noise inherent in the background [22] and would depend on factors such as pump fluctuations, sample introduction irregularities, and flame turbulence; k is an intrinsic property of a particular experimental system.

The measured ratio of the background photocurrent ($\bar{i}_b$) with and without Li^+ bleed is 30, suggesting that S/N and therefore detection limits should be thirty-fold more in the presence of the measured bleed. Moreover, the three-column r.i.c. device decreased the Li^+ peak height (i_s) by a factor of approximately 2 compared to the value obtained from the direct anion column injection. At a given S/N (2 at the detection limit), the increase in background level caused by Li^+ bleed coupled with the decrease in peak signal caused by band broadening with three columns accounts for most of the difference in the molar sensitivities in Figs. 4 and 5.

Literature values for the detection limit of lithium in flames are near 0.5 nM (3 ng l^{-1}) [16]. The difference between this value and that shown in Fig. 5 is, of course, related to the flicker factor (k) and the sensitivity of the photometric system. Pump noise, turbulence in the flame produced by the total-consumption burner, and limited sample-injection volume all affect (increase) k compared to values found in most conventional spectrometric systems.

Calibration of r.i.c.

Importantly, equimolar concentrations of eluting ions produce peaks of equal area in r.i.c. Figure 3 illustrates this useful feature. The chromatogram in Fig. 3 of an equimolar mixture of halides contains three peaks whose areas are the same to within the precision of manual measurement (±5%).

The construction of working curves for anions is also simple in r.i.c. because only the replacement ion (Li^+) is calibrated by using the flame photometer. Figure 6 illustrates that peak area can be used reliably for universal quantitation of ions on a molar basis. Of course, the detection limit for an individual ion will be determined by its peak broadening and therefore by retention time; that is, the peak must be detectable above drift and noise in the baseline. As expected, the calibration graph produced with this method was nearly identical to those of conventional flame photometers for alkali metals [15]. At very low lithium concentrations ($<10^{-6}$ M), the classical ionization upward curvature is found, while at high lithium concentrations ($>10^{-2}$ M), self-absorption is observed. The net result is a sigmoidal-shaped working curve with its linear region between 10^{-6} and 10^{-2} M. The straight-line portion of the calibration curve of Fig. 6 fits the equation $A = (1.3 \pm 0.2) \times 10^5 C_i + (15 \pm 2)$, where A is the relative peak area (in the appropriate ampere—time units) and C_i is the ion concentration (in molarity). The standard error of estimate is 0.3×10^5 and the correlation coefficient is $r^2 = 0.99$. The linear section of Fig. 6 has a slope of 0.97 ± 0.01.

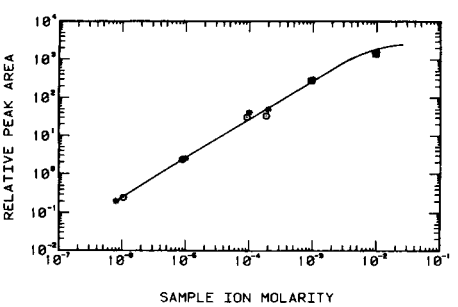

Fig. 6. Universal calibration graph for r.i.c. with flame photometric detection of lithium: (*) F^-; (○) Cl^-; (□) Br^-. The data for 1—10 mM were obtained under the conditions described in Fig. 3; all other data were obtained under the conditions described in Fig. 4.

Other replacement ions

Different cations can be used as the replacement ion in r.i.c., regardless of their relative affinity for the replacement cation-exchange resin. Table 2 lists the order of relative affinity of various cations for a typical high-capacity cation-exchange resin. Figure 7, which shows results obtained using a replacement column prepared in the K^+ form, should be compared to Fig. 4. As in Fig. 4, the replacement-ion (K^+) bleed in Fig. 7 was measured to be 3 μM and reflects the concentration of ionic impurities in the eluent. Unfortunately, these contaminants could not be practically removed with our conventional deionizing equipment.

Cation replacement ion chromatography

Cation concentrations can be measured with r.i.c. in a manner similar to that used in anion concentration measurements; however, sample cations can be replaced directly in the cation-exchange replacement column. A chromatogram of monovalent cations is shown in Fig. 8. In this system, the separated sample cations are injected into and eluted from the separating column in the nitrate salt form. In the basic suppressor column, the acidic eluent is neutralized and the sample cations exit in the hydroxide form. In the replacement column, sample cations displace lithium ions while the hydroxide counter-ions elute unretained.

The reproducible nature of the replacement processes is evident from the equivalence (±5%) of the peak areas of Fig. 8. Conveniently, the calibration graph for these cations is the same as that used for anions (Fig. 6). The precision and detection limits provided by the cation r.i.c. arrangement, like those with anion r.i.c. are limited by Li^+ bleed from the three-column system. Eluent fractions collected at various points in the system indicated that the 12.5-cm suppressor column changed the pH of the 3.14 mM nitric acid solvent from 2.5 (entering) to 5.5 (leaving). However, the replacement column then raised the pH to 6.5, indicating that hydrogen ion attack of the replacement column was responsible for the background lithium bleed. As before, the source of the residual hydrogen ion was traced to micromolar ionic impurities in the laboratory deionized water used to prepare the eluent.

TABLE 2

Relative affinities of various cations for the ion-exchange resin used in the replacement column[a]

Ion	Relative selectivity for 5OW-X8	Ion	Relative selectivity for 5OW-X8
Li^+	0.85	K^+	2.5
H^+	1.0	Mg^{2+}	2.5
Na^+	1.5	Cu^{2+}	2.9
NH_4^+	1.95	Ca^{2+}	2.9

[a]Data from Bio-Rad Laboratories, 1982.

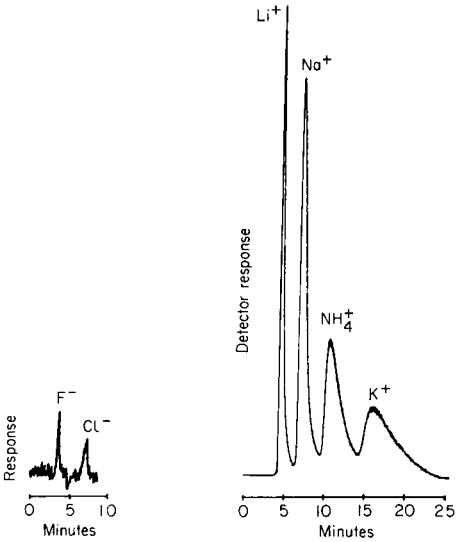

Fig. 7. Detection of 10 μM each of fluoride and chloride using K^+ as the replacement ion. Potassium emission is measured at 760 nm. Eluent 0.01 M NaOH; flow rate 2 ml min^{-1}; injection volume 0.100 ml.

Fig. 8. Detection of monovalent cations (1 mM each) by r.i.c. Eluent, HNO_3 at pH 2.5 and 1.2 ml min^{-1}. Suppressor column, 12.5 cm × 3 mm i.d., 100—200 mesh particle size anion-exchange resin. Replacement column, 12.5 cm × 3 mm i.d., 20—50 mesh particle size cation-exchange resin.

Under ideal conditions, the sensitivity for monovalent ions in cation r.i.c. would be comparable to that seen for anions when water is the suppressor-column reaction product (i.e., where $[H^+] \approx 1\ \mu M$).

Other aspects of r.i.c.

Early experimental results obtained with a lithium 670-nm interference filter (bandpass 8 nm) are similar to those presented here. An r.i.c. instrument using such a filter would obviously be more compact and less expensive to construct. However, in the present system, the narrow bandpass of the monochromator was useful in rejecting unwanted light from room illumination.

A present limitation of r.i.c. is that the lowest detection limits are obtained when H^+ and OH^- eluents are used. These eluting agents are effectively suppressed so that minimum replacement ion bleed occurs; however these eluting agents are rather weak and have limited practical application.

In preliminary experiments, magnesium and calcium ions were separated by using a hydroxide-suppressed 4 mM copper(II) nitrate eluent system. Unfortunately, the $Cu(OH)_2$ precipitate quickly raised the column pressure. In addition, some free copper ion was found to reach the replacement column and created a background Li^+ signal similar to that described earlier for the HCO_3^-/CO_3^{2-} eluent (cf. Fig. 2). The use of three columns in r.i.c. has several additional drawbacks. Chromatographic resolution is superior with

one or two column systems. Also, retention times are somewhat longer when three columns are used. The replacement column requires special preparation, but does not need regeneration as often as suppressor columns. Conveniently, when the suppressor column nears exhaustion, a sharp increase in replacement-ion bleed is seen. In contrast, if the replacement column should become exhausted first, a gradual lessening in replacement-ion bleed is noticed.

CONCLUSION

In this first example of replacement ion chromatography, it is demonstrated that the measurement of replacement ion concentration is a quantitative and reliable method of indirectly measuring sample-ion concentration. In addition, the r.i.c. detector can provide a universal means of quantifying either cations or anions with a single calibration graph. The detection limits of r.i.c. with flame photometric detection, here in its infancy, are in general comparable and in some cases superior to those of conventional conductivity detectors. For example, the detection limit for chloride ion using conductometric detectors has been reported to be between 5 and 50 μM [11, 23—25], without preconcentration. One notable exception [20] reports a remarkable detection limit of 0.1 μM for chloride using essentially the same technology reported elsewhere [23]; such detection requires a successful discrimination of 1 part in 1600 in residual background conductance. With r.i.c., a detection limit of 1 μM is noted, even with the addition of a third column. In addition, flame photometric detection has a usable working curve of four orders of magnitude, similar to that of suppressed-conductometric detectors and superior to non-suppressed detection [21].

With the current r.i.c. instrument, precision and detection limits are limited by system flicker noise, eluent purity and the dissociation constant of suppressor-column reaction products. These limitations might be reduced by use of less noisy spectroscopic detectors (e.g., laminar flames or ion fluorimetry), smoother, constant-flow pumps, improved solvent purity, or better suppressor-column technology.

This work was supported in part by the National Science Foundation through grant CHE 79-18073 and by the Office of Naval Research. The loan of chromatographic supplies from The Upjohn Company and the research groups of John Hayes, Dennis Peters, and Mark Wightman and technical advice from Jim Cleary and Lowry Caudill are greatly appreciated. The generous gift of separator columns and ion-exchange columns from the Dionex Corporation is also appreciatively acknowledged.

REFERENCES

1 H. Small, T. S. Stevens and W. C. Bauman, Anal. Chem., 47 (1975) 1801.
2 J. S. Fritz, D. T. Gjerde and R. M. Becker, Anal. Chem., 52 (1980) 1519.
3 D. T. Gjerde, J. S. Fritz and G. Schmuckler, J. Chromatogr., 186 (1979) 509.
4 D. T. Gjerde, J. S. Fritz and G. Schmuckler, J. Chromatogr., 187 (1980) 35.
5 D. T. Gjerde and J. S. Fritz, Anal. Chem., 53 (1981) 2324.

6 F. C. Smith, Jr. and R. C. Chang, Crit. Rev. Anal. Chem., 9 (1980) 197.
7 C. A. Pohl and E. L. Johnson, J. Chromatogr. Sci., 18 (1980) 442.
8 H. H. Willard, L. L. Merritt, Jr., J. A. Dean and F. A. Settle, Jr., Instrumental Methods of Analysis, 6th edn., Van Nostrand, New York, 1981, Ch. 26.
9 R. P. W. Scott, Liquid Chromatography Detectors, Elsevier, Amsterdam, 1977, p. 83.
10 H. Small and T. E. Miller, Jr., Anal. Chem., 54 (1982) 462.
11 R. A. Cochrane and D. E. Hillman, J. Chromatogr., 241 (1982) 392.
12 D. J. Freed, Anal. Chem., 47 (1975) 186.
13 D. Eubanks, A. W. Fitchett, K. Haak and J. Riviello, FACSS Conference, Philadelphia, PA, 1982 Abstr. No. 443.
14 F. R. Nordmeyer, L. D. Hansen, D. J. Eatough, D. K. Rollins and J. D. Lamb, Anal. Chem., 52 (1980) 852.
15 J. D. Lamb, L. D. Hansen, G. G. Patch and F. R. Nordmeyer, Anal. Chem., 53 (1981) 749.
16 G. D. Christian and F. J. Feldman, Appl. Spectrosc., 25 (1971) 660.
17 C. Th. J. Alkemade and R. Herrmann, Fundamentals of Analytical Flame Spectrometry, Wiley, New York, 1979.
18 G. Herzberg, Atomic Spectra and Atomic Structure, Dover Publications, New York, 1944.
19 D. G. Peters, J. M. Hayes and G. M. Hieftje, Chemical Separations and Measurements, W. B. Saunders Co., Philadelphia, PA, 1974.
20 Y. Hanaoka, T. Murayama, S. Muramoto, T. Matsuura and A. Nanba, J. Chromatogr., 239 (1982) 537.
21 C. Th. Alkemade, W. Snelleman, G. D. Boutilier, B. D. Pollard, J. D. Winefordner, T. L. Chester, and N. Omenetto, Spectrochim. Acta, Part B, 33 (1978) 383.
22 J. D. Winefordner and T. J. Vickers, Anal. Chem., 36 (1964) 1939.
23 T. S. Stevens, J. C. Davis and H. Small, Anal. Chem., 53 (1981) 1488.
24 C. A. Pohl and E. L. Johnson, J. Chromatogr., 18 (1980) 442.
25 J. A. Glatz and J. E. Girard, J. Chromatogr. Sci., 20 (1982) 266;

Analytica Chimica Acta, 153 (1983) 15—22
Elsevier Science Publishers B.V., Amsterdam — Printed in The Netherlands

AN ATOMIC ABSORPTION SPECTROMETRIC METHOD FOR THE INDIVIDUAL DETERMINATION OF CHROMIUM(III) AND CHROMIUM(VI) BY ATOMIZATION OF CHROMIUM FROM A CHELATING RESIN IN A GRAPHITE TUBE

AKINORI ISOZAKI*, KAZUHIRO KUMAGAI and SATORI UTSUMI

Department of Industrial Chemistry, College of Science and Technology, Nihon University, 1-8-14, Kanda-Surugadai, Chiyoda-ku, Tokyo (Japan)

(Received 14th March 1983)

SUMMARY

A method for the determination of $\mu g\ l^{-1}$ levels of chromium(III) and chromium(VI) by electrothermal atomic absorption spectrometry is described. Chromium(III) is quantitatively adsorbed onto Chelex-100 (<400 mesh) from 250 ml of sample solution (pH 4.0). After collection of the resin on a membrane filter, 5.0 ml of an aqueous suspension of the resin is prepared, and 10 μl is injected into a carbon furnace. The chromium peak area is measured. Chromium(VI) remains in the filtrate, and is completely reduced to Cr(III) with hydrochloric acid and hydrogen peroxide, and measured as before. The relative standard deviations for 1.0 $\mu g\ l^{-1}$ Cr(III) and Cr(VI) are 2.3% and 3.7%, respectively.

Chromium is one of the elements that is present in natural waters in two main oxidation states. Because of the difference in toxicity of chromium(III) and chromium(VI), there have been many attempts in recent years to discriminate between these two oxidation states in natural waters [1]. For example, total chromium was measured by extraction with ammonium pyrrolidinedithiocarbamate in 4-methyl-2-pentanone after oxidation of chromium(III) [2], and chromium(VI) was determined with diethyldithiocarbamate in 4-methyl-2-pentanone [3]. De Jong and Brinkman [4] reported a method based on electrothermal atomic absorption spectrometry (a.a.s.) based on selective liquid—liquid extraction of chromium(VI) from sea water; chromium(VI) was quantitatively extracted with Aliquat-336 from weakly acidic (pH 2) sample solutions, whereas chromium(III) was extracted as chromium(VI) after oxidation by ammonium peroxodisulfate. Other studies of chromium speciation [5, 6] relied on the ability of hydrated iron(III) oxide selectively to co-precipitate chromium(III), with chromium(VI) being determined after reduction. Separation and preconcentration of chromium species by ion-exchange have also been investigated. Pankow and Janauer [7] proposed a method for the preconcentration of chromium(VI) from aqueous solutions by an anion-exchange resin. By combining the anion-exchange process with a.a.s., Cresser and Hargitt [8] proposed a method for

0003-2670/83/$03.00

the rapid determination of chromium in each of its two main oxidation states in a soil extract.

The chelating resin, Chelex-100, has frequently been applied for the separation and preconcentration of trace metal ions because it readily forms stable chelates. A sensitive method for the determination of copper has been described [9, 10] in which Chelex-100 is introduced as a suspension into a carbon tube for electrothermal a.a.s., after the adsorption of copper ions in a batch process. Similar methods have been reported for lead [11] and aluminum [12] ions. A highly purified chelating resin contains no metals, and smoke does not interfere if a suitable ashing temperature is selected. These methods do not require drying and weighing of the resin, nor elution of the metal from the resin.

This paper describes a sensitive and simple method for the individual determination of chromium(III) and chromium(VI) in a sample solution. As chromium(VI) is not adsorbed by Chelex-100, it is necessary to convert chromium(VI) to chromium(III) before the resin technique can be applied. Chromium(III) is first separated from the sample solution by using the Chelex-100; chromium(VI) in the filtrate is then reduced to chromium(III) with hydrochloric acid and hydrogen peroxide, and collected on a separate portion of the resin.

EXPERIMENTAL

Apparatus

A Nippon Jarrell-Ash FLA-100 carbon tube atomizer was used in conjunction with a Nippon Jarrell-Ash Model AA-8500 two-channel atomic absorption spectrometer. A single-element chromium hollow-cathode lamp (Hamamatsu TV L-233) was employed as the line source in order to determine chromium at 357.9 nm, and the neon line at 352.0 nm from this lamp was used for the measurement of background absorption. Peak areas were measured by using a Tokyo Kagaku RD-202 digital integrator. The numerical values of peak area and peak height were recorded with a Tokyo Kagaku RD-10-21 digital printer. The peak atomic absorption signals of chromium during atomization were stored in a Tokyo Kagaku TM-707 sampling memory, and the signals were recorded with a Hitachi 056 recorder after amplification. The resin suspension was injected into the atomizer with a micropipette (Eppendorf Model 4700) fitted with disposable plastic tips.

A 15-ml polystyrene centrifuge tube with a screw cap was used for treatment with the resin; a 5.0-ml mark was etched on the tube. A Sartorius suction bottle with a membrane filter (2.0-μm pore size) was used for separation of the resin from the sample solution. Apparatus such as polyethylene beakers and centrifuge tubes, were washed thoroughly with 10% nitric acid, and with water.

Reagents

All chemicals were of super-special grade. Fresh distilled-deionized water was used throughout.

Standard chromium(III) and chromium(VI) solutions (1000 mg l^{-1}). Dissolve 0.500 g of chromium metal (99.99%) in 10 ml of 6 M hydrochloric acid, and dilute to 500 ml with 0.1 M hydrochloric acid. Dissolve 1.414 g of potassium dichromate in 500 ml of water. Prepare working solutions by appropriate dilution, and store these solutions in glass bottles in the dark.

Chelating resin. Chelex-100 (Bio-Rad Laboratories, Richmond, CA; Na-form) prepared to a grain size below 400 mesh was used. After the removal of fine particles in the resin by decantation, add 500 ml of 2 M hydrochloric acid to 50 g of the resin in a beaker. Stir the mixture for about 2 h with a magnetic stirrer, and wash the resin with water by decantation. Add 500 ml of 2 M ammonia to the resin, and stir the mixture for 2 h. Filter the resin through a 2.0-μm membrane filter, wash with water, and dry in vacuum for 6 h at 60°C. (The resin was used in the NH_4-form because in its H^+-form it tends to lose its chelating capacity.)

Buffer solution (pH 4.0). Purify a 0.8 M sodium acetate solution by passing it through a column packed with Chelex-100 (Na-form), and dilute to 0.4 M. Use a 0.2 M acetic acid—0.05 M sodium acetate solution as buffer.

Recommended procedure

Transfer 250 ml of sample solution containing less than 0.50 μg of chromium(III + VI) to a polyethylene beaker. Adjust the sample solution to pH 4 with ammonia solution or acetic acid. Add 5 ml of pH 4.0 buffer solution and 0.10 g of Chelex-100, and stir for 20 min with a magnetic stirrer. Separate the resin from the aqueous phase with the membrane filter, retain the filtrate (see below), transfer the resin with water to a centrifuge tube and centrifuge. Decant the supernatant liquid from the tube, taking care to leave the resin, and prepare 5.0 ml of resin suspension by adding water to the tube. After mixing thoroughly to form a uniform suspension, inject 10 μl (0.2 mg of resin) of the suspension into the carbon tube atomizer. Measure the atomic absorption of chromium (peak area) under the instrumental conditions shown in Table 1.

TABLE 1

Instrumental operating conditions
(Wavelength 357.9 nm, lamp current 10 mA, argon gas flow rate 3 l min^{-1}, damping 1, sensitivity 1)

Operating steps	Current (A)	Time (s)	Mode	Approximate final temp. (°C)
Drying	40	15	Ramp	300
Ashing	120	75	Ramp	1200
Atomization	270	10	Flash	2500

For the determination of chromium(VI), transfer the filtrate to a polyethylene beaker. Add 5 ml of 3 M hydrochloric acid and 5 ml of 3% hydrogen peroxide to the filtrate, and stir for 20 min. Adjust to about pH 4 with ammonia solution. Measure the peak area chromium absorbance as described above, after treatment with Chelex-100, etc.

RESULTS AND DISCUSSION

Adsorption of chromium(III) ion by Chelex-100 resin

In the above procedure, the extent of adsorption of chromium(III) by the Chelex-100 was examined. A 250-ml sample solution containing 0.25 μg of chromium(III) was treated as in the above procedure, and chromium(III) in the filtrate was measured again by the same procedure. The peak area absorbance obtained from the filtrate was the same as that from a blank; therefore, adsorption is about 100%, indicating a concentration ratio of 50:1. Experiments were also done on 500 and 1000 ml of solution each containing 0.25 μg of chromium(III). Since the adsorption from these solutions was about 100%, it is possible to raise the concentration ratio.

Optimization of experimental conditions

Effect of ashing current. To obtain satisfactory atomization of chromium after complete ashing of the resin, the atomic absorption signals from chromium taken up by the resin and from pure resin were measured at various ashing currents. The results are shown in Fig. 1 and are compared to the signals obtained from an aqueous chromium(III) solution. The peak areas for chromium on the resin at an ashing current of 70 A were high and erratic, because of absorption by smoke from the resin, as is evident from the signal produced by the pure resin at this current. The decrease in signal at 170 A was due to the loss of chromium by volatilization during ashing; this also occurred with the aqueous solution of chromium(III). As the peak areas for chromium on the resin were constant for ashing currents between 90 A and 150 A, an ashing current of 120 A for 75 s was used before atomization.

The resin increased chromium atomization. The peak area signal at an ashing current of 120 A was 10% greater than that of chromium in the aqueous solution (Fig. 1). The carbon in the resin seems to be effective for reduction of chromium oxide during the atomization step. This effect was also observed for copper [10] and aluminum [12].

Atomic absorption signals from chromium adsorbed on resin. Some peak atomization signals expanded by use of the transient memory, obtained after applying different ashing currents, are shown in Fig. 2. When the ashing current was 80 A, a small peak appeared early in the atomization because of smoke emitted from the residual resin, before the second peak was obtained from chromium atoms. This is responsible for the apparent increase in peak area at 70 or 80 A shown in Fig. 1. At 100—160 A, this small initial peak does not appear. When the ashing current is increased from 100 to 160 A, the

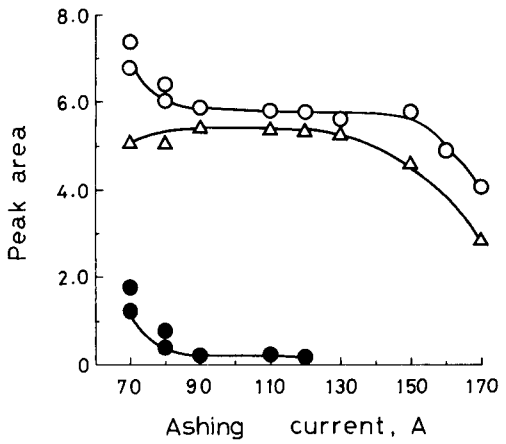

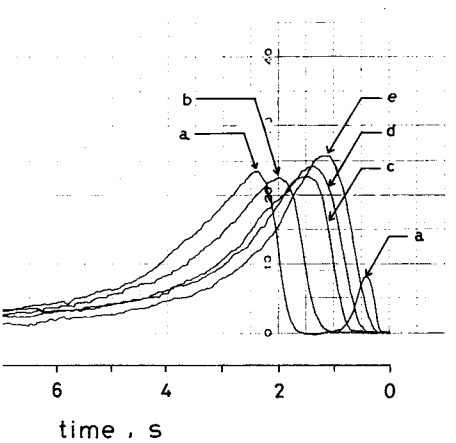

Fig. 1. Effect of ashing current on the peak area of chromium (resin suspension was 0.10 g/5.0 ml H_2O; injected volume 10 μl): (○) Cr(III) on resin (0.25 μg Cr/5.0 ml); (●) pure resin; (△) aqueous chromium(III) (0.25 μg Cr/5.0 ml). (A peak area of 10 is ascribed to a signal of 1.0 absorbance for 1 s.)

Fig. 2. Atomic absorption signals of Cr(III) (0.25 μg/5.0 ml) added on the resin. Ashing current: (a) 80; (b) 100; (c) 120; (d) 140; (e) 160 A.

chromium signals become gradually higher, but the peak areas are constant except at 170 A.

The background absorption was measured by using the neon line at 352.0 nm. No molecular or any other absorption was found at this wavelength during the atomization step. Therefore, no correction was necessary for background absorption in measuring the chromium peak area. It is also apparent from Fig. 2 that the atomization of chromium takes place increasingly rapidly with an increase in ashing current, i.e., with increasing temperature of the furnace before atomization, provided that the ashing current is <170 A.

Effect of argon flow rate. An argon atmosphere is necessary to extend the life of the carbon tube and to achieve satisfactory atomization of chromium by thermal dissociation. Argon flow rates of 0.5—2.0 l min^{-1} gave peak areas that varied by about 10% on repeated runs, and the carbon tube became more fragile. At 4.0 l min^{-1}, the peak areas had decreased appreciably, because of the dilution of chromium vapor by the gas. Constant peak areas were obtained from 2.5 to 3.5 l min^{-1} and an argon flow rate of 3.0 l min^{-1} was used in subsequent work.

Effect of amount of resin and stirring time. The adsorption of chromium(III) ions by Chelex-100 depends on the amount of resin, reaction time and pH. Tests with 250 ml of a 2.0 μg l^{-1} chromium(III) solution buffered at pH 4.0 showed that a constant peak area was obtained for chromium absorbance when 0.05—0.20 g of resin was used. Thus 0.1 g of resin was added in sub-

sequent experiments. Stirring for 5—30 min at the same speed produced the same chromium peak area, thus 20 min was selected for the recommended procedure.

Effect of pH. Below pH 3.0, chelation was increasingly inhibited by increasing concentrations of hydrogen ions. Above pH 6.0, there was incomplete collection of chromium(III) because of formation of chromium-hydroxide species such as $Cr(OH)^{2+}$ and $Cr(OH)_2^+$ [13]. The chromium signal was at a constant maximum over the pH range 3.5—5.5, and a pH 4.0 acetate buffer was selected for further use.

Conditions for reduction of chromium(VI). In order to establish conditions for the complete reduction of chromium(VI), the amounts of hydrogen peroxide and hydrochloric acid and the reaction time were examined for 1.0 $\mu g\ l^{-1}$ chromium(VI) with 250-ml samples. Figure 3 shows the % reduction after various reaction times, at various concentrations of hydrochloric acid. With increasing concentration of hydrochloric acid, the rate of reduction rises. After 15—20 min, almost 100% reduction is achieved in 0.04 and 0.10 M acid. In addition, 5 ml of 3% hydrogen peroxide was found to be sufficient for complete reduction.

Results for Cr(III) and Cr(VI)

Results obtained by the recommended procedure for some simple mixtures of chromium(III) and chromium(VI) are given in Table 2. The recoveries of chromium(III) and chromium(VI) were correct to within ±4%. The relative standard deviations obtained for 7 determinations of 0.25 μg of both chromium(III) and chromium(VI) in a 250-ml sample solution were 2.3% and 3.7%, respectively. Total chromium can be determined simply by reducing chromium(VI) to chromium(III) with hydrochloric acid and hydrogen peroxide before addition of the resin. The results for total

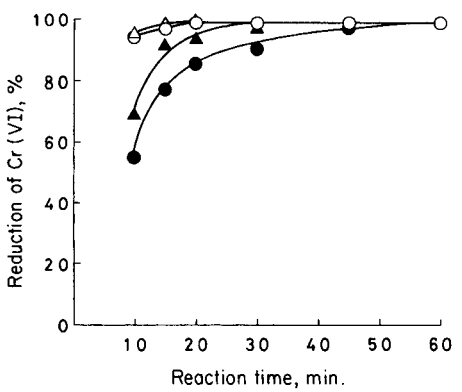

Fig. 3. Effect of reaction time on the % reduction of chromium(VI) (0.25 μg/250 ml) using 5.0 ml of 3% H_2O_2 and HCl of the following concentration: (△) 0.10; (○) 0.04; (▲) 0.012; (●) 0.008 M.

TABLE 2

Results for chromium(III) and chromium(VI) in synthetic mixtures (250-ml samples)

Added (μg)		Found (μg)		
Cr(III)	Cr(VI)	Cr(III)	Cr(VI)	Cr (total)[a]
0.25	0.25	0.24	0.25	0.48
0.45	0.05	0.45	0.04	0.50
0.15	0.35	0.15	0.34	0.49
0.25	0.00	0.24	—[b]	0.24
0.00	0.25	—[b]	0.25	0.25

[a]Obtained by pre-reduction of chromium(VI) (see text). [b]Not detected.

chromium are also shown in Table 2; they compare well with the sum of chromium(III) and chromium(VI) taken.

The procedure is relatively simple and requires few chemicals. The resin suspension is injected directly into the carbon tube atomizer with a micropipette, without weighing the resin or eluting the chromium from the resin. In addition, the method removes all anions before measurement of the peak-area signal. The effect of foreign ions was examined in the presence of both chromium(III) and chromium(VI) (1.0 μg l^{-1} each). Most common cations at the 100-ppm level, except aluminum and iron(III), did not influence the determination of chromium. Aluminum and iron(III) precipitated at pH 4. When 1 mg l^{-1} iron(III) was present, for example, the filter was clogged by the hydrated iron oxide. The interferences of these ions could be eliminated by adding 1.0 ml of 0.01 M cyclohexanediaminetetraacetic acid to the sample solution. Chloride, nitrate and sulfate did not interfere at 1000 mg l^{-1} concentrations.

The successive determination of chromium(III) and chromium(VI) in natural waters will be discussed in a subsequent paper.

This work was supported in part by a Grant-in-Aid for Scientific Research from the Ministry of Education, Science and Culture of Japan.

REFERENCES

1 T. M. Florence and G. E. Batley, C. R. C. Crit. Rev. Anal. Chem., 9 (1980) 219.
2 T. R. Gilbert and A. M. Clay, Anal. Chim. Acta, 67 (1973) 289.
3 K. Hiiro, T. Owa, M. Takaoka, T. Tanaka and A. Kawahara, Bunseki Kagaku, 25 (1976) 122.
4 G. J. de Jong and U. A. Th. Brinkman, Anal. Chim. Acta, 98 (1978) 243.
5 R. Fukai and D. Vas, J. Oceanogr. Soc. Jpn., 23 (1967) 298.
6 H. Elderfield, Earth Planet. Sci. Lett., 9 (1970) 10.
7 J. F. Pankow and G. E. Janauer, Anal. Chim. Acta, 69 (1974) 97.
8 M. S. Cresser and R. Hargitt, Anal. Chim. Acta, 81 (1976) 196.
9 A. Isozaki, N. Soeda, T. Okutani and S. Utsumi, Nippon Kagaku Kaishi, (1979) 549.
10 A. Isozaki, N. Soeda and S. Utsumi, Bull. Chem. Soc. Jpn., 54 (1981) 1364.

11 A. Isozaki, Y. Fukuda and S. Utsumi, Bunseki Kagaku, 31 (1982) 404.
12 A. Isozaki, T. Kawakami and S. Utsumi, Bunseki Kagaku, 31 (1982) E 311.
13 Y. Nakamura, E. Yamada, E. Nakayama, T. Kuwamoto and T. Fujinaga, Bunseki Kagaku, 31 (1982) 52.

Analytica Chimica Acta, 153 (1983) 23—31
Elsevier Science Publishers B.V., Amsterdam — Printed in The Netherlands

RAPID DETERMINATION OF LEAD, BISMUTH, ANTIMONY AND SILVER IN STEELS BY FLAME ATOMIC ABSORPTION SPECTROMETRY COMBINED WITH FLOW INJECTION ANALYSIS

NANGEN ZHOU[a], WOLFGANG FRECH* and ERIK LUNDBERG
Department of Analytical Chemistry, University of Umeå, S-901 87 Umeå (Sweden)
(Received 24th May 1983)

SUMMARY

A procedure based on pulse-nebulization flame atomic absorption spectrometry (a.a.s.) is shown to give considerably lower detection limits than conventional flame a.a.s. for the direct determination of trace elements in steels, because more concentrated sample solutions can be aspirated. Optimum conditions with respect to injected sample volume, total salt concentration in sample solution, (i.e., dilution factor) and selected resonance wavelengths were investigated. Results for a variety of low and high alloy steels are presented. The detection limits in the solid steel were as follows: Pb 2.5, Bi 2.5, Sb 10 and Ag 0.3 $\mu g\, g^{-1}$.

It is well known that trace or residual elements, such as Pb, Sn, Bi, Sb, As, Te, Ag, have adverse effects on the mechanical properties of steels [1]. Lead and bismuth are of special interest, because they have strongly deleterious effects even at very low concentrations. For example, Zou and Grinder [2] reported a pronounced decrease in hot ductility if a steel contained more than 20 $\mu g\, g^{-1}$ Pb or 6 $\mu g\, g^{-1}$ Bi.

Its simplicity and convenience make atomic absorption spectrometry (a.a.s.) the most frequently-used technique for the determination of the above-mentioned elements. The use of electrothermal atomizers generally permits direct determination of volatile trace elements in solid steel samples [3]. Because the dissolution step is omitted, the direct methods are both rapid and sensitive. It is, for example, possible to determine elements like bismuth in the ng g^{-1} range in the solid material. In spite of these impressive results, the solid-sampling technique has not been employed extensively. This is due to limitations mainly with regard to standardization [4] and narrow dynamic working range [3]. Therefore, in many applications, it is necessary to dissolve the steel samples prior to analysis. For flame work, such samples have to be further diluted (1 g of steel to 100 ml) in order to avoid clogging of the burner head. The concentrations of interest are then so low that a direct determination with the flame is practically impossible. For that reason

[a]Permanent address: Luoyang Bearing Factory, Luoyang, Henan, People's Republic of China.

0003-2670/83/$03.00

an extraction procedure, which is time-consuming, has to be included in order to concentrate the elements. The extraction can be omitted if the more sensitive graphite furnace [5] or hydride generation [6] techniques are used. However, these techniques are more complex than the flame and more subject to interference effects. Therefore it would be desirable to be able to use the simplicity of the flame without having to include a preconcentration step. To a certain extent this can be achieved by using more concentrated sample solutions, e.g., only 10 times dilution. In order to avoid clogging of the burner head, such samples have to be introduced into the flame by the so-called pulse-nebulization technique [7]. However, the detection limits obtained with this approach will be poorer than those reported with extraction—flame a.a.s. [8] or the graphite furnace [5] or hydride generation [6].

The pulse-nebulization technique has recently been reviewed by Cresser [9]. This technique is suitable for solutions that contain high salt concentrations, because the burner can be used for a considerably longer time before it is clogged. This advantage must be weighed against the main disadvantage, namely that the atomizer background absorption and/or emission spectra may change appreciably when a pulse of sample is nebulized, because more concentrated solutions are used and because solvent is not nebulized continuously between each sample. The latter drawback can be overcome by introducing the sample into a continuous stream of solvent [10] or by using flow injection analysis (f.i.a.) [11—13]. By use of the latter technique, memory effects as well as corrosion of the burner head and nebulizer are minimized. This paper deals with the potentialities of a combination of flame a.a.s. and f.i.a. for direct determination of trace elements in steels.

EXPERIMENTAL

Instrumentation

Figure 1 shows a block diagram of the instrumentation used. A flow-injection analysis system FIA 05 (BIFOK AB, Box 124, S-191 22 Sollentuna, Sweden) was connected to the nebulizer of a Varian-Techtron AA-875 atomic absorption spectrometer, provided with background corrector. In the f.i.a.

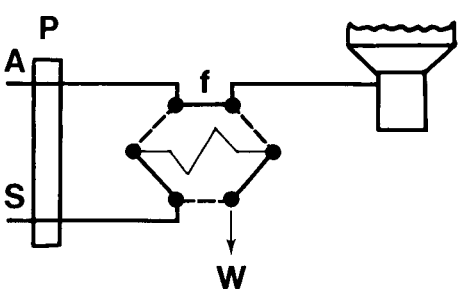

Fig. 1. Block diagram of instrumentation. P, pump; f, injector with 90-μl sample loop (— filling, --- inject position); A, aqueous carrier stream; S, sample; W, waste.

system was included an eight-channel peristaltic pump (FIA 08) with adjustable speed and a sample injector valve with exchangeable sample loops. The tubings used were made from Tygon and teflon. A Perkin-Elmer model 56 recorder was connected to the spectrometer. The instrumental parameters are summarized in Table 1. Lamp currents, slit widths and recorder damping were chosen for optimum signal-to-noise ratio.

Reagents and materials

The metallurgical standard materials used were supplied by British Chemical Standards (BCS), National Bureau of Standards (NBS) and Institutet för Metallforskning, Sweden (JK).

All reagents were analytical reagent-grade products. The 1000 μg g^{-1} stock solutions were prepared from lead nitrate, silver nitrate, bismuth metal and antimony metal. Nitric acid (65%) and hydrochloric acid (37%) were Merck products.

Procedures

Preparation of sample solutions. Samples (1.00 g) were dissolved in 7.0 ml of concentrated hydrochloric acid and 3.5 ml of concentrated nitric acid (added slowly) in a 100-ml Erlenmeyer flask. The solution was then filtered through a glass filter paper (GF/A, Whatman), which was washed with the minimum volume of (1 + 19) hydrochloric acid. Dilution was then made with (1 + 19) hydrochloric acid to a final mass of 12.5 g, which means that the total metal concentration in the sample solution was 8% (w/w).

Preparation of standard solutions. Four standard solutions were prepared for use with low-alloy steels. Solution A was prepared containing 100 μg g^{-1} each of Pb, Bi and Sb, and 10 μg g^{-1} silver in (1 + 99) nitric acid. For

TABLE 1

Instrumental parameters

	Pb	Bi	Ag	Sb
Wavelength (nm)	283.3	223.1	328.1	206.8
Slit width (nm)	1.0	1.0	1.0	1.0
Lamp current (mA)	5	5	5	11.5 W[a]
Air flow rate (l min^{-1})	11			
Acetylene flow rate (l min^{-1})	1.3			
Aspiration rate (ml min^{-1})[b]	5.8			
Pump rate (ml min^{-1})	5.6			
Sample volume (μl)	90			
Inner diam. of sample coil (mm)	0.5			
Length of tubing between valve and nebulizer (mm)	250			
Recorder damp mode	normal			

[a]Electrodeless discharge lamp. [b]Measured with the f.i.a. system disconnected.

solution B, 193.60 g of iron(III) chloride hexahydrate was dissolved in 100.00 g of (1 + 99) nitric acid and the solution was diluted with (1 + 19) hydrochloric acid to a final mass of 500.00 g, to produce an 8% (w/w) iron solution. Solution C was prepared in the same way as solution B, except that the 100.00 g of diluted nitric acid was replaced by 100.00 g of solution A, thus producing an 8% (w/w) iron solution containing 20 $\mu g\ g^{-1}$ each of Pb, Bi and Sb and 2 $\mu g\ g^{-1}$ silver. For solution D, appropriate amounts of solutions B and C were measured out, to produce a set of multielement standards (see Fig. 4).

The standards for use with high-alloy steels were the same as for low-alloy steels except for solution B, which was prepared by dissolving 128.26 g of iron(III) chloride hexahydrate, 41.00 g of chromium(III) chloride hexahydrate and 26.32 g of nickel(II) chloride hexahydrate in 100.00 g of (1 + 99) nitric acid followed by addition of (1 + 19) hydrochloric acid to a final mass of 500.00 g, to produce a 5.3% (w/w) iron, 1.6% (w/w) chromium and 1.1% (w/w) nickel solution.

Atomic absorption procedure. The instrumental parameters are given in Table 1. The concentrations of Pb, Bi, Sb and Ag were determined in steels and blanks: the sample loop was filled by aspirating 200 μl of sample or standard solutions; 90-μl plugs were pumped into the flame in triplicate at a rate of 120 h^{-1}. The carrier stream was distilled water. After every two hours, the burner head had to be cleaned mechanically. After each such cleaning procedure, the burner was conditioned by aspirating ten 90-μl portions of a steel sample, after which the system was recalibrated. Peak height values were evaluated throughout, using a strip-chart recorder with 5—10× scale expansion. In order to check for impurities of the trace elements in the iron, chromium and nickel chlorides, the low-alloy ultrapure steel JK 1C was used as a blank (8% w/w solution).

RESULTS AND DISCUSSION

Optimization of analytical conditions

The optimum dilution factor with respect to signal increase and interfering effects from the steel matrix was investigated. Figure 2 shows the decrease in signal height for constant amounts of Pb, Bi and Sb on aspiration with increasing concentrations of iron. The fact that the signals decrease means that possible improvements with regard to detectability of trace elements in steels are not as large as expected. This is clarified in Fig. 3 where the relative signal increase is shown as a function of the dilution, and thus iron concentration. As can be seen, an optimum for all three elements is obtained at an iron concentration of 12% (w/w). It should be noted that baseline noise was not significantly affected with increasing salt concentration and hence the signal increase does to a certain extent reflect improvements in the detection limit of the trace elements in steel. A dilution corresponding to 8% (w/w) of iron was used in order to minimize the risk of clogging and to avoid problems

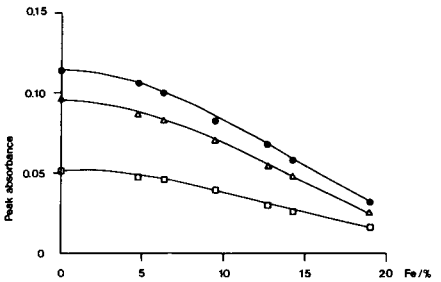

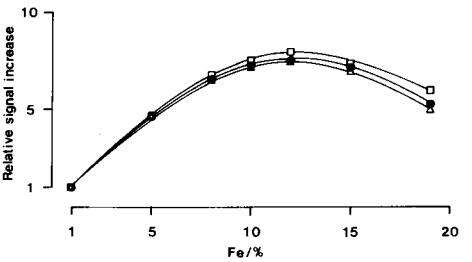

Fig. 2. Peak height absorbance values for 0.9 μg of Pb (•), Bi (△) and Sb (□), as a function of the iron concentration in solution.

Fig. 3. Signal increases (1—10-fold) relative to 1% Fe (100 times dilution) for Pb (•), Bi (△) and Sb (□) as a function of increasing iron concentration (decreasing dilution factor) when the interfering effects seen in Fig. 2 are taken into account.

in filtering and diluting more concentrated solutions. The fact that the maxima coincide means that the interfering effects obtained are not element-specific and so the same dilution factor is adequate for these three elements.

A sample volume of 90 μl was used throughout, because further increase in volume resulted in only minor gain in signal height [7] but increased the risk of clogging. A pump rate slightly less than the normal aspiration rate of the nebulizer system was found to give maximum peak height signal.

When solutions containing high concentrations of iron, chromium or nickel were aspirated, baseline shifts were obtained at most of the resonance wavelengths of the trace elements investigated, although the solutions did not contain measurable amounts of those elements, and the background corrector was used. This problem has been discussed by Cresser [9], who suggested that the reasons could be fine structure on the background spectra or changes in the flame stoichiometry or geometry. In this work, the wavelengths and flame stoichiometry were selected so that minimum baseline shifts and acceptable sensitivities were obtained.

Standardization

Calibration graphs for all four elements in the presence of iron or iron—chromium—nickel matrices are shown in Fig. 4 (a—d). These lines were found to be parallel to the lines obtained by making standard additions to low- and high-alloy steels, and for that reason standardization against synthetic standards is possible. However, for Ag, Bi and Sb, different standard graphs have to be used for low- and high-alloy steels, because of differences in sensitivity (silver) or differences in baseline shift (Sb, Bi, Ag). This baseline shift must of course be considered in the evaluation of sample concentrations. It should be observed that the fact that negative signals can occur, results in an increased uncertainty in the zero level and so the detection limits will deteriorate.

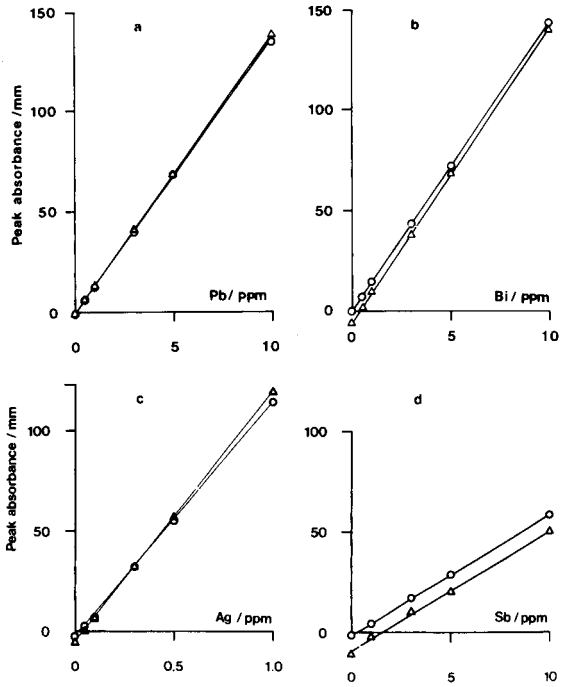

Fig. 4. Calibration curves for Pb (a), Bi (b), Ag (c) and Sb (d) in the presence of iron (○) or iron—chromium—nickel (△) matrices. 100 mm = 0.087 absorbance units.

Results for standard steels

Several low- and high-alloy steels were analyzed by the procedure described, and the results are given in Tables 2—5. For comparison, reference [5—6, 14—22] or certified values are also included. In general, the accuracy and precision are acceptable considering that many of the trace element concentrations of these materials are close to the detection limits of the procedure. These limits were calculated as twice the standard deviation obtained for repeated analyses of samples containing low concentrations of the trace elements. In order to illustrate the performance of the procedure, recorder traces are given for the most difficult (antimony) and the easiest (silver) element in Fig. 5. The previously discussed baseline shift is exemplified for both elements.

As has been demonstrated in this paper, the combination of flame a.a.s. and f.i.a. comprises a significant improvement with regard to sensitivities and detection limits compared with conventional flame a.a.s. This means that rapid and convenient determinations of trace elements in steels are possible, provided that the detection limits of the procedure can be accepted.

This work was supported by grants from the Swedish Natural Science Research Council. We thank Dr. Neil Clark of Varian-Techtron Pty. for

TABLE 2

Determination of lead in a variety of low- and high-alloy steels

Designation	Value found[a] ($\mu g\ g^{-1}$)	n	Certified value ($\mu g\ g^{-1}$)	Reference value[b] ($\mu g\ g^{-1}$)
JK 1C	<2.5	4	<1[c]	0.3[18]; 0.2[19]
2C	4.8; 3.8; 4.8	3	4[c]	4.9[14]; 4[18]
8C	<2.5; 2.9; <2.5	3	2[c]	2.6[14]; 2[18]; 1.9[19]
16A	10.0 ± 1.2	6	10	9[18]; 11[14]
BCS 330	26.2 ± 1.4	6	30	27[18]
331	4.2 ± 1.1	5	—	5.8[14]; 5.4[22]
332	6.1 ± 1.2	5	—	7.6[14]
333	4.3 ± 1.4	6	—	6.0[14]; 6.0[22]
334	10.1 ± 1.2	6	11	10.6[14]; 11.3[22]; 12[19]
335	13.7 ± 1.3	5	15	15.3[22]; 15[18]; 14.6[14]
336	5.0; 5.6; 4.7	3	7	7.4[22]; 7.1[14]
273	35.7; 36.9; 36.2	3	30[c]	
277	85.2; 82.8; 85.1	3	65[c]	75[18]
NBS 361	2.8; <2.5; 2.5; <2.5	4	—	1[14]; 0.24[22]
362	3.5 ± 0.9	4	4.8	4.7[14]
363	17.6 ± 1.5	5	18.6	18[14]

[a]With standard deviation where appropriate.
[b]Numbers in square brackets are literature references.
[c]Recommended value from analysis certificate.

TABLE 3

Determination of bismuth in a variety of low- and high-alloy steels

Designation	Value found[a] ($\mu g\ g^{-1}$)	n	Certified value ($\mu g\ g^{-1}$)	Reference value[b] ($\mu g\ g^{-1}$)
JK 16A	16.5 ± 0.5	4	18	17[16]; 17[14]
BCS 330	3.2 ± 1.2	4	—	2.9[22]; 2.8[16]; 3.0[15]
335	<2.5	2	—	0.062[17]; 0.06[22]; 0.06[14]; 0.1[15]
336	2.7	1	—	3.4[17]; 3.3[22]; 3.5[14]; 3.2[16]
NBS 361	5.5 ± 0.7	4	4[c]	4.8[22]; 6.4[14]; 5[6]
362	23.4; 18.8	2	20[c]	30[6]
363	5.0 ± 1.0	4	8[c]	5.2[22]; 7.4[14]; 8[6]
364	12.5 ± 1.1	4	9[c]	24[14]; 15[6]

[a–c]See Table 2.

TABLE 4

Determination of antimony in a variety of low- and high-alloy steels

Designation	Value found[a] ($\mu g\ g^{-1}$)	n	Certified value ($\mu g\ g^{-1}$)	Reference value[b] ($\mu g\ g^{-1}$)
JK 2C	35; 32	2	30[c]	29[5]; 35[14]
8C	19; 17	2	18[c]	19[14]; 20[5]
16A	<10	4	—	10[5]; 7[14]
BCS 330	166 ± 6	4	180	174[5]
331	44 ± 5	4	—	42[14]; 45[22]
332	40 ± 3	4	—	39[14]; 35[22]
333	35 ± 4	4	—	36[14]; 43[22]
334	19 ± 1	4	—	21[14]; 22[22]; 18[5]
335	29 ± 4	4	—	30[14]; 35[22]; 27[5]
336	31; 30	2	—	28[14]; 34[22]; 28[5]; 31[21]
NBS 361	37 ± 4	4	42	43[14]; 41[21]; 40[6]
362	119; 112	2	130	135[21]; 130[6]
363	21 ± 5	4	20	21[14]; 16[21]; 20[6]
364	339; 303; 318	3	340	337[21]; 340[6]

[a—c]See Table 2.

TABLE 5

Determination of silver in a variety of low- and high-alloy steels

Designation	Value found ($\mu g\ g^{-1}$)	Certified value ($\mu g\ g^{-1}$)	Reference value ($\mu g\ g^{-1}$)
JK 2C	0.3; 0.3	—	0.36[20]
8C	0.7; 0.7	2.5[a]	0.85[15]
16A	4.5; 4.5	—	—
BCS 273	0.4; 0.3	—	—
277	<0.3; 0.3; 0.3	—	—
330	0.3; 0.4	—	—
331	<0.3; <0.3	—	0.24[14]; 0.25[22]
336	0.5; 0.7	—	0.71[14]; 0.70[22]; 0.63[15]
NBS 361	3.9; 3.9; 3.8	4	4.2[14]
362	11.0; 11.2; 11.0; 11.3	11	9[14]

[a]Recommended value.

providing the model 875 AA spectrophotometer on loan and Dr. Bo Karlberg of BIFOK AB for the loan of the f.i.a. equipment. We also thank Prof. Dr. Eberhardt Hasenteufel for valuable discussions and his interest in this work.

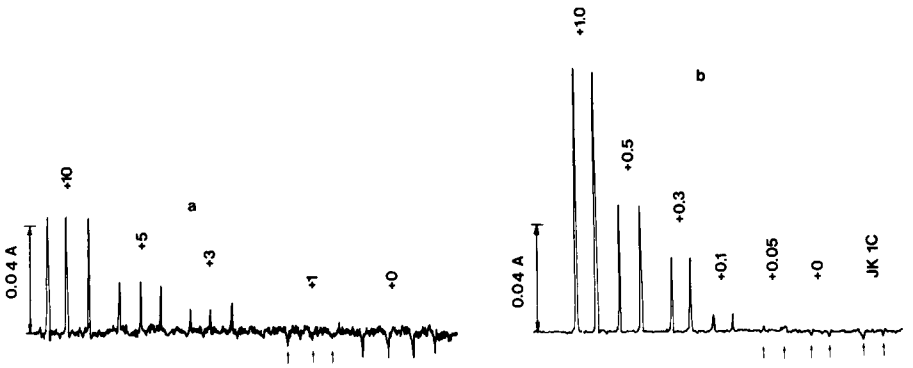

Fig. 5. Recorder traces for Sb (a) in high-alloy and Ag (b) in low-alloy matrix. The precision for repeated injections of 0.5 $\mu g\ g^{-1}$ Ag solution (n = 11) was ±2.9%.

REFERENCES

1 G. Mayer and C. A. Clark, The Metallurgist and Materials Technologist, Nov. 1974, p. 491.
2 Z. Zou and O. Grinder, Scand. J. Metall., 11 (1982) 79.
3 J. B. Headridge, Spectrochim. Acta, Part B, 35 (1981) 785.
4 W. Frech, E. Lundberg and M. Barbooti, Anal. Chim. Acta, 131 (1981) 45.
5 W. Frech, Talanta, 21 (1974) 565.
6 B. Welz and M. Melcher, Spectrochim. Acta, Part B, 35 (1981) 439.
7 H. Berndt and E. Jackwerth, Spectrochim. Acta, Part B, 30 (1975) 169.
8 K. F. Burke, Analyst, 97 (1972) 19.
9 M. S. Cresser, Prog. Anal. At. Spectrosc., 4 (1981) 219.
10 P. E. Wilson, At. Absorpt. Newsl., 18 (1979) 115.
11 W. R. Wolf and K. K. Stewart, Anal. Chem., 51 (1979) 1201.
12 J. Růžička and E. H. Hansen, Flow Injection Analysis, Wiley, New York, 1981.
13 B. Karlberg, in R. W. Frei and J. F. Lawrence (Eds.), Chemical Derivatization in Analytical Chemistry, Vol. 2, Plenum, New York, 1982, p. 1.
14 B. Thelin, Appl. Spectrosc., Part B, 35 (1981) 302.
15 E. Lundberg and W. Frech, Anal. Chim. Acta, 108 (1979) 75.
16 W. Frech, Fresenius Z. Anal. Chem., 275 (1975) 335.
17 D. G. Andrews and J. B. Headridge, Analyst, 102 (1977) 436.
18 W. Frech, Anal. Chim. Acta, 77 (1975) 43.
19 E. Lundberg and W. Frech, Anal. Chim. Acta, 104 (1979) 75.
20 A. M. Aziz-Alrahman and J. B. Headridge, Talanta, 25 (1979) 413.
21 A. M. Aziz-Alrahman and J. B. Headridge, Analyst, 104 (1979) 944.
22 S. Bäckman and R. W. Karlsson, Analyst, 104 (1979) 1017.

Analytica Chimica Acta, 153 (1983) 33—40
Elsevier Science Publishers B.V., Amsterdam — Printed in The Netherlands

DETERMINATION OF ANTIMONY IN ATMOSPHERIC PARTICULATE MATTER BY HYDRIDE GENERATION AND ATOMIC ABSORPTION SPECTROMETRY

K. DE DONCKER, R. DUMAREY, R. DAMS and J. HOSTE*

Institute for Nuclear Sciences, Rijksuniversiteit Gent, Proeftuinstraat 86, B-9000 Gent (Belgium)

(Received 4th May 1983)

SUMMARY

Antimony-124 is used as tracer in the development of a procedure for the wet digestion of atmospheric particulates collected on cellulose filters. The samples are decomposed with sulphuric acid and hydrogen peroxide, followed by hydrofluoric acid to dissolve residual silicates. The yield of the dissolution for antimony is almost 100%. The chemical and instrumental parameters for the hydride generation and subsequent atomic absorption spectrometry were optimized. The precision of the entire procedure is generally better than 10% with a sensitivity for antimony of 1 ng m^{-3} of air. Excellent agreement was found between the results obtained by the proposed method and those from instrumental neutron activation analysis for concentrations of 4—2500 ng m^{-3}.

Various techniques are available for the determination of traces of antimony in environmental samples, instrumental neutron activation analysis (i.n.a.a.) and electrothermal atomic absorption spectrometry (a.a.s.) probably being the most accurate methods [1—3]. If hydride generation is combined with a.a.s., the determination of antimony and other volatile hydride-forming elements (e.g., As, Se, Te, Ge, Bi) offers selectivity and sensitivity because most matrix interferences are eliminated. In this technique, the hydride is separated from the digested sample solution after addition of sodium tetrahydroborate and then thermally decomposed in a heated quartz cell placed in the optical path of the spectrometer [4—7].

The present paper describes a digestion procedure for antimony in atmospheric particulate materials. This is a prerequisite as losses were encountered with a standard digestion procedure using nitric and perchloric acids [8].

Tracer experiments with antimony-124 were done, to quantify and subsequently avoid such losses. Additionally, the analytical parameters were optimized. To check for accuracy, results obtained with the technique described are compared with data obtained by i.n.a.a. for air samples with a wide range of antimony concentrations.

0003-2670/83/$03.00

EXPERIMENTAL

Apparatus and reagents

A Perkin-Elmer model 503 spectrometer was equipped with the mercury/hydride system MHS-1 and an antimony electrodeless discharge lamp. The output signal was monitored with a Perkin-Elmer Model 56 recorder operated at a range of 10 mV full scale and a 20 mm min^{-1} chart speed.

All reagents were of at least analytical grade: hydrofluoric acid (50%, analytical-grade), hydrogen peroxide (30%, UCB), hydrochloric acid (Suprapur, 30%, Merck), sulfuric acid (95—98%, J. T. Baker), nitric acid (70%, J. T. Baker). Solutions required are: 10% (w/v) hydroxylammonium chloride, 2% (w/v) hydrazinium sulfate, 10% (w/v) sodium iodide with ascorbic acid (1 g l^{-1}) added for stabilization, 5% (w/v) sodium tetrahydroborate (Aldrich) stabilized with 2% sodium hydroxide.

The antimony stock solution (1000 mg l^{-1}) in 3% (v/v) hydrochloric acid was prepared from antimony trichloride. The ^{124}Sb tracer had a specific activity of 32 C μg^{-1} s^{-1}.

Optimization of the hydride generation

Chemical and instrumental parameters influencing the formation of stibine from antimony, present in particulate matter collected on Whatman 41 cellulose filters, were studied to optimize the analytical method.

Valence state. Antimony can be present as Sb(III) or Sb(V) depending on the oxidizing properties of the solution. As is well known, the valence state plays an important role in the formation of hydrides. The difference in peak shape obtained from Sb(III) and Sb(V) solutions is illustrated in Fig. 1. Sb(V) decreases the sensitivity by ca. 60%, because of the much faster conversion of Sb(III) to stibine. The difference in reaction rate increases with increasing pH [9]. This problem may be overcome by preconcentrating the stibine in a cold trap. However, in the MHS-1 arrangement, the stibine is carried continuously to the optical cell during generation. Therefore, any Sb(V) present in the sample solution must be pre-reduced to Sb(III). Several reducing agents were tested for a solution containing 0.1 μg Sb ml^{-1} obtained after digestion of an antimony-spiked blank Whatman 41 cellulose filter in a mixture of nitric and perchloric acids. Sodium iodide showed good prereducing properties, when 1 ml of 10% (w/v) NaI per 10 ml of sample solution was used.

Addition of sodium tetrahydroborate. In the MHS-1, the tetrahydroborate can be added as a solution or as a pellet. The use of the solution gave the best results. The addition of a fixed volume (2.50 ml) can be done very reproducibly, whereas the production of equal pellets is tedious and time-consuming. Moreover, the blank values when a pellet (125 mg) was used, were 6—7 ng Sb, whereas the use of the reducing solution gave a blank of only 3.3 ± 1 ng. For all further measurements, 2.5 ml of 5% (w/v) sodium tetrahydroborate solution was used for a 10-ml sample. This solution was

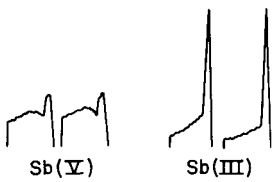

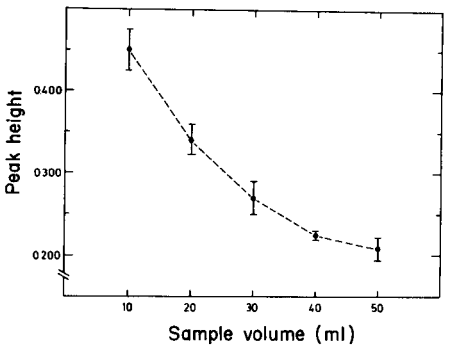

Fig. 1. Effect of the valence state on the absorbance signal (100 ng Sb).

Fig. 2. Effect of sample volume on the peak height for 100 ng Sb. Peak height is given as absorbance.

stabilized with 2% (w/v) sodium hydroxide and stored at 4°C. During analyses, the solution was cooled with ice to prevent decomposition of the tetrahydroborate, which led to an irregular introduction of the reagent into the cell, resulting in multiple peaks.

Sample volume. Figure 2 illustrates the influence of the sample volume on the peak height. The optimal volume was 10 ml; below 10 ml, incomplete mixing of the reductant and sample gave irreproducible signals. Higher volumes gave broadened peaks caused by the increasing time needed to sweep the stibine out of the sample solution at the argon flow rate of 250 ml min^{-1} fixed by the manufacturer. Before the measurements, argon at 500 ml min^{-1} is used to expel oxygen from the system.

Cell temperature. The influence of the atomization temperature on the absorbance signal is given in Fig. 3. Below 400°C, stibine was not decomposed. Between 600 and 800°C, only partial atomization was achieved, whereas above 950°C, the signal decreased slightly. Therefore 950°C was selected for all further experiments.

MHS-1 program. The MHS-1 control module permits the choice of four programs which differ only in the timing of the purge and measurement cycle. No significant effects on the absorbance signals were found with the different programs, hence the short program (I) was used (total analysis time 70 s).

Background correction. No improvement was found when deuterium background correction was applied, whether for aqueous standard solutions or for digested samples.

The optimal operating parameters are summarized in Table 1.

Optimization of the digestion procedure

When the standard digestion procedure with nitric and perchloric acids recommended for atmospheric particulate matter collected on filters [8] was

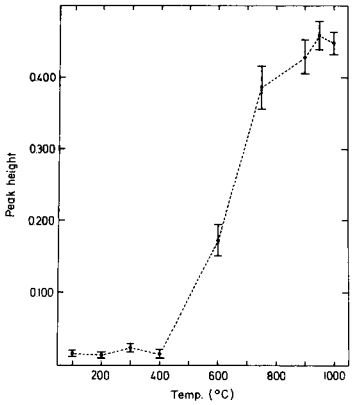

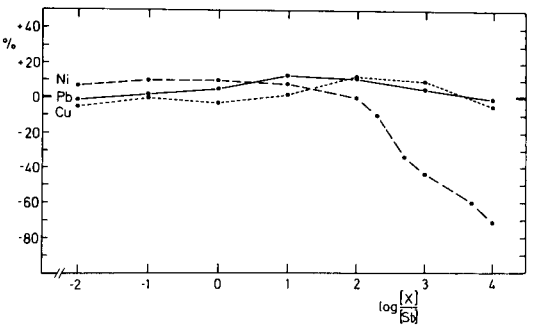

Fig. 3. Effect of cell temperature on the peak height (100 ng Sb).

Fig. 4. Interferences on the determination of antimony: (— — —) Ni; (——) Pb; (···) Cu.

applied, losses occurred ranging from 13 to 54%. This was established by comparing the results to those obtained with i.n.a.a. Accordingly, a two-step radiotracer study with the γ-emitting isotope ^{124}Sb ($t_{1/2}$ = 60.2 d) was conducted to check the efficiency of other possible digestion mixtures. In the first step, a blank cellulose filter spiked with ^{124}Sb was digested to investigate for losses caused by the possible formation of slightly soluble antimony compounds. In the second step, these experiments were repeated with particulate-loaded filters to check for sorption effects on the undissolved residue of the material.

Tracer-spiked blank filters. An aliquot containing 10 μg of ^{124}Sb was spiked on a Whatman 41 filter (5.5-cm diameter), which was subsequently digested in different mixtures: (A) H_2SO_4—HNO_3; (B) H_2SO_4—H_2O_2; and (C) H_2SO_4—HCl—HNO_3. In all cases, the digest was filtered on a Whatman 41 filter. The filtrate was diluted to volume in a 100-ml volumetric flask with deionized water. After measurement on a NaI scintillation detector, the γ-ray activity of the final solution was compared with a diluted undigested aliquot of the original radiotracer solution. In no case were losses encountered.

In subsequent experiments, the residual ^{124}Sb activity was measured after hydride generation, for samples digested with mixtures A or B. It was found

TABLE 1

Operating parameters

Reductant	2.5 ml of 5% $NaBH_4$	Background correction	Off
Sample volume	10 ml	Damping	2
Argon flow	250 ml min^{-1}	Wavelength	217.6 nm
Cell temperature	950°C	Spectral bandwidth	0.2 nm (slit 3)
Hydride program	I	Lamp	8 W

that 13% and 82% of the antimony remained in solution when the digest contained nitric acid and peroxide, respectively, because the oxidant removed the iodide needed for reduction of Sb(V) to Sb(III). These interfering traces of nitric acid or peroxide could be removed with 3 ml of 10% (w/v) hydroxylammonium chloride or 2 ml of 2% (w/v) hydrazinium sulfate on heating for about 20 min. After these additions, the antimony was quantitatively recovered during the hydride generation step (99.0% ± 1.2%).

Although both modified procedures A and B yielded excellent recoveries, method B was preferred because the digestion was much faster.

Tracer-spiked particulate-loaded filters. When the above digestion technique was applied to filters loaded with atmospheric particulates, negative results (up to 35%) were obtained. In these tests, 10 μg of ^{124}Sb radiotracer was spiked on a Whatman 41 filter (5.5-cm diameter) loaded with about 300 μg of particulate matter per cm^2. After digestion, the solution was filtered and both residue and filtrate were examined for γ-ray activity. The results are listed in Table 2. The undissolved fraction still contained an important amount of antimony. This was probably caused by adsorption of antimony on the insoluble fraction. For this reason, the procedure was modified by adding 4 ml of hydrofluoric acid after the initial reaction with H_2SO_4/H_2O_2 had subsided. Because all traces of hydrofluoric acid must be removed before the addition of the hydrazinium sulfate, 2 ml of sulfuric acid and 2 ml of hydrogen peroxide were added. Following this method, the residue contained less than 2% Sb. However, in some cases, the recovery was not quantitative, probably because of incomplete dissolution of the sample. This could easily be avoided by using larger amounts of acid and peroxide at the beginning of the digestion step, 8 ml and 4 ml, respectively. The hydride generation step, applied to samples digested in this way, yielded complete recoveries of the antimony (99.0% ± 0.3%).

Recommended procedure

Place a filter (Whatman 41, diameter 11 cm) in a 100-ml teflon beaker, containing 8 ml of concentrated sulfuric acid and add dropwise 4 ml of 30% hydrogen peroxide. After the initial reaction has subsided, heat the digest for

TABLE 2

Recovery of ^{124}Sb activity after digestion of spiked particulate-loaded filters

Mixture	^{124}Sb activity (%)	
	In filtrate	In residue
H_2SO_4—H_2O_2—$NH_2NH_2H_2SO_4$ (3:2:2)	75—100	6—15
H_2SO_4—H_2O_2—HF (3:3:4)	90—95	2
H_2SO_4—H_2O_2—$NH_2NH_2H_2SO_4$ (2:2:3)		
H_2SO_4—H_2O_2—HF (8:4:4)	100—101	2
H_2SO_4—H_2O_2—$NH_2NH_2SO_4$ (2:2:4)		

about 20 min. After cooling, add 4 ml of hydrofluoric acid and evaporate to half the initial volume. Remove traces of hydrofluoric acid by heating after the addition of 2 ml of sulfuric acid and 2 ml of hydrogen peroxide. Finally, add 4 ml 2% (w/v) hydrazinium sulfate to remove all the peroxide.

After the digestion, filter the solution on a Whatman 41 filter paper and dilute with 0.1% (w/v) sodium iodide to 50 ml or 100 ml, depending on the antimony content of the digested air samples. Quantify antimony in the final sample solutions by hydride generation, using the parameters given in Table 1.

Interferences

The interfering effects of Ni^{2+}, Cu^{2+} and Pb^{2+} were established by determining the antimony content in the presence of increasing amounts of these ions. The percent enhancement or suppression of the signal, obtained for metal ion/antimony ratios varying from 10^{-2} to 10^{4}, is given in Fig. 4. The only significant interference is encountered for Ni^{2+} in 200-fold amounts.

RESULTS AND DISCUSSION

The recommended procedure was used to determine the antimony content in a number of particulate samples collected in the vicinity of a non-ferrous plant producing antimony alloys and oxides. The samples were taken by passing daily approximately 400 m^3 of air over a 11-cm diameter Whatman 41 filter [10]. The high-volume samplers were of the LIB type [11].

Calibration and precision

For calibration of the a.a.s. measurements, two procedures were applied to check for possible systematic errors. When standard solutions in the range 20—100 ng of antimony were measured, the calibration plot of absorbance (A) against ng Sb gave the equation $y = x(0.0046 \pm 0.0001)\ A\ ng^{-1} - (0.0081 \pm 0.0039)\ A$. When standard additions were made by adding known amounts (25 and 50 ng) of antimony to portions of a digested solution of a particulate sample, the equation of the straight line then obtained was $y = x(0.0047 \pm 0.0003)\ A\ ng^{-1} + (0.1857 \pm 0.0093)\ A$. The correlation coefficients for these two equations were 0.9990 and 0.9804, respectively.

When both methods were applied to the same sample of particulate matter, the agreement was within 10%, as expected from the standard deviation. The result obtained from the calibration plot was (37.0 ± 3.2) ng, whereas the result by standard additions was (40.0 ± 6.7) ng of antimony.

To check further the precision of the technique, several filters were quartered and each part was analyzed. The results (Table 3) show the precision, calculated as the relative standard deviation. These figures include uncertainties arising from inhomogeneity of the filters as well as those from the digestion and measurement procedure.

TABLE 3

Analysis of quartered filters for antimony in air samples with mean ($\bar{x}$) and relative standard deviation

Filter No.	Sb found (ng m^{-3})				$\bar{x}$	RSD (%)
	1	2	3	4		
1	27.0	27.0	23.0	32.0	27.0	14.0
2	130.0	147.0	146.0	146.0	142.0	6.0
3	789.0	731.0	634.0	726.0	720.0	8.9
4	2265.0	2455.0	2468.0	2556.0	2436.0	5.0

Accuracy

The accuracy of the method was evaluated by treating separate quarters of the same filter by the proposed a.a.s. technique and by instrumental neutron activation analysis. For the latter analysis, a quarter of the filter was pressed to a pellet and irradiated for 7 h at a neutron flux of 1.5×10^{12} n cm^{-2} s^{-1}. After a decay time of 10—15 days, ^{124}Sb was counted for 15 min on a Ge(Li) detector, using the photopeaks at 602.7 and 1691.0 keV. The standard deviation on this technique varied from 1 to 10%, depending on the antimony concentration.

In Fig. 5, the data obtained by the two methods are compared. The agreement is good. The equation of the line is $y = x(0.963 \pm 0.023) + (7.3 \pm 22.4)$ ng m^{-3}, with a correlation coefficient of 0.995. The mean percent difference between the two methods is 10% for the 19 results which vary over a concentration range of three orders of magnitude.

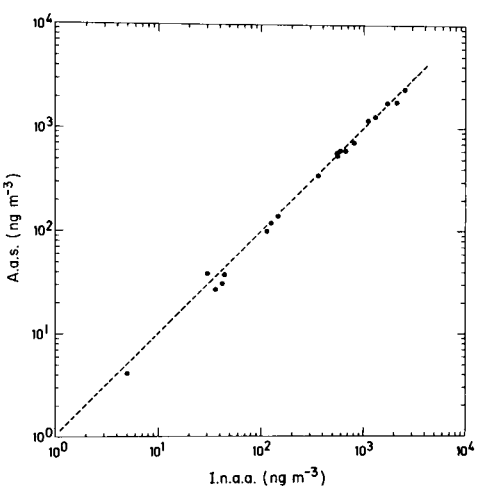

Fig. 5. Correlation between i.n.a.a. and hydride generation a.a.s.

Sensitivity

The detection limit, defined as the antimony concentration corresponding to three times the standard deviation of the blank, was calculated to be about 4 ng. It must, however, be emphasized that this value and also the precision depend on the optical quality of the cell. Because of deterioration of its inner walls after repeated use, the precision decreases rapidly.

A sensitivity of 4 ng per 2-ml of sample injected into the reaction vessel corresponds to 100 ng in the 50-ml solution of the digest. This is equivalent to 1 ng m^{-3} if at least 100 m^3 of air has been filtered, which is normally sufficient for all urban, industrial and normal continental samples. Only at extremely pure background stations would larger volumes of air need to be filtered.

This work was supported by the "Interuniversitair Instituut voor Kernwetenschappen" to whom we are sincerely grateful.

REFERENCES

1 G. C. Kunselman and E. A. Huff, At. Absorpt. Newsl., 15 (1976) 29.
2 B. W. Haynes, At. Absorpt. Newsl., 17 (1978) 49.
3 T. Kamada and Y. Yamamoto, Talanta, 24 (1977) 330.
4 K. C. Thompson and D. R. Thomerson, Analyst, 99 (1974) 595.
5 Y. Yamamoto and T. Kumamaru, Z. Anal. Chem., 281 (1976) 355.
6 W. B. Robbins and J. A. Caruso, Anal. Chem., 51 (1979) 889 A.
7 R. G. Godden and D. R. Thomerson, Analyst, 105 (1980) 1137.
8 Belgisch Instituut voor Normalisatie, NBN T 94-401, Determination of the Lead Mass in Particles Collected by Air Filtration — Atomic Absorption Spectrophotometry, 1977.
9 M. Yamamoto, K. Urata and Y. Yamamoto, Anal. Lett., 14 (1981) 21.
10 R. Dams, R. Vanderborght and F. Adams, Environ. Technol. Lett., 3 (1982) 337.
11 Verein Deutscher Ingenieure, VDI 2463-Blatt 4, VDI Verlag GmbH, Düsseldorf, 1976.

Analytica Chimica Acta, 153 (1983) 41—51
Elsevier Science Publishers B.V., Amsterdam — Printed in The Netherlands

MOLECULAR EMISSION CAVITY ANALYSIS
Part 25. The Determination of Silicon

MARCELA BURGUERA[a] and S. L. BOGDANSKI[b]

Chemistry Department, University of Birmingham, PO Box 363, Birmingham B15 2TT (Gt. Britain)

ALAN TOWNSHEND*

Chemistry Department, University of Hull, Hull HU6 7RX (Gt. Britain)

(Received 10th March 1983)

SUMMARY

Silicon is rapidly converted to volatile silicon tetrafluoride in 98% sulphuric acid at 135°C in the presence of chloride. The gases are carried by nitrogen to a m.e.c.a. oxy-cavity, and the intensity of the white SiO continuum emission is measured. The detection limit is 0.2 μg Si, and linear calibration is achieved up to 500 mg l^{-1} silicon. Few ions interfere. The procedure is applied to an iron ore.

The determination of silicon is a necessary step in the analysis of natural and synthetic silicates, ores, ferrous and non-ferrous metals, organosilicon compounds and other silicon-containing substances. Silicon compounds are common in air contaminants. Exposure to silica occurs in hard rock mining, and in manufacture of porcelain, pottery, silica firebricks, etc.

This paper presents a new method for the determination of silicon, by molecular emission cavity analysis (m.e.c.a.) [1]. The formation of an effective population of silicon atoms requires a high-temperature flame [2—6]. The low temperature hydrogen—nitrogen diffusion flame does not provide enough energy to volatilize most inorganic silicon compounds, so that direct injection of such compounds (silicates, for instance) into the m.e.c.a. cavity does not produce any emission. However, an oxy-cavity [7] placed in a hydrogen—nitrogen flame was found to stimulate an emission when gaseous silicon tetrafluoride was swept into it. It was decided therefore to examine the possibility of determining silicon by converting it to volatile silicon tetrafluoride and measuring the emission produced in the m.e.c.a. oxy-cavity.

---

[a]Present address: Chemistry Department, University of the Andes, Apartado Postal 542, Merida 5101-A, Venezuela.
[b]PAT Centre International, Royston, Herts., Gt. Britain.

0003-2670/83/$03.00

EXPERIMENTAL

Apparatus

All the emission measurements were made with a Unicam SP900 flame spectrophotometer, modified to record in the m.e.c.a. mode [8]. A Servoscribe 1S recorder, connected to the output of the instrument, and a premixed hydrogen—nitrogen flame were used. The instrument was operated with a slit width of 0.5 mm (≡11 nm) at 540 nm and at gain 5.

A duralumin cavity was found to be suitable for these experiments. This cavity, shown in Fig. 1, had two stainless steel tubes (1 mm o.d.) screwed into the rear of the cavity at opposite sides, one for supplying oxygen and the other connected to the vaporisation reactor. The cavity was inserted into a specially designed holder (Fig. 2), which permits adjustments of the vertical and horizontal cavity positions, as well as cavity angle, in order to obtain the optimal cavity position in line with the detector. During the preliminary

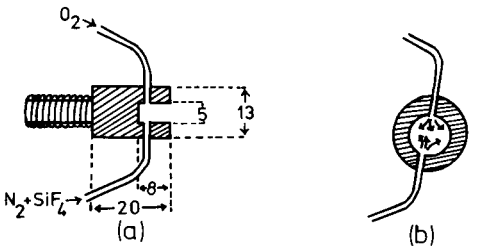

Fig. 1. Aluminium oxy-cavity: (a) cross section; (b) front view (dimensions in mm).

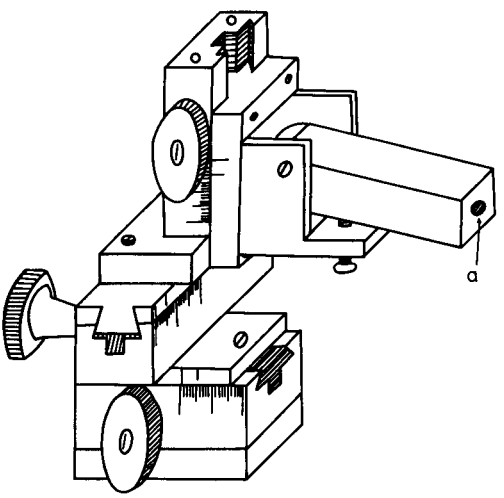

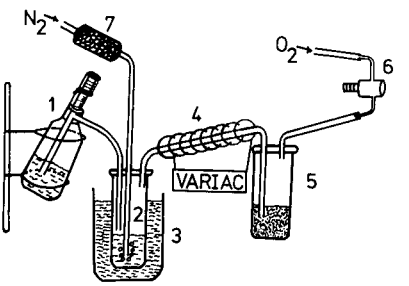

Fig. 2. Sample holder assembly: the cavity is screwed into hole *a*.

Fig. 3. Volatilization system for silicon: (1) sulphuric acid reservoir; (2) reaction tube, containing sample; (3) oil bath; (4) resistance tape; (5) sulphuric acid trap; (6) duralumin cavity; (7) drying tube.

work, the flame composition was 1.0 l H_2 min^{-1}, 4.5 l N_2 min^{-1}, 80 ml O_2 min^{-1} and carrier gas, 60 ml N_2 min^{-1}.

The volatilization system used for the production of silicon tetrafluoride is shown in Fig. 3. The reaction vessel was a teflon tube (10 cm long, 10 mm i.d.) closed by a polyethylene stopper having three holes, one for injecting concentrated sulphuric acid, another for passing nitrogen carrier gas and the third for transport of gases to the cavity. The generator tube containing the aqueous reaction mixture (see below) was placed in a paraffin oil bath maintained at 135°C. Concentrated sulphuric acid was added through the top from an automatic Zippette reservoir.

Reagents

The water used throughout was double-distilled from glass apparatus. A sodium silicate solution was prepared by dissolving 3.7726 g of sodium metasilicate ($Na_2SiO_3 \cdot 5H_2O$) in 100 ml of water and 42.4 ml of 36% hydrochloric acid, and water was added to give a final concentration of 1.0 mg Si ml^{-1} in 500 ml. A neutral silicate solution was prepared by dissolving the same amount of sodium metasilicate in 500 ml of water. Sodium fluoride solutions were prepared by dissolving 8.102 g of sodium hydrogenfluoride in 500 ml of 1 M hydrochloric acid or water to give a final fluoride concentration of 10.0 mg ml^{-1}. A 100.0 g l^{-1} chloride solution was prepared by dissolving 164.89 g of sodium chloride (analytical reagent) in 1 l of water. Working solutions were prepared daily from these stock solutions.

Recommended procedure for determination of silicon

(A) For 50—500 mg l^{-1} silicon. A set of calibration solutions containing 0—500 μg Si ml^{-1} was prepared from the acidic standard sodium silicate solution (1000 μg Si ml^{-1}) in six 50-ml polyethylene volumetric flasks. To each flask, 6.5 ml of the acidic sodium fluoride solution and 5 ml of the sodium chloride solution were added, the final concentrations of fluoride and chloride being 1.5 mg ml^{-1} and 10 mg ml^{-1}, respectively, in each of the flasks. The solutions were diluted to volume with water. For each measurement, a 0.2-ml aliquot of one of these solutions was transferred to the reaction tube and 1 ml of 98% sulphuric acid was injected. The tube was firmly closed and heated at 135°C for 35 s. The gases formed were carried to the cavity by nitrogen at 100 ml min^{-1}. The emission intensity was measured at 540 nm for 20 s. The flame composition used was 1.2 l H_2 min^{-1} and 4.7 l N_2 min^{-1}, with 80 ml O_2 min^{-1} supplied to the cavity. The peak height was measured for each silicon concentration and a graph of peak height vs. amount of silicon was plotted (Fig. 4).

(B) For 0—50 mg l^{-1} silicon. A set of calibration solutions containing 0—50 μg Si ml^{-1} was prepared in a similar way to that described above. The concentrations of fluoride and chloride were again 1.5 mg ml^{-1} and 10.0 mg ml^{-1}, respectively. The procedure described above was followed, except that the nitrogen carrier gas flow was increased to 140 ml min^{-1}.

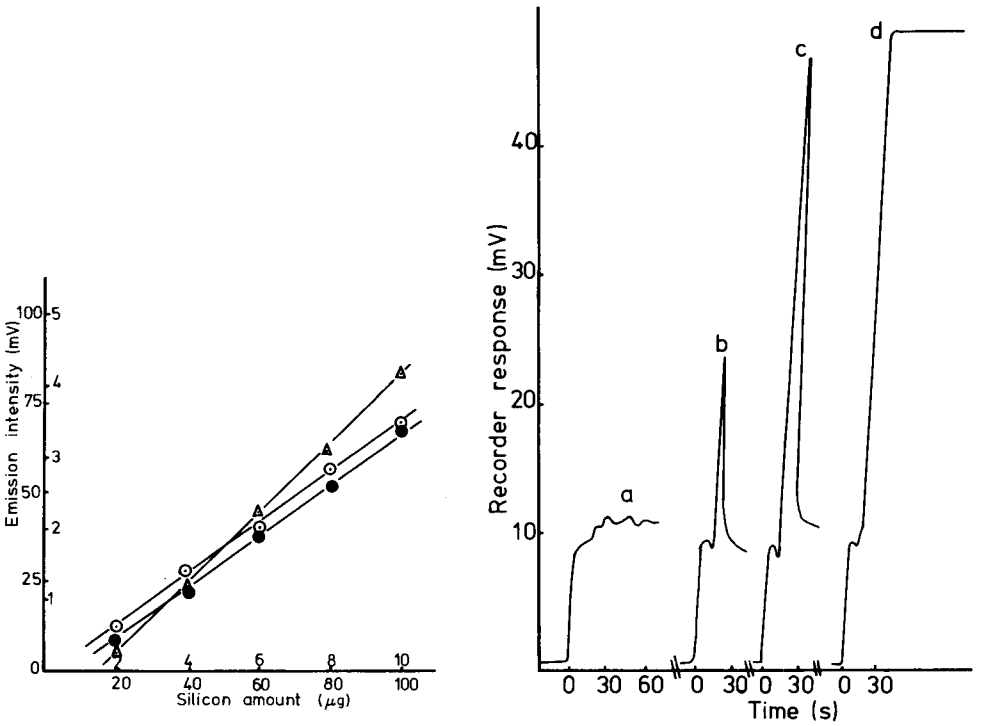

Fig. 4. Calibration graphs for silicon: (○) 20—100 μg; (●) 20—100 μg (after dehydration); (△) 2—10 μg.

Fig. 5. Effect of the trap saturation on emission intensity: (a) blank with new trap; (b) emission from 20 μg of silicon; (c) as (b) after 15 experiments using the same trap; (d) blank using the same trap after 25 experiments.

Determination of silicon in iron ore. A 0.5-g or 1.0-g sample of powdered iron ore sinter was placed in a porcelain dish and treated with 10.0 ml of concentrated hydrochloric acid. The solution of the decomposed sample was evaporated to dryness on a hot plate to separate hydrated silica. The residue was heated at 110°C for at least 1 h. The porcelain dish was cooled and the ash moistened with 10 ml of hot 10% hydrochloric acid to dissolve iron, aluminium and alkali metal salts. The residue was filtered off on a Whatman No. 40 filter paper and washed with 5 ml of cold 1% hydrochloric acid. A second evaporation and dehydration of the filtrate was made to recover the small amount of silica that escaped the first separation. The second portion of silica was filtered off onto a fresh filter and washed with 5 ml of cold 1% hydrochloric acid. The two washed precipitates were dissolved in 5 ml of cold 48% hydrofluoric acid. The solution was quantitatively transferred to a 100-ml polyethylene volumetric flask and diluted to the mark with double-distilled water, after addition of 10 ml of the 100 g l^{-1} chloride solution. A

0.2-ml portion of the final solution was transferred to the reaction tube, and the procedure described above was followed for the measurement of the silicon emission intensity. The same dehydration procedure was applied to standard silicate solutions in order to give a calibration graph from results obtained under the same conditions as the sample (Fig. 4).

RESULTS

Emission spectra

The spectrum of the silicon emission in the oxy-cavity was obtained from silicon tetrafluoride generated by adding 0.5 ml of 1 M hydrochloric acid containing 0.5 mg of silicon (as $Na_2SiO_3 \cdot 5H_2O$) and 2 mg of fluoride (as sodium hydrogenfluoride) to the generator. The system was closed, and 1 ml of 98% sulphuric acid was injected. The gas generated when the system was heated at 135°C was carried to the cavity by a steady stream of nitrogen (60 ml min^{-1}). A constant white emission was maintained in the oxy-cavity for at least 2 min. The spectrum showed a broad, featureless emission band with the apparent maximum intensity between 540 and 620 nm. The only emissions recorded when the spectrum of the flame alone was scanned were from OH around 306 nm and sodium atoms at 590 nm. The region between 320 and 580 nm was practically free of emission bands, but there was a small background increase with increasing wavelength. To avoid the effect of sodium emission on the background, all subsequent measurements were made at 580 nm.

Dagnall et al. [9] published the spectra obtained from several volatile fluorides introduced into a nitrogen—hydrogen diffusion flame. The spectrum obtained for silicon tetrafluoride had six principal band heads over the range 400—700 nm. The authors claimed that at least part of the spectrum could be attributed to SiF, which has been obtained previously in discharge tubes [10—12]. Shanker et al. [13] obtained excited SiO in a flame by chemiluminescent reaction of silicon tetrachloride vapo · with oxygen atoms in an argon atmosphere. Various SiO band systems wei identified in the region 230—460 nm. By comparing the values for the dissociation energy [14] of the possible silicon molecules in the cavity (187 kcal mol^{-1} for SiO and 115 kcal mol^{-1} for SiF), it was assumed that the emitting species was the more stable SiO.

To prove that the white emission was due only to silicon species, volatile silicon tetrachloride and hexamethyldisilazane (HMDS) were used for obtaining spectra. When about 1.0 ml of $SiCl_4$ or HMDS was placed in the reaction tube and the vapours were carried by hot nitrogen through the sealed system to the cavity, a strong emission was obtained in the cavity for long enough to scan the spectrum. In both cases, the spectra were similar to the spectrum obtained from silicon tetrafluoride.

Development of procedure for determination of silicon

The reaction taking place in the generator can be represented as follows [15—17]:

$$SiO_3^{2-} + 6\ F^- + 8\ H^+ \rightarrow H_2SiF_6 + 3\ H_2O$$

$$H_2SiF_6 \xrightarrow{heat} SiF_4 + 2\ HF$$

It has been reported [18, 19] that the evolution of silicon tetrafluoride starts when the reaction mixture reaches the temperature of decomposition of sulphuric acid (>150°C) into sulphur trioxide and water. The time required for complete evolution of silicon tetrafluoride is said to vary from several hours to a few minutes. In this investigation, the evolution of the gas was accelerated by the addition of chloride ions, so that silicon tetrafluoride was evolved within a few seconds. The maximum amount of chloride which did not show any effect on the blank response (2.0 mg) was used for all experiments. With the aim of not changing considerably the concentration of sulphuric acid and of preventing its violent reaction with water, mixtures of known amounts of silicon, chloride (2.0 mg in 0.2 ml of solution) and excess of fluoride were prepared; 0.2-ml aliquots of those solutions were pipetted into the generator, and 1 ml of 98% sulphuric acid was injected when the system was closed. The volatile products formed during the heating period (35 s) were carried to the cavity by a stream of nitrogen.

Quantitative recovery of volatilized silicon tetrafluoride is complicated, owing to its strong water affinity. Therefore, the construction and use of the vaporization system must be such that the silicon tetrafluoride along with some hydrochloric and sulphuric acid vapours, can be transferred from the sample solution and discharged into the cavity without retention by aqueous condensate along the way. To achieve this, the teflon tube connecting the generator with the cavity was jacketed with a resistance tape controlled by a Variac variable resistance, which maintained the tube above 100°C.

Under these conditions, acid vapours and silicon tetrafluoride were generated, which gave rise to an emission that flashed out of the cavity causing an immediate off-scale recorder deflection. This could be prevented if a sulphuric acid trap containing 10 ml of 98% sulphuric acid and maintained at room temperature was placed in the system between the heated outer tube and the cavity. The trap absorbed water and sulphuric and hydrofluoric acid vapours. The emission intensity from a certain amount of silicon started to increase (Fig. 5) after 10—12 consecutive experiments. Thus, the sulphuric acid in the trap was changed every ten experiments.

Effect of amount of fluoride. The minimum amount of fluoride required for the maximum response from silicon tetrafluoride was established. The amounts of fluoride calculated to react with 20 μg and 100 μg of silicon for the formation of silicon tetrafluoride are 54 μg and 271 μg, respectively. The amounts obtained by experiments and extrapolation (Fig. 6) are 55 and 275 μg respectively. For subsequent experiments, an excess of fluoride was

always used to ensure complete conversion of silicon to silicon tetrafluoride (i.e., 300 μg of fluoride for ⩽100 μg of Si).

Effect of sulphuric acid injected. Table 1 shows the effect of sulphuric acid on the emission from 10 μg and 100 μg of silicon at 135°C; 0.8 ml of 98% sulphuric acid was sufficient to give maximum emission intensity from ⩽100 μg of silicon. Larger amounts of sulphuric acid had no effect on the emission intensity but the trap placed in the system became easily saturated. The injection of a maximum volume of only 1.0 ml of 98% sulphuric acid prevents frequent changes of the sulphuric acid in the trap having to be made.

Under these conditions (oil bath temperature = 135°C) the time between the injection of sulphuric acid and measurement was only 35 s. At 110°C, however, 70 s was required to achieve maximum intensity.

Optimization of gas flow rates. The gas flow rates were optimized for a determination of a constant amount of silicon under the optimum reaction conditions found for complete conversion to silicon tetrafluoride. At a hydrogen flow of 0.8 l min^{-1}, the intensity from silicon and from the flame background decreased markedly as the nitrogen flow rate increased. Increasing the hydrogen flow rate at constant nitrogen flow rates increased both emission intensities. These observations indicate that the intensity increases

TABLE 1

Effect of sulphuric acid on maximum emission intensity

H_2SO_4 (ml)		0.2	0.4	0.6	0.8	1.0	1.2	1.5
Intensity	10 μg Si	2.0	5.5	7.0	7.0	6.8	7.1	7.0
(mV)	100 μg Si	0	5.0	38.0	64.0	65.0	65.0	65.0

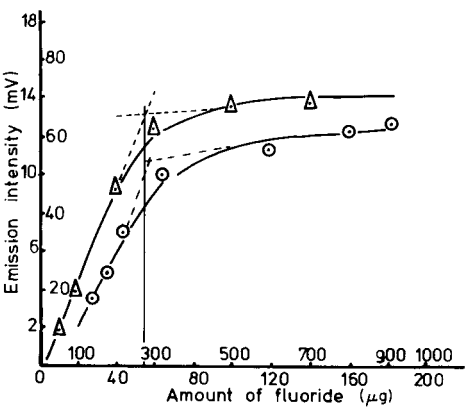

Fig. 6. Effect of amount of fluoride on the emission from: (△) 20 μg of silicon; (○) 100 μg of silicon.

with increasing flame and cavity temperature. This was confirmed by studying the effect of cooling the cavity. Before every experiment, the flame was burned for 60 s, and then the cavity was cooled by an air blower. The time which elapsed between turning off the flame and turning it on again for the measurement of SiO emission was varied. The results in Table 2 show that as the cavity temperature increases (i.e. as the cooling time decreases) the emission intensity becomes greater.

The hydrogen flow could not be increased above 2.0 l min^{-1} because the aluminium cavity employed became red hot and started to deform. Therefore, different combinations of nitrogen and hydrogen flow rates were used in order to obtain the highest signal-to-background ratio. A combination of 4.7 l N_2 min^{-1} and 1.2 l H_2 min^{-1} was best whilst providing a flame sufficiently cool to prevent deformation of the aluminium cavity. The flame was kept burning during the experiments to ensure a constant cavity temperature.

The effect of the flow rate of oxygen to the cavity on the emission of silicon is shown in Table 3. In the absence of oxygen, S_2 emission appears from sulphuric acid vapours. An oxygen flow rate of 80 ml min^{-1} was used in all further experiments.

The variation in the emission intensity from 20 and 100 μg of silicon with carrier gas flow rate is shown in Table 4. The carrier gas flow rate was not critical in the range 140—200 ml min^{-1} for 20 μg of silicon, so that a flow of 140 ml min^{-1} was used for the determination of $\leqslant 20$ μg of silicon. For larger amounts of silicon, the flow rate used was 100 ml min^{-1}. For >100 μg of silicon, the peaks tended to broaden and peak area measurements are advisable.

TABLE 2

Effect of cavity cooling time on silicon emission

Time of cooling (s)	0	20	45	75	105	120
Peak height (mV)	23.0	18.0	16.5	13.0	8.5	7.5

TABLE 3

Effect of oxygen flow rate on the emission intensity of 20 μg of silicon[a]

Oxygen flow rate (ml min^{-1})	0	60	80	100	120	160	200
Peak height (mV)	(S_2)	140	170	160	155	105	90

[a] N_2 carrier = 140 ml min^{-1}; H_2 = 1.2 l min^{-1}; N_2 = 4.7 l min^{-1}.

TABLE 4

Effect of carrier gas flow rate on net silicon emission intensity

Nitrogen flow rate (ml min^{-1})[a]		60	80	100	140	160	200	240
Intensity (mV)	20 μg Si	11	14	15	16	16	15	11
	100 μg Si	58	64	70	52	46	—	—

[a] O_2 = 80 ml min^{-1}; H_2 = 1.2 l min^{-1}; N_2 = 4.7 l min^{-1}; 0.2-ml injected.

Analytical performance

Linear calibration plots were obtained for both concentration ranges (Fig. 4). From the slope of the calibration graph, the sensitivity for the determination of silicon was 0.5 mV μg^{-1}. The relative standard deviation for seven measurements on 0.2 ml of solution containing 20 μg of silicon was 2.3%. For 1.0 μg of silicon in the same volume, the relative standard deviation increased to 12%. The detection limit, considered as the absolute amount of silicon required to give a signal-to-noise ratio of 2, was 0.2 μg of silicon in 0.2 ml of solution.

Several cations and anions were tested for interference. The emission intensity from 20 μg of silicon in 0.2 ml of solution was measured before and after measuring the emission intensity from 0.2 ml containing 20 μg of silicon and the ion to be studied for interference. Various amounts of interfering ions (10—1000 μg) were added. In each instance, a solution containing 1 mg of the interfering ion was added in the absence of silicon, to check the emission arising from the blank. An interference was defined as significant if the signal from silicon was different by two standard deviations (i.e., 5%) from the signal obtained for silicon in the absence of any interfering ion. The anions were added as their acids and most of the cations as their nitrates. The results are shown in Table 5.

Strong positive interferences were caused by arsenic and ammonium, both giving an emission in the absence of silicon. Under the conditions of this experiment, arsenic probably forms arsenic trifluoride which carried to the cavity, and causes the blue arsenic—oxide emission in the flame [20]; ammonia causes the whitish NO—O continuum [21]. Both these emissions interfere spectrally with the measurement of the SiO emission, but arsenic and the slight boron interference can be avoided by using a narrower (0.2 mm) slit, and measuring at 580 nm. Most of the other elements had no significant effect on the determination of silicon. Sulphate and sulphite did not interfere at low concentrations. The problem of trap saturation (see above) appeared after every five experiments when more than 100 μg of sulphate or sulphite ions was added. Therefore the sulphuric acid in the trap was changed every two experiments during the study of such interferences.

TABLE 5

Effect of other ions on the determination of 20 μg of silicon

Amount of ion added (μg)	Change in emission intensity (%)									
	Interfering ion									
	Pb^{2+}	Hg^{2+}	Co^{2+}	Ni^{2+}	Mn^{2+}	Zn^{2+}	Ba^{2+}	Cr^{3+}	Al^{3+}	Ge^{4+}
10	+3	+4	+6	−2	+6	+5	−2	2.5	0	0
100	+6	+5	−4	+2	+6	+4	+3	+5	+2	−3
1000	+8	+10	+8	+5	+7	+6	+5	+6	+2	−4
Blank	0	0	0	0	0	0	0	0	0	0
	NH_4^+	$C_2O_4^{2-}$		ClO_4^-	PO_4^{3-}		SO_4^{2-}	NO_3^-	BO_3^{3-}	AsO_3^{3-}
10	+28	−5		+3	−34		+2	+4	+4	+80
100	+44	−7		+4	−37		+6	+7	+6	>100
1000	>100	−30		+6	−100		+10	+15	+37	OS[a]
Blank	OS[a]	2		0	0		0	0	16	OS[a]

[a]Off scale.

Determination of silica in an iron ore

Because of difficulty in obtaining standard samples of low silicon content, the m.e.c.a. method was applied to the determination of silica in an iron ore sinter sample (Bureau of Analysed Samples). The sample was also reported to contain Al, Ti, Mn, Ca, Mg, S, P and V. Possible interferences from the elements present were eliminated by the separation of silicon as insoluble silica [17]. The results obtained by m.e.c.a. (8.48% SiO_2 for a 0.5-g sample, 8.52% for a 1.0-g sample) were similar to the certified value (8.55% SiO_2).

DISCUSSION

The technique applied was found to be suitable for the determination of silicon at microgram levels. The vaporisation procedure applied for the generation of silicon tetrafluoride was successful when a few parameters were strictly controlled. For example, a constant temperature (135°C) must be achieved during the experiment for providing rapid generation of the gas. The composition of the reaction medium must be carefully controlled, especially the chloride concentration. Condensation must not be present in the exit tubing from the generator to the cavity, lest silicon tetrafluoride be prematurely absorbed. An analogous procedure has been applied to the determination of fluoride [22].

REFERENCES

1 S. L. Bogdanski, M. Burguera and A. Townshend, CRC Crit. Rev. Anal. Chem., 10 (1981) 185.
2 W. J. Price and J. F. H. Roos, Analyst, 93 (1968) 709.
3 J. S. Cartwright, C. Sebens and D. C. Manning, At. Absorpt. Newsl., 5 (1966) 91.
4 L. Capacho-Delgado and D. C. Manning, Analyst, 92 (1967) 563.
5 J. J. McAuliffe, At. Absorpt. Newsl., 6 (1967) 69.
6 G. F. Kirkbright, M. Sargent and T. S. West, Talanta, 16 (1969) 245.
7 S. A. Ghonaim, Ph.D. Thesis, Birmingham University, 1974.
8 R. Belcher, S. L. Bogdanski, I. H. B. Rix and A. Townshend, Anal. Chim. Acta, 81 (1976) 325.
9 R. M. Dagnall, B. Fleet, T. H. Risby and D. R. Deans, Talanta, 18 (1971) 155.
10 R. C. Johnson and H. G. Jenkins, Proc. R. Soc., 116 (1927) 327.
11 R. K. Asundi and R. Samuel, Proc. Indian Acad. Sci., 3 (1936) 346.
12 E. H. Eyster, Phys. Rev., 51 (1937) 1078.
13 R. Shanker, C. Linton and R. D. Verma, J. Mol. Spectrosc., 60 (1976) 197.
14 A. G. Gaydon, Dissociation Energies and Spectra of Diatomic Molecules, Chapman and Hall, London, 1968.
15 I. M. Kolthoff and E. B. Sandell, Textbook of Quantitative Inorganic Analysis, MacMillan, New York, 1946, pp. 398—406.
16 C. Hodzic, Anal. Chem., 38 (1966) 1626.
17 R. P. Curry and M. G. Mellon, Anal. Chem., 29 (1957) 1632.
18 R. P. Curry and M. G. Mellon, Anal. Chem., 28 (1956) 1567.
19 B. D. Hold, Anal. Chem., 32 (1960) 124.
20 S. A. Ghonaim, Proc. Soc. Anal. Chem., 11 (1974) 138.
21 R. Belcher, S. L. Bogdanski, A. C. Calokerinos and A. Townshend, Analyst, 102 (1977) 220; 106 (1981) 625.
22 S. L. Bogdanski, M. Burguera and A. Townshend, Anal. Chim. Acta, 117 (1980) 247.

Analytica Chimica Acta, 153 (1983) 53—60
Elsevier Science Publishers B.V., Amsterdam — Printed in The Netherlands

DETERMINATION OF SOME ORGANOHALOGEN COMPOUNDS BY MOLECULAR EMISSION CAVITY ANALYSIS AFTER GAS CHROMATOGRAPHIC SEPARATION

M. BURGUERA and J. L. BURGUERA

Departamento de Quimica, Facultad de Ciencias, Universidad de Los Andes, Apartado Postal 542, Mérida 5101-A (Venezuela)

(Received 18th March 1983)

SUMMARY

Emissions from InCl, InBr and InI, generated in an indium-lined m.e.c.a. cavity, are used to determine organic halogen compounds separated by g.c. Emissions are measured at 360, 376 and 410 nm, respectively. Linear calibration ranges are 5—60, 10—150 and 5—500 mg l^{-1} for chloro-, bromo- and iodo-alkanes, respectively. Mutual interference effects are evaluated.

Hydrogen diffusion flames have been examined by several workers for the determination of non-metals, many of which are difficult to determine by other flame methods [1]. In these flames, hydrogen is diluted with an inert gas such as nitrogen or argon to lower the flame temperature and make the flame more rigid and transparent. The background emission and noise of such flames in the ultraviolet and visible regions are extremely low and their structure and composition promotes the formation of diatomic species which emit as a result of chemiluminescent reactions. Molecular emission cavity analysis (m.e.c.a.) in which the emission from the analyte is generated within a small cavity, has the advantage of concentrating the emission in a small, predetermined region of the flame. In this way, sensitive determinations of many non-metals can be achieved rapidly and often very selectively [2].

It is well known that the m.e.c.a. cavity is an excellent medium for producing metal halide emissions [2]. Of the various metal halides known to emit in the cavity, those of indium were found to give the most sensitive emissions [3, 4]. This is because, in the presence of hydrogen, indium forms relatively stable monohalides, unlike other elements, which form stable oxides. Two m.e.c.a. methods have been developed for the determination of halides in aqueous samples; one consists of injecting the halide solution containing indium directly into a steel cavity [3]; the other involves the use of an indium-lined cavity [4].

Recently, m.e.c.a. was used as a gas chromatographic detector for chlorinated solvents and pesticides [5]. An indium-lined cavity was connected to the exit of a chromatographic column and the InCl emission formed when

0003-2670/83/$03.00

the chloro-compounds reached the cavity was measured. This paper describes studies to improve this instrumentation and to extend it to the detection of bromo- and iodo-compounds.

EXPERIMENTAL

Apparatus and reagents

The instrumentation used was a Varian 1475-BD atomic absorption spectrometer operated in the emission mode and equipped with a specially designed sample holder support device and a circular emission burner. The cavity assembly (Fig. 1) was made from brass, and was situated between the lamp and burner compartments. It was firmly positioned by screwing it into the burner mounting device of the instrument. Adjustment screws on the assembly allowed horizontal, vertical, lateral and angular variations, so as to place the cavity in the best position in the flame in line with the detector.

The water-cooled cavity support (Fig. 2), made from a brass rod, was placed around the cavity. It had four holes drilled inside its body, surrounding the orifice of the cavity, so that the water could circulate freely. Two brass side-tubes (a few mm long) for cooling water inlet and outlet were inserted into two threaded holes 2 mm away from the closed ends of the rod. The water-cooling system allowed the flame to be kept on as long as was necessary without overheating the cavity material. A screw was fitted to the side of the rod so that the cavity was firmly attached. The device supporting the cavity was fitted to the sample holder in such a way as to permit the whole rod to be raised to the vertical position when necessary.

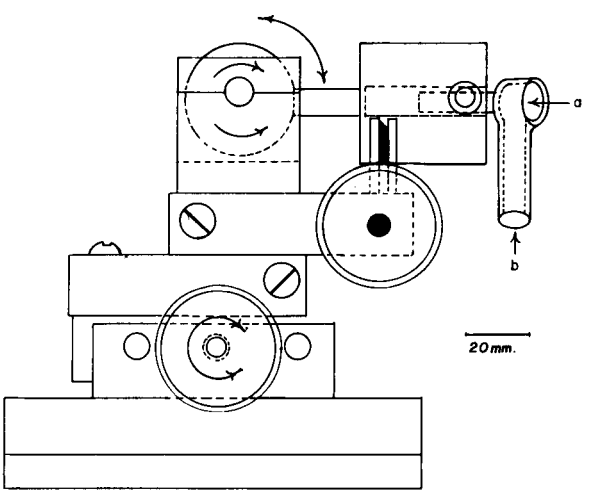

Fig. 1. Sampler holder assembly: (a) indium-lined cavity; (b) input from gas chromatograph.

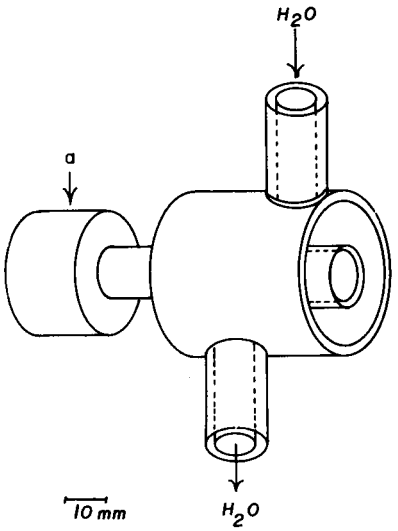

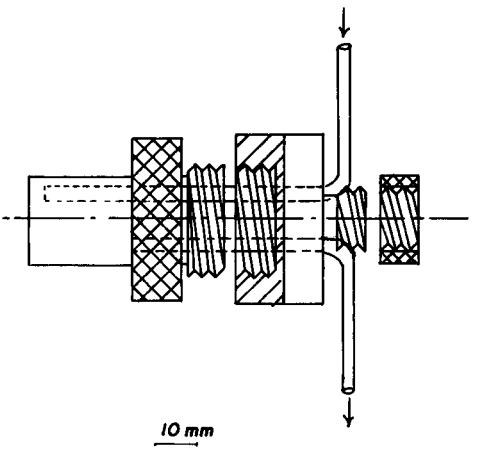

Fig. 2. Water-cooling system fitted onto the cavity rod: (a) cavity.

Fig. 3. All-teflon vapour generator.

The steel cavity used had a side tube (2 mm i.d.) fixed by pressure into a hole drilled in its wall, in order to connect it to a gas chromatograph, as described previously [3]. The inner surface of the cavity was covered with high-purity indium (99.9999%).

A circular burner was used which had separate entrances at the base for nitrogen and hydrogen. Its head (1.5 cm diameter) had 40 holes (1 mm diameter each) drilled symmetrically into it, so as to provide a steady, almost transparent flame.

Vapours of halogen compounds were generated in an all-teflon apparatus (Fig. 3).

All the halogen compounds used were from B.D.H. Chemicals. Some of their properties are given in Table 1. Pure 2-chlorobutane, bromoethane and iodomethane were chosen as standards for scanning spectra and optimizing m.e.c.a. parameters. Ethanolic solutions were used in all other studies.

Procedure

For scanning spectra and optimizing m.e.c.a. parameters, 3 ml of a solution of the compound studied was placed in the teflon generator at 120°C. The vapour was carried to the cavity by a slow flow of nitrogen (5 ml min^{-1}) so that a constant emission was obtained inside the cavity. All experiments with the m.e.c.a.—gas chromatography system were done as described previously [3].

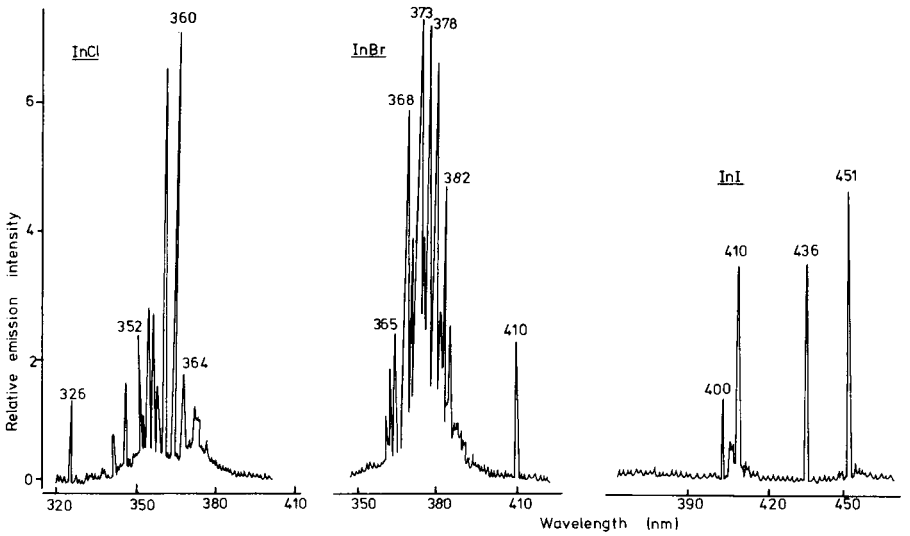

Fig. 4. Emission spectra obtained in the indium-lined cavity from vapours of C_4H_9Cl, C_2H_5Br and CH_3I.

TABLE 2

Optimal conditions and analytical characteristics of the m.e.c.a.—g.c. system

Parameter	Species		
	InCl	InBr	InI
Wavelength (nm)[a]	360	376	410
Compound used	C_4H_9Cl	C_2H_5Br	CH_3I
Hydrogen (l min^{-1})[b]	1.0	1.2	2.8
N_2 carrier gas (ml min^{-1})	16	20	25
Cooling water (ml min^{-1})	150	150	400
Oven temperature (°C)[c]	80	110	80
Linear range (mg l^{-1} halogen)	5—60	10—150	5—500
2σ detection limit (mg l^{-1} halogen)	0.23	0.8	1.8
Relative standard deviation (%)[d]	2.4	2.2	3.6

[a]0.2 nm slit-width. [b]Nitrogen at 5.5 l min^{-1} also supplied to flame. [c]Column 0.2 cm i.d., 200 cm long containing 3% OV-101 on Chromosorb W, 80—100 mesh, AW-HMDS. [d]5 results.

because of the increased cavity temperature. A flow of 150 ml min^{-1} was used in all subsequent studies.

The response for InI was different. When the water flow rate was increased, the In emission decreased and that of InI increased continuously. A water flow of 400 ml min^{-1} was used because that was the maximum capacity of the system. This gave the greatest difference in emission intensities between InI and In.

Effect of ethanol

All compounds used in the m.e.c.a.—g.c. system were used as ethanolic solutions. A significant decrease in the intensity obtained from most eluted compounds was observed when the solution had stood for 1 h compared to freshly prepared solutions (Table 3). This effect was also observed with other solvents (Table 3). Moreover, only acetone and ethanol solutions could be used. The low results obtained for benzene and n-hexane solutions can be attributed to the low solubility of the compounds in these solvents or overlapping with solvent peaks, or both. These last two solvents also produced incandescence when they were eluted to the cavity.

Mutual interferences

The mutual effect of the three halides, without g.c. separation, was studied, using the standard compounds. The iodide had no significant effect on the signal from the chloride and bromide. The effect of large amounts of iodomethane and bromoethane on the determination of chlorobutane at 360 nm is shown in Fig. 5. In the presence of bromoethane, with the oven at 150°C, there was an increase in the blank signal at 360 nm, caused mainly by the presence of a weak InBr band, which increased the apparent InCl signal. Above ca. 400 mg l^{-1} bromide, however, the InCl intensity decreased considerably, probably because of competition between the two halogens for the available indium in the cavity. By decreasing the temperature of the oven to 100°C, and maintaining the concentration of bromide below 400 mg l^{-1}, the mutual interference was eliminated. Chlorobutane was without effect on InBr emission at 376 nm.

The analytical characteristics of the m.e.c.a.—g.c. system listed in Table 2 were obtained under the optimal operating conditions. The calibration graphs obtained under these conditions are shown in Fig. 6.

TABLE 3

Effect of some solvents on the m.e.c.a.—g.c. response[a]

Solvent	Ethanol		Benzene		n-Hexane		Acetone	
	A	B	A	B	A	B	A	B
Chloroethane	27	23.5	21	20	12	9	27.5	25
Chloropropane	29	27	20	14	4	3	25.5	25
Chlorobutane	27	21.5	7	5	3.5	3	25	23
Bromoethane	21	19	12	9	14	12	25	23
Bromopropane	21	17	9.5	7	10	9.5	23	22
Bromobutane	20	12.5	7	5	2	1.5	22	20
Iodomethane	21	18	10	9.5	7	6.5	24	23
Iodoethane	20	15	7	5	2	1.5	22	20

[a]The numbers represent peak heights (mm) corresponding to emission intensities from 50 mg l^{-1} halogen immediately after preparation (A) and after 1 h (B).

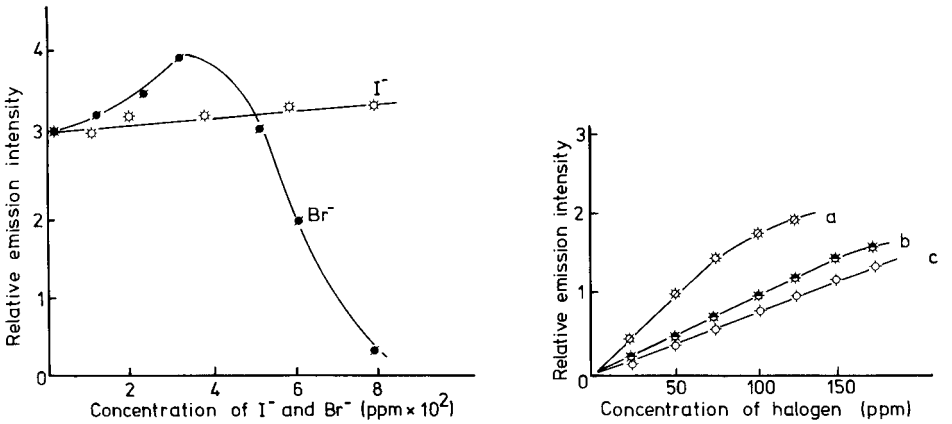

Fig. 5. Effect of bromoethane and iodomethane on the determination of 100 mg l^{-1} chloride as chlorobutane using the m.e.c.a.—g.c. system under optimal experimental conditions (oven temperature 150° C).

Fig. 6. Calibration graphs for: (a) chlorine; (b) bromine and (c) iodine.

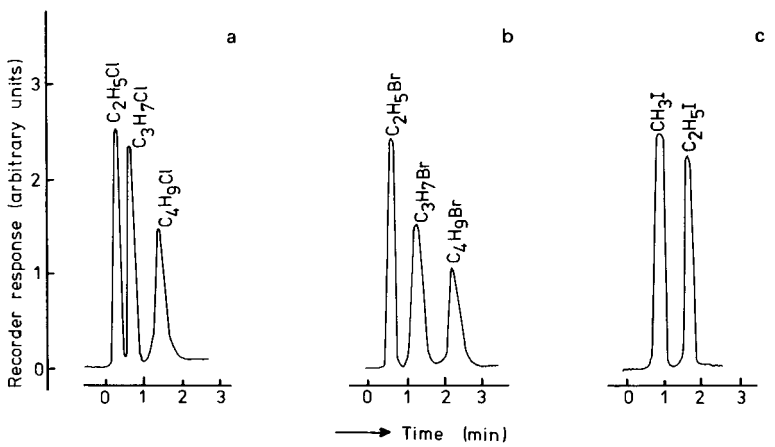

Fig. 7. Chromatograms from mixtures of halo-compounds recorded at: (a) 360 nm; (b) 376 nm; (c) 410 nm. (5 μl of mixture injected; column temperature 150° C. Other conditions as in Table 2.)

Mixtures of the three types of compounds (Table 1) were prepared in ethanol to contain 50 mg l^{-1} halogen in the final solution for each compound. The m.e.c.a. chromatograms shown in Fig. 7 are the results of injecting 5 μl of the mixtures into the column and recording the responses at 360, 376 and 410 nm for the chloro-, bromo- and iodo-compounds, respectively. These experiments show that the m.e.c.a. detector should be useful for the detection of mixtures of organic halogen compounds at mg l^{-1} concentrations, providing a useful extension to the existing methods for the analysis of halogen-containing organic mixtures.

The authors gratefully acknowledge the financial support given by CDCH, Universidad de Los Andes, Mérida, Venezuela.

REFERENCES

1 J. A. Dean and Th. C. Rains (Eds.), Flame Emission and Atomic Absorption Spectrometry, Vol. 3, M. Dekker, New York, 1975.
2 M. Burguera, S. L. Bogdanski and A. Townshend, CRC Crit. Rev. Anal. Chem., 10 (1980) 185.
3 R. Belcher, S. L. Bogdanski, Z. M. Kassir, D. A. Stiles and A. Townshend, Anal. Lett., 7 (1974) 751.
4 D. R. Narine, M. E. Peach and D. A. Stiles, Anal. Lett., 9 (1976) 767.
5 M. Burguera, J. L. Burguera and M. Gallignani, Anal. Chim. Acta, 138 (1982) 137.
6 R. C. Weast (Ed.), Handbook of Chemistry and Physics, 57th edn., CRC Press, New York, 1976—1977.
7 R. W. B. Pierce and A. G. Gaydon, The Identification of Molecular Spectra, 4th edn., Chapman and Hall, London, 1976.

Analytica Chimica Acta, 153 (1983) 61—67
Elsevier Science Publishers B.V., Amsterdam — Printed in The Netherlands

THE DETERMINATION OF DISSOLVED AND PARTICULATE VANADIUM IN SEA WATER BY X-RAY FLUORESCENCE SPECTROMETRY

P. C. COLE, J. M. ECKERT* and K. L. WILLIAMS

Department of Inorganic Chemistry, University of Sydney, Sydney, NSW 2006 (Australia)

(Received 24th May 1983)

SUMMARY

Vanadium is coprecipitated from filtered sea water with a cobalt—pyrrolidinedithiocarbamate carrier complex at pH 4.0. The precipitate is collected as a thin film on a membrane filter (0.4-μm pore size) and, with the particulate material from the initial filtration, analysed directly for vanadium by x-ray fluorescence spectrometry. The detection limit, for 100-ml water samples and a counting time of 100 s, is 0.02 μg V l^{-1}. The coprecipitation efficiency in the 0—5 μg l^{-1} range is 95% for vanadium(IV) or vanadium(V). Results for the determination of dissolved and particulate vanadium in sea-water samples are 1.4—1.7 μg l^{-1} and 0.06—0.61 μg l^{-1}, respectively.

Tris(pyrrolidinedithiocarbamato)cobalt(III), the complex formed by mixing cobalt(II) and ammonium pyrrolidinedithiocarbamate (APDC) solutions, has been used previously as a carrier in the preconcentration of Mn, Ni, Cu, Zn, Cd and Pb(II), Fe(II,III) and Cr(VI), prior to acid digestion and measurement by atomic absorption spectrometry (a.a.s.) [1—3] and in the separation of Cr(VI) from Cr(III) prior to measurements by thin-film x-ray fluorescence (x.r.f.) spectrometry [4]. Reported now is a method for the determination of dissolved and particulate vanadium in sea water, based on coprecipitation of the dissolved fraction with this carrier system and measurement of the precipitates, and of particulate material from the water samples, as thin films by x.r.f.

Optimum x.r.f. operating conditions are defined and the effects of vanadium oxidation state, the major ions of sea water and dissolved organic matter are assessed. The combination of coprecipitation and thin-film x.r.f. appears to have been used only once before in the determination of vanadium at μg l^{-1} levels, the carrier metal being iron(III) [5]. The study reported then, however, was of an exploratory nature and no information about either particulate vanadium or possible interference by dissolved organic matter was presented.

0003-2670/83/$03.00

EXPERIMENTAL

Reagents

Distilled-deionized water was used for all solution preparations and dilutions.

Cobalt solution (100 mg Co(II) l^{-1}). Dissolve 0.247 g of cobalt(II) nitrate hexahydrate in water and dilute to 500 ml.

Ammonium pyrrolidinedithiocarbamate solution. Dissolve 2 g of APDC in water and dilute to 100 ml. Filter through a membrane filter and remove trace metal impurities from the filtrate by addition of 1 ml of cobalt solution and filtration after 1 h through a membrane filter. The resulting filtrate should normally be used within 24 h but may be kept for up to a week if stored at 4°C.

Buffer pH 4.0. Dissolve 20.4 g of potassium hydrogenphthalate in water and dilute to 500 ml. Purify the solution by addition of 1-ml quantities of the cobalt and APDC solutions and filtration after 1 h through a membrane filter.

Nitric acid was of Suprapur grade (65%; Merck) and the vanadium metal was puriss. (Fluka).

Procedures

Membrane filters and filtration apparatus. Particulate material and precipitates were collected on Nuclepore polycarbonate membrane filters (0.4-μm pore size, 37 mm diameter) with a Sartorius vacuum filtration unit (3.1-cm^2 filtration area).

Separation of particulate material. Filter 500 ml of the freshly-collected water for analysis through a membrane filter. Retain the loaded filter for the determination of particulate vanadium and if possible proceed immediately with the coprecipitation of dissolved vanadium from the filtrate. If the filtrate cannot be treated immediately, reduce the pH to below 2 by the addition of nitric acid (5 ml Suprapur nitric acid per litre of filtrate should be sufficient). The acidified filtrate may be kept (at 4°C) for several weeks.

Coprecipitation procedure. Place 100 ml of the filtrate in a 250-ml polythene bottle fitted with a screw cap and, if necessary, adjust the pH to between 3 and 5. Add 5 ml of phthalate buffer. The pH should now be 4.0 (±0.5). Add 1 ml of cobalt solution, followed by 5 ml of APDC solution. Cap the bottle, swirl the mixture for 15 s and allow it to stand for 1 h. Filter the suspension through a membrane filter and rinse the bottle and filtration funnel with 5—10 ml of water.

Preparation of thin-film standards. Prepare a set of thin-film standards, including a blank, from standard vanadium solutions using the recommended coprecipitation procedure. For the studies described here, the standard solutions were prepared from a stock standard, obtained by dissolving high-purity metal in approximately 5 M nitric acid and diluting.

The precipitates are stable and thin-film standards prepared on polycarbonate filters can be used repeatedly.

Treatment of loaded membrane filters. Place the loaded filters in plastic boxes with hinged lids and allow them to dry, with the lids partly open, first in an air oven at 50°C for 12 h and then in a vacuum desiccator.

X.r.f. spectrometry. The particulate material and precipitates were analysed with a Philips PW1450 automatic sequential x-ray spectrometer. The loaded filters were mounted, with the sample side towards the x-ray beam, in standard holders (Philips type PW1527), fitted with adaptor rings to suit the PW1450 sample changer. To reduce the scattered background intensity, teflon sleeves, 2 mm thick, were fitted inside the sample holders.

The following working conditions were used: gold anode tube operated at 60 kV and 45 mA, coarse collimator, LiF_{200} crystal, 2θ values of 76.94° (for peak) and 76.04° and 77.84° (for background), automatic pulse-height selection, flow and scintillation detectors in tandem and counting times of 100 s and 20 s for peak and background, respectively.

RESULTS AND DISCUSSION

Oxidation states of vanadium

The stable oxidation states of vanadium in well-aerated aqueous solution are V(IV) and V(V) [6]. In the development of the proposed method, experiments to determine a suitable carrier complex and to optimise the chemistry of the coprecipitation were conducted on separate solutions of V(IV) and V(V). The V(IV) solutions were prepared from oxovanadium(IV) sulphate pentahydrate, and the V(V) solutions from the V(IV) solution by boiling gently with hydrogen peroxide and sodium hydroxide. The responses of vanadium in the two oxidation states were indistinguishable in all tests. The proposed method measures the combined concentration of dissolved V(IV) and V(V).

Subsequent tests were performed on standard vanadium solutions prepared by dissolving the high-purity metal in nitric acid. These solutions appear to contain a mixture of V(IV) and V(V) in proportions which change with time. For example, a stock standard solution, containing 500 mg V l^{-1} in approximately 0.3 M nitric acid, was blue when freshly prepared (this is the colour of the oxovanadium(IV) ion, VO^{2+}) but turned pale green, then greenish-yellow on standing. Solutions of the VO^{2+} ion in water have an absorption peak at 765 nm (ϵ_{max} = 16.5 l mol^{-1} cm^{-1} in 1 M perchloric acid [7]) whereas V(V) species do not absorb in this wavelength region. Absorbance measurements on the stock standard at 765 nm indicated that the proportion of V(IV) in the solution was 90% initially, 80% after a week and less than 50% at the end of six weeks, V(IV) presumably oxidizing to V(V) on standing. Because the proposed method does not distinguish between the two oxidation states in solution, the change of one into the other in the standards does not affect the analysis.

Calibration, precision and limit of detection

The calibration graph was linear in the concentration range 0—5 μg V l^{-1}. Values obtained for m (sensitivity) and b (background), parameters of the equation for the regression line $y = mx + b$, are presented in Table 1; y is the net count rate and x the amount of metal, in μg, in the precipitate.

Table 1 also includes estimates of precision at the 1 and 5 μg l^{-1} levels and the lower limit of detection, calculated as $(3/m)\ (b/t_b)^{1/2}$ where t_b is the background counting time (20 s).

Coprecipitation efficiency

A knowledge of the coprecipitation efficiency is not essential in the determination of dissolved vanadium, involving as it does a comparison of x.r.f. count rates for precipitates obtained by treating the test waters and standard solutions in an identical manner. It is, however, necessary to know the absolute amounts of vanadium in the precipitates obtained from the standard solutions if these are to be used as thin-film standards in the determination of particulate vanadium; and also to establish that matrix effects are not significant.

At the 100 μg l^{-1} level, coprecipitation was shown to be quantitative, by atomic absorption spectrometry (a.a.s.) of acid-digested precipitates. A detailed x.r.f. calibration graph over the range 0—100 μg l^{-1} exhibited slight curvature, the slope of the straight line of best fit between 0 and 5 μg l^{-1} (the concentration range of interest for natural waters) being 95% of the slope between 50 and 100 μg l^{-1}. The curvature is barely significant but probably indicates that the coprecipitation efficiency falls off marginally at the lower levels. In the determination of particulate vanadium, the amounts of metal in the standard precipitates were taken to be 95% of the amounts available for coprecipitation.

The near-linearity of the x.r.f. calibration graph over a wide concentration range supports the claim by previous workers in this field [8] that absorption of primary and secondary radiation by thin films is often negligible. Further evidence that matrix effects are not serious was provided by tests in which carrier complex blanks were added to membrane filters already loaded

TABLE 1

Sensitivity, background and limit of detection

Sensitivity and background[a]	m (c s^{-1} μg^{-1})	506
	b (c s^{-1})	2.30
Precision[b]	s_r (%) for 1 μg l^{-1}	5
	s_r (%) for 5 μg l^{-1}	3
Lower limit of detection[c]	(μg l^{-1})	0.02

[a]Slope and intercept of regression line in a typical calibration run; 20 standards in the range 0—5 μg l^{-1} were determined. [b]Six precipitates were measured at each concentration. [c]Based on count rates of precipitates from 100-ml samples.

with particulate material; the net count rates increased by approximately the amount expected for the blank.

Interferences

Interference by the major ions of sea water was studied by measuring precipitates obtained from standard vanadium solutions in artificial sea water, prepared from analytical-reagent grade salts [9]. In Table 2, the slope and intercept of the resulting regression line are compared with values obtained from standard solutions in distilled—deionized water. The slopes are in good agreement, the intercepts are not. The high background in the case of the artificial sea water data indicates a blank value in that medium of 0.6 (±0.1) μg V l^{-1}. This value, however, was reduced to 0.3 (±0.1) μg l^{-1} by doing a second coprecipitation on the filtrate from the artificial sea water blank and to <0.2 μg l^{-1} by a third coprecipitation. The high blank from the initial coprecipitation is evidently due to contaminant vanadium in the salts used to prepare the artificial sea water and not to some constant (positive) interference by the major ions in sea water. It is concluded that sea salts do not interfere with the proposed method.

The method was also tested in the presence of a number of trace metal ions (Cr^{3+}, Cr(VI), Mn^{2+}, Fe^{2+}, Fe^{3+}, Ni^{2+}, Cu^{2+}, Zn^{2+} and Pb^{2+}) separately at the 1000 μg l^{-1} level, and no significant interferences were observed.

Analysis of sea water

Surface sea-water samples were collected (in polyethylene bottles) from Oak Park, a small beach 20 km south of Sydney, N.S.W. and from North Maroubra Beach, situated between Port Jackson and Botany Bay. The samples were filtered within 4 h of collection, the loaded filters were retained for the determination of particulate vanadium, and aliquots of the filtrate were treated immediately to coprecipitate dissolved vanadium. The rest of the filtrate was treated within 24 h to release bound metal.

This was done in two ways: (i) by irradiating the filtrate with a 35-W U-tube immersion lamp for 6 h after addition of nitric acid (5 ml l^{-1} of filtrate) and hydrogen peroxide (0.5 ml of 30% (w/v) solution per litre) [10]; and (ii) by gently boiling the filtrate for 10 min after addition of hydrochloric acid (10 ml l^{-1} of filtrate; Merck Suprapur) and ammonium

TABLE 2

Effect of major ions in sea water

Medium	Distilled-deionized water	Artificial sea water
m (c s^{-1} μg^{-1})[a]	472	473
b (c s^{-1})[a]	0.53	30.8

[a]Slope and intercept of regression lines; 20 determinations, in each medium, in the range 0—2 μg V l^{-1}.

TABLE 3

Vanadium in sea water

Collected	Source	Salinity (‰)	Dissolved vanadium[c] ($\mu g\ l^{-1}$)	Particulate vanadium[c] ($\mu g\ l^{-1}$)
July, 1982	a	35.0	1.6 ± 0.1	0.06 ± 0.01
Aug., 1982	a	34.9	1.7 ± 0.2	0.07 ± 0.01
	a	34.9	1.6 ± 0.1	0.14 ± 0.03
Sept., 1982	b	34.9	1.7 ± 0.1	0.09 ± 0.01
Nov., 1982	a	35.0	1.7 ± 0.1	0.12 ± 0.01
	b	35.2	1.7 ± 0.1	0.61 ± 0.04
	b	35.4	1.4 ± 0.1	0.10 ± 0.02
Dec., 1982	b	35.3	1.4 ± 0.1	0.39 ± 0.02

[a]Surface waters from Oak Park. [b]Surface waters from North Maroubra. [c]Mean and standard deviation of 4 determinations.

peroxodisulphate (2.5 g l^{-1}) [11]. The excess of peroxide or peroxodisulphate was removed before addition of APDC solution, by gently boiling the digested samples for several hours.

Results for dissolved and particulate vanadium in the fresh unacidified seawater samples are given in Table 3. Concentrations of dissolved vanadium were found to lie in a quite narrow range, 1.4—1.7 $\mu g\ l^{-1}$ (r.s.d. 5—10%). In no case did u.v. irradiation or peroxodisulphate oxidation significantly increase the value obtained. The method therefore appears to measure total dissolved vanadium in sea water directly, without a preliminary digestion step. This observation suggests that, at least in sea water, vanadium is not tightly bound to dissolved organic matter.

Particulate vanadium was present in the range 0.06—0.14 $\mu g\ l^{-1}$ (r.s.d. 5—15%) except on two days, in samples from North Maroubra, when substantially higher levels were observed. The sea on these days was choppy, the turbulence evidently keeping extra particulate material in suspension. An appealing feature of the proposed method is the ease with which particulate vanadium can be measured, even at levels below 0.1 $\mu g\ l^{-1}$, without any treatment other than the initial filtration.

The work described in this paper was supported by the Australian Research Grants Scheme. The x.r.f. equipment was made available by the Department of Geology and Geophysics of the University of Sydney, and we gratefully acknowledge the help provided by Dr. Michael Hough of that Department.

REFERENCES

1 E. A. Boyle and J. M. Edmond, in T. R. P. Gibb (Ed.), Analytical methods in oceanography, Advances in Chemistry Series, No. 147, American Chemical Society, Washington, DC, 1975, p. 44.

2 E. A. Boyle and J. M. Edmond, Anal. Chim. Acta, 91 (1977) 189.
3 K. V. Krishnamurty and M. M. Reddy, Anal. Chem., 49 (1977) 222.
4 A. J. Pik, J. M. Eckert and K. L. Williams, Anal. Chim. Acta, 124 (1981) 351.
5 A. H. Pradzynski, R. E. Henry and J. S. Stewart, J. Radioanal. Chem., 32 (1976) 219.
6 See, e.g., H. T. Evans and R. M. Garrels, Geochim. Cosmochim. Acta, 15 (1958) 131.
7 C. K. Jørgensen, Acta Chem. Scand., 11 (1957) 73.
8 See, e.g., R. Jenkins and J. L. de Vries, Practical X-ray Spectrometry, 2nd edn., Macmillan, London, 1970, sect. 7.4.
9 J. P. Riley and G. Skirrow (Eds.), Chemical Oceanography, Vol. 1, 2nd edn., Academic Press, London, 1975, p. 559.
10 G. E. Batley and Y. J. Farrar, Anal. Chim. Acta, 99 (1978) 283.
11 E. Nakayama, T. Kuwamoto, H. Tokoro and T. Fujinaga, Anal. Chim. Acta, 131 (1981) 247.

Analytica Chimica Acta, 153 (1983) 69—82
Elsevier Science Publishers B.V., Amsterdam — Printed in The Netherlands

MASS SPECTROMETRIC ANALYSIS OF THERMAL DECOMPOSITION PRODUCTS OF GRAPHITE FLUORIDES AND ELECTROGENERATED CARBON—FLUORINE COMPOUNDS

DIDIER DEVILLIERS, MICHEL VOGLER, FREDERIC LANTELME and MARIUS CHEMLA*

Laboratoire d'Electrochimie, Université Pierre et Marie Curie, 4 Place Jussieu, 75230 Paris Cedex 05 (France)

(Received 23rd May 1983)

SUMMARY

Graphite fluoride is generally described as a stable compound at temperatures up to 400°C. It is shown that thermal decomposition starts below 100°C, leading to the formation of several gaseous fluorocarbons and some other compounds, e.g., CO, CO_2, SiF_4, when the reaction proceeds in a quartz tube. Comparison of the spectra of several graphite fluorides with those of samples obtained from the surface layers of carbon electrodes used as anodes in molten 2HF—KF, confirms the hypothesis of the formation of a CF_x passivating surface film. Its stoichiometric ratio is estimated to be $x \approx 1.1$, for a carbon anode maintained for several hours at +6 V vs. a Pt—H_2 electrode. The formation of graphite fluoride is responsible for the high anodic overvoltage and contributes to the disintegration of the carbon anode. Analysis of the anodic gases evolved from a laboratory fluorine cell shows that gaseous fluorocarbons are evolved at a potential lower than that of fluorine evolution, in agreement with thermodynamic calculations. These results explain why fluorine always contains trace amounts of fluorocarbons.

Electrolysis is the only method for the production of elemental fluorine [1]; molten 2HF—KF at 85—100°C is used in nearly all industrial processes. Although the thermodynamic potential of hydrofluoric acid decomposition in this electrolyte is 2.9 V [2], a voltage of 10—14 V is necessary for the working current density of 30 A dm^{-2}. Such a large loss of energy is accepted only because of the considerable added value of the compounds (e.g., uranium hexafluoride) that are produced with fluorine.

This situation is mainly due to the anodic overpotential of the fluorine evolution reaction at the carbon electrode; and, although this is the highest overvoltage ever observed in electron-transfer reactions, little work has been reported concerning the electrochemical kinetics of fluorine evolution [3] on carbon anodes. Watanabe et al. [4] and Arvia and Bebczuk de Cusminsky [5], studying respectively the 2HF—KF and HF—KF melts, determined the ohmic potential drop by the current commutation technique. They both suggested the formation of a layer of a C $\cdots$ F compound, which means that fluorine atoms are bound on the carbon surface; an F_2 molecule is formed

0003-2670/83/$03.00

by the combination of two chemically adsorbed species or by an electrochemical reaction involving a fluorine atom adsorbed on the electrode and a fluoride ion from the electrolyte.

From thermodynamic data, however, the formation of gaseous as well as solid fluorocarbons should appear before fluorine evolution [6]. Table 1 shows the free enthalpy and the corresponding thermodynamic potential ΔE, for the formation of some fluorocarbon compounds in the molten 2HF—KF electrolyte at 85°C according to the reaction

$$C + x\ \mathrm{HF\ (liq)} \rightarrow \mathrm{CF}_x + \frac{x}{2}\mathrm{H}_2 \qquad (1)$$

As the values for fluorine evolution and for the formation of CF_x are 2.89 V and 1.45 V, respectively, the appearance of an insulating layer of CF_x at the surface of the anode can be predicted. Indeed, in the previous work [6], a passivation peak was observed at +2.2 V (vs. Pt—H_2 reference electrode) by linear voltammetry at a scan rate of 1 V s^{-1}. This passivation peak appears only during the first sweep with a new electrode; it is difficult to restore the initial surface state because the reduction peak can only be observed at about 0 V. In agreement with Imoto and Watanabe [7], it can be assumed that the CF_x film is always present under normal electrolysis conditions, and it acts as a high potential barrier which is responsible for the large energy loss in the electron transfer at the anode.

The aim of this paper is to confirm the existence of fluorocarbon compounds at the surface of carbon anodes issuing from fluorine cells, and to establish the chemical composition of these compounds by a study of their thermal behavior, comparatively with various graphite fluorides. For this purpose, the work was divided into three parts. First, mass spectrometry was used to analyze the gaseous products evolved during the thermal decomposition of some graphite fluorides of well-known stoichiometric composition. These first experiments showed that the decomposition reaction cannot be neglected even at temperatures as low as 100°C. Secondly, under the same experimental conditions, we analyzed the gases evolved from surface samples of carbon electrodes used as anodes in the 2HF—KF melt. Comparison of the spectra gave information on the stoichiometry of the carbon—fluorine layers. Thirdly, the anodic gases produced during the electrolysis of 2HF—

TABLE 1

Free enthalpy and thermodynamic potential corresponding to the formation of some fluorocarbon compounds by reaction (1)

Compound	ΔG (kJ)	ΔE (V)
F_2	279.2	2.89
CF_4 (g)	489.7	1.27
$CF_{1.25}$ (s)	156.1	1.44
$CF_{0.597}$ (s)	83.3	1.45

KF at several applied potentials were analyzed. Gaseous fluorocarbons, which could be ascribed to the thermal decomposition of the CF_x layer, were found. An evaluation of the corrosion process of the anode was deduced. The experimental procedure was based on preliminary trapping of the corrosive gases (F_2, F_2O, HF), followed by further spectroscopic determination of the remaining "inert gases".

THERMAL DECOMPOSITION OF SOME GRAPHITE FLUORIDES

The name "graphite fluorides" is assigned to non-stoichiometric solid fluorocarbons with the general formula CF_x, where $0 < x \leqslant 1.24$. The structure of some of these compounds is known, corresponding to simple F/C ratios such as CF [8, 9] or $CF_{0.5}$ [9]. Kamarchik and Margrave [10] have reviewed the general properties and thermodynamic data concerning CF_x compounds. These materials are used as lubricants under extreme conditions of temperature and vacuum [11], and also as cathodic depolarizers for high-energy batteries [9, 12]. Many investigators have examined their thermal stability [13—18]. The thermal decomposition of CF_x was studied from 420 to 580°C by Kuriakose and Margrave [13], who analyzed the gaseous products in a time-of-flight mass spectrometer. Later, Kamarchik and Margrave [14], using thermogravimetry, concluded that the kinetics of decomposition is satisfactorily fitted by the Avrami equation [19]: $\ln(1-\alpha) = -kt^n$, where α is the decomposed fraction, k the rate constant, and n the dimensionality of nucleus growth ($n = 2$). These kinetics results were confirmed and supplemented by Watanabe and co-workers for various samples of CF_x prepared under different conditions [15—18]. The decomposition rates were studied in vacuum as well as in oxygen [16], nitrogen or fluorine [18] atmospheres for the temperature range 430—700°C.

Many papers deal with the kinetics of the thermal decomposition, but little information is available concerning the evolved gaseous products; only Kuriakose and Margrave [13] using mass spectrometry, and Watanabe et al. [17] using i.r. spectroscopy, have reported some results.

It is useful to complete the previous studies by analysis of the behavior of graphite fluorides with a well-known F/C ratio in a wide range of temperatures.

Experimental

Nature of the samples. Five samples of graphite fluorides corresponding to different F/C stoichiometric ratios were examined:

A, $CF_{0.5}$, black in color, obtained by fluorination of artificial graphite (donated by Professor Watanabe, Kyoto University);
B, $CF_{0.8}$, grey compound (Alfa Products);
C, CF, white, obtained by fluorination of petroleum coke (donated by Professor Watanabe, Kyoto University);
D, CF_x ($x > 1$), white (Alfa Products);
E, $CF_{1.1}$, white ("Foracarb"; P.C.U.K., France).

Measurements. The samples (50—200 mg) were introduced into quartz tubes and maintained under vacuum (10^{-5} torr) at room temperature, for at least 3 h.

At each temperature step, the sample was heated in a furnace for 15 h; then, the gases were collected and analyzed with an Atlas Werke CH4 mass spectrometer; the ionizing energy was 70 eV. When thermal decomposition was done at low temperature (i.e., 100 or 300°C), the small amount of released gas was evaluated from the intensity of the spectral lines, because the pressure was too low for measurement with a manometer. The gases were pumped off the quartz tubes between two temperature steps. At the end of the experiments, a black powder remained in the tubes.

Results

Amounts of released gas. Figure 1 shows the volume of the mixture of gases, referred to 10 mg of sample, obtained by the thermal treatment at each temperature step: 100°C, 300°C, 450°C and 700°C. The scales used are not the same for the four steps because the corresponding volumes were quite different. The small quantity of gases released at low temperature is probably why it has not been mentioned by other authors. For example, the total volume of gas evolved from 10 mg of $CF_{0.5}$ (sample A) is $V_0 = 1.67\ cm^3$ under standard conditions of temperature and pressure. Table 2 shows the distribution of this volume among the four temperature steps.

Composition of the released mixtures of gases. The mass spectra indicated that the mixtures of gases contain mainly CO, CO_2, SiF_4 and fluorocarbons, denoted by C_xF_y, characterized by the CF_3^+ ion peak at mass 69; other minor components, chiefly H_2O, are also present, but only in the gases released at low temperature.

It would be interesting to determine the composition of the C_xF_y mixtures of compounds. Unfortunately, for all the perfluoroparaffins, the most intense peak is that from CF_3^+ at mass 69, and, in all cases, the molecular ion is vanishingly small; the mass spectra of high-molecular-weight perfluoroparaffins are very similar, and it is difficult to analyze mixtures of these compounds [20]. The spectra of perfluoro-olefins are distinctive, with no obvious common features; but for heavy compounds, the mass 69 peak is also the most intense one, as for the perfluoroparaffins.

Hence, like other authors [13], we cannot determine the exact composition of all the mixtures of C_xF_y compounds. However, examples of characteristic mass spectra are given, as they are useful for comparison with spectra obtained from compounds produced by electrochemical anodization of carbon. Table 3 lists the main ions observed in the mass spectra of the complex mixtures of fluorocarbons released by samples A, E and I. The ions are listed in order of increasing mass to mass 200, and the intensities are relative to that of the CF_3^+ ion taken as 1000. Sample I (fluorinated carbon anode) at 100°C will be discussed below. The second part of the spectra (not presented) corresponding to heavy fragments with masses ranging between

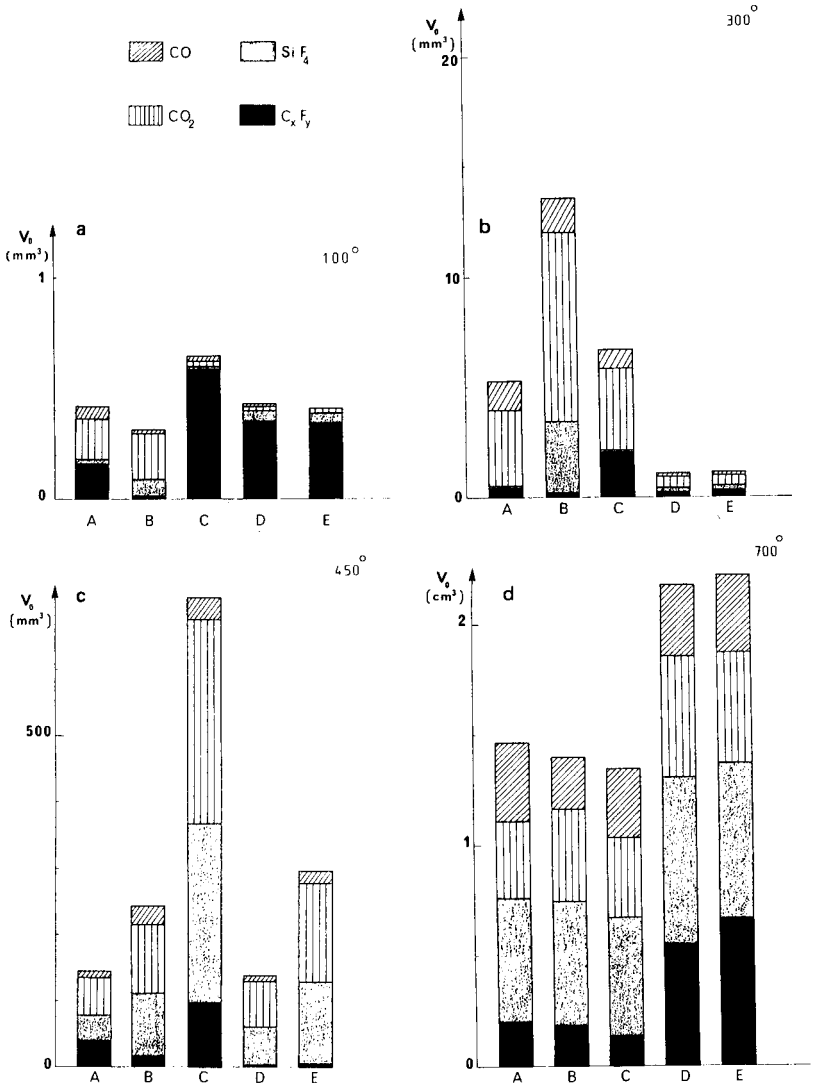

Fig. 1. Volumes of gases (CO, CO_2, SiF_4, C_xF_y) evolved from samples of graphite fluorides (A, B, C, D, E) at the four temperature steps: (a) 100°C; (b) 300°C; (c) 450°C; (d) 700°C.

TABLE 2

Amounts of gases evolved from sample A ($CF_{0.5}$)

Temperature (°C)	100	300	450	700
Volume (%)	0.2	0.8	15.6	83.4

TABLE 3

$C_xF_y^+$ ions of the mass spectra (m/z <200) of some graphite fluorides (samples A, E, I) at 100°C and 700°C

Mass	$C_xF_y^+$ ion		Peak intensity[a]				
	x	y	A(100)	A(700)	E(100)	E(700)	I(100)
31	1	1	72	83	61	114	107
50	1	2	22	71	13	47	16
69	1	3	1000	1000	1000	1000	1000
70	1[b]	3	13	11	17	12	12
74	3	2	7	1	21	7	24
81	2	3	9	1	9	21	9
93	3	3	49	4	109	37	137
98	5	2	5	0	18	1	18
100	2	4	107	17	111	60	64
112	3	4	8	3	20	8	26
117	5	3	6	1	108	5	92
119	2	5	199	236	68	199	74
124	4	4	7	1	55	8	53
131	3	5	242	12	158	86	160
143	4	5	13	2	60	21	71
148	6	4	6	0	29	1	28
150	3	6	14	1	5	22	8
155	5	5	7	1	87	7	69
162	4	6	15	1	17	12	30
167	6	5	1	2	41	1	34
169	3	7	97	41	21	46	27
181	4	7	119	4	81	21	73
186	6	6	3	1	47	2	41
193	5	7	11	1	29	17	47

[a]Relative to the CF_3^+ peak taken as 1000. [b]Isotopic $^{13}CF_3^+$ ion.

200 and 400, showed very few heavy fragments from sample A ($CF_{0.5}$), whereas the spectrum from sample E ($CF_{1.1}$) was characterized by a large number of lines, indicating that decomposition at 100°C leads to several heavy fluorocarbon molecules. Similar results were obtained, also at 100°C, with CF_x compounds for which $x \geqslant 1$.

For the same samples, the decomposition patterns at higher temperatures, say 700°C, showed much lower amounts of heavy components, especially for sample A. Thus, from the literature data on fluorocarbon spectra [20], and from the cracking patterns of CF_4 and C_2F_6 evaluated with the mass spectrometer used here, it was possible to find the composition of the C_xF_y gas mixtures when the contribution of heavy components was small. As an example, Table 4 indicates the composition of gases evolved from A ($CF_{0.5}$) at 700°C.

The other samples of CF_x with $x \approx 1$ released at 700°C larger amounts of heavy fluorocarbons than sample A, but CF_4 and C_2F_6 remained the most

TABLE 4

Fluorocarbons evolved from sample A ($CF_{0.5}$) at 700°C

Components	CF_4	C_2F_6	C_3F_8	C_xF_y ($x > 3$)
Mole (%)	44	44	8	⩽4

abundant products. But, at the 100°C step, the percentage of heavy fluorocarbons increased as the F/C ratio of the sample increased.

Discussion

The minor products, mainly water, which are observed at the low-temperature steps, are assigned to the contribution of gaseous molecules adsorbed at the surface of the solid samples. They must not be considered as products of thermal decomposition. Likewise, at least part of the CO and CO_2 can be considered as deriving from chemisorbed oxygenated compounds. The presence of silicon tetrafluoride is due, at least mainly, to the reaction of the primary gases with the quartz vessel. Watanabe et al. [17] reported i.r. absorption bands of SiF_4 and CO_2 in the spectra corresponding to the decomposition of $(CF)_n$ at 586°C, whereas Kuriakose and Margrave [13] did not report these components. Kamarchik and Margrave [10] suggested that C_2F_4 is the initial product and that it changes to various other gaseous compounds by secondary reactions.

Steunenberg and Cady [21] investigated the thermal behavior of several fluorocarbons and found that the most stable compounds are CF_4, C_2F_6, cyclo-C_5F_{10}, hexafluoropropene and octafluoromethyl-propene. The other gases studied, including C_2F_4, $C_3F_8 \cdots$, are transformed to more stable fluorocarbons on heating, although Atkinson and Atkinson [22] reported that C_2F_4 cannot be decomposed to CF_4 at temperatures below 700°C. Pyrolysis of each of the compounds listed above gives rise to: (1) gaseous products, CO, SiF_4, stable fluorocarbons, but not CO_2; (2) a high polymer such as teflon, and (3) traces of carbon residue.

Some other authors report that the pyrolysis of CF_4 can give CO_2 and SiF_4 by reaction with SiO_2, but the dissociation is only 0.006% at 1000°C and 0.04% at 1200°C [23]. The thermal reaction of C_2F_6 with quartz has been studied in 1947 by White and Rice [24]:

$$C_2F_6 + 3/2\ SiO_2 \rightarrow CO + CO_2 + 3/2\ SiF_4 \qquad (2)$$

but the test at 589°C gave no measurable pressure increase in 40 min, while 710°C produced a barely perceptible reaction. In order to confirm this result under the present experimental conditions by mass spectrometry, pure C_2F_6 was heated in a quartz tube for 15 h at 700°C, the initial pressure being p_0 = 62 torr. The mixture of gases obtained was 98.37% C_2F_6, 0.84% CO, 0.42% CO_2 and 0.37% SiF_4. Thus the decomposition of C_2F_6 may be neglected under the present experimental conditions. At 700°C, reaction (2) is just starting, which could explain the presence of some CO, CO_2 and

SiF_4, but this reaction cannot be taken into account at lower temperatures. The formation of silicon tetrafluoride can result from the reaction of quartz with HF [25] or F_2 [26], but it is also possible that reactive species such as CF_2, reported by Watanabe et al. [17], could react with quartz and give SiF_4, CO and CO_2; they could also account for the simultaneous formation of heavy fluorocarbons. At high temperature, as heavy fluorocarbons are themselves pyrolyzed, only light compounds such as CF_4, C_2F_6 ...are observed.

Finally, this study has shown a phenomenon previously unobserved: thermal decomposition of graphite fluorides starts at 100°C; it releases reactive chemical species able to react with quartz. The final gaseous phase contains SiF_4, CO, CO_2 and a mixture of various gaseous fluorocarbons that is characteristic of the F/C ratio of the compounds.

This method of thermal decomposition can be used to verify the formation of a passivating layer of CF_x on a carbon anode during the electrolysis of molten 2HF—KF. The patterns described above will serve to identify this layer of solid fluorocarbons generated in the electrochemical cell.

THERMAL DECOMPOSITION OF ELECTROGENERATED SAMPLES

The electrolysis of 2HF—KF requires non-graphitized carbon anodes. In this laboratory, C-205 (Carbone Lorraine) was used. During fluorine evolution, the electrode/molten fluoride interface is altered and the carbon is no longer wetted by the electrolyte, as a result of the formation of a graphite fluoride film [27]. It is possible to collect, by mechanical erosion, the surface layers from electrodes immediately after they have been used as anodes for fluorine evolution.

Thermal decomposition of these samples was studied using the same experimental procedure as described above, including mass spectrometric analysis of the evolved gases.

Nature of the samples

The argument is based on the study of the following species:

G, a sample of a new C-205 carbon electrode;

H, surface layers of a carbon electrode which has been exposed to the 2HF—KF melt for 24 h;

I, surface layers of a carbon electrode that had been used as anode in the molten 2HF—KF, for fluorine evolution at +6 V (vs. $Pt—H_2$);

J, a sample of solid residues resulting from the disintegration of a carbon anode, collected in an industrial fluorine production cell.

Results

Amounts of released gases. Figure 2 shows the volume of the mixture of gases, referred to 10 mg of materials, at the four temperature steps considered above. The results obtained for sample G, pure carbon, are not given,

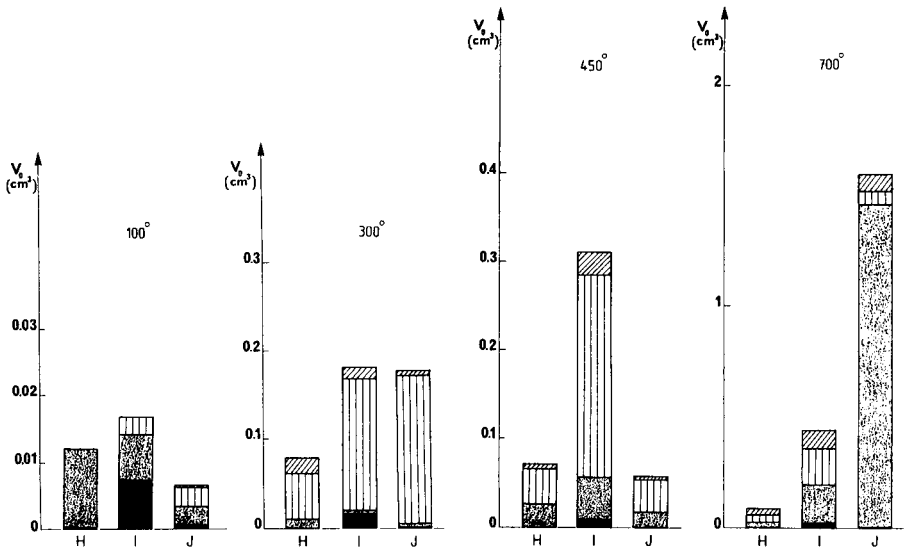

Fig. 2. Volumes of gases evolved from electrogenerated samples H, I, J, at the four temperature steps (100, 300, 450, 700°C).

because the amount of gases, mainly H_2O, CO_2, CO, CH_4 and H_2, was not significant at temperatures below 900°C. In fact, the spectrum observed with sample G can be considered as a blank.

For samples H, I and J, the average volume of the released gas is about the same at each temperature step; this was not the case for the graphite fluorides (samples A—E). As an example, Table 5 shows the results obtained with 10 mg of sample I; the total volume was 1.09 cm^3.

Description of the mass spectra and discussion. As for the graphite fluorides, CO, CO_2, SiF_4 and C_xF_y were observed as well as some other minor components (not presented in Fig. 2) consisting mainly of water; small amounts of methane and hydrogen appeared only in sample H. Because mechanical erosion does not provide homogeneous materials, depending on the relative amounts of surface and inner layers, the results in Fig. 2 are average values.

For sample H, the large silicon tetrafluoride content is assigned to the reaction of quartz with hydrogen fluoride released from the remaining salt crystallized at the surface of the electrode. This electrode had just been

TABLE 5

Amounts of gases evolved from sample I
(Surface layers of a carbon anode used in the 2HF—KF melt)

Temperature (°C):	100	300	450	700
Volume (%)	2.1	24.5	33.3	40.1

dipped in the molten fluorides; nevertheless, some gaseous fluorocarbons C_xF_y can be observed at the 100°C step, together with some hydrogen and methane. This means that, when carbon is in contact with molten 2HF—KF, a chemical reaction takes place, probably leading to the formation of the salt-like compound described by Rüdorff [28].

Sample I, corresponding to an electrode effectively used as anode in the molten 2HF—KF, released a large amount of gaseous C_xF_y, mostly at the 100°C temperature step. In order to specify the composition of the mixture of fluorocarbons, Table 3 (column 8) lists the principal ions of the corresponding mass spectrum, after discarding the contributions of H_2O, CO, CO_2 and SiF_4; the intensities are relative to the most intense peak, that of CF_3^+ at *m/z* 69, taken as 1000. Comparison of columns 6 and 8 of Table 3 shows the analogy between samples I and E: thermal decomposition of these two materials leads to the same heavy fluorocarbons at the first temperature step. The only difference is the reduced quantity of C_xF_y for I at the 700°C step. As the corresponding spectra of the other graphite fluorides, A—D, are quite different, it can be concluded that sample I contains a graphite fluoride similar to E, i.e., with a stoichiometric F/C ratio close to 1.1.

Likewise, the spectrum of sample J, pieces of carbon electrode collected in a fluorine production cell, shows the presence of the same fluorocarbons, together with silicon tetrafluoride arising from salt contamination. It may be concluded that the formation of CF_x at the carbon anode is responsible for its disintegration. On electrochemical reaction, some fluorine atoms penetrate into the bulk of the electrode and contribute to expanding the carbon matrix; some bits of surface layers of the anode, resulting from this splitting of the structure, fall down in the electrolytic cell.

ANALYSIS OF THE GASES EVOLVED DURING THE PRE-ELECTROLYSIS OF 2HF—KF AT A CARBON ANODE

The above work indicated that the carbon anode in the fluoride melt is covered by a CF_x film, and that this material is continuously decomposed into gaseous fluorocarbons at the usual temperature of electrolysis. It was worthwhile to confirm this conclusion by analysis of the fluorine evolved at the anode.

The direct analysis of anodic gases is possible by i.r. spectroscopy, using a special gas cell with silver chloride or calcium fluoride windows. Calcium fluoride is more resistant to corrosion but cannot be used for wavelengths greater than 10 μm; the silver chloride windows become cloudy and need to be polished after each measurement.

Mass spectrometric investigations require a special spectrometer insensitive to fluorine corrosion. Alternatively, and preferably, the corrosive gases (F_2, F_2O, HF) are trapped and the remaining "inert compounds" are measured. Usually, hydrogen fluoride is trapped in a bed of sodium fluoride [29—31] which gives the NaF—HF compound; further acid—base titration gives the

initial amount of hydrogen fluoride [31]. In the present electrochemical cell, there is an important temperature gradient between the body and the head of the vessel, so that the vapor pressure of hydrogen fluoride is low at the head of the cell. This small amount of hydrogen fluoride is then trapped by solid 2HF—KF before leaving the anodic compartment. Fluorine oxide, F_2O, is trapped by potassium iodide [25], the resulting iodine being titrated by thiosulfate. For determination of fluorine, several methods are possible [32]. Fluorine can be trapped by aqueous solutions of hydriodic acid [31] or by metals such as mercury [33]. The most reliable method consists of the displacement of another halogen:

$$1/2\ F_2 + MX \rightarrow 1/2\ X_2 + MF$$

The temperature of reaction must be carefully defined to avoid the formation of interhalogenated compounds such as IF_5, IF_7 [34], BrF_5 or ClF_5 [35]. Very often an alkali chloride is chosen. The released chlorine can be determined in several ways: spectrophotometry at 0.36 μm [36], oxidation of iodide [31], or liquid—gas chromatography on halocarbon oil supported on Kel-F [29, 37, 38]. After elimination of the corrosive gases, the remaining components are easily evaluated by i.r. spectroscopy, mass spectrometry, or gas chromatography.

Experimental

The electrolysis experiments were done at 85°C, in the cell described previously [2]. The gas-tight anode compartment was swept by pure argon. The electrical system comprised an AMEL 555 potentiostat driven by a potential adder-amplifier, which can deliver potentials of −10 V to + 10 V vs. Pt—H_2 [39, 40]. The counter electrode material was graphite so as to prevent any pollution of the melt.

The purpose was to determine the composition of the anodic gases evolved from the electrolytic cell, in order to prove the presence of gaseous fluorocarbons as minor components. Only two techniques are suitable for the range of concentration of these samples, mass spectrometry and i.r. spectroscopy, after F_2 and F_2O have been trapped on a polytetrafluoroethylene column packed with potassium chloride and sodium iodide. Fluorine is quantitatively absorbed, and the chlorine produces iodine from sodium iodide, while F_2O reacts only with iodide:

$$F_2 + 2\ Cl^- \rightarrow Cl_2 + 2\ F^-$$

$$Cl_2 + 2\ I^- \rightarrow I_2 + 2\ Cl^-$$

$$3\ F_2O + 7\ I^- \rightarrow 3\ I_2 + IO_3^- + 6\ F^-$$

After dissolution of the contents of the chemical trap in an acetic acid—acetate buffer, the conventional reaction proceeds:

$$IO_3^- + 6\ H^+ + 5I^- \rightarrow 3I_2 + 3H_2O$$

All the iodine is titrated with thiosulfate, and the fluoride concentration of

the solution is measured with an Orion 94-09 fluoride-selective electrode. Overall reactions are

$$F_2 + 2\,I^- \rightarrow 2\,F^- + I_2$$

$$F_2O + 4\,I^- + 2\,H^+ \rightarrow 2\,F^- + 2\,I_2 + H_2O$$

Thus when the amounts of fluoride and iodine are known, the initial amounts of F_2 and F_2O in the gas mixture can be calculated.

A Beckman IR-10 spectrophotometer was used to analyze the residual gases; the length of the cell was 10 cm. Generally, the Beer—Lambert law can be applied, but for several light gases (CO, CO_2, CH_4, etc.) at a constant partial pressure p, the absorbance increases with increasing total pressure of the sample [41, 42]. Thus, to determine carbon dioxide in the mixtures, at 2350 cm^{-1}, it is necessary to use standards. Many fluorocarbons absorb in the range 1200—1300 cm^{-1} [43], so that i.r. spectroscopy of a mixture of fluorocarbons is difficult. In the present samples, only CF_4, with a very sharp absorption band at 1283 cm^{-1}, and C_2F_6 at 1250 cm^{-1}, can be determined, again with standards.

Mass spectrometric analysis of the gas mixtures was done with the Atlas Werke CH4 instrument; the composition of a fluorocarbon mixture is difficult to determine because the mass spectra of these compounds lack distinguishing features (see first section).

Results

Mass spectrometry and i.r. spectroscopy are complementary for this analysis of the "inert gases". With mass spectrometry, one can deduce the composition of the whole sample, but minor components are evaluated imprecisely; it is only possible to find the total percentage of C_xF_y compounds (including CF_4 and heavier molecules). In contrast, some gases show strong i.r. bands (CF_4, C_2F_6); thus their partial pressure can be calculated more precisely. The results obtained for carbon dioxide, easily determined by both methods, were in good agreement.

Table 6 shows the results obtained for various potentials applied at the working electrode, during the pre-electrolysis of a 2 HF—KF melt. At +4.3 V, a very small amount of gas was evolved, even for a twelve-hour experiment; thus the results are less precise. For all the samples, the important contents of CO, CO_2, O_2 and F_2O are related to the discharge of water on the carbon anode. The large quantity of oxygenated gases (in agreement with the results obtained with industrial cells during pre-electrolysis [44]) decreases with time, because water is consumed by electrochemical reactions. The F_2 and F_2O evolution is significant only for potentials greater than +6.5 V, revealing the large anodic overvoltage. For all the experiments, several fluorinated gases are detected: SO_2F_2, SiF_4, CF_4 and other fluorocarbons. The first two of these gases arise from electrochemical reactions involving impurities of the melt (sulfates and hexafluorosilicates).

In industrial cells, CF_4 is known as a contaminant in the fluorine and

TABLE 6

Composition of the anodic gases during pre-electrolysis at different potentials applied at the working carbon electrode

E(V)	Composition (%)								
	F_2O	F_2	CO	CO_2	O_2	SiF_4	SO_2F_2	C_xF_y	
								total	as CF_4
4.3	0		2.6	13.4	80.6		3.4		0.12
5.5	1.1		0.6	5.0	93.2	0.01	0.08	0.04	0.03
6.0	1.8		0.8	8.3	89.2	0.01	0.10	0.11	0.01
6.5	6.3	5.1	0.4	11	77	0.02	0.07	0.13	0.07
7.0	2.6	14.4	0.9	15	65.7	0.07	0.06	0.11	0.035

must be determined on line [45]. These observations and the present gas analysis prove the systematic presence of CF_4 in anodic gases for a large range of potentials applied to the carbon anode.

The evolved fluorocarbons can be related to thermal decomposition of the solid layer of CF_x formed at the surface of the carbon anode. These gaseous compounds appear at a potential as low as +4.3 V, i.e., before the evolution of fluorine. Hence, the presence of CF_4 cannot be due only to oxidation of the carbon anode with fluorine.

CONCLUSION

This study leads to a better understanding of the discharge mechanisms of fluoride ions at the carbon anode during the electrolysis of 2HF—KF melts. The first step is the formation of a semi-conducting CF_x layer as soon as a sufficiently positive potential is applied. Then, the fluorine evolution occurs by electron transfer across the barrier-layer film which is responsible for the high anodic overvoltage. The energy dissipated in this process may increase the local temperature and allow partial thermal decomposition of the CF_x compounds. In industrial electrolysis cells, the steady-state thickness of the layer is a consequence of simultaneous electrochemical formation and thermal decomposition of graphite fluorides. In this mechanism, the electrogenerated fluorine is not in direct contact with the carbon electrode.

The authors are grateful to Professor Watanabe, Kyoto University, for providing the samples of C_2F and CF compounds and for fruitful discussions.

REFERENCES

1 D. Pletcher, Industrial Electrochemistry, Chapman and Hall, London, 1982, Ch. 5, p. 132.
2 D. Devilliers, F. Lantelme and M. Chemla, J. Chim. Phys., 76 (1979) 428.

3 A. T. Kuhn, in A. J. Bard (Ed.), Encyclopedia of Electrochemistry of the Elements, Vol. IV, Dekker, New York, 1975, Ch. 2.
4 N. Watanabe, M. Inoue and S. Yoshizawa, J. Electrochem. Soc. Jpn., 31 (1963) 168.
5 A. J. Arvia and J. Bebczuk de Cusminsky, Trans. Faraday Soc., 58 (1962) 1019.
6 D. Devilliers, F. Lantelme and M. Chemla, J. Chim. Phys., 80 (1983) 267.
7 H. Imoto and N. Watanabe, Bull. Chem. Soc. Jpn., 49 (1976) 1736.
8 R. J. Lagow, R. B. Badachhape, J. L. Wood and J. L. Margrave, J. Chem. Soc., Dalton Trans., (1974) 1268.
9 N. Watanabe, Solid State Ionics, 1 (1980) 87.
10 P. Kamarchik, Jr. and J. L. Margrave, Acc. Chem. Res., 11 (1978) 296.
11 H. Gisser, M. Petronio and A. Shapiro, Lubr. Eng., 28 (1972) 161 (Chem. Abstr., 77 (1972) 37289 s).
12 H. F. Hunger and G. J. Heymach, J. Electrochem. Soc., 120 (1973) 1161.
13 A. Kuriakose and J. L. Margrave, Inorg. Chem., 4 (1965) 1639.
14 P. Kamarchik, Jr. and J. L. Margrave, J. Thermal Anal., 11 (1977) 259.
15 N. Watanabe and S. Koyama, Bull. Chem. Soc. Jpn., 53 (1980) 3093.
16 N. Watanabe and S. Koyama, Bull. Chem. Soc. Jpn., 53 (1980) 3100.
17 N. Watanabe, S. Koyama and H. Imoto, Bull. Chem. Soc. Jpn., 53 (1980) 2731.
18 S. Koyama, Thesis, Kyoto, Japan, 1980.
19 M. Avrami, J. Chem. Phys., 8 (1940) 212.
20 J. R. Majer, in M. Stacey, J. C. Tatlow and A. G. Sharpe (Eds.), Advances in Fluorine Chemistry, Vol. II, Butterworths, London, 1961, Ch. 3.
21 R. K. Steunenberg and G. H. Cady, J. Am. Chem. Soc., 74 (1952) 4165.
22 B. Atkinson and V. A. Atkinson, J. Chem. Soc., (1957) 2086.
23 Gmelin Handbuch der Anorganischen Chemie, Vol. Kohlenstoff D2, Springer-Verlag, Berlin, 1974, p. 131.
24 L. White Jr. and O. K. Rice, J. Am. Chem. Soc., 69 (1947) 267.
25 P. Pascal, Nouveau Traité de Chimie Minérale, Vol. XVI, Masson, Paris, 1960, p. 17.
26 R. O'D. Teston and F. E. McKenna, Anal. Chem., 19 (1947) 193.
27 A. J. Rudge, Chem. Ind. (London), (1966) 482.
28 W. Rüdorff, Z. Anorg. Chem., 254 (1947) 319.
29 O. Rochefort, Anal. Chim. Acta, 29 (1963) 350.
30 A. J. Rudge, in A. T. Kuhn (Ed.), Industrial Electrochemical Processes, Elsevier, Amsterdam, 1971, Ch. 1.
31 S. G. Turnbull, A. F. Benning, G. W. Feldmann, A. L. Linch, R. C. McHarness and M. K. Richards, Ind. Eng. Chem., 39 (1947) 286.
32 N. S. Nikolaev, S. N. Suvorova, E. I. Gurovich, I. Peka and E. K. Korchemnaya, Analytical Chemistry of Fluorine, Halsted Press, New York, 1972.
33 W. T. Miller and L. A. Bigelow, J. Am. Chem. Soc., 58 (1936) 1585.
34 H. Selig, C. W. Williams and G. J. Moody, J. Phys. Chem., 71 (1967) 2739.
35 G. A. Hyde and M. M. Boudakian, Inorg. Chem., 7 (1968) 2648.
36 C. W. Weber and O. H. Howard, Anal. Chem., 35 (1963) 1002.
37 R. Foon and G. P. Reid, J. Chromatogr. Sci., 14 (1976) 421.
38 S. Sugikawa and T. Tsujino, J. Nucl. Sci. Technol., 14 (1977) 147.
39 J. Giner, J. Electrochem. Soc., 111 (1964) 376.
40 M. Chemla, in A. J. Bard (Ed.), Encyclopedia of Electrochemistry of the Elements, Vol. IX (A), Dekker, New York, 1982, p. 386.
41 L. J. Brady, in M. G. Mellon (Ed.), Analytical Absorption Spectroscopy, Wiley, New York, 1950, Ch. 8, p. 497.
42 N. D. Coggeshall and E. L. Saier, J. Appl. Phys., 17 (1946) 450.
43 D. G. Weiblen, in J. H. Simons (Ed.), Fluorine Chemistry, Vol. II, Academic Press, New York, 1954, Ch. 7.
44 R. C. Downing, A. F. Benning, F. B. Downing, R. C. McHarness, M. K. Richards and T. W. Tomkowit, Ind. Eng. Chem., 39 (1947) 259.
45 A. Level, Chim. Ind. Génie Chimique, 102 (1969) 1077.

Analytica Chimica Acta, 153 (1983) 83—92
Elsevier Science Publishers B.V., Amsterdam — Printed in The Netherlands

THE SYMMETRY-CONTROLLED SIMPLEX OPTIMIZATION PROCEDURE

P. F. A. VAN DER WIEL*, R. MAASSEN and G. KATEMAN

Department of Analytical Chemistry, Faculty of Science, University of Nijmegen, Toernooiveld, 6525 ED Nijmegen (The Netherlands)

(Received 27th December 1982)

SUMMARY

The degeneracy problem in a simplex procedure can be solved by introducing a symmetry criterion. The determinant of the simplex can be used to monitor the optimization process when the symmetry of the simplex is controlled. This monitoring of the optimization process is valuable when more than two parameters are involved. The symmetry criterion can be used in any variable-size simplex. A Super Modified Simplex procedure with a symmetry criterion and a boundary violation procedure is described fully.

The performance of any sophisticated analytical method depends strongly on the correct choice of the experimental parameters. In flow injection analysis, for instance, these parameters may include temperature, flow rates of reagent, reaction coil lengths, concentrations of reagents, etc. The desired performance of a particular method is influenced by the goal of the analysis (e.g., accuracy vs. speed).

One method of optimization applied for this kind of problem is the simplex technique. This sequential technique, which also accounts for interactions between the parameters, has found widespread use [1—6]. The history of the development of simplex optimization procedures has been described [7]. This paper formulates rules that may be applied in order to enhance the performance and to circumvent some problems of the Super Modified Simplex procedure (SMS) [2, 8]. One of the major problems, degeneracy, is solved by introducing a "symmetry" restriction.

GENERAL OUTLINE OF A SIMPLEX PROCEDURE

The optimization is started by supplying start parameters to the simplex procedure (Fig. 1). The output of the procedure forms a set of parameters to be used in the system. When a response is obtained from the system, new parameter settings are calculated, aiming for a better response. In the SMS procedure, the geometric figure formed by $N + 1$ vertices (N being the number of parameters involved) is called the simplex. The vertices are given by the value of the parameters. The vertices of the start simplex can be

0003-2670/83/$03.00

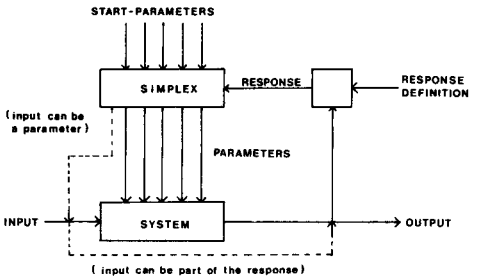

Fig. 1. General outline of a simplex procedure.

calculated as described by Spendley et al. [9]. As shown in Fig. 2, the vertex yielding the worst response (V_w) is reflected through the centroid (V'_w) in order to obtain a reflected vertex (V_n). When a Y factor is defined as in Fig. 2, the reflected vertex can be calculated by using $Y = 2$ in the equation

$$V = Y * V'_w + (1 - Y) * V_w \tag{1}$$

where $V'_w = (\sum_{i \neq w}^{N+1} V_i)/N$.

Based on the responses at V_w, V'_w (which can be estimated from the mean of the responses minus the response at V_w) and V_n (measured), an "optimal" Y factor is calculated by using Gaussian or second-order curve-fitting. The "optimal" vertex is calculated by using this Y factor in Eqn. (1) and the response is measured. This vertex replaces the worst vertex and the procedure can be started again.

Restrictions to the Y *factor*

To prevent excessive movement of the simplex, the Y factor must be restricted between two pre-set limits. With a minimum value of -1 and a maximum value of 3, the size of the new simplex may grow until it becomes,

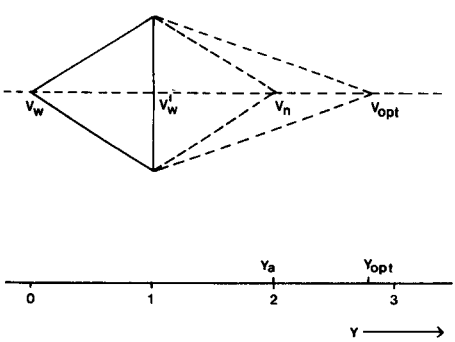

Fig. 2. Nomenclature of vertices and definition of the Y factor. V_w is the vertex giving the worst response, V'_w the centroid, V_n the reflected vertex and V_{opt} the optimal vertex.

maximally, twice the size of the current simplex. This can be written as: $Y <$ minimum Y: $Y =$ minimum Y and $Y >$ maximum Y: $Y =$ maximum Y. Another restriction to the Y factor is needed. When $Y = 1$, the optimal vertex is the centroid; here the simplex loses the ability to move in a certain direction. When $Y = 0$, the optimal vertex equals the (old) worst vertex and no progress is made. This restriction can be considered as a safety margin around $Y = 1$ and $Y = 0$ and can be written as:

$1 + Sy > Y >= 1$: $Y = 1 + Sy$

$1 > Y > 1 - Sy$: $Y = 1 - Sy$

$Sy > Y >= 0$: $Y = Sy$

$0 > Y > -Sy$: $Y = -Sy$

where Sy is the safety margin ($0.5 > Sy > 0$) (see Fig. 3).

Boundary violation

Another problem is encountered from boundary violation. Usually the value of a parameter is restricted between given minimum and maximum values, imposed by the system (e.g., temperature, pressure). If it can be assumed that the parameters of all vertices of the current simplex are within the boundaries, there are two cases of boundary violation.

A, A parameter of the reflected vertex (V_n) is out of range. This is the most complicated case of boundary violation. The assignment of a very bad response to the violating vertex is not a cure because the movement of the simplex is determined by the response itself. Therefore, first the Y factor corresponding to the violated boundary is calculated (see Fig. 4):

$$Y_a = (B_j - V'_{w,j})/(V'_{w,j} - V_{w,j}) + 1 \qquad (2)$$

where Y_a is the boundary Y factor and B_j is the violated boundary for parameter j. Because the reflected vertex is involved in the calculation of the optimal vertex (V_{opt}) by a second-order or Gaussian estimator, Y_a is restricted as follows: if $Y_a \geqslant 1.5$, Y_a is accepted, and if $Y_a < 1.5$, $Y_a = 0.5$. The restriction $Y_a \geqslant 1.5$ is made to ensure a reasonable spacing between V_w, V'_w and V_n. A calculated value $Y_a > 0$ AND $Y_a < 1$ indicates a logical error, because in this situation the boundary for one of the parameters lies within the simplex which is in conflict with the assumption made above.

A new reflected vertex can be calculated by using Eqn. (1): $Y = Y_a$. The troublesome parameter is located exactly at the parameter boundary when $Y_a \geqslant 1.5$.

Fig. 3. Restrictions to the Y factor. The shaded regions are forbidden.

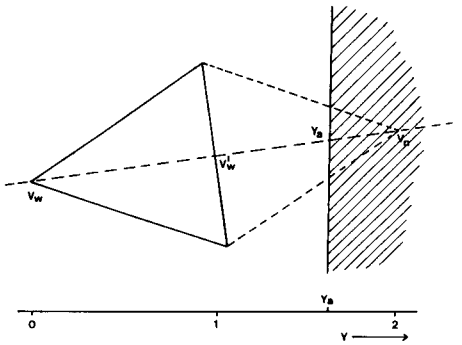

Fig. 4. Boundary violation of the reflected vertex.

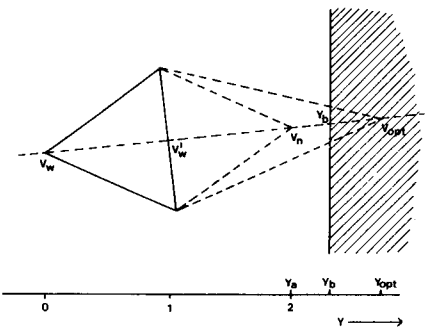

Fig. 5. Boundary violation of the "optimal" vertex.

The equations used to calculate the optimal Y factor [8] with the response of a reflected vertex which is not located at $Y_a = 2$ (the undisturbed position of this vertex) can be written in two ways. For second-order estimates:

$$Y_{opt} = 0.5(Y_a^2 - Y_a) * (R_w - R'_w)/[(Y_a - 1) * R_w - Y_a * R'_w + R_n] + 0.5 \tag{3}$$

with the additional conditions

if $Y_a > 1, R'_w > [R_n + (Y_a - 1) * R_w]/Y_a$

if $Y_a \leqslant 1$ AND $Y_a \neq 0, R'_w < [R_n + (Y_a - 1) * R_w]/Y_a$

For Gaussian estimates:

$$Y_{opt} = 0.5(Y_a^2 - Y_a) * (\ln R_w - \ln R'_w)/[(Y_a - 1) * \ln R_w - Y_a * \ln R'_w + \ln R_n] + 0.5 \tag{4}$$

with the additional conditions

if $Y_a > 1, R'_w > R_n^{(1/Ya)} * R_w^{(1-1/Y_a)}$

if $Y_a \leqslant 1$ AND $Y_a \neq 0, R'_w < R_n^{(1/Ya)} * R_w^{(1-1/Y_a)}$

These equations can be used even if no boundary violation occurs for a preset Y_a value of 2. The conditions given for the estimators ensure that a Y factor is calculated for a maximum response optimization. If a condition is not met, the estimator cannot be used. Here the Y factor is set to the maximum or minimum value, depending on the responses at the reflected vertex and the worst vertex.

B, A parameter of the optimal vertex (V_{opt}) is out of range. First, the Y factor corresponding to the violated boundary is calculated with Eqn. (2) (see Fig. 5). This Y factor could be used to calculate a new optimal vertex

(Eqn. 1); however, this Y factor should be checked for the safety margins (bearing in mind that the Y factor is not allowed to increase). As a result, the troublesome parameter is located exactly at the parameter boundary when $Y \geqslant 1 + Sy$.

IMPROVEMENT OF THE SIMPLEX MOVEMENT MECHANISM

The success of the SMS procedure is based on two features. First is the progress made by simple reflection of the worst vertex. This is the only mechanism used in the earlier versions of the simplex procedure. Second is a correction on this reflection by an optimum estimator. This estimator yields an "optimal" Y factor for the calculation of the next vertex. This correction can be unsuccessful so the "optimal" rule is stated: if the response at the "optimal" vertex is worse than the response at the reflected vertex, and if the response at the reflected vertex is not the worst response in the resulting simplex, the optimal vertex (which in fact was not very optimal) is replaced by the reflected vertex. This rule forces the SMS to act as a Modified Simplex [10].

An unsuccessful correction is possible in three situations: (a) the response surface cannot be estimated properly by a second-order or Gaussian estimator; (b) the vertices do not give a useful description of (part of) the response surface (e.g., because the simplex is large); and (c) noise imposed on the response.

Noise imposed on the responses

When the responses are subject to error, the $N + 1$ rule can be applied to reduce the risk that the simplex becomes anchored to some erroneous high response. This rule was stated by Spendley et al. [9]: if a vertex persists in $N + 1$ simplexes, the response of this vertex should be evaluated again; the response of this vertex can be this evaluated response or a combination of all or some of the responses evaluated so far for this vertex.

Without altering the purpose of the rule, it can be re-stated as: if a vertex is the best vertex in $N + 1$ simplexes, the response of this vertex should be evaluated again. This re-statement is made for sake of simplicity in programming a simplex procedure.

The degeneracy problem

The most important problem in the described simplex procedure is the degeneracy of the simplex (i.e., loss of the ability to search in all directions of the parameter space). Interest in the degeneracy of a simplex also arises from the observation that a weighted centroid simplex [8, 11] can follow the "steepest" ascent of a response surface very closely but soon degenerates. The weighted centroid (see Fig. 6) is as follows:

$$V'_w = \{\sum_{i=1}^{N+1} [V_i * (R_i - R_w)]\} / \{\sum_{i=1}^{N+1} (R_i - R_w)\}$$

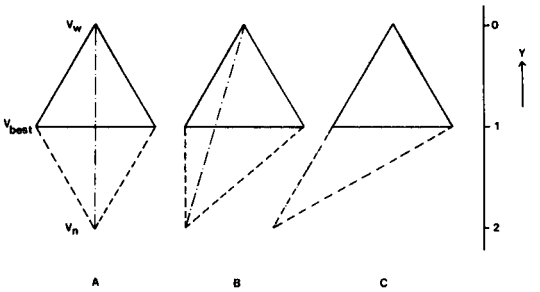

Fig. 6. A, Normal centroid; B, weighted centroid; *C*, extreme weighted centroid.

This degeneracy can be caused by repeated movement of the simplex in one direction; when the optimal vertex is the worst vertex in the new simplex. This can be solved by rejecting the next-to-worst vertex instead of the worst vertex. In simpler simplex procedures, this rule must be applied to prevent oscillation and to force the simplex to circle eventually around an optimum [9]. In the SMS procedure, it is applied to reduce the risk of degeneracy. This rule can be stated as follows: if a vertex is the worst vertex in K simplexes, the next-to-worst vertex should be used as the worst vertex in the calculation of vertices. A situation where this rule is applied successfully is shown in Fig. 7.

A more effective solution of the degeneracy problem is the introduction of a "symmetry" restriction. Application of a symmetry restriction to the SMS procedure yields the symmetry-controlled simplex procedure. Ryan et al. [11] used the determinant of the simplex in their OJWC procedure to

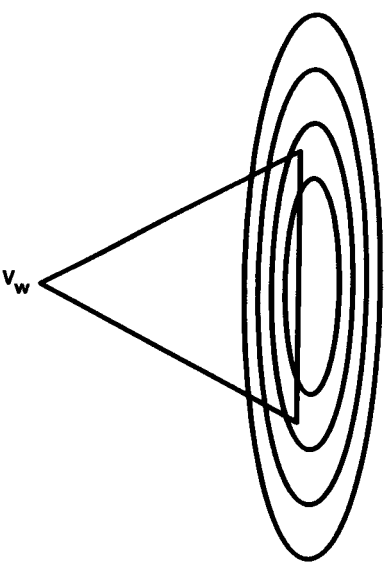

Fig. 7. Situation where repeated movement of the simplex in one direction can cause degeneracy.

detect degeneracy and correct the simplex by means of an "orthogonal jump". The determinant is calculated from the scaled simplex (0 1), using one of the vertices as a base. One of the vertices is subtracted from all the other vertices. This operation yields a $N \times N$ matrix from which the determinant is calculated. The determinant is related to the volume of the simplex: Vol = ABS (determinant)/$N!$. The rationale behind this approach is based on the observation that on degeneration of a simplex, the determinant decreases to very small values. Because it is immaterial which vertex is used as base, the determinant only depends on the Y factor applied for the calculation of the simplex. Thus the determinant can be calculated prior to the calculation of a new vertex:

$$(\text{Determinant})_i = \text{ABS}\ (1 - Y) * (\text{Determinant})_{i-1} \tag{5}$$

This equation clearly demonstrates the necessity of the safety margin around $Y = 1$ but unfortunately also shows that the determinant is independent of the centroid, weighted or not. A decrease in the determinant may be caused by shrinking of the simplex in all OR some directions and thus cannot be used to avoid degeneracy as proposed by Ryan et al. [11]. However, the determinant can be used conveniently to monitor the optimization process and can be incorporated in a stop criterion.

In order to distinguish between the size of the simplex and its ability to move in a certain direction, the "symmetry" is defined as follows. The symmetry equals the Nth root of the absolute value of the determinant divided by the radius of the sphere passing through all vertices of the simplex. This symmetry is scaled between 0 and 1, where the scaling factor depends on the number of parameters involved in the optimization. The symmetry of a perfect regular simplex equals 1 (Fig. 8).

Calculation of the symmetry

The determinant is readily available (Eqn. 5). The radius of the sphere is calculated as being the distance between the center of the sphere and one of the vertices. The condition that all distances must equal the radius yields N

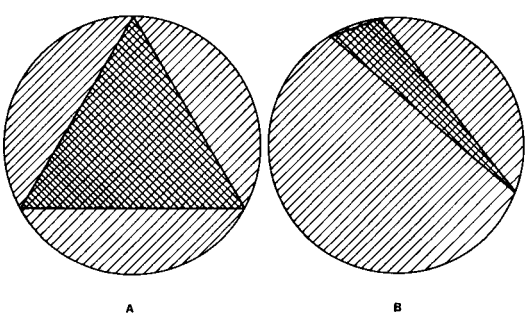

Fig. 8. Definition of the symmetry: the symmetry can be visualized as the ratio of the shaded surfaces.

equations with N unknowns. The scaling factors to be used are: 2 parameters, 0.6204; 3 parameters, 0.6874; 4 parameters, 0.7314; 5 parameters, 0.7631; 6 parameters, 0.7872; 7 parameters, 0.8063; 8 parameters, 0.8218.

Figure 9 shows the symmetry as a function of the Y factor starting with a perfect regular simplex ($Y = 0$), and with a perfect regular simplex and one of the vertices as the centroid (extreme weighted). When the symmetry thus defined can be kept above a pre-set minimum value, there will be no degeneracy problem and a weighted centroid simplex procedure can be used.

The symmetry restriction overrules the safety margins described earlier. If it can be assumed that the symmetry of the current simplex is above the minimum, a general procedure for the preservation of the symmetry can be given. A new vertex will be located on the line passing through V_w and V'_w. Considering only a Y factor greater than 1 and less than the maximal allowable Y factor, the first step is to examine whether a resulting simplex will have a symmetry above the criterion or not. If there is no such simplex, the procedure is repeated with the next-to-worst vertex, until a resulting simplex meets the symmetry criterion. If the tests fail for a weighted centroid, the tests should be repeated for an unweighted centroid. These tests can be made without evaluating a response. The only case where examining the symmetry curve is not necessary is the two-dimensional unweighted case.

When the optimal Y factor has been calculated (corrected for minimum and maximum Y factors but not corrected for a safety margin), a symmetry check is made. Eventually, the Y factor is corrected for the symmetry and the optimal vertex is calculated. The previous tests for the existence of a resulting simplex which has symmetry above the criterion, ensure that the symmetry correction for the optimal vertex cannot fail. The only situation where the symmetry could fall below the criterion is when the simplex results from a boundary violation of the optimal vertex. Here the safety criterion should be used.

The symmetry restriction should be taken into account when the optimal rule is applied. This rule should not be applied when the symmetry (using

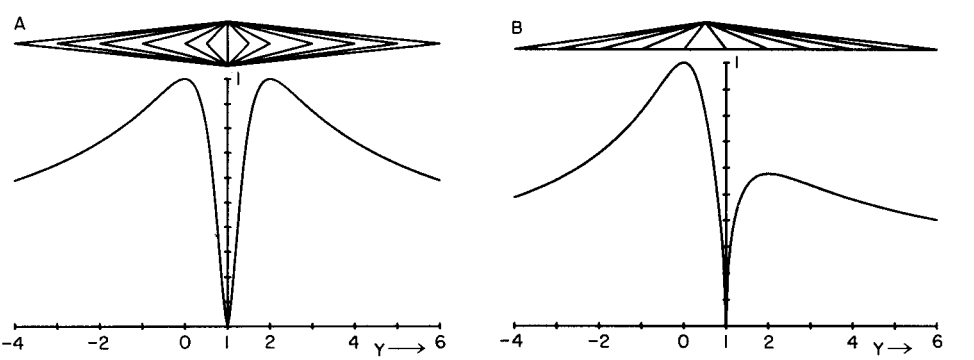

Fig. 9. The symmetry as a function of the Y factor: (A) starting with a perfect regular simplex ($Y = 0$) using a normal centroid; (B) starting with a perfect regular simplex ($Y = 0$) using an extreme weighted centroid. The resulting simplexes are shown on top.

the reflected vertex) falls below the criterion, unless the symmetry of the current simplex is below the criterion and the symmetry is improved by applying this rule.

The effect of increasing the symmetry criterion on the behaviour of a simplex in a simulated optimization with a fixed number of measurements on response surface B4 [8] is shown in Fig. 10. The "optimal" symmetry criterion in this experiment seems to be in the range 0.3—0.5.

To find an optimal symmetry criterion, it is obvious that a simplex procedure can be used. Some test runs were made where a simplex controlled the maximal allowable Y factor and the symmetry criterion of a sub-simplex. The response surface for the sub-simplex was B4 [8]. The response for the

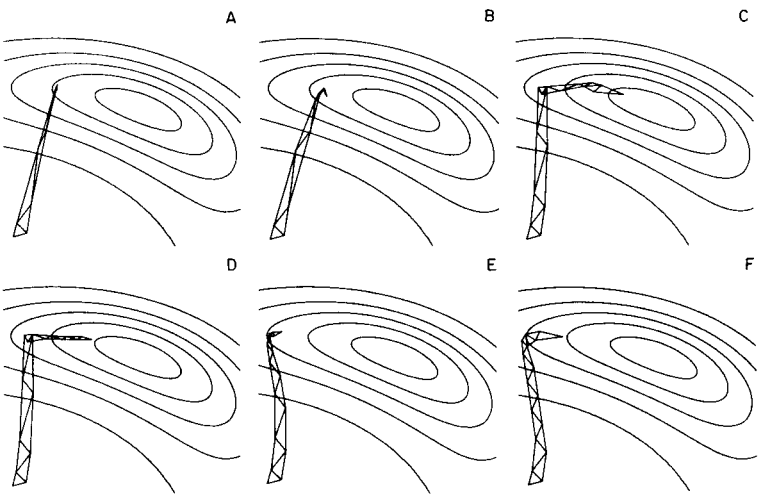

Fig. 10. Effect of increasing the symmetry criterion on the behaviour of a simplex: A, no symmetry criterion; B, C, D, E, F, symmetry criterion 0.2, 0.3, 0.4, 0.5 and 0.6, respectively.

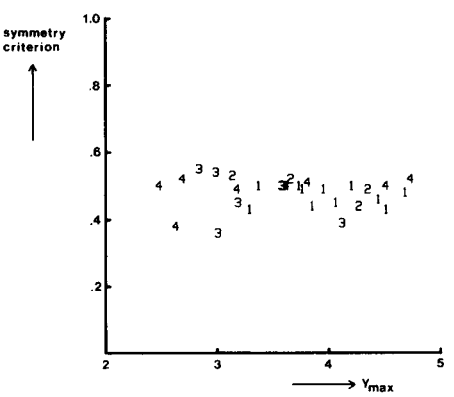

Fig. 11. Results of optimization of the symmetry criterion and the maximal allowable Y factor, with different start parameters and noise levels. Maximum response = 10, standard deviation of noise is 0, 0.1, 0.5 and 1.0, respectively (1, 2, 3, 4, n).

controlling simplex was defined as the mean response of 100 runs of the sub-simplex after 15 measurements. The runs were made with different noise levels on the response surface for the sub-simplex. The results are shown in Fig. 11. A somewhat surprising conclusion from these results is that there is an optimal symmetry criterion (about 0.5) which is independent of the noise level. There is no distinct optimum for the maximal allowable Y factor, because this parameter controls the simplex in exceptional cases only.

An optimization program in FORTRAN IV or BASIC (HP9845B) is commercially available from the authors.

REFERENCES

1 A. S. Olanski, L. R. Parker, Jr., S. L. Morgan and S. N. Deming, Anal. Chim. Acta, 95 (1977) 107.
2 M. W. Routh, P. A. Swartz and M. B. Denton, Anal. Chem., 49 (1977) 1422.
3 M. L. Rainey and W. C. Purdy, Anal. Chim. Acta, 93 (1977) 211.
4 R. C. Michel, J. Coleman and J. D. Winefordner, Spectrochim. Acta, Part B, 33 (1978) 195.
5 B. B. Jablonski, W. Wegscheider and D. E. Leyden, Anal. Chem., 51 (1979) 2359.
6 L. Ebdon, M. R. Cave and D. J. Mowthorpe, Anal. Chim. Acta, 115 (1980) 179.
7 S. N. Deming and L. R. Parker, C.R.C. Crit. Rev. Anal. Chem., (1978) 187.
8 P. F. A. van der Wiel, Anal. Chim. Acta, 122 (1980) 421.
9 W. Spendley, G. R. Hext and F. R. Himsworth, Technometrics, 4 (1962) 441.
10 J. A. Nelder and R. Mead, Comput. J., 7 (1965) 308.
11 D. B. Ryan, R. L. Barr and H. D. Todd, Anal. Chem., 52 (1980) 1460.

Analytica Chimica Acta, 153 (1983) 93—101
Elsevier Science Publishers B.V., Amsterdam — Printed in The Netherlands

UTILITY FUNCTIONS AS OPTIMIZATION CRITERIA FOR SEPARATIONS BY HIGH-PERFORMANCE LIQUID CHROMATOGRAPHY

J. W. WEYLAND*, C. H. P. BRUINS, H. J. G. DEBETS, B. L. BAJEMA and D. A. DOORNBOS

Optimization Research Group, Laboratory for Pharmaceutical and Analytical Chemistry, Anton Deusinglaan 2, 9713 AW Groningen (The Netherlands)

(Received 23rd March 1983)

SUMMARY

Several response functions have been proposed as optimization criteria for sequential optimization methods in chromatography. Studies of their behaviour indicate that several unresolved problems are associated with the use of these criteria for optimization purposes. All the proposed criteria suffer from the disadvantage that they do not give an unequivocal optimum. The present study illustrates this for some of the proposed criteria by actually mapping the response surface for several separations in a ternary mobile phase on a reversed-phase column.

Optimization of chromatographic separations has been attempted along various lines by several authors. Promising approaches are those by Laub et al. [1], who optimized the lowest separation factor in a chromatogram and Glajch et al. [2] who used resolution mapping. These methods have in common that they are simultaneous, based on an appropriate experimental design that is commonly laid out after some preliminary experiments. In general, they depend on the judgement of the experimenter for their interpretation and success. Other authors who used a similar approach are Belinky [3], Issaq [4] and Weyland et al. [5].

Sequential methods like the simplex algorithm have also been tried. In sequential methods, experiments already done are used to calculate new settings of the experimental parameters in the general direction of a better response, sequentially climbing the response surface until an optimum is reached. Sequential methods are well suited for automation, because little preliminary knowledge is needed [6]. The algorithm is simply started somewhere in the factor space, after which it locates the optimum on the response surface automatically, provided that the response surface is well behaved. Sequential methods require a response criterion, a quantity that summarizes in a single numerical value the quality that has to be optimized.

In chromatography, it is separation that should be optimized, preferably within a certain elution time. Thus the optimization criterion should measure

0003-2670/83/$03.00

the quality of the separation in the chromatogram. Separation can only be measured between pairs of peaks, e.g., as resolution. Generally, there are many peaks to be separated in a chromatogram, so that any attempt to optimize a separation is really a multicriteria optimization, i.e., an attempt to optimize several resolutions at the same time.

The best known approach to multicriteria analysis is to define a "utility function". If there are n criteria to be optimized (resolutions between pairs of peaks, time, etc.), $f_1(x), f_2(x), \ldots f_n(x)$, then for a particular set of experimental conditions x^* (a decision), these functions will take the definite values $f_1(x^*), f_2(x^*), \ldots f_n(x^*)$. The utility function $F(x)$ is defined [7] as

$$F(x) = \sum_{i=1}^{N} \lambda_i f_i(x) \tag{1}$$

in which λ_i is the weight given to criterion i. Comparing Eqn. (1) to the criteria (chromatographic response functions) published so far, the utility function can easily be recognized (Table 1). Most response functions used ignore the weighting factors, in effect giving equal importance to all criteria: every peak is as important as all the others in the chromatogram. Indeed, when weighting factors are given to the different criteria, an implicit choice is made favouring some decisions above others. It is questionable, however, whether weighting will accomplish what it is intended to do, because weighting one criterion twice as heavily can be offset by greater improvement of the less important criteria. This shows one distinct disadvantage of all utility functions: for any arbitrary decision x^*, there is an indefinite number of utility functions that have this solution as the optimum; vice versa, for any definite value of the function, there is an indefinite number of decisions that can yield this function value. Any decision can be justified in retrospect with a certain utility function. Some ten criteria of the form of

TABLE 1

Response functions used in this study[a,b]

Total overlap	$\phi = \sum_{i=1}^{k} \exp(-2R_i)$	[8]
CRF	$\mathrm{CRF} = \sum_{i=1}^{k} w_i \ln(p_i)$	[9]
COF	$\mathrm{COF} = \sum_{i=1}^{k} w_i \ln(R_i/R_d) + \beta(t_m - t_l)$	[2]

[a]An extensive list of chromatographic response functions is available [10]. [b]R_i, resolution of the ith pair of peaks. p_i, peak separation of the ith pair of peaks (see Fig. 6). w_i, weighting factor; in this study $w_i = 1.0$. R_d, desired resolution; in this study $R_d = 1.5$. β, weighting factor for the total time required; in this study $\beta = 0$. t_m, maximal allowed separation time. t_l, retention time of the last eluting peak.

Eqn. (1) have been described and tried for optimization of separations [8, 9, 11–13]. Debets et al. [10] conducted a comparative study from which they concluded that all proposed criteria suffered severe disadvantages. The response surfaces obtained when these criteria are used, are inherently complicated and it is impossible to link the value of the criteria to a notion of what to expect from the chromatogram. It is not clear whether the response surfaces yielded are suitable for sequential optimization, but it seems doubtful. Debets et al. [10] studied the behaviour of the criteria by simulating a hypothetical situation in which every imaginable difficulty (crossing of peaks, etc.) was taken into account. One can wonder, however, whether the objections raised against this hypothetical situation are of great importance in actual optimizations in practice. Of course, peak crossing caused by changing the experimental parameters has been observed. Nor is it uncommon for the worst separated pair to change in response to the experimental settings, giving rise to multiple optima. In order to gain some insight into the importance of these effects and their influence on the response surfaces obtained for practical separations, it was decided to construct response surfaces for several reversed-phase h.p.l.c. separations, using the composition of the mobile phase as the experimental variable. Taking mobile phase composition as the optimizing variable is justified by the fact that mobile phase composition is by far the most important means of influencing the separation in reversed-phase h.p.l.c., once the column has been chosen. The criteria used in this study were chosen from the list by Debets et al. [10] because they seemed the most promising, either because of ease of calculation, or because they promise to give a relatively smooth surface.

Methods

Because a complicated response surface can be expected, it is impossible to obtain an accurate description of the surface by direct measurement. The number of measurements needed would be prohibitive, so that a different approach is clearly needed. From a knowledge of the hold-up time of the column, the number of plates and the capacity factor of the compounds in the chromatogram, it is possible to construct the chromatogram, assuming a Gaussian peak shape. The simulated chromatogram can then be used to calculate the response criteria. A disadvantage of this method is that all information regarding peak shape is lost. The consequence for the calculated response is that it will be slightly overestimated with respect to the real measured chromatogram, because Gaussian peaks will have better separation than tailing peaks for the same separation factors. This is not considered to be a serious limitation, however, in view of the difficulties in measuring, for instance, resolutions from tailed peaks: these measurements will also be in error by an unknown amount. The problem is now reduced to finding a description of the capacity factors of all the compounds in the chromatogram over the available factor space.

The dependence of capacity factor on the content of organic modifier in a

ternary mobile phase presents a smooth continuous surface, so that it can readily be represented by a polynomial. Regression techniques are used to estimate the polynomial coefficients. A suitable model is:

$$\ln k = \beta_1\phi_1 + \beta_2\phi_2 + \beta_3\phi_3 + \beta_{12}\phi_1\phi_2 + \beta_{13}\phi_1\phi_3 + \beta_{23}\phi_2\phi_3 + \beta_{123}\phi_1\phi_2\phi_3 \qquad (2)$$

in which ϕ_1, ϕ_2 and ϕ_3 are the volume fractions of the components of the ternary mobile phase.

There are seven regression parameters to be estimated in Eqn. (2), so that a minimum of seven measurements is necessary to obtain the β values. Preferably some extra measurements should be made to gain an impression of the goodness of fit of the model. Once the models for all the compounds of the mixture have been found, it is possible to simulate chromatograms of the mixture over the complete feasible factor space. From the simulated chromatograms, the response criteria can then be calculated, using the functions from Table 1, whereafter the response surface can be plotted.

EXPERIMENTAL

Chemicals and chromatographic equipment

Mobile phases were made from deionized water and analytical-grade methanol and acetonitrile (Merck). Analytical-grade acetic acid (Merck) was also used. Sulfonamides, obtained from different manufacturers, were used as received.

The instrument used was a Spectra Physics model SP740 pump with pump control and pressure monitor (type 3500B) fitted with the following accessories: a Chromatronix model 220 dual-wavelength detector, a Rheodyne injection valve fitted with a 20-μl injection loop and a Houston Omniscribe recorder.

Data acquisition and integration were done with an Autolab system IVb chromatography data analyzer (Spectra Physics). The column used was 150 mm × 4.6 mm stainless steel, packed with Nucleosil 5-RP8.

Chromatographic procedures

Mobile phases were prepared by mixing 1% (v/v) solutions of acetic acid in the organic modifiers and water to give the desired composition. Mixtures were degassed in an ultrasonic bath under vacuum for 3 min. Stock solutions (1 mg ml^{-1}) of the individual sulfonamides were prepared in ethanol, from which samples were prepared by dilution with the eluent (1 ml/100 ml).

Dead time was measured as the first baseline distortion peak obtained with the mobile phase slightly enriched with water. Capacity factors given are the average of at least three determinations. The flow was maintained at 0.8 ml min^{-1} throughout.

Calculations were done on the CDC760/120 computer of the Groningen University Computing Centre.

Simulation of chromatograms and calculation of criteria values

For the simulations, a Gaussian peak shape was assumed for all peaks. For peak i:

$$Y(t) = f_i(t) = (C_i^0/(2\pi\sigma^2)^{1/2} \exp[-\tfrac{1}{2}(t - t_{r(i)})^2/\sigma_i^2] \quad (3)$$

where, for component i, C_i^0 is the peak height factor, σ_i is the peak variance, and $t_{r(i)}$ is the retention time. For the complete chromatogram, consisting of several peaks, the peaks are considered to be additive:

$$G(t) = \sum_{i=1}^{n} f_i(t) + g(t) \quad (4)$$

where n is the number of peaks, and $g(t)$ the background (noise, drift, etc.); $g(t)$ was taken as zero in all simulations.

The functions $f_i(t)$ were found by calculating the capacity factor from the model of Eqn. (2) and the data of Table 2. For a column with known dead volume and number of plates, $t_{r(i)}$ was calculated from $k_i = (t_{r(i)} - t_0)/t_0$ and σ_i from $N = t_{r(i)}^2/\sigma_i^2$. C_i^0 was taken as 1.0 for all peaks. Criteria values were calculated from the simulated chromatogram by a computer program in PASCAL (INTEGR) that located the peak maxima (apparent retention times) and the valleys between peaks by means of derivative monitoring. These data allowed the calculation of peak separations between pairs of peaks as in Fig. 6. Resolutions were calculated from

$$R_i = \tfrac{1}{2}[t_{r(i)} - t_{r(i-1)}]/[\sigma_i + \sigma_{(i-1)}]$$

The number of plates was $N = 2600$ for all the calculations. From the data thus obtained, INTEGR calculated the criterion value according to the utility functions of Table 1.

RESULTS AND DISCUSSION

In order to estimate the regression parameters of Eqn. (1), the capacity factors of all compounds used in this study were measured at ten different eluent compositions. The useful part of the factor space is restricted, because very high water contents give capacity factors that are too large to be of

TABLE 2

Regression parameters in Eqn. (2) calculated for the five sulfonamides (ϕ_1 water, ϕ_2 methanol, ϕ_3 acetonitrile)

	β_1	β_2	β_3	β_{12}	β_{13}	β_{23}	β_{123}
Sulfanilamide	−0.050769	−2.641673	1.283201	1.0721	−4.011466	−46.362615	72.851137
Sulfacetamide	0.726300	−2.106178	1.484036	0.1637	−5.630925	−31.774128	49.331779
Sulfadiazine	1.011663	−2.557096	1.975988	0.8435	−6.954371	−25.664066	38.519619
Sulfisomidine	1.012637	−2.572678	1.595561	−0.2621	−8.882957	−31.865905	51.676445
Sulfaguanidine	−0.287494	−4.927794	−8.114966	4.5488	6.740631	−24.564083	51.029447

practical value, while high organic modifier contents yield capacity factors that are so low as to interfere with solvent peaks. Figure 1 shows the region of the factor space where measurements were made, and where the models hold (shaded area). These measurements are more or less regularly spread, but were not made according to a strict experimental design. Adherence to an experimental design may be important with regard to ease of calculations; however, this was not considered to be important, because of the computer used. Care was taken that the experiments were laid out so that at least three levels for every factor were measured; this is necessary for quadratic models.

Table 2 gives the regression coefficients that were obtained for the five sulfonamides. Figure 2 gives a three-dimensional view of log k vs. composition for one of the sulfonamides. Once the behaviour of the k's over the factor space had been defined, the response map was constructed as follows. Starting with 0% methanol, chromatograms were simulated for all the mixtures at increments of 0.5% acetonitrile up to 40% acetonitrile. For every composition, the chromatograms were simulated and the criteria calculated, the response being stored in the corresponding array element. Next, the methanol content was incremented by 0.5% and this procedure was repeated with acetonitrile varying between 0 and 39%, and so on up to 40% methanol. This gave a triangular array with response values on a regular grid, which was used to plot the response surfaces of Figs. 3—5. Shown are the response surfaces obtained with Giddings' ϕ, the CRF and the COF (Glajch) [2]. The first of these should be minimized; the other two should be maximized.

It can be seen from these figures that the criteria do agree with regard to the local and global optimum compositions; the criteria that should be maximized give ridges at the same places where the total overlap gives a

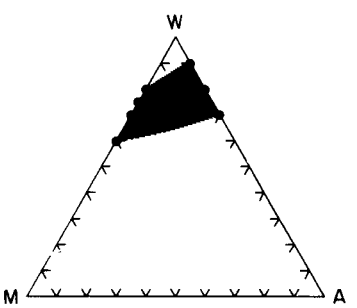

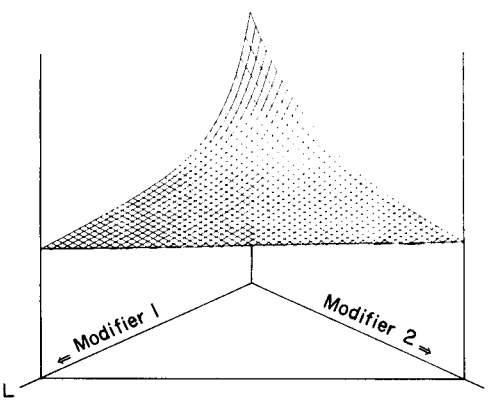

Fig. 1. Compositions where the capacity factors of the five sulfonamides were measured. The regions over which the models are valid are shaded.

Fig. 2. Three-dimensional plot of the capacity factor of one of the sulfonamides vs. composition. Modifier 1, methanol; modifier 2, acetonitrile.

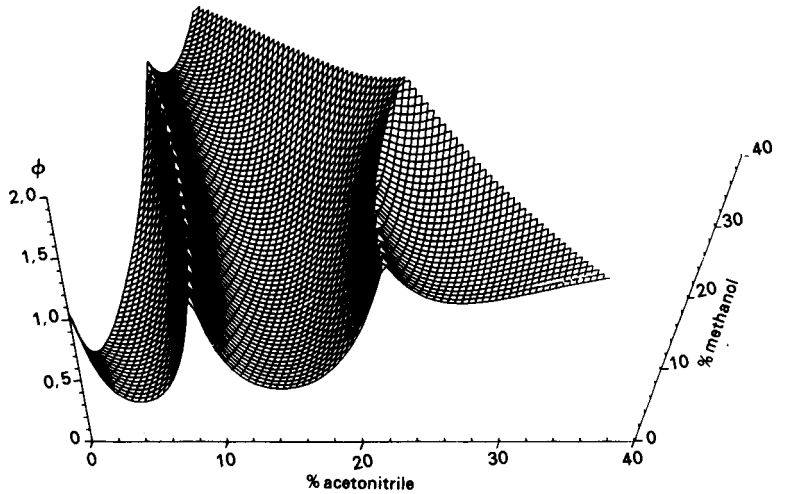

Fig. 3. Three-dimensional plot of Giddings' total overlap vs. composition.

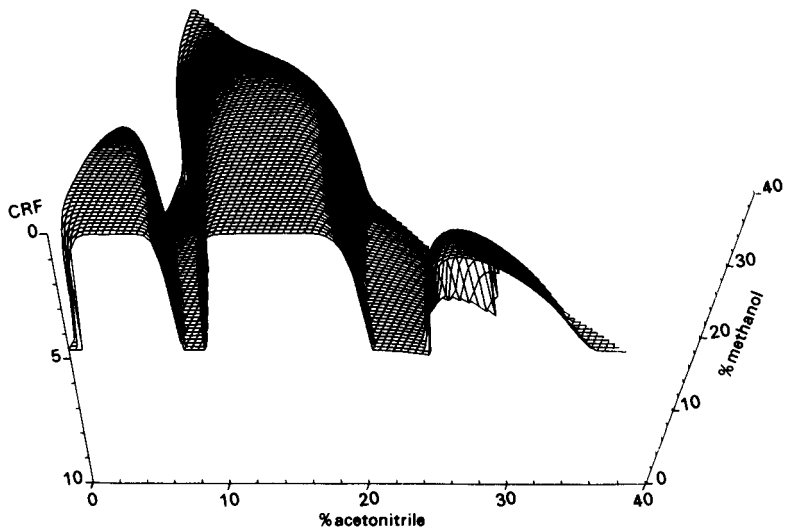

Fig. 4. Three-dimensional plot of the CRF vs. composition.

valley. Also the greatest problem associated with the use of these functions in reversed-phase h.p.l.c. becomes very clear: the response surfaces have many local optima. This reflects the actual situation for chromatographic separations (where different chromatograms may be evaluated as equally well separated); however, when sequential methods of optimization are used, there is no guarantee that the global optimum will be found. Which local optimum will be located depends solely on the starting position of the algorithm.

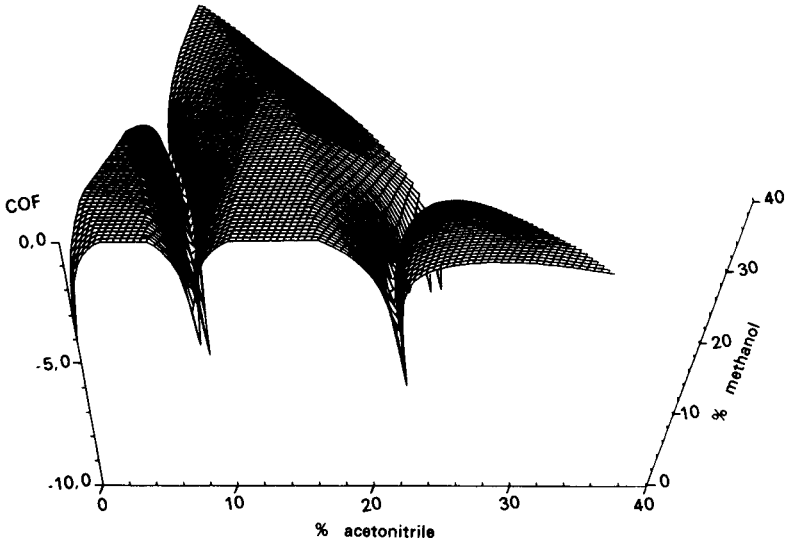

Fig. 5. Three-dimensional plot of the COF vs. composition.

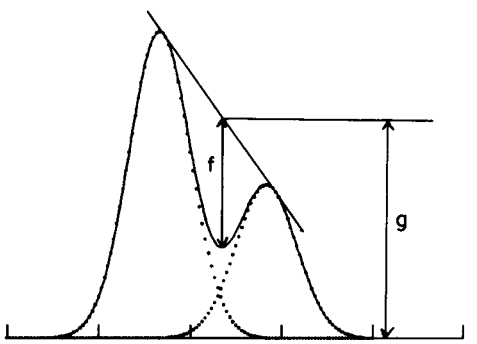

Fig. 6. Peak separation, defined as $p = f/g$.

Apart from the fact that the worst local optimum in terms of separation could be found, there are other important differences between the different optima. The optimum nearest 100% water, for instance, is expensive in terms of separation time. The optimum near 30% methanol is very fast, but might interfere with the solvent front, leaving only the central ridge as a practical proposition. It is questionable, however, if the simplex will end there, because the algorithm has no way of knowing the response surface, and neither has the experimentalist. Only the starting coordinates of the simplex define where the algorithm will end up.

The response surfaces shown here do not differ very much amongst each other. It seems that those based on resolution are slightly smoother than the CRF and the COF, which are based on peak separation. This can be ex-

plained by the fact that, in a simulation, it remains possible to calculate resolutions of peaks that overlap completely, while the peak separation cannot be calculated when the distance between the peak maxima is less than 2σ, for the simple reason that no valley can be detected when the distance is less.

This shows in the three-dimensional plots as a flat valley, which could present serious problems for a simplex algorithm. The algorithm might stop here, because it does not detect any change in response if the step size is small.

It should be noted that a knowledge of the identity and retention times of all components is presumed here; this allows precise calculation of the criteria, even for overlapping peaks. For reliable operation of the simplex algorithm, it is essential that these data are known, because misjudging the number of peaks will be catastrophic in calculating the criterion value [10], giving an erroneous response surface. In practice, this knowledge can be hard to obtain, which presents a serious problem for the successful application of sequential methods based on utility functions.

The results of this study confirm the conclusions of Debets et al. [10, 14] that there are severe disadvantages connected with the use of chromatographic response functions. These conclusions can be summarized as follows: the multiple local optima obtained when the elution order changes present serious difficulties when used in conjunction with a sequential optimization method. Further, in order to give the right response value, the functions need prior information that might be hard to obtain.

REFERENCES

1 R. J. Laub, J. H. Purnell and P. S. Williams, J. Chromatogr., 134 (1977) 249.
2 J. L. Glajch, J. J. Kirkland, K. M. Squire and J. M. Minor, J. Chromatogr., 199 (1980) 57.
3 B. R. Belinky, Occupational Health Chemistry, A.C.S. Symp. Ser. 120, American Chemical Society, Washington, DC, 1980, p. 149.
4 H. Issaq, J. Liq. Chromatogr., 4 (1981) 2091.
5 J. W. Weyland, H. Rolink and D. A. Doornbos, J. Chromatogr., 247 (1982) 221.
6 J. C. Berridge, J. Chromatogr., 244 (1982) 1.
7 D. L. Massart, A. Dijkstra and L. Kaufman, Evaluation and Optimization of Laboratory Methods and Analytical Procedures, Elsevier, Amsterdam, 1980.
8 J. C. Giddings, Anal. Chem., 32 (1960) 1707.
9 S. L. Morgan and S. N. Deming, J. Chromatogr., 112 (1975) 267.
10 H. J. G. Debets, B. J. Bajema and D. A. Doornbos, Anal. Chim. Acta, 151 (1983) 131.
11 M. Watson and P. W. Carr, Anal. Chem., 51 (1979) 1835.
12 S. L. Morgan and C. H. Jacques, J. Chromatogr., 16 (1978) 501.
13 R. Smits, C. Vanroelen and D. L. Massart, Anal. Chem., 273 (1975) 1.
14 H. J. G. Debets, J. W. Weyland and D. A. Doornbos, Anal. Chim. Acta, 150 (1983) 259.

Analytica Chimica Acta, 153 (1983) 103—109
Elsevier Science Publishers B.V., Amsterdam — Printed in The Netherlands

NON-LINEAR TRANSFORMATION OF FACTORS IN THE DESIGN OF EXPERIMENTS

P. KOŚCIELNIAK and A. PARCZEWSKI*
Department of Analytical Chemistry, Jagiellonian University, 30-060 Krakow (Poland)
(Received 25th February 1983)

SUMMARY

The application of nonlinear transformations of factors in empirical modelling based on experimental design is proposed. The utility of the polynomial model: $\hat{R} = \Sigma_i B_i \tilde{x}_i + \Sigma_{i,j} B_{ij} \tilde{x}_i \tilde{x}_j + \ldots$ in empirical modelling may be considerably increased when nonlinear relationships between the coded, $\tilde{x}$, and actual, x, factors are applied, in addition to the linear (conventional) ones. The logarithmic transformation, $\tilde{x}_i = \log_{q_i} (a_i + b_i x_i)$, is presented as an example and its application in modelling of interference effects in atomic absorption spectrometry is suggested.

The design of experiments and empirical modelling [1, 2] are widely used in analytical chemistry (see, e.g. [2—14]). The polynomial model normally used approximates the dependence between the response R (a measured signal or its function) and the controlled factors $x_1, \ldots, x_n$ (experimental conditions such as temperature, pressure, concentrations of reagents and/or sample components):

$$\hat{R} = \sum_{i=0}^{n} b_i x_i + \sum_{\substack{i,j=1 \\ (i \leqslant j)}}^{n} b_{ij} x_i x_j + \ldots \quad (x_0 \stackrel{df}{=} 1) \tag{1}$$

where n is the number of factors considered.

The regression coefficients b in model (1) are determined by fitting this model to the results of measurements at the experimental points, the points being arranged according to a selected plan, e.g., a k^n factorial (k is the number of levels of values assumed by each factor in the plan) or a composite rotatable design. In Fig. 1 some selected plans for $n = 2$ are presented in natural, x, and coded, $\tilde{x}$, variables. Each point in a plan represents experimental conditions. Coded variables, $\tilde{x}$, are related to the natural variables, x:

$$\tilde{x}_i = (x_i - x_i^{(0)})/\Delta x_i \tag{2}$$

where $x_i^{(0)} = (x_i^{(l)} + x_i^{(u)})/2$ and $\Delta x_i = (x_i^{(u)} - x_i^{(l)})/2$; $x_i^{(l)}$ and $x_i^{(u)}$ are explained in Fig. 1. Model (1) can be expressed by coded variables:

0003-2670/83/$03.00

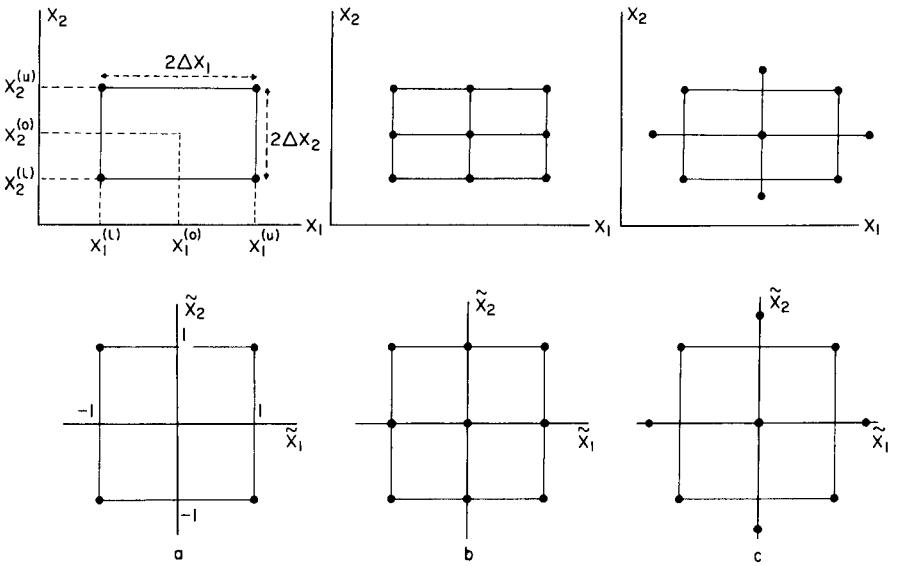

Fig. 1. Some of the experimental plans used in the conventional design of experiments: (a) 2^2 factorial, (b) 3^2 factorial, (c) composite rotatable design in natural, x, and coded, $\tilde{x}$, coordinate systems.

$$\hat{R} = \sum_{i=0}^{n} B_i \tilde{x}_i + \sum_{\substack{i,j=1 \\ (i \leqslant j)}}^{n} B_{ij} \tilde{x}_i \tilde{x}_j + \ldots \; (x_0 \stackrel{df}{=} 1) \tag{3}$$

Because of the high symmetry of the plans in the $\tilde{x}$ coordinates, the determination of the coefficients B in model (3) and the analysis of variance are straightforward [1, 2].

From the practical point of view, polynomial models of the first or second order are most attractive on account of their simplicity. In the formulation of these models, simple plans are applied, e.g., 2^n or 3^n factorials or a central rotatable design. However, a polynomial of the first or second degree can adequately approximate the true function $R = f(x_1, \ldots, x_n)$ only in relatively narrow intervals of factors x; it usually fails when broad intervals of the factors are considered. An example for $n = 1$ is presented in Fig. 2 [15]. The solid line exemplifies the typical interference of phosphoric acid on the atomic absorption spectrometry of calcium. Curve 2 in Fig. 2(a) is the second-order model: $\hat{R} = B_0 + B_1\tilde{c}_1 + B_{11}\tilde{c}_1^2$ fitted to the experimental results, R, read from the solid line at the points of a 3^1 factorial: $c_1^{(l)} = 0$ ($\tilde{c}_1 = -1$), $c_1^{(u)} = 5$ ($\tilde{c}_1 = 1$), and $c_1^{(0)} = 2.5$ ($\tilde{c}_1 = 0$), where the coded concentration, $\tilde{c}_1$, of the interferent (phosphoric acid) is related to the actual concentration, c_1(% v/v), according to Eqn. (2), by $\tilde{c}_1 = (c_1 - 2.5)/2.5$. This formula transforms the above second-order model into a parabola in a natural coordinate, c_1. The model fails, as seen in Fig. 2(a), because the experimental line in Fig. 2 does not have a parabolic shape in the concentration interval

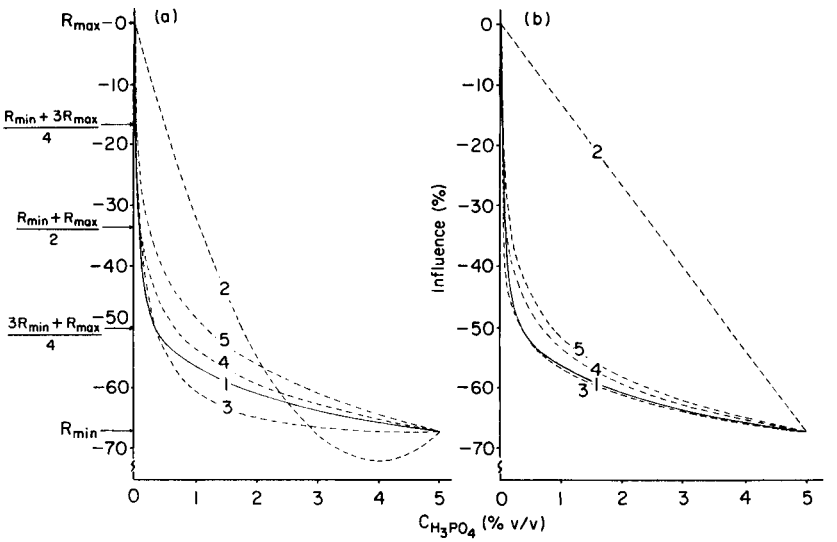

Fig. 2. Effect of phosphoric acid on the determination of calcium by a.a.s. (experimental line 1): (a) second-order models; (b) first-order models (dashed lines 2—5). For detailed information, see text.

(0, 5), although it could be considered as a "deformed" parabola. However, the locus of the central point $c_i^{(0)} = 2.5$ in the 3^1 factorial is unsuitable in this case because it is far from the concentration range (0, 0.5) over which the experimental curve changes most rapidly.

The method described below enables the simple experimental plans and polynomials of low degree to be successfully applied in modelling the surfaces $R = f(x_1, \ldots, x_n)$ which significantly differ from a plane or paraboloid.

METHOD

The following generalized transformation of factors is proposed:

$$\tilde{x}_i = f_i(x_1, \ldots, x_n); i = 1, \ldots, n \tag{4}$$

In particular:

$$\tilde{x}_i = f_i(x_i); i = 1, \ldots, n \tag{5}$$

In conventional design of experiments functions f_i are the linear transformations given by Eqn. (2). When they fail, other functions f_i can be sought. The idea is that an assumed polynomial model (Eqn. 3) after conversion to natural variables, x, should resemble, as closely as possible, the examined response $R = f(x_1, \ldots, x_n)$. Thus if the transformations f_i are selected properly, the response R in coded variables, $\tilde{x}$, can be successfully approximated by the polynomial Eqn. (3).

Equations (4) or (5) transform the symmetrical experimental plans in

coded coordinates, $\tilde{x}$ (Fig. 1) to the asymmetrical plans in natural coordinates, x (see Fig. 3 below).

Logarithmic transformation of factors

As an example of the use of Eqn. (5), the following transformation of factors is presented. It proved to be very effective in an examination of matrix effects in atomic absorption spectrometry [16]:

$$\tilde{x}_i = \log_{q_i}(a_i + b_i x_i) = M_i \log_{10}(a_i + b_i x_i) \tag{6}$$

where $M_i = 1/\log_{10} q_i$, x_i denotes, for example, the concentration of a sample component i. The appropriate parameters a_i, b_i and q_i in transformations (6) follow from the following requirements: $\tilde{x}_i = 1$ for $x_i = x_i^{(u)}$, $\tilde{x}_i = -1$ for $x_i = x_1^{(l)}$ and $\tilde{x}_i = 0$ for $x_i = x_i^*$, where $x_i^{(l)} < x_i^* < x_i^{(u)}$. Hence

$$q_i = (x_i^{(u)} - x_i^*)/(x_i^* - x_i^{(l)}) \tag{7}$$

$$\tilde{x}_i = \log_{q_i}[(q_i^2 - 1)(x_i - x_i^{(l)}) + (x_i^{(u)} - x_i^{(l)})]/q_i(x_i^{(u)} - x_i^{(l)}) \tag{8}$$

Equation (8) transforms the symmetrical experimental designs in Fig. 1(b) to the asymmetrical designs of Fig. 3.

It follows from Eqn. (7) that q_i is the ratio of the lengths of two segments on the axis x_i resulting from division of the interval $(x_i^{(l)}, x_i^{(u)})$ by the point x_i^*. However, the coordinate x_i^* cannot be placed at the centre of this interval $(x_i^{(0)})$ because q_i must not be equal to unity. For $x_i^* = x_i^{(0)}$, Eqn. (8) is replaced by the linear transformation Eqn. (2).

The adequacy of model (3) expressed by variables (8) depends strongly on the base q_i, and then on coordinates x_i^*. Because q_i and x_i^* are interrelated according to Eqn. (7), only one of these parameters can be sought at a time.

Selection of coordinates x_i^*

The selection of the coordinates x_i^* is preferred (to q_i) when the second-order model, $\hat{R} = \Sigma_{i=0}^{n} B_i \tilde{x}_i + \Sigma_{i,j=1\,(i<j)}^{n} B_{ij} \tilde{x}_i \tilde{x}_j$, is applied based on a 3^n factorial (or a rotatable design). In this case, the coordinates x_i^* define the

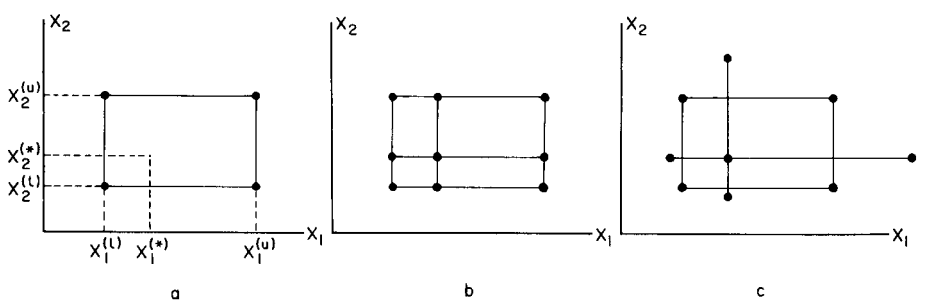

Fig. 3. Asymmetrical experimental plans in the coordinate system of natural variables, x; Eqn. (8) transforms these plans to symmetrical plans in coded coordinates $\tilde{x}$ presented in Fig. 1.

arrangement of the internal experimental points in the 3^n factorial, as seen in Fig. 3. Hence, the regression coefficients B in the model $\hat{R}$ are influenced by the choice of coordinates x_i^*. The values of x_i^* determine the parameters q_i in Eqn. (8) as stated above.

The success in selection of the proper coordinates x_i^* depends on the amount of preliminary information available on the shape of the surface examined $R = f(x_1, \ldots, x_n)$. When a monotonic function (Fig. 2) is to be approximated, then the result R obtained with the properly selected coordinates x_i^* satisfies the following inequality:

$$(3R_{\min} + R_{\max})/4 \leqslant R \leqslant (R_{\min} + 3R_{\max})/4 \tag{9}$$

where $R_{\min}$ and $R_{\max}$ denote the minimum and maximum values of R in the interval $(x_i^{(l)}, x_i^{(u)})$ in a section R vs. x_i. If inequality (9) is not fulfilled, then an extreme appears in the second-order model R (in a section $\hat{R}$ vs. x_i). This condition also holds in the case of conventional modelling, when the linear transformation, Eqn. (2), is applied; i.e., if the response R for $x_i = x_i^{(0)}$ does not satisfy inequality (9), then the conventional approach will fail too. In this case, the nonlinear transformation, Eqn. (8) should be applied.

If the shape of the curve (section) R vs. x_i is known, at least approximately, then x_i^* can be read from this curve for R satisfying the above inequality. In particular, x_i^* may correspond to $R = (R_{\min} + R_{\max})/2$. In this case, the coefficient B_{ii} in model $\hat{R}$ disappears.

Selection of parameters q_i

The selection of parameters q_i is preferred when a first-order model $\hat{R} = \Sigma_{i=0}^{n} B_i \tilde{x}_i + \Sigma_{i,j=1\,(i<j)}^{n} B_{ij} \tilde{x}_i \tilde{x}_j$ is applied, based on a 2^n factorial. In this case, the regression coefficients B in the model do not depend on the q_i parameters; the experimental points in the 2^n factorial are combinations of the lower, $x^{(l)}$, and upper, $x^{(u)}$, levels of the factors only. After coefficients B have been determined, the "best" parameters q_i are obtained by fitting the model $\hat{R}$ to the results of measurements made at the additional experimental points (one point for each q_i suffices). The points do not belong to the 2^n arrangement. In general, these results are substituted into the model $\hat{R}$ and the resulting set of equations is solved in order to obtain parameters q_i.

However, parameters q_i can simply be determined independently of each other if the coordinates x_i of an additional point, selected with the aim of determining q_j, satisfy the following conditions: (a) $x_i = x_i^{(l)}$ or $x_i^{(u)}$ ($\tilde{x}_i = -1$ or 1), for $i = 1, \ldots, n$; $i \neq j$; (b) $x_j^{(l)} < x_j < x_j^{(u)}$ (all variables except x_j assume their lower or upper levels). When a monotonic function (Fig. 2) is examined, then the result R obtained at the properly selected coordinate x_j satisfies the inequality (9) (note, however, that in this case x_j is not the coordinate x_j^* which is calculated from Eqn. (7) after q_j has been determined). For a point selected according to the above rules (a) and (b), model $\hat{R}$ is expressed by the coordinate $\tilde{x}_j$ only (other coordinates $\tilde{x}$ are equal to -1 or 1). Hence, the fitting procedure (searching for q_j) is very simple.

If the procedures outlined above lead to the conclusion that $x_i^* \approx x_i^{(0)}$, or $q_i \approx 1$, then the linear transformation, Eqn. (2), should be applied instead of the logarithmic Eqn. (8).

EXAMPLES

The examples presented in Fig. 2 are based on the methodology described above.

In Fig. 2(a), four quadratic models are presented: $\hat{R} = B_0 + B_1\tilde{c}_1 + B_{11}\tilde{c}_1^2$. Coefficients B_0, B_1 and B_{11} were obtained by fitting these models to the values of R corresponding to $c_1^{(l)} = 0$, $c_1^{(u)} = 5$ and $c_1 = c_1^*$ (3^1 factorial). Curve (2) has already been commented on; in this case, $\tilde{c}_1$ is related to c_1 according to the linear transformation Eqn. (2) ($c_1^* = c_1^{(0)} = 2.5$). This model failed. Curves (3), (4), and (5) present the models $\hat{R}$ in which $\tilde{c}_1$ are related to c_1 according to the logarithmic Eqn. (8), where coordinates c_1^* (parameters q_i) were obtained for: $R = (3R_{\min} + R_{\max})/4 = 4.95$, $R = (R_{\min} + 3R_{\max})/4 = 11.65$, and $R = (R_{\min} + R_{\max})/2 = 8.3$, respectively (see inequality 9).

In Fig. 2(b), four first-order models: $\hat{R} = B_0 + B_1\tilde{c}_1$ are presented. Coefficients $B_0 = 8.3$ and $B_1 = -6.7$ (which are the same in all models $\hat{R}$) were obtained by fitting these models to the values of R corresponding to $c_1^{(l)} = 0$ and $c_1^{(u)} = 5$ (2^1 factorial). Curve (2) presents the model $\hat{R}$ in which $\tilde{c}_1$ is related to c_1 according to the linear Eqn. (2). The model is useless. In models (3), (4), and (5), $\tilde{c}_1$ is related to c_1 according to Eqn. (8). The parameters q_1 in these models were obtained by fitting of the above model $\hat{R}$ to the following additional experimental points: $c_1 = 0.375$ ($R = 4.95$), $c_1 = 0.025$ ($R = 11.65$), and $c_1 = 0.1$ ($R = 8.3$), respectively.

CONCLUSIONS

As can be seen from Fig. 2, the proposed method of empirical modelling is much more effective than the conventional approach. The models obtained by this procedure approximate the experimental curve tolerably well in cases when the conventional models failed. Even the first-order models obtained by the proposed methodology (curves (3—5) in Fig. 2b) are much better than the conventional second-order model (curve (2) in Fig. 2a). It can be deduced from Fig. 1 that there exists a coordinate c_1^* (or a parameter q_1) for which an excellent fit of a model to the experimental curve can be achieved.

When various methods of empirical modelling are compared for their effectiveness then, apart from the adequacy of the model, the number of experiments that will be necessary in order to formulate a model should be considered. In formulation of a first-order model, $(2^n + n)$ experiments are needed (n additional measurements are necessary to determine parameters q_i in Eqn. 8). In the second-order modelling, a 3^n factorial or the composite rotatable designs are usually applied. In this case, it is necessary to run 3^n or $(2^n + 2n + n_0)$ experiments where n_0 is the number of experiments corres-

ponding to the centre of the plan. The above numbers satisfy the inequality: $(2^n \dot{+} n) < (2^n + 2n + n_0) < 3^n$ (for $n > 2$).

In the proposed modelling, some preliminary information on the shape of the examined response $R = f(x_1, \ldots, x_n)$ is necessary. Such information is usually easily attainable from published data or can be deduced from the preliminary experiments which are normally done at the first stage of examination. The more prior information that is available, the more precise the rules of selection of the coordinates x_i^* (parameters q_i) that can be formulated and thus the more adequate the $\hat{R}$ models that can be obtained.

An example for $n = 2$ is described in the following paper [16].

REFERENCES

1 W. G. Cochran and G. M. Cox, Experimental Designs, Wiley, New York, 1950.
2 D. L. Massart, A. Dijkstra and L. Kaufman, Evaluation and Optimization of Laboratory Methods and Analytical Procedures, Elsevier, Amsterdam, 1978.
3 M. L. Parsons and J. D. Winefordner, Appl. Spectrosc., 21 (1967) 368.
4 V. T. Si'akova, Zh. Anal. Khim., 29 (1974) 9.
5 A. Parczewski and A. Rokosz, Chem. Anal., (Warsaw), 20 (1975) 267.
6 V. Z. Krasilsčik and G. A. Steinberg, Zh. Anal. Khim., 31 (1976) 5.
7 V. V. Nalimov and T. I. Golikova, Zavod. Lab., 43 (1977) 1247.
8 M. N. Gusinsky, N. N. Zavadska and L. N. Filimonov, Zh. Anal. Khim., 33 (1978) 421.
9 C. Różycki, Chem. Anal., (Warsaw), 24 (1979) 129.
10 P. Kościelniak, S. Walas and A. Parczewski, Fresenius Z. Anal. Chem., 302 (1980) 402.
11 R. J. Matthews, Anal. Chim. Acta, 133 (1981) 169.
12 J. Kragten and A. Parczewski, Talanta, 28 (1981) 901.
13 A. Parczewski, Anal. Chim. Acta, 130 (1981) 221.
14 A. Rokosz and P. Strycharski, Fresenius Z. Anal. Chem., 313 (1982) 316.
15 M. Pinta, Spectrometrie D'Absorption Atomique. Masson, Paris, 1971.
16 P. Kościelniak and A. Parczewski, Anal. Chim. Acta, 153 (1983) 111.

Analytica Chimica Acta, 153 (1983) 111—119
Elsevier Science Publishers B.V., Amsterdam — Printed in The Netherlands

EMPIRICAL MODELLING OF THE MATRIX EFFECT IN ATOMIC ABSORPTION SPECTROMETRY
Determination of Calcium in Presence of Aluminium

P. KOSĆIELNIAK AND A. PARCZEWSKI*
Department of Analytical Chemistry, Jagiellonian University, 30-060 Krakow (Poland)
(Received 25th February 1983)

SUMMARY

A generalized method of empirical modelling based on experimental design is adapted and applied in an examination of the interfering effect of aluminium on the determination of calcium by atomic absorption spectrometry. Both 2^2 and 3^2 factorials, as well as first-order and second-order models are considered with linearly and logarithmically transformed concentrations of calcium and aluminium. The logarithmic transformations are shown to be more effective in modelling the interfering effect, i.e., fewer experiments are necessary to obtain an adequate mathematical description of the effect than are needed after linear transformations.

In the previous paper [1] a generalized approach to empirical modelling based on experimental design was proposed. For application of this model in examinations of matrix (interference) effects, the proposed methodology can be adapted as follows. The relationship between the measured signal (or its function), R, and the concentrations of n sample components is approximated by the polynomial model $\hat{R}$ [1]

$$\hat{R} = \sum_{i=0}^{n} B_i \tilde{c}_i + \sum_{\substack{i,j=1 \\ (i \leqslant j)}}^{n} B_{ij} \tilde{c}_i \tilde{c}_j + \ldots \quad (c_0 \stackrel{df}{=} 1) \tag{1}$$

where $\tilde{c}_i$ denotes the coded concentrations which are related to the actual concentrations, c_i, by appropriate transformations:

$$\tilde{c}_i = f_i(c_i) \quad (i = 1, \ldots, n) \tag{2}$$

Model (1) can be expressed by actual concentrations, c, by inserting Eqn. (2) into Eqn. (1). The regression coefficients B in model (1) are calculated on the basis of the results of measurements made on standard solutions which have compositions corresponding to a selected plan, e.g., 2^n or 3^n factorials [2]. In Fig. 1, 2^2 and 3^2 factorials, which are applied in the present paper, are presented in coded (Fig. 1b) and actual (Fig. 1a and Fig. 1c) coordinates. Each point in the plan represents the composition of a standard solution. These plans permit formulation of the first-order and second-order models

0003-2670/83/$03.00

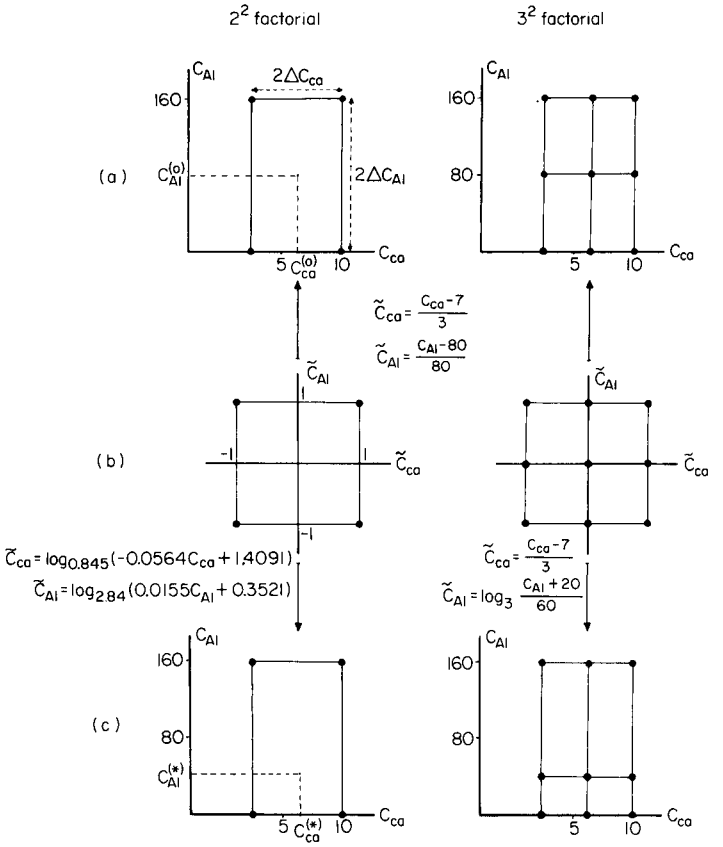

Fig. 1. 2^2 and 3^2 factorials applied in examination of the effect of aluminium on the determination of calcium. In all cases, $c_{Ca}^{(l)} = 4$ μg ml^{-1}, $c_{Ca}^{(u)} = 10$ μg ml^{-1}, $c_{Al}^{(l)} = 0$ μg ml^{-1} and $c_{Al}^{(u)} = 160$ μg ml^{-1}.

(Eqn. 1). The transformations (Eqn. 2) applied are also indicated in Fig. 1. The linear (conventional) transformation can be formulated as follows:

$$\tilde{c}_i = (c_i - c_i^{(0)})/\Delta c_i \tag{3}$$

where $c_i^{(0)}$ and Δc_i are explained in Fig. 1(a). The first-order or second-order models usually fail when broad intervals of concentrations are considered [1]. More effective is the following logarithmic transformation [1]:

$$\tilde{c}_i = \log_{q_i}[(q_i^2 - 1)(c_i - c_i^{(l)}) + (c_i^{(u)} - c_i^{(l)})]/q_i(c_i^{(u)} - c_i^{(l)}) \tag{4}$$

$$q_i = (c_i^{(u)} - c_i^*)/(c_i^* - c_i^{(l)}) \tag{5}$$

where $c_i^{(l)}$ and $c_i^{(u)}$ denote the lower and upper concentration level of an ith sample component, respectively, and c_i^* is explained in Fig. 1(c). The adequacy of model (1) expressed by the coded concentrations (Eqn. 4) depends on parameters q_i, and then on the coordinates c_i^* (see Eqn. 5). These parameters can be selected as described before [1].

Because of high symmetry of the plans in coded coordinates $\tilde{c}$ (Fig. 1b) and the way in which the concentration levels are coded, the coefficients B in model (1) and their errors are calculated from the same simple formulae, regardless of the applied transformation (Eqn. 2). An example of modelling of the interfering effect of aluminium in the determination of calcium by atomic absorption spectrometry (a.a.s.) is presented below.

EXPERIMENTAL

Standard stock solutions of Ca (0.5 mg Ca ml^{-1}) and Al (1.25 mg Al ml^{-1}) were prepared from analytical-grade calcium chloride and aluminium chloride. Working solutions were obtained by mixing and suitable dilutions of the stock solutions.

The atomic absorption spectrometer (AAS-1; C. Zeiss-Jena) was used under standard conditions with an air-acetylene flame. Duplicate readings of the absorbance of calcium at 422.67 nm were taken for each solution.

The compositions of the standard solutions used in examination of the interfering effect are outlined in Fig. 2.

The a.a.s. measurements R (relative absorbances) are shown in Fig. 3 by points. Each measurement is the ratio of two absorbances: one obtained for a standard sample (Fig. 2) and the second on a solution of constant composition: $c_{Ca} = 10\ \mu g\ ml^{-1}$ and $c_{Al} = 160\ \mu g\ ml^{-1}$.

RESULTS

The first- and second-order models (Eqn. 1) were applied in this study. In formulation of a model $\hat{R}$, results selected from those presented in Fig. 3 were used; the remaining m results served in testing the model for its adequacy. To this end, the mean absolute error e was calculated for each model from

$$e = \frac{1}{m} \sum_i |R_i - \hat{R}_i| \tag{6}$$

where R_i is the result measured on solution i (which was not taken into account in formulation of the model) and $\hat{R}_i$ is the corresponding result predicted by the model.

First-order modelling based on the 2^2 factorial

In this case, the following model was formulated:

$$\hat{R} = B_0 + B_1\tilde{c}_{Ca} + B_2\tilde{c}_{Al} + B_3\tilde{c}_{Ca}\tilde{c}_{Al} = 52.61 + 23.76\tilde{c}_{Ca} - 15.88\tilde{c}_{Al} - 6.2\tilde{c}_{Ca}\tilde{c}_{Al} \tag{7}$$

(For simplicity, the coefficients B_{ij} in Eqn. (1) are denoted by single indices in Eqns. (7) and (13)).The regression coefficients B in Eqn. (7) were calculated on the basis of the data presented in Table 1 in which the 2^2 factorial

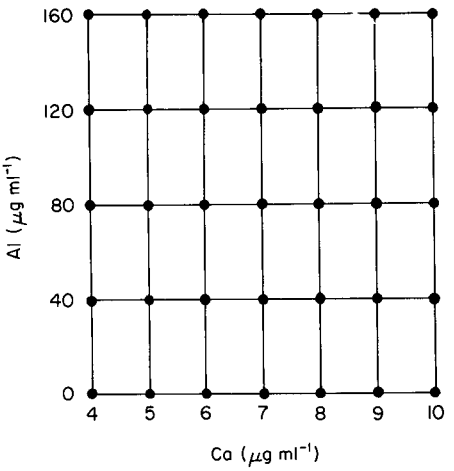

Fig. 2. Compositions of the standard solutions used. Each point corresponds to the composition of a solution.

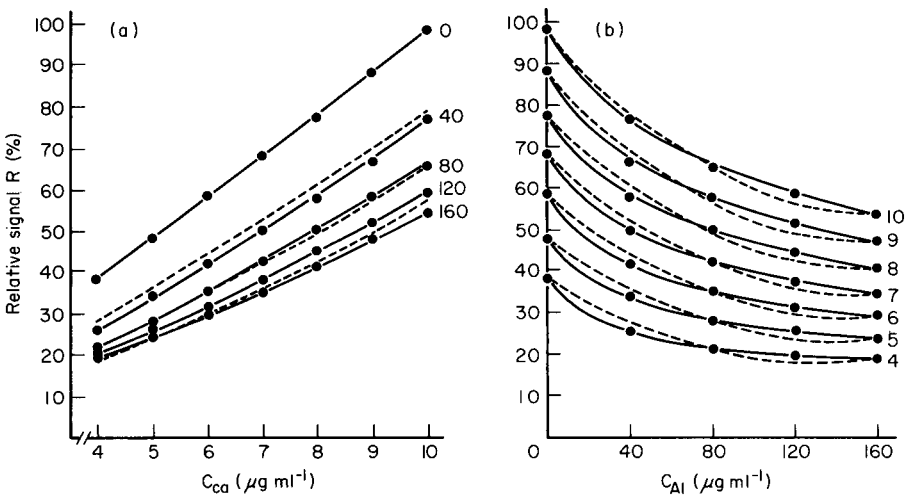

Fig. 3. The dependence of R on (a) c_{Ca} and (b) c_{Al}. (•) Experimental points; (---) calculated from Eqn. (14); (—) calculated from Eqn. (16). The numbers on the curves correspond to: (a) μg Al ml^{-1}; (b) μg Ca ml^{-1}. The dashed and solid lines R vs. c_{Ca} coincide for $c_{Al} = 0$ and 160 μg ml^{-1}.

(design matrix) is presented (see also Fig. 1). The coefficient B_i is the scalar product of the column vector of the experimental results R and the respective (ith) column vector of the design matrix divided by the squared absolute value of the latter vector. The variance $s^2_{B_i}$ of coefficient B_i can be calculated as the ratio of the variance of the response measurements s^2_R and the squared absolute value of the ith column vector of the design matrix. In case of the 2^2 factorial presented in Table 1, the error of all coefficients B is the same: $s^2_{B_i} = s^2_R/4$. The coefficients B in model (7) do not depend on the transform-

TABLE 1

2^2 factorial

No. of standard solution	Design matrix				c_{Ca} (μg ml^{-1})	c_{Al} (μg ml^{-1})	R
	$\tilde{c}_0$	$\tilde{c}_{Ca}$	$\tilde{c}_{Al}$	$\tilde{c}_{Ca}\tilde{c}_{Al}$			
1	1	1	1	1	10	160	54.29
2	1	1	−1	−1	10	0	98.44
3	1	−1	1	−1	4	160	19.18
4	1	−1	−1	1	4	0	38.53

ations by Eqn. (2) [1]. However, the adequacy of the model depends on the applied transformations $\tilde{c} = f(c)$. Two cases are considered below.

Conventional approach. The following transformations of concentrations were applied:

$$\tilde{c}_{Ca} = (c_{Ca} - 7)/3; \quad \tilde{c}_{Al} = (c_{Al} - 80)/80 \tag{8}$$

(compare Eqn. 3 and Fig. 1). Substitution of these into model (7) gives

$$\hat{R} = -1.41 + 9.985c_{Ca} - 0.0176c_{Al} - 0.0258c_{Ca}c_{Al} \tag{9}$$

The corresponding error e (Eqn. 6) is 6.0.

Unconventional approach. The following nonlinear transformations of concentrations were applied:

$$\tilde{c}_{Ca} = \log_{q_{Ca}}[(q_{Ca}^2 - 1)(c_{Ca} - 4) + 6]/6q_{Ca};$$
$$\tilde{c}_{Al} = \log_{q_{Al}}[(q_{Al}^2 - 1)c_{Al} + 160]/160q_{Al} \tag{10}$$

In order to determine the parameters q_{Ca} and q_{Al} in Eqn. (10), two additional standard solutions were selected, according to the rules presented earlier [1]. One of these, with the composition $c_{Ca} = 6$ and $c_{Al} = c_{Al}^{(u)} = 160$ ($\tilde{c}_{Al} = 1$; $R = 29.62$) served in the determination of q_{Ca}; after substitution of these data into Eqn. (10), model (7) gave

$$29.62 = 52.61 - 15.88 + (23.78 - 6.2)\log_{q_{Ca}}(q_{Ca}^2 + 2)/3q_{Ca} \tag{11}$$

which was solved numerically, to give $q_{Ca} = 0.845$. In an analogous way, $q_{Al} = 2.84$ was found on the basis of the data corresponding to the second additional solution, which had the composition $c_{Ca} = c_{Ca}^{(u)} = 10$ ($\tilde{c}_{Ca} = 1$) and $c_{Al} = 40$ ($R = 76.92$). Hence:

$$\hat{R} = 52.61 + 23.76\log_{0.845}[(0.845^2 - 1)(c_{Ca} - 4) + 6]/6 \times 0.845$$
$$- 15.88\log_{2.84}[(2.84^2 - 1)c_{Al} + 160]/160 \times 2.84$$
$$- 6.2\log_{0.845}[(0.845^2 - 1)(c_{Ca} - 4) + 6]/6 \times 0.845$$
$$\log_{2.84}[(2.84^2 - 1)c_{Al} + 160]/160 \times 2.84$$
$$= 52.61 + 23.78\log_{0.845}(-0.0564c_{Ca} + 1.4091) -$$

$$-15.88 \log_{2.84}(0.0155c_{Al} + 0.3521) - 6.2 \log_{0.845}(-0.0564c_{Ca} + 1.4091) \log_{2.84}(0.0155c_{Al} + 0.3521) \quad (12)$$

The corresponding error e is 1.2.

Second-order modelling based on the 3^2 factorial

In this case, the following model was formulated:

$$\hat{R} = B_0 + B_1\tilde{c}_{Ca} + B_2\tilde{c}_{Al} + B_3\tilde{c}_{Ca}\tilde{c}_{Al} + B_4\tilde{c}'_{Ca} + B_5\tilde{c}'_{Al} + B_6\tilde{c}'_{Ca}\tilde{c}_{Al} + B_7\tilde{c}_{Ca}\tilde{c}'_{Al} + B_8\tilde{c}'_{Ca}\tilde{c}'_{Al} \quad (13)$$

where $\tilde{c}' = \tilde{c}^2 - 2/3$. The regression coefficients B in model (13) were determined on the basis of the data presented in Table 2. In this table, the 3^2 factorial (design matrix) is presented in coded concentrations, $\tilde{c}$ (the use of variables $\tilde{c}'$ ensures the orthogonality of the design), together with the corresponding actual concentrations of calcium and aluminium in the standard solutions. Then the coefficients B were calculated independently from each other by the simple formulae as outlined for first-order modelling above. It can be seen from the data presented in Table 2 that the concentrations c_{Ca} and c_{Al} in conventional and unconventional 3^2 factorials are not the same (compare Fig. 1); consequently, the corresponding vectors of the results R differ from each other. Hence the regression coefficients B in model (13) depend on the applied transformation (Eqn. 2). The conventional and proposed approaches are considered below.

Conventional approach. The transformations (Eqns. 8) were applied. From the data presented in Table 2, the following model (13) was formulated:

$$\hat{R} = 49.22 + 23.13\tilde{c}_{Ca} - 16.18\tilde{c}_{Al} - 6.2\tilde{c}_{Ca}\tilde{c}_{Al} + 1.06\tilde{c}'_{Ca} + 9.12\tilde{c}'_{Al} + 0.92\tilde{c}'_{Ca}\tilde{c}_{Al} + 1.82\tilde{c}_{Ca}\tilde{c}'_{Al} - 0.02\tilde{c}'_{Ca}\tilde{c}'_{Al} \quad (14)$$

where $\tilde{c}'_{Ca} = \tilde{c}^2_{Ca} - 2/3$ and $\tilde{c}'_{Al} = \tilde{c}^2_{Al} - 2/3$. Model (14) may be expressed by the actual concentrations c_{Ca} and c_{Al} by inserting Eqns. (8). The corresponding error e is 1.4.

Unconventional approach. In this case, the coordinates c^*_{Ca} and c^*_{Al} (see Eqn. 5) were sought, in accordance with the rules presented earlier [1]. The result R corresponding to the properly selected coordinate c^* should satisfy the inequality, $(3R_{min} + R_{max})/4 \leqslant R \leqslant (R_{min} + 3R_{max})/4$, where R_{min} and R_{max} denote the minimum and maximum values of R in the considered concentration interval; in particular $R = (R_{min} + R_{max})/2$.

The following coordinates c^* were selected. First, $c^*_{Ca} = c^{(0)}_{Ca} = 7\ \mu g\ ml^{-1}$; because in this case $q_{Ca} = 1$, the linear transformation (Eqn. 8) of calcium concentration was applied in this case. (For all lines R vs. c_{Ca}, for $c_{Al} = 0$, 40, 80, 120 and 160 $\mu g\ ml^{-1}$, $R \approx (R_{min} + R_{max})/2$ for $c_{Ca} = c^{(0)}_{Ca} = 7\ \mu g\ ml^{-1}$, as seen in Fig. 3.)

Secondly, $c^*_{Al} = 40\ \mu g\ ml^{-1}$, for which

$$q_{Al} = (160 - 40)/(40 - 0) = 3, \text{ and } \tilde{c}_{Al} = \log_3(c_{Al} + 20)/60 \quad (15)$$

TABLE 2

3^2 factorial

No. of standard solution	Design matrix[a]									Conventional approach			Unconventional approach		
	$\tilde{c}_0$	$\tilde{c}_{Ca}$	$\tilde{c}_{Al}$	$\tilde{c}_{Ca}\tilde{c}_{Al}$	$\tilde{c}'_{Ca}$	$\tilde{c}'_{Al}$	$\tilde{c}'_{Ca}\tilde{c}_{Al}$	$\tilde{c}_{Ca}\tilde{c}'_{Al}$	$\tilde{c}'_{Ca}\tilde{c}'_{Al}$	c_{Ca}	c_{Al}	R	c_{Ca}	c_{Al}	R
1	1	1	1	1	$\frac{1}{3}$	$\frac{1}{3}$	$\frac{1}{3}$	$\frac{1}{3}$	$\frac{1}{9}$	10	160	54.29	10	160	54.29
2	1	1	−1	−1	$\frac{1}{3}$	$\frac{1}{3}$	$-\frac{1}{3}$	$\frac{1}{3}$	$\frac{1}{9}$	10	0	98.44	10	0	98.44
3	1	−1	1	−1	$\frac{1}{3}$	$\frac{1}{3}$	$\frac{1}{3}$	$-\frac{1}{3}$	$\frac{1}{9}$	4	160	19.18	4	160	19.18
4	1	−1	−1	1	$\frac{1}{3}$	$\frac{1}{3}$	$-\frac{1}{3}$	$-\frac{1}{3}$	$\frac{1}{9}$	4	0	38.53	4	0	38.53
5	1	1	0	0	$\frac{1}{3}$	$-\frac{2}{3}$	0	$-\frac{2}{3}$	$-\frac{2}{9}$	10	80	65.43	10	40	76.92
6	1	−1	0	0	$\frac{1}{3}$	$-\frac{2}{3}$	0	$\frac{2}{3}$	$-\frac{2}{9}$	4	80	21.56	4	40	25.61
7	1	0	1	0	$-\frac{2}{3}$	$\frac{1}{3}$	$-\frac{2}{3}$	0	$-\frac{2}{9}$	7	160	34.77	7	160	34.77
8	1	0	−1	0	$-\frac{2}{3}$	$\frac{1}{3}$	$\frac{2}{3}$	0	$-\frac{2}{9}$	7	0	68.35	7	0	68.35
9	1	0	0	0	$-\frac{2}{3}$	$-\frac{2}{3}$	0	0	$\frac{4}{9}$	7	80	42.42	7	40	50.21

[a] $\tilde{c}'_{Ca} = \tilde{c}^2_{Ca} - 2/3$, $\tilde{c}'_{Al} = \tilde{c}^2_{Al} - 2/3$.

(For all the examined range of R vs. c_{Al}, for $c_{Ca} = 4, 5, 6, \ldots, 10\ \mu g\ ml^{-1}$, R satisfies the inequality presented above, as seen in Fig. 3.)

The corresponding unconventional 3^2 arrangement is presented in Fig. 1 and Table 2. On the basis of the data presented in Table 2, the following model (13) was formulated:

$$\hat{R} = 51.81 + 24.39\tilde{c}_{Ca} - 16.18\tilde{c}_{Al} - 6.2\tilde{c}_{Ca}\tilde{c}_{Al} + 1.05\tilde{c}'_{Ca} + 1.34\tilde{c}'_{Al} + 0.92\tilde{c}'_{Ca}\tilde{c}_{Al} - 1.9\tilde{c}_{Ca}\tilde{c}'_{Al} - 0.01\tilde{c}'_{Ca}\tilde{c}'_{Al} \quad (16)$$

where $\tilde{c}'_{Ca}$ and $\tilde{c}'_{Al}$ are as explained above. The model may be expressed by the actual concentrations c_{Ca} and c_{Al} by substitution of Eqn. (8) for $\tilde{c}_{Ca}$ and Eqn. (15) for $\tilde{c}_{Al}$. The corresponding error e is 0.4.

DISCUSSION

The proposed method is aimed primarily at formulation of adequate polynomial models on the basis of a minimal number of experiments. It should be remembered that the empirical polynomial model is an interpolation formula and, in general, physical meaning should not be ascribed to the individual terms in the model (unless there are sound theoretical reasons, as in the case of spectrophotometric methods where Beer's law and the additivity principle are valid).

Models $\hat{R}$ discussed in this paper can be applied for several purposes: (a) to compare the characteristics of analytical methods with respect to their resistance to interfering or matrix effects; (b) to correct the results of analysis for a matrix effect; (c) to formulate a criterion for elimination of a matrix effect (e.g., in optimization of a procedure); (d) in multicomponent analysis. The requirement is that model $\hat{R}$ should adequately approximate the true relationship R vs. $c_1, \ldots, c_n$. The adequacy of the models considered here was estimated on criterion (6), i.e., each model was compared with the results of measurements taken on the additional test solutions which were not used in formulation of the model. This criterion was acceptable because few results were used in formulation of the models (actually, all possible terms in the presented models were determined).

The results presented above demonstrate the effectiveness of the proposed method compared with conventional empirical modelling. The use of the proposed logarithmic transformation of concentrations, instead of the linear transformation, reduced the inadequacy (error), e, of the model from 6.0 to 1.2 in the case of the first-order modelling, and from 1.4 to 0.4 in the case of the second-order modelling. The unconventional first-order model (Eqn. 12) and the conventional second-order model (Eqn. 14) are comparable with respect to adequacy. In Fig. 3, the second-order models are compared with the experimental results. The unconventional second-order model (Eqn. 16) fits the experimental data excellently. In the formulation of model (16), various transformations (Eqn. 2) were applied for calcium and aluminium concentrations. In general, the linear transformation of concentration of

an element to be quantified may be anticipated, as the calibration diagram for the analyte is usually a straight or slightly curved line. In the case of interfering sample components, logarithmic (or other) transformations of concentrations may turn out to be much more effective than the linear ones. Such cases are frequently met in atomic emission and absorption spectrometry.

REFERENCES

1 P. Kościelniak and A. Parczewski, Anal. Chim. Acta, 153 (1983) 103.
2 D. L. Massart, A. Dijkstra and L. Kaufman, Evaluation and Optimization of Laboratory Methods and Analytical Procedures, Elsevier, Amsterdam, 1978.

Analytica Chimica Acta, 153 (1983) 121—131
Elsevier Science Publishers B.V., Amsterdam — Printed in The Netherlands

FACTORS AFFECTING THE PRECISIONS OF POTENTIOMETRIC STRONG ACID—STRONG BASE AND OTHER ISOVALENT ION-COMBINATION TITRATIONS WITH DATA HANDLING BY NON-LINEAR REGRESSION ANALYSIS

H. C. SMIT and LOUIS MEITES*[a]

Laboratorium voor Analytische Scheikunde, Universiteit van Amsterdam, Nieuwe Achtergracht 166, 1018 WV Amsterdam (The Netherlands)

G. KATEMAN

Laboratorium voor Analytische Scheikunde, Universiteit van Nijmegen, Toernooiveld, 6525 ED Nijmegen (The Netherlands)

(Received 23rd May 1983)

SUMMARY

When non-linear regression analysis is applied to data obtained in titrations of the class specified by the above title, it is possible to evaluate two important parameters: the initial concentration c_A^0 of the substance titrated, and the equilibrium constant K_t for the reaction on which the titration is based. It is shown how the standard errors of these parameters depend on the standard errors of measurement of the independent variable (the volume of reagent) and the dependent variable (the pH or its equivalent), and on the values of c_A^0, K_t, and the dilution ratio r. Although in general the precision with which c_A^0 can be evaluated improves as K_t increases and the titration curve becomes steeper around the equivalence point, as the common belief indicates that it should, there are conditions under which the opposite is true. There are other conditions under which the precisions of the results are made worse by increasing the precision of measurement of one of the experimental variables.

A recent paper [1] from these laboratories discussed the problem of weighting in the analysis by non-linear regression of data obtained in potentiometric acid—base titrations, and argued that the proper procedure is to minimize the quantity $\Sigma_n W_n\ (\mathrm{pH}_{c,n} - \mathrm{pH}_{m,n})^2$, where $\mathrm{pH}_{c,n}$ is the calculated and $\mathrm{pH}_{m,n}$ the measured value of the pH at the nth experimental point; W_n is a weighting factor that is given by the equation

$$W_n = 1/[\sigma_{\mathrm{pH}}^2 + \sigma_{V_b}^2\ (\mathrm{dpH}/\mathrm{d}V_b)_n^2] \qquad (1)$$

where σ_{pH}^2 and $\sigma_{V_b}^2$ are the variances of the measured values of the pH and the volume of reagent, respectively; and $(\mathrm{dpH}/\mathrm{d}V_b)_n$ is the slope of the

[a]Permanent address: 22, Circle Drive, Potsdam, NY 13676 (U.S.A.).

0003-2670/83/$03.00

titration curve at the nth point. The form of the weighting factor reflects the fact that the uncertainty in V_b gives rise to an uncertainty in the pH-value that is largest in the region where the titration curve is steepest: for example, in the vicinity of the equivalence point in the titration of a moderately strong acid. This diminishes the significance of points close to the equivalence point, which would be more useful than any others in evaluating the concentration of such an acid if all of the pH-values were equally reliable, and causes the precisions of the calculated values of the parameters to depend in a complex way on the precisions of the experimental measurements and on the dissociation constant K_a of the acid. The significance of those points is further diminished by the well-known fact that the standard error of a measured pH-value (or e.m.f.) increases as the buffer (or poising) capacity of the solution decreases, as is illustrated by the behaviors of glass electrodes in unbuffered neutral media and of redox electrodes in solutions containing only very small concentrations of the ionic or molecular substances that govern their potentials. Two factors are involved: one reflects the effect of the concentration(s) of the potential-determining species on the exchange current and on the slope of the current—potential curve at zero current; the other reflects the resulting increase of sensitivity to traces of foreign acids or bases (or reducing and oxidizing agents) that might be present as impurities. Allowance for the first of these factors might be made on the basis of fundamental electrochemical information, but allowance for the second could not be attempted without knowing the natures and concentrations of the impurities that are present, and these will of course vary from one titration to another in practical work. Hence the problem is ignored here, but the reader should be aware that this paper, like its predecessor, is founded on overestimates of the significance of points in the steepest portions of the curves, even despite the use of a weighting factor that would be theoretically correct if the problem did not arise.

This paper describes the consequences of these ideas in potentiometric titrimetry based on isovalent ion-combination titrations. As defined by Goldman and Meites [2], these involve reactions of the form

$$A^{m+} + B^{m-} = AB(a = \text{constant}) \qquad (2)$$

Titrations of strong acids with strong acids belong to this class when AB is used as the solvent; precipitation titrations also belong to it if the two reacting ions have equal charges, if the solution is saturated with AB at the very start of the titration, if side-reactions such as $AB(s) + B^{m-} = AB_2{}^{m-}$ do not occur, and if the reacting ions do not undergo adsorption onto the surface of the precipitate AB. Unfortunately, these conditions are so restrictive that it is doubtful whether there are many precipitation titrations in which the data conform exactly to the simple algebraic equations that describe isovalent ion-combination titrations.

THEORY AND PROCEDURE

It is assumed that V_A^0 cm^3 of a c_A^0 M solution of A^{m+} is titrated with a c_B M solution of B^{m-} and that the value of pA is measured as a function of the total volume V_B of reagent that has been added. The titration curve is described by the equations

$$[A] = c_A^0 \, (1 - f)/(1 + rf) + 1/(K_t[A]) \tag{3a}$$

and

$$pA = -\log_{10} (y_A [A]) \tag{3b}$$

from which ionic charges are omitted for simplicity; f is the titration parameter defined by $f = V_B c_B / V_A^0 c_A^0$; r is the dilution ratio defined by $r = c_A^0 / c_B^0$; K_t is the conditional equilibrium constant of reaction (2) defined by $K_t = 1/[A][B]$ in the medium in which the titration is carried out; y_A is formally the single-ion activity coefficient of A^{m+} in that medium but also depends on the liquid–junction potential involved in the measurements. To ensure that the experimental data will conform to these equations, a titration must be carried out in the presence of a swamping electrolyte that will prevent variations of the activity coefficients and the liquid–junction potential.

Defining a subsidiary variable α by the equation

$$\alpha = c_A^0 \, (1 - f)/(1 + rf) \tag{4}$$

makes it possible to express the solution of Eqn. (3a) in the compact and convenient forms

$$\begin{aligned} &[A] = \{\alpha + (\alpha^2 + 4/K_t)^{1/2}\}/2 && (f < 1) \\ &[B] = \{-\alpha + (\alpha^2 + 4/K_t)^{1/2}\}/2; \; [A] = 1/K_t \, [B] && (f > 1) \end{aligned} \tag{5}$$

from which, together with Eqn. (3b), it is easy to compute the value of $pA_{c,n}$ at each experimental point. The corresponding slope is obtained by writing

$$\begin{aligned} dpA/dV_B &= (dpA/dpcA)(dpcA/d[A])(d[A]/df)(df/dV_B) \\ &= (1)(-0.4343/[A])\langle -c_A^0 \, [A](1 + r)/ \\ &\quad (1 + rf)\{2[A](1 + rf) - c_A^0 \, (1 - f)\}\rangle \, (1/[V_A^0 r]) \\ &= (0.4343/V_A^0)\langle c_A^0 \, (1 + r)/ \\ &\quad r(1 + rf)\{2[A](1 + rf) - c_A^0 (1 - f)\}\rangle \end{aligned} \tag{6}$$

Assuming that the volume of solution titrated and the concentration of the reagent are known, there are three parameters to be evaluated: c_A^0, K_t, and y_A. Their variances, and the ways in which they depend on the values of σ_{pA}, σ_{V_B}, c_A^0, K_t, and r, were estimated by means of a computer program that has been described elsewhere [1, 3].

That program operates in the following way. A set of synthetic data was first obtained by combining Eqns. (3b) and (5) with a set of arbitrarily chosen values of V_A^0 (which was always 25 cm^3), c_A^0, K_t, and r, and with an arbitrarily chosen data-acquisition schedule designed to simulate the possible actions of a human analyst performing an actual titration, or of an autotitrator in which the additions of reagent are controlled by the results of on-line predictive non-linear regression analysis or something equivalent to it [4]. There were 25 points in all: one at the very start of the titration (where $f = 0$), then four more at small increments (0.05 unit) of f to provide an indication of the shape of the curve and some crude basis for estimating the location of the equivalence point, and finally twenty more governed by the algorithm

$$\Delta f = 0.4\,|1 - f|; \quad \Delta f_{min} = 0.002 \tag{7}$$

where f denotes the current value, Δf represents the next increment of reagent to be added, and Δf_{min} is an arbitrary lower limit to that increment. With $r = 1$, so that $c_B = c_A^0$ and the equivalence point corresponds to V_B = 25.00 cm^3, this gives points at V_B = 0, 1.25, 2.50, 3.75, 5.00, 13.00, 17.80, 20.68, ..., 24.98, 25.03, 25.08, 25.13, 25.18, 25.25, 25.35, ..., 25.69 cm^3. All the results given below would be changed if a different schedule were adopted, and the discussion therefore emphasizes their trends rather than their exact values.

When these values of V_B and the corresponding ones of pA had been stored, the value of V_B at the first point was incremented by $5\sigma_{V_B}$ and the resulting data were subjected to non-linear regression to find the best values of c_A^0, log K_t, and y_A. Because of the error deliberately introduced into the value of V_B at the first point, those values differed from the ones used in synthesizing the data. The differences served to estimate the partial derivatives $\partial c_A^0/\partial V_B$, $\partial(\log K_t)/\partial V_B$, and $\partial y_A/\partial V_B$ at the first point. The original value of V_B at the first point was then restored, the value at the second point was incremented and a new fit was performed, and so on. The entire procedure was repeated with the original values of V_B but with each value of pA in turn incremented by $5\sigma_{pA}$. Finally, the variance σ_{Vj}^2 of the ith parameter was computed by combining the estimates of the partial derivatives with the values of σ_{V_B} and σ_{pA} and with the equation

$$\sigma_{Vi}^2 = \sigma_{V_B}^2 \sum_n (\partial V_i/\partial V_B)_n^2 + \sigma_{pA}^2 \sum_n (\partial V_i/\partial\ pA)_n^2 \tag{8}$$

The computations were done with a Hewlett-Packard HP-1000 computer operated in a time-sharing configuration. Because only three parameters had to be evaluated, and because Eqns. (5) are simpler than the corresponding equations for the titration of a weak acid, these computations were both faster and less affected by round-off and termination errors than those described previously [1], and replicate calculations initialized in different ways gave standard errors that were reproducible within 1%. Some error is of

course introduced by the finite-difference approximations to the partial derivatives that appear in Eqn. (8), but it must have been held to reasonable values by the consistent use of the value $\sigma_{pA} = 0.001$ unit, and it is believed to be inappreciable for any practical purpose.

Provision for estimating the standard errors of the parameters for other values of σ_{pA}, and for values of σ_{V_B} that differ from those used in the calculations, is most easily made by rewriting Eqn. (8) in the form [1]

$$\sigma_{V_i} = F\{0.001\ [\ \sum_n (\partial V_i/\partial\ pA)_n^2 + (G/F)^2\ \sum_n (\partial V_i/\partial\ V_B)_n^2]^{1/2}\} = F\ \sigma_{V_i}^* \qquad (9)$$

where $\sigma_{V_i}^*$ denotes the quantity within braces while the factors F and G are given by

$$F = \sigma_{pA}/0.001;\quad G = \sigma_{V_B}/0.001\ [= F\ \sigma_{V_B}/\sigma_{pA}] \qquad (10)$$

Values of $\sigma_{V_i}^*$ for various values of G/F under different conditions are listed in the tables that follow. Those for the value of G/F relevant to any particular titration will, of course, often have to be found by interpolation, but once found they need only be multiplied by the appropriate value of F in accordance with Eqn. (9).

RESULTS AND DISCUSSION

The general trends are illustrated by Table 1, which portrays the behavior observed when $c_A^0 = 0.1$ M and $r = 1$, so that c_B is also equal to 0.1 M. If G/F is very small, so that the measurements of the volume of reagent are very precise, the precisions of both c_A^0 and log K_t improve steadily as the value of log K_t increases. The rate of improvement is greatest for small values of log K_t. If log K_t is only 4, there is no point of maximum slope on the titration curve [5], and it is not surprising that the appearance of such a point is accompanied by a substantial increase of precision. If log K_t is large, the precisions of both c_A^0 and log K_t become steadily worse as σ_{V_B} (and consequently G/F) increases, as is of course to be expected.

Subtler effects are superimposed on this general pattern. The most striking one is that, if G/F is moderately large, the precisions become non-monotonic functions of log K_t. If, for example, $G/F = 10$, the relative standard error of c_A^0 decreases from 0.23% when log $K_t = 4$ to 0.013% when log $K_t = 8$, and then increases again to 0.026% when log $K_t = 22$. This behavior arises because points in the immediate vicinity of the equivalence point receive less weight as the titration curve becomes steeper in that region. It contradicts the customary generalization that the precision of a titration of this sort is always improved by increasing the value of K_t. Another striking effect is that, if G/F is large, the precision of log K_t becomes steadily worse as its value increases, in contrast to the steady improvement that occurs if G/F is small. This reflects the fact that the value of log K_t is chiefly determined by the difference between the values of pA at the start and at the end

TABLE 1

Effects of K_t and G/F on the standard errors of the parameters for c_A^0 = 0.1 M and r = 1
(This table gives values of $\sigma^*_{V_i}$ (Eqn. 9) for various values of log K_t and G/F (Eqn. 10) in the titration of 0.1 M A^{m+} with 0.1 M B^{m-}. The value of $\sigma^*_{c_A^0}$ is expressed as a percentage of the initial concentration of A^{m+}. Throughout these tables F = 1)

log K_t	G/F = 100		10		1		0.1		0.01	
	$\sigma^*_{c_A^0}$	$\sigma^*_{\log K_t}$	$\sigma^*_{c_A^0}$	$\sigma^*_{\log K_t}$	$\sigma^*_{c_A^0}$	$\sigma^*_{\log K_t}$	$\sigma^*_{c_A^0}$	$\sigma^*_{\log K_t}$	$\sigma^*_{c_A^0}$	$\sigma^*_{\log K_t}$
22	0.274	0.715	0.0264	0.00754	0.00148	0.000813	0.000343	0.000479	0.000178	0.000421
18	0.276	0.512	0.0262	0.00749	0.00146	0.000820	0.000336	0.000487	0.000176	0.000432
14	0.281	0.313	0.0251	0.00729	0.00149	0.000827	0.000303	0.000467	0.000181	0.000429
10	0.291	0.134	0.0176	0.00605	0.00153	0.000824	0.000317	0.000471	0.000207	0.000442
8	0.250	0.0872	0.0127	0.00547	0.00170	0.000857	0.000664	0.000553	0.000643	0.000540
7	0.185	0.0708	0.0152	0.00558	0.00280	0.000972	0.00203	0.000755	0.00206	0.000765
6	0.231	0.0463	0.0272	0.00486	0.00952	0.00146	0.00927	0.00140	0.00948	0.00141
5	0.412	0.0253	0.0643	0.00341	0.0443	0.00220	0.0444	0.00218	0.0438	0.00217
4	0.952	0.0118	0.228	0.00246	0.209	0.00232	0.208	0.00227	0.215	0.00234

of the titration. The slope of the titration curve is always small near the beginning of the titration, and if the value of log K_t is small the slope is small near the end of the titration as well. However, if the value of log K_t is fairly large, the slope of the titration curve is still appreciable at the last point (where $f = 1.028$ according to the data-acquisition schedule described above), and a large value of G/F causes so much deweighting of the data in this important region that there is a substantial deterioration in the precision with which log K_t can be evaluated.

In practical acid—base titrimetry, the value of σ_{pH} usually lies between about 0.002 and 0.02 unit, depending largely on the nature of the pH meter and electrodes that are used. If the reagent is dispensed from a 50-cm^3 buret, the value of σ_{V_B} is typically 0.01—0.02 cm^3, and may be significantly larger if the buret is uncalibrated. Hence the value of G/F is likely to lie between about 0.5 and 20 in a titration made with such apparatus, and the phenomena described in the preceding paragraph can therefore be expected to arise in much practical work. Their practical importance is that, for the chemist confronted by a titration curve that is only moderately steep in the vicinity of the equivalence point, it may be a serious mistake to take steps (e.g., decreasing the temperature of the titration mixture or adding a non-aqueous solvent to decrease its dielectric constant, both of which have often been recommended and adopted) designed to increase the value of K_t without ascertaining that these will actually improve the results instead of making them worse.

The interaction of all these effects causes the minimum on a plot of $\sigma^*_{c^0_A}$ against log K_t to become shallower and shift toward higher values of log K_t as G/F decreases. There is some indication, which is more prominent in Table 1 than in Tables 2—5, that the minimum is followed by a very small maximum at still higher values of log K_t, so that a further increase of a large slope around the equivalence point slightly overcompensates for the resulting further diminution of the already negligible weights assigned to points in that region. However, even if this effect is real, it is certainly too small to have any practical importance.

Tables 1—3 portray the effect of r. The ranges of values of G/F included in these tables differ in proportion to the value of r. If $r = 1$, the equivalence point is attained when 25.00 cm^3 of reagent has been added, and the value $G/F = 10$ (or, since $F = 1$ for all these results, $G = 0.01$ cm^3) corresponds to a standard error of V_B that is equal to 0.04% of that volume. However, if $r = 0.01$, only 0.2500 cm^3 of reagent is needed to reach the equivalence point, and 0.04% of that volume corresponds to $G = 10^{-4}$ cm^3 or to $G/F = 0.1$. When this effect is taken into account, the influence of r on the precision of either c^0_A or log K_t is negligible if log K_t is large. For example, if $r = 1$, $\sigma_{pA} = 0.001$, $G/F = 10$ (so that $\sigma_{V_B} = 0.01$ cm^3), and log $K_t = 22$, the relative standard error of c^0_A is 0.0264% while the absolute standard error of log K_t is 0.00754 unit; both of these figures are identical with those for $r = 0.1$ and $G/F = 1$.

TABLE 2

Effects of K_t and G/F on the standard errors of the parameters for c^0_A = 0.1 M and r = 0.1
(As for Table 1, except that the titration is done with 1 M B^{m-})

log K_t	G/F = 10.0		1.0		0.1		0.01		0.001	
	$\sigma^*_{c^0_A}$	$\sigma^*_{\log K_t}$	$\sigma^*_{c^0_A}$	$\sigma^*_{\log K_t}$	$\sigma^*_{c^0_A}$	$\sigma^*_{\log K_t}$	$\sigma^*_{c^0_A}$	$\sigma^*_{\log K_t}$	$\sigma^*_{c^0_A}$	$\sigma^*_{\log K_t}$
22	0.272	0.747	0.0264	0.00759	0.00153	0.000782	0.000347	0.000455	0.000184	0.000416
18	0.275	0.542	0.0261	0.00755	0.00150	0.000814	0.000333	0.000465	0.000190	0.000426
14	0.279	0.340	0.0253	0.00736	0.00153	0.000820	0.000323	0.000480	0.000182	0.000429
10	0.288	0.155	0.0195	0.00638	0.00147	0.000822	0.000327	0.000471	0.000154	0.000424
8	0.270	0.0952	0.0130	0.00554	0.00161	0.000842	0.000454	0.000511	0.000412	0.000503
7	0.207	0.0810	0.0131	0.00558	0.00198	0.000895	0.00108	0.000622	0.00102	0.000586
6	0.179	0.0587	0.0193	0.00547	0.00473	0.00115	0.00400	0.000955	0.00407	0.000985
5	0.273	0.0333	0.0396	0.00420	0.0203	0.00187	0.0203	0.00187	0.0202	0.00187
4	0.576	0.0186	0.121	0.00328	0.0984	0.00265	0.102	0.00272	0.103	0.00273

TABLE 3

Effects of K_t and G/F on the standard errors of the parameters for c^0_A = 0.1 M and r = 0.01
(As for Table 1, except that the titration is done with 10 M B^{m-})

log K_t	G/F = 1.0		0.1		0.01		0.001		0.0001	
	$\sigma^*_{c^0_A}$	$\sigma^*_{\log K_t}$	$\sigma^*_{c^0_A}$	$\sigma^*_{\log K_t}$	$\sigma^*_{c^0_A}$	$\sigma^*_{\log K_t}$	$\sigma^*_{c^0_A}$	$\sigma^*_{\log K_t}$	$\sigma^*_{c^0_A}$	$\sigma^*_{\log K_t}$
22	0.272	0.751	0.0264	0.00756	0.00152	0.000819	0.000333	0.000473	0.000210	0.000417
18	0.274	0.547	0.0261	0.00752	0.00152	0.000821	0.000318	0.000466	0.000186	0.000433
14	0.278	0.344	0.0253	0.00739	0.00151	0.000827	0.000325	0.000474	0.000196	0.000439
10	0.287	0.158	0.0197	0.00645	0.00153	0.000826	0.000317	0.000475	0.000196	0.000430
8	0.271	0.0965	0.0131	0.00554	0.00160	0.000841	0.000428	0.000504	0.000366	0.000480
7	0.211	0.0824	0.0130	0.00559	0.00196	0.000885	0.000997	0.000590	0.000970	0.000597
6	0.174	0.0607	0.0182	0.00543	0.00427	0.00110	0.00362	0.000938	0.00364	0.000932
5	0.264	0.0354	0.0371	0.00434	0.0186	0.00186	0.0186	0.00183	0.0184	0.00181
4	0.528	0.0192	0.108	0.00328	0.0968	0.00287	0.0928	0.00272	0.0915	0.00271

TABLE 4

Effects of K_t and G/F on the standard errors of the parameters for c^0_A = 0.01 M and r = 0.1
(As for Table 1, except that 0.01 M A^{m+} is titrated with 0.1 M B^{m-})

log K_t	G/F = 10		1		0.1		0.01		0.001	
	$\sigma^*_{c^0_A}$	$\sigma^*_{\log K_t}$	$\sigma^*_{c^0_A}$	$\sigma^*_{\log K_t}$	$\sigma^*_{c^0_A}$	$\sigma^*_{\log K_t}$	$\sigma^*_{c^0_A}$	$\sigma^*_{\log K_t}$	$\sigma^*_{c^0_A}$	$\sigma^*_{\log K_t}$
22	0.273	0.643	0.0263	0.00757	0.00152	0.000809	0.000329	0.000479	0.000222	0.000418
18	0.276	0.440	0.0259	0.00750	0.00154	0.000820	0.000335	0.000468	0.000226	0.000419
14	0.282	0.244	0.0238	0.00709	0.00154	0.000808	0.000327	0.000466	0.000222	0.000431
12	0.287	0.155	0.0195	0.00637	0.00152	0.000820	0.000343	0.000469	0.000225	0.000432
10	0.269	0.0952	0.0131	0.00555	0.00161	0.000830	0.000476	0.000505	0.000423	0.000485
8	0.178	0.0586	0.0190	0.00544	0.00475	0.00115	0.00412	0.00101	0.00405	0.000966
7	0.274	0.0336	0.0404	0.00421	0.0206	0.00188	0.0202	0.00187	0.0201	0.00188
6	0.554	0.0178	0.120	0.00324	0.104	0.00274	0.104	0.00280	0.0984	0.00258
5	1.80	0.00959	0.861	0.00418	0.697	0.00332	0.842	0.00412	0.874	0.00429

TABLE 5

Effects of K_t and G/F on the standard errors of the parameters for c^0_A = 0.001 M and r = 0.1
(As for Table 1, except that 0.001 M A^{m+} is titrated with 0.01 M B^{m-})

log K_t	G/F = 10		1		0.1		0.01		0.001	
	$\sigma^*_{c^0_A}$	$\sigma^*_{\log K_t}$	$\sigma^*_{c^0_A}$	$\sigma^*_{\log K_t}$	$\sigma^*_{c^0_A}$	$\sigma^*_{\log K_t}$	$\sigma^*_{c^0_A}$	$\sigma^*_{\log K_t}$	$\sigma^*_{c^0_A}$	$\sigma^*_{\log K_t}$
22	0.274	0.542	0.0261	0.00749	0.00156	0.000828	0.000333	0.000471	0.000231	0.000431
18	0.279	0.341	0.0253	0.00736	0.00153	0.000819	0.000323	0.000471	0.000229	0.000432
14	0.288	0.155	0.0195	0.00638	0.00152	0.000824	0.000342	0.000473	0.000248	0.000431
12	0.269	0.0952	0.0131	0.00554	0.00162	0.000847	0.000489	0.000495	0.000414	0.000494
10	0.178	0.0588	0.0191	0.00543	0.00483	0.00117	0.00404	0.000990	0.00387	0.000978
9	0.278	0.0340	0.0399	0.00412	0.0206	0.00185	0.0200	0.00183	0.0203	0.00180
8	0.577	0.0185	0.116	0.00311	0.106	0.00280	0.0958	0.00244	0.0961	0.00257
7	1.98	0.0107	0.898	0.00442	0.710	0.00352	0.783	0.00381	0.891	0.00434

Appreciable effects do, however, appear as the value of log K_t decreases. If log $K_t = 4$, the standard errors of c_A^0 and log K_t are roughly halved by the same changes of r and G/F. Although those changes do not affect the relative errors in V_B and f at any point, they do improve the precision with which the total volume of the titration mixture is known, and this is more important when the overall variation of pA is small than when it is large.

Tables 2, 4 and 5 portray the effect of c_A^0. Defining a dimensionless variable β by $\beta = c_A^0 K_t^{1/2}$ makes it possible to describe the normalized titration curve by the equation

$$[A]/[A]_{f=0} = \langle (1-f)/(1+rf) + \{[(1-f)/(1+rf)]^2 + 4/\beta^2\}^{1/2} \rangle / \{1 + [1 + 4/\beta^2]^{1/2}\} \quad (11)$$

If r were equal to zero, the value of $[A]/[A]_{f=0}$ would depend only on f and β. That is not exactly true for finite values of r, but the shape of the titration curve is governed chiefly by the value of β [6] unless r is quite large. For example, if $G/F = 1$ and $\beta = 1 \times 10^4$, the values of $\sigma^*_{c_A^0}$ and $\sigma^*_{\log K_t}$ correspond to 0.0195% and 0.00638 unit, respectively, if $c_A^0 = 0.1$ M and log $K_t = 10$ (Table 2); to 0.0195% and 0.00637 unit if $c_A^0 = 0.01$ M and log $K_t = 12$ (Table 4); and to 0.0195% and 0.00638 unit if $c_A^0 = 0.001$ M and log $K_t = 14$ (Table 5).

Two other effects, both relatively small, complicate this general picture a little further. Decreasing c_A^0 causes $\sigma^*_{c_A^0}$ and $\sigma^*_{\log K_t}$ to increase slightly if log K_t is large and if G/F is very small, but to decrease slightly if log K_t is small regardless of the value of G/F, even though β is kept constant by appropriately changing the value of K_t. These effects arise because the shape of the titration curve is influenced by the value of r as well as by that of β. If K_t is very large, the quantity $4/\beta^2$ in Eqn. (11) is very small, and the effect of dilution is relatively prominent; but if K_t is very small, the value of pA at any point is much less dependent on the value of r. Similar phenomena can of course be observed in Tables 1–3.

All these results have important, and occasionally surprising, consequences for the design of experiments. Suppose that a 0.01 M solution of a strong acid is to be titrated with 0.1 M strong base in a dilute aqueous solution at 25°C, so that $r = 1$ and log $K_t = 14$. If $\sigma_{pH} = 0.001$ unit and $\sigma_{V_B} = 0.001$ cm^3, Table 4 shows that the standard errors of c_A^0 and log K_t will correspond to 0.024% and 0.0071 unit, respectively. If σ_{pH} were decreased to 0.0001 unit (so that $F = 0.1$ and $G/F = 10$), these numbers would change to 0.028% and 0.024 unit. Improving the precision of measurement thus yields a less precise result, for it leads to severe deweighting of points that contain useful and important information. However, if σ_{V_B} were decreased to 0.0001 cm^3 while σ_{pH} remained equal to 0.001 unit (so that $F = 1$ and $G/F = 0.1$), the relative standard error of c_A^0 would decrease to 0.0015% while the standard error of log K_t would decrease to 0.00081 unit. The decrease in the first of these figures would exceed, and that in the second would nearly

equal, a full order of magnitude. Only if either log K_t (i.e., β) or G/F is very small can an improvement in the precision of measurement of pA be beneficial; under all other conditions it will not be worth the effort and will frequently be detrimental, and expedients that will improve the precision of measurement of the volume of reagent will be far more rewarding.

The conclusions described in the preceding paragraph were so unexpected that special pains were taken to ensure that they did not arise from errors in the calculations. The computations were repeated in double precision, with conditions for the termination of each fit that were far more stringent than those used in the original single-precision computations, but with identical increments applied to the individual values of V_B and pA in computing the finite-difference approximations to the partial derivatives that appear in Eqn. (8). They gave $\sigma^*_{c^\circ_A}$ = 0.0238% and $\sigma^*_{\log K_t}$ = 0.00713 unit with σ_{pA} = 0.001 unit and σ_{V_B} = 0.001 cm^3 (that is, with F = 1 and G/F = 1), and $\sigma^*_{c^\circ_A}$ = 0.282% and $\sigma^*_{\log K_t}$ = 0.244 unit with σ_{pA} = 0.001 unit and σ_{V_B} = 0.01 cm^3 (that is, with F = 1 and G/F = 10). These results are nearly identical with the ones given in Table 4. The agreement shows that round-off and termination errors were insignificant in the single-precision computations, as was asserted above. The sizes of the increments were then decreased, and the results were extrapolated to increment widths of zero to eliminate the finite-difference approximation. The extrapolated values differed appreciably from those given in Table 4, but led to exactly the same conclusion.

This work was made possible by the generous support of the Nederlandse Organisatie voor Zuiver Wetenschappelijk Onderzoek, and was aided in part by grant number CHE-8106103 from the National Science Foundation.

REFERENCES

1 G. Kateman, H. C. Smit and L. Meites, Anal. Chim. Acta, 152 (1983) 61.
2 J. A. Goldman and L. Meites, Anal. Chim. Acta, 30 (1964) 280.
3 L. Meites, Anal. Chim. Acta, 74 (1975) 177.
4 G. Kateman, H. C. Smit, P. C. Thyssen and L. Meites, work in progress.
5 L. Meites and J. A. Goldman, Anal. Chim. Acta, 29 (1963) 472.
6 L. Meites, Polarographic Techniques, 2nd edn., Wiley-Interscience, New York, 1965, pp. 470—474.

Analytica Chimica Acta, 153 (1983) 133—139
Elsevier Science Publishers B.V., Amsterdam — Printed in The Netherlands

THE APPLICATION OF STRONGLY REDUCING AGENTS IN FLOW INJECTION ANALYSIS
Part 2. Chromium(II)

R. C. SCHOTHORST and G. DEN BOEF*

Laboratory for Analytical Chemistry, University of Amsterdam, Nieuwe Achtergracht 166, 1018 WV Amsterdam (The Netherlands)

(Received 17th May 1983)

SUMMARY

The application of chromium(II) as strongly reducing reagent in flow injection analysis is described in detail. Results of the determination of a number of organic and inorganic substances are presented. With spectrophotometric detection, based on the absorption of chromium(III)—EDTA at 600 nm, limits of determination were of the order 10^{-4} mol l^{-1}. Polarographic detection was studied for nitrate and nitrite, for which the limit of determination was decreased with respect to spectrophotometric detection by factors of about 3 for nitrate and 10 for nitrite.

As has been reported [1], it is possible to use reagents which are unstable under atmospheric conditions in a flow injection analysis (f.i.a.) system. Examples are the strongly reducing agents chromium(II) and vanadium(II). Although partial oxidation of these reagents in such a flowing system cannot be avoided completely, the extent to which this occurs is highly reproducible. Hence, by generating the reagent and letting the analytical reaction proceed in a flowing system, fast and convenient quantitative procedures based on these strongly reducing reagents become feasible.

In the present paper, the analytical applications of divalent chromium in f.i.a. are extensively studied. Numerous reducible substances were tested. Apart from the spectrophotometric detection described in the previous paper [1], for which the absorbance by Cr(III)—EDTA at 600 nm was chosen, electrochemical detection was studied in order to achieve lower limits of determination.

Mainly two types of electrochemical detector have been applied in flowing systems. Voltammetric detectors have been proposed with stationary electrodes like glassy carbon, carbon paste, platinum and the hanging mercury drop electrode (HMDE). The principal drawback of these electrodes is contamination of the electrode surface, mainly by products of the reaction at the electrode, which cause changes in the sensitivity and in the baseline levels. Polarographic detectors, with a dropping mercury electrode (DME) do not suffer from this disadvantage of the stationary electrodes, because of the

0003-2670/83/$03.00

continuous renewal of the electrode surface. The principal disadvantage of the DME is the periodic growth of the mercury drops. The limit of determination is determined mainly by the charging currents, resulting from the flow of mercury. Recently a new type of dropping mercury electrode was introduced, the so-called static mercury drop electrode (SMDE). This electrode combines the advantages of a stationary electrode and the DME, i.e., constant area during the current sampling period and a periodically renewed electrode surface.

Bond and Jones [2] made an extensive evaluation of the analytical performance of the SMDE in batch polarography. They found limits of determination for the SMDE of the same magnitude in the sampled d.c., the normal pulse and the differential pulse polarographic modes. The same result was obtained by Bond et al. [3] for the analytical performance of the SMDE as working electrode in some home-made flow-through cells. A commercially available adaptation of the SMDE for flow-through detection is based on the wall jet principle [4] with a vertical flow pattern and an effective cell volume of less than 1 μl [5]. The flow-through detector with the SMDE as working electrode, combined with high-performance liquid chromatography, has been evaluated by van Oort et al. [6] and by Vohra and Harrington [7]. These authors reported extensive investigations of the influence of the various electrochemical parameters on the analytical performance.

The SMDE flow-through detector was used in the present investigation for the electrochemical part of the work.

EXPERIMENTAL

The polarographic detector consisted of an EG & G Princeton Applied Research Corp. (Princeton, NJ, U.S.A.) model 310 polarographic detector. Potentials were applied with a PARC model 174-A polarographic analyzer. All potentials are reported with respect to a silver/silver chloride reference electrode. In order to improve the jet function, the nozzle diameter of the model 310 was reduced to 0.5 mm by insertion of a piece of stainless-steel tube with that inner diameter.

The instrumentation for the spectrophotometric part of the work and the dimensions of the flow system (Fig. 1) were as described earlier [1].

The reagents used for the spectrophotometric part of the work were described before [1].

In the case of polarographic detection, the concentration of chromium(III) chloride entering the reductor (zinc, with a 5% degree of amalgamation) was 2×10^{-3} mol l^{-1} in 10^{-2} mol l^{-1} hydrochloric acid. The buffer solution contained 7×10^{-2} mol NH_4Cl, 2×10^{-1} mol KCl and 10^{-2} mol EDTA per litre; the pH was adjusted to 9.3 with concentrated ammonia liquor. The carrier stream was distilled water. All solutions were carefully deaerated with nitrogen, because oxygen interfered with the determinations.

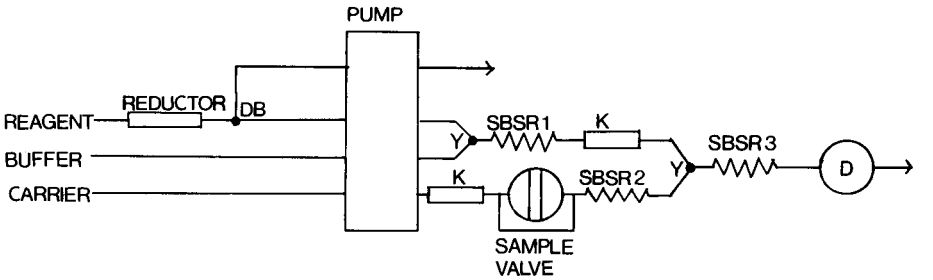

Fig. 1. Flow diagram. Length of single bead string reactors (SBSR): (1) 0.2 m; (2) 0.2 m; (3) 0.4 m. DB, debubbler; K, damping coil, see text; D, detector. All connecting and SBSR tubing is 1-mm i.d. nylon. SBSRs are packed with 0.6-mm glass beads. Sample size, 32 μl.

SPECTROPHOTOMETRIC DETECTION

The choice of substances examined spectrophotometrically was based on the work of Groeneveld and den Boef [8], who determined several reducible substances with chromium(II)—EDTA as reagent in excess in a batch procedure. The reaction time was made long enough to complete various different reductions.

In Table 1, the results of the determination of the chosen substances by f.i.a. are summarized for nine inorganic and organic species. The absorbance (A) depended linearly on the concentration of the analyte in the sample solution (C) over realistic working ranges. The limit of determination is defined here as the analyte concentration for which the absorbance change equals ten times the peak-to-peak noise. The fact that maleic acid and formaldehyde caused no absorbance changes when determined in the flowing system must be ascribed to the very short reaction time in f.i.a. In the mentioned batch procedures (with a reaction time of 5 min), these substances were quantitatively reduced.

TABLE 1

Calibration lines for the flow injection system with spectrophotometric detection (Reagent concentration 10^{-2} mol l^{-1})

Sample	Concentration range (mol l^{-1})	Regression line	Regression coefficient r	Limit of determination (mol l^{-1})
$VOSO_4$	10^{-3}—7.5×10^{-3}	$A = (293 \pm 0.4)\,C$	0.9994	3.9×10^{-4}
NH_4VO_3	5×10^{-4}—7.5×10^{-3}	$A = (43.6 \pm 0.2)\,C$	0.9999	2.4×10^{-4}
$UO_2(Ac)_2$	2.5×10^{-4}—5×10^{-3}	$A = (41.1 \pm 0.3)\,C$	0.9997	2.4×10^{-4}
$K_3Fe(CN)_6$	5×10^{-4}—10^{-2}	$A = (120.4 \pm 0.1)\,C$	0.9999	4.9×10^{-4}
KIO_3	1.66×10^{-4}—1.66×10^{-3}	$A = (120.2 \pm 1)\,C$	0.9997	8.3×10^{-5}
Methyl red	1.25×10^{-4}—1.25×10^{-3}	$A = (59.5 \pm 0.6)\,C$	0.9995	2.5×10^{-4}
o-Nitrophenol	1.66×10^{-4}—1.66×10^{-3}	$A = (57.9 \pm 1)\,C$	0.9988	1.7×10^{-4}
Maleic acid	10^{-3}—10^{-2}	No signal	—	—
Formaldehyde	10^{-3}—10^{-2}	No signal	—	—

Electrochemical parameters

The working potential of the detector (−1.5 V) was selected from the polarogram obtained in flow conditions. The potential was chosen in the limiting current region of the chromium(III)—EDTA reduction wave. Selecting a potential in the limiting current region of the chromium(II)—EDTA oxidation wave was also possible. However, the current generated by the oxidation of chromium(II)—EDTA was very large and pump pulsations therefore had a great influence on the baseline. This potential was therefore not very attractive.

Some experiments were done with the SMDE in the hanging mercury drop mode. Working with a hanging mercury drop electrode has some advantages (no problems with changing drop size), but at the selected potential a rapid fall of the electrode response occurred, probably because of contamination of the electrode surface with chromium(III) hydroxide. With the SMDE in the dropping mode, these problems did not occur. Therefore the experiments were carried out with a dropping SMDE.

In a flowing system, the diffusion layer around the electrode is very thin and depletion is not appreciable, especially at low drop times. This was concluded from the fact that current measurements in the sampled d.c. and pulse mode gave the same sensitivity. Of the three possible drop sizes (small, medium and large), the smaller mercury drop (1.1×10^{-2} cm^{-2} [4]) gave the highest signal-to-noise ratio. Drop times of 0.5 or 1 s gave well-developed peaks. Drop times longer than 1 s caused lowering of peaks, probably because of contamination of the electrode surface by chromium(III) hydroxide; it is also possible for the peak maximum to be missed at large drop times.

Pump noise

Pump pulsations cause fluctuations in the mass transfer towards the electrode surface, which in turn cause fluctuations in the current. Therefore it is necessary to minimize pump pulsation. Van Oort et al. [6] found good results with a combination of an empty column, a coil and a pressure gauge; this combination gives a large increase in the volume of the flow system, which causes a longer residence time of the reagents. That is not very desirable in the case of unstable reagents. Therefore several other devices were examined: a coil (length 3 m, inner diameter 1 mm); an empty column (length 14 cm, inner diameter 4 mm); a combination of these two; a packed column (length 14 cm, inner diameter 4 mm, packed with 1-mm glass beads).

In the flow system the place of these devices is indicated by the symbol K (Fig. 1). The results are presented in Table 2. All devices gave a slight increase in the baseline level, because of the longer residence time. The packed column gave the best results. All further experiments were therefore carried out with two packed columns (K) in the flow system (Fig. 1).

TABLE 2

The influence of different damping devices in the flow system on the baseline fluctuations

Device	Baseline fluctuations (nA)
None	200
Coil	75
Empty column	50
Coil and empty column	25
Packed column	12.5

Dependence of the signal on the flow rate

When the flow rate is raised, four effects may influence the peak height resulting from injection of a sample: an increase of the mass transfer rate; a decrease in reagent decomposition, because of the shorter residence time; a decrease in the reaction yield, especially for slowly reacting compounds; and a fall in reduction efficiency of the Jones reductor. Only the first effect influences the peak height independently of the kind of analyte in the sample. As the dilution is independent of the flow rate for SBSRs [9], the corresponding influence of flow rate on peak height can be neglected.

In the case of nitrate, the dependence of the signal on the flow rate was investigated. Peak heights resulting from the injection of 10^{-3} M sodium nitrate were recorded at different flow rates. The resulting peak height as a function of the flow rate is presented in Fig. 2. The baseline level showed a slight decrease with increasing flow rate. At the highest flow rate, the highest signal was obtained, whereas the fluctuations in the baseline were minimal. All experiments were therefore carried out with the highest flow rate (about 1.25 ml min^{-1}) that could be achieved with the pump (Gilson Minipuls-II) and pump tubes used. It must be kept in mind, however, that the situation may be different for other analytes.

Results and discussion

Nitrate, nitrite and iodate were chosen to test the performance of the polarographic detector. Because nitrate and nitrite were not completely reduced to ammonia, possible intermediates in this reduction, viz., hydrazine and hydroxylamine, were also examined. The polarographic detector, at a working potential of −1.5 V, records changes in the chromium(III)—EDTA concentration. When the analyte itself is electroactive at this potential, current signals are no longer the result of the reaction of the analyte and the reagent only. If this occurs, the substance cannot be determined by this method. Therefore a polarogram was run for all five test substances. Iodate showed a reduction wave with a half-wave potential of −1.0 V and was therefore not further investigated. The other four substances were not electroactive at −1.5 V.

Results of the determinations are summarized in Table 3. The correlations

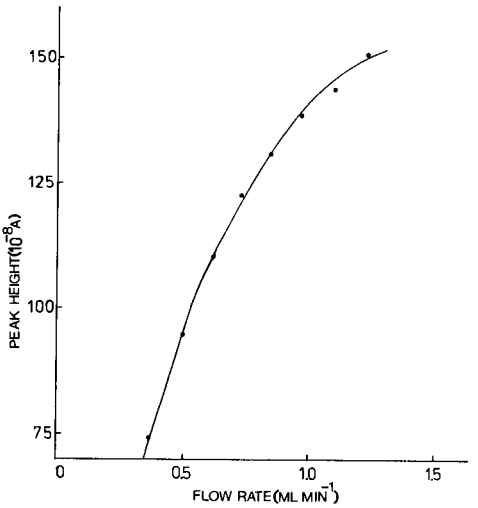

Fig. 2. Peak height as a function of the flow rate for the polarographic measurement of 10^{-3} mol l^{-1} sodium nitrate.

for the current (I) and the concentration of the analyte in the sample solution (C) show good linearity for nitrate and nitrite in the concentration range 2.5 × 10^{-5}—10^{-4} M. The maximum sampling rate [10] is: S_{max} = $3600/4\sigma_t$ = 170 h^{-1}, for σ_t = 5.3 s (σ_t is the variance in seconds).

From the moments of a peak resulting from the injection of 10^{-3} M sodium nitrate, the number of tanks to which the flow system corresponds can be calculated. The mean equals 24 s and the variance 36 s^2, so that the number of tanks is 16. Hydrazine and hydroxylamine do not react with chromium(II)—EDTA under these conditions. Thus if the reduction of nitrate and nitrite has one of these compounds as intermediate, the reduction stops under these conditions.

In comparison with the spectrophotometric detection, the limit of determination with polarographic detection is lower, for nitrate by a factor of

TABLE 3

Calibration lines for the flow injection system with polarographic detection (Reagent concentration 2 × 10^{-3} mol l^{-1})

Sample	Concentration range (mol l^{-1})	Regression line	Regression coefficient r	Limit of determination (mol l^{-1})
$NaNO_3$	2.5 × 10^{-5}—10^{-4}	$I = (2.20 \pm 0.04)10^{-3}\ C$	0.9997	3.4 × 10^{-5}
$NaNO_2$	2.5 × 10^{-5}—10^{-4}	$I = (4.06 \pm 0.11)10^{-3}\ C$	0.9992	1.5 × 10^{-5}
NH_2NH_2	10^{-4}—7.5 × 10^{-4}	No signal	—	—
NH_2OH	10^{-4}—7.5 × 10^{-4}	No signal	—	—

about 3 and for nitrite by a factor of about 10. However, spectrophotometric detection may be applicable in cases where electrochemical detection is not.

The authors thank Mr. W. Ozinga for experimental aid with the spectrophotometric part of the work.

REFERENCES

1 R. C. Schothorst, J. M. Reijn, H. Poppe and G. den Boef, Anal. Chim. Acta, 145 (1983) 197.
2 A. M. Bond and R. D. Jones, Anal. Chim. Acta, 121 (1980) 1.
3 A. M. Bond, H. A. Hudson and P. A. van den Bosch, Anal. Chim. Acta, 127 (1981) 121.
4 R. Samuelsson and J. Osteryoung, Anal. Chim. Acta, 123 (1981) 97.
5 M. R. Hackman and M. A. Brooks, J. Chromatogr., 222 (1981) 179.
6 W. J. van Oort, J. den Hartigh and R. J. Driebergen, Proc. Joint Meeting UK/CZ, London, September, 1981; T. Ryan (Ed.), Fundamentals and Applications of Electrochemical Detectors, Pergamon, Oxford, in press.
7 S. K. Vohra and G. W. Harrington, J. Chromatogr. Sci., 18 (1980) 379.
8 E. R. Groeneveld and G. den Boef, Fresenius Z. Anal. Chem., 237 (1968) 85.
9 J. M. Reijn, W. E. van der Linden and H. Poppe, Anal. Chim. Acta, 126 (1981) 1.
10 J. Růžička and E. H. Hansen, Flow Injection Analysis, Wiley-Interscience, New York, 1981.

Analytica Chimica Acta, 153 (1983) 141—147
Elsevier Science Publishers B.V., Amsterdam — Printed in The Netherlands

THE REDUCTION OF PROPYLENEGLYCOL DINITRATE, NITROGLYCERIN, DINITROTOLUENE, AND TRINITROTOLUENE ON SILVER ELECTRODES

D. A. FINE* and M. H. MILES

Chemistry Division, Research Department, Naval Weapons Center, China Lake, CA 93555 (U.S.A.)

(Received 1st March 1983)

SUMMARY

The nitrate esters propyleneglycol 1,2-dinitrate and nitroglycerin, as well as the aromatic nitro compounds, dinitrotoluene and trinitrotoluene, are electrochemically reducible on silver electrodes. Concentrations as low as 0.5 mg l^{-1} are readily detectable at scan rates of 5 mV s^{-1} in unstirred solutions. Peak potentials vary with the nature of the electrolyte anion. The *ortho*, *meta*, and *para* isomers of dinitrotoluene yield different voltammograms; the *ortho* and *para* isomers show two reduction peaks but only a single peak is found for the three *meta* isomers. Constant-current, exhaustive electrolysis studies of 2,5-dinitrotoluene show two distinct reduction stages, corresponding to three-electron and five-electron reductions.

The toxic nature of certain nitrate esters and aromatic nitro compounds used in explosives has created a need on the part of ordnance facilities for detection of these compounds in effluent waters. Of particular importance are the two nitrate esters, propyleneglycol 1,2-dinitrate (PGDN) and nitroglycerin, and aromatic nitro compounds such as dinitrotoluene (DNT) and trinitrotoluene (TNT) [1—3].

The electrochemical reduction of nitrate esters at dropping mercury electrodes has been studied [4, 5] and polarographic methods for detecting and quantifying the esters have been devised [6, 7]. There have also been studies of the reduction of aromatic nitro compounds at dropping mercury electrodes [8—11]. For purposes of field and bench testing at ordnance facilities, the dropping mercury electrode poses problems connected with handling, maintenance and toxicity; hence, suitable solid working electrodes have been sought.

Aromatic nitro compounds are known to be reduced at numerous solid electrodes [12—14]; nitrate esters, in contrast, are much more sensitive to the choice of electrode materials and show no evidence of reduction on most transition metal electrodes, including platinum [15]. A previous paper [15] reported the reduction of PGDN, nitroglycerin and n-propyl nitrate on silver wire electrodes. Propyleneglycol dinitrate and nitroglycerin were found to

undergo four- and six-electron reductions per molecule, respectively. This paper describes further studies of the behavior of PGDN and nitroglycerin on silver electrodes and some new studies of the behavior of DNT and TNT.

EXPERIMENTAL

Solutions

All electrolyte solutions were prepared from reagent-grade chemicals and distilled water. In most of the voltammetric and electrolysis studies, the supporting electrolyte was 0.50 M NaCl, buffered to pH 10 with 0.01 M $Na_2CO_3/NaHCO_3$. Anion effects were investigated in 0.2 M solutions of sodium salts.

Aqueous stock solutions of PGDN were prepared by weighing aliquots of a mixture of 10 g of PGDN dissolved in 200 g of acetone, followed by dilution to yield final concentrations of 100—1000 mg l^{-1}. Solutions of nitroglycerin were prepared from pharmaceutical tablets (Nitrostat, Parke-Davis) containing 0.6 mg of nitroglycerine. Solutions of DNT and TNT were prepared by weighing the pure solids and dissolving in water with agitation. Concentration and purity of stock solutions were checked by chromatographic methods. Solutions in the 0—10 mg l^{-1} range were prepared by pipetting the calculated amount of stock solution into the electrolyte solution; in most cases, the volume of the electrolyte solution was 40 ml.

Electrodes

The silver wire electrodes were prepared as described previously [15]. The wire in most of the electrodes was about 1.5 cm long (0.10-cm diameter), yielding a surface area of 0.48 cm^2. The electrodes were usually cleaned with Orion polishing strips before a set of experiments; however, as noted previously [15], omission of this mechanical cleaning produced no detectable adverse effects. The most important factor in achieving reproducible behavior was electrochemical conditioning. In voltammetric measurements, the electrode was subjected to three rapid potential scans (50 mV s^{-1} or 100 mV s^{-1}), starting at —0.1 to —0.3 V vs. SCE and finishing at —1.1 to —1.3 V, before each recorded voltammetric scan.

Measurements

Electrochemical measurements were made in cylindrical glass cells fitted with a cap that supported the electrodes and the inert gas purging tubes. The electrode system consisted of the silver-wire working electrode, a platinum-wire counter electrode, and a commercial Ag/AgCl or SCE reference electrode. Unless otherwise noted, potentials listed in subsequent sections are relative to SCE. Solutions were deaerated with nitrogen or helium. For voltammetric scans, a long deaeration period (15—20 min) was found to be necessary in order to obtain reproducible baselines. This deaeration period could be shortened by use of strong agitation during the bubbling [15, 16].

Inert gas was passed over the surface of the solution during the actual measurements. All experiments were conducted at room temperature (23—25°C). Experiments involving exhaustive electrolysis in stirred solutions were conducted as previously reported [15].

Most voltammetric measurements were obtained with a Princeton Applied Research (PAR) model 174 polarographic system. Results were recorded with an X-Y recorder (Hewlett-Packard 7005A or 7047A). In some studies, such as exhaustive electrolysis and cyclic voltammetry, a PAR model 173 potentiostat/galvanostat equipped with a model 176 current follower plug-in and a PAR model 175 programmer was used.

RESULTS AND DISCUSSION

Linear sweep voltammetry

All of the current—potential traces discussed in this section were obtained at a scan rate of 5 mV s^{-1}, in 0.5 M NaCl buffered to pH 10. At higher pH values, some flattening of the waves occurred; at lower pH values, interference from the hydrogen evolution wave became significant.

For PGDN (Fig. 1), only one reduction wave is seen in the region from 0.0 to −1.3 V; the peak potential E_p for this wave occurs at about −0.57 V. The behavior of nitroglycerin is very similar to that of PGDN.

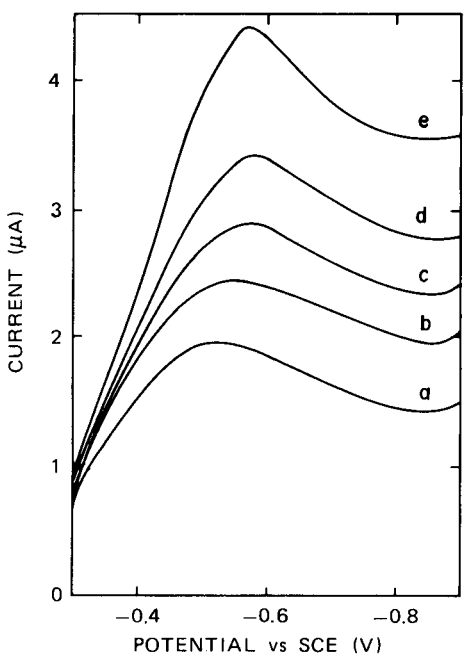

Fig. 1. Linear sweep voltammetric traces at a silver wire electrode at 5 mV s^{-1} for solutions of PGDN in 0.5 M NaCl, buffered to pH 10 with 0.01 M $NaHCO_3$/0.01 M Na_2CO_3: (a) 0.0; (b) 1.0; (c) 2.0; (d) 3.0; (e) 5.0 mg l^{-1}.

In the case of DNT, the voltammetric behavior at the silver wire electrode is dependent on isomeric composition. All three *meta* isomers show a single reduction wave, with E_p between —0.52 and —0.56 V. The two *ortho* isomers and the *para* isomer show two definite waves. The first wave occurs at approximately the same potential for all concentrations, but the position of the more negative wave shows a concentration-dependence. In the case of 2,3-DNT, the first E_p is at —0.52 V; at concentrations $\leqslant$2.0 mg l^{-1}, the second E_p is at —0.56 V, and at concentrations $\geqslant$4.5 mg l^{-1} this second E_p shifts to —0.76 V. Curves suggesting the possible occurrence of three reduction processes are obtained for intermediate concentrations. Typical traces are shown in Fig. 2. The 3,4-isomer shows the same behavior, with the first E_p at —0.45 V, the second at —0.59 V for concentrations $\leqslant$1.5 mg l^{-1} and at —0.79 V for concentrations $\geqslant$2.5 mg l^{-1}. In the case of the *para* isomer (2,5-DNT), the first E_p is at —0.40 V; the shift of the second E_p occurs at higher concentrations than for the *ortho* isomers, E_p = —0.64 V for concentrations $\leqslant$7 mg l^{-1}, and —0.80 V for concentrations $\geqslant$12 mg l^{-1}. Traces for 2,5-DNT are shown in Fig. 3.

For TNT, only one reduction wave appears at concentrations <3 mg l^{-1}, with E_p about —0.52 V. At higher concentrations, this wave broadens, with hints of another wave at more negative potentials.

The effects of variation of the supporting electrolyte anion were similar to those reported previously for PGDN [15]. In the present study, the anions

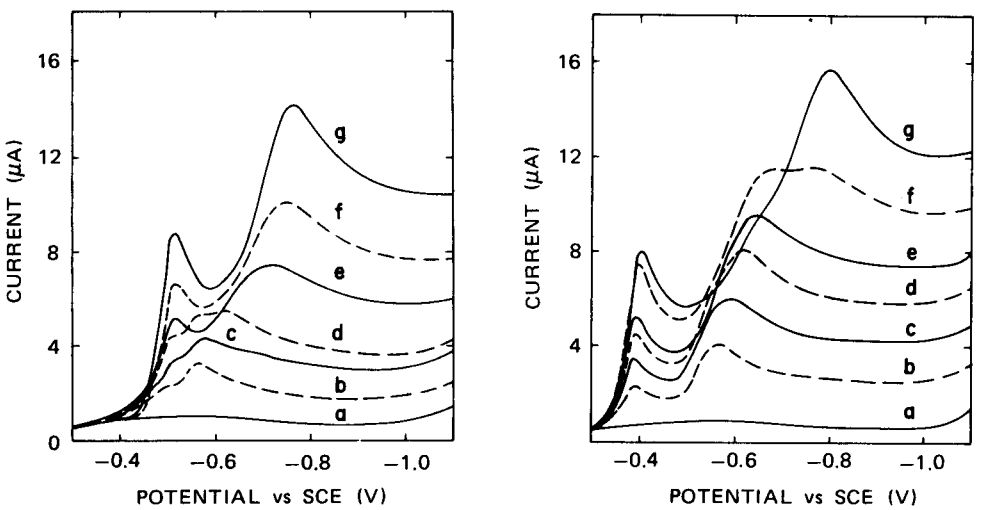

Fig. 2. Linear sweep voltammetric traces at a silver wire electrode at 5 mV s^{-1} for solutions of 2,3-DNT in 0.5 M NaCl, buffered to pH 10 with 0.01 M $NaHCO_3$/0.01 M Na_2CO_3: (a) 0.0; (b) 1.1; (c) 2.2; (d) 3.3; (e) 6.3; (f) 8.3; (g) 12.0 mg l^{-1}.

Fig. 3. Linear sweep voltammetric traces at a silver wire electrode at 5 mV s^{-1} for solutions of 2,5-DNT in 0.5 M NaCl, buffered to pH 10 with 0.01 M $NaHCO_3$/0.01 M Na_2CO_3: (a) 0.0; (b) 2.0; (c) 3.9; (d) 5.8; (e) 7.6; (f) 10.1; (g) 12.5 mg l^{-1}.

investigated were fluoride, chloride, bromide, iodide, and nitrate. Very broad reduction waves were observed for sodium fluoride and sodium nitrate solutions; resolution of multiple reduction waves was difficult. The best resolution was obtained with sodium chloride or bromide solutions. It is interesting that three distinct peaks were seen for TNT in sodium bromide solutions, whereas only one or two peaks were observed in chloride solutions. In sodium iodide solutions, the waves shifted to potentials sufficiently negative to make interference from the hydrogen evolution wave a significant problem. Peak potentials for the different electrolyte solutions are summarized in Table 1. No appreciable variation in sensitivity of detection of the nitro compounds was observed for the different anions. The results in Table 1 show the same order of increasingly negative reduction potentials as specific anion adsorption ($NO_3^- \sim F^- < Cl^- < Br^- < I^-$). As reported previously for PGDN [15], the potential region for the reduction of aromatic nitro compounds on silver electrodes can be correlated with potentials at which the surface coverage by adsorbed anions is decreasing [17].

The results with linear-sweep voltammetry indicate the usefulness of the silver wire electrode in the quantitation of PGDN, nitroglycerin, DNT, and TNT in waste waters. For each compound, 0.5 mg l^{-1} is readily detectable. For PGDN and nitroglycerin, plots of i_p vs. concentration are linear for concentrations <10 mg l^{-1}. In the case of PGDN, plots from ten different runs, each with 6—10 different PGDN concentrations, showed an average slope of 0.50 μA mg^{-1} l (1.0 μA cm^{-2} mg^{-1} l), with a standard deviation (s) of ±0.06. This is almost identical to previous results in 0.01 M NaOH solutions containing 0.5 M NaCl [15]. Plots for 7 different runs with nitroglycerin showed an average slope of 0.65 μA mg^{-1} l (s = ±0.10). For DNT and TNT, not all of the observed waves yielded linear plots of i_p vs. concentration, but the current at certain fixed potentials, especially in the region —0.8 to —1.0 V, did show linearity with concentration. In the case of DNT, plots using the current peak at —0.90 V for 12 different runs with solutions of varying isomeric composition yielded an average slope of 1.0 μA mg^{-1} l

TABLE 1

Anion effects on the reduction of PGDN, nitroglycerin (NG), DNT, and TNT on silver wire electrodes at concentrations ≤5 ppm. Potential sweep rate = 5 mV s^{-1}, electrode area = 0.48 cm^2, pH = 10 unless otherwise noted

Electrolyte (0.20 M)	E_p (V vs. SCE)			
	PGDN	NG	DNT[a]	TNT
NaF	—0.5[b]	—0.5[b]	—0.6[b]	—0.5[b], —0.7[b]
NaCl	—0.52	—0.52	—0.52	—0.49, —0.7[b]
NaBr	—0.70	—0.71	—0.64	—0.49, —0.66, —0.75
NaI[c]	—0.97	—0.95	—0.8[b]	—0.8[b], —0.96[b]
$NaNO_3$	—0.5[b]	—0.5[b]	—0.6[b]	—0.5[b], —0.6[b], —0.8[b]

[a] 2,6-isomer. [b] Peak poorly defined because of broadness of reduction wave. [c] pH 12.

(s = ±0.15). In the case of TNT, plots for 7 different runs, based on the current peak at —0.80 V, yielded an average slope of 0.79 μA mg^{-1} l (s = ±0.06).

Exploratory measurements with pyrolytic graphite and glassy carbon electrodes showed these materials to be much less sensitive to PGDN than the silver electrode. Also, the reduction of PGDN occurs at highly negative potentials on carbon (ca. —0.9 V vs. SCE), and it would be necessary to work in strongly alkaline solution in order to avoid interference from the hydrogen evolution wave. Another disadvantage of carbon electrodes is the need for frequent mechanical cleaning.

Cyclic voltammetry

Cyclic voltammetric studies of the meta isomers of DNT showed that the potential scan rate had no effect on E_p over the range of 5—1000 mV s^{-1}. Studies of 2,5-DNT showed that the potential of the first peak shifted to more negative values as the potential sweep rate increased ($\Delta E_p/\Delta \log v$ = —20 ± 5 mV), while the second E_p showed no change over the range 5—1000 mV s^{-1}. The first peak showed the expected behavior for a diffusion-controlled irreversible reaction: $i_p \propto C^0 v^{1/2}$, $E_p = f(v)$, $E_p \neq f(C^0)$, as found previously for the reduction of PGDN on silver electrodes [15].

Exhaustive electrolysis

Exhaustive electrolysis studies of the *ortho* and *para* isomers at a large silver electrode (A = 50 cm^2) at constant current (0.06 mA cm^{-2}) showed two distinct waves, in agreement with the potential scan experiments. For 2,5-DNT, the first reduction wave began at —0.41 V and the second reduction wave began at —0.7 V. Dramatic color changes were observed in this experiment, involving a 60-mg l^{-1} solution of 2,5-DNT in 0.5 M NaCl/0.1 M $NaHCO_3$/0.1 M Na_2CO_3. The solution rapidly became pink as current was applied and deepened to a bright reddish orange during the first wave. The color gradually faded during the second wave until the solution became almost colorless. The first wave required three electrons per DNT molecule while the second wave involved five electrons per molecule to give a total of eight electrons for the reduction of each molecule of 2,5-DNT. The experimental error in these values is estimated to be ±10%. Similar results were obtained with 2,3-DNT and 3,4-DNT except that the color produced in the first wave was deep violet rather than reddish orange. All three *meta* isomers showed a single reduction wave that yielded eight electrons per DNT molecule and produced no significant color changes. A possible explanation for these results is the formation of resonance-stabilized free-radical anions during the initial reduction wave for the *ortho* and *para* isomers.

The dependence of the polarographic behavior of DNT on isomeric composition has been noted [9]. A detailed study of the kinetic behavior of the different DNT isomers at the silver-wire electrode is currently in progress, and results will be published separately.

The authors thank Dr. Arnold T. Nielsen for helpful discussions of this work.

REFERENCES

1 D. G. Clark and M. H. Litchfield, Toxicol. Appl. Pharmacol., 15 (1969) 175.
2 R. D. Stewart, J. E. Peterson, P. E. Newton, C. L. Hake, M. H. Hosko, A. J. Lebrun and G. M. Lawton, Toxicol. Appl. Pharmacol., 30 (1974) 377.
3 M. E. Andersen and R. G. Mehl, J. Am. Ind. Hyg. Assoc., 34 (1973) 526.
4 F. Kaufman, J. H. Cook and S. M. Davis, J. Am. Chem. Soc., 74 (1952) 4997.
5 G. C. Whitnack, J. M. Nielsen and E. St. Clair Gantz, J. Am. Chem. Soc., 76 (1954) 4711.
6 A. R. Holland and A. G. S. Benham, Analyst, 93 (1968) 817.
7 G. C. Whitnack, Anal. Chem., 47 (1975) 618.
8 J. Pearson, Trans. Faraday Soc., 44 (1948) 683.
9 A. Tallec, Ann. Chim., 3 (1968) 155, 164, 347.
10 M. Heyrovsky, S. Vavricka and L. Holleck, Collect. Czech. Chem. Commun., 36 (1971) 971.
11 R. Ratan and M. Singh, Indian J. Chem., Sect. A, 18 (1979) 140.
12 V. M. Artemova and V. G. Govorukha, Electrokhimiya, 4 (1968) 246.
13 R. Chandra, P. N. Anantharaman and H. V. K. Udupa, J. Indian Chem. Soc., 53 (1976) 627.
14 J. Marquez and D. Fletcher, J. Appl. Electrochem., 10 (1980) 567.
15 M. H. Miles and D. A. Fine, J. Electroanal. Chem., 127 (1981) 143.
16 A. Navarro and C. Gutiérrez, J. Electroanal. Chem., 109 (1980) 361.
17 G. Valette and A. Hamelin, J. Electroanal. Chem., 45 (1973) 301.

Analytica Chimica Acta, 153 (1983) 149—159
Elsevier Science Publishers B.V., Amsterdam — Printed in The Netherlands

DESIGN AND CHARACTERIZATION OF AN ELECTROCHEMICAL RING-DISK FLOW-THROUGH DETECTOR FOR LIQUID CHROMATOGRAPHY

J. C. HOOGVLIET*, F. ELFERINK, C. J. VAN DER POEL and W. P. VAN BENNEKOM

Department of Pharmaceutical Analysis and Analytical Chemistry, Subfaculty of Pharmacy, State University, Gorlaeus Laboratories, Wassenaarseweg 76, 2333 AL Leiden (The Netherlands)

(Received 14th March 1983)

SUMMARY

An electrochemical flow-through detector of the confined wall-jet type with a ring-disk electrode pair opposite the auxiliary electrode is described. The detector has a geometric cell volume of 2—8 μl, dependent on the spacer thickness used and is suitable for application in high-performance liquid chromatography (h.p.l.c.). The disk and ring currents depend on volumetric flow rate (v), determined with hexacyanoferrate(II); currents are proportional to $v^{0.331}$ (disk) and $v^{0.280}$ (ring). Collection and shielding efficiency depends on cell geometry and flow rate. Collection efficiency lies in the range 20—65%, depending on electrode dimensions and spacer thickness, and becomes independent of flow rate at >0.25 ml min^{-1}. In a h.p.l.c. system, adrenaline is oxidized at the disk and the product is then reduced at the ring electrode. Calibration graphs are linear for the disk electrode (0.6—600 ng), and the ring electrode (6—600 ng).

Reduction of oxygen at the ring-disk detector is discussed for aqueous media of pH 10.0, 5.0 and 3.5 and in methanol. In methanol, the ring current is small; in all solutions, the ring current is at least 100 times less than the disk current caused by dissolved oxygen. In a h.p.l.c. system with methanol as eluent, vitamin K_1 is reduced at the disk with, and the product is oxidized at the ring without, interference from oxygen in the eluent. The calibration graph (ring, collection mode) is linear for 10—10000 ng.

Electrochemical detection has been used successfully in high-performance liquid chromatography (h.p.l.c.). Selectivity and the ability to obtain low detection limits are the major advantages. Recently, detectors with two working electrodes (dual or twin electrode cells) have received increased attention [1—5]. The advantages of these detectors lie mainly in their increased selectivity. Various applications are possible, dependent on the orientation of the two working electrodes with respect to each other. Three types have been described in the literature, all in a thin-layer cell configuration: two electrodes in series, parallel or opposite to each other.

Theoretically, wall-jet detectors have better signal-to-noise (S/N) ratios than have thin-layer detectors [6]. However, dual electrode detectors of the confined wall-jet type and applicable in h.p.l.c. have not yet been described. Two working electrodes in series can consist of a disk and concentric ring

0003-2670/83/$03.00

electrode. Hydrodynamics and mass transfer of a ring-disk flow-through cell of the free wall-jet type have been described by Do Duc [7] and Chin and Chandran [8]. These cells are not applicable as detectors in h.p.l.c.

In this paper, a new ring-disk electrochemical detector of the confined wall-jet type is described, in which the working and auxiliary electrodes are placed opposite each other. An important application of this detector could be the determination of compounds reducible at the disk with formation of a product oxidizable at the ring electrode, without the need to remove oxygen from eluent and sample solutions. Usually, the problems of a high background current and resulting baseline noise in reductive detection in h.p.l.c., caused by dissolved oxygen in the eluent, are solved by purging the eluent with oxygen-free nitrogen, helium or argon. Other ways to lower the background current are the use of an on-line electrochemical scrubber [10] or a differential detector [11].

In this study, characteristics concerning hydrodynamics, mass transfer, collection and shielding efficiency of the ring-disk detector are examined. In order to establish optimum conditions for the detection of reducible compounds, the reduction of oxygen was studied in aqueous and non-aqueous solutions. To assess determinations of electrochemically reducible and oxidizable substances, vitamin K_1 and adrenaline were used as test compounds.

EXPERIMENTAL

Electrochemical detector and instrumentation

The PB-2 detector, shown in Fig. 1, is of the confined wall-jet type. Both working electrodes (ring and disk) and the auxiliary electrode (AE) are made of glassy carbon (V10, Le Carbone-Lorraine, Paris, France) and sealed in glass. A home-made saturated calomel reference electrode (SCE) was used. The ring-disk and auxiliary electrodes are positioned, centered and opposite to each other, at a distance defined by the thickness of a three-point PVC spacer (typically 50 μm). In the centre of the auxiliary electrode (10-mm diameter), a hole is drilled, in which a PTFE capillary (300 μm i.d.) is mounted. The eluent impinges normally on the disk electrode and flows radially away between the sandwich, along the ring electrode (Fig. 2A). The electrodes are placed in a glass housing. An advantage of this design is the low uncompensated resistance (typically 10—20 ohm) and therefore the great linear dynamic range.

Two ring-disk electrodes were used (Fig. 2B). The dimensions were as follows: for RDE_1, r_1 = 3.0 mm, r_2 = 3.6 mm and r_3 = 4.4 mm; and for RDE_2, r_1 = 2.4 mm, r_2 = 2.8 mm and r_3 = 5.3 mm. Geometric cell volume was 2—8 μl, depending on the thickness of the spacer (25—100 μm).

A ring-disk potentiostat (Bruker E 350, Brussels, Belgium) was used to control the potentials of the ring and disk electrodes independently of each other. For continuous flow experiments, constant flow pumps (Labotron 13A, Gelting, G.F.R.) were used, allowing the adjustment of six fixed flow

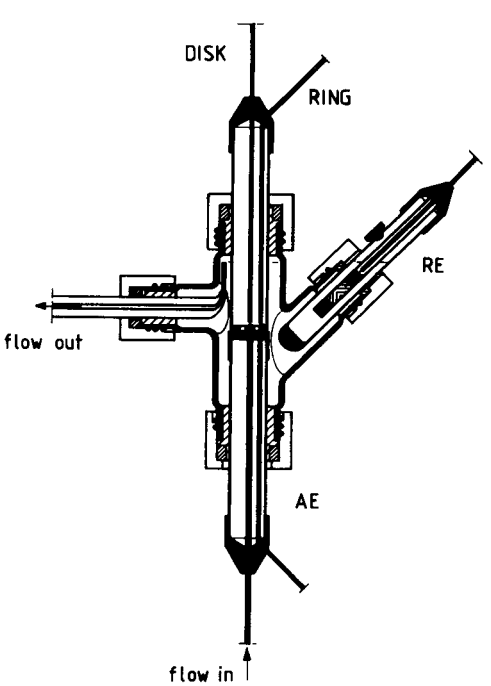

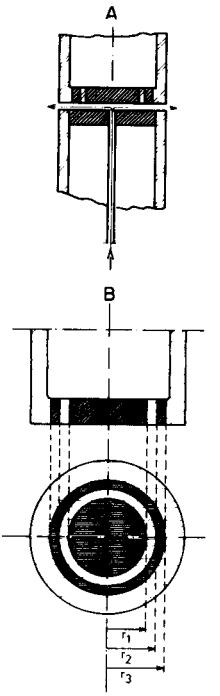

Fig. 1. The PB-2 detector, shown with a ring-disk electrode.

Fig. 2. (A) Schematic representation of the fluid flow in the PB-2 detector with a ring-disk electrode. (B) Cross section and frontview of a ring-disk electrode. For dimensions see text.

rates between 0.025 and 1.33 ml min^{-1}. The disk and ring currents were recorded simultaneously (Kipp BD 41 double-pen recorder, Delft, The Netherlands).

Before the experiments, the ring-disk electrodes were polished with 1-μm diamond spray. For measurements with hexacyanoferrate(II) and adrenaline, the electrodes were pretreated by scanning the potential from 0 to +1.5 V vs. SCE until a stable voltammogram was obtained. This pretreatment was not used for the experiments with vitamin K_1 in methanol, because no significant improvement in the *I/E* relationship could be obtained.

Chemicals

Demineralized water, additionally purified with a Millipore Milli-Q water purification system, was used. All solvents and chemicals were of analytical grade (Merck or Baker) and were used as received. Adrenaline hydrogen tartrate (Boehringer Ingelheim; B.P. 73, U.S.P. XIX) and vitamin K_1 (Merck; B.P. 73) were of pharmacopoeial quality. The oxygen reduction studies were done with an ammonia/ammonium chloride buffer pH 10.0 (4.5 M), an

ammonium acetate/hydrochloric acid buffer pH 3.5 (5.8 M) and an unbuffered 0.1 M KCl solution (pH 5.0).

Liquid chromatography

For measurements of adrenaline, a stainless steel column (100 × 2.8 mm i.d.) was packed with LiChrosorb RP-8 (5 μm; Merck) using the pressurized slurry method with tetrachloromethane as dispersing solvent and n-hexane as displacing solvent. The column was coated in situ with tri-n-butylphosphate (TBP). The eluent used was an aqueous 0.05 M phosphate/0.1 M perchloric acid solution, which was adjusted with sodium hydroxide to pH 3.5 and finally saturated with TBP [12].

For measurements of vitamin K_1, Zorbax C-8 (5 μm; Dupont) was used as stationary phase. The eluent was methanol with 0.05 M sodium perchlorate as supporting electrolyte, acidified with perchloric acid to an apparent pH of 1.5.

In both h.p.l.c. systems, an Orlita TW 1515 pump (Giessen, G.F.R.) and an injection valve with a fixed 20-μl loop (Rheodyne 70-10) were used. The eluents were thermostatted at 25°C.

RESULTS AND DISCUSSION

Hydrodynamics and mass transfer

The mass transfer characteristics of the disk and ring electrode (RDE_1) in the PB-2 detector were established for a spacer thickness of 50 μm. The limiting current of each electrode was measured as a function of the volumetric flow rate (v). The measurements for the disk and ring electrode were done independently of each other, i.e., in a three-electrode configuration. For these experiments, the continuous flow technique was used. A solution of 0.001 M potassium hexacyanoferrate(II) in 0.1 M KCl was pumped through the detector and the response at +0.8 V vs. SCE was recorded. This electrode reaction is fast and chemically reversible. From five $\log I$ vs. $\log v$ plots, slopes of 0.315, 0.330, 0.339, 0.336 and 0.336 were found for the disk electrode (standard error of slope 0.003, intercept 1.340 ± 0.002, standard error of estimate 0.004, correlation coefficient 0.9998, $n = 6$; all mean values of 5 lines). For the ring electrode, slopes of 0.280, 0.279, 0.277, 0.280 and 0.275 were measured (standard error of slope 0.003, intercept 1.230 ± 0.002, standard error of estimate 0.004, correlation coefficient 0.9998, $n = 6$; all mean values of 5 lines).

Theoretical studies of Van der Meer et al. [13] predict a linear relationship between the disk or ring current and the cubic root of the volumetric flow rate. This corresponds very well with the results obtained here for the disk. The discrepancy between the theoretical and experimental flow dependency of the ring current cannot be explained at present.

Collection and shielding efficiency

Rotating ring-disk electrodes can be characterized by their collection and the shielding efficiency. For the ring-disk detector, the collection and shielding efficiencies are defined by $N_d = (n_D/n_R)(|I_R|/|I_D|)$ and $S_d = I_{R,sh}/I_{R(0)}$; here I_D and I_R are the disk current and ring current, respectively, n_D and n_R are the numbers of electrons involved in the disk and ring electrode reactions, respectively, $I_{R,sh}$ is the shielded ring current and $I_{R(0)}$ is the ring current when the disk electrode circuit is open, i.e., $I_D = 0$. It is assumed that the ring and disk electrodes are at the same potential for shielding.

For the rotating ring-disk electrode (RRDE), both the collection and shielding efficiencies depend only on the geometry (the radii of disk and ring) of the RDE [14, 15]. For a stationary ring-disk electrode in the PB-2 detector, N_d and S_d, defined as above, depend on v and on the distance b between the ring-disk and the auxiliary electrode. The influence of the flow rate and b on collection and shielding efficiency was investigated by continuous flow experiments with 5×10^{-4} M potassium hexacyanoferrate(II) in 0.1 M KCl (Figs. 3, 4). At higher flow rates, both collection and shielding efficiency tend to become constant, caused by the predominant convective term. The large influence of the flow rate on the collection and shielding efficiencies at low flow rates can be explained by the relatively high contribution of diffusion of the reaction product formed at the disk to the ring signal, compared with convection. The ratio of the thickness of the hydrodynamic boundary layer to the diffusion boundary layer is altered by changing b. This causes a change in the ratio of convection of mass along the electrode surfaces to the diffusion of mass in the direction perpendicular to the surface.

At flow rates exceeding 0.25 ml min^{-1}, a constant fraction of the product formed at the disk reacts at the ring. This means that when the ring-disk detector is used in h.p.l.c., it can be assumed that the collection efficiency is independent of the flow rate and is a function only of the ring and disk radii and of b. As can be concluded from Fig. 3, a smaller distance between disk

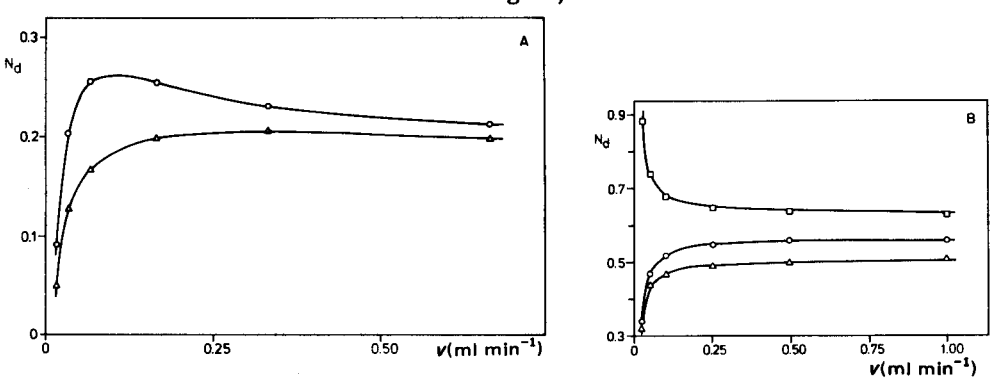

Fig. 3. Collection efficiency vs. flow rate for different spacer thicknesses. (A) RDE_1: (○) b = 50 μm; (△) 25 μm. (B) RDE_2: (□) b = 100 μm; (○) 50 μm; (△) 25 μm. Conditions: 5×10^{-4} M $K_4Fe(CN)_6$ in 0.1 M KCl, E_D = +0.8 V vs. SCE, E_R = −0.1 V vs. SCE.

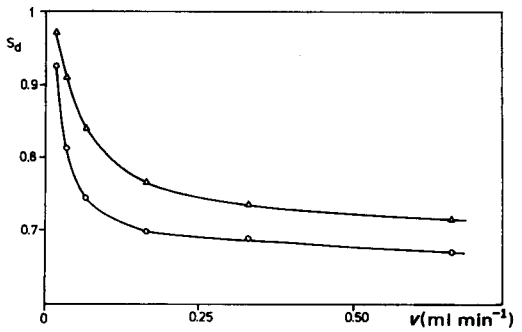

Fig. 4. Shielding efficiency vs. flow rate for two spacer thicknesses. RDE_1: (○) b = 50 μm; (△) 25 μm. Conditions: 5 × 10^{-4} M $K_4Fe(CN)_6$ in 0.1 M KCl, $E_D = E_R$ = +0.8 V vs. SCE.

and ring ($r_2 - r_1$) and a larger ring ($r_3 - r_2$) will give a better collection efficiency (the collection efficiency for RDE_1 is about 20%, whereas it is up to 65% for RDE_2), as will a greater value of b. Although high collection efficiencies can be obtained, its use as a detector in h.p.l.c. depends not only on the collection efficiency of the ring-disk detector (which determines its applicability) but particularly on the S/N ratio of the ring electrode; cell volume must also be considered. Studies with a computer simulation program are in progress to explain the effects of these various parameters and to optimize the geometry of the ring-disk detector.

Reduction of oxygen

To investigate the possibility of reductive detection with the ring-disk detector without the need to remove oxygen from eluent and sample, the reduction of oxygen was studied. Investigation of the reduction mechanism of oxygen is complicated by the fact that it is strongly dependent on the electrode material, pretreatment of the electrode and the kind of electrolyte solution used. Several different mechanisms have been proposed [16—19]. Like the rotating ring-disk electrode, the ring-disk detector can be a powerful tool for such investigations.

For these experiments, a continuous constant flow of solution was passed through the detector. All solutions were in equilibrium with air. The disk potential was scanned in the cathodic direction, and the ring potential was fixed at a positive potential. Figure 5 (a) shows the reduction of oxygen in alkaline solution (buffer pH 10.0) at the disk, while re-oxidation of a reduction product occurs at the ring. Two distinctly separated cathodic waves are observed at the disk. The increasing ring current is correlated with the first wave at the disk, the most likely explanation being formation of hydrogen peroxide at the disk and its oxidation at the ring. At more cathodic disk potentials, the ring current decreases, indicating that less peroxide is formed at the disk. At the same time, the disk current increases. Probably two reduction processes, the reduction of oxygen to hydrogen peroxide and the reduction

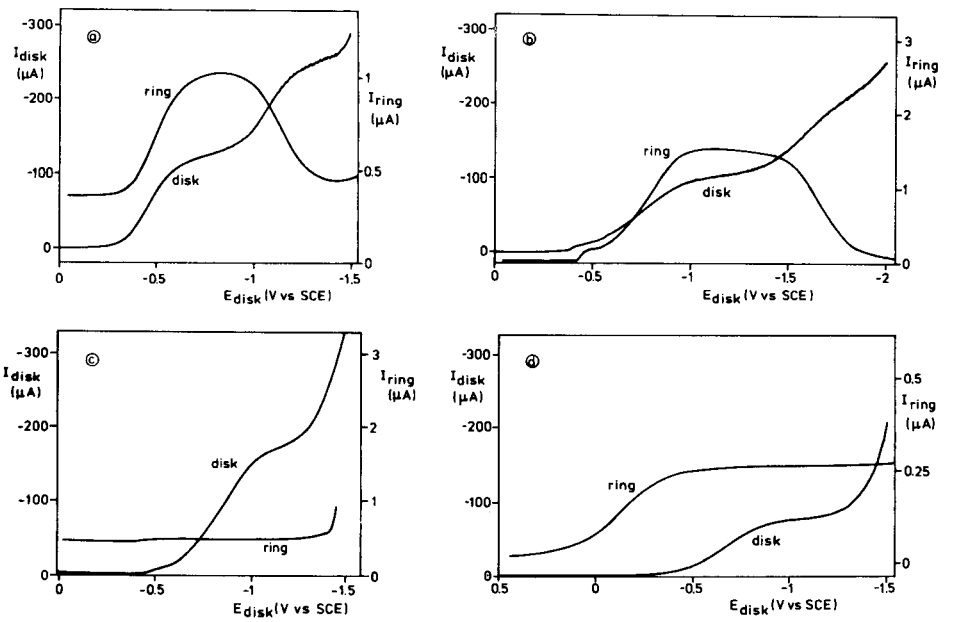

Fig. 5. Oxygen reduction in the ring-disk detector in various media in equilibrium with air (b = 50 μm). (a) RDE_1, buffer pH 10.0, E_R = +0.5 V vs. SCE, flow rate 0.5 ml min^{-1} and scan rate (disk) 10 mV s^{-1}. (b) RDE_1, 0.1 M KCl solution (pH 5.0), E_R = +0.5 V vs. SCE, flow rate 0.25 ml min^{-1}, scan rate (disk) 1 mV s^{-1}. (c) RDE_2, methanol eluent (apparent pH = 1.5), E_R = +0.8 V vs. SCE, flow rate 1.0 ml min^{-1}, scan rate 2 mV s^{-1}. (d) RDE_1, buffer pH 3.5, E_R = +0.5 V vs. SCE, flow rate 0.5 ml min^{-1}, scan rate (disk) 10 mV s^{-1}.

of hydrogen peroxide to hydroxide ions or water, take place consecutively, while reduction of oxygen to water is an important parallel reaction, accounting for the fact that the collection efficiency is very much lower than expected.

In an (unbuffered) solution of 0.1 M KCl (pH 5.0) a similar, although less pronounced, behaviour is shown and the waves shift to more cathodic potentials (Fig. 5b). In acidic solution (pH 3.5) no second wave is found at the disk and I_R does not decrease at more cathodic disk potentials (Fig. 5d). A different behaviour is found in non-aqueous solutions; in methanol eluent, only one wave is observed at the disk, which can be ascribed to reduction of oxygen, and the ring current does not increase until the disk potential becomes more negative than −1.5 V vs. SCE, i.e., no hydrogen peroxide is formed (Fig. 5c). In all these solutions, at disk potentials where oxygen is reduced, I_R is 100—300 times smaller than I_D.

Applications

If the ring-disk PB-2 detector is to be suitable for detection in h.p.l.c., there must be a linear relation between the ring current and the amount of sample injected. With a single working electrode, the PB-2 detector was

applied successfully for catecholamines [9]. Because adrenaline is electrochemically reversible under the conditions used:

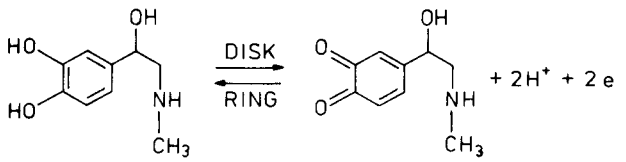

and because the ring potential can be set at a value where there is no interference from oxygen, this compound was chosen as a test compound to demonstrate the linearity of the ring-disk detector.

In continuous flow experiments, adrenaline hydrogentartrate solution in phosphate buffer pH 3.5 was pumped through the detector. The ring potential was scanned from —0.5 to +1.0 V vs. SCE, once with the disk potential circuit disconnected (Fig. 6, upper curve) and once with the disk potential at +0.75 V vs. SCE (Fig. 6, lower curve). Both collection and shielding effect are apparent. For detection of adrenaline in h.p.l.c., potentials of +0.75 V vs. SCE for the disk and of 0 V vs. SCE for the ring were chosen. Linear relationships were observed between the amount of adrenaline injected and the disk and ring currents (Table 1).

To study the applicability of the ring-disk detector for reducible substances, vitamin K_1 was examined as the test compound. Direct electrochemical detection is possible at negative potentials at glassy carbon, but reduction of oxygen interferes and causes a high background current. Without removing oxygen from the eluent, reductive detection of vitamin K_1 at the disk was not possible in amounts smaller than 400 ng. To test the electro-

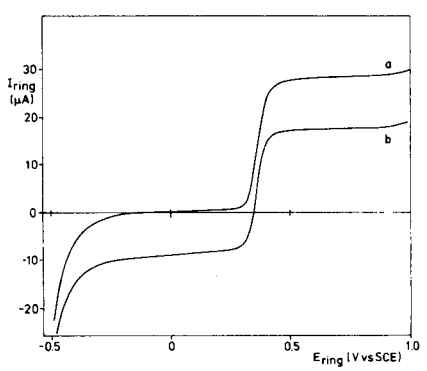

Fig. 6. The *I/E* relationship for 10^{-4} M adrenaline. Conditions: RDE_1, b = 50 μm, buffer pH 3.5, flow rate 0.7 ml min^{-1}. Potential of the ring electrode is scanned from —0.5 to +1.0 V vs. SCE (scan rate 1 mV s^{-1}) (a) with disk electrode circuit disconnected, and (b) with the disk electrode at +0.75 V vs. SCE.

TABLE 1

Calibration graphs recorded with the ring-disk electrochemical flow-through detector

				Slope	Intercept	Standard error of estimate	Correlation coefficient	n	Range (ng)
Adrenaline	Disk	RDE_1	log—log	1.004 ± 0.005	+0.923 ± 0.009	0.01	0.99992	7	0.6—600
			lin—lin	8.71 ± 0.01[a]	—6 ± 3[b]	6[b]	0.999995		
	Ring	RDE_1	log—log	1.023 ± 0.002	+0.264 ± 0.003	0.003	0.999995	5	6—600
			lin—lin	2.139 ± 0.005[a]	—4 ± 1[b]	2[b]	0.999992		
Vitamin K_1	Ring	RDE_2	log—log	0.96 ± 0.01	—0.94 ± 0.04	0.04	0.9995	7	10—10000
			lin—lin	0.079 ± 0.001[a]	+4 ± 5[b]	10[b]	0.9996		

[a] nA ng^{-1}. [b] nA.

chemical reversibility of the electrode reaction

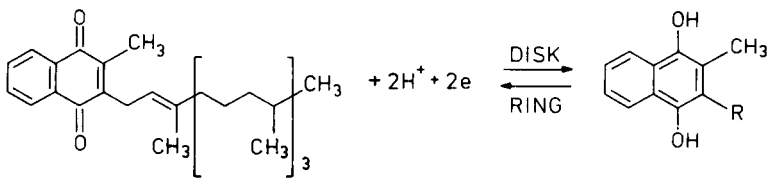

a hydrodynamic voltammogram of vitamin K_1 was constructed from recordings in methanol eluent from which dissolved oxygen had been removed by purging with nitrogen (Fig. 7). The optimum disk and ring potentials selected for the h.p.l.c. measurements were E_D = —0.5 V and E_R = +0.4 V vs. SCE. A typical example of the chromatograms obtained at disk and ring is shown in Fig. 8. These chromatograms were recorded without removal of oxygen from

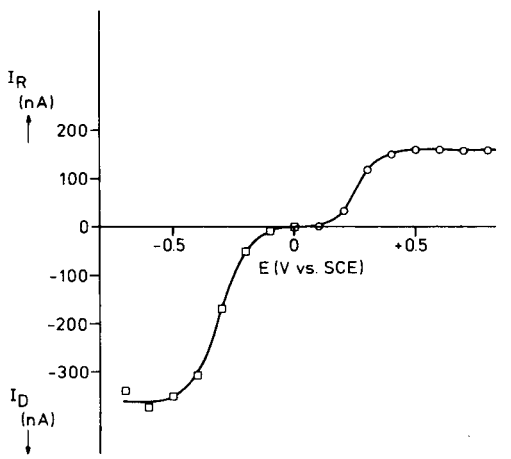

Fig. 7. Hydrodynamic voltammograms of vitamin K_1 (disk) and reduction product (ring), constructed from chromatograms. Conditions: RDE_2, b = 50 μm, flow rate 1.0 ml min^{-1}. (□) E_D from 0 to —0.6 V vs. SCE (in steps); (○) E_R from +0.1 to +0.8 V vs. SCE (in steps), with E_D = —0.6 V vs. SCE. About 2.5 μg vitamin K_1 was injected.

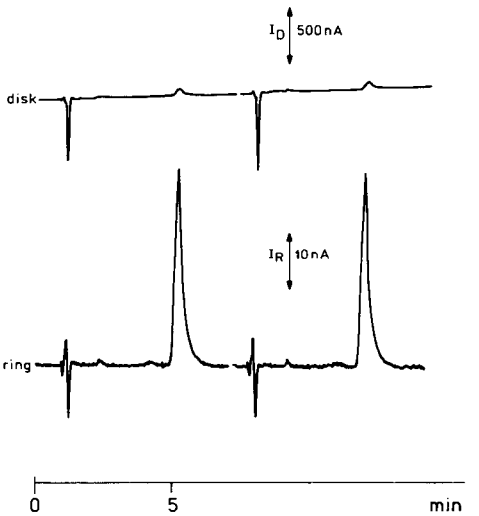

Fig. 8. Chromatograms of 412 ng of vitamin K_1. Conditions: RDE_2, b = 50 μm, E_D = −0.5 V vs. SCE, E_R = +0.4 V vs. SCE, flow rate 1.0 ml min^{-1}. Horizontal axis is the zero of both disk and ring signals; no time constant is used.

eluent or sample solutions. The calibration graph for the injected amount of vitamin K_1 is linear (Table 1). Preliminary measurements suggest a detection limit of about 5 ng for vitamin K_1, detected at the ring (S/N ratio is 3 times the standard deviation of the recorded noise). Other applications of the detector will be published in a later paper.

Conclusions

From the results obtained with hexacyanoferrate(II) as test substance, it can be concluded that the ring-disk detector described shows flow dependency of the disk ($v^{0.331}$) and ring ($v^{0.280}$) current, and of the collection (20—65%) and shielding efficiencies. At the usual flow rates in h.p.l.c. (v >0.25 ml min^{-1}) N_d is independent of v. The performance of the detector was tested in h.p.l.c. for adrenaline (oxidation/reduction) and vitamin K_1 (reduction/oxidation mode). In the latter mode, determinations were possible without removal of oxygen from eluent and sample. Calibration graphs were linear over the range 10—10000 ng.

The influence of dissolved oxygen, which was studied with the detector in aqueous and non-aqueous solutions, can be reduced greatly. The ring current is at least 100 times smaller than for an amperometric detector with a single electrode. Thus the dual detector offers better selectivity, and should also be useful for application in flow-injection analysis with reductive detection, and for studying reaction mechanisms and electrode kinetics.

The authors thank Mrs A. C. J. Hermans-Lokkerbol for the determinations of vitamin K_1, Mr J. A. G. van Bezooyen for skilful technical assistance in

the construction of electrodes, and Ir. Th. H. van der Meer for stimulating discussions on hydrodynamics.

REFERENCES

1 C. L. Blank, J. Chromatogr., 117 (1976) 35.
2 R. J. Fenn, S. Siggia and D. J. Curran, Anal. Chem., 50 (1978) 1067.
3 W. A. MacCrehan and R. A. Durst, Anal. Chem., 53 (1981) 1700.
4 D. A. Roston and P. T. Kissinger, Anal. Chem., 54 (1982) 429.
5 M. Goto, E. Sakurai and D. Ishii, J. Chromatogr., 238 (1982) 357.
6 H. B. Hanekamp and H. G. de Jong, Anal. Chim. Acta, 135 (1982) 351.
7 H. Do Duc, J. Appl. Electrochem., 10 (1980) 385.
8 D. T. Chin and R. R. Chandran, J. Electrochem. Soc., 128 (1981) 1904.
9 W. P. van Bennekom, Ph.D. Thesis, State University of Leiden, Leiden, The Netherlands, 1981.
10 H. B. Hanekamp, W. H. Voogt, P. Bos and R. W. Frei, Anal. Chim. Acta, 118 (1980) 81.
11 K. Brunt, C. H. P. Bruins and D. A. Doornbos, Anal. Chim. Acta, 125 (1981) 85.
12 H. J. L. Janssen, U. R. Tjaden, H. J. de Jong and K.-G. Wahlund, J. Chromatogr., 202 (1980) 223.
13 Th.H. van der Meer, W. P. van Bennekom and C. J. Hoogendoorn, Physicochemical Hydrodynamics, Europhys. Conf. Abstr., 3F (1980) 30g.
14 Y. B. Ivanov and V. G. Levich, Dokl. Akad. Nauk. SSSR, 126 (1959) 1029.
15 W. J. Albery and S. Bruckenstein, Trans. Faraday Soc., 62 (1966) 1920.
16 A. N. Frumkin, L. N. Nekrassov, V. G. Levich and Y. B. Ivanov, J. Electroanal. Chem., 1 (1959) 84.
17 M. Brezina, Z. Anal. Chem., 224 (1967) 74.
18 R. J. Taylor and A. A. Humffray, J. Electroanal. Chem., 64 (1975) 63, 85, 95.
19 P. Fischer and J. Heitbaum, J. Electroanal. Chem., 112 (1980) 231.

Analytica Chimica Acta, 153 (1983) 161—168
Elsevier Science Publishers B.V., Amsterdam — Printed in The Netherlands

CONSTRUCTION, CHARACTERISTICS AND APPLICATION OF A DICHLOROACETATE-SELECTIVE ELECTRODE IN THE DETERMINATION OF CHLORAMPHENICOL IN PHARMACEUTICALS

J. G. PENTARI and C. E. EFSTATHIOU*

University of Athens, Laboratory of Analytical Chemistry, 104 Solonos St., Athens 144 (Greece)

(Received 8th March 1983)

SUMMARY

A dichloroacetate-selective electrode with a liquid membrane of tetraoctylammonium dichloroacetate dissolved in *o*-nitrotoluene is described. The electrode exhibits near-Nernstian response to dichloroacetate activity from 0.01 to 2×10^{-5} M, in the pH range 3.5—10. A potentiometric determination of chloramphenicol in pharmaceutical preparations is reported; the dichloroacetate released from the antibiotic after alkaline hydrolysis at 30°C is measured directly. Chloramphenicol in the range 5—15 mg can be determined with an average error of about 2.1%. The results obtained for real samples compare favorably with those obtained by a polarographic procedure.

Many ion-selective electrodes of the liquid membrane type have been suggested, but not all of these provide acceptable sensitivity and selectivity for the ion of interest. Ion-sensitive liquid-membrane electrodes for anions of the lower aliphatic acids can be prepared by using heavily substituted quaternary ammonium as the counter-ion [1]. Unfortunately, the ion-pairs formed are rather unstable in the organic phase so that back-extraction to the aqueous phase is easy by exchange with other anions present in the sample solution. This means that such electrodes show limited ranges of linear response and moderate or poor selectivity. Halogenated aliphatic acids tend to form more stable ion-pairs. A trifluoroacetate-selective electrode has been prepared from the trifluoroacetate ion-pair with crystal violet dissolved in nitrobenzene [2].

This paper deals with the preparation of a dichloroacetate-selective electrode, in which a solution of tetraoctylammonium dichloroacetate in *o*-nitrotoluene serves as the ion-exchanger. Dichloroacetic acid is a fairly strong acid ($pK_a = 1.26$) and the broad-spectrum antibiotic chloramphenicol (I) appears to be its only naturally occurring derivative (amide). The possibility of developing a dichloroacetate-selective electrode that could be used in a potentiometric procedure for the determination of chloramphenicol was therefore studied. Such a method could be based on measurement of the dichloroacetate released by alkaline hydrolysis of the drug:

0003-2670/83/$03.00

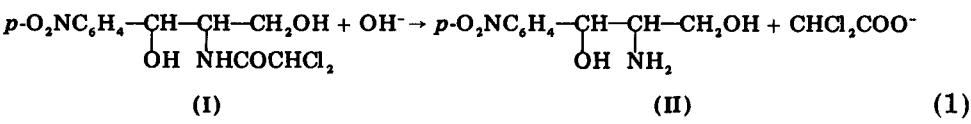

(I) (II) (1)

Chloramphenicol is usually determined either spectrophotometrically by direct measurements at 280 nm [3] or polarographically through the electroactive nitro group in the molecule [4]. An indirect potentiometric procedure can be based on the reduction of the nitro group with cadmium and measurement of the resulting cadmium ions with a cadmium(II)-selective electrode [5]. These procedures fail to differentiate between chloramphenicol and the free base of chloramphenicol (II).

The potentiometric procedure developed here allows the determination of $\geqslant 5$ mg of chloramphenicol in pharmaceuticals without any prior separation, with an average error of about 2.1%.

EXPERIMENTAL

Apparatus

The dichloroacetate-selective electrode was used with an Orion 90-01-00 Ag/AgCl single-junction reference electrode; its chamber was filled with a 0.1 M KCl solution saturated with silver chloride. Potentials were measured with an Orion Ion-Analyzer (Model 801 digital pH/pIon meter) and pH with a Metrohm pH meter (Model E350B). All solutions were measured at ambient temperature with constant magnetic stirring.

Reagents

All solutions were prepared with deionized distilled water from reagent-grade materials.

Standard 0.2000 M sodium dichloroacetate. Dissolve the necessary amount of dichloroacetic acid (Fluka; puriss. ~99%) in water to give a 0.3—0.4 M solution. Determine the exact titer of this solution by titration with 0.1000 M sodium hydroxide. Neutralize a suitable amount of the dichloroacetic acid solution and dilute to the necessary volume (solution A). Store this solution at 4°C when not in use. It is stable for at least three months; some molding may be observed thereafter.

Dichloroacetate liquid ion-exchanger. Dissolve 0.69 g of tetraoctylammonium bromide (Eastman Kodak) in 25 ml of *o*-nitrotoluene. Extract the resulting solution with three 25-ml portions of solution A to achieve complete replacement of bromide by dichloroacetate in the organic phase. Filter the organic layer through a filter paper containing 1—2 g of anhydrous sodium sulfate. The filtrate should be clear and light yellow. This solution is approximately 0.050 M in tetraoctylammonium dichloroacetate.

Procedures

Electrode preparation. An Orion liquid-membrane electrode barrel (Model 92) was used for electrode assembly with a porous membrane (Orion 92-07-

04). The internal reference solution was 0.010 M NaCl—0.010 M sodium dichloroacetate (saturated with silver chloride). After assembly of the electrode, the internal reference solution and the liquid ion-exchanger were injected into the appropriate ports. When not in use the electrode was kept immersed in a 10^{-2} M solution of sodium dichloroacetate.

Determination of calibration slope. Mark a suitable vessel at a volume of 20.0 ml. Add by pipet 5.00 ml of 0.10 M sodium hydroxide, followed by a drop of an ethanolic 0.1% (w/v) phenolphthalein solution. Add 0.70 M phosphoric acid until the solution is discolored. Dilute to the 20.0-ml mark with water (solution B). Pipet 15.00 ml of solution B into a 50-ml beaker. Immerse the electrodes in the solution, start stirring at a speed such that air bubbles are not formed, and add 40 μl of standard solution A. Read the e.m.f. to the nearest 0.05 mV by observing the relative appearance of the last digit (0.1 mV) of the Ion-Analyzer. Continue with four more increments of solution A (40, 80, 80, and 200 μl) and read the meter after each addition. Calculate the slope, S, of the graph of E (mV) vs. logarithm of dichloroacetate concentration. Repeat the measurements if the correlation coefficient is more than —0.999.

Determination of chloramphenicol in pharmaceuticals. Homogenize the samples (capsules or suppositories) if necessary. Use vessels calibrated at the 20.0-ml mark, with well-fitting stoppers. Weigh appropriate amounts of the homogenized samples (or 1.00 ml of the eye drops) containing 5—15 mg of chloramphenicol into the vessels. Pipet 5.00 ml of 0.100 M sodium hydroxide into each vessel, stopper tightly, shake and immerse in a water bath thermostated at 30 ± 1°C for 70—80 min with frequent shaking. Neutralize each solution with 0.70 M phosphoric acid as before. Dilute to 20.0 ml with water (solution C). Transfer 15.00 ml of solution C to the 50-ml beaker, immerse the electrodes in the solution, and record the corresponding potential, E_1. Add 50.0 μl of solution A and record the new potential, E_2. Calculate the amount of chloramphenicol in the weighed sample from the equation: chloramphenicol (mg) = $4.309/(1.0033 \times 10^{(E_1 - E_2)/S} - 1)$.

RESULTS AND DISCUSSION

Characteristics of the electrode

Effect of pH. To check the pH dependence of the potential of the dichloroacetate electrode, potential—pH curves at various dichloroacetate concentrations were constructed. The pH of the initial dichloroacetic acid solutions was altered by adding very small volumes of 5 M sodium hydroxide. The plots (Fig. 1) show that the potential is almost independent of pH in the range 4.0—10. The movement of the electrode response below pH 3.5 was inconsistent for the three concentration levels tested. Prolonged immersion of the electrode in alkaline solutions (pH >10) caused deterioration of its response, probably because the dichloroacetate anion was back-extracted to the aqueous phase substituted by hydroxide anion.

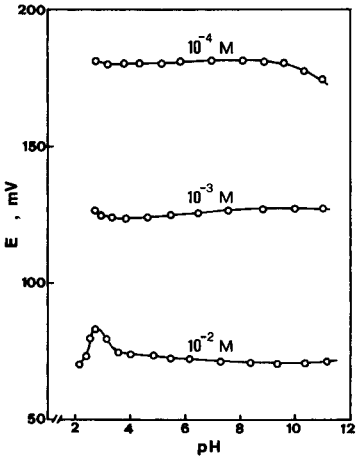

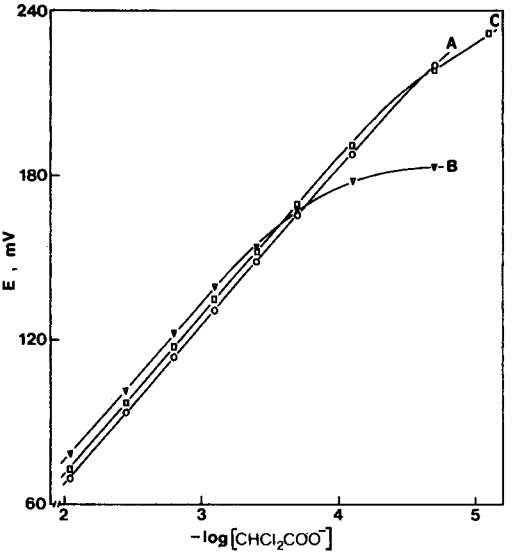

Fig. 1. Effect of pH on the potential of the dichloroacetate-selective electrode.

Fig. 2. Calibration plots for the dichloroacetate-selective electrode: (A) in pure sodium dichloroacetate solutions; (B) in a 0.03 M K_2CO_3—0.01 M $KHCO_3$ buffer solution (pH 10.5); (C) in aqueous 10% (v/v) propyleneglycol solution.

Linear response range. Typical calibration graphs for the electrode under different experimental conditions are shown in Fig. 2. The response is linear in the range 10^{-2}—2×10^{-5} M for pure dichloroacetate solutions (curve A). In the presence of a 0.03 M K_2CO_3—0.01 M $KHCO_3$ buffer solution (pH 10.5) (curve B), the linear range decreases because of electrode response to carbonate and hydrogencarbonate. The electrode can be used in aqueous 10% (v/v) propyleneglycol solution (a good solvent of chloramphenicol) with a slight decrease in the linear range (curve C).

Selectivity coefficients. The interference of various anions was studied by the mixed solution method and the corresponding potentiometric selectivity coefficients, $K^{pot}_{i,j}$, were calculated. The results are summarized in Table 1. The increased interference of acetate anions when hydrogen atoms of the methyl group are replaced by chlorine should be noted.

Response times. The electrode provides stable potential readings (±0.05 mV) within 30 s to 2 min, depending on the dichloroacetate concentrations, presence of interferences, pH, etc. Generally, fast response (less than 1 min) is observed when the electrode is used in the proposed phosphate buffer.

Stability of response. The electrode exhibited a day-to-day reproducibility within ±2 mV for dichloroacetate concentrations in the range 5×10^{-4}—2×10^{-2} M, actually used in the proposed application, provided that the electrode was not used under unfavorable extreme conditions, i.e., in highly acidic or alkaline solutions or in the presence of strong interferences. The

TABLE 1

Potentiometric selectivity coefficients for the dichloroacetate-selective electrode

Interfering anion, j	Conc. added (M)	$K_{i,j}^{pot}$ [a]	Interfering anion, j	Conc. added (M)	$K_{i,j}^{pot}$ [a]
CCl_3COO^-	1×10^{-4}	0.96	HPO_4^{2-}	1×10^{-2}	0.0087
CH_2ClCOO^-	1×10^{-3}	0.14	CH_3COO^-	1×10^{-2}	0.0072
Cl^-	1×10^{-2}	0.038	$(COO)_2^{2-}$	1×10^{-2}	0.0016
OH^-	2×10^{-3}	0.035	CO_3^{2-}	1×10^{-2}	0.0012
$HOCH_2COO^-$	1×10^{-2}	0.025	SO_4^{2-}	1×10^{-2}	0.0010
HCO_3^-	1×10^{-2}	0.012			

[a] i = dichloroacetate.

electrodes tested had an initial slope of 57.0—58.5 mV/concentration decade, depending on the solution used, and the presence of interferences and ageing (up to one month) had practically no effect on the slope value. Anyway, the slope should be determined before each series of measurements in order to obtain more accurate results.

The electrode should be refilled when the liquid ion-exchanger becomes exhausted or the supporting membrane has been damaged and stable potentials are no longer obtainable.

Stability of the dichloroacetate anion in alkaline solutions

The dichloroacetate anion is hydrolyzed in alkaline solutions at elevated temperatures yielding glyoxylate [6]. Glyoxylate may then undergo a Cannizzaro reaction, yielding glycolate and oxalate:

$$Cl_2CHCOO^- \underset{-2Cl^-}{\overset{2OH^-}{\longrightarrow}} (HO)_2CHCOO^- \rightleftharpoons CH(O)COO^- + H_2O \quad (2)$$

$$2CH(O)COO^- \xrightarrow{OH^-} HOCH_2COO^- + (COO)_2^{2-} \quad (3)$$

A thorough kinetic study of the alkaline hydrolysis of dichloroacetate has been published [7]. In the present work, an important point is the stability of dichloroacetate at the temperature and alkalinity used for the hydrolysis of chloramphenicol. When solutions of dichloroacetate (up to 0.02 M) in 0.1 M sodium hydroxide were examined, there was no decrease in the dichloroacetate activity after a 2-h reaction period at temperatures up to 70°C. With solutions of 0.02 M dichloroacetate in 0.1 M and 0.5 M sodium hydroxide at 90°C (±1°C), the dichloroacetate activity decreased by 2.7% and 7.5%, respectively, after a 1.5-h reaction period. These results agree well with those predicted from earlier data [7]. All measurements were made with the dichloroacetate-selective electrode in neutralized aliquots of the reacting mixtures.

Alkaline hydrolysis of chloramphenicol

The hydrolysis of chloramphenicol is a general acid/base-catalyzed reaction and the drug is highly unstable in alkaline media [8—10].

When known amounts of pure chloramphenicol (Fluka; pure >99%) were used, it proved impossible to obtain quantitative release of dichloroacetate by hydrolysis at elevated temperatures in 0.1 M sodium hydroxide. Decreasing the temperature to 30°C gave almost quantitative release of dichloroacetate. Figure 3 shows the percentage release of dichloroacetate as a function of reaction time at 30, 50 and 70°C.

Dichloroacetate proved to be stable under these conditions, therefore its reduced release from chloramphenicol has to be explained. One plausible explanation may be that, as the uncharged chloramphenicol molecule does not repulse the hydroxide ion, the latter may attack the dichloromethyl group more easily in the drug than it does in the free dichloroacetate. Another possible explanation is the partial formation of a lactam ring by self-condensation of chloramphenicol, which resists further hydroxide attack. It appears that the activation energies of the competing reactions differ so much that lower temperatures favor only hydrolysis of the amide link.

Treatment of the samples and results

The proposed treatment of samples releases dichloroacetate almost quantitatively from chloramphenicol. Erratic results were obtained when the electrodes were immersed directly in the alkaline hydrolysate, therefore the neutralization step with phosphoric acid was necessary. Problems arising from variations of ionic strength and the presence of various excipients (such as the polyethylene glycols) were overcome by using the standard addition technique instead of a calibration graph.

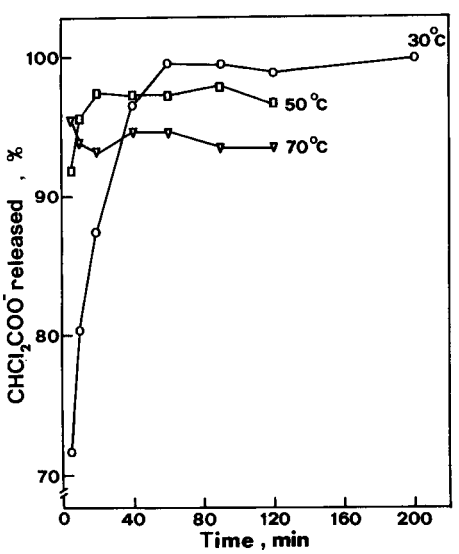

Fig. 3. Percentage release of dichloroacetate during alkaline hydrolysis of chloramphenicol (in 0.10 M NaOH) at three different temperatures.

TABLE 2

Potentiometric determination of pure chloramphenicol

Amount of chloramphenicol (mg)		Error (%)	Amount of chloramphenicol (mg)		Error (%)
Taken	Found		Taken	Found	
5.24	5.39	2.9	9.60	9.65	0.5
6.33	6.40	1.1	10.1	10.5	−4.0
7.01	7.05	0.6	12.2	11.7	−4.1
7.73	7.68	−0.6	13.9	13.5	−2.9
					Av. 2.1

TABLE 3

Determination of chloramphenicol in pharmaceutical products

Sample	Chloramphenicol found	
	Present method (N = 5)	Polarographic method (N = 3)[a]
Capsules ($\bar{w}$ = 0.3513 g)	239 ± 3 mg/cap.	233 ± 11 mg/cap.
Suppositories ($\bar{w}$ = 6.113 g)	250 ± 8 mg/sup.	256 ± 12 mg/sup.
Eye drops	6.50 ± 0.03 mg ml^{-1}	6.61 ± 0.27 mg ml^{-1}

[a]Measurements in 0.70 M acetate buffer, pH 4.7, using the (single) standard addition technique.

Results for the determination of pure chloramphenicol samples (weighed to the nearest 0.01 mg) are shown in Table 2. The average error found was about 2.1%. Chloramphenicol was also determined in capsules, suppositories and eye drops by the proposed method and the polarographic method. The results obtained (Table 3) agree well. The accuracy of the proposed method was further checked by means of recovery experiments with the capsules. The average recovery found was 104% (range 96—110%).

Conclusions

The potentiometric method for the determination of chloramphenicol eliminates prior separation steps and may be applied directly to colored and turbid solutions. The selectivity and sensitivity of the dichloroacetate-selective electrode are sufficient for the determination of chloramphenicol in pharmaceuticals. The accuracy of the method is typical of most direct potentiometric techniques.

The dichloroacetate electrode should be useful in determining the degree of decomposition of various pharmaceuticals containing chloramphenicol, by direct measurement of the liberated dichloroacetate. Hitherto, these determinations have been based on spectrophotometric determination of

free chloramphenicol base after tedious chromatographic separations from the parent compound.

The possibility of obtaining kinetic data on the hydrolysis of chloramphenicol under a variety of conditions, and for other compounds containing the dichloroacetate group, is under investigation.

REFERENCES

1 C. J. Coetzee and H. Freiser, Anal. Chem., 41 (1969) 1128.
2 N. Ishibashi and A. Jyo, Microchem. J., 18 (1973) 220.
3 See, e.g., R. C. Shah, P. V. Raman and B. M. Shah, J. Pharm. Sci., 52 (1963) 167.
4 K. Fossdal and E. Jacobsen, Anal. Chim. Acta, 56 (1971) 530.
5 S. S. M. Hassan and M. H. Eldesouki, Talanta, 26 (1979) 531.
6 E. Larsson, Trans. Chalmers Univ. Technol. Gothenburg, Swed., 51 (1946) 3.
7 H. Dautzenberg and B. Philipp, Z. Phys. Chem., Leipzig, 260 (1979) 298.
8 T. Higuchi, A. D. Marcus and C. D. Bias, J. Am. Pharm. Assoc., Sci. Ed., 43 (1954) 129.
9 T. Higuchi and A. D. Marcus, J. Am. Pharm. Assoc., Sci. Ed., 43 (1954) 530.
10 K. A. Connors, G. L. Amidon and L. Kennon, Chemical Stability of Pharmaceuticals, Wiley, New York, 1979, p. 201.

Analytica Chimica Acta, 153 (1983) 169—174
Elsevier Science Publishers B.V., Amsterdam — Printed in The Netherlands

FLOW INJECTION ANALYSIS FOR CHOLINESTERASE IN BLOOD SERUM BY USE OF A CHOLINE-SENSITIVE ELECTRODE AS AN AMPEROMETRIC DETECTOR

TOSHIO YAO

Department of Applied Chemistry, College of Engineering, University of Osaka Prefecture, Mozu-Umemachi, Sakai, Osaka 591 (Japan)

(Received 18th November 1982)

SUMMARY

A platinum electrode chemically modified with choline oxidase is used as an electrochemical detector for cholinesterase. The flow injection system for the determination of cholinesterase in blood serum comprises a copper(II) dithiocarbamate-modified silica gel column for removing interfering substances, a mixing coil to allow hydrolysis of acetylcholine chloride in phosphate buffer at pH 7.5 in the carrier stream, and the choline-sensitive electrode in a flow cell. The peak current caused by the hydrogen peroxide produced is linearly related to the cholinesterase activity in the range 2.5×10^{-4}—0.1 IU; 40 samples per hour can be processed with a r.s.d. below 2% without interference. The electrode is stable for about two months.

Immobilized enzyme electrodes that are highly selective for a wide variety of substrates are now widely used. Most electrodes are formed by holding a thin enzyme layer over an electrode with some type of membrane [1]. There remains, however, a need to develop enzyme membranes which have a rapid response and long-term stability. The preparation of a chemically modified enzyme membrane electrode (c.m.e.) which has a fairly rapid response, long-term stability and good reproducibility as an amperometric glucose sensor has recently been described [2]. This c.m.e. was also used as an electrochemical detector in a flow injection system [3].

Cholinesterase in serum is an important indicator of liver disease [4]. Some enzymatic methods, based on spectrophotometric [5], potentiometric [6] and amperometric [7] measurements, have been proposed for its determination. In this paper, a choline-sensitive c.m.e. which has a rapid response for choline is used as the electrochemical detector in a flow injection system for the determination of cholinesterase in serum. Injected cholinesterase hydrolyzes acetylcholine to choline in the flow stream and choline is oxidized in the immobilized choline oxidase layer, producing hydrogen peroxide.

0003-2670/83/$03.00

EXPERIMENTAL

Reagents

Choline oxidase (EC 1.1.3.17, 12.7 IU mg^{-1}, from *Alcaligenes sp.*; Toyobo Co.) was used. Bovine serum albumin (BSA; 96—99% albumin), glutaraldehyde, and 3-aminopropyltriethoxysilane were as described previously. Control human serum (ORTHO Control Serum; Ortho Diagnostic Systems) was used as the standard for cholinesterase (1038 IU l^{-1}). Choline chloride, acetylcholine chloride and the other reagents (analytical-reagent grade; Wako Pure Chemical Co.) were used as received.

Preparation of flow-type choline-sensitive c.m.e.

The method was similar to that described previously [2]. A platinum sheet (1 cm × 2 cm, 0.1 mm thick) was anodized, refluxed for 5 h with 3-aminopropyltriethoxysilane in toluene, and rinsed as before. On one side of the resulting alkylamino-bonded platinum sheet, a 6-μl aliquot of aqueous 20% (w/v) BSA and an 8-μl aliquot of 4% (w/v) choline oxidase solution in 0.1 M phosphate buffer at pH 8.0, were mixed with 4 μl of aqueous 4% (v/v) glutaraldehyde solution; mixing was done rapidly with a fine glass rod. The membrane was left open to air overnight. The resulting enzyme membrane was covalently bonded to some part of the platinum surface [2].

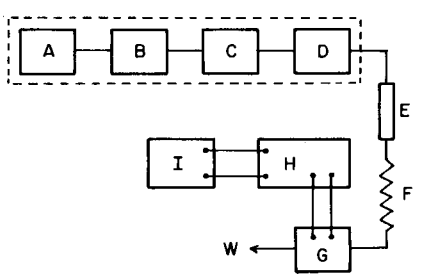

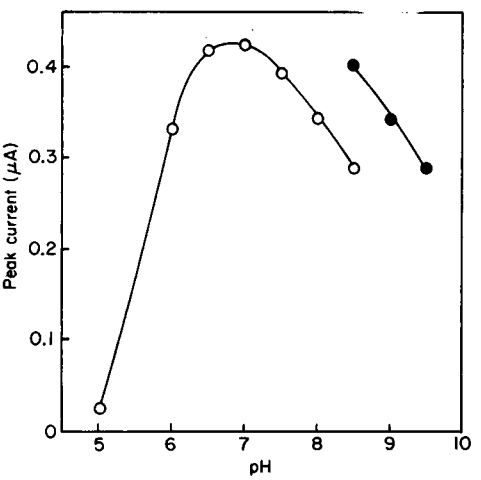

Fig. 1. Block diagram of flow system. The boxed parts are a Yanagimoto L-2000 performance liquid chromatograph. A, Carrier reservoir; B, pump; C, damper; D, sample injector; E, precolumn (5 cm × 4 mm i.d.) packed with copper(II) dithiocarbamate-modified silica gel; F, mixing coil (0.5 mm i.d., 2.00 m); G, choline-sensitive electrode; H, potentiostat; I, recorder; W, waste.

Fig. 2. Effect of pH of the carrier solution on the peak current for choline. (○) 0.1 M phosphate buffers; (●) 0.1 M pyrophosphate buffers. Conditions: flow rate 2.9 ml min^{-1}; applied potential 0.8 V; 5-μl injections of 7.2 mM choline chloride.

The amperometric flow cell was assembled as described before [3] with the choline oxidase-BSA membrane attached to the platinum sheet over the graphite anode.

Flow system and procedures

The flow system is shown schematically in Fig. 1. The flow-type choline-sensitive c.m.e. was inserted as shown. A constant potential (0.8 V) was applied with a Yanagimoto potentiostat (VMD-101) and current was measured with a strip-chart recorder (Hitachi 056-3001). Carrier solution (0.1 M phosphate buffer at pH 7.5 containing 1.0 mM acetylcholine chloride) from the reservoir was pumped at a flow rate of 0.9 ml min^{-1} to the injection valve, equipped with a 100-μl sample loop, and thence to the stainless steel column (5 cm × 4 mm i.d.) packed with copper(II) dithiocarbamate-modified silica gel to remove the interfering substances in sera [3]. A teflon mixing coil (0.5 mm i.d., 2.00 m) was placed between the column and the flow electrode to provide suitable dispersion of the sample zone. This was necessary so that the injected cholinesterase had time to hydrolyze the acetylcholine to choline. Enzymatic oxidation of the choline proceeded in the immobilized choline oxidase layer, and the hydrogen peroxide produced was monitored amperometrically.

RESULTS AND DISCUSSION

Response of the electrode to choline

The above determination of cholinesterase is based on monitoring choline, thus the response of the electrode to choline (as chloride) was first examined in the flow system without the mixing coil. Phosphate and pyrophosphate buffers (0.1 M) at various pH values were used as the carrier solution. Figure 2 shows the effect of pH on the peak current; maximum response was obtained at about pH 7. The effects of flow rate on the peak current and on the peak width (at half-height of the signal) are shown in Fig. 3. As the flow rate increased, the peak current decreased, but the decrease was slight at higher flow rates. Maximum sensitivity was obtained at applied potentials above 0.8 V, and so this potential was applied to the flow electrode for hydrogen peroxide monitoring.

A linear calibration graph was obtained over a wide concentration range (0.07—70 mM) for 5-μl injections; slope, y-intercept and linear correlation coefficient were 75.6 nA mM^{-1}, —2.79 nA and 0.9997, respectively. The minimum concentration of choline which could be determined was ca. 15 μM ($S:N = 2$). Reproducibility was tested by repeated 5-μl injections of 0.36, 1.8 and 7.2 mM choline chloride solutions; the relative standard deviations for sets of 10 injections were 2.8, 1.6 and 1.2%, respectively.

Optimization of experimental conditions for the cholinesterase determination

In the mixing coil, acetylcholine in the carrier solution is hydrolyzed to choline by the enzymatic action of cholinesterase. Therefore, experiments

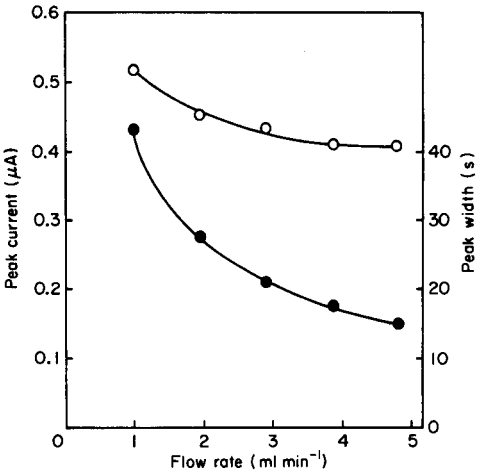

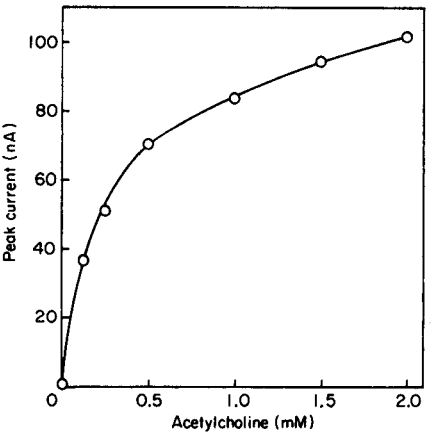

Fig. 3. Effect of flow rate on the peak current (○) and the peak width at half-height (●). Conditions as in Fig. 2 except for pH (0.1 M phosphate buffer at pH 7.5) and flow rate.

Fig. 4. Effect of acetylcholine concentration in carrier solution (0.1 M phosphate buffer at pH 7.5) on the peak current. Conditions: mixing coil length 1.00 m; flow rate 0.9 ml min^{-1}; applied potential 0.8 V; 5-μl injections of ORTHO control serum (5.19×10^{-3} IU cholinesterase).

were conducted to establish the optimum acetylcholine concentration, pH, coil length and flow rate for the determination of cholinesterase. Figure 4 shows the effect of the acetylcholine concentration on the peak current. As the acetylcholine concentration in the carrier solution was increased, the peak current increased, but the increase was slight at higher concentrations, whereas the background current became large, probably because choline was present as an impurity in acetylcholine. Figure 5 evaluates the effect of pH of the carrier stream in terms of peak current; maximum response was obtained at pH 8.1. At pH values above 8, however, the background current became progressively larger with increase in pH, probably because of non-enzymatic hydrolysis of acetylcholine. Therefore, 0.1 M phosphate buffer at pH 7.5 containing 1.0 mM acetylcholine was selected as the carrier solution in this work.

An investigation of the effect of the length of the mixing coil (0.5 mm i.d.) between the copper(II) dithiocarbamate column and the flow electrode (Fig. 6) showed that both peak current and peak width increased with increasing coil length, but the increase was slight at longer lengths. Therefore, a mixing coil 2.00 m in length was selected in order to obtain a reasonable sampling rate. Figure 7 shows the effect of the flow rate on the signal peak. As the peak current decreased sharply with increasing flow rate, 0.9 ml min^{-1} is recommended as the most suitable flow rate for achieving good sensitivity and a reasonable sample throughput.

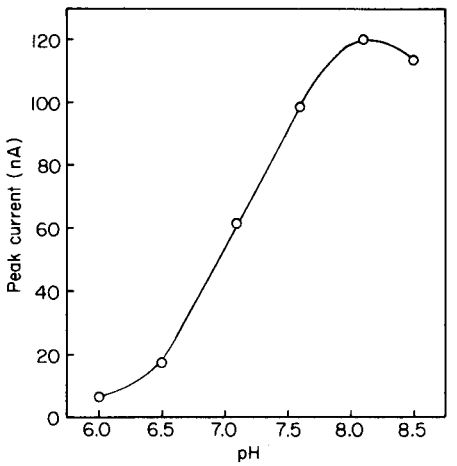

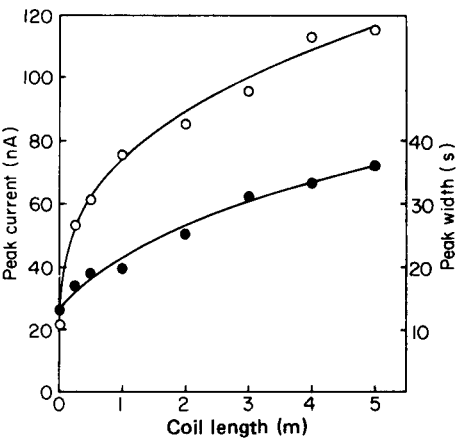

Fig. 5. Effect of pH of the carrier solution on the peak current for cholinesterase. Conditions as in Fig. 4 except for acetylcholine concentration (1.0 mM) and pH of carrier solution.

Fig. 6. Effect of the length of mixing coil on the peak current (○) and the peak width at half-height (●). Conditions as in Fig. 4 except for acetylcholine concentration (1.0 mM) and coil (0.5 mm i.d.) length.

Calibration graph for cholinesterase, interferences and reproducibility

Typical signal peaks at two different activities of cholinesterase injected are shown in Fig. 8. The peak current increased with increasing activity of cholinesterase and one sample could be determined in ca. 1.5 min. Linear calibration graphs were obtained over the range of 2.5×10^{-4}—0.1 IU cholinesterase; the slope, y-intercept and linear correlation coefficient were 1.63×10^{4} nA IU^{-1}, '—0.610 nA and 0.9995, respectively. The activity of cholinesterase in human serum is about 1—4 IU ml^{-1}, so that 5 μl of serum contains $(0.5—2) \times 10^{-2}$ IU cholinesterase, well within the linear range of the calibration graph. The detection limit of the method is 4×10^{-5} IU ($S:N = 2$).

Electroactive species such as ascorbate, urate, tyrosine, cysteine, glutathione and bilirubin are usually present in human sera and are oxidized at the same potential as hydrogen peroxide. However, most of these substances could be eliminated [3] by introducing the copper(II) dithiocarbamate-modified silica gel column just before the mixing coil and did not interfere with the measurement of cholinesterase activity.

Reproducibility was tested by repeated 25-μl injections of an ORTHO control serum (2.6×10^{-2} IU cholinesterase) at an injection rate of 40 samples per hour. The relative standard deviation was 1.80%.

The electrode was used repeatedly to confirm its stability over a long period. A slight increase in response was observed over the first 2 or 3 days. This behavior has been observed in the past [8] with enzyme electrodes and may be mainly attributed to the establishment of diffusion channels in the

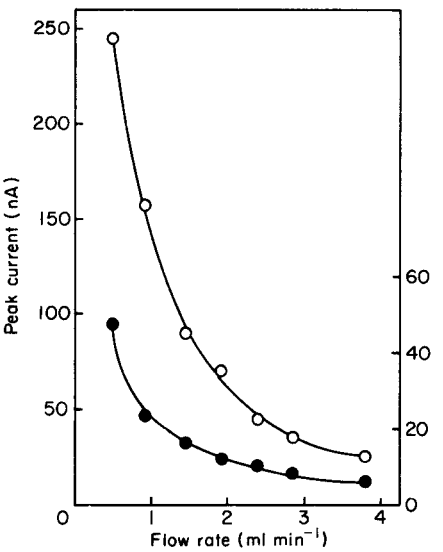

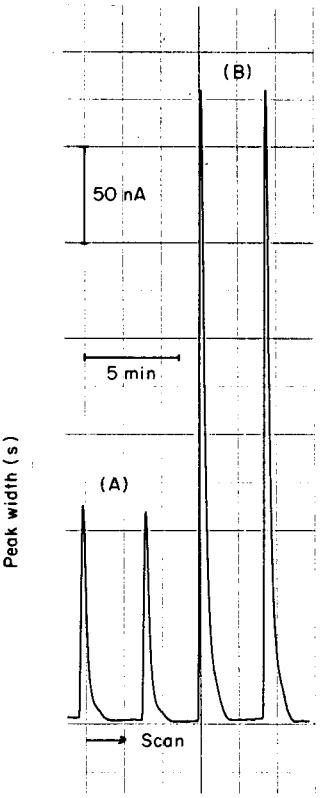

Fig. 7. Effect of flow rate on the peak current (○) and the peak width at half height (●). Conditions: coil length 2.00 m; 0.1 M phosphate buffer pH 7.5 containing 1.0 mM acetylcholine as carrier; applied potential 0.8 V; 10-μl injections of ORTHO control serum (1.04×10^{-2} IU cholinesterase).

Fig. 8. Typical signal peaks: (A) 5.19×10^{-3} IU; (B) 1.56×10^{-2} IU cholinesterase in serum.

membrane. However, the stability of the electrode was high and even after repetitive use for two months the electrode retained 95% of its original activity when it was stored in the recommended carrier solution while not in use.

The author thanks Mr. Minoru Sato for his help in the experimental work.

REFERENCES

1 M. Koyama, Y. Sato, M. Aizawa and S. Suzuki, Anal. Chim. Acta, 116 (1980) 307.
2 T. Yao, Anal. Chim. Acta, 148 (1983) 27.
3 T. Yao, Anal. Chim. Acta, (1983) in press.
4 V. Fintelmann and H. Linder, Dtsch. Med. Wochenschr., 95 (1970) 469.
5 H. Okabe, K. Sagehara, N. Nakajima and A. Noma, Clin. Chim. Acta, 80 (1977) 87.
6 K. Gibson and G. G. Guilbault, Anal. Chim. Acta, 76 (1975) 245.
7 F. Mizutani and K. Tsuda, Anal. Chim. Acta, 139 (1982) 359.
8 G. G. Guilbault and G. J. Lubrano, Anal. Chim. Acta, 64 (1973) 439.

Analytica Chimica Acta, 153 (1983) 175—180
Elsevier Science Publishers B.V., Amsterdam — Printed in The Netherlands

AMPEROMETRIC DETERMINATION OF GLUCOSE IN BLOOD SERUM WITH A CHEMICALLY MODIFIED ENZYME MEMBRANE ELECTRODE IN A CONTINUOUS FLOW SYSTEM

TOSHIO YAO

Department of Applied Chemistry, College of Engineering, University of Osaka Prefecture, Mozu-Umemachi, Sakai, Osaka 591 (Japan)

(Received 18th November 1982)

SUMMARY

Glucose oxidase cross-linked with bovine serum albumin and chemically immobilized on silanized platinum is used as the electrochemical detector for glucose in a continuous flow system. The peak current is linearly related to the glucose concentration in the range 1—800 mg dl^{-1}, for injections of 5-μl samples. Glucose in blood serum can be determined at 100 samples per hour with satisfactory precision (1% r.s.d.); interferences are removed with a precolumn containing copper(II) diethyldithiocarbamate-modified silica gel. The flow sensor retains most of its original activity after repetitive use for two months.

Most enzyme electrodes have generally been formed by immobilizing a thin layer of enzyme over an electrode with some type of membrane [1—6]. Recently, a chemically modified enzyme electrode (c.m.e.) has been reported as an amperometric glucose sensor [7]. This c.m.e. was constructed by cross-linking glucose oxidase with bovine serum albumin (BSA) using glutaraldehyde on a platinum sheet silanized with 3-aminopropyltriethoxysilane. The characteristics of the c.m.e. were response within 10 s, long-term stability and high reproducibility.

In this paper, a flow-type c.m.e. based on this principle is proposed as an electrochemical detector in flow injection and applied to the specific determination of glucose in human serum.

EXPERIMENTAL

Reagents

Glucose oxidase (EC.1.1.3.4., 43.4 IU mg^{-1}, from *Aspergillus niger*; Amano Pharmaceutical Co.) was used. The BSA powder was 96—99% albumin (Sigma Chemical Co.; fraction V), glutaraldehyde was an aqueous 20% solution (Wako Pure Chemical Co.), and 3-aminopropyltriethoxysilane and *N*-(2-aminoethyl)-3-aminopropyltrimethoxysilane was obtained from Tokyo Kasei Kogyo Co. Control human serum (ORTHO Control Serum; Ortho

0003-2670/83/$03.00

Diagnostic Systems Inc.) was used as a standard. All other chemicals were of analytical reagent grade. Aqueous stock solution (1000 mg dl^{-1}) of D-glucose was allowed to mutarotate overnight before use. All dilutions were made in the appropriate buffers.

Immobilization of the glucose oxidase—BSA membrane on a platinum sheet. A platinum sheet (1 cm × 2 cm, 0.1 mm thick) was prepared for modification and silanized as described previously [7]. On one side only of this alkylamino-bonded platinum sheet, a 6-μl aliquot of aqueous 20% (w/v) BSA solution and an 8-μl aliquot of 4% (w/v) glucose oxidase solution (pH 5.5, acetate buffer) were spread and 4 μl of aqueous 2% (v/v) glutaraldehyde solution was added. The solutions were mixed rapidly with a glass capillary rod. The membrane was allowed to form overnight at room temperature open to air. In this way, glucose oxidase cross-linked with BSA is fixed with glutaraldehyde on the alkylamino-bonded platinum by covalent binding [7].

Construction of the amperometric flow glucose sensor

The amperometric flow cell is shown in Fig. 1. The body consisted of two acrylic plates (5 cm × 3 cm, 5 mm thick). A 0.62-cm diameter hole was machined in the center of each plate to contain the graphite rods which were sealed in with a non-conducting epoxy cement. The solution inlet and outlet holes were drilled to accept teflon tubing (0.5 mm i.d., 1.5 mm o.d.) which was press fitted and sealed with epoxy cement. One of the graphite disks was covered with the enzyme-modified platinum sheet. A channel cut in the spacer extended from the inlet hole to the outlet hole; this resulted in a working volume of about 12 μl.

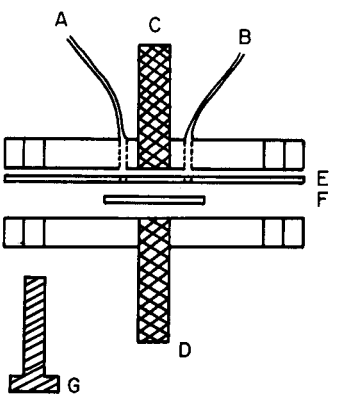

Fig. 1. Amperometric flow sensor. A, Solution inlet; B, solution outlet; C, graphite rod (cathode); D, graphite rod (anode); E, spacer; F, enzyme-modified platinum sheet; G, assembly screw.

Flow system and procedure for glucose determination

The amperometric flow glucose sensor was inserted into the flow line of a continuous flow system. The carrier reservoir, pump, pulse damper and sample injector (100-μl sample loop) formed part of a Yanagimoto L-2000 liquid chromatograph. Constant potential (0.8 V) was applied with a Yanagimoto potentiostat (VMD-101) and current was measured with a strip-chart recorder (Hitachi 056-3001). A phosphate buffer (0.1 M, pH 7.5) served as carrier solution at 2.9 ml min^{-1}. A stainless steel precolumn (5 cm × 4 mm i.d.) packed with copper(II) dithiocarbamate-modified silica gel [8] was positioned just before the amperometric flow cell to remove the interfering substances in sera. Sample solutions were injected in the usual way and glucose was estimated from the current peak height. A calibration graph was prepared from the results obtained with standard glucose solutions.

RESULTS AND DISCUSSION

Optimization of experimental conditions

Experiments were conducted to establish the optimum pH, under flow conditions, for the determination of glucose. Phosphate buffers (0.1 M) at various pH values were used as the carrier solution; a maximum response was obtained at a pH close to 7.5. Therefore, subsequent work was done at this pH because the pH of serum is about this value.

Figure 2 shows the effect of the buffer flow rate on the peak current and on the peak width (t_{rb} = time to return to baseline). As the peak current increased with a decrease in the flow rate, 2.9 ml min^{-1} is recommended as a suitable flow rate for achieving relative good sensitivity and a reasonable sample throughput (about 100 determinations per hour under these conditions).

The optimum applied potential for the flow sensor was determined by 10-μl injections of a 100 mg dl^{-1} glucose solution. A plateau region was obtained at applied potentials above 0.8 V, and so this potential was applied for hydrogen peroxide monitoring.

Linear calibration range

Figure 3 is a typical recording for injections of five standards, followed by two sera and repeated calibration. Reproducibility is good and there is no carry-over from high to low concentrations. The calibration graph was linear over the range 0.04—40 mg dl^{-1} for 100-μl injections, but the range was 1—800 mg dl^{-1} for 5-μl injections. Slope, y-intercept, and linear correlation coefficient were 2.596 nA(mg dl^{-1})$^{-1}$, 0.268 nA, and 0.9999, respectively, for 5-μl injections. The normal concentration of glucose in human blood serum ranges between 50 and 100 mg dl^{-1}, well within the range of this calibration graph, although diabetic sera contain glucose at higher concentrations. The lowest glucose concentration which could be detected by the present method was 0.2 mg dl^{-1}, when the signal-to-noise ratio was 2.

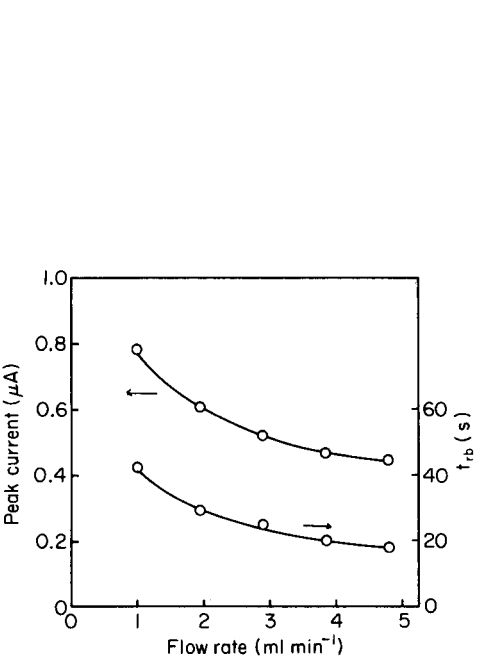

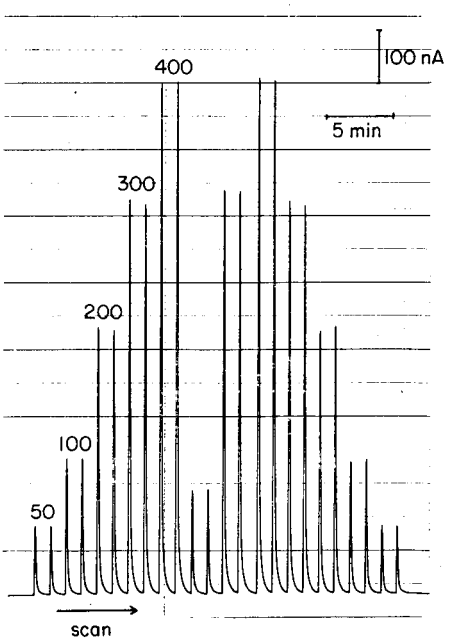

Fig. 2. Effect of flow rate on signal peak height and time to return to baseline (t_{rb}).

Fig. 3. Typical signals for duplicate injections (5 μl) of five standard solutions of glucose (50—400 mg dl^{-1}) followed by two sera and repetition of the five standard solutions.

Selectivity, reproducibility and accuracy

The selectivity depends on both the enzyme and the electrochemical detection. Glucose oxidase itself is highly selective for β-D-glucose, so the sensor under flow conditions offers high selectivity for glucose compared to other sugars (Table 1).

Because species other than enzymatically generated hydrogen peroxide may diffuse through the membrane and be oxidized on platinum at the same potential (0.8 V), there were some interferences of electroactive species such as ascorbate, urate, tyrosine, cysteine, glutathione, and bilirubin. How-

TABLE 1

Substrate selectivity

Sugars	Relative response	Sugars	Relative response
Glucose	100	Arabinose	0.03
Galactose	0.72	Fructose	0.07
Xylose	0.43	Sucrose	0.01
Mannose	1.34	Lactose	0.00

TABLE 2

Effect of addition of foreign substances on the response to 100 mg dl^{-1} glucose solution

Substance added	Level tested (mM)	Relative response	Substance added	Level tested (mM)	Relative response
None		100	Urea	20	99
Ascorbic acid	1.0	101	L-Lactic acid	20	100
Uric acid	1.0	100	Creatine	1.0	99
Glutathione	1.0	100	Creatinine	1.0	99
Tyrosine	1.0	101	Albumin	(5000)[a]	99
Cysteine	1.0	100	NaCl	100	100
Bilirubin	1.0	100	KCl	50	99
Pyruvic acid	1.0	100	$NaHCO_3$	20	100

[a]mg dl^{-1}.

TABLE 3

Reproducibility of measurements of glucose solutions and control serum

	Glucose solution (mg dl^{-1})[a]			Control serum (mg dl^{-1})	
	50	100	200	91	317
N	7	10	10	10	10
Mean[a]	129.9	259.6	515.1	85.6	307.3
S.d.	1.28	1.57	3.23	0.86	1.91
R.s.d. (%)	0.99	0.60	0.62	1.00	0.62

[a]Mean and standard deviation (s.d.) given in nA, with relative standard deviation for *N* measurements.

ever, most of these reducing substances that are usually present in blood sera, can be eliminated by introducing the copper(II) dithiocarbamate column just before the amperometric sensor. Table 2 lists some of the substances that might interfere with the measurement of glucose but did not when the precolumn was in position. The present method can therefore be applied to the specific determination of glucose in human blood sera.

Reproducibility of the results was tested by repeated injections of 5-μl aliquots of glucose standard solutions and control sera, at an injection rate of 100 samples per hour. The results are shown in Table 3. The relative standard deviations were less than 1% for all samples. Also the average amount found for glucose in the control human serum agreed well with the data from the manufacturer.

The sensor was used repeatedly to confirm its stability over a long period. The stability of the sensor was good; even after repetitive use for two months,

the enzyme sensor retained 95% of its original activity when it was stored in phosphate buffer pH 7.5 between series of measurements.

The author thanks Mr. Minoru Sato for his help in the experimental work.

REFERENCES

1 G. G. Guilbault and G. J. Lubrano, Anal. Chim. Acta, 64 (1973) 439; 69 (1974) 183; 97 (1978) 229.
2 G. Nagy, L. H. Von Storp and G. G. Guilbault, Anal. Chim. Acta, 66 (1973) 443.
3 D. R. Thevenot, R. Sternberg, P. R. Coulet, J. Laurent and D. C. Gautheron, Anal. Chem., 51 (1979) 96.
4 M. Koyama, Y. Sato, M. Aizawa and S. Suzuki, Anal. Chim. Acta, 116 (1980) 307.
5 J. J. Kulys, M. V. Pesliakiene and A. S. Samalius, Bioelectrochem. Bioenerg., 8 (1981) 81.
6 C. Bertrand, P. R. Coulet and D. C. Gautheron, Anal. Chim. Acta, 126 (1981) 23.
7 T. Yao, Anal. Chim. Acta, 148 (1983) 27.
8 T. Yao, M. Akino and S. Musha, Bunseki Kagaku, 30 (1981) 740; 31 (1982) 409.

Analytica Chimica Acta, 153 (1983) 181—190
Elsevier Science Publishers B.V., Amsterdam — Printed in The Netherlands

REPETITIVE ENZYMATIC DETERMINATION OF GLUCOSE WITH REGENERATION AND RECYCLING OF COENZYME AND ENZYMES

P. ROEHRIG, C.-M. WOLFF* and J. P. SCHWING

Laboratoire de Chimie Physique et d'Electrochimie, Equipe de Recherche Associée au C.N.R.S. No. 166, Ecole Nationale Supérieure de Chimie de Strasbourg, 1 rue Blaise Pascal, 67008 Strasbourg (France)

(Received 2nd December 1982)

SUMMARY

The use of closed-loop systems in flow injection analysis allows recycling and regeneration of reagents which are present in excess. Enzymatic determination of glucose with glucose dehydrogenase, which requires NAD^+ as coenzyme, was chosen as a model system. The NADH produced is spectrophotometrically determined by kinetic measurements. Glutamate dehydrogenase added to the circulating solution slowly oxidizes NADH back to NAD^+. Maximum rate of glucose determination ($\leqslant 500$ mg dl^{-1}) is 120 h^{-1} with an r.s.d. of 2.5%. Results for samples of human blood serum were compared to results obtained with a Technicon AutoAnalyzer. The correlation coefficient was 0.98. Regeneration and recycling of the NAD^+ and enzymes allowed 300 determinations of glucose in serum with the same 40-ml circulating solution.

Speed and simplicity are major advantages of flow injection analysis (f.i.a.) [1—4]. A possibility which has not been much exploited is the automatic recirculation of reagents, which can lead to appreciable economies [5—7], particularly when expensive materials such as enzymes are used. In enzymatic determination of substrates involving dehydrogenases, nicotinamide adenine dinucleotide (NAD^+) or its reduced form (NADH) is used as the coenzyme, according to the following general reaction:

$$S\ (\text{substrate}) + NAD^+ \overset{E}{\rightleftharpoons} \text{Product(s)} + NADH + H^+$$

where E is the enzyme. The NADH absorbs strongly at 340 nm whereas NAD^+ does not. For this reason, such reactions are utilized for the direct determination of substrate S or for the determination of another substrate, in which the above reaction is used as the final step (indicator reaction). The high cost of coenzymes and enzymes justifies efforts to regenerate and reuse them. In 1980, Blaedel and Engstrom [8] reported an experiment with a membrane electrode in which NAD^+ was automatically regenerated by electrochemical oxidation of NADH. A determination with this electrode took 5 min.

The major object of the present work is rapid determination of glucose

0003-2670/83/$03.00

with automatic regeneration and recycling of NAD^+ and glucose dehydrogenase, GlucDH [9, 10], a highly selective enzyme. The enzymatic reaction is

$$\beta\text{-D-glucose} + NAD^+ \xrightarrow{\text{GlucDH}} \text{Glucono-}\delta\text{-lactone} + NADH + H^+$$

Hansen et al. [11] used this reaction for glucose determination in an "open" flow injection system, in which the circulating solution, containing the enzyme, NAD^+ and product NADH, were passed to waste. In the present work, the NADH formed was converted back to NAD^+ by glutamate dehydrogenase, GlDH:

$$NADH + NH_4^+ + \alpha\text{-ketoglutarate} \xrightarrow{\text{GlDH}} NAD^+ + \text{glutamate} + H_2O$$

Experimental conditions for the determination of glucose in human serum were determined and the results obtained were compared with those obtained independently with a Technicon AutoAnalyzer.

EXPERIMENTAL

Apparatus

Two different arrangements of the apparatus were used (Fig. 1). The enzyme solution flowed from a reservoir through two identical optical cells. Between these cells, the sample was injected into the stream by means of a rotary valve injector, a simplified version of that described by Hansen and Růžička [12, 13], and mixed with the solution in a helical glass coil. The circulating solution, after emerging from the second optical cell, returned to the reservoir. The two arrangements differed principally in the arrangement for achieving solution circulation. In system I (Fig. 1), there was gravity flow from A to B at a constant rate in the range 0.06—0.17 ml s^{-1}. The solution

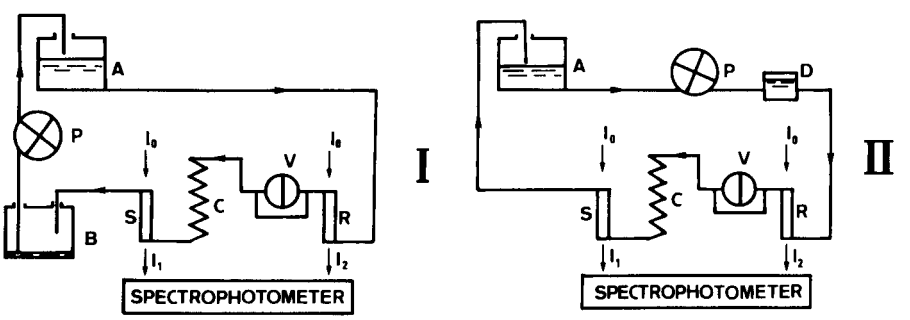

Fig. 1. Schematic diagrams of the two flow systems (I and II) tested. (A) Reservoir; (B) second reservoir; (V) injection valve; (C) mixing coil; (P) pump; (D) flow-rate damping cell; (R) spectrophotometric reference cell; (S) spectrophotometric sample cell; (I_0) incident radiation intensity; (I_1) intensity transmitted by the sample; (I_2) intensity transmitted by reference. The length of the optical cells was 2 or 4 cm. The mixing coil was made from a glass tube of elliptical cross section (1 × 2 mm) and of 30 cm total length. The average diameter of the coil was 6 mm.

was pumped back to the reservoir at a slightly faster rate so as to avoid overflow from B. In system II (Fig. 1), the peristaltic pump (Masterflex, with SRC Model 7020 speed controller and 7014 pump head) was located before the optical cells and forced the solution through these and back to the reservoir. The rate of the pump had to be controlled carefully and the pulses caused by the pump were attenuated but not completely eliminated by a damping cell. The damping cell was a vertical glass tube (13 mm i.d., 10 ml total volume) through which the solution circulated. Apart from the inlet (top) and outlet (bottom), the cell was closed, and always contained 5 ml of the circulating solution, the 5-ml air gap above the surface of the solution in the tube acting as the pulse-damper. The two optical cells were identical flow cells of cylindrical internal section (5 mm i.d.). All tubing was Tygon (1.6 mm i.d.). The difference in absorbance between the two cells was measured at 340 nm with a Beckman DB spectrophotometer and recorded on a Beckman chart recorder. Preliminary work on the kinetics of the enzymatic reactions was done with a Durrum-Gibson stopped-flow spectrophotometer.

Reagents and solutions

Glucose dehydrogenase, purified from *Bacillus megatherium* M 1286, was supplied by Merck (Darmstadt, F.R.G.) as part of a complete kit (Merckotest No. 3389). In the kit, GlucDH is mixed with mutarotase to accelerate the equilibrium between α- and β-glucose. Glutamate dehydrogenase used for NAD^+ regeneration was purified from beef liver (Boehringer, Mannheim, F.R.G.). All other reagents were of analytical-reagent grade (Merck). Water used for preparation of solutions was twice-distilled. A typical circulating solution was made up of 40 ml of a solution containing phosphate buffer (pH 7.4, 0.10 M total phosphate), 10 IU ml^{-1} GlucDH, 0.2 units GlDH (one unit is defined as the activity which transforms 1 μmol of α-ketoglutarate to glutamate per min, under the present conditions, in the presence of 1×10^{-4} mol l^{-1} NADH), 2.25×10^{-3} mol l^{-1} α-ketoglutarate, 2.5×10^{-2} mol l^{-1} ammonium acetate and 3.9×10^{-3} mol l^{-1} NAD^+. When not in use, the enzyme solution was stored stoppered at 4°C in darkness. Foaming was prevented by placing an antifoaming agent (Ref. A-8267, Sigma Chemical Company) on the surface of the solution in the reservoir. All standard glucose solutions were used more than 30 min and less than 6 h after preparation; within this period no noticeable change in glucose concentration was detected.

Activities of GlucDH and GlDH were determined experimentally. It was not actually possible to measure the activity of mutarotase in the solutions because this enzyme was always mixed with GlucDH and the reaction of the latter enzyme was the kinetically limiting step. According to the manufacturer's specification, the activity of mutarotase was 0.2 U ml^{-1}. When a sample of freshly dissolved glucose (nearly 100% α-D-glucose) was added to the GlucDH and mutarotase solution containing an excess of NAD^+, the rate of NADH formation was not significantly different from that obtained with

a 2-h old glucose solution (36% α- and 64% β-D-glucose). Hence, the equilibrium between α- and β-glucose can be considered to be very fast compared to the later reactions.

Procedure for glucose determination

Serum samples or glucose standard solutions were injected in volumes of 23 μl just before the mixing coil by means of the rotary valve. The total volume necessary for one glucose determination was 50 μl. This volume was sufficient to rinse the injection valve and to carry out the determination. A blank injected after a glucose sample gave a zero signal. For security, 60—70-μl samples were added to the injection valve. The glucose concentration in the serum samples was determined by reference to a calibration graph constructed from the results obtained from standard sera of known glucose concentrations. During a series of determinations, an occasional injection of a standard serum allowed periodic re-calibration and dispensed with the necessity of precise temperature control.

Deproteinization of the samples by perchloric acid, as recommended in the Merckotest 3389 kit based on the classical equilibrium method using glucose dehydrogenase, was not applicable. After a few injections of such deproteinized samples, the circulating solution lost all enzymatic activity. For that reason, human serum samples were directly injected for glucose assay without further treatment.

RESULTS AND DISCUSSION

Rate considerations

After injection, the glucose sample is mixed with the flowing solution by passing through the coil. As the sample reaches the detection cell, it produces a transient absorbance signal (Fig. 2). The peak height is dependent on the time between injection and detection, and is proportional to the amount of NADH present in the cell after that period. The peak height is used initially for glucose determination.

The reactions occurring in the mixing zone after injection are summarised in Fig. 3. Mutarotase catalyses the equilibrium between α- and β-glucose, which is very fast compared to the later reactions. If it is assumed that mixing of glucose with the enzyme solution is instantaneous, under the experimental conditions used, the concentrations of glucose and NADH are always less than one tenth of the Michaelis constants for these substrates, and all other reagents are in excess compared to the corresponding Michaelis constants. In addition, the concentration of glucose is always very small compared to that of NAD^+. Under these conditions, the reactions involving GlucDH and GlDH may be assumed to be pseudo-first order [14]. Thus, if C_0 is the total initial concentration of glucose when mixed (proportional to the glucose concentration in the sample), A_t is the absorbance measured at time t after injection, k_1 is the apparent rate constant for the glucose—GlucDH reaction and k_2 is the apparent rate constant for the α-ketoglutarate—GlDH reaction:

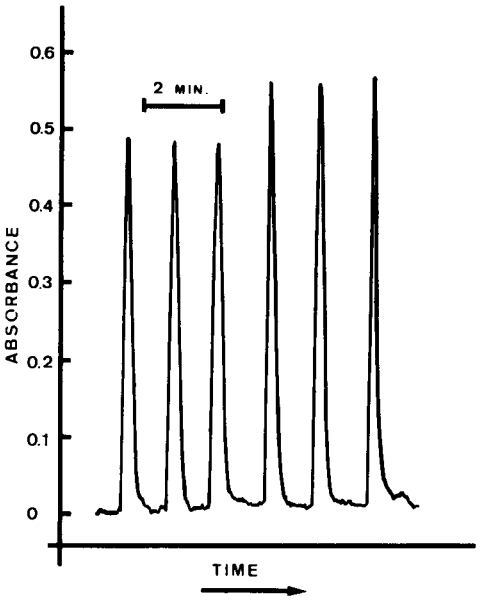

Fig. 2. Signals obtained with two samples of glucose (105 and 120 mg dl^{-1}). (Sample volumes, 23 μl; optical pathlength, 4 cm.)

$$A_t \propto [\text{NADH}]_t = C_0[k_1/(k_2 - k_1)]\,[\exp(-k_1 t) - \exp(-k_2 t)]$$

Figure 4 shows the experimental verification of this equation, by using stopped-flow spectrophotometry for different GlDH activities. For lower activities, there is good agreement between calculated and experimental values. For higher activities agreement is good only within the first 30 s of reaction. Under these conditions, at a given time, provided that $t < 30$ s, the concentration of NADH is proportional to the initial concentration of glucose.

Selection of experimental conditions

The GlucDH activity chosen was 10 IU ml^{-1}. This was satisfactory for making glucose oxidation sufficiently fast, while using the enzyme economically. The choice of GlDH activity depends on the time elapsed before the measurement is made and on the volume in the reservoir where NADH

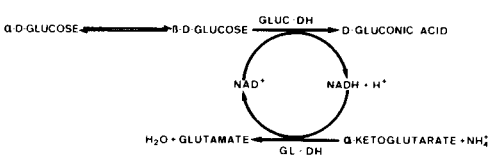

Fig. 3. Enzymatic system used for glucose determination and NAD^+ regeneration. Mutarotase is added to speed up the equilibrium between α- and β-glucose.

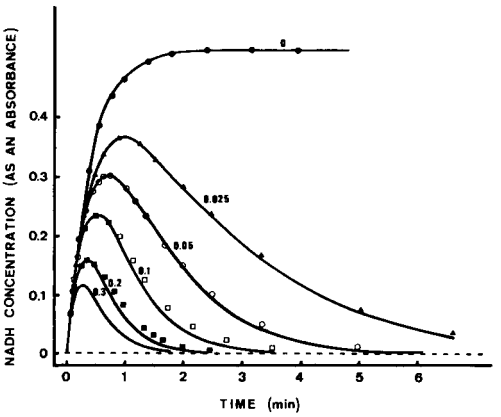

Fig. 4. Stopped-flow kinetic curves for NADH formation. (GlucDH = 10 IU ml^{-1}, GlDH activity is given in U ml^{-1} beside each curve, 25°C.) Curves represent experimental values. Theoretical values, given by the points, were computed on the assumption of two consecutive pseudo-first order reactions.

is diluted and NAD^+ regenerated. After an injection, the NADH produced must be completely eliminated from the solution, so that it is not recycled to the spectrophotometric reference cell to interfere with later measurements. To allow a significant amount of reaction to occur before measurement and to use a reservoir of reasonable size, the activity of this enzyme was chosen as 0.2 U ml^{-1}. A typical volume of circulating solution was 30—40 ml.

For mixing the sample and enzyme solutions, a helical glass coil was used. Different kinds of injection systems were tested. Best results were obtained with a modified rotary valve injector. Forty injections of the same sample of aqueous glucose gave a relative standard deviation (r.s.d.) of 2.5% with system I and 1.5% with system II. When a serum sample was used, the corresponding deviations were 4% and 2.5%, respectively. The flow rate of the circulating solution was 0.14 ml s^{-1}.

Calibration

Calibration graphs were constructed by injecting aqueous solutions containing 0—500 mg dl^{-1} glucose or standard sera with glucose concentrations ranging from 40 to 350 mg dl^{-1}. Glucose concentrations in these standard sera were verified by two enzymatic methods, the first based on glucose oxidase and peroxidase with 4-aminophenazone [15] as recommended by the Boehringer Diagnostica (124001), and the second being the end-point method based on glucose dehydrogenase [9, 10]. These two methods have been selected by the Swiss Society of Clinical Chemistry for the determination of glucose in blood [16].

With system I, the peak height was proportional to the glucose concentration in aqueous samples only at low glucose levels (<50 mg dl^{-1}). At higher

levels there was a significant deviation from linearity. For serum samples, the calibration graph was similar but was shifted 0.03 absorbance higher because of the presence of bilirubin. This serum calibration graph is shown in Fig. 5. No satisfactory explanation was found for the curvature.

With system II, the two calibration graphs, for aqueous and serum samples, were linear over the whole range of glucose concentrations tested. For aqueous standards, this graph passed through the origin. For serum standards, the graph was again shifted to higher absorbances, because of the bilirubin content (Fig. 5). The linear calibration shows the superiority of system II.

The delay time between injection of the sample and start of the transient signal was 5.5 s with both arrangements when the sample was an aqueous glucose standard. When the sample was serum, the delay time was 6 s when system I was used but 5.5 s when system II was used. This difference is due to the higher viscosity of the serum compared to aqueous solution. In both cases, the time between the beginning of the peak and its maximum was 6 s, with a further 19 s for return to the baseline. This allowed about 100 measurements per hour.

Because of the use of double-beam spectrophotometric detection, the baseline was not affected by slow changes in the absorbance of the circulating solution, which can occur when slightly absorbing samples are repetitively injected.

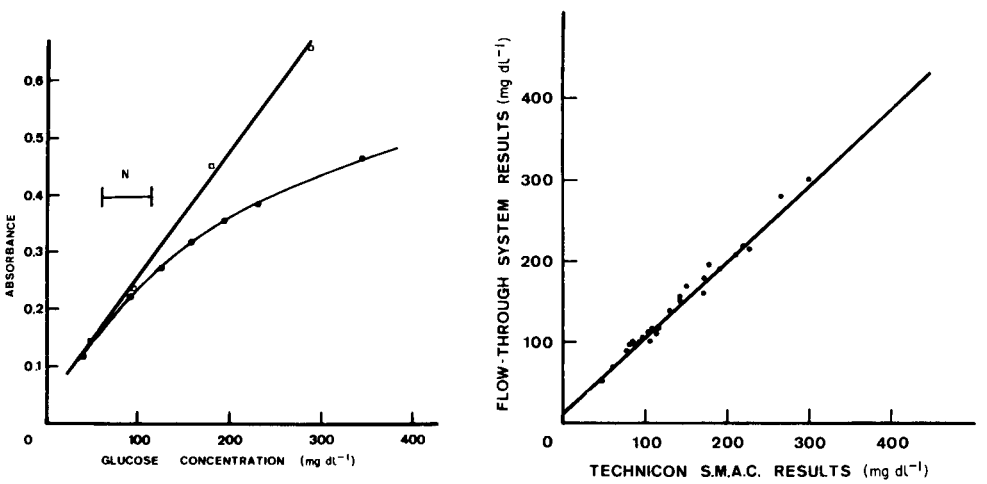

Fig. 5. Calibration graphs for glucose obtained by injecting standard serum samples: (•) system I; (□) system II. 23-μl samples, 2-cm optical pathlength. N indicates the normal fasting level of glucose in blood.

Fig. 6. Comparison of results obtained for 26 human serum samples obtained from system II and from the Technicon Auto-Analyzer (line drawn by linear regression; $r = 0.986$).

Interferences

Interferences with the enzyme-catalyzed reaction are well documented [9] and will not be discussed further. For human blood serum, bilirubin interferes with the spectrophotometric detection as it absorbs at 340 nm. The error introduced by bilirubin in the present method is positive and corresponds to about 10 mg dl^{-1} glucose. Hansen et al. [11] described a two-point detection method to eliminate this kind of interference. In their method, the difference between two peak heights is used as the analytical signal. In similar experiments on the present system, the second peak was not reproducible and the uncertainty of the results was higher than the error caused by the presence of bilirubin. For that reason, in this work, single-point detection and comparison with standard sera were used.

In the circulating solution, glutamate and gluconic acid are accumulating products, as a consequence of repeated injections. No interference from these species was detected.

The α-ketoglutarate reduction is an equilibrium which lies far towards NAD^+ formation [17]. This makes the regeneration of NAD^+ essentially complete, even after hundreds of determinations. This was confirmed experimentally; the spectrum of the circulating solution after 300 injections of serum did not show any evidence for NADH.

In serum, the principal metals present that could interfere are zinc, copper, iron, aluminium and manganese. Although in serum they are complexed by organic moieties, their effects were tested at high levels. The results obtained are summarized in Table 1.

Application to human blood serum samples

Glucose concentrations were determined with systems I and II by direct comparison to standard sera in 58 and 26 human serum samples, respectively. The results were compared to those obtained for the same samples,

TABLE 1

Effect of some metal species on the determination of glucose (160 mg dl^{-1}) in serum

Metal added[a]	Normal range in plasma[b] (mg dl^{-1})	Metal added (mg dl^{-1})	Glucose found (mg dl^{-1})
None	—	—	160
Zinc	0.08—0.4	3.9	154
Copper	0.04—0.17	1.4	163
Iron	0.07—0.15	2.3	176
Aluminium	0.0004—0.14	0.9	142
Manganese	0.00005—0.003	8.2	168
Bismuth	—	2.1	160
Lead	—	2.1	149

[a]As nitrate. [b]Data from Versieck and Cornelis [18], except those for iron which were from Florin and Stotz [19].

with the use of the Technicon AutoAnalyzer SMAC system [20] following standard procedures with the glucose oxidase—peroxidase—aminophenazone system [16]. Graphical comparison of the results obtained with system II is shown in Fig. 6. Correlation coefficients were found to be 0.981 and 0.986 between the AutoAnalyzer results and the results with systems I and II, respectively. Results for glucose obtained with a Boehringer Precipath S control serum by comparison with standard sera were 295 ± 15 mg dl^{-1}. This result is within the tolerance given by the manufacturer for different methods (reported range is 275—350 mg dl^{-1}).

Comparison of the two correlation coefficients found above, the reproducibilities, and the calibration curves obtained, demonstrates the superiority of system II over system I.

Operating conditions

Under the conditions used in this work, with a reservoir volume of 40 ml, 300 glucose determinations in blood serum samples were done in one day. By periodic injection of the same standard serum, a slow decrease in peak height was noted; the total loss in height was about 10% after the 300 determinations. It was mainly due to dilution as 23 μl of the solution are replaced by the same volume of sample for each injection. Because control samples were injected periodically, this decrease was of no consequence other than a small decrease in sensitivity of the method. After several hundred injections, the baseline began to fluctuate (development of turbidity in the solution) resulting in poor reproducibility. Thus the 40-ml solution was not normally used for more than 300 determinations. Because NAD^+ slowly decomposes and enzyme activities decrease at room temperature, the circulating solution, when used every day, was changed every 3 days. This solution was stored overnight at 4°C in darkness. Results indicate that recycling of reagents allows a 20-fold reduction in the consumption of glucose dehydrogenase, with respect to the normal method [9, 10]. Consumption of NAD^+ is decreased 7—10 times. Only a small part of this coenzyme effectively participates in the enzyme reaction; most is present to ensure maximum rate. Immobilization of the enzymes in some regions of the apparatus should increase the stability of the system and allow regeneration and recycling of NAD^+ for a longer period of time.

The authors are indebted to Maurice Offner (Laboratoire de Biochimie, Pavillon Poincarré, Hospices Civils de Strasbourg) for samples of human blood serum and the results from the Technicon AutoAnalyzer. P. Roehrig gratefully acknowledges the financial support of the Direction Générale de la Recherche Scientifique et Technique in the form of a Fellowship.

REFERENCES

1 J. Růžička and E. H. Hansen, Flow Injection Analysis, Wiley, New York, 1981.
2 H. A. Mottola, Anal. Chem., 53 (1981) 1312A.
3 C. B. Ranger, Anal. Chem., 53 (1981) 20A.
4 H. A. Mottola and H. B. Mark, Jr., Anal. Chem., 54 (1982) 62R.
5 V. V. S. Eswara Dutt, D. Scheller and H. A. Mottola, Anal. Chim. Acta, 94 (1977) 289.
6 C. M. Wolff and H. A. Mottola, Anal. Chem., 50 (1978) 94.
7 S. M. Ramasamy and H. A. Mottola, Anal. Chim. Acta, 127 (1981) 39.
8 W. J. Blaedel and R. C. Engstrom, Anal. Chem., 52 (1980) 1691.
9 K. Gerbig, Tec. Lab., 45 (1975) 410.
10 W. Brummer and W. Ebeling, Kontakte, 2 (1976) 3.
11 E. H. Hansen, J. Růžička and B. Rietz, Anal. Chim. Acta, 89 (1977) 241.
12 E. H. Hansen and J. Růžička, J. Chem. Educ., 56 (1979) 677.
13 J. Růžička and E. H. Hansen, Anal. Chim. Acta, 106 (1977) 207.
14 H. W. Bergmeyer, Methods of Enzymatic Analysis, 2nd edn., Vol. 1, Academic Press, New York, 1974, p. 101.
15 P. Trinder, Ann. Clin. Biochem., 6 (1969) 24.
16 H. Horak and A. Scholer, Bull. Schweiz. Ges. Klin. Chem., 22/1 (Suppl.) (1981).
17 H. W. Bergmeyer, Methods of Enzymatic Analysis, 2nd edn., Vol. 2, Academic Press, New York, 1974, p. 650.
18 J. Versieck and R. Cornelis, Anal. Chim. Acta, 116 (1980) 217.
19 M. Florin and E. H. Stotz (Eds.), Comprehensive Biochemistry, Vol. 21, Elsevier, Amsterdam, 1971, p. 185.
20 G. G. Guilbault, Handbook of Enzymatic Methods of Analysis, Dekker, New York, 1976, p. 590.

Analytica Chimica Acta, 153 (1983) 191—197
Elsevier Science Publishers B.V., Amsterdam — Printed in The Netherlands

HIGHLY SENSITIVE ENZYMATIC SPECTROPHOTOMETRIC DETERMINATION OF HYDROGEN PEROXIDE WITH WATER-SOLUBLE DIPHENYLMETHANE-BASED DERIVATIVES

MASANOBU SHIGA*, MIKIHIKO SAITO and KENYU KINA
Dojindo Laboratories, 2861, Kengun-machi, Kumamoto-shi, 862 (Japan)
(Received 10th May 1983)

SUMMARY

Five water-soluble diphenylmethane derivatives were synthesized. They give colored products by condensation with 3-methylbenzothiazolinonhydrazone in the presence of hydrogen peroxide and peroxidase. These reactions are useful for the enzymatic determination of hydrogen peroxide. The absorption maxima and the molar absorptivities of the chromogens lie in the ranges 560—600 nm and 5—9 × 10^4 l mol^{-1} cm^{-1}, respectively. The optimum pH range for color formation is 6.5—7.5. Calibration graphs for the determination of hydrogen peroxide are linear for 3—20 × 10^{-6} mol H_2O_2 l^{-1}. Di[4-(3-sulfopropylethylamino)phenyl]methane, disodium salt, is the best of the reagents tested.

Determinations of clinically important substances in serum, such as glucose, cholesterol or uric acid, are now mostly based on enzymatic reactions. The enzymatically generated hydrogen peroxide is determined spectrophotometrically after reaction with a chromogenic hydrogen donor and a coupling agent in the presence of peroxidase. While various hydrogen donors have been proposed for this purpose [1, 2], none is completely satisfactory for practical applications. For example, the absorption maximum of the resulting chromogen is often in the 500—520-nm region where interference by bilirubin is expected [3—5], or the water-solubility of the hydrogen donor is poor [6, 7]; the enzymatic reaction of peroxide with 4-aminoantipyrine and phenol proceeds only in acidic solution.

Recently, Tamaoku et al. [8, 9] reported a series of new water-soluble hydrogen donors derived from *N*-sulfopropylaniline, which developed a color over a wider pH range, giving chromogens with absorption maxima at longer wavelengths. The present investigation was undertaken to develop more sensitive water-soluble hydrogen donors than the *N*-sulfopropylaniline derivatives. The synthesis of a series of highly sensitive water-soluble diphenylmethane-based derivatives is reported, together with their chromogenic reaction with 3-methylbenzothiazolinonhydrazone (MBTH) in the presence of peroxidase and hydrogen peroxide.

0003-2670/83/$03.00

EXPERIMENTAL

Syntheses of diphenylmethane-based derivatives

The compounds prepared are shown in Table 1.

Di[4-(3-sulfopropylethylamino)phenyl] methane,disodium salt (Bis-ALPS, Compound 2). Under nitrogen, 5.47 g (2.06×10^{-2} mol) of *N*-ethyl-*N*-(3-sulfopropyl)aniline, sodium salt [8] was dissolved in 10 ml of water, to which was added a mixture of 0.89 ml (1.10×10^{-2} mol) of 37% formaldehyde and 0.10 ml of 90% formic acid. While the solution was warmed at 35—40°C, a few drops of *N*-methylaniline were added and the mixture was stirred for 4 h. The mixture was poured into 200 ml of acetone, and the resulting white crystals were separated and recrystallized from a mixture of tetrahydrofuran and methanol. [Yield 4.95 g (88%), m.p. 246—250°C. ^{1}H-n.m.r. (d_6-DMSO:ppm for internal TMS): 1.10(6H, t, CH_3), 1.68—2.18 (4H, m, CH_2), 2.40—2.75(4H, m, CH_2), 3.05—3.60(8H, m, CH_2), 4.35(2H, s, benzyl-CH_2), 6.47(4H, d, aromatic-H), 6.90(4H, d, aromatic-H). I.r.: 3480, 1600, 1260 cm^{-1}. Found: 49.3% C, 6.3% H, 5.0% N; calc. for $C_{23}H_{32}N_2O_6S_2Na_2 \cdot H_2O$, 49.3% C, 6.1% H, 5.0% N. T.l.c. (silica gel, n-butanol saturated with aqueous 0.2 M ammonia), $R_f = 0.30$.]

The other derivatives were prepared under similar conditions. The data for the yield, m.p., ^{1}H-n.m.r., i.r., elemental analysis and R_f value (obtained on silica gel plates, with n-butanol saturated with aqueous 0.2 M ammonia) were as follows.

Di[4-(3-sulfopropylamino)phenyl] methane, disodium salt (Bis-HALPS, Compound 1). Yield 84%, m.p. 210—231°C (dec.). ^{1}H-n.m.r. (d_6-DMSO): 1.60—2.16(4H, m, CH_2), 2.38—2.75(4H, m, CH_2), 3.02—3.70(4H, m, CH_2), 4.28(2H, s, benzyl-CH_2), 6.45(4H, d, aromatic-H), 6.87(4H, d, aromatic-H). I.r.: 3320, 1610, 1263, 1170, 1050 cm^{-1}. Found: 47.1% C, 5.1% H, 5.5% N; calc. for $C_{19}H_{24}N_2O_6S_2Na_2$, 46.9% C, 5.0% H, 5.1% N. T.l.c., $R_f = 0.25$.

TABLE 1

Methane-based derivatives

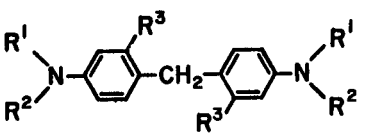

Compound	No.	R^1	R^2	R^3
Bis-HALPS	1	H	—$(CH_2)_3SO_3Na$	H
Bis-ALPS	2	ethyl	—$(CH_2)_3SO_3Na$	H
Bis-ALOS	3	ethyl	—$CH_2CH(OH)CH_2SO_3Na$	H
Bis-TOPS	4	ethyl	—$(CH_2)_3SO_3Na$	methyl
Bis-BLPS	5	n-butyl	—$(CH_2)_3SO_3Na$	H

Di[4-(2-hydroxy-3-sulfopropylethylamino)phenyl] methane, disodium salt (Bis-ALOS, Compound 3). Yield 77%, m.p. 214—222°C (dec.). ^{1}H-n.m.r. (d_6-DMSO): 1.12(6H, t, CH_3), 2.41—2.75(4H, m, CH_2), 3.13—3.54(10H, m, CH_2), 4.30(2H, s, benzyl-CH_2), 6.42(4H, d, aromatic-H), 6.85(4H, d, aromatic-H). I.r.: 3500, 1605, 1257, 1160 cm^{-1}. Found: 48.3% C, 5.7% H, 4.6% N; calc. for $C_{23}H_{32}N_2O_8S_2Na_2$, 48.1% C, 5.6% H, 4.9% N. T.l.c., R_f = 0.30.

Di[4-(3-sulfopropylethylamino)-2-methylphenyl] methane, disodium salt (Bis-TOPS, Compound 4). Yield 83%, m.p. 235—247°C (dec.). ^{1}H-n.m.r. (d_6-DMSO): 1.10(6H, t, CH_3), 1.70—2.15(4H, m, CH_2), 2.40—2.73(4H, m, CH_2), 3.70(6H, s, benzyl-CH_3), 3.11—3.85(8H, m, CH_2), 4.38(2H, s, benzyl-CH_2), 6.40—7.08(6H, m, aromatic-H). I.r.: 3450, 1600, 1275 cm^{-1}. Found: 49.5% C, 6.7% H, 4.4% N; calc. for $C_{25}H_{36}N_2O_6S_2Na_2 \cdot 2H_2O$, 49.5% C, 6.7% H, 4.6% N. T.l.c., R_f = 0.33.

Di[4-(3-sulfopropyl-n-butylamino)phenyl] methane, disodium salt (Bis-BLPS, Compound 5). Yield 64%, m.p. 220—235°C (dec.). ^{1}H-n.m.r.(d_6-DMSO) = 1.05 (6H, t, CH_3), 1.65—2.30(12H, m, CH_2), 2.40—2.85(4H, m, CH_2), 3.06—3.65(8H, m, CH_2), 4.35(2H, s, benzyl-CH_2), 6.48(4H, d, aromatic-H), 6.90(4H, d, aromatic-H). I.r.: 3460, 1610, 1366, 1260 cm^{-1}. Found: 54.7% C, 6.8% H, 4.3% N; calc. for $C_{27}H_{40}N_2O_6S_2Na_2$, 54.4% C, 6.8% H, 4.5% N. T.l.c., R_f = 0.35.

Reagents and apparatus

All reagents were of analytical grade, unless otherwise stated. Hydrogen donors and MBTH were stored as aqueous 1.0 mM solutions. Aqueous hydrogen peroxide solutions (0.1—1.0 mM) were standardized by acidic permanganate titration. An aqueous peroxidase solution was prepared from commercial peroxidase (820 U mg^{-1}; BDH Chemicals) and stored under refrigeration. MoniTrol-II (DADE Division, American Hospital Supply Corp.) was used as a control serum. Good's buffers or phosphate buffer solution were used to cover the pH ranges of 4.8—9.0 (phosphate), 5.2—7.2 (MES, 2-(*N*-morpholino)-ethane sulfonic acid), 6.0—7.5 (HEPES, *N*-(2-hydroxyethyl)-1-piperazine-*N'*-ethane sulfonic acid) and 8.3—8.8 (glycine); *N,N*-bis(2-hydroxyethyl)-2-aminoethane sulfonic acid (BES) was also tested.

All spectrophotometric measurements were done with a Shimadzu model UV-210A double-beam recording spectrophotometer using 1-cm cells.

Standard procedure for the color development

A mixture consisting of 2.0 ml of 0.1 M buffer solution (pH 7), 300 µl of the hydrogen donor solution and 300 µl of peroxidase solution was incubated at 37°C. To this solution, were added 200 µl of MBTH solution and 100 µl of hydrogen peroxide solution, and the mixture was incubated at 37°C for 10 min. The absorption spectrum of the resulting chromogen was observed against a reagent blank prepared in a similar manner without hydrogen peroxide.

The optimum pH range for the color development was investigated by incubating the reaction mixture at different pH values. The time dependence of the chromogenic reaction was investigated by measuring the absorbance after incubating for 5—60 min.

Calibration graphs for hydrogen peroxide in the presence of the control serum

A mixture of 50 µl of control serum, 300 µl of peroxidase solution, 300 µl of hydrogen donor solution, 200 µl of MBTH solution and 100 µl of hydrogen peroxide solution (0.1—1.0 mM), was diluted to 3.0 ml with 0.1 M buffer solution (pH 7). After the solution had been incubated at 37°C for 10 min, the absorbance at the wavelength of maximum absorption was measured against the reagent blank.

RESULTS AND DISCUSSION

Syntheses of the water-soluble diphenylmethane-based derivatives

The derivatives were prepared according to the reaction scheme

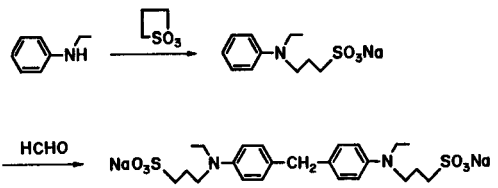

The reaction must proceed under nitrogen to prevent oxidation. The condensation reaction is quantitative; the extent of the reaction can be followed by separating a drop of the reaction mixture by t.l.c. (developing on a silica gel layer with n-butanol saturated with aqueous 0.2 M ammonia). The derivatives were obtained as white crystals and were highly soluble in water. Their aqueous solutions were stable for several weeks if stored under nitrogen.

Chromogenic reactions

In order to investigate the effect of pH on the color development for each derivative, the oxidative condensation with MBTH in the presence of hydrogen peroxide and peroxidase was examined in media of various pH values. As a typical example, the results for Bis-ALPS are shown in Fig. 1. The other derivatives gave similar pH dependences.

It can be seen in Fig. 1 that the reaction is most sensitive around neutral pH values, and is decreased at both lower and higher pH regions. It is interesting to note that the sensitivity is affected by the buffering agents, Good's buffers giving the highest sensitivity. The oxidative condensation of these derivatives with MBTH can be considered to proceed as follows:

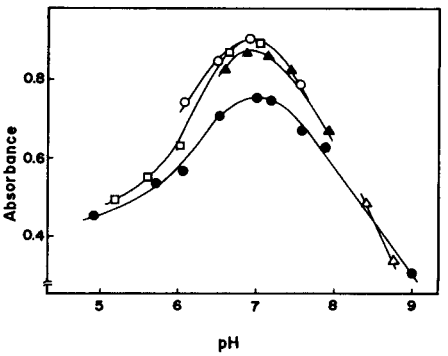

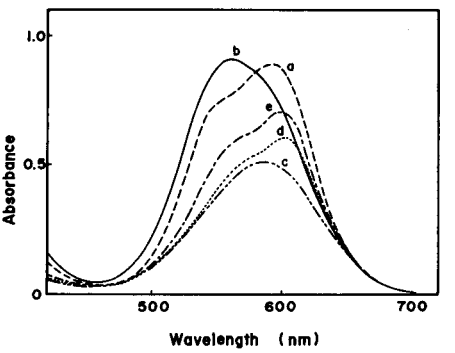

Fig. 1. Effect of pH of various buffers on color development at 598 nm for Bis-ALPS and MBTH. (0.1 M buffer, 0.1 mM Bis-ALPS, 1.3 U ml^{-1} peroxidase, 0.067 mM MBTH, 20 μM H_2O_2). (○) BES; (▲) HEPES; (□) MES; (△) glycine; (●) phosphate.

Fig. 2. Absorption spectra of dyes formed by oxidative condensation of hydrogen donors with MBTH at pH 7.0 (conditions as Fig. 1): (a) Bis-ALPS; (b) Bis-TOPS; (c) Bis-HALPS; (d) Bis-ALOS; (e) Bis-BLPS.

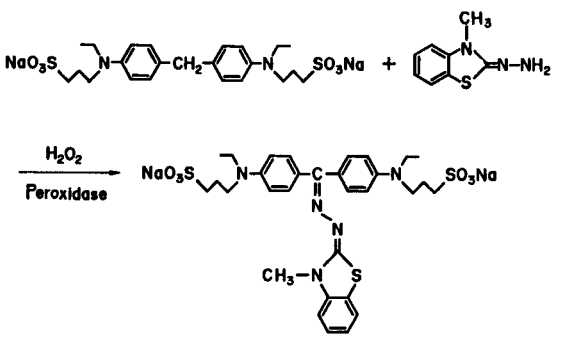

The absorption spectra of the chromogens are shown in Fig. 2 and their spectral characteristics are summarized in Table 2. Although there is no experimental evidence to prove the structure of the chromogen as shown above, the unusually high molar absorptivity and the distinct bathochromic shift may be attributed to such a conjugated structure.

Table 2 indicates that the absorption maximum of the chromogen derived from Bis-TOPS is at 561 nm, and is the band most shifted to shorter wavelengths among the derivatives investigated in this study. This suggests that the 3-methyl group of the phenyl ring of Bis-TOPS interferes with the coplanarity of the phenyl ring and the methylidenamino group, resulting in the blue shift.

The absorbance of the chromogens increases with the *N*-substituted group on the methane base in the following order: hydrogen < n-butyl < ethyl, hydroxysulfopropyl < sulfopropyl. The *N*-substituent also evidently activates the oxidative condensation of the methane base with MBTH, regardless of the size and kind of alkyl group. These results may be explained by the elec-

TABLE 2

Absorption maxima and molar absorptivities of the dyes formed

Compound	λ_{max} (nm)	Molar absorptivity ($\times 10^4$ l mol^{-1} cm^{-1})	
		Phosphate	BES
Bis-HALPS	583	5.48	5.35
Bis-ALPS	598	7.52	9.00
Bis-ALOS	601	5.14	6.72
Bis-TOPS	561	7.06	9.24
Bis-BLPS	600	6.35	7.02

tronic effect of the *N*-substituted groups. The addition of a non-ionic surfactant, such as Triton X-100, retards the formation of the chromogen by 10—20%.

Optimum condition for color development

The time dependences of the color development with methane-based derivatives are illustrated in Fig. 3. The absorbances reach their maxima within 10 min, and are constant for the succeeding 60 min, with the exception of Bis-TOPS. As shown in Fig. 4, the blank values also increase linearly with time, through oxidation by atmospheric oxygen. Therefore, it is desirable to measure the absorbance as quickly as possible. Although the blank value can be minimized by the addition of a non-ionic surfactant, some sensitivity has to be sacrificed.

In order to establish the feasibility of using these diphenylmethane derivatives for the enzymatic determination of clinically important substances in

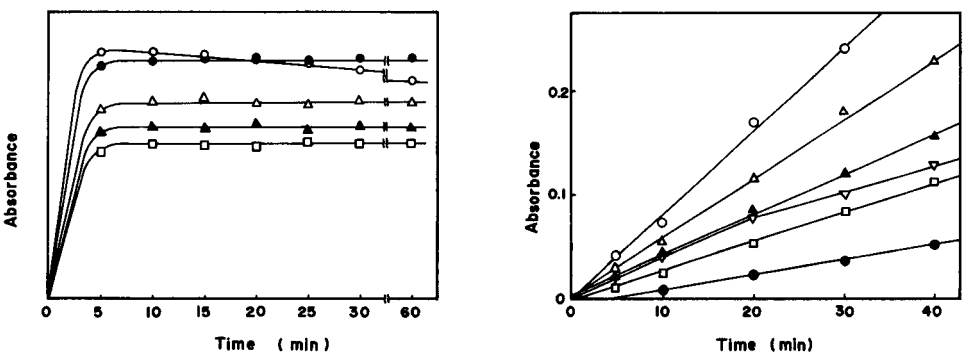

Fig. 3. Effect of time on the oxidative condensation at pH 7.0 (conditions as in Fig. 1): (●) Bis-ALPS; (○) Bis-TOPS; (△) Bis-BLPS; (▲) Bis-ALOS; (□) Bis-HALPS.

Fig. 4. Effect of time on the blank absorbance measured at λ_{max} (0.1 M BES buffer; 0.1 mM hydrogen donor; 1.3 U ml^{-1} peroxidase; 0.067 mM MBTH). (○) Bis-TOPS; (△) Bis-ALPS; (□) Bis-ALOS; (●) Bis-HALPS; (▲) Bis-ALPS (with 0.1% Triton X-100); (▽) Bis-ALPS (with 0.1% Brij 35).

serum, the determination of hydrogen peroxide in the presence of a control serum was examined. The calibration graphs were linear over the concentration range 3—20 × 10^{-6} mol H_2O_2 l^{-1}. The highest sensitivity was obtained with Bis-ALPS using MBTH as a coupler, being 1.5—2 times higher than the values obtained with *N*-sulfopropylaniline derivatives. Thus, Bis-ALPS seems to be the most successful hydrogen donor for use in the enzymatic determination of hydrogen peroxide in serum. Applications of these water-soluble derivatives to the analysis of serum will be the subject of a later paper.

The authors express their gratitude to Professor Keihei Ueno for helpful discussions.

REFERENCES

1 P. Trinder, Ann. Clin. Biochem., 6 (1969) 24.
2 N. Gochman and J. M. Schmitz, Clin. Chem., 17 (1971) 1154.
3 P. G. Cole, G. H. Lathe and B. H. Billing, Biochem. J., 57 (1954) 514.
4 B. H. Billing, J. Clin. Pathol., 8 (1955) 126.
5 G. W. Stevenson, S. L. Jachobs and R. J. Henry, Clin. Chem., 10 (1964) 95.
6 G. S. Rautela and R. J. Leidtke, Clin. Chem., 24 (1978) 108.
7 S. Hashimoto, H. Horiki, S. Nishina, M. Tsuda and T. Tatano, Jpn. J. Clin. Pathol., 26 (1978) 199.
8 K. Tamaoku, Y. Murao, K. Akiura and Y. Ohkura, Anal. Chim. Acta, 136 (1982) 121.
9 K. Tamaoku, K. Ueno, K. Akiura and Y. Ohkura, Chem. Pharm. Bull., 30 (1982) 2492.

Analytica Chimica Acta, 153 (1983) 199—206
Elsevier Science Publishers B.V., Amsterdam — Printed in The Netherlands

SPECTROPHOTOMETRIC DETERMINATION OF TRACES OF IRON WITH 2-(3,5-DIBROMO-2-PYRIDYLAZO)-5-[*N*-ETHYL-*N*-(3-SULFOPROPYL)AMINO]PHENOL AND ITS APPLICATION IN FLOW INJECTION ANALYSIS

H. WADA* and G. NAKAGAWA

Laboratory of Analytical Chemistry, Nagoya Institute of Technology, Showa-ku, Nagoya (Japan)

K. OHSHITA

Laboratory of Chemistry, Daido Institute of Technology, Minami-ku, Nagoya (Japan)

(Received 15th February 1983)

SUMMARY

2-(3,5-Dibromo-2-pyridylazo)-5-[*N*-ethyl-*N*-(3-sulfopropyl)amino]phenol reacts with iron(II) to form a water-soluble chelate, which gives two absorption maxima at 568 nm (ϵ = 88000 l mol^{-1} cm^{-1}) and 748 nm (ϵ = 39000 l mol^{-1} cm^{-1}). A spectrophotometric determination of 1—35 μg of iron is described. Interferences from other metals are eliminated with *N*-(dithiocarboxy)sarcosine and EDTA; Cu (15 or 30 μg), Ni (3 or 60 μg), Zn (30 or 130 μg) and Co (20 or 150 μg) do not interfere when the absorbances are measured at 570 nm or 750 nm, respectively. For the flow-injection procedure, the calibration graph is linear for 20—440 μg l^{-1} iron at 750 nm. Total iron in potable waters can be determined after some preliminary treatment. The sample rate is 30 h^{-1}.

Various organic reagents such as 1,10-phenanthroline, bathophenanthroline and 2,4,6-tri-2-pyridyl-*s*-triazine (TPTZ) have been widely used for spectrophotometric determinations of iron. These reagents are very selective for iron, but are not very sensitive so that long optical paths are needed for analysis of water samples. A flow-injection method based on 1,10-phenanthroline has been reported for iron (0.1—30 mg l^{-1}) in natural waters and plant materials [1].

Pyridylazo- and thiazolylazophenols generally react with iron(II) to form chelates having two absorption maxima around 550 and 750 nm. Sensitivity is higher at 550 nm, at which many metal chelates also absorb, but absorption at 750 nm is highly selective for the iron(II) chelate. Iron(II) determinations with 4-(2-pyridylazo)resorcinol (PAR) [2], 4-(2-thiazolylazo)-resorcinol [3], 2-(2-thiazolylazo)-5-dimethylaminophenol [4] and 2-(2-thiazolylazo)-4-methylphenol [5] have been reported. With PAR, the absorbance was measured at 500 nm; although the sensitivity is good (ϵ = 50000 l mol^{-1} cm^{-1}), reagent blanks are large. With the other reagents, the sensitivity is similar to that with TPTZ (2.26×10^4 l mol^{-1} cm^{-1}) [6].

0003-2670/83/$03.00

Various water-soluble thiazolylazo and pyridylazo compounds have recently been synthesized, and spectrophotometric determinations of cobalt with 2-(2-thiazolylazo)-4-methyl-5-(sulfomethylamino)benzoic acid [7] and of uranium with 2-(3,5-dibromo-2-pyridylazo)-5-[*N*-ethyl-*N*-(3-sulfopropyl)amino]phenol (3,5-diBr-PAESPAP) [8] have been developed. These reagents, having a sulfoalkylamino group in the *p*-position to the azo group, are not only very sensitive but water-soluble.

The present paper deals with the sensitive and selective determination of iron with 3,5-diBr-PAESPAP (I) and its application in flow-injection analysis.

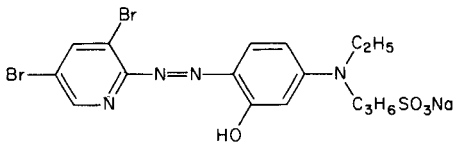

(I)

EXPERIMENTAL

Reagents and apparatus

Compound I was synthesized as before [8]. An aqueous 10^{-3} M solution was used.

Standard solutions of iron(III) and iron(II) were prepared from analytical reagent-grade iron(III) ammonium sulfate and iron(II) ammonium sulfate and were standardized against EDTA in the presence of ascorbic acid with xylenol orange as an indicator. Other metal—ion solutions were prepared from their analytical reagent-grade nitrates, sulfates or chlorides. β-Dithiocarbamino-propionic acid, diammonium salt (β-DTCPA) was synthesized as described by Russeva and Budevsky [9]. *N*-(Dithiocarboxy)sarcosine, diammonium salt (DTCS) was synthesized as described by Sakai and Kurogi [10]. All other chemicals used were of reagent-grade. All water was redistilled from a hard-glass vessel. Acetic acid—sodium acetate (2 M, pH 3—6) and 2 M ammonia—ammonium chloride (pH 8—10) buffer solutions were used.

A Union Giken Model SM-401 spectrophotometer and a Hitachi-Horiba Model F-7 pH meter were used. A Gilson Model HP-4 peristaltic pump and a JASCO spectrophotometer (UVIDEC-100IIW; Japan Spectroscopic Co.) were suitable for the flow-injection system.

Recommended manual procedure for iron

To the sample solution (in a 25-ml volumetric flask) containing 0—20 μg of iron, add 0.2 ml of 1% DTCS solution and 2 ml of 10^{-3} M 3, 5-diBr-PAESPAP solution. Adjust the pH to 6 with acetic acid—sodium acetate buffer solution and leave for 30 min. Then add 2 ml of 10^{-2} M EDTA. Dilute to the mark with water. Measure the absorbance at 570 or 750 nm against the reagent blank.

Recommended flow-injection procedure

The manifold is shown in Fig. 1. The teflon tubing used was of 0.5 mm i.d., except for the back-pressure coil which was 0.25 mm i.d. (20 cm length). The 10^{-4} M 3,5-diBr-PAESPAP solution, buffer solution (1 M NH_3—NH_4Cl) and an ascorbic acid solution (0.1%, w/v) were delivered, each at 0.81 ml min^{-1}, through tubes R, B and A respectively. The sample was injected into the ascorbic acid stream via a rotary valve to which a loop of given volume (usually 200 μl) was attached. Sample and reagent were mixed in the 200-cm coil. The absorbance was measured at 570 or 750 nm and recorded.

RESULTS AND DISCUSSION

Absorption spectra

Many metal ions form chelates with 3,5-diBr-PAESPAP [8]. In the presence of reducing agents such as ascorbic acid or DTCS, iron(III) forms the iron(II)—3,5-diBr-PAESPAP chelate. The absorption spectra are shown in Fig. 2. The absorbance at 570 nm (ϵ = 88000 l mol^{-1} cm^{-1}) or at 750 nm (ϵ = 39000 l mol^{-1} cm^{-1}) can be employed manually for the determination of iron. The absorbances at 750 nm caused by other metal chelates were almost negligible.

Effects of pH and reagent strength; calibration graph

The absorbance of the iron(II) chelate at different pH values was measured manually at 570 nm. The absorbance increased rapidly with increasing pH in the range 2.5—4.0, and reached a constant value over the pH range 5.0—9.5. This range is wider than that with PAR (pH 8.8—10.3) or 4-(2-thiazolylazo)-resorcinol (pH 8.9—10.3).

The results of the molar ratio method showed that iron(II) formed a 1:2 chelate with the reagent. The absorbance of the chelate was constant in the presence of more than a three-fold excess of the reagent, therefore 2 ml of 10^{-3} M solution was employed for the manual method.

Beer's law was obeyed up to 15 μg/25 ml at 570 nm and 35 μg/25 ml at 750 nm. The Sandell sensitivities were 6.3 × 10^{-4} μg cm^{-2} at 570 nm and 1.4 × 10^{-3} μg cm^{-2} at 750 nm. The sensitivity even at 750 nm is almost twice that available with the other reagents mentioned in the introduction.

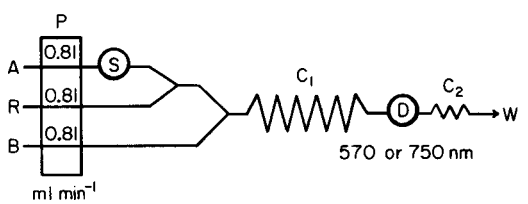

Fig. 1. Flow diagram: P, peristaltic pump with flow rates (ml min^{-1}); S, sample injector with loop (200 μl); C_1, mixing coil (200 cm); C_2, back-pressure coil (20 cm); D, flow-through cell (volume 8 μl, light path 10 mm). See text for reagents.

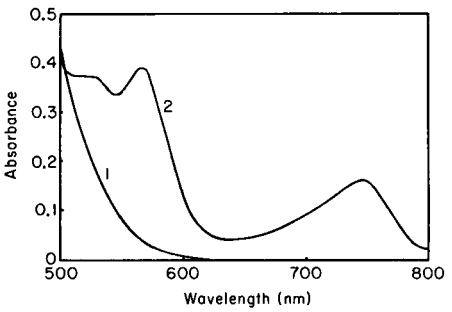

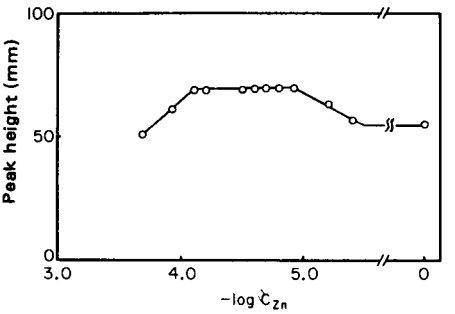

Fig. 2. Absorption spectra of 3,5-diBr-PAESPAP and its Fe(II) chelate: (1) 2×10^{-5} M 3,5-diBr-PAESPAP, pH 2.5—9.5; (2) iron(II) chelate for 4×10^{-6} M Fe(II), pH 6.0.

Fig. 3. Effect of zinc concentration in sample on the peak height for 220 $\mu g\ l^{-1}$ iron.

Interferences

The absorbances of the chelates formed with 3,5-diBr-PAESPAP and copper(II), nickel, cobalt and zinc are large at 570 nm, and their interferences are serious. At 750 nm interferences are small. To eliminate such interferences, masking agents such as thiourea, β-DTCPA, β-mercaptopropionic acid (MPA), *N,N*-dihydroxyethylglycine (DHG), DTCS, thioglycolic acid (TGA), sodium thiosulfate, nitrilotriacetic acid (NTA) and triethylenetetramine (trien) were examined (Table 1). Copper could be completely masked by thiourea, trien, DTCS, thiosulfate or β-DTCPA, nickel by DTCS, cobalt by DTCS or β-DTCPA, zinc by NTA, TGA or DHG (but incompletely by DTCS). Iron(III) readily formed the iron(II)—DTCS complex, but this was broken up by 3,5-diBr-PAESPAP to form the iron(II)-3,5-diBr-PAESPAP chelate. These results indicate that DTCS is a versatile masking agent for copper, nickel and cobalt. A large excess of DTCS slowed down the rate of chelate formation, but when 0.2 ml of 1% DTCS solution was used, 30 min was sufficient for complete colour development.

In addition, the copper(II) and zinc chelates formed with 3,5-diBr-PAESPAP were immediately decomposed by adding EDTA. When 4 ml of 10^{-2} M EDTA was added, the absorbance of the iron(II)—3,5-diBr-PAESPAP chelate remained constant for at least 90 min. Interferences by diverse metal ions could thus be eliminated by masking some metals with DTCS and decomposing other undesired chelates with EDTA. The tolerable amounts of various ions are listed in Table 2. There was no interference from 50 mg of Cl^-, I^-, NO_3^-, SO_4^{2-}, ClO_4^- or $S_2O_3^{2-}$, from 20 mg of phosphate, or from 10 mg of fluoride.

Application in flow-injection analysis

The flow-injection manifold is shown in Fig. 1. The rate of formation of the iron(II) chelate was found to increase with increasing pH. Complete colour development in the presence of ascorbic acid required a few minutes

TABLE 1

Absorbances at 570 nm of metal—3,5-diBr-PAESPAP chelates in the presence of masking agents (pH 6)[a]

Masking agent[b]	Cu(II) (μg)		Ni(II) (μg)		Co(II) (μg)		Zn(II) (μg)	
	6.3	12.7	5.9	11.8	5.9	11.8	6.5	13.0
None	0.290		0.564		0.380		0.180	
Thiourea (1 M, 1.0 ml)	0	0	>0.5	>0.5	0.335	>0.5	0.040	0.085
β-DTCPA (1%, 0.2 ml)	0.005	0.020	>0.5	>0.5	0.010	0.015	0.160	0.190
MPA (1%, 0.2 ml)	0.045	0.084	>0.5	>0.5	0.330	>0.5	0.030	0.058
DHG (0.1 M, 2.0 ml)	0.175	0.290	>0.5	>0.5	0.285	>0.5	0.010	0.020
DTCS (1%, 0.2 ml)	0.002	0.004	0.008	0.016	0.002	0.002	0.038	0.086
TGA (0.1%, 0.5 ml)	0.020	0.040	>0.5	>0.5	0.335	>0.5	0.001	0.015
Thiosulfate (1 M, 1.0 ml)	0.004	0.010	>0.5	>0.5	0.335	>0.5	0.090	0.150
NTA (10^{-2} M, 0.5 ml)	0.098	0.178	0.138	0.256	0.232	0.393	0	0
Trien (0.5%, 1.0 ml)	0	0.006	0.465	>0.5	0.110	0.211	0.041	0.064

[a]Abbreviations: β-DTCPA, β-dithiocarbaminopropionic acid; MPA, β-mercaptopropionic acid; DHG, *N*,*N*-dihydroxyethylglycine; DTCS, *N*-(dithiocarboxy)sarcosine; TGA, thioglycolic acid; NTA, nitrilotriacetic acid; trien, triethylenetetramine. [b]In the presence of each masking agent at the concentration examined, iron (5.6 μg) formed the 3,5-diBr-PAESPAP chelate completely.

at pH 6 but was almost immediate at pH 9; an ammonia/ammonium chloride buffer was therefore employed.

When the concentration of the chromogenic reagent was reduced from 10^{-4} to 10^{-5} M, the peak height for the iron(II) chelate decreased. When the concentration exceeded 10^{-4} M the baseline was unstable.

Peak heights were not affected by changes in the concentration of ascorbic acid solution between 0.05 and 0.5% and so a 0.1% solution was used.

Increasing the flow rate of each solution from 0.81 to 1.0 ml min^{-1} enhanced the peak heights but did nothing for reproducibility. At the flow rates chosen, the sample throughput was 30 h^{-1}. With a 100 cm mixing coil, the iron(II) chelate was incompletely developed. With a 300 cm coil, dispersion decreased the peak heights by 12% compared with the 200 cm coil.

Under the optimum conditions, with 200-μl injections, the calibration graph was linear for 10—330 μg l^{-1} iron at 570 nm and 20—440 μg l^{-1} iron at 750 nm. Although the sensitivity of the detector was almost doubled at

TABLE 2

Effect of diverse ions on the determination of 5.6 μg of iron in the presence of 4×10^{-4} M DTCS and 8×10^{-4} M EDTA

Determination at 570 nm		Determination at 750 nm	
Ion added	Tolerance limit (μg)	Ion added	Tolerance limit (μg)
Cu(II)	15	Cu(II)	30
Ni(II)	3	Ni(II)	60
Zn(II)	30	Zn(II)	130
Co(II)	20	Co(II)	150

570 nm, the signal became unstable owing to the increased reagent blank, whereas at 750 nm reproducible peaks were readily obtained.

Effects of foreign metals. For masking of some metals, DTCS was again examined but it was unsuitable; the peak heights at both 570 and 750 nm increased, probably because of absorbance by DTCS—copper or DTCS—cobalt complexes. Therefore, when various interfering metals are present, measurements must be done at 750 nm. In the determination of 200 $\mu g\ l^{-1}$ iron at 750 nm, no effects were observed from copper(II), cobalt(II), nickel, manganese(II) or cadmium at about the same concentration as iron. Although the absorbance of the zinc—3,5-diBr-PAESPAP chelate was negligible at 750 nm, the peak height of iron was enhanced and the reproducibility was improved in the presence of zinc. As can be seen in Fig. 3, the peak heights for iron became constant in the zinc concentration range $1.2—8 \times 10^{-5}$ M zinc, but then decreased because of excessive reagent consumption. Thus prior addition of zinc to a final concentration of 2×10^{-5} M in the sample solution is recommended. The addition of zinc had no effect on the rate of the reaction between iron(II) and 3,5-diBr-PAESPAP, as judged by the stopped-flow method. The reason for this enhancement of iron peak heights by zinc ion in the flow system is not clear.

Determination of total iron in drinking water

Potable water was collected in a polyethylene bottle (1 l) containing 10 ml of concentrated hydrochloric acid. Two aliquots of the sample were taken in 100-ml beakers (pyrex) and evaporated to less than 1 ml on a sand bath. Then 0.5 ml of 10^{-3} M zinc nitrate solution was added and the solution was diluted to 25 ml with 0.01 M HCl. The resulting solutions were injected into the flow-injection system. Some results are shown in Fig. 4 together with the results for iron(III) standard solutions treated with acid in the same way. The same samples were also analyzed by the usual batch methods with 3,5-diBr-PAESPAP and with TPTZ. The results given in Table 2 show that the values are in good agreement.

The proposed method is more sensitive than those with ferroin-type reagents or with PAR and its analogs mentioned earlier. Both the iron(II)

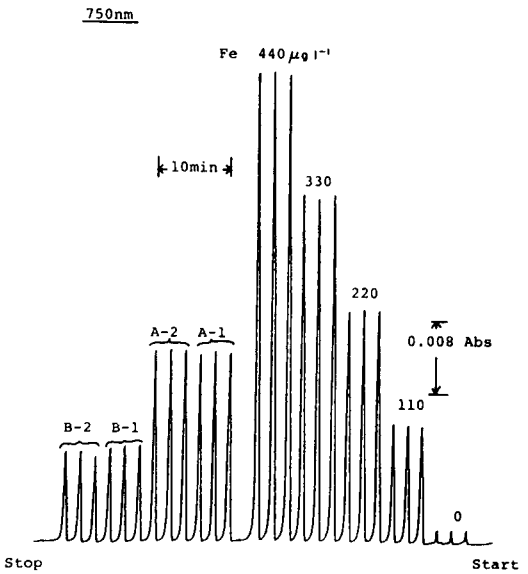

Fig. 4. Calibration graph and the determination of iron in potable water. All standards and samples are injected three times each. A-1,2: tap water (Daido Inst. Technol.) B-1,2: tap water (Nagoya).

TABLE 3

Comparison of procedures for the determination of iron in tap waters

	Iron content ($\mu g\ l^{-1}$)	
	Water A (Daido Inst. Technol.)	Water B (Nagoya)
Flow-injection method[a]	89	43
Batch method[a]	90	44
TPTZ batch method	89	44

[a]Proposed methods.

chelate with 3,5-diBr-PAESPAP and the reagent itself are very soluble in water, so that their use in flow-injection analysis is advantageous. Applications to various samples such as natural waters, boiler water, serum, etc. should pose no problems.

REFERENCES

1 J. Mortatti, F. J. Krug, L. C. R. Pessenda and E. A. G. Zagatto, Analyst, 107 (1982) 659.
2 T. Yotsuyanagi, K. Goto and M. Nagayama, Jpn. Analyst, 18 (1969) 184; T. Yotsuyanagi, R. Yamashita and K. Aomura, Anal. Chem., 44 (1972) 1091.

3 K. Ueda and Y. Yamamoto, Nippon Kagaku Kaishi, (1980) 1713.
4 K. Ueda, Y. Kiyota and Y. Yamamoto, Bull. Chem. Soc. Jpn., 54 (1981) 3763.
5 K. Ueda, S. Sakamoto and Y. Yamamoto, Nippon Kagaku Kaishi, (1981) 1111.
6 P. F. Collins, H. Diehl and G. F. Smith, Anal. Chem., 31 (1959) 1862.
7 H. Wada, T. Ishizuki and G. Nakagawa, Anal. Chim. Acta, 135 (1982) 333.
8 K. Ohshita, H. Wada and G. Nakagawa, Anal. Chim. Acta, 149 (1983) 269.
9 E. Russeva and O. Budevsky, Talanta, 20 (1973) 1329.
10 Y. Sakai and K. Kurogi, Bunseki Kagaku, 28 (1979) 429.

Analytica Chimica Acta, 153 (1983) 207—212
Elsevier Science Publishers B.V., Amsterdam — Printed in The Netherlands

DETERMINATION OF CADMIUM IN HUMAN URINE BY EXTRACTION WITH DITHIZONE IN A FLOW INJECTION SYSTEM[a]

J. L. BURGUERA and M. BURGUERA

Departamento de Quimica, Facultad de Ciencias, Universidad de Los Andes, Apartado Postal 542, Mérida 5101-A (Venezuela)

(Received 18th March 1983)

SUMMARY

A method for the rapid determination of cadmium in human urine by extraction with dithizone and flow injection analysis (f.i.a.) is described. The method could be used for the direct determination of ≥ 0.2 μg Cd l^{-1}, with a coefficient of variation of $\leq 3\%$. Results were in good agreement with those obtained by atomic absorption spectrometry, whereas f.i.a. was appreciably faster. A novel phase separator is described.

Cadmium is virtually absent from the human body at birth and accumulates with age for at least 50 years. At this age the average person not exposed to abnormal amounts of cadmium has a total body burden of 20—30 mg of cadmium, of which one-half to two-thirds occurs in the liver and kidneys [1]. The urinary cadmium excretion of individuals with no known abnormal exposure to cadmium is low and variable, and according to Perry and Schroeder [2], and Gardiner and Ottaway [3] is usually <5 μg l^{-1}. Cadmium is toxic to every system in the human body, whether ingested, injected or inhaled. There is a correlation between urinary cadmium excretion and the toxicity of cadmium [4]. For these reasons, the determination of cadmium at the low concentrations which may be of toxicological significance requires a highly sensitive method, such as spectrophotometry with dithizone [5], or atomic absorption spectrometry [6].

Usually, existing methods for the determination of cadmium in urine involve pre-concentration or ashing procedures, which are time-consuming [3, 6]. Klinghoffer et al. [7] studied the determination of lead and cadmium by liquid—liquid extraction with dithizone in chloroform using flow injection analysis (f.i.a.). However, their procedure was not sufficiently sensitive for use in the analysis of most clinical samples. Hence, the most important objectives of this work were to increase the sensitivity and selectivity of this procedure. As part of the investigation, two phase separators were constructed and their performance was compared.

---

[a] Presented at the XV Congreso Latinoamericano de Química, San Juan, Puerto Rico, 24—29 Oct., 1982.

0003-2670/83/$03.00

EXPERIMENTAL

Apparatus

The equipment conprised the following items: a five-channel peristaltic pump [model 375, Sage (Orion Research) Cambridge, MA, U.S.A.]; an injector with a self-sealing rubber septum [8]; a conventional segmentor [9] with two adjustable Acidflex tubes, and an extraction coil of Acidflex tubing; a phase separator of new design as described in detail below; and a spectrophotometer (UV-110-02, Shimadzu, Japan) with a 0.5-ml quartz flow cell (10-mm optical pathlength). Pump tubes were of Tygon for aqueous solutions and Acidflex for the organic phase. Figure 1 shows a schematic diagram of the manifold used.

Description of the phase separators. Figure 2 shows diagrams of the two phase separators used. Separator (a) makes use of the difference in density of the two phases and employs phase-separating papers to complete the separation of the phases. The aqueous phase, after being forced upward, passes to waste through a hydrophilic phase-separating paper disc (Whatman, cellulose, 10 mm diam.) held between two washers. The organic phase was carried into the flow cell, after passing through a hydrophobic phase-separating paper

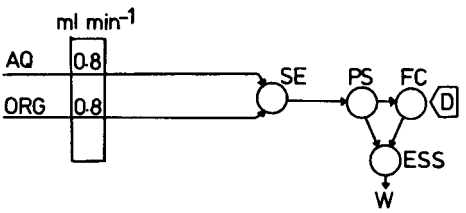

Fig. 1. Diagram of the extraction–flow injection system. (AQ) Aqueous phase; (ORG) organic phase; (SE) segmentor; (PS) phase separator; (FC) flow cell; (D) detector; (ESS) exit sucking system; (W) waste.

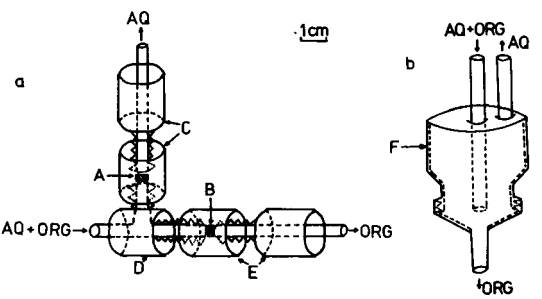

Fig. 2. Phase separators. (A) Hydrophilic phase-separating paper; (B) hydrophobic phase-separating paper; (C) joints for outlet of aqueous phase; (D) Daiflon body; (E) joints for outlet of organic phase; (F) brass body.

disc (silicone-treated Whatman paper, 10 mm diam.) also held between two washers. Both phase-separating papers had a durability of at least 1.5 h. After this time the papers were changed.

Phase separator 6 merely takes advantage of the difference in density between the two phases. The organic phase was forced downwards and thence to the flow cell. The aqueous phase flowed to waste.

Reagents

All reagents were of analytical reagent grade unless otherwise stated. The water used was doubly distilled. The chloroform used was passed as "suitable for use in the dithizone test" by adding a minute amount of dithizone to a portion of the chloroform in a stoppered test tube so that a faint green was produced; the green color should be stable for a day.

Stock cadmium solutions (100 μg ml^{-1}) were prepared by dissolving 100 mg of pure cadmium metal in a solution composed of 20 ml of water and 1 ml of concentrated nitric acid, transferred quantitatively to a 1-l volumetric flask and diluted to the mark with water.

Procedures

Sample collection. Urine samples were collected in polypropylene flasks which had previously been cleaned by rinsing with dilute nitric acid and water. The samples were quickly frozen after collection with a minimum of air space above the urine. Before analysis, the frozen urine was allowed to come to room temperature and thoroughly mixed.

Procedure for cadmium determination. The urine or standard solution was injected via the self-sealing rubber septum into a flowing stream of 3×10^{-3} M hydroxylamine, 5×10^{-3} M sodium potassium tartrate, 10^{-2} M potassium hexacyanoferrate(II) and 10^{-2} M tartaric acid adjusted to pH 10.5. Cadmium was extracted by 3.9×10^{-5} M dithizone in chloroform. After phase separation, the absorbance of the organic phase was measured at 518 nm against time. All absorbance values were based on peak-height measurements.

RESULTS AND DISCUSSION

The first step was to investigate the performances of the phase separators. For this purpose the above basic procedure was followed. As can be seen in Table 1, the separating efficiency of separator (b) was never >70%. This is probably because, even at low flow rates, the flow is too fast to allow time for complete phase segregation. Table 1 also shows that separator (a) can give complete segregation. This separator was therefore investigated in more detail.

The influence of sample volume injected is shown in Fig. 3. The peak height increases with increasing sample volume, but peak broadening and

TABLE 1

Effect of flow rate on the proportion of organic phase reaching the flow cell

Flow rate (ml min^{-1})[a]	Proportion of organic phase reaching flow cell (%)	
	Separator (a)	Separator (b)
0.6	100	70
0.8	100	66
1.0	100	63
1.2	95	60
1.4	92	54
1.6	90	46
1.8	87	40

[a]Same for both phases.

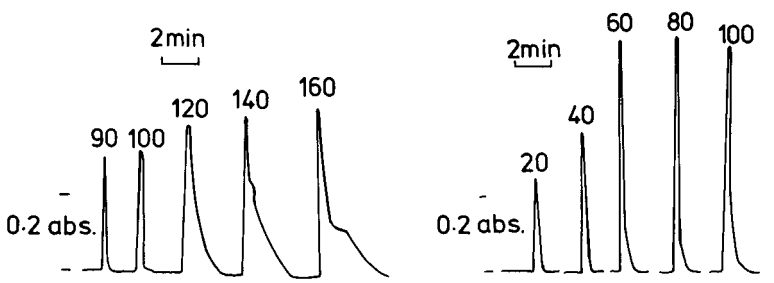

Fig. 3. Influence of injected sample volume. Numbers on the peaks indicate μl injected (1 μg Cd l^{-1}, 0.8 ml min^{-1} for both phases, 90-cm extraction coil, 50-cm mixing coil).

Fig. 4. Effect of extraction coil length on the peak height. Numbers indicate coil length in cm. (2 μg Cd l^{-1}; other conditions as in Fig. 3.)

tailing occur above 90 μl of sample, thus this volume is the largest that can be recommended. The effect of extraction coil length on the peak height is shown in Fig. 4. The peak height increases with increasing coil length up to ca. 60 cm. Very short coil lengths (<30 cm) give poor mixing so that extraction is incomplete. The length of the extraction coil was found to be unimportant between 60 and 90 cm. Above 90 cm, the peak height decreased slightly, probably because of degradation of the cadmium dithizonate on prolonged contact with strong alkali saturated with chloroform.

The effect of flow rate on the proportion of the organic phase reaching the flow cell is shown in Table 1. The proportion was obtained by measuring the difference between the volume of organic phase entering the flowing system and that leaving the flow cell. A better phase separation was achieved by decreasing the flow rate. This was later confirmed by measuring the absorbance, which markedly decreased as the flow rate of both phases was increased above 1.0 ml min^{-1}.

Interferences

Table 2 lists the metals normally present in urine which were tested for possible interference in the f.i.a. procedure. The metals were added to 5-ml samples of urine, which contained 0.7 μg Cd l^{-1}. The aqueous stream was a buffer containing 10^{-2} M tartaric acid or a mixture of masking agents (see below). An interference was defined as a deviation of more than two standard deviations from the mean cadmium value of the control sample. Varying the pH of the aqueous buffer stream was one of the most important ways of changing the degree of interference, but even at pH 12 (Table 2) the presence of other metal ions remained a problem. However, a mixture of hydroxylamine, sodium potassium tartrate and potassium hexacyanoferrate(II) in the aqueous stream [5] successfully masked the interfering ions at pH $\geqslant$10 (Table 2). Therefore, this mixture, at the concentrations described in the basic procedure was used in all subsequent studies.

Cadmium in urine

Cadmium was determined in urine to check the applicability of the method. No sample pre-treatment was required. The urine samples were injected directly into the flow-injection system, precalibrated in the normal manner. The calibration graph was linear up to 12 μg Cd l^{-1}, at which concentration the peak height absorbance was 1.16. The procedure was applied with 90-μl injections taken from 50-ml portions of urine to which known amounts of cadmium had been added, to check the recovery. Table 3 shows that good recoveries of cadmium were achieved.

The accuracy of the method was checked against samples analyzed by conventional atomic absorption spectrometry (a.a.s.) [6]. The results are shown in Table 4. The results obtained by f.i.a. are in good agreement with those obtained by a.a.s. Precision was established by replicate analysis of 5

TABLE 2

Effect of pH on the masking action of a hydroxylamine—tartrate—hexacyanoferrate(II) mixture

Ion studied	Interference (%)[a]				
	Without masking agents	With masking agents			
	pH 12	pH 8	pH 9	pH 10	pH 11
Co(II)	22	20	5	0	0
Fe(II)	18	18	18	2	0
Ni(II)	8	7	3	0	0
Pb(II)	14	10	12	3	0
Zn(II)	14	11	9	1	0

[a]Interference (%) denotes the % increase in absorbance obtained from 1.0 μg l^{-1} interferent and 0.7 μg Cd l^{-1}. Other conditions as in Table 3.

TABLE 3

Recovery of cadmium added to urine samples[a]

Cd in original sample ($\mu g\ l^{-1}$)	Cd added ($\mu g\ l^{-1}$)	Cd found ($\mu g\ l^{-1}$)	Recovery (%)
0.84	0.50	1.22	91
0.82	0.60	1.42	100
0.95	0.70	1.85	113
0.94	0.80	1.63	94
0.78	0.70	1.58	107
0.77	0.80	1.57	100

[a]Flow rates: 0.8 ml min^{-1}; 80-cm extraction coil; 50-cm mixing coil; 90-μl sample; aqueous and organic streams as in the Procedure.

TABLE 4

Determination of urine cadmium ($\mu g\ l^{-1}$) by f.i.a. and a.a.s.

Sample	F.i.a.			A.a.s.		
	Cd[a]	S.d.	R.s.d.	Cd	S.d.	R.s.d.
1	0.5	0.01	2	0.5	0.02	4
2	3.4	0.10	3	2.9	0.06	2
3	5.1	0.10	2	5.2	0.16	3
4	1.5	0.04	3	1.7	0.04	2
5	2.6	0.07	3	2.5	0.07	3
6	4.9	0.15	3	4.8	0.14	3
7	4.3	0.12	3	4.0	0.12	3
8	4.6	0.11	2	4.4	0.11	3

[a]Mean of 5 measurements with standard deviation and relative standard deviation.

samples over several months. The standard deviation and relative standard deviation were 0.10 μg Cd l^{-1} and 2.5%, respectively.

The procedure described is simple and rapid. The phase separator is efficient, and should be applicable to a wide range of extraction procedures.

REFERENCES

1 E. J. Underwood, Trace Elements in Human and Animal Nutrition, Academic Press, New York, 1977, pp. 243–257.
2 H. M. Perry, Jr. and H. A. Schroeder, Circulation, 12 (1955) 758.
3 P. E. Gardiner and J. M. Ottaway, Talanta, 26 (1979) 841.
4 H. M. Perry, Jr., H. A. Schroeder and A. F. Frederickson, J. Lab. Clin. Med., 44 (1953) 758.
5 B. E. Saltzman, Anal. Chem., 25(3) (1953) 493.
6 J. B. Willis, Anal. Chem., 34 (1962) 614.
7 O. Klinghoffer, J. Růžička and E. H. Hansen, Talanta, 27 (1980) 169.
8 J. L. Burguera and M. Burguera, Anal. Quim., Part B, 78 (1982) 307.
9 B. Karlberg and S. Thelander, Anal. Chim. Acta, 98 (1978) 1.

Analytica Chimica Acta, 153 (1983) 213—218
Elsevier Science Publishers B.V., Amsterdam — Printed in The Netherlands

THE USE OF ABSORBANCE RATIOS IN pK MEASUREMENTS BY SPECTROPHOTOMETRIC METHODS

ANTHONY J. WARING

Chemistry Department, University of Birmingham, P.O. Box 363, Birmingham B15 2TT (Gt. Britain)

(Received 19th April 1983)

SUMMARY

In order to improve the precision of the determination of pK values by spectrophotometric methods, the ratios of absorbance values at two or more wavelengths can be used. It is shown that these ratios can be handled in exactly the same way as absorbance values, provided that a simple correction is applied to the pK value calculated from them. The method is illustrated for the determination of protonation equilibria of weak organic bases, using acidity functions, by visible—u.v. spectrophotometry. Data are given for the protonation of the sesquiterpene, α-santonin, and the advantages of the method are discussed: it eliminates experimental scatter caused by variations in concentrations and cell pathlengths. The method applies equally to the protonation of bases in acids defined by the pH scale, and to the deprotonation of acids.

The ionization constants (pK values) of organic acids and bases are often determined by measuring the variation of the visible—ultraviolet spectrum of the compound with the acidity/basicity of solutions containing it. In the pH region, the protonation equilibrium is given by

$$BH^+ \rightleftharpoons B + H^+;\ K = [B][H^+]/[BH^+];\ pK = pH + \log[BH^+]/[B] \quad (1)$$

In dilute solutions the pK is a thermodynamic value [1]. In concentrated acids, where pH is inapplicable, an appropriate acidity function, H_B, can be used to define the acidity, with an analogous equation $pK = H_B + \log[BH^+]/[B]$. For many classes of compounds, the "correct" acidity function varies linearly with Hammett's acidity function, H_0, which is used in the general equation

$$\log[BH^+]/[B] = m_0[(H_0)_{1/2} - H_0] = pK - m_0H_0 \quad (2)$$

The value taken for pK is $m_0(H_0)_{1/2}$, where $(H_0)_{1/2}$ is the acidity at half-protonation: it is a thermodynamic value [2, 3]. The measurement of pK therefore simplifies to the measurement of the concentration ratio $[BH^+]/[B]$. The equation

$$\log[(\epsilon_1 - \epsilon_{B,1})/(\epsilon_{BH^+,1} - \epsilon_1)] = pK - m_0H_0 \quad (3)$$

0003-2670/83/$03.00

applies if the Beer law is obeyed: here ϵ_1 is the effective molar absorptivity of the stoichiometric compound at wavelength λ_1, and any known acidity, and $\epsilon_{B,1}$ and $\epsilon_{BH^+,1}$ are the molar absorptivities of pure B and BH^+ at λ_1.

In practice, stock solutions of the compound are often made in water or other solvents, aliquots are diluted to constant known volume with acids of known strength, and the absorbances D are measured in uniform silica cells. At constant concentration and cell length:

$$\log[(D_1 - D_{B,1})/(D_{BH^+,1} - D_1)] = pK - m_0H_0 \quad (4)$$

Alternatively, aliquots of stock solutions in a suitable organic solvent can have the solvent evaporated and then be made up to the required volume with acid, or the compound may be accurately weighed into the acid directly for absorbance measurement, especially if it has limited solubility. Clearly, there are numerous implied constants to relate the experimental absorbance D to ϵ: sample weight, solution volumes, optical pathlengths, and the assumptions of complete solubility and stability in solution. Since up to 20 solutions may be needed for a pK determination, there will be inevitable and sometimes important variations.

When the use of the ratios of absorbance at two or more suitably chosen wavelengths is adopted, any lack of consistency in solution concentrations or spectrophotometric cell pathlength ceases to be of importance. (Prudent technique would aim for consistency, so that absorbances would remain similar and have similar errors, but careful multiple-matching of u.v. cells, for example, is not necessary.) The accuracy of measurement becomes that of measuring absorbance, with the appropriate cell—solvent baseline corrections (see later), at preset wavelengths. Modern instrumentation is particularly well suited to the purpose, with highly reproducible wavelength setting or multiple fixed wavelength detection. The theory derived in the Appendix shows that if the ratio R of absorbance at wavelength λ_1 to that at λ_2 ($R = \epsilon_1/\epsilon_2 = D_1/D_2$) is used, then the equation obtained is

$$\log[(R - R_B)/(R_{BH^+} - R)] = pK - m_0H_0 + \log(\epsilon_{BH^+,2}/\epsilon_{B,2}) \quad (5)$$

which has the same form as Eqns. (3) and (4) except that any calculation gives (pK + log $\epsilon_{BH^+,2}/\epsilon_{B,2}$) from Eqn. (5) in place of pK. The correcting quantity should be easily defined and is generally small. If ϵ_{BH^+} cannot easily be experimentally determined (e.g., if the compound reacts rapidly at high conversion to the protonated form), the method outlined in the Appendix can be used to define it.

The method was used in measuring the basicity equilibria of a number of steroidal and sesquiterpenoid ketones in aqueous sulphuric acid. Typical data, and the parameters derived from them, are given for α-santonin in Table 1. This compound is extremely sparingly soluble, so that the preparation of aqueous stock solutions at the 20 mg l^{-1} level was unreliable; solution by direct weighing was slow and at high acidities decomposition set in.

Calculation based on the absorbance ratio at 250/268 nm gave a value of

TABLE 1

Basicity data for α-santonin, using absorbance ratios, at 25°C in aqueous sulphuric acid medium

Acidity ($-H_0$)[a]	1.11	1.50	1.50	1.95	1.98	2.25	2.33	2.43	2.67	2.76	3.10
R 250/268[b]	1.602	1.556			1.540		1.494	1.423	1.338	1.320	1.192
Calculated[c]	1.579	1.559			1.511		1.450	1.427	1.360	1.332	1.205
R 310/268[d]	0.025	0.039	0.073	0.058	0.089	0.109	0.130	0.159	0.223	0.224	0.316
Calculated[e]	0.040	0.055	0.055	0.090	0.093	0.130	0.144	0.162	0.214	0.235	0.323
(Calculated[f])	0.077	0.084	0.084	0.104	0.106	0.132	0.142	0.156	0.201	0.221	0.310
Acidity ($-H_0$)[a]	3.47	3.52	3.86	4.10	4.58	4.94	5.73	5.74	6.04	6.40	6.53
R 250/268[b]	1.026	1.038	0.896	0.787	0.754	0.691	0.622	0.580	0.534	0.608	0.600
Calculated[c]	1.049	1.028	0.895	0.816	0.705	0.656	0.608	0.608	0.601	0.596	0.595
R 310/268[d]	0.406	0.407	0.506	0.506	0.555	0.559	0.568	0.567	0.611	0.567	0.571
Calculated[e]	0.412	0.423	0.484	0.514	0.550	0.564	0.575	0.575	0.576	0.577	0.577
(Calculated[f])	0.410	0.423	0.490	0.522	0.556	0.567	0.574	0.574	0.575	0.576	0.576

[a]Acidity on Hammett's acidity function, H_0, as tabulated by Johnson et al. [4]. [b]Ratio of absorbance at 250 nm/268 nm. Errors ±0.001 on each absorbance value would give an error in the ratio of about 0.016 to 0.008, increased by any irreproducibility in wavelength setting. [c]Calculated using $R_{BH^+} = 0.590, R_B = 1.602, m_0 = 0.73, m_0(H_0)_{1/2} + \log(\epsilon_{BH^+}/\epsilon_B)_{268} = -2.45$ = "uncorrected" $m_0(H_0)_{1/2}$. RMS error of each point is 0.027. [d]Ratio of absorbance at 310 nm/268 nm. [e]Calculated using $R_{BH^+} = 0.578$, $R_B = 0.025$, $m_0 = 0.86$, $m_0(H_0)_{1/2} + \log(\epsilon_{BH^+}/\epsilon_B)_{268} = -2.61$ = "uncorrected" $m_0(H_0)_{1/2}$. RMS error of each point is 0.016. [f]Calculated using $R_{BH^+} = 0.576$, $R_B = 0.072$, $m_0 = 0.97$, $m_0(H_0)_{1/2} + \log(\epsilon_{BH^+}/\epsilon_B)_{268} = -3.06$ = "uncorrected pK". RMS error of each point is 0.020. Given to show the sensitivity of the optimised value of m_0 to relatively small changes in the parameter R_B, and to variations in the experimental data.

-2.45 for $pK + \log(\epsilon_{BH^+,2}/\epsilon_{B,2})$. The ratio of ϵ values, $\epsilon_{BH^+}/\epsilon_B$ at 268 nm is $1.12 \times 10^4/0.79 \times 10^4$ (i.e., 1.418), the logarithm of which is 0.15. The corrected pK value is then $-2.45 - 0.15 = -2.60$. Similarly, the ratio of absorbances at 310/268 nm gave an uncorrected value -2.61, which is corrected to a pK value of -2.76. Division of the results by the appropriate m_0 values gives corrected acidities at half-protonation, $(H_0)_{1/2} = -3.56$ and -3.21, respectively. Variations in results of this order are commonly found. The particular sensitivity of m_0 values to minor variations in data or other parameters is shown in the last line of Table 1 and is not uncommon. The smallness of the correction factor, $\log(\epsilon_{BH^+}/\epsilon_B)_2$ should be noted: in this case, it is within the experimental error of the results.

EXPERIMENTAL

Method

A Pye-Unicam SP8-100 visible—u.v. spectrophotometer, with thermostatted cells, was interfaced to a Hewlett-Packard HP-97S printing calculator. To correct each absorbance to its value relative to pure acid (solvent) in the sample cell, a program (Baseline) was written which allows up to 16 baseline absorbances (solvent in sample cell vs. solvent in reference cell) to be stored for up to four cell pairs and four wavelengths. The highest wavelength, measured first, is chosen to be a "no absorbance" value. For each solution measured thereafter, the same pair of cells is retained and the output from the spectrophotometer is corrected at each wavelength to give a printed, serialised absorbance value. (This correction is not required if the spectrophotometer makes it routinely, or if minor baseline variations are ignored. However, it is useful and easy, as part of checks against contamination and normal careful practice.) The appropriate ratios are calculated separately and plotted according to Eqn. (5), or fitted iteratively to the theoretical curve (see Appendix).

The normal considerations [5] apply when wavelengths are selected for measurement. They are particularly critical when medium effects are present (shown as a lateral movement or sharpening of the peaks with changes in the medium, even when there is no significant change in the ionisation ratio). Measurements should be made at, or close to, λ_{max} in the solutions where the medium effect is greatest. This is almost always λ_{max} for the protonated form, BH^+, at high acidities. It is advantageous also to measure at λ_{max} for B, and at any isosbestic points (for use in the ratios). If a medium effect is seen on a peak, two wavelengths chosen should be on the same side so that both absorbances rise or fall together. Previous methods that have been applied to mitigate the problem include mathematical procedures involving absorbance values [6, 7], the use of differences between absorbance values at two wavelengths [8], and the use of the integrated areas [9] or half-widths [10] of spectral bands. All, however, require the assumptions of constancy between absorbances D and ϵ outlined earlier.

It may be noted that other measures of acidity have been advanced; for example, Bunnett and Olsen [11] introduced the use of $(H_0 + \log[H^+])$ instead of H_0, and Cox and Yates [12] have developed the use of "excess acidities". All, however, require measurement of $\log[BH^+]/[B]$ for their application. The method suggested here is applicable in all cases: as a source of $\log[BH^+]/[B]$, $\log[(R - R_B)/(R_{BH^+} - R)] - \log(\epsilon_{BH^+,2}/\epsilon_{B,2})$ simply replaces $\log[(\epsilon - \epsilon_B)/(\epsilon_{BH^+} - \epsilon)]$.

Description of program

When the absorbance (molar absorptivity) or absorbance ratio for the completely-formed protonated species BH^+ is not quite accessible with sufficient reliability, the following program can be used. It may be needed if the species reacts very rapidly, so that extrapolation of readings to the time of mixing is unreliable, or if there is a heat-of-mixing effect, or if a significant medium effect starts to intrude at high acidities. It can also be used for curve-fitting to Eqns. (3), (4), or (5) in any case.

The three quantities m_0, R_{BH^+} (or ϵ_{BH^+}), and $pK + \log \epsilon_{BH^+,2}/\epsilon_{B,2}$ (Eqn. 5) or pK (Eqns. 3 and 4) are treated as disposable constants. The program used here is written for the HP-97S calculator, and is easily reformulated for a microcomputer. Approximate, trial values of the three constants are input, followed by the values of experimental R or ϵ at each H_0 which are stored on magnetic cards. The residuals from the calculated R or ϵ are found, together with the partial differentials of R or ϵ at each point with respect to variation of each of the three "constants". The matrices (3×3 and 3×1) for application of a first-order Newton—Raphson curve-fitting procedure are then filled [13]. The standard matrix-inversion and multiplication routine (Hewlett-Packard Standard Pac program) gives corrections to be applied to each constant parameter. Repeating the process rapidly converges to final values for m_0, pK and R_{BH^+} or ϵ_{BH^+}. Experience has shown that two or three passes allow convergence within the accuracy of the experimental values. Annotated listings of this program (Newton—Raphson Basicity from u.v.), and of the unrelated baseline-correction program for the Pye-Unicam SP8-100 (Baseline) are available from the author. Clearly, in the pH region, m_0 has the value unity, and H_0 is directly replaced by pH. The general method also applies, with trivial modification to terminology, to measurements in solutions for which the basicity must be defined by basicity functions.

APPENDIX

R is defined as the ratio of absorbance at λ_1 to that at λ_2: $R = D_1/D_2$. At λ_1, $D_1/l = [B]\epsilon_{B,1} + [BH^+]\epsilon_{BH^+,1}$ and at λ_2, $D_2/l = [B]\epsilon_{B,2} + [BH^+]\epsilon_{BH^+,2}$, where l is the cell pathlength (cm); [B] and $[BH^+]$ are molar concentrations.

For the pure protonated form: $R_{BH^+} = \epsilon_{BH^+,1}/\epsilon_{BH^+,2}$; and for the unprotonated form: $R_B = \epsilon_{B,1}/\epsilon_{B,2}$. Thus at λ_1:

$$D_1/l = R_B[B]\epsilon_{B,2} + R_{BH^+}[BH^+]\epsilon_{BH^+,2}$$

and

$$R = (R_B[B]\epsilon_{B,2} + R_{BH^+}[BH^+]\epsilon_{BH^+,2})/([B]\epsilon_{B,2} + [BH^+]\epsilon_{BH^+,2})$$

$$(R - R_B)/(R_{BH^+} - R) = ([BH^+]\epsilon_{BH^+,2})/([B]\epsilon_{B,2})$$

$$\log[BH^+]/[B] = \log[(R - R_B)/(R_{BH^+} - R)] - \log[\epsilon_{BH^+,2}/\epsilon_{B,2}]$$

From Eqn. 2

$$\log[(R - R_B)/(R_{BH^+} - R)] = pK - m_0H_0 + \log(\epsilon_{BH^+,2}/\epsilon_{B,2}) \quad (5)$$

This equation is of the same form as Eqns. (3) and (4), except that a correction quantity, $\log(\epsilon_{BH^+}/\epsilon_B)_2$ must be applied to the normally-calculated pK value. If, for example, a linear plot is made of $\log[(R - R_B)/(R_{BH^+} - R)]$ against H_0, it has gradient $(-m_0)$ and intercept on the axis $H_0 = 0$ with value $[pK + \log(\epsilon_{BH^+,2}/\epsilon_{B,2})]$. An interpolated, and possibly more accurate result, is gained by determining the value of H_0 at which $R = 0.5(R_B + R_{BH^+})$, i.e., $\log(R - R_B)/(R_{BH^+} - R) = 0$. This value, multiplied by m_0, is $pK + \log(\epsilon_{BH^+,2}/\epsilon_{B,2})$. A similar plot based on absorbances, according to Eqns. (3) or (4), gives pK as the intercept.

REFERENCES

1 A. Albert and E. P. Serjeant, The Determination of Ionization Constants, Chapman and Hall, London, 1971.
2 L. P. Hammett, Physical Organic Chemistry, 2nd edn., McGraw-Hill, New York, 1970, Ch. 9.
3 C. H. Rochester, Acidity Functions, Academic Press, London, 1970; M. Liler, Reaction Mechanisms in Sulphuric Acid, Academic Press, London, 1971.
4 C. D. Johnson, A. R. Katritzky and S. A. Shapiro, J. Am. Chem. Soc., 91 (1969) 6654.
5 K. L. Cook and A. J. Waring, J. Chem. Soc., Perkin Trans. II, (1973) 84.
6 A. R. Katritzky, A. J. Waring and K. Yates, Tetrahedron, 19 (1963) 465.
7 L. A. Flexser, L. P. Hammett and A. Dingwall, J. Am. Chem. Soc., 57 (1935) 2103.
8 C. T. Davis and T. A. Geissman, J. Am. Chem. Soc., 76 (1954) 3507.
9 W. M. Schubert and R. H. Quacchia, J. Am. Chem. Soc., 85 (1963) 1278.
10 T. S. Sorensen, Can. J. Chem., 42 (1964) 724.
11 J. F. Bunnett and F. P. Olsen, Can. J. Chem., 44 (1966) 1899.
12 R. A. Cox and K. Yates, J. Am. Chem. Soc., 100 (1978) 3861.
13 See, e.g., K. J. Johnson, Numerical Methods in Chemistry, M. Dekker, New York, 1980, pp. 279 et seq.

Analytica Chimica Acta, 153 (1983) 219—227
Elsevier Science Publishers B.V., Amsterdam — Printed in The Netherlands

SENSITIVE FLOTATION—SPECTROPHOTOMETRIC DETERMINATION OF PLATINUM BASED ON SYSTEMS WITH CHLOROSTANNATE(II) AND BASIC DYES

Z. MARCZENKO* and K. KALINOWSKI

Department of Analytical Chemistry, Technical University, 00-664 Warsaw (Poland)

(Received 3rd March 1983)

SUMMARY

Sensitive flotation—spectrophotometric methods are based on the ion-associates formed by the anionic chlorostannate(II) complex of platinum with the basic dyes rhodamine 6G, Victoria blue B, Victoria blue 4R and Capri blue. The ion-associates finally formed are sparingly soluble in water; when shaken with a suitable organic liquid, they accumulate quantitatively at the phase boundary or on the wall of the separatory funnel. The compound with rhodamine 6G, separated and washed, is dissolved in acetone; those ones with the other basic dyes are dissolved in methanol. In the best method, with rhodamine 6G, the molar absorptivity is 2.8×10^5 l mol^{-1} cm^{-1}; with the other dyes, the molar absorptivities are $2.0—2.45 \times 10^5$. Beer's law is obeyed over the range 0.08—0.6 μg Pt ml^{-1}. The separated ion-associate formed with rhodamine 6G (R6G) is considered to have the formula $[(R6G^+)_3][Pt(SnCl_3)_5^{3-}]$. The effects of other platinum metals on the determination of platinum with rhodamine 6G were examined; some interference was found from palladium and rhodium. Trace amounts of platinum in palladium could be determined after separation of platinum by extraction with triphenylphosphine oxide in 1,2-dichloroethane.

Ion-pairs of monovalent anionic complexes of many elements with univalent cations of basic dyes (1:1 type), sparingly soluble in aqueous phases, are extracted into slightly polar solvents. This forms the basis of extraction—spectrophotometric methods for the determination of various elements [1]. In the case of multivalent anionic complexes, the ion-associates formed are not extracted but, after the aqueous phase has been shaken with a suitable organic solvent, accumulate quantitatively at the phase boundary or on the wall of the separatory funnel. After careful decantation of both liquid phases the washed precipitate (which adheres to the wall of the separatory funnel) can be dissolved in a small volume of a polar organic solvent. The operation of separating the sparingly soluble ion-associate from the aqueous phase by shaking with a non-polar solvent has been called flotation by Babko et al. [2]. This operation combined with measurement of the absorbance of coloured solutions of the ion-associate in polar organic solvents leads to very sensitive (molar absorptivities $1.5—5 \times 10^5$ l mol^{-1} cm^{-1}) flotation—spectrophotometric methods [3].

0003-2670/83/$03.00

Flotation consists in collection of solid particles of pseudosolution (suspension) on the surface of gas bubbles in a liquid (water phase) or of liquid droplets in a water phase. Carrying the component to be concentrated to a phase boundary is the common feature of flotation processes. Flotation of ion-associates can occur in the absence of a surfactant; the associates discussed here contain basic dyes with multiple aromatic rings, which form hydrophobic particles. The bubbling processes used in classical industrial flotation and in its analytical application [4] are replaced by shaking the aqueous suspension of the ion-associate with a slightly polar organic solvent.

In hydrohalic acid medium and in the presence of tin(II), platinum metals form multivalent anionic complexes, called cluster compounds [5—9]. These anionic complexes give floatable ion-associates with some basic dyes, which have already been used to advantage in flotation—spectrophotometric methods for the determination of rhodium [10] and iridium [11, 12]. In the present paper, the possibility of flotation isolation and spectrophotometric determination of platinum is discussed.

EXPERIMENTAL

Reagents and apparatus

Platinum standard solution (1 mg Pt ml^{-1}) was prepared by dissolving the pure metal in aqua regia. The solution was evaporated several times with concentrated hydrochloric acid and the residue was dissolved in 4 M hydrochloric acid.

The radioisotopes (OPiDI Świerk) used were ^{193}Pt as the metal, and ^{113}Sn as tin(II) chloride in 6 M hydrochloric acid.

Rhodamine 6G (R6G) was used as an aqueous 1×10^{-3} M solution. The preparation was purified by dissolving in ethanol and precipitating by addition of a five-fold volume of diethyl ether. Other basic dyes were used as 1×10^{-3} M solutions of the analytical-reagent grade chemicals. Tin(II) chloride dihydrate was used as a 10% solution in 2 M hydrochloric acid.

A SPECORD UV—VIS recording spectrophotometer and VSU-2P spectrophotometer were used with 1-cm cells.

Procedure with rhodamine 6G

Evaporate to dryness the acidic (HCl) sample solution, containing not more than 15 μg of platinum, on a boiling water bath. Add 2 ml of the tin(II) chloride solution. Transfer the solution to a separatory funnel. Add appropriate amounts of concentrated hydrochloric acid and water to obtain 20 ml of solution 0.8—1.2 M in hydrochloric acid. Then add 1 ml of rhodamine 6G solution and 5 ml of di-isopropyl ether and shake for 1 min. Open the separatory funnel from the top, allow the phases to separate and slowly discard the aqueous layer. Wash the ether phase and the separated precipitate by shaking with two successive 20-ml portions of 1 M hydrochloric acid for 30 s each. Carefully remove the aqueous and the organic layers and dissolve

the isolated ion-associate in acetone. Transfer the solution to a 25-ml volumetric flask and dilute to the mark with acetone. Measure the absorbance of the solution at 530 nm against a reagent blank prepared in the same way.

For preparation of the standard curve, apply the same procedure to suitable portions of the platinum standard solution.

RESULTS AND DISCUSSION

Preliminary studies

Preliminary studies were designed to find basic dyes forming floatable ion-associates with anionic chloride or chlorostannate(II) platinum complexes. The dyes tested were rhodamine 6G, rhodamine B, malachite green, brilliant green, crystal violet, Victoria blue B, Victoria blue 4R, methylene blue, Capri blue, Nile blue A, safranine T, Meldola's blue, Bindschedler's green.

The reactions were examined in the range 0.4—4 M hydrochloric acid for 30—60-fold molar excesses of the basic dye with respect to platinum (10 μg). The aqueous solutions (pseudo-solutions) were shaken with benzene, toluene, di-isopropyl ether, xylene and chloroform. In none of the systems examined was precipitation of the ion-associate of the anionic chloride complex of platinum(IV) with the basic dye observed. Addition of the basic dye to a solution containing the chlorostannate(II) complex of platinum resulted in the formation of a precipitate dispersed in the aqueous phase. After the aqueous phase had been shaken with di-isopropyl ether, benzene or toluene, the sparingly soluble ion-associate accumulated at the phase boundary or on the wall of the separatory funnel.

The absorbance of the solutions obtained by dissolving the isolated precipitates in polar solvents was proportional to the concentration of platinum (the central atom of the anionic complex). This fact forms the basis of the proposed spectrophotometric determination of platinum. Methanol, ethanol, acetone and dimethylformamide (DMF) were tested as solvents for the precipitates. The absorbance of the blanks was also measured because basic dyes may accumulate as sparingly soluble precipitates (at the phase boundary or on the wall of the funnel), not only as ion-associates with the anionic chlorostannate(II) complex of platinum but also as ion-pairs with $SnCl_3^-$. The isolated precipitates were washed with a suitable solution in order to remove the dye bound to the chlorostannate(II) complex.

Rhodamine 6G, crystal violet, Capri blue, Victoria blue B and Victoria blue 4R, used with suitable floating agents at suitable acidity, provided systems in which quantitative separation of platinum-containing ion-associates took place. These five systems can be utilized for flotation—spectrophotometric methods with molar absorptivities exceeding 2×10^5. Such a method with crystal violet was proposed several years ago [13]. The most promising system was that with rhodamine 6G. In the case of the other eight dyes tested, the systems were of no analytical use: the flotation of platinum was not quantitative, or simultaneous extraction occurred, or the ion-associate

decomposed when the precipitate was washed in order to reduce the blank (removal of the dye ion-pair with $SnCl_3^-$).

The system with platinum and rhodamine 6G

In hydrochloric acid medium, platinum forms anionic complexes with $SnCl_3^-$ and chloride ions. The composition of these complexes depends on the molar excess of tin(II) (with respect to platinum), acidity and chloride concentration. It was found that all platinum complexes, occurring in the range 0.4—4 M hydrochloric acid, formed sparingly soluble compounds with rhodamine 6G. These complexes separated on shaking with di-isopropyl ether. The best solvent for the separated precipitate was acetone.

Optimal conditions. The final absorbance of the acetone solution depended on the acidity of the aqueous solution in which the complex of platinum with tin(II) and chloride was formed, as well as on the acidity during shaking with the floating agent. This indicates that ion-associates of various anionic complexes of platinum are formed and floated depending on the conditions. When the platinum complex was formed in ca. 1 M hydrochloric acid and the same acid concentration was maintained during flotation, the absorbances of the acetone solutions were reproducible and attained a maximum (Fig. 1).

The absorbances of acetone solutions of the ion-associate with rhodamine 6G also depend on the excess of the dye, concentration of tin chloride and shaking time. For quantitative separation of platinum from the aqueous phase as a sparingly soluble ion-associate, a 40—60-fold molar excess of rhodamine 6G (with respect to platinum) is necessary. Further increase in the dye concentration results in higher blank values (Fig. 2). The amount of the organic liquid required to float the precipitate has no effect on the

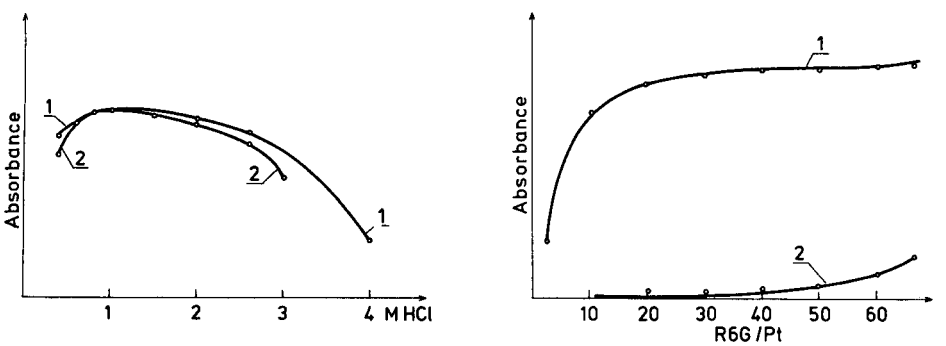

Fig. 1. The effect of the hydrochloric acid concentration on the absorbance of the acetone solution of the ion-associate with rhodamine 6G (flotation with di-isopropyl ether): (1) on formation of the Pt complex with $SnCl_3^-$ (1 M HCl concentration during flotation); (2) on flotation (the acidity during formation of the Pt complex with $SnCl_3^-$ was about 1 M HCl).

Fig. 2. Dependence of the absorbance of the acetone solution of the ion-associate on the excess of rhodamine 6G (flotation with di-isopropyl ether): (1) absorbance of the solutions measured against the blank; (2) absorbance of the blank measured against acetone.

effectiveness of separation of the platinum ion-associate. For quantitative separation, the shaking time must be at least 60 s.

In this system, the ion-pair of $SnCl_3^-$ with the dye forms a bulky precipitate which coprecipitates and floats with the platinum-containing ion-associate. However, the latter complex is more stable. When the precipitate is washed with 1 M hydrochloric acid, the rhodamine 6G—$SnCl_3^-$ complex decomposes (the dye passes to the aqueous phase); decomposition is rapid and after two washes with 20-ml portions of 1 M acid (shaking time 30 s), the absorbance of the blank does not exceed 0.04. Washing the precipitate causes slight losses of platinum by partial decomposition of the platinum-containing associate.

The flotation process is affected by the concentration of tin(II). Large amounts of tin(II) in the aqueous phase yield a bulky precipitate. When the mass of the precipitate of the rhodamine 6G—$SnCl_3^-$ ion-pair is insufficient, the separation of platinum is incomplete. The maximum and reproducible absorbances of the acetone solutions were obtained when the concentration of tin(II) in the aqueous phase was in the range 0.02—0.04 M; at higher tin(II) chloride concentrations, the blank increased. The effect of tin(II) on the absorbance of the acetone solutions is shown in Fig. 3.

The platinum-containing ion-associate can be floated with benzene or toluene from about 3.5 M hydrochloric acid. When these solvents are used, the precipitate accumulates mainly at the phase boundary and not on the wall of the separatory funnel as in the case of di-isopropyl ether. This makes it difficult to remove benzene or toluene from the funnel without losses of the required ion-associate.

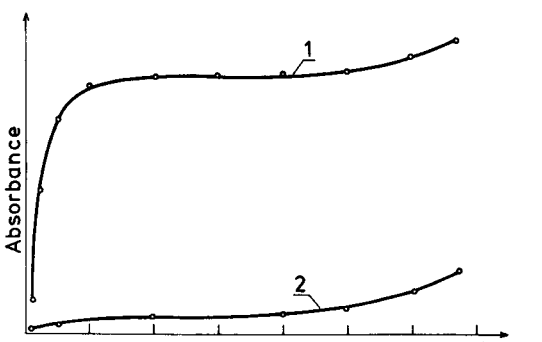

Fig. 3. Dependence of the absorbance of the acetone solution of the ion-associate on the concentration $SnCl_2$ (flotation with di-isopropyl ether): (1) absorbance of the solutions measured against the blank; (2) absorbance of the blank measured against acetone.

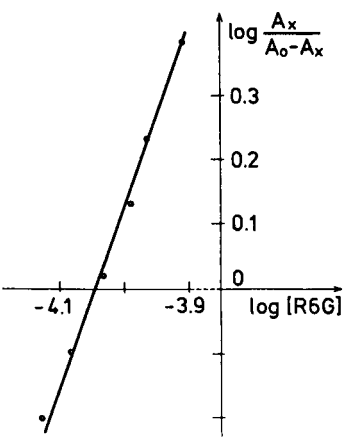

Fig. 4. Determination of the Pt:R6G molar ratio in the floated compound by the Bent and French method.

Calibration. The above studies made it possible to prepare a calibration graph. Beer's law is obeyed in the concentration range 0.08—0.6 μg Pt ml^{-1}. Molar absorptivity is 2.8×10^5 l mol^{-1} cm^{-1} (specific absorptivity $a = \epsilon$/atomic mass × 1000 = 1.43). The precision and accuracy of the method were verified by analysing solutions containing known amounts of platinum. The results are shown in Table 1.

Interferences. The effects of other platinum metals on the determination of platinum by the proposed method were examined. The results are shown in Table 2. Significant effects were found for rhodium and palladium. Complexes of the other platinum metals with $SnCl_3^-$ are formed more slowly and therefore their effects on the separation and determination of platinum are less significant.

The method was applied to the determination of platinum in palladium wire. Platinum was separated from palladium by extraction with triphenylphosphine oxide (TPPO) in 1,2-dichloroethane [14] and the proposed method was applied after back-extraction into 1 M hydrochloric acid. The platinum content was found to be 3.6 ± 0.3 × 10^{-3}% (for seven determinations). A recovery of 103% was obtained on adding 6 μg of platinum. Owing to the high sensitivity of the method, platinum was determined from small samples (e.g., 0.1 g) of the preparation examined.

TABLE 1

Statistical evaluation of the results of the determination of platinum with rhodamine 6G

Platinum (μg)		Standard deviation[a]	Relative standard deviation (%)	Confidence limits (probability level 0.95)
Added	Found			
4.00	4.07	0.13	3.2	4.07 ± 0.10
8.00	7.92	0.10	1.3	7.92 ± 0.17
12.00	12.20	0.09	0.8	12.20 ± 0.21

[a]For seven determinations.

TABLE 2

Effect of metal ions on the determination of platinum (4 μg) with rhodamine 6G

Metal	Mass ratio of metal to Pt	Platinum recovery (%)	Metal	Mass ratio of metal to Pt	Platinum recovery (%)
Palladium	1	99, 101	Iridium	5	101, 100
	5	104, 105		10	108, 112, 113
	10	108, 110, 107		20	130, 132
Rhodium	2	102, 103	Osmium	5	104
	5	105, 109, 110		10	110, 111, 115
	10	124, 128	Ruthenium	5	101, 102
				10	116, 118

Composition of the complex. The molar ratio of platinum to rhodamine 6G in the separated and washed ion-associate was determined by comparing the absorbance of acetone solutions of the ion-associate containing a known amount of platinum with the absorbances of acetone solutions of the dye taken in 3-fold molar excess with respect to platinum in the former solution. The absorbances were similar in both cases. The spectrum of the acetone solution of the ion-associate was identical with the spectrum of rhodamine 6G in this solvent. This result is in agreement with the data obtained with the aid of Bent and French's logarithmic method [15] (Fig. 4). It can be accepted that the molar ratio of platinum to rhodamine 6G in the separated and washed associate is 1:3.

The molar absorptivity for the proposed method is a little less than thrice the value for rhodamine 6G in acetone. This result is somewhat lower than the expected one, which can be attributed to losses of the ion-associate during handling. Tests with the radioisotope ^{193}Pt showed that about 98.5% of platinum was floated. After two washings of the compound (and inevitable mechanical losses) about 88% of the original platinum remains in the precipitate.

In order to establish the number of tin atoms per platinum atom in the ion-associate, tin was determined radiometrically by using the radioisotope ^{113}Sn. Nine determinations of tin in the washed precipitate gave a mean value of Pt:Sn = 1:5.8. It follows from literature data [5, 7, 9] that, in about 1 M hydrochloric acid medium, platinum forms the anionic complex $Pt(SnCl_3)_5^{3-}$. If the formula $[(R6G^+)_3][Pt(SnCl_3)_5^{3-}]$ is ascribed to the separated associate, the positive bias of the results may be attributed to contamination of the precipitate with tin not bound in the platinum ion-associate, or to the presence (in the washed precipitate) of a mixture of associates of rhodamine 6G with anionic platinum complexes of different composition.

Systems of platinum with other basic dyes

The possibility of the application of Capri blue, Victoria blue B and Victoria blue 4R to the flotation—spectrophotometric determination of platinum was examined. The platinum-containing ion-associates with these dyes can be floated with di-isopropyl ether, benzene and toluene, but only benzene gives reproducible results. After the aqueous phase had been shaken with benzene, the sparingly soluble ion-associates of platinum accumulated mostly on the wall of the separatory funnel (above the level of the aqueous phase) and in small amounts at the phase boundary. When toluene was used, the precipitate accumulated mainly at the phase boundary, which makes quantitative separation awkward. With benzene and toluene, flotation proceeded well even at 1:4 solvent/water ratios. With di-isopropyl ether, the effectiveness of the flotation separation depended on the ratio of the phase volumes. At a di-isopropyl ether/water volume ratio of 1:4, the flotation of platinum was not quantitative; at a ratio of 1:1, the precipitate separated in the correct manner. The mass of the precipitate formed in these systems was larger than that observed with rhodamine 6G.

Methanol was the best solvent for the platinum-containing ion-associates with Capri blue, Victoria blue 4R and Victoria blue B. Dissolution was total after brief shaking. The absorbances of the solutions obtained were somewhat higher than those of solutions in acetone and dimethylformamide. The precipitates floated out were washed with hydrochloric acid of the same concentration as used during the flotation. The absorbances of the blank did not exceed 0.08 for Victoria blue B and Victoria blue 4R, or about 0.1 for Capri blue.

The most effective platinum separations and reproducible absorbances of the methanol solutions were obtained for hydrochloric acid concentrations of 0.4—1 M for all the three dyes. As in the case of rhodamine 6G, the necessary molar excess of the dye was 40—60-fold with respect to platinum.

Characteristics of these flotation—spectrophotometric methods for the determination of platinum are summarized in Table 3. Undoubtedly, the system with rhodamine 6G is the best for platinum. It should be stressed that all the methods exhibit much higher sensitivity than the known spectrophotometric methods of determining platinum.

For each of the blue dyes (Victoria B, Victoria 4R and Capri), the calibration graphs were linear over ranges similar to that for rhodamine 6G. Considering the molar absorptivities of the dyes in methanol, the molar ratio of the dye to platinum was 3:1 for Victoria blue B and Victoria blue 4R, but was higher for Capri blue.

Unlike the system with crystal violet, the other systems were not affected by light. Reduction (decolorization) of the dyes by tin(II) under the influence of light, observed in the systems with triphenylmethane dyes [12, 13], did not take place.

Hydrophobic particles of the discussed ion-associates, which are wetted better by lighter-than-water nonpolar solvent than by water, are pushed out

TABLE 3

Characteristics of the proposed flotation—spectrophotometric determinations of platinum

Basic dye	Floating agent (solvent)	Acidity (M HCl)	λ_{max} (nm)	ε (10^5 l mol^{-1} cm^{-1})
Rhodamine 6G	Di-isopropyl ether (acetone)	0.8—1.2	530	2.80
Victoria blue B	Benzene (methanol)	0.6—1.0	598	2.45
Victoria blue 4R	Benzene (methanol)	0.4—0.8	590	2.20
Capri blue	Benzene (methanol)	0.6—1.0	620	2.00
Crystal violet[a]	Benzene (ethanol)	0.4—0.8	585	2.10

[a]Ref. [13].

to the phase boundary. These particles agglomerate with a suitable solvent on the wall of the funnel and adhere to it. In this way, good conditions can be obtained for quantitative separation of the aqueous phase and the organic solvent from the precipitate.

This work was supported by Research Program MR-I-32.

REFERENCES

1 Z. Marczenko, Mikrochim. Acta, (II) (1977) 651.
2 A. K. Babko, Z. I. Chalaya and V. F. Mikitchenko, Zavod. Lab., 32 (1966) 270.
3 Z. Marczenko, CRC Crit. Rev. Anal. Chem., 11 (1981) 195.
4 A. Mizuike and M. Hiraide, Pure Appl. Chem., 54 (1982) 1555.
5 R. D. Cramer, E. L. Jenner, R. V. Lindsey, Jr. and V. G. Stolberg, J. Am. Chem. Soc., 85 (1963) 1691.
6 J. F. Young, R. D. Gillard and G. Wilkinson, J. Chem. Soc., (1964) 5176.
7 V. I. Baranovskii, V. P. Sergeev and B. E. Dzevitskii, Dokl. Akad. Nauk S.S.S.R., 184 (1969) 632.
8 A. I. Gorbanov, V. P. Sergeev, B. E. Dzevitskii and V. B. Margulis, Proc. Int. Solvent Extraction Conf., ISEC 1974, Lyon, Society of Chemical Industry, London, 1974, p. 19.
9 E. N. Yurchenko, E. T. Devyatkina, T. S. Khodashova, M. A. Poray-Koshits, V. I. Konnov, V. A. Vornek, P. G. Antonov and Yu. N. Kukushkin, Koord. Khim., 5 (1979) 552.
10 Z. Marczenko and E. Kowalczyk, Anal. Chim. Acta, 108 (1979) 261.
11 Z. Marczenko and K. Kalinowski, Anal. Chim. Acta, 144 (1982) 173.
12 Z. Marczenko and K. Kalinowski, Mikrochim. Acta, (II) (1983) 169.
13 Z. Marczenko and J. Maruszak, Chem. Anal. (Warsaw), 24 (1979) 341.
14 M. Mojski and K. Kalinowski, Microchem. J., 25 (1980) 507.
15 M. Bent and C. French, J. Am. Chem. Soc., 63 (1941) 568.

Analytica Chimica Acta, 153 (1983) 229—236
Elsevier Science Publishers B.V., Amsterdam — Printed in The Netherlands

A COMPARATIVE STUDY OF SOME METHODS FOR THE SPECTROFLUORIMETRIC DETERMINATION OF TERBIUM IN AQUEOUS SOLUTIONS CONTAINING OTHER LANTHANIDES AND YTTRIUM

SAMUEL J. LYLE* and NIDAL A. ZA'TAR
The Chemical Laboratory, University of Kent at Canterbury, Kent CT2 7NH (Gt. Britain)
(Received 17th May 1983)

SUMMARY

Published methods based on the use of water-soluble binary and ternary complexes for the spectrofluorimetric determination of terbium(III) are compared. The complexes formed by terbium(III) with (1) ethylenediamine-*N*,*N*'-bis-*o*-hydroxyphenylacetic acid, (2) *o*-hydroxyphenyliminodiacetic acid, (3) EDTA and sulphosalicylic acid, (4) EDTA and Tiron, and (5) iminodiacetic acid and Tiron were examined. In each system, the characteristic sharp-line emission from terbium(III) at around 545 nm is measured. On the basis of emission spectra from 400 to 600 nm, fluorescence intensity in relation to variation in terbium/reagent mole ratios, sensitivity and some interference tests involving other lanthanides, yttrium, thorium and dioxouranium(VI) ions, it is concluded that the system represented by (4) is best, followed by (1), (5) and (3) in that order; (2) is least satisfactory on account of the strong dependence of fluorescence intensity on the terbium(III)/reagent mole ratio.

The analytical problems encountered in the determination of the lanthanides arise from the similarity of chemical properties of these elements. Selective and sensitive reactions are not readily available and it is usually necessary to resort to physical properties of the ions of individual elements. Spectrophotometric methods, using the near-ultraviolet and visible spectral region, are satisfactory only for relatively high concentrations, because molar absorptivities arising from *f*-electron excitation within the metal ion tend to be low. Spectrofluorimetric methods, where applicable, can give higher sensitivities and are potentially more suitable for the determination of trace amounts. However, it can still be difficult to find conditions whereby interference from other lanthanides is not a seriously confining factor.

Among the methods described for the spectrofluorimetric determination of terbium(III), those involving the use of aminopolycarboxylate ligands, which produce stable water-soluble complexes, are attractive in that they tend to give good sensitivity and promise of spectral discrimination against other lanthanides. Ethylenediamine-*N*,*N*'-bis(*o*-hydroxyphenylacetic acid) (EDBHPA) [1] and *o*-hydroxyphenyliminodiacetic acid (HPIDA) [2] have been used as complexing agents for this purpose. However, others have pre-

0003-2670/83/$03.00

ferred to use mixtures of complexing agents giving ternary complexes. Thus, EDTA with either sulphosalicylic acid [3] or disodium 1,2-dihydroxybenzene-3,5-disulphonate (Tiron) [4] and iminodiacetic acid with Tiron [5] have been proposed for terbium determination. Two of the reagent mixtures producing ternary complexes can also be used for the determination of dysprosium [4, 5].

These methods are compared here in an attempt to determine which reagent system is most suitable for the determination of terbium in the presence of other lanthanides and yttrium. Absorption and emission spectra, metal ion/reagent ratios and, for ternary complex formation, reagent/reagent ratios, and sensitivity of fluorescent emission at 545 nm were examined. Interferences from other lanthanides and yttrium were also tested for comparison with related published data. The selection of a reagent system suitable for the development of an automated method of analysis was a major objective of the study.

EXPERIMENTAL

Reagents and equipment

Unless otherwise stated, all chemicals used were of analytical-reagent grade (Fisons Scientific, Loughborough). Those reagents used to form complexes with terbium are listed in Table 1.

HPIDA was obtained from the related lactone, 2,3-dihydro-2-oxobenzomorpholine-4-acetic acid in alkaline solution. The lactone was prepared by the method of Irving and Da Silva [6]. (M.p. 178—179°C (lit. 178—179°C). Required for $C_{10}H_9NO_4$, 58.0% C, 4.4% H, 6.8% N; found 57.5% C, 4.0% H, 6.6% N.)

Iminodiacetic acid, Tiron (97% pure; Lancaster Synthesis, Lancaster, England) and EDBHPA (95% pure; Fluka/Fluorochem) were further purified, iminodiacetic acid by recrystallisation from water, Tiron from ethanol and EDBHPA by dissolution in dilute aqueous ammonia followed by precipitation at pH 4 with mineral acid [7].

The aqueous reagent solutions prepared were 10^{-1} M EDTA (disodium salt), 10^{-3} M iminodiacetic acid, 10^{-3} M Tiron, and 2.5×10^{-3} M EDBHPA. A 10^{-1} M sulphosalicylic acid solution was prepared by dissolving 12.7 g of the dihydrate in 500 ml of water containing 20 ml of buffer solution (see below). The 10^{-3} M HPIDA solution was prepared by dissolving the corresponding lactone in hot water.

The buffer solution was prepared by adding 70 ml of diethylamine (laboratory reagent, 99% purity) to 400 ml of water and adjusting the pH to 11.9 with concentrated hydrochloric acid.

Standard 10^{-3} M terbium(III) solution. Terbium oxide (Tb_4O_7; 99.9% pure; Rare Earth Products, Widnes, England) was dissolved in the minimum quantity of hydrochloric acid. The solution was evaporated to dryness and the residue dissolved in 1 l of water. The terbium concentration was determined by EDTA titration [8].

TABLE 1

Published conditions for spectrofluorimetric determinations of terbium

Range of linearity[a] (ng Tb ml^{-1})	Reagent R_1 added		Reagent R_2 added		Mole ratio[b] R_1:R_2:Tb	pH range	Wavelength (nm)		Ref.
	R_1	Mole	R_2	Mole			λ_{ex}	λ_{em}	
1—1500	EDBHPA	1.25×10^{-5}	—	—	1:1	7.5—7.8	295	545	1
6—3200	EDTA	1.00×10^{-4}	SSA[c]	5.00×10^{-5}	1:1:1	11.6—11.9	320	545	3
>0.008	EDTA	2.50×10^{-6}	Tiron	2.50×10^{-6}	1:1:1	11.5—12.5	320	546	4
0.004—790 000	IDA[d]	2.50×10^{-6}	Tiron	2.50×10^{-6}	1:1:1	12.5—13.0	320	546	5
0.01—16	*o*-HPIDA	3.75×10^{-6}	—	—	1:1	11.0—12.0	294	544	2

[a]For the solution as measured with reagents added. [b]In the complex undergoing excitation and emission. [c]Sulphosalicylic acid. [d]Iminodiacetic acid.

Solutions of other lanthanides (except cerium) and yttrium were prepared from the corresponding oxides (Rare Earth Products, Widnes). Each oxide was ignited at a dull red heat and cooled, and an appropriate amount was weighed out and dissolved in the minimum quantity of hydrochloric acid. The solution was evaporated to dryness and the residue dissolved in a known volume of water. Cerium(III) nitrate (Hopkin and Williams) was dissolved in water and standardised with EDTA [8]. Ammonium iron(II) sulphate, iron(III) chloride, thorium nitrate, dioxouranium(VI) acetate, sodium chloride, sodium perchlorate, sodium sulphate, sodium oxalate and calcium nitrate were used in the interference tests.

Apparatus. Either an Aminco-Bowman or a Perkin-Elmer MPF3 spectrofluorimeter was used with a quartz cell (1 × 1 cm). Absorption spectra were obtained with a Unicam SP800 spectrophotometer.

General procedure for the determination of terbium

A portion of solution containing an amount of terbium within the range recommended for each method (Table 1) was transferred to a 25-ml beaker. Appropriate amounts (Table 1) of the essential complexing agents were added. The pH was then adjusted by adding dilute hydrochloric acid and sodium hydroxide [1, 2], or buffer solution [3, 4], or 10% (w/v) sodium hydroxide and 4 M sodium perchlorate to adjust the pH and the final ionic strength to 0.2 [5]. The solution was transferred to a 25-ml volumetric flask and diluted to volume with water. The fluorescence was measured after 10 min. The pH, excitation and emission wavelengths recommended in each method are listed in Table 1.

RESULTS AND DISCUSSION

Absorption spectra of blank solutions

The absorptions of terbium-free (i.e., blank) solutions prepared as in the above general procedure, with the solution compositions set out in Table 1, were checked over the range 450—600 nm. Only solutions containing HPIDA absorbed; additional experiments showed that this reagent was unstable in solution above pH 7. The absorbance of the solution containing HPIDA at pH 11.5 was studied at 544 nm (the wavelength of maximum emission of its terbium(III) complex) as a function of time. The absorbance increase was roughly rectilinear over the first 40 min from preparation of the solution and then remained approximately constant. However, addition of a reducing agent such as hydrazine hydrate prevented formation of the coloured decomposition product and the absorbance at 544 nm remained negligible over a period of at least one month.

Fluorescence spectra of terbium-containing solutions

The fluorescence spectra of complexes of terbium with the reagents listed in Table 1, prepared as prescribed, were recorded from 400 to 650 nm. Typical spectra are presented in Fig. 1 except for the terbium—EDBHPA system which gave a spectrum very similar to that for terbium—HPIDA. The resolution of the emission peaks depended on the reagents; the best separa-

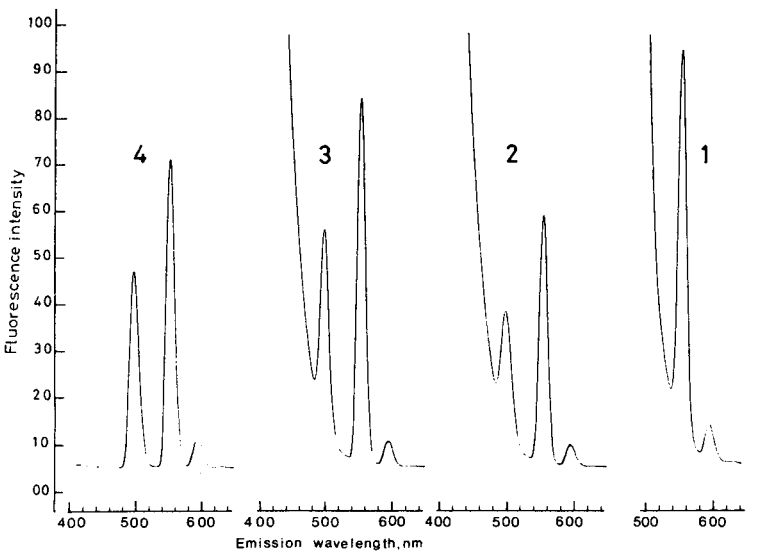

Fig. 1. Emission spectra from terbium(III) with: (1) EDTA and sulphosalicylic acid; (2) iminodiacetic acid and Tiron; (3) EDTA and Tiron; (4) HPIDA. Conditions: 4.61×10^{-6} M terbium(III) with 9.16×10^{-5} M EDTA, 9.12×10^{-5} M iminodiacetic acid, 8.00×10^{-5} M sulphosalicylic acid, 4.61×10^{-5} M Tiron and 4.70×10^{-6} M HPIDA as appropriate. Excitation wavelengths and pH of the solution are those recommended in Table 1.

tion of the peak at around 545 nm was obtained with HPIDA and EDBHPA. The spectra from EDTA/Tiron and iminodiacetic acid/Tiron complexes showed superior resolution of this peak when compared with those of the corresponding sulphosalicylic acid complexes. The spectrum of the terbium—iminodiacetic acid/sulphosalicylic acid complex (not shown) was similar to that of the corresponding EDTA ternary complex. The presence of 10^{-1} M hydrazine did not appear to affect the terbium—HPIDA fluorescence.

Effect of reagent concentration

Fluorescence intensity from metal complexes of the type considered here often exhibits a dependence on reagent concentrations. Dagnall et al. [3] studied the effect of changing molar ratios of metal ion to reagents in the terbium—EDTA/sulphosalicylic acid system. They found that keeping the concentration of sulphosalicylic acid fixed (Tb:SSA = 1:2000 at 10^{-6} M Tb) and varying the EDTA concentration resulted in an increase in fluorescence intensity up to a terbium/EDTA mole ratio of 1:2; further increase in EDTA relative to metal ion did not affect fluorescence intensity. However, with a fixed mole ratio of terbium to EDTA (10^{-6} M Tb), the fluorescence intensity increased logarithmically with increasing sulphosalicylic acid concentration. Taketatsu and Yoshida [1] examined the effect of changing molar ratios of terbium to EDBHPA for a fixed metal ion concentration (5×10^{-6} M Tb) and found that fluorescence output was almost constant over terbium/EDBHPA ratios of 1:20 to 1:100 but further increase in relative reagent concentration decreased the intensity. Observations in the work described here confirmed these results except that a somewhat more marked dependence (quenching) was found for ratios beyond 1:20 (Fig. 2) than in the original work [1].

Other terbium—reagent systems were studied further and representative results are presented in Fig. 2 for fixed terbium concentrations. Fluorescence intensity increases in the terbium—HPIDA system up to a 1:1 mole ratio beyond which marked quenching occurs; thus HPIDA is a much less satisfactory reagent than EDBHPA. The system containing EDTA is less dependent on the terbium: Tiron ratio than the corresponding iminodiacetic acid system. Fluorescence intensities were maximum in the terbium/Tiron ranges 1:4 to 1:30 and 1:4 to 1:20 for the EDTA and iminodiacetic acid systems, respectively. A mole ratio of terbium/EDTA or iminodiacetic acid of 1:2 is necessary for maximum fluorescence intensity but further increases in relative EDTA or iminodiacetic acid concentrations, at least to ratios of 1:100, do not affect the fluorescence yield.

Relative intensity of fluorescence and comparison of reagent utility

The ranges of linearity (Table 1) of fluorescence intensity as a function of terbium(III) concentration provide a rough measure of the sensitivity of each system. However, because different instruments each with its own light source were used, the results do not provide a strict comparison of sensitivity of the

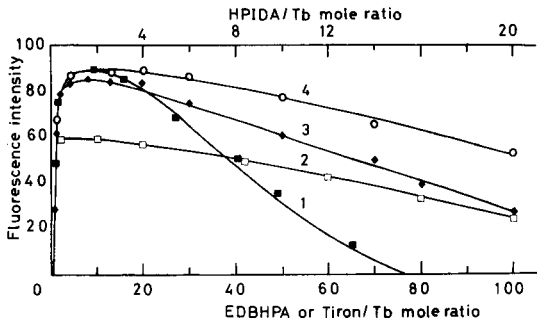

Fig. 2. Effect of changing the terbium(III)/reagent mole ratio on the fluorescence intensity of terbium complexed with: (1) HPIDA; (2) EDBHPA; (3) iminodiacetic acid and Tiron; (4) EDTA and Tiron. Conditions: 6.15×10^{-5} M terbium(III) in (1) and 4.61×10^{-6} M terbium(III) in (2—4); 5.55×10^{-5} M EDTA and 5.52×10^{-5} M iminodiacetic acid. The excitation and emission wavelengths and reaction conditions are those recommended in Table 1.

methods. Such a comparison was made by using the Perkin-Elmer spectrofluorimeter with a single light source, a fixed terbium concentration, and the prescribed procedure in each case. The results are summarised in Table 2. It can be seen that the terbium—HPIDA system is the most sensitive but unfortunately the strong dependence on reagent/metal concentration ratio greatly detracts from the practical utility of HPIDA.

The ternary systems with EDTA and sulphosalicylic acid or Tiron exhibit similar sensitivities but the latter is preferable because of the better-resolved terbium emission peak. The system with iminodiacetic acid and Tiron is somewhat less sensitive than the EDTA/Tiron system although otherwise as attractive for terbium determination. The EDBHPA binary system is also satisfactory in most respects, but the sensitivity is relatively low and, unlike the EDTA/Tiron system, it cannot be used for the fluorimetric determination of dysprosium(III). Thus, on balance, it can be concluded that the

TABLE 2

Relative intensity of fluorescence for the terbium(III) systems studied (4.61×10^{-6} M Tb was used; pH, excitation and emission wavelengths are those recommended in Table 1)

System		Mole ratio	Relative
R_1	R_2	Tb:R_1:R_2	intensity
HPIDA	—	1:1	100
EDBHPA	—	1:5	12
EDTA	SSA	1:20:17	37
EDTA	Tiron	1:20:20	35
IDA	Tiron	1:20:10	24

ternary system based on EDTA and Tiron is the best of the five systems tested for use in standard commercial spectrofluorimeters. Of the other reagent systems studied, EDBHPA would be second choice followed by iminodiacetic acid/Tiron and EDTA/sulphosalicylic acid. Only HPIDA is unsatisfactory for terbium determinations under the conditions set out in the literature.

Interference from other metal ions and common anions

Interference from other lanthanides, scandium, yttrium, thorium or dioxouranium(VI) cations was not detected in the EDTA/sulphosalicylic acid system by Dagnall et al. [3] for at least 50-fold molar amounts of a single metal ion relative to 10^{-6} M terbium. The present work confirmed these observations but interferences did occur at somewhat greater relative concentrations.

Taketatsu and Yoshida [1] reported that in their method with EDBHPA, of the elements listed above, cerium(III), praesodymium, neodymium, samarium and europium interfered slightly and thorium seriously; adequate quantitative data were not provided to enable a precise comparison to be made. The present work with EDTA/Tiron showed that in the range 0.02—0.24 μg ml^{-1} terbium (1.2×10^{-7}—1.5×10^{-6} M), up to the 200 μg ml^{-1} level of a given lanthanide ion, yttrium or a mixture of lanthanides, except for cerium(III), produced $\leqslant$6% quenching. Cerium(III) at the 150 μg ml^{-1} level depressed the fluorescence intensity by 5.7%. Uranium(VI) and thorium did not interfere seriously at 200 μg ml^{-1} and 450 μg ml^{-1}, respectively. Thus tolerance for these metal ions is relatively good. Quantitative information on interferences by the same metal ions is not available from the literature for the iminodiacetic acid/Tiron system. It was claimed [2] that the presence of lanthanide/terbium ratios up to 1000:1 did not decrease the fluorescence intensity when HPIDA was used. In view of the conclusions drawn above, interferences on these systems were not tested in the present work.

The EDTA/Tiron reagent system should be used only after a group separation of lanthanides and yttrium from other elements present. For example, iron(II) and iron(III) give intense colours with Tiron and greater than 10-fold molar amounts of either relative to terbium cannot be tolerated. A 4000-fold molar amount of chloride, perchlorate, sulphate, nitrate or oxalate relative to 8×10^{-7} M terbium does not interfere. Except for nitrate, a 5000-fold molar amount of any of these anions can be tolerated.

With the EDTA/Tiron system, equilibrium is attained in reaction with terbium(III) in the concentration range 1.2×10^{-7}—1.5×10^{-6} M within 1 min, under conditions which should be suitable for automation with the segmented flow technique.

One of us (N. Z.) gratefully acknowledges financial assistance from the Arab—British Chamber Charitable Foundation.

REFERENCES

1 T. Taketatsu and S. Yoshida, Bull. Chem. Soc. Jpn., 45 (1972) 2921.
2 M.A. Tishchenko, N. S. Poluektov, G. F. Yaroshenko, R. P. Lastovskii, G.L. Gerasimenko, I. I. Zheltvai and L. M. Timakova, Zh. Anal. Khim., 33 (1978) 2368.
3 R. M. Dagnall, R. S. Smith and T. S. West, Analyst, 92 (1967) 358.
4 N. S. Poluektov, M. A. Tishchenko and L. A. Alakaeva, Tr. Khim. Khim. Tekhnol., 5 (1973) 104.
5 M. A. Tishchenko, G. I. Gerasimenko and N. S. Poluektov, Zavod Lab., 40 (1974) 935.
6 H. Irving and J. J. R. F. Da Silva, J. Chem. Soc., (1963) 3308.
7 H. Kroll, M. Knell, J. Powers and J. Simonian, J. Am. Chem. Soc., 79 (1957) 2024.
8 S. J. Lyle and Md. M. Rahman, Talanta, 10 (1963) 1177.

Analytica Chimica Acta, 153 (1983) 237—247
Elsevier Science Publishers B.V., Amsterdam — Printed in The Netherlands

SORPTION OF COPPER(II) BY SOME COMPLEXING AGENTS LOADED ON VARIOUS SUPPORTS

KIKUO TERADA*, KEN MATSUMOTO and HITOSHI KIMURA

Department of Chemistry, Faculty of Science, Kanazawa University, Kanazawa, Ishikawa 920 (Japan)

(Received 12th April 1983)

SUMMARY

2-Mercaptobenzothiazole, 2-mercaptobenzimidazole and 2,5-dimercapto-1,3,4-thiadiazole loaded on silica gel, activated carbon and polytrifluorochloroethylene powder are compared for sorption and desorption of copper(II) ions. The separations are compared with those based on precipitation or extraction with these reagents. Columns of 2-mercaptobenzothiazole and 2-mercaptobenzimidazole on silica gel are particularly efficient for quantitative sorption of copper(II) from aqueous solutions at very high flow rates. 2-Mercaptobenzothiazole on silica gel is considered to be the most useful, as it reacts at pH 4.0, instead of pH 6.0 for 2-mercaptobenzimidazole. 2,5-Dimercapto-1,3,4-thiadiazole on silica gel removed copper from highly acidic solutions, but silica gel adsorbed this ligand only poorly, so that column capacity was severely restricted.

Many methods have been developed for preconcentration of trace metals from natural waters. They include coprecipitation, electrodeposition, liquid—liquid extraction, chelating ion-exchange and filtration through a filter paper impregnated with a chelating agent. Leyden et al. [1, 2] reported the use of chelating functional groups attached to silylated silica gel. This method requires no previous addition of chemicals, and can be used for online collection at the natural pH of the sample. Several methods based on activated carbon have also been reported. The sample is either filtered through an activated carbon layer on filter paper or is mixed with activated carbon, which is filtered off after shaking or standing for a given time. Except for mercury and iron, it is necessary to add another reagent for complete adsorption of trace metals on activated carbon. Chelation with 8-quinolinol followed by adsorption onto carbon gave high and reproducible collection yields for a large variety of water samples and elements [3, 4].

In the authors' laboratory, several exchange materials have been prepared by loading water-insoluble inorganic ion-exchangers or chelating precipitants on silica gel. Rapid preconcentration/determination methods for several trace metals in natural waters have been established by using columns packed with these materials [5—9]. Such columns are superior to conventional columns because of their high sorption efficiency even at very high flow rates (1—5 l h^{-1}).

0003-2670/83/$03.00

In the present study, the retention and elution behaviour of copper(II) were examined with several organic precipitants loaded on silica gel, activated carbon and polytrifluorochloroethylene (PTFCE) used in batch and column modes. In the batch mode, the reactivity between the reagents and the metal ion was determined and compared with that obtained by precipitation and extraction methods. The precipitants studied were 2-mercaptobenzothiazole (MBT), 2-mercaptobenzimidazole (MBI) and 2,5-dimercapto-1,3,4-thiadiazole (DMT). Previously MBT loaded on silica gel has been shown

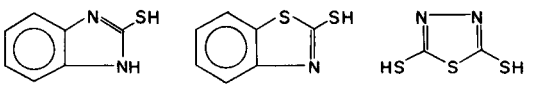

MBI MBT DMT

to be useful for the rapid preconcentration and determination of several heavy metals in sea water [6, 7]. The collection of traces of cadmium, silver, gold and mercury by MBI has been reported [10, 11]. Further, DMT (bismuthiol I) has been used for the precipitation of copper, iron, lead, silver, gold and cadmium, the necessary selectivity being obtained by pH control and by the use of suitable masking agents [12]. Extraction of metal—DMT complexes into organic solvents makes it possible to use this reagent in spectrophotometric methods [10]. In the present study, copper(II) was chosen as a representative metal ion because of its high reactivity with these reagents.

EXPERIMENTAL

Reagents

The ligands MBT, MBI and DMT were of analytical-reagent grade. Deionized water was used throughout. A standard solution of copper(II) (756 mg l^{-1}) was prepared by dissolving 0.3780 g of copper metal (99.99%) in a mixture of sulphuric and nitric acids, evaporating almost to dryness, and dissolving in 0.1 M nitric acid to make 500 ml. For buffering, the aqueous solution was adjusted with 0.2 M sodium acetate and 0.2 M hydrochloric acid for pH 0—5, or with 0.2 M potassium dihydrogenphosphate and 0.2 M sodium hydroxide for pH 5—8. Chloroform, benzene and ethanol were used after purification. Pyridine, 1,4-dioxan and methyl acetate (all analytical-reagent grade) were used without purification.

Silica gel (chromatographic grade, Wakogel C-100) was sieved through a stainless steel sieve (60—80 mesh), soaked with twice its volume of (1 + 1) hydrochloric acid for 1 day at 90°C, and washed with water until free from chloride. The washing was repeated twice. The gel was activated at 110°C for 1—2 days. Activated carbon (gas chromatographic grade, 60—80 mesh; Wako) was soaked in hydrochloric acid for 1 day; it was then washed with water until free from chloride and dried at 110°C for 1—2 days. A commercial polytrifluorochloroethylene (Daikin Kogyo Co.; molding powder)

was ground to 60—80 mesh and soaked in ethanol—hydrochloric acid mixture (1 + 1, v/v) for 1 day; the powder was washed with water until free from chloride, and dried at 50°C for 1—2 days under reduced pressure.

Preparation of the exchangers. About 70 g of silica gel was stirred with 100 ml of a mixture of 1,4-dioxan and methyl acetate (4 + 1, v/v) containing MBT (10 g). After 1 day, the impregnated gel was dried at 60°C under reduced pressure for 20 h to expel the solvents. The dry material was washed repeatedly with water until the washings were clear. Finally, the product was dried at 60°C under reduced pressure for 20 h and stored in a polyethylene bottle [6, 7].

The preparation of MBI or DMT loaded on silica gel, and these reagents loaded on activated carbon or PTCFE was similar to the preparation of MBT on silica gel, except for the solvent used, i.e., 1,4-dioxan for MBI and 1 M potassium hydroxide solution for DMT. It was found, however, that pyridine dissolved larger amounts of all these reagents; 10 ml dissolved up to 10, 4 and 2 g of MBT, MBI and DMT, respectively. This solvent was therefore used where possible.

Apparatus

A Hitachi 170-50 atomic absorption spectrometer with Hamamatsu TV hollow-cathode lamp was used to quantify copper. The pH of the aqueous solutions was checked by a Hitachi-Horiba pH meter (M-5). A Jasco UNIDEC-505 u.v.—visible recording digital spectrophotometer and a Hitachi Model-239 digital spectrophotometer were used for the spectral measurements. An Iwaki VS electric shaker operating at 340 strokes/min was used for the batch experiments and a Toyo E-E SF-100A fraction collector was used for the column experiments. The columns were the bodies of plastic syringes (13 mm i.d., 65 mm long).

Procedures

Batch experiments. To a 30-ml glass centrifuge tube were added 10 ml of copper(II) test solution, 5 ml of buffer solution and 0.5 g of the chelating exchanger. The contents were shaken vigorously by an electric shaker for 30 min at room temperature. After the gel had settled, the supernatant solution was filtered through dry Toyo No. 5C filter paper. Copper(II) was determined in aliquots of the filtrate by atomic absorption spectrometry (a.a.s.) at 324.8 nm, and the pH of each solution was also measured. The percent retention of copper was calculated by comparison of the absorbance measured for the filtrate and the untreated solution.

For comparison, copper(II) was extracted with MBT in chloroform or benzene (10 ml containing 20 mg of MBT), or precipitated by addition of each ligand (10 mg of solid) or an ethanolic solution of each ligand (1 ml containing 10 mg of reagent) under conditions similar to those described above.

Column experiments. The column was filled with 1.0 g of the exchanger

to give a bed height of 10 mm. Small discs of Toyo No. 5C filter paper were placed at the bottom and on the top so that the gel was not disturbed during sample passage. A given volume of an aqueous sample containing copper(II) was adjusted to a suitable pH and percolated through the column at 1.0—40 ml min^{-1} under mild suction. The column was washed with 10—20 ml of water. The copper concentration in the effluent was measured as described above. The percent retention of copper was calculated. A given volume of an eluant was passed through the column and the amount of copper eluted was determined in a similar manner to that described above.

Measurement of amount of complexing agent loaded on the support. Dry exchanger (1 g) was placed in a 30-ml glass centrifuge tube and 10 ml of ethanol (for MBT or MBI) or pyridine (for DMT) was added to dissolve the reagent completely by shaking. The supernatant liquid was filtered into a volumetric flask and diluted with the same solvent to the mark. The absorbances of the solutions were measured at 325, 306 and 348 nm for MBT, MBI and DMT, respectively, using the appropriate solvent as a reference.

RESULTS AND DISCUSSION

Amount of reagents loaded on supporting materials

The data in Table 1 indicate that the sorption of the complexing agents on silica gel increases in the order DMT < MBI < MBT, when they were prepared from pyridine solution. This order corresponds to that of the solubility of each reagent in pyridine. In order to prepare an exchanger containing a large amount of the reagent, the reagent should be dissolved in the best solvent. A modified procedure involving vacuum degassing of silica gel prior to addition of the reagent solution has been recommended [13]. This method seems to be effective, because it helps to remove air trapped in the pores of the silica gel, so that the reagent solution can contact all parts of the surface.

Recovery of copper(II) with MBT

The recovery of copper(II) with MBT from an aqueous solution was examined by the batch method at various pH values for 10 ml of 1.5 mg l^{-1}

TABLE 1

Amount of reagents loaded on various supporting materials (mg g^{-1})

Reagent	Solvent	Amount loaded (mg g^{-1})		
		Silica gel	Activated carbon	PTFCE
MBT	Dioxan—methyl acetate	14	115	173
	Pyridine	102	415	—
MBI	Pyridine	77	279	—
DMT	Pyridine	3	198	—

copper(II) solution, 5 ml of a buffer solution, and 1 ml of ethanol containing 5 mg of MBT, or 0.5 g of MBT on silica gel containing about 5 mg of MBT, or 50 mg of MBT on activated carbon containing 5 mg of MBT, or 10 ml of MBT (20 mg) in chloroform or in benzene. The results are illustrated in Fig. 1. As shown in the figure, the curve obtained on precipitation of copper(II) by adding MBT in ethanol agrees fairly well with those retention curves obtained by shaking with MBT on silica gel or activated carbon. Therefore, these supporting materials are considered to have no effect on retention of copper(II) with MBT. The curves corresponding to extractions into chloroform and benzene were shifted to more acidic conditions, probably because of the increased MBT concentration. The effect of MBT concentration in chloroform on extraction of copper(II) was therefore examined. As shown in Fig. 2, complete extraction of copper was achieved with >5.5 mg of MBT in 10 ml of chloroform. The MBT concentration of 20 mg in 10 ml of chloroform generally employed in the present study is sufficient for extraction of 25 μg of copper. In contrast, only 50 mg of MBT on silica gel (actually 0.5 mg of MBT) was required to retain copper quantitatively under the same conditions.

As shown in Fig. 1, the extent of extraction of copper tends to decrease under alkaline conditions, probably because of the formation of copper hydroxide. Thus, subsequent experiments were carried out at pH 4.0.

Properties of columns of MBT on different supports

Since PTFCE could adsorb larger amounts of complexing reagents than silica gel or activated carbon, it was expected to be the best support. However, a column packed with MBT on PTFCE was completely useless, because an aqueous solution could hardly pass through the column without applying pressure. In addition, the results of retention recoveries obtained from repeated runs varied from 34% to 60%, even when the experiments were done under apparently the same conditions. These results may be due to the hydrophobic nature of PTFCE which inhibits close contact between sample solution and the complexing groups on the PTFCE surface. Therefore, if a

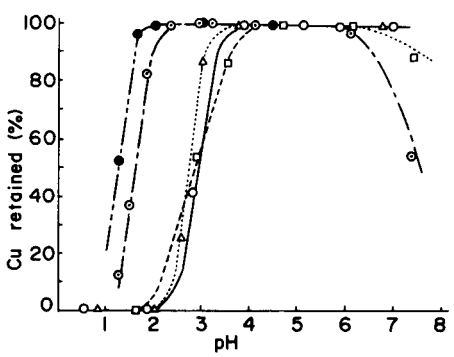

Fig. 1. Effect of pH on retention of copper(II) with MBT in various forms: (○) on silica gel; (△) in ethanol; (□) on activated carbon; (⊙) in chloroform; (●) in benzene.

sample solution becomes more hydrophobic, solution transport and the retention of the metal ion may be improved. In fact, the flow rate of the sample solution was much improved when the solution was made 30% in ethanol, and the retention of copper(II) increased to 100%. However, since such a procedure is impractical, PTFCE is inadequate as a supporting material for the present purpose.

Although activated carbon could sorb larger amounts of the complexing agents than silica gel, it also had inferior properties. Figure 3 shows the effect of the flow rate on the retention of copper(II) by MBT on silica gel and activated carbon. The silica gel column quantitatively retained copper at flow rates up to ca. 30 ml min^{-1}, whereas flows as small as 1 ml min^{-1} resulted in less than quantitative retention on the activated carbon column. However, when 5 ml of a 3.8 mg l^{-1} copper(II) solution (pH 4.0) was passed through a column packed with 0.5 g of MBT on activated carbon at 0.3 ml min^{-1}, copper was quantitatively retained. This difference in retention may be caused by the interaction of the surface of the supporting material with an aqueous solution. Activated carbon, like PTFCE, is scarcely wetted by water [14]. Thus, activated carbon also seems to be an unsuitable support for rapid preconcentration of copper from a large volume of sample. The surface of silica gel strongly interacts with polar solvents [15], so that an aqueous solution achieves sufficient contact with a silica gel column for quantitative retention of copper to be achieved at very high flow rates.

Retention of copper(II) by MBI and DMT

The percent retentions of copper(II) with MBI and DMT at various pH values were examined as described for MBT. The results are shown in Fig. 4. The precipitation of Cu—MBI by adding the reagent in ethanol gives results almost identical to those obtained by using MBI on silica gel. In general, the retention curves obtained with MBI appear to be shifted to more alkaline

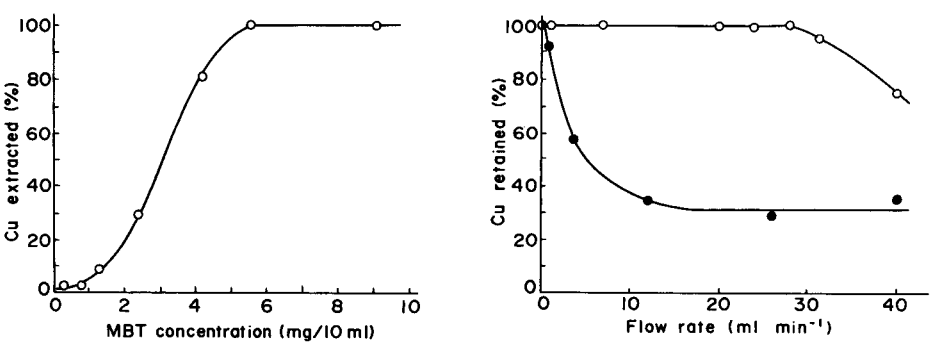

Fig. 2. Effect of MBT concentration in chloroform on extraction of 25 μg of copper(II).

Fig. 3. Effect of flow rate on retention of 7 mg l^{-1} copper(II) from 100 ml of solution at pH 4.0 by 10-mm long columns of MBT on: (○) silica gel; (●) activated carbon.

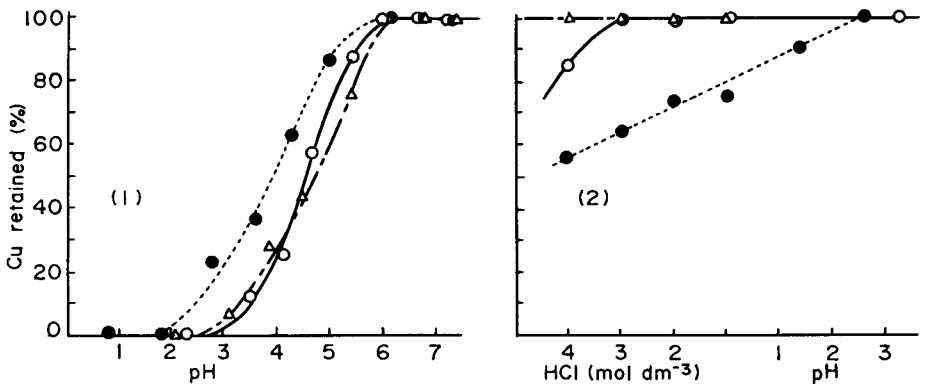

Fig. 4. Effect of pH on retention of copper(II) with (1) MBI and (2) DMT in various forms: (△) in ethanol; (○) on silica gel (6 mg DMT); (●) solid MBI or DMT on silica gel (0.6 mg DMT).

conditions compared to those with MBT. MBT seems to bind copper more strongly than MBI. Subsequent experiments with MBI were done at pH 6.0.

Figure 4 shows that DMT can react quantitatively with copper(II) even in 2—3 mol dm^{-3} hydrochloric acid. But if a small amount of DMT on silica gel (which contained 0.6 mg of DMT) is used, the retention of copper does not reach 100% even at pH 2.0. This is probably due to the decreased activity of DMT at higher acidities. Thus, subsequent experiments with DMT were done at pH 2—3.

In the course of the studies described above, the complex stability for copper(II) with the three ligands was found to be in the order MBI < MBT < DMT. As DMT contains two active sites, while MBT and MBI contain one, DMT would be expected to bind copper more strongly.

Elution of copper(II)

The elution of copper from MBT on silica gel was examined by both batch and column methods. In the column method, 25 ml of hydrochloric acid of varying concentration (1—12 mol dm^{-3}) was passed through the column (which had retained 225 μg of copper) at less than 1 ml min^{-1}, and the amount of copper in the effluent was measured. The elution recoveries at various acidities are shown in Fig. 5. The batch method showed that when MBT on silica gel (with 76 μg of copper) was shaken with 10 ml of hydrochloric acid of various concentrations for 30 min, the plot of dissolution recovery vs. acid concentration obtained was identical with that obtained by the column method. Figure 5 indicates that the copper cannot be eluted quantitatively from MBT on silica gel even with concentrated hydrochloric acid. The back-extraction behaviour of copper in MBT—chloroform solution was similar but more pronounced, varying from 2.7% at pH 0 to 2.0% at pH 2.3. Thus, the reaction of copper with MBT is almost irreversible.

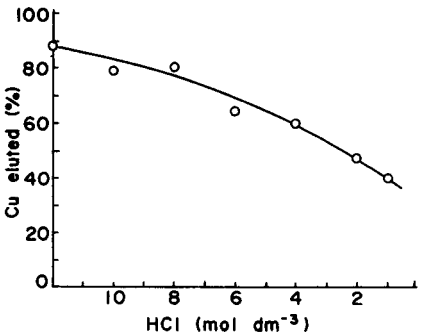

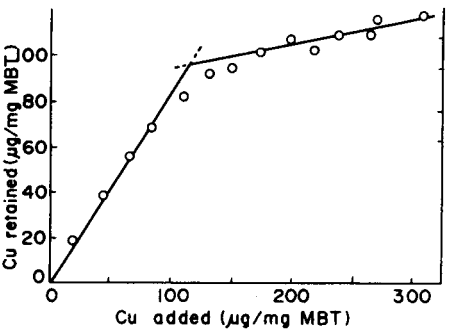

Fig. 5. Effect of hydrochloric acid concentration on elution of copper (225 μg) retained on a column of MBT on silica gel.

Fig. 6. Sorption isotherm of copper(II) on MBT on silica gel (0.5 g).

For Cu—MBI, only 20% of the copper was released at pH 1.0, although complexation did not occur at this pH.

Of the solutions tested, 0.2 mol dm^{-3} thiourea in 0.1 mol dm^{-3} hydrochloric acid was found to be best for elution of copper from columns of MBT, MBI or DMT on silica gel. A mixture of acetone and hydrochloric acid (9:1 v/v) also eluted the copper [6, 7]. This solution, however, also released the ligand from the column, which made measurement of copper by a.a.s. difficult because of interaction with the ligand and acetone. Thiourea in hydrochloric acid did not dissolve the reagent. This was confirmed by passing 5 ml of 1.5 mg l^{-1} copper(II) solution through the column and washing with water; copper was eluted with 20 ml of the above acidic thiourea solution and the column was washed with water. Another 5 ml of 1.5 mg l^{-1} copper solution was percolated through the column; no copper was detected in the effluent.

The effective elution of copper from the column is due to the strong complexing ability of thiourea with copper. A column of DMT on silica gel could retain only 25% of the copper(II) from an aqueous solution containing 0.1 mol dm^{-3} thiourea at pH 2—3, and did not retain copper from a solution of 0.2 mol dm^{-3} thiourea in 0.1 mol dm^{-3} hydrochloric acid. However, copper was retained on an MBT silica gel column from a 0.2 mol dm^{-3} thiourea solution adjusted to pH 4 or 6. The extent of elution of copper from columns packed with 0.5 g of the exchangers which had retained about 50 μg of copper are given in Table 2. Complete elution of copper from an MBT/silica gel column was achieved with only 20 ml of the eluting solution at a flow rate of 1 ml min^{-1}. However, for MBT columns on activated charcoal, 50 ml of eluant at 0.5 ml min^{-1} was needed for complete elution.

Comparison of copper(II) complexes

The copper(II) complexes of MBT, MBI and DMT were precipitated by the procedure described above, and a given weight of each was shaken with

TABLE 2

Release of copper from the silica gel and activated carbon columns

Eluant (ml)[a]	Flow rate (ml min^{-1})	Support	Recovery (%)		
			MBT	MBI	DMT
20	1.0	Silica gel	100	100	100
50	0.5	Activated carbon	100	72	0 70[b]

0.2 mol dm^{-3} thiourea in 0.1 mol dm^{-3} hydrochloric acid. The copper concentration in the solution was directly measured by a.a.s. The mole ratios of the complexing reagent to copper in the precipitates were calculated and found to be 2.2, 1.8 and 1.7 for MBT, MBI and DMT, respectively. As the magnetic susceptibility of Cu—MBT | (-0.444×10^5 cm^3 g^{-1}) indicates that this complex is diamagnetic, copper should be present as copper(I). Consequently, the reaction of MBT with copper(II) can be represented in its simplest form as [16]:

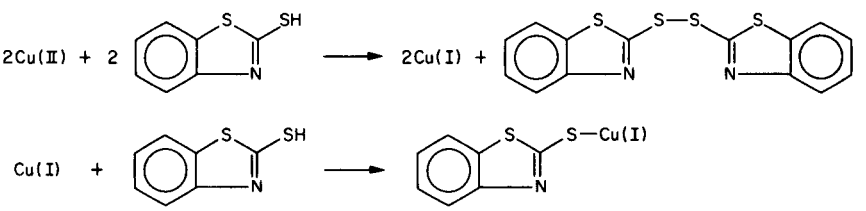

although the copper(I) complex is unlikely to have such a simple structure. Accordingly, in the MBT/silica gel column, the inactive disulphide is formed in an equivalent amount to the retained copper, and the complexing capacity of the column is gradually decreased with use.

Retention capacity

An accurately weighed amount of MBT/silica gel (0.5 g) was shaken with 10 ml of pH 4.0 buffer solution containing copper(II) in the range 0.7—13 mg l^{-1} at room temperature, and the unreacted copper in the solution was measured. The sorption isotherm calculated is shown in Fig. 6. When the total amount of copper in a sample solution is less than equivalent to that of MBT, all the copper is retained on the column (the slope in Fig. 6 is unity). In the vicinity of the equivalence point, at which MBT sites are completely occupied by copper, the slope is less than unity, and beyond this point, it is about 0.08, but not zero, because of over-loading by secondary sorption. The intersection of the two straight lines indicates that the mole ratio of MBT to copper on the saturated column is 3.7. As the ratio should be 2.0, some of the MBT may not react with the copper, perhaps because of the

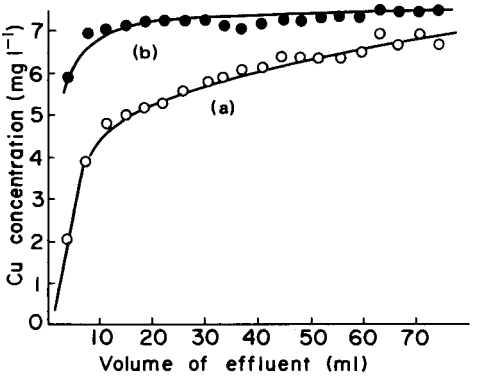

Fig. 7. Break-through curves for 7.6 mg l^{-1} copper(II) with columns of: (a) MBT/silica gel, 0.3 g, flow rate 2.6 ml min^{-1}; (b) MBT/activated carbon, 0.25 g, flow rate 1.0 ml min^{-1}.

porous structure of the silica gel surface. Most of the surface area of porous silica gel is within the pores, and access to some of these may be restricted by the ligand or its copper complex [13, 17].

The break-through curves of copper(II) with columns of MBT on silica gel and activated carbon are shown in Fig. 7. Each 3.7-ml portion of effluent was collected and copper was measured in each fraction by a.a.s. The MBT/activated carbon column was expected to retain copper quantitatively only at low flow rates; it was shown that, although this column contained a larger amount of MBT than did the silica gel column, its retention capacity was much smaller than that of the silica gel column. The amount of copper required to saturate each column was evaluated from the difference between the concentrations of the element in the test solution and the combined effluent. At the saturation points, the mole ratios of MBT to copper retained were 7 and 243 for the MBT/silica gel and MBT/activated carbon, respectively. Thus, silica gel greatly surpasses activated carbon as a support material.

The break-through curves for columns of MBT, MBI and DMT on silica gel with copper(II) are shown in Fig. 8. The saturation capacities for copper

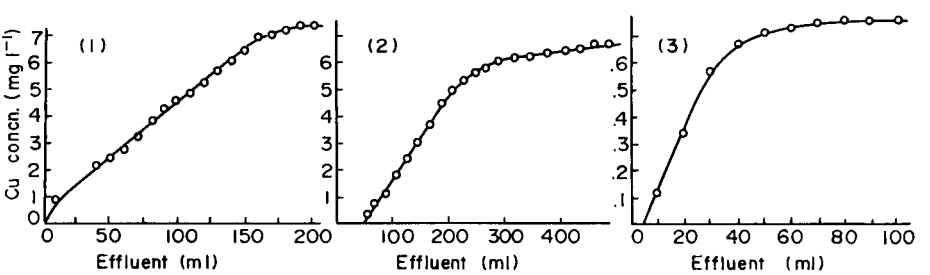

Fig. 8. Break-through curves for copper(II) with 10-mm columns of: (1) MBT/silica gel, 0.7 g, 7.6 mg l^{-1} Cu; (2) MBI/silica gel, 0.5 g, 7.6 mg l^{-1} Cu; (3) DMT/silica gel, 0.5 g, 0.76 mg l^{-1} Cu. Flow rate 1.5 ml min^{-1}.

were calculated from these results; thus the mole ratios of the ligand to copper retained were found to be 6.5, 7.6 and 35 for MBT, MBI and DMT columns, respectively. The poor efficiency of the DMT column may be due to the rather smaller amount of reagent loaded on the gel.

Conclusion

Silica gel columns supporting MBI or MBT allow quantitative retention of copper(II) from solution at high flow rates. The MBI/silica gel column is very similar to the MBT/silica gel column with respect to its sorption efficiency and capacity for copper(II). However, because the latter reacts with copper(II) at pH 4.0, while the former requires pH 6.0, the MBT column is considered to be more useful. DMT has a high reactivity with copper(II) and retains copper even from highly acidic solutions. Unfortunately, silica gel adsorbs DMT only poorly, thus the MBT/silica gel column is again superior.

REFERENCES

1 D. E. Leyden and G. H. Luttrell, Anal. Chem., 47 (1975) 1612.
2 D. E. Leyden, G. H. Luttrell, W. K. Nonidez and D. B. Werho, Anal. Chem., 48 (1976) 67.
3 B. M. Vanderborght and R. E. Van Grieken, Anal. Chem., 49 (1977) 311.
4 J. Smits, J. Nerissen and R. E. Van Grieken, Anal. Chim. Acta, 111 (1979) 215.
5 K. Terada, H. Hayakawa, K. Sawada and T. Kiba, Talanta, 17 (1970) 955.
6 K. Terada, A. Inoue, J. Inamura and T. Kiba, Bull. Chem. Soc. Jpn., 50 (1977) 1060.
7 K. Terada, K. Morimoto and T. Kiba, Bull. Chem. Soc. Jpn., 53 (1980) 1605; Anal. Chim. Acta, 116 (1980) 127.
8 K. Terada and K. Nakamura, Talanta, 28 (1981) 123.
9 K. Terada, K. Matsumoto and Y. Taniguchi, Anal. Chim. Acta, 147 (1983) 411.
10 D. D. Perrin, Organic Complexing Reagents: Structure, Behavior, and Application to Inorganic Analysis, Wiley, New York, 1964, p. 220.
11 H. V. Weiss and M. G. Lai, Anal. Chim. Acta, 28 (1963) 242.
12 J. V. Dubsky and A. Okac, Z. Anal. Chem., 96 (1934) 267.
13 C. Fulcher, M. A. Crowell, R. Bayliss, K. B. Holland and J. R. Jezorek, Anal. Chim. Acta, 129 (1981) 29.
14 H. Corin, C. Eon and G. Guiochon, J. Chromatogr., 119 (1976) 41.
15 R. P. W. Scott, J. Chromatogr. Sci., 18 (1980) 297.
16 F. Feigl, Chemistry of Specific, Selective and Sensitive Reactions, Academic Press, New York, 1949, p. 236.
17 H. Jenett, J. Knecht and G. Stock, Fresenius Z. Anal. Chem., 304 (1980) 362.

Analytica Chimica Acta, 153 (1983) 249—255
Elsevier Science Publishers B.V., Amsterdam — Printed in The Netherlands

SPECTROPHOTOMETRIC TITRATION OF TRACES OF IODIDE IN CONCENTRATED CHLORIDE SOLUTION

MARIA PESAVENTO

Istituto di Chimica Generale e Inorganica, Università di Pavia, Viale Taramelli 12, 27100 Pavia (Italy)

(Received 12th July 1982)

SUMMARY

The classical Andrews titration of iodide with iodate in strong hydrochloric acid is applied to the determination of 10^{-7}—10^{-5} M iodide, by using spectrophotometric monitoring based on the high molar absorptivity of the I^+ species at 230 nm. Interferences are discussed, and methods for avoiding them are suggested.

Many methods have been proposed for the determination of traces of iodide in different materials [1]. The two most used methods, neutron activation and the kinetic spectrophotometric procedure based on the iodide-catalyzed reduction of cerium(IV) by arsenic(III) have been critically reviewed by Malvano et al. [2]. Potentiometric methods with an iodide-selective electrode have also been proposed [3, 4]. Recently, Gifford and Bruckenstein [5] described a new pneumatoamperometric method. Many of the previously described methods are satisfactory with regard to sensitivity and accuracy, but they often require sophisticated apparatus. Moreover, chloride can interfere seriously, so that time-consuming separation procedures are necessary (e.g., ion-exchange on a strongly basic anion-exchange resin, followed by selective precipitation with palladium(II) [6], or coprecipitation with silver chloride [7]).

The titration proposed in this paper is simple and requires only a conventional u.v. spectrophotometer. Time, temperature and solution preparation are not critical and the sensitivity is satisfactory for many purposes. There are relatively few interferences. Dilute iodide solutions, containing $\geqslant 10$ μg I^{-1} iodide, are titrated with iodate in strong hydrochloric acid, following the well-known Andrews—Jamieson method for more concentrated solutions [8, 9]. Two reactions take place successively and quantitatively, even at the very low concentrations studied:

$$5\ I^- + IO_3^- + 6\ H^+ \rightarrow 3\ I_2 + 3\ H_2O \quad (1)$$

$$2\ I_2 + IO_3^- + 6\ H^+ \rightarrow 5\ I^+ + 3\ H_2O \quad (2)$$

0003-2670/83/$03.00

the overall reaction being

$$2\,I^- + IO_3^- + 6\,H^+ \rightarrow 3\,I^+ + 3\,H_2O \qquad (3)$$

Because the titration is done in the presence of hydrochloric acid, both I_2 and I^+ are partially or totally converted to chloride complexes, such as I_2Cl^-, ICl and ICl_2^- [10, 11]. An equilibrium which must also be taken into account in order to understand what happens during the titration of iodide at very low concentration is the disproportionation reaction

$$I_2Cl^- + Cl^- \rightleftharpoons ICl_2^- + I^- \qquad (4)$$

for which Cason and Neumann [10] suggested the possible constant $K = [ICl_2^-][I^-][I_2Cl^-]^{-1}[Cl^-]^{-1} = 7.3 \times 10^{-7}$. In the 5 M hydrochloric acid solutions usually employed in the Andrews titration, equilibrium (4) is displaced to the right when the iodide concentration is less than 1.6×10^{-7} M, and to the left when the iodide concentration exceeds 6.5×10^{-5} M. Therefore, for the concentrations of iodide here considered (10^{-7}—10^{-5} M), reactions (1) and (2) are never clearly separated in 5 M hydrochloric acid. In the first part of the titration of iodide, both I_2 and I^+ are present simultaneously.

In the work described here, the Andrews titration was studied not only as usual in 5 M hydrochloric acid, but also in 0.5 M. It was possible to demonstrate that even at this lower acidity the titration was quantitative. This is important, because many substances are only slightly soluble in 5 M hydrochloric acid. The chloride complexation equilibria are of course differently displaced in solutions of different hydrochloric acid concentration. Thus reaction (4) is drawn to the left in more dilute chloride solutions. This reaction seems to occur only at iodide concentrations less than 3.3×10^{-6} M, so that a sharper separation between reactions (1) and (2) is expected in 0.5 M hydrochloric acid than in 5 M hydrochloric acid.

Figure 1 presents the spectra obtained for a dilute iodide solution in 0.5 M hydrochloric acid on titration with a standard iodate solution. Initially there

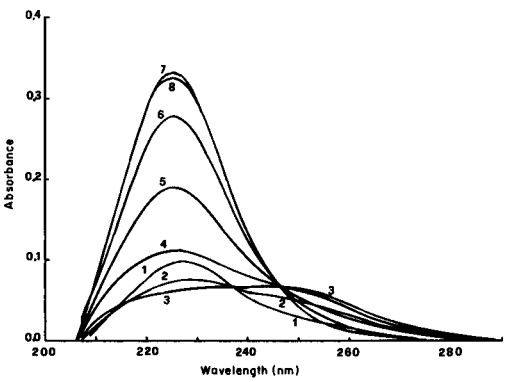

Fig. 1. Spectrum of a 8.40×10^{-6} M iodide solution (5 ml) in 0.5 M HCl, titrated with 1.00×10^{-4} M KIO_3. Volume of added titrant: (1) 30; (2) 60; (3) 90; (4) 120; (5) 150; (6) 180; (7) 210; (8) 240 µl.

is only the absorption band of iodide (λ_{max} = 227 nm, ϵ_{230} = 1.2 × 10^4 l mol^{-1} cm^{-1}). On addition of the iodate, this maximum decreases, and an isosbestic point is formed at 238 nm. At the same time, the absorption maximum of I_2Cl^-, not very intense, is formed at 250 nm. After iodide has been quantatively oxidized to I_2, a peak at 224 nm, distinctive of I^+, appears, as is expected on the basis of reaction (2), and another isosbestic point is formed at 245 nm. On the basis of these spectra, it was decided to follow the titration spectrophotometrically at 230 nm.

A titration curve obtained for 0.5 M hydrochloric acid solution is shown in Fig. 2. The first and second equivalence points are easily detectable. A titration curve for iodide in 5 M hydrochloric acid is also given in Fig. 2. In this case, only the second end-point is sharp and useful. This is probably due to the disproportionation reaction (4) that occurs to a considerable extent in 5 M chloride solutions. After the second end-point the slope of the titration graph is different in 0.5 and 5 M acid. Iodate itself absorbs only slightly at 230 nm, so that a line nearly parallel to the abscissa is expected when an excess of iodate is added to the solution. This is obtained in 0.5 M hydrochloric acid, but in 5 M acid the linear plot after the end-point has a positive slope. The spectrum of iodate alone in 5 M hydrochloric acid solu-

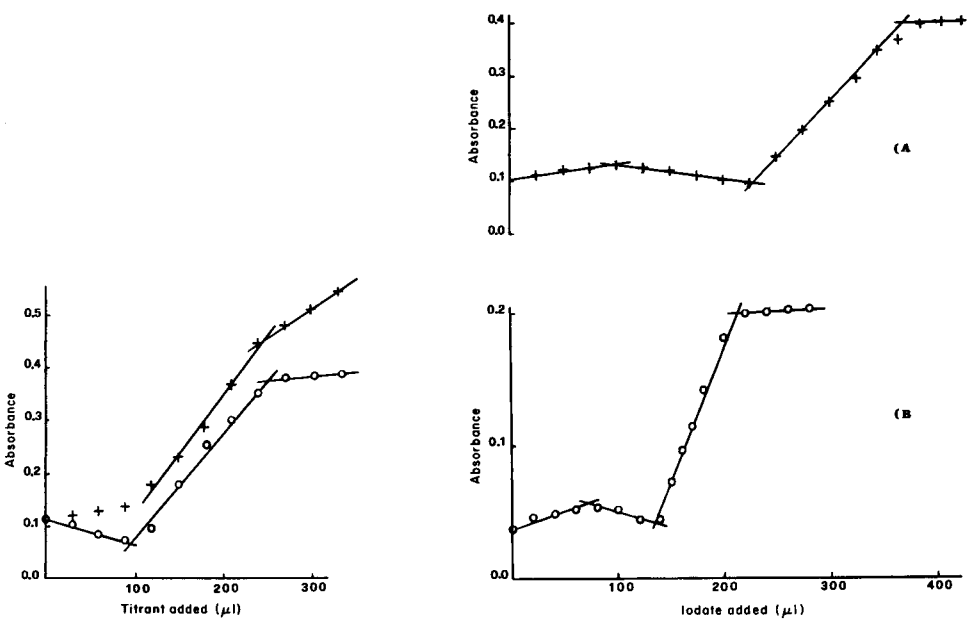

Fig. 2. Spectrophotometric titration curves for 1.00 × 10^{-5} M iodide (5 ml) titrated with 1.00 × 10^{-4} M iodate in (+) 5 M HCl and (○) 0.5 M HCl.

Fig. 3. Spectrophotometric titration curves for iodide in presence of sulphide or sulphite in 0.5 M HCl (5 ml) with 1.00 × 10^{-4} M iodate: (A) sulphide (initial conc. 1.00 × 10^{-3} M, 9.50 × 10^{-6} M I^-); (B) sulphite (initial conc. 1.00 × 10^{-3} M, 3.30 × 10^{-6} M I^-).

tion shows the distinctive peak of ICl_2^- at 224 nm, which is formed quantitatively some minutes after the reagent addition. The reduction of iodate to I^+ may be attributed to chloride: $IO_3^- + 6\ Cl^- + 6\ H^+ \rightarrow ICl_2^- + 2\ Cl_2 + 3\ H_2O$. Indeed iodate, even at a concentration as high as 0.01 M, is quantitatively reduced to I^+ in 5 M hydrochloric acid. Iodide may be titrated by means of the Andrews method in 5 M hydrochloric acid because the reduction potential of the I^+/I_2 couple is lower than that of Cl_2/Cl^-, and the oxidation of iodide or iodine is faster than that of chloride. Another difference between the two titrations shown in Fig. 2 is that the absorbance of the second end-point is lower in 0.5 M than in 5 M hydrochloric acid. The calculated molar absorptivities of the final product containing I^+ are 2.8×10^4 and 3.5×10^4 l mol^{-1} cm^{-1}, respectively, for the 0.5 M and 5 M acid. This is completely unexpected on the basis of the previously discussed reactions. It was observed that the molar absorptivity for the I^+ species depends on both the chloride and I^+ concentrations.

EXPERIMENTAL

Apparatus and reagents

The absorbance measurements were done with a Bausch and Lomb Spectronic 200 u.v. spectrophotometer, equipped with quartz cells (0.5, 1 and 4 cm). The titrations were made with micropipettes (Eppendorf Varipette 4710), which were standardized weekly.

All the reagents were of analytical grade. Potassium iodate stock solutions were prepared directly by weighing the solid.

Procedure

To a known volume of sample, concentrated hydrochloric acid was added, so that the required concentration is finally present. As shown in Fig. 2, the titration may be done in 0.5 or in 5 M acid. Any intermediate concentration is of course also suitable, and may be chosen by considering the particular analysis concerned, particularly the solubility of the sample and the presence of interfering substances. As many substances strongly absorb at 230 nm, it is necessary to check if the absorbance of the blank is less than about 1.5, and to dilute if it is not. An aliquot of this final solution is used as blank. Another measured aliquot is titrated with standard iodate, by recording the absorbance at 230 nm after each addition. The end-point is detected graphically by plotting absorbance vs. volume of iodate added. The iodide concentration is calculated from the second end-point, which corresponds to the overall reaction (3).

The molar absorptivity of the I^+ species can be calculated from the absorbance at the second end-point (A_2), on the basis of the following equation:

$$A_2 + 2\ \epsilon_{I^-}\ V_2 M\ V_t^{-1} = 3\ \epsilon_{I^+}\ V_2 M\ V_t^{-1}$$

where $\epsilon_{I^-} = 1.2 \times 10^4$ l mol^{-1} cm^{-1} at 230 nm, V_2 is the volume of the titrant added at the second end-point, V_t is the total volume of the solution at this

end-point, and M is the concentration in mol l^{-1} of the titrant. The second term takes into account the iodide absorbance included in the blank. The ϵ values for the I^+ species calculated in this way lie between 2.0×10^4 and 4.0×10^4 l mol^{-1} cm^{-1}. As discussed above, the lowest values are obtained when the titration is made in 0.5 M hydrochloric acid. The iodide concentration is also important, because lower ϵ_{I^+} values are obtained when lower concentrations of iodide are titrated. If the ϵ_{I^+} value is found to be significantly lower than 2.0×10^4 l mol^{-1} cm^{-1}, this provides strong evidence that reducing substances other than iodide have been titrated.

RESULTS

The recoveries of added iodide in different solutions are reported in Table 1.

Interferences

All substances having a reduction potential higher than that of I_2/I^- or of I^+/I_2 in 0.5—5 M hydrochloric acid can be expected to interfere in the proposed titration by oxidizing iodide to iodine or to iodine monochloride. Fortunately, many potential interferences are somewhat inert. For example, dissolved oxygen, iron(III) [12], nitrate and perchlorate do not interfere if the titration is done within 15 min after the preparation of the final solution. Chromium(VI) reacts slowly, but causes low results even if the titration is done immediately. Other oxidants, such as permanganate, iodate and nitrite, react immediately with iodide. Nitrite interferes even at extremely low concentrations, via a cyclic oxidation process [13].

A negative interference can also be expected from copper(II) [14]. However, in 5 M hydrochloric acid, this ion does not interfere, even at concentrations as high as 1×10^{-3} M, probably because in 5 M chloride, copper is quantitatively converted to $CuCl^+$ [15]. Higher copper concentrations could not be investigated, because of the absorbance of copper itself in this medium

TABLE 1

Recoveries of iodide under different conditions

Composition of solution	Iodide added (mol l^{-1})	Iodide found (mol l^{-1})[a]	ϵ[b] (l mol^{-1} cm^{-1})
0.5 M HCl	1.00×10^{-5}	$0.97 \pm 0.03 \times 10^{-5}$	2.8×10^4
	1.00×10^{-7}	$1.06 \pm 0.04 \times 10^{-7}$	2.5×10^4
5 M HCl	1.00×10^{-5}	$1.02 \pm 0.04 \times 10^{-5}$	3.4×10^4
	1.00×10^{-7}	$0.98 \pm 0.03 \times 10^{-7}$	3.2×10^4
5.13 M NaCl, 0.5 M HCl	1.00×10^{-6}	$0.98 \pm 0.04 \times 10^{-6}$	2.8×10^4

[a]Mean of 3 determinations ± standard deviation. [b]Calculated for the I^+ species as described in the text.

($\epsilon_{230} = 1.5 \times 10^3$ l mol^{-1} cm^{-1}). In 0.5 M hydrochloric acid, 5×10^{-3} M copper gave results 20% low for 5×10^{-6} M iodide, because in this more dilute chloride medium $CuCl^+$ is partially dissociated.

Some reducing substances could cause high results. Examples are sulphide and sulphite; in the acidic solutions studied, these exist as hydrogen sulphide and sulphur dioxide and so can be removed simply by vigorously stirring the solution, or, better, by passing a stream of inert gas (nitrogen or carbon dioxide). A few minutes are sufficient to remove concentrations up to 10^{-5} M from 5 M acid. It is easy to check if these gases have been completely removed, because they absorb strongly at 230 nm. Therefore, if the absorbance of the blank decreases with time, the gases are still being evolved. Even when the absorbance of the blank is apparently constant, small amounts of sulphite or sulphide can remain dissolved in the 0.5 M acid. However, as can be seen from Fig. 3, resolution of the components is possible. The first end-point corresponds to the reduction of iodate by sulphur dioxide or hydrogen sulphide:

$$3\ SO_2 + IO_3^- + 3\ H_2O \rightarrow I^- + 3\ HSO_4^- + 3\ H^+$$

$$3\ H_2S + IO_3^- \rightarrow I^- + 3\ S + 3\ H_2O$$

It is fairly sharply defined, and allows the subsequent iodide end-point to be evaluated.

On the basis of the reduction potential for Fe(III)/Fe(II) given by Latimer [16], an interference from iron(II) could be expected. In practice, this was not observed for concentrations up to 2×10^{-3} M iron(II) for 2×10^{-6} M iodide solutions. Iodine itself gives a positive interference by reacting with iodate as described in reaction (2). Clearly, iodine and iodide mixtures can be resolved if the chloride concentration is so low (about 0.5 M) that a sharp end-point for reaction (1) can be obtained.

Conclusions

The spectrophotometric titration here proposed is particularly suitable for the determination of traces of iodide in fairly concentrated chloride solutions. As already pointed out, high concentrations of chloride constitute a serious interference in many of the previously proposed methods, including the potentiometric, neutron activation and catalytic procedures. The usual separation via oxidation to iodine and solvent extraction is not successful in very concentrated chloride media, chiefly because the oxidation very easily produces oxidation states higher than 0. Therefore, other separation techniques have been proposed, but they are slow and not easy to perform [6, 7]. In the present method chloride is added to the final sample, with the aim of enhancing reaction (2).

The determination of iodide in table salt is made easier by this method. Concentrations as low as 0.08 mg kg^{-1} can be determined with high precision (±3%) by dissolving 15 g of salt in 50 ml of 0.5 M hydrochloric acid, and titrating this solution spectrophotometrically.

REFERENCES

1 B. R. Clark and R. Skoog, Anal. Chem., 47 (1975) 2458.
2 R. Malvano, G. Buzzigoli, M. Scarlattini, G. Cenderelli, C. Gandolfi and P. Grosso, Anal. Chim. Acta, 61 (1972) 201.
3 W. J. Williams, Handbook of Anions Determination, Butterworths, London, 1979, pp. 358—399.
4 V. A. Nikashina and A. N. Krachak, Zh. Anal. Khim., 34 (1979) 2236.
5 P. R. Gifford and S. Bruckenstein, Anal. Chem., 52 (1980) 1024.
6 G. T. F. Wong and P. G. Brewer, Anal. Chim. Acta, 81 (1976) 81.
7 A. D. Matthews and J. P. Riley, Anal. Chim. Acta, 51 (1970) 295.
8 L. W. Andrews, J. Am. Chem. Soc., 25 (1903) 756; Z. Anorg. Chem., 36 (1903) 76.
9 G. S. Jamieson, Volumetric Iodate Methods, Chemical Catalog Co., New York, 1926.
10 D. L. Cason and H. M. Neumann, J. Am. Chem. Soc., 83 (1961) 1822.
11 J. H. Faull, J. Am. Chem. Soc., 56 (1934) 522.
12 J. N. Brønsted, Z. Physik. Chem., 102 (1922) 169.
13 I. M. Kolthoff and R. Belcher, Volumetric Analysis, Vol. III, Interscience, New York, 1957, p. 203.
14 S. Popov, M. Jones, C. Rucker and W. W. Becker, J. Am. Chem. Soc., 51 (1929) 1299.
15 L. G. Sillen and A. E. Martell, Stability Constants of Metal—Ion Complexes, Spec. Publ. 17, The Chemical Society, London, 1964, pp. 285—286.
16 W. M. Latimer, Oxidation Potentials, Prentice-Hall, New York, 1953, pp. 340—345.

Analytica Chimica Acta, 153 (1983) 257—260
Elsevier Science Publishers B.V., Amsterdam — Printed in The Netherlands

Short Communication

CLUSTERING ON A MICROCOMPUTER WITH AN APPLICATION TO THE CLASSIFICATION OF COALS

L. KAUFMAN, A. PIERREUX and P. ROUSSEEUW

Department of Statistics, Vrije Universiteit Brussel, Pleinlaan 2, B-1050 Brussels (Belgium)

M. P. DERDE, M. R. DETAEVERNIER and D. L. MASSART*

Pharmaceutical Institute, Vrije Universiteit Brussel, Laarbeeklaan 103, B-1090 Brussels (Belgium)

G. PLATBROOD

LABORELEC, P.O. Box 11, B-1640 Sint-Genesius-Rode (Belgium)

(Received 6th June 1983)

Summary. The widespread introduction of microcomputers in laboratories where large data sets are more and more frequently gathered, makes it necessary to be able to use adapted statistical software. This paper describes a BASIC program for the Macnaughton-Smith clustering method adapted to the Apple II microcomputer. Experience is reported of an application of the program to the classification of a set of coals.

Clustering programs have the reputation of needing a lot of computer memory and time. This is due to the need for working with a large dissimilarity matrix ($n \times n$ for n objects). The usual agglomerative hierarchical methods reduce the matrix one unit at a time, while nonhierarchical methods need the whole matrix all the time. For use with microcomputers, this is an important handicap. In view of the growing number of microcomputers in laboratories, it seemed worthwhile to examine the possibility of using microcomputers for clustering.

Macnaughton-Smith's algorithm [1] was selected to achieve this. Macnaughton-Smith's algorithm is of the hierarchical type but, in contrast to the better-known agglomerative algorithms, it is divisive. This means that one starts out with all the objects to be clustered and divides them first in two groups, each of these groups is then further divided into two, etc. This leads to the kind of result shown in Fig. 1. A more convenient way of representing the results is given in Fig. 2. In this way, one immediately more or less halves the matrix and keeps on doing so, so that the algorithm should be more readily adapted to microcomputers.

0003-2670/83/$03.00

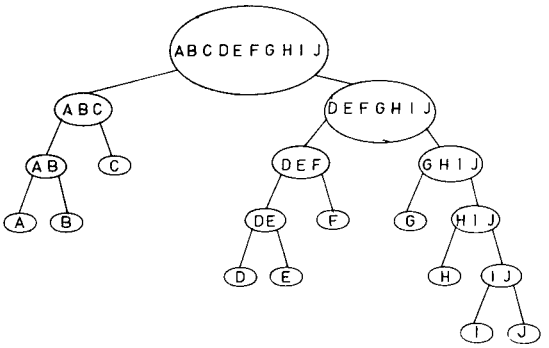

Fig. 1. Sample output of a divisive clustering algorithm.

Methodology

A set of n objects is considered; each of them is measured on p variables. The dissimilarity between the ith and the jth object is denoted by dist(i,j).

The whole set of objects, A, has to be divided into two subsets. Therefore a splinter group B is constructed by sequential addition of one object at a time.

Initiation of the splinter group. For each k belonging to A, calculate

$$G_k = (|A| - 1)^{-1} \Sigma_{i \in A} \text{dist}(k,i)$$

where $|A|$ is the number of objects in set A. Call m the object which maximizes G_k:

$$G_m = \max_{k \in A} G_k .$$

When m is not unique, it is chosen arbitrarily. Now m is the object with the greatest total dissimilarity from the rest of the group. Then construct a new set A by taking away object m. Object m goes to the splinter group B.

Allocating new objects to the splinter group and setting up a stopping rule. For each k belonging to A, calculate

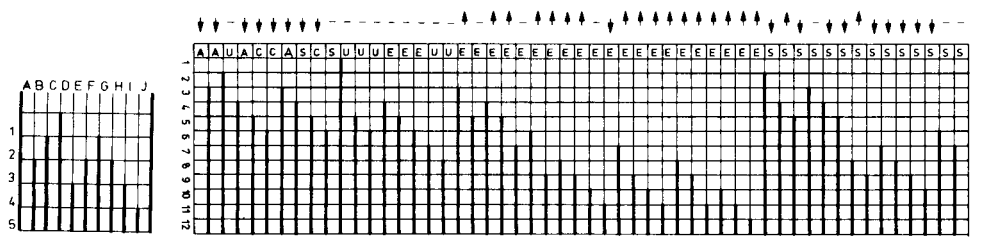

Fig. 2. Graphical representation of the output of Fig. 1.

Fig. 3. Graphical representation of the program output of the classification of coals. For symbols, see text.

$DA_k = (|A| - 1)^{-1}\Sigma_{i \in A}\text{dist}(k,i)$ if A contains at least 2 objects.
$= 0$ if A contains a single object.

$DB_k = |B|^{-1}\Sigma_{i \in B}\text{dist}(k,i)$

$D_k = DA_k - DB_k$.

Call m the object which maximizes D_k: $D_m = \max_{k \in A} D_k$.

There are two possibilities.

(1) If $D_m > 0 \Leftrightarrow DA_m > DB_m$, the object m is more similar to B than to the rest of the set A; object m is taken away from A and placed in B; repeat the allocation step.

(2) If $D_m \leqslant 0 \Leftrightarrow DA_m \leqslant DB_m$, no more objects will be transferred to the splinter group (stopping rule).

The set A is now divided into two subsets, namely B and a new set A. These subsets can be split up again until each subset consists of only one object.

The method and applications are discussed in a book about clustering applied to analytical chemistry [2]. As for all clustering applications, a dissimilarity measure is needed. In the present instance, this is the Euclidian distance. The program was written in Applesoft and implemented on an Apple II with 48K. The output is a list of clusters. Figures are not provided by the program and must be made manually.

Data

To test the program, a set of data about coals was used. The data set consisted of the results of the determination of the elements Al, Si, Fe, Ca, Mg, Na, K and S and the minerals illite, dolomite, kaolinite, gypsum, pyrite, calcite, silica for 53 coals of different origin and quality. Coals from the following origins were present: Australia (A), Canada (C), the U.S.A. (U), Western Europe (E) and South Africa (S). These coals were also subjected to a sintering test and divided into three categories. These categories are related to the possible use of the coals and are symbolized by ↓ (low sintering value), ↑ (high sintering value) and — (intermediate sintering value).

Results

The clustering was obtained in 96 min of computation time. The result is given in Fig. 3. The first division separates a cluster containing all the Australian and Canadian coals together with two South Africans and one U.S. coal. All these coals have a low or intermediate sintering value. The larger cluster is split up in two subclusters, the smaller of which contains all the South African coals. The larger subcluster then splits again in two: one of the resulting clusters contains only intermediate quality coals and all the remaining U.S. coals; the other contains only European coals. The clustering was repeated on a CDC CYBER 170/750 mainframe computer with the MASLOC clustering program, the quality of which is well proven [3, 4]. Very similar results were obtained. As a result, the following conclusions can be drawn.

TABLE 1

Computer time required for problems of different size

Number of objects	10	20	30	40	50
Required computing time (minutes excluding output)	1	6	17	39	83

First, the clustering program developed for the microcomputer performs well. In order to estimate the upper limit of objects that can be handled with the present program, the required computing time was noted for several problems. The dissimilarity matrix was used as the starting point for the program. The results are given in Table 1. In view of the results in Table 1, it seems reasonable to say that up to approximately 60 objects can be clustered with this program on the Apple II computer. The rapid increase of performance of present day microcomputers makes it reasonable to expect that clustering programs for a few hundred objects will be available quite soon.

Secondly, the clustering of coals reveals that geographical origin is a very important factor in determining the mineral content of coal. The coincidence of sintering values with the clustering is somewhat less good and, in fact, it is not impossible that the relation is fortuitous.

REFERENCES

1 P. Macnaughton-Smith, W. T. Williams, M. B. Dale and L. G. Mockett, Nature, 202 (1964) 1034.
2 D. L. Massart and L. Kaufman, The Interpretation of Analytical Chemical Data by the Use of Cluster Analysis, Wiley, New York, 1983.
3 A. M. Massart-Lëen and D. L. Massart, Biochem. J., 196 (1981) 611.
4 D. L. Massart, L. Kaufman and K. H. Esbensen, Anal. Chem., 54 (1982) 911.

Analytica Chimica Acta, 153 (1983) 261—263
Elsevier Science Publishers B.V., Amsterdam — Printed in The Netherlands

Short Communication

ULTRATRACE PHOTOMETRIC DETERMINATION OF PHOSPHATE WITH A SOLID-STATE EMITTER AS LIGHT SOURCE

TOTARO IMASAKA, TIICHIRO KAMIKUBO, YUJI KAWABATA and NOBUHIKO ISHIBASHI*

Faculty of Engineering, Kyushu University, Hakozaki, Fukuoka 812 (Japan)

(Received 26th April 1983)

Summary. The stability of the output power of a solid-state emitter (814 nm) is so great when operated from two 1.5-V batteries that an absorption photometer equipped with this emitter as light source can be used to measure absorbances down to 1.5×10^{-6}. A detection limit of 15 ng l^{-1} is obtained for the determination of phosphorus by a molybdenum blue method.

Spectrophotometric molybdenum blue methods are most frequently used for the determination of phosphorus. However, the phosphorus concentration in lake and sea waters is normally only 0.1—100 μg l^{-1} [1], so that conventional direct spectrophotometry is sometimes not sensitive enough for determinations at the lower levels. Recently, a new type of high-power solid-state emitter has been developed, which involves technology related to that in a semiconductor laser for data communication systems. It provides a large output power (>30 mW) at around 800 nm. The output is very stable; there is no discharge noise and no ripple from a power line as it can be operated from batteries. This implies that a solid-state emitter should be quite promising as a light source for photometry in ultratrace analysis, as very small absorbance changes should be measurable. This communication describes the construction and operation of a photometer incorporating a solid-state emitter as light source. Its application is demonstrated in the ultratrace determination of phosphorus by the molybdenum blue method.

Experimental

Apparatus. A block diagram of the apparatus is shown in Fig. 1. The solid-state emitter (Hitachi HLP60RL) provides emission at 814 nm with an output power of 36 mW. The power supply is two conventional 1.5-V batteries, and the electronic current is adjusted by changing a resistor connected in series to the emitter. The emitted beam is split by a quartz plate. The reflected (reference) beam is detected by a photodiode (Hamamatsu TV, S-780-8BQ). The transmitted beam passes through the sample cell and is detected by another photodiode (HTV, S-1190). Slight deviation of the optical path

0003-2670/83/$03.00

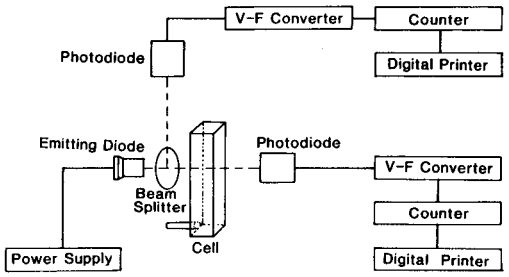

Fig. 1. Block diagram of the photometer.

causes serious errors, thus the sample solution must be changed without moving the cell. The detected voltage signals are converted to frequency, accumulated by an electronic counter (NF Circuit Design Block Co., Ltd., PC-545A), and printed out by a printer (Nada Electronic Lab., Ltd., DP102). Slight long-term drift of the emitted intensity was compensated by measuring the ratio of the transmitted intensity to the reference intensity.

Procedure. Mix in a beaker 0—1 ml of 1 μg ml^{-1} phosphorus solution (as KH_2PO_4; Wako), 1 ml of 0.1 M sodium molybdate solution (Na_2MoO_4; Wako) in 5 M sulphuric acid, 2 ml of 0.01 M hydrazinium sulphate (Kishida), 5 ml of 5 M sulphuric acid (Kishida), and distilled water to make the total volume slightly less than 100 ml. Heat the solution to 100°C over 20 min and cool immediately in water. Transfer the solution to a 100-ml volumetric flask and dilute to volume with distilled water. Transfer the solution to the optical cell and accumulate the transmittance signal for 50 s.

Results and discussion

The absorption maximum of molybdenum blue is at 824 nm, which is close to the emission wavelength of the solid-state emitter (814 nm). The short-term stability of the output power of the emitter was 0.01%. The long-term drift was much larger (2%), but was compensated by the ratio measurement. This drift seems to arise from variation of the emitter temperature. A calibration graph for phosphorus was constructed; it was linear from 0 to 10 μg l^{-1}. The background signal corresponded to 0.6 μg P l^{-1}. This seemed to arise mainly from phosphorus in the sodium molybdate or residual contamination by phosphate adsorbed on the glassware or both. The detection limit (signal:noise = 2) was 15 ng l^{-1}, which corresponded to an absorbance of 1.5×10^{-6}. This value is at least two orders of magnitude less than that achieved in a conventional spectrophotometer.

The regulation limits for phosphorus in Japan and the detection limits for various spectrophotometric techniques are summarized in Table 1. The detection limit obtained with the new equipment is sufficiently low for the determination of phosphate in the environment, and is a considerable improvement on most spectrometric techniques. The photometer is very simple, and will find use in many areas.

TABLE 1

Regulation limits for phosphorus in water samples and detection limits of various spectrometric techniques

Method	Phosphorus conc. ($\mu g\ l^{-1}$)	Regulatory limit in Japan
Inductively-coupled plasma spectrometry [2]	100	Water for industrial use
	30	
	10	Tap water
	5	Lakes and marshes high clarity)
Conventional absorption photometry [2]	2	
Photoacoustic spectrometry [3][a]	2	
This work	0.015	
Thermal lens spectrometry [1]	0.005	

[a]Semiconductor laser as light source.

This research was partly suppported by a Grant-in-Aid for Scientific Research from the Ministry of Education of Japan and a Research Grant from the Kajima Foundation.

REFERENCES

1 K. Fujiwara, W. Lei, H. Uchiki, F. Shimokoshi, K. Fuwa and T. Kobayashi, Anal. Chem., 54 (1982) 2026.
2 Handbook of Analytical Chemistry, Ed. Jpn. Soc. Anal. Chem., 3rd edn., Maruzen, Tokyo, 1981, p. 168.
3 Y. Kawabata, T. Kamikubo, T. Imasaka and N. Ishibashi, Anal. Chem., 55 (1983) in press.

Analytica Chimica Acta, 153 (1983) 265—269
Elsevier Science Publishers B.V., Amsterdam — Printed in The Netherlands

Short Communication

DETERMINATION OF LOW LEVELS OF URANIUM(VI) IN WATER SOLUTIONS BY MEANS OF THE LASER-INDUCED THERMAL LENSING EFFECT

T. BERTHOUD and P. MAUCHIEN

CEA, Centre d'Etudes Nucleaires, Fontenay aux-Roses (France)

N. OMENETTO* and G. ROSSI

Joint Research Centre, Chemistry Division, Commission of the European Communities, Ispra-Varese (Italy)

(Received 16th March 1983)

Summary. Thermal lensing spectrometry based on a pulsed, excimer-pumped, tunable dye laser as heating beam and a He—Ne laser as probe is described for the determination of low concentrations of uranyl ions in water solution. The dye laser, tuned at 414 nm, has a peak power of about 200 kW and a bandwidth of 0.02 nm. The smallest detectable sorptivity was 3×10^{-5} cm^{-1} and the limit of detection for uranium was 4×10^{-6} M.

Knowledge of the migration mechanisms of actinide ions in ground waters is necessary for safety assessments of nuclear waste deposits in rock formations. Classical analytical techniques are usually too insensitive to detect very low concentrations of these elements. For example, counting techniques are unsuitable for plutonium and neptunium, because of their very long lifetimes. Determination of the oxidation state of these elements is also of major interest for the understanding of their physico-chemical behavior at trace levels. New techniques that could detect and possibly identify the oxidation state of specific actinide ions in solutions are therefore being sought.

Thermal lensing spectroscopy, based on laser excitation, seems to be a very promising approach for actinide determinations [1]. This technique, first described by Gordon et al. [2], has been developed extensively in recent years [3—11]. As in classical absorption spectrophotometry, incident radiation is absorbed by the species to be determined; if the resulting fluorescence is weak, the absorbed energy is converted to heat which is then dissipated into the medium. When a laser is used for excitation, the beam can be focused into the absorbing medium, creating a strong local temperature gradient and so a refractive index gradient. Gordon et al. [2] showed that in the case of a gaussian laser beam (TEM_{00}), spatial redistribution of the refractive index makes the absorbing medium behave as a thin optical lens. Absorption of the incident beam can then be detected by monitoring the

0003-2670/83/$03.00

focusing or defocusing of the light beam passing through the absorbing medium. This is usually done by sensing the relative variation of the intensity of the laser beam passing through a small pinhole at some distance from the absorbing medium. The intensity change can be observed on the beam causing the absorption or on a probe beam, collinear with the primary beam but not absorbed by the medium. In the latter case, the creation of the thermal lens may be observed by deflection of the probe beam [12, 13] or by its defocusing. Thorough theoretical descriptions are available [2, 3, 5, 7].

Different experimental arrangements have been based on continuous wave lasers (argon ion) or pulsed dye lasers. These earlier studies have demonstrated that the technique can detect absorptions 2—3 orders of magnitude lower than is possible by conventional spectrophotometry. Further, it has been shown that water is the worst medium for development of the thermal lens effect, because of its high heat conductivity and the small temperature dependence of its refractive index compared to organic solvents such as chloroform or carbon tetrachloride. In the present case, however, water solutions were obligatory because the primary goal was to investigate the direct applicability of the technique to ground waters, without dilution or chemical treatment of the samples.

This communication presents some preliminary results obtained with pulsed dye laser excitation on uranium in pure water solutions. The choice of uranium is based on the similarity of its behavior with that of the other actinides and the fact that it does not require measures for radioprotection. Of course, the thermal lens technique cannot compete with laser-induced fluorescence of uranium in terms of sensitivity, but the results obtained with uranium indicate what can be expected for similar non-fluorescent species.

Experimental

The complete experimental set-up is schematically depicted in Fig. 1. The heating laser beam was a pulsed tunable dye laser pumped by an excimer laser. The dye laser [14] (Jobin Yvon, Longjumeau, France) consists of an oscillator cavity and one amplifier section; the excimer laser (Lambda Physik, Göttingen, Germany) was operated at the XeCl emission (308 nm). A solution of stilbene provided the necessary output in the 420-nm region and the grating was tuned to select the excitation wavelength of 414 nm with a spectral bandwidth of approximately 0.02 nm. The duration of the excitation pulse, measured with a vacuum photodiode (Model F-4000; ITT, Fort Wayne, IN, U.S.A.) and a fast oscilloscope (Tektronix Model 7904) was found to be about 6 ns. A peak power of 200 kW ($\approx$1 mJ per pulse) was measured with a volume absorbing calorimeter (Model 380101; Scientech, Boulder, CO, U.S.A.). The dye laser beam, after spatial filtering, was focused into a quartz cell containing the uranyl solution. The thermal effect was measured by means of a He—Ne laser (Spectra Physics, Model 47430), the divergence of which was compensated by a lens. The excitation and probe beams were made collinear before crossing the sample cell by means of a

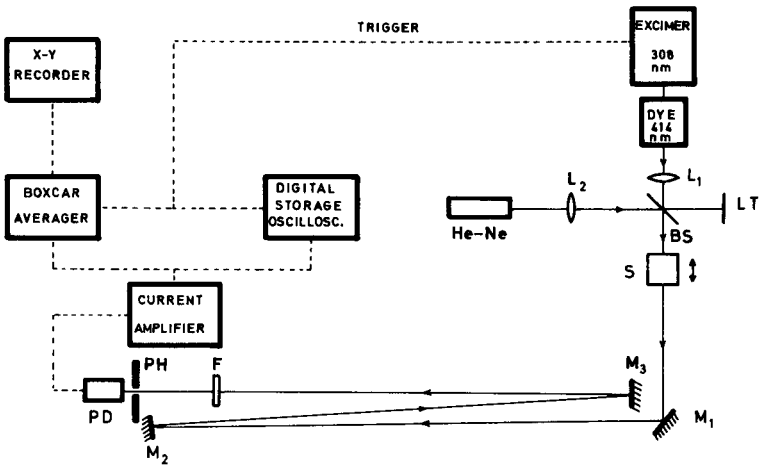

Fig. 1. Schematic layout of the system: L_1, L_2, quartz lenses; BS, beam splitter; LT, light trap; S, sample cuvette; M_1, M_2, M_3, plane mirrors; F, filter; PH, pin-hole; PD, photodiode.

quartz beam splitter. After passing through the absorbing solution, the 414-nm radiation was filtered out and the He—Ne beam was directed throughout a pinhole to a photodiode after an optical path of about 4 m. The current from the photodiode was amplified with a current amplifier (Keithley Model 427) and then sent either to a digital storage oscilloscope with averaging facilities (Tektronix Model 468) or to a boxcar integrator (Princeton Applied Research Model 162/165) connected to an X-Y recorder (Hewlett-Packard Model 7045-B). This set-up allowed retrieval of the temporal behavior of the signal and recording of the absorption spectrum by rotating the grating in the laser oscillator cavity.

Results and discussion

In order to investigate the physical characteristics of the effect caused on the probe beam by the absorbing uranyl solution when the dye laser was tuned at 414 nm, the concentration of uranium was kept at 10^{-2} M in 0.01 M nitric medium. By careful adjustment of the beam splitter, the heating and probing laser beams could be directed collinearly and/or slightly displaced throughout the absorbing volume. For 10^{-2} M uranyl nitrate, the thermal effect appeared to be a combination of both defocusing and deflection processes. This was substantiated by the clearly seen behavior of the He—Ne spot on a white screen at the position of the pinhole, and by the critical dependence of the signal observed on the pinhole position. When the concentration of the absorbing solution was decreased, no deflection effect could be seen. Beam collinearity was therefore optimized to maximize the varization of the signal which was then attributed solely to the defocusing effect, the more so because the best results were obtained when the He—Ne spot was centered on the pinhole.

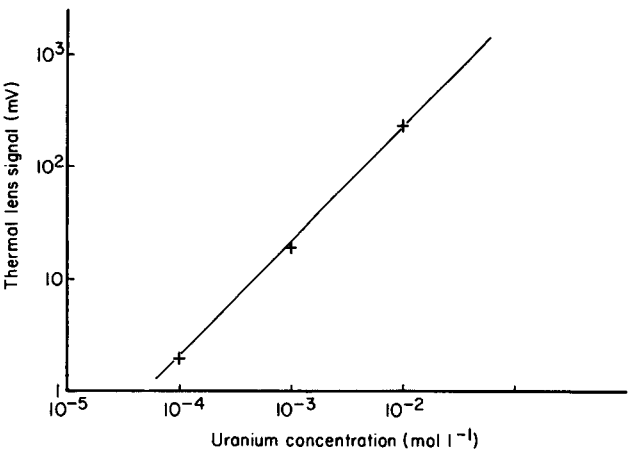

Fig. 2. Calibration graph for uranium. The thermal lensing signals were obtained with a 1-cm absorption path.

In order to assess the sensitivity of the above technique, several less concentrated solutions were tested for the thermal effect. With the 1-cm path length cell, a linear calibration curve (see Fig. 2) was easily obtained down to 10^{-4} M. With a 3-cm cell, the signal-to-noise ratio was 7 for a concentration of 10^{-5} M, averaging 256 laser pulses. This corresponds to an absorptivity of 7×10^{-5} cm^{-1}, assuming a value of 7 for the molar absorptivity of uranium at 414 nm [15]. If the detection limit is set at a signal-to-rms noise ratio equal to 3, then the minimum detectable absorptivity (3×10^{-5} cm^{-1}) corresponds to 4×10^{-6} M uranium. Needless to say, it is the product of the molar absorptivity and the molar concentration (i.e., the absorption coefficient) that matters here: considering that an aqueous medium was used, it can be seen that these measurements are within an order of magnitude of the best results previously reported [1] and obtained with more dedicated electronic data processing.

The main limitations of the present equipment are the poor stability of the He—Ne probe laser (±2%) and the limited number of pulses averaged to reduce the random noise associated with the signal. Both parameters, if properly optimized, should improve sensitivity considerably. In addition, the pulsed laser beam was not optimized in terms of its spatial structure; this could be done, for example, by inserting a small aperture in the oscillator cavity [10]. Nevertheless, the results obtained without sample treatment demonstrate that the technique is viable for the detection of actinides, and certainly worthy of further investigation.

The authors thank Dr. G. Baudin, whose interest made this work possible. The experimental help of P. Cavalli and useful discussions with Dr. H. Human are gratefully acknowledged. The work was done at the Joint Research Centre at Ispra, and was partly supported by the C.E.E. under contract WAS 210-481-7-Ss.

REFERENCES

1 J. V. Beitz and J. P. Hessler, Nucl. Technol., 51 (1980) 169.
2 J. P. Gordon, R. C. C. Leite, R. S. Moore, S. P. Porto and J. R. Whinnery, J. Appl. Phys., 36 (1965) 3.
3 C. Hu and J. R. Whinnery, Appl. Opt., 12 (1973) 72.
4 N. J. Dovichi and J. M. Harris, Anal. Chem., 52 (1980) 2338; Anal. Chem., 53 (1981) 106.
5 J. M. Harris and N. J. Dovichi, Anal. Chem., 52 (1980) 695A.
6 K. Fujiwara, H. Uchiki, F. Shimokoshi, K. Tsunoda, K. Fuwa and T. Kobayashi, Appl. Spectrosc., 36 (1982) 157.
7 S. J. Sheldon, L. V. Knight and J. M. Thorne, Appl. Opt., 21 (1982) 1663.
8 T. Imasaka, K. Miyaishi and N. Ishibashi, Anal. Chim. Acta, 115 (1980) 407.
9 K. Miyaishi, T. Imasaka and N. Ishibashi, Anal. Chim. Acta, 124 (1981) 381.
10 K. Mori, T. Imasaka and N. Ishibashi, Anal. Chem., 54 (1982) 2034.
11 K. Fujiwara, W. Lei, H. Uchiki, F. Shimokoshi, K. Fuwa and T. Kobayashi, Anal. Chem., 54 (1982) 2026.
12 D. Fournier, A. C. Boccara, N. M. Amer and R. Gerlach, Appl. Phys. Lett., 37 (1980) 519.
13 A. Rose, J. D. Pyrum, C. Muzny, G. J. Salamo and R. Gupta, Appl. Opt., 21 (1982) 2663.
14 F. Bos, Appl. Opt., 20 (1981) 3553.
15 E. Rabinowitch and R. L. Belford, Spectroscopy and Photochemistry of Uranyl Compounds, Macmillan, New York, 1964.

Analytica Chimica Acta, 153 (1983) 271—275
Elsevier Science Publishers B.V., Amsterdam — Printed in The Netherlands

Short Communication

DETERMINATION OF TOTAL AMMONIACAL NITROGEN IN WATER BY FLOW INJECTION ANALYSIS AND A GAS DIFFUSION MEMBRANE

M. VAN SON, R. C. SCHOTHORST and G. DEN BOEF*

Laboratory for Analytical Chemistry, University of Amsterdam, Nieuwe Achtergracht 166, 1018 WV Amsterdam (The Netherlands)

(Received 1st June 1983)

Summary. A simple flow injection method for the spectrophotometric determination of ammonia and ammonium ions is described. Ammonia diffuses through a gas-permeable membrane, causing an absorbance change of an acid—base indicator solution (bromothymol blue). The detection limit is about 10^{-6} mol l^{-1}, the response is linear in the concentration range 10^{-6}—10^{-4} mol l^{-1}, the sample rate is 100 h^{-1}, and the standard deviation at 10^{-5} mol l^{-1} is about 3%.

Several potentiometric and spectrophotometric methods of flow injection analysis (f.i.a.) have been described for the determination of ammonia. For potentiometric detection, an air-gap electrode has been used [1]. This method is suitable for the determination of low concentrations (down to 7×10^{-6} mol l^{-1}) but the method is rather slow: the sample rate is 60 h^{-1}. For spectrophotometric detection, indophenol blue and Nessler's reagent have been applied. The method involving indophenol blue is fast (120 samples per hour) but the detection limit is rather high; concentrations down to 3.5×10^{-4} mol l^{-1} can be determined [2—4]. With a computer-controlled system [5], concentrations down to 10^{-5} M can be determined with an accuracy of 3%. With the method involving Nessler's reagent [6, 7], concentrations down to 3.5×10^{-5} mol l^{-1} can be determined at a sample rate of 100 h^{-1}.

In the present communication, a method is described for the determination of ammonia with a gas-permeable membrane. The sample is injected into an alkaline stream in which the ammonium ions present are converted to ammonia molecules. This solution is fed to a cell with a gas-permeable membrane in which reproducible exchange of ammonia with a flowing solution of the acidic form of bromothymol blue occurs. The resulting absorbance change is measured spectrophotometrically in a flow-through cell.

Experimental

Reagents. A 10^{-3} mol l^{-1} stock solution of ammonium chloride was used for the preparation of solutions for the calibration graph. The indicator solution was aqueous 10^{-4} mol l^{-1} bromothymol blue, the pH of which was

0003-2670/83/$03.00

adjusted to 6.5 with 10^{-2} mol l^{-1} sodium hydroxide. The alkaline stream into which samples were injected was 10^{-2} mol l^{-1} sodium hydroxide.

The deionized water, used for preparation of the ammonium chloride and bromothymol blue solutions, was made carbon dioxide-free by boiling for approximately 15 min. In order to avoid uptake of carbon dioxide, the solutions were kept under nitrogen during the experiments, and stored in bottles with soda-lime guard tubes.

Apparatus. The flow system used is shown in Fig. 1. A peristaltic pump (Gilson Minipuls 2) pumps both sodium hydroxide and bromothymol blue solutions at a flow rate of 0.72 ml min^{-1}. The injection valve (BIFOK FIA5 with an injection volume of 29 μl) is connected via a single bead string reactor (SBSR 1, tube length 16 cm, i.d. 1 mm containing glass beads with a diameter of 0.6 mm) with the under inlet of a perspex block containing a membrane. The perspex block is composed of two equal halves, each with a groove (width 2 mm, length 8 cm and depth 75 μm), between which the membrane (a piece of teflon tape with a thickness of 45 μm) is placed. The channels connecting the groove with the tubing are 12 mm long (0.9 mm i.d.). The upper outlet of the block is connected via SBSR 2 (same dimensions as SBSR 1 except for length, 5 cm) to a home-made flow-through cell (optical pathlength 0.4 cm, volume 3 μl).

The absorbance change of the bromothymol blue solution is measured spectrophotometrically with a Zeiss PMQ II spectrophotometer with a digital readout device at 620 nm, the wavelength of maximum absorption for the basic form of the indicator. The light was conducted to the flow cell by glass fibers (Fiberoptic-Heim AG-LC-1/1, length 1 m).

Theory

The relationship between the total ammonium concentration and the concentration of the basic form of the indicator in the indicator solution can be derived from the equations $K_I = [I^{2-}][H^+]/[HI^-] = 10^{-7.1}$, $K_{am}\ [NH_3][H^+]/[NH_4^+] = 10^{-9.3}$, $K_w = [H^+][OH^-] = 10^{-14}$, and the electroneutrality equation

$$[NH_4^+] + [Na^+] + [H^+] = 2[I^{2-}] + [HI^-] + [OH^-]$$

The relationship derived from these equations is

$$C_{am} = \left\{C_I + [I^{2-}] - [Na^+] + \underbrace{\left[\frac{K_w}{K_I}\frac{[I^{2-}]}{(C_I - [I^{2-}])} - K_I\frac{(C_I - [I^{2-}])}{[I^{2-}]}\right]}_{1}\right\} \times \left\{1 + \underbrace{\left[\frac{K_{am}}{K_I}\frac{[I^{2-}]}{(C_I - [I^{2-}])}\right]}_{2}\right\} \quad (1)$$

in which C_{am} is the total ammonia concentration present in the indicator solution ($[NH_4^+] + [NH_3]$), C_I is the total indicator concentration ($[I^{2-}] + [HI^-]$), and $[Na^+]$ is the sodium hydroxide concentration in the indicator solution required to adjust the pH of the solution to the desired value.

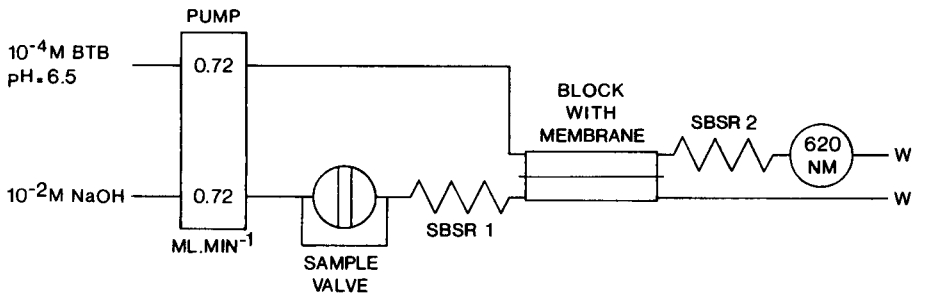

Fig. 1. Flow system.

This relationship is derived on the assumption that the indicator solution is carbon dioxide-free, which can be ensured during experiments. It can easily be verified that terms 1 and 2 of Eqn. (1) will be negligible within a certain concentration range of the basic form of the indicator (and so within a certain pH range). Within that range, there is a linear relationship between the total ammonia concentration and the concentration of the basic form of the indicator in the indicator solution.

For a 10^{-4} mol l^{-1} bromothymol blue solution (the concentration actually used) there is a linear relationship for the pH range 6.4—7.3. For the experiments, a pH of 6.5 was chosen as the starting pH of the bromothymol blue solution. The absorbance change will then be proportional to the total ammonia concentration in the bromothymol blue solution. The theoretical relationship between the total ammonia concentration in a 10^{-4} mol l^{-1} bromothymol blue solution at pH 6.5 and the absorbance change derived from the given formula, is shown in Fig. 2. The curve is linear up to a total ammonia concentration in the bromothymol blue solution of 3×10^{-5} M. Provided that a reproducible fraction of the ammonia diffuses through the membrane, the absorbance change will be proportional to the total ammonia concentration in the sample.

TABLE 1

Relationship between the total ammonia concentration in the samples and the absorbance change for different membranes

Membrane No.	Slope[a] (l mol^{-1})	Conc. range in sample (mol l^{-1})	Permeability (%)
1	959.7 ± 3.7	10^{-5}—10^{-4}	27.6
2	761.7 ± 2.5	10^{-5}—10^{-4}	21.9
3	796.3 ± 3.0	10^{-5}—10^{-4}	22.9
4	1011.7 ± 12.3	10^{-6}—10^{-5}	29.1

[a]Slope with standard deviation, see text.

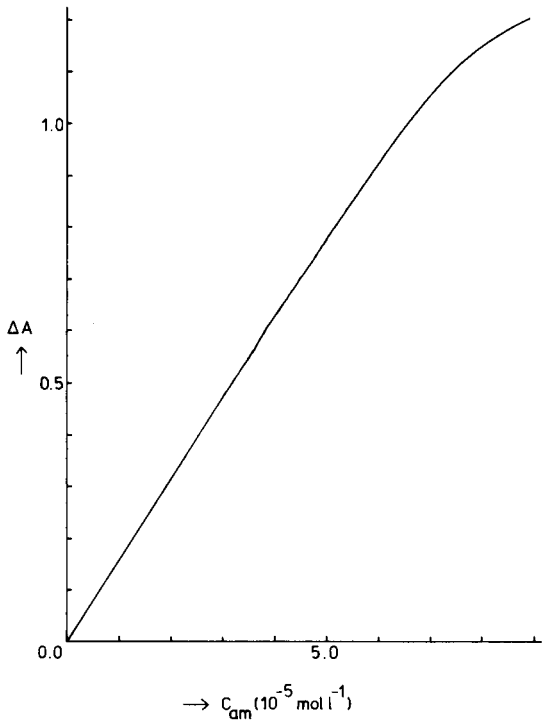

Fig. 2. Theoretical relationship between the total ammonia concentration in a 10^{-4} mol l^{-1} bromothymol blue solution at pH 6.5 and the absorbance change.

Results and discussion

The relationship between the total ammonia concentration in the sample and the absorbance change was determined experimentally for different membranes of the same material. The relationship was indeed linear, as can be seen in Table 1. The given slopes (the ratio of the absorbance change and the total ammonia concentration in the samples) and their standard deviations were calculated by linear regression of 24 data points (six different concentrations, each concentration injected four times). The different slopes for different membranes of the same material are due to the difference in permeability of the membranes, which is caused by the inhomogeneity of the teflon tape used. The permeability was calculated by measuring the peak area.

The influence of carbon dioxide. Carbon dioxide in the sample diffuses quickly through the membrane, resulting in a decrease of the absorbance. Carbon dioxide also has a buffering action, which causes a decrease in sensitivity. Thus both the sample and the bromothymol blue solution must be freed and kept free from carbon dioxide.

Practical applicability. To test the practical applicability of the method, the total ammonia concentration in a sample of Amsterdam canal-water was

determined. The concentration found was $6.48 \times 10^{-5} \pm 0.09 \times 10^{-5}$ mol l^{-1} (99% reliability interval). The concentration of the sample was also determined by the Nessler method [8], which gave $6.51 \times 10^{-5} \pm 0.22 \times 10^{-5}$ mol l^{-1} (99% reliability interval). It can be concluded that the method is promising for practical applications. Another advantage of this method, compared with other spectrophotometric methods, would be that clarification of turbid samples is not necessary.

REFERENCES

1 J. Růžička and E. H. Hansen, Anal. Chim. Acta, 78 (1975) 145.
2 J. W. B. Stewart, J. Růžička, J. Bergamin and H. Zagatto, Anal. Chim. Acta, 81 (1976) 371.
3 J. W. B. Stewart and J. Růžička, Anal. Chim. Acta, 82 (1976) 137.
4 E. H. Hansen, F. J. Krug, A. K. Ghose and J. Růžička, Analyst, 102 (1977) 714.
5 J. Slanina, F. Bakker, A. Bruijn-Hes and J. J. Mols, Anal. Chim. Acta, 113 (1980) 331.
6 E. A. G. Zagatto, B. F. Reis, H. Bergamin and F. J. Krug, Anal. Chim. Acta, 109 (1979) 45.
7 F. J. Krug, J. Růžička and E. H. Hansen, Analyst, 104 (1979) 47.
8 Z. Marczenko, in G. Svehla (Ed.), Spectrophotometric Determination of Elements, Wiley, New York, 1976, p. 391.

Analytica Chimica Acta, 153 (1983) 277—280
Elsevier Science Publishers B.V., Amsterdam — Printed in The Netherlands

Short Communication

THE SPECTROPHOTOMETRIC DETERMINATION OF HYDROXYLAMINE ALONE AND IN THE PRESENCE OF HYDRAZINE BY FLOW INJECTION ANALYSIS

G. C. M. BOURKE, G. STEDMAN* and A. P. WADE

The Chemistry Department, University College, Singleton Park, Swansea SA2 8PP (Gt. Britain)

(Received 18th April 1983)

Summary. The spectrophotometric determination of hydroxylamine based on ferrozine is adapted for flow injection analysis. The sample concentration range is 1×10^{-5}—1×10^{-4} M. The optimised method allows 25 measurements per hour with a repeatability of 0.7%. For 5×10^{-5} M hydroxylamine, hydrazine present in up to 20-fold amounts caused errors of not more than 2%.

The determination of hydroxylamine in the presence of hydrazine is made difficult by their similar chemical properties. Both species behave as weak bases, with pK_a values of 6.04 for NH_3OH^+ [1] and 8.11 for $N_2H_5^+$ [2] at 20°C, and as reducing agents, so that these properties cannot be used to determine hydrazine and hydroxylamine in mixtures. A satisfactory selective method for hydrazine has been published [3], but determination of hydroxylamine has proven to be more difficult. A colorimetric procedure for the latter which makes use of the difference in rates of reaction has been proposed by Dias et al. [4]. Manual operation of their method involves the addition of four solutions followed by an absorbance measurement 7 min later. Tests showed that the repeatability was not satisfactory. It was hoped that the repeatability could be improved by adapting the system to allow semi-automation. Flow injection analysis (f.i.a.) [5] is widely accepted as one such method; the mixing of the sample with the reagents and the reaction time are not operator-dependent, and the flow rate has a repeatability of 1—2%.

Adoption of such a dynamic method as opposed to the static manual method significantly increases the number of system parameters that affect the final sensitivity. Thus it was decided to optimise the system for sensitivity by use of a modified simplex procedure [6], which is a variation of that developed by Nelder and Mead [7] and applied by Morgan and Deming [8].

This communication reports the development and optimisation of an f.i.a. procedure for the determination of hydroxylamine alone and in the presence of up to 200-fold amounts of hydrazine.

0003-2670/83/$03.00

Experimental

Reagents. All chemicals were of reagent grade unless otherwise specified. Fresh ferrozine solutions (0.01 M) were prepared from the commercially available reagent, 3-(2-pyridyl)-5,6-diphenyl-1,2,4-triazine-*p,p'*-disulphonic acid, monosodium salt monohydrate (Aldrich Chemical Co.). The disodium salt was found to be unsuitable because it degraded on mixing with hydroxylamine. Iron(III) ammonium sulphate solution (0.03 M) was prepared by dissolving 14.466 g of the salt in sulphuric acid (2 M) and diluting to 1 l with water. Monochloracetic acid solution (1.5 M) was prepared in water.

A hydroxylamine stock solution (0.02 M) was prepared from the sulphate salt, standardised by acidimetry, and diluted to give solutions in the range 10^{-5}—10^{-4} M. Hydrazine sulphate solutions (0.02 M) were prepared similarly, standardised and diluted to give solutions in the range 5×10^{-5}—10^{-2} M.

Apparatus. The apparatus consisted of a single-channel f.i.a. system and separate microcomputer (Fig. 1). The flow rate was controlled by a peristaltic pump (Desaga 132100; Desaga, Heidelberg, W. Germany). The injection valve was a Rheodyne type 5020 teflon rotary valve. A 2-ml disposable plastic syringe and sample loops of assorted sizes were also required. Polytetrafluoroethylene (PTFE) tubing (0.8 mm i.d.) was used except where otherwise specified. A coil consisting of 35 cm of PTFE tubing and 40 cm of 1.0 mm i.d. silicone tubing was positioned between the peristaltic pump and the injection valve to minimise pulsation. The detector was made in this department and had a tubular flow cell. The light source was a green light-emitting diode (LED) with emission maximum at 565 nm, thus matching the 562-nm absorption maximum of the purple reaction product. The source and phototransistor sensor were mounted transversely across the flow stream giving a path length of 1.4 mm. Construction and performance details have been reported elsewhere [9]. The temperature of the carrier stream

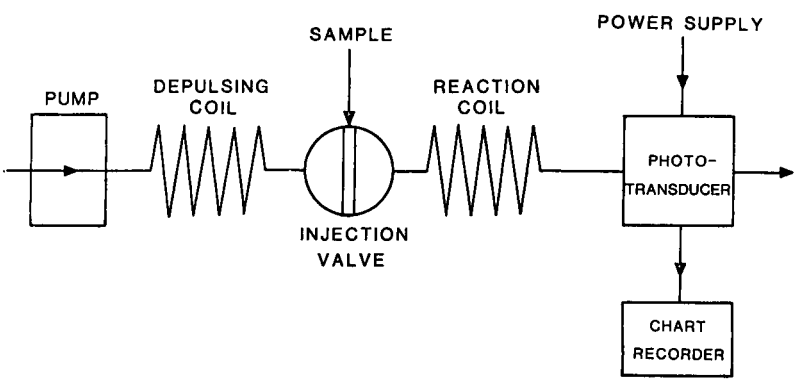

Fig. 1. Schematic diagram of the apparatus. The experimental parameters used were: sample, 410 μl containing 1 volume of hydroxylamine (10^{-4}—10^{-5} M) to 3 volumes of 0.01 M ferrozine; reaction coil, 180 cm; carrier stream, 0.3 M in monochloroacetic acid, 0.273 M in sodium hydroxide and 3.1×10^{-3} M in iron(III); flow rate 1.19 ml min^{-1}.

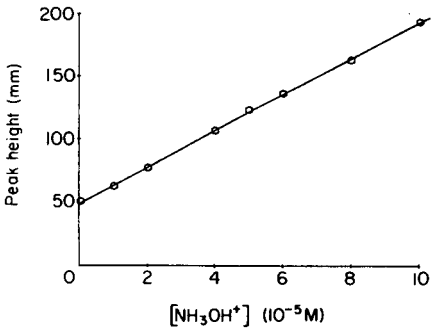

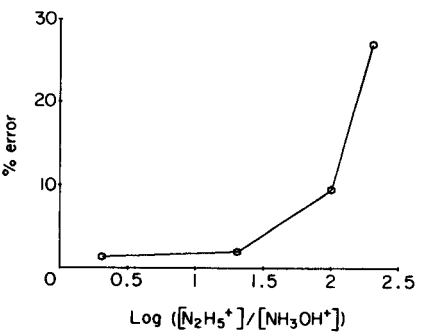

Fig. 2. Peak height (mm) vs. hydroxylamine concentration ($\times 10^{-5}$ M).

Fig. 3. Percentage error for hydrazine interference in hydroxylamine determination vs. log ($[N_2H_5^+]/[NH_3OH^+]$) for 5×10^{-5} M hydroxylamine.

reservoir and reaction coil was kept at 25°C by a thermostatted water bath. The chart recorder used was a Gallenkamp Euroscribe. The microcomputer was a Commodore PET 3032 with 4040 disk drive, 3022 printer and software in BASIC.

Procedure. The apparatus and the chemical compositions of the carrier stream and sample solution are outlined in Fig. 1. A colour was found to develop in the thermostatted carrier stream reservoir if ferrozine was present. Ferrozine was therefore added to the hydroxylamine sample solution. Hydroxylamine samples could have been injected without this stage if a two-stream system had been used, but it was preferred to keep the apparatus as simple as possible. In development of the method, each peak was replicated 4—5 times; agreement was good (±1 mm).

Results and discussion

Optimisation. A subset of the experimental variables was considered, these being the carrier stream pH, iron(III) concentration and flow rate, the sample size and the length of tubing between the points of injection and detection. The initial experimental conditions were as follows: carrier stream, 0.3 M monochloracetic acid/0.171 M sodium hydroxide/9×10^{-4} M iron(III); sample solution, 3 volumes of 1×10^{-2} M ferrozine to 1 volume of 1×10^{-4} M hydroxylamine; sample size, 330 μl (250 μl sample loop and 80 μl of connection tubing); flow rate 1.85 ml min^{-1}; length of tubing between points of injection and detection, 100 cm. These gave a peak height of 47 mm. The optimisation procedure was continued for twelve experiments only. This resulted in conditions which gave a peak height of 168 mm, but repeatability was poor because of precipitation of hydrated iron(III) oxide. Thus a sub-optimal set (giving a peak height of 148 mm) was adopted as the potential method. The conditions used are given in the legend to Fig. 1.

The instrument gain was adjusted to give peak heights of about 193 mm

for a 1×10^{-4} M hydroxylamine sample (as above); 15 consecutive peaks gave a repeatability of 0.7%, the peak heights falling in the range 192.5—194.5 mm, with a fairly flat baseline.

Calibration. Calibration of the system gave a straight line graph (Fig. 2) for hydroxylamine concentrations in the range 10^{-5}—10^{-4}; the slope was 14.3 mm/M $\times 10^5$ and intercept 49.2 mm, suggesting a hydroxylamine detection limit of 10^{-6} M at the baseline noise level observed.

Interference of hydrazine. Hydroxylamine solutions (5×10^{-5} M) containing up to 200-fold amounts of hydrazine were tested. The results were plotted in terms of percentage error in the hydroxylamine determination (Fig. 3). Hydrazine present in up to 20-fold amounts gave rise to errors of $\leqslant 2\%$ in the hydroxylamine results. Where larger amounts are known to be present, hydrazine may be determined specifically by using *p*-dimethylaminobenzaldehyde [3] and then appropriate f.i.a. hydroxylamine calibration experiments can be run to facilitate the analysis.

Interference of reducing agents. The repeatability and sensitivity of the analysis is impaired when reducing agents (e.g. ferrous ion) are present in the solutions, these causing an increased absorbance for the blank.

We thank BNFL, Sellafield, for the provision of a grant to G. C. M. B., The British Petroleum Company for an industrial studentship award to A. P. W., and Prof. D. Betteridge (B.P. Research Centre, Sunbury on Thames, U.K.) for valued discussion.

REFERENCES

1 R. A. Robinson and V. E. Bower, J. Phys. Chem., 65 (1961) 1279.
2 G. Schwarzenbach and A. Zobrist, Helv. Chim. Acta, 19 (1936) 178.
3 G. Watt and J. D. Chrisp, Anal. Chem., 24 (1952) 2006.
4 F. Dias, A. S. Olojola and B. Jaselskis, Talanta, 26 (1979) 47.
5 J. Růžička and E. H. Hansen, Flow Injection Analysis, Wiley, New York, 1981.
6 D. Betteridge and A. P. Wade, unpublished work.
7 J. A. Nelder and R. Mead, Comput. J., 7 (1965) 308.
8 S. L. Morgan and S. N. Deming, Anal. Chem., 46 (1974) 1170.
9 T. J. Sly, D. Betteridge, D. Wibberley and D. G. Porter, J. Automatic Chem., 4(4) (1982) 186.

Analytica Chimica Acta, 153 (1983) 281—284
Elsevier Science Publishers B.V., Amsterdam — Printed in The Netherlands

Kurze Mitteilung

DIE EXTRAKTION—SPEKTROPHOTOMETRISCHE BESTIMMUNG VON MAGNESIUMSPUREN MIT 5,7-DIIODOCHINOLIN-8-OL UND RHODAMIN S

G. RÖBISCH* und A. RERICHA

Sektion Chemie/Biologie der Pädagogischen Hochschule "Karl Liebknecht" Potsdam, DDR-1500 Potsdam (D.D.R.)

(Eingegangen den 26 April 1983)

Summary. (Extraction—spectrophotometric determination of traces of magnesium with 5,7-diiodo-8-quinolinol and rhodamine S). The extraction of magnesium as an ion-associate with 8-quinolinol derivatives is investigated. Traces of magnesium (24—240 ng ml^{-1}) can be determined by extraction with 5,7-diiodo-8-quinolinol and rhodamine S into toluene and absorbance measurements at 540 nm. The molar absorptivity is 6.53×10^4 l mol^{-1} cm^{-1}.

Zusammenfassung. Untersucht wurde die Extrahierbarkeit von Magnesium als Ionenassoziat. Eine extraktionsphotometrische Bestimmung von Magnesiumspuren (20 ppb) mit 5,7-Diiodochinolin-8-ol/Rhodamin S/Toluen wurde entwickelt.

Bei der Bildung der Ionenassoziate von Chinolinolaten des Typs $[MOx_3]^-$ (Ox = deprotoniertes Chinolin-8-ol) mit ungefärbten, positiv geladenen Gegenionen ist eine für photometrische Zwecke wünschenswerte Erhöhung des Extinktionskoeffizienten nicht zu erwarten, weil die ^1L_a-Bande des Chinolinolats [1] durch das Gegenion nicht wesentlich beeinflußt wird. Dagegen ist mit Hilfe der farbintensiven Rhodamine ein drastischer Effekt zu erwarten, denn hier werden die Energieverhältnisse im Chromophor durch das Chinolinolat verändert. Das wird durch eine Reihe von Untersuchungen bestätigt. Übersichten dazu publizierten Marczenko [2] und Shcherbov und Plotnikova [3]. Die Rhodaminbande bei 550 nm erlaubt eine Steigerung der photometrischen Empfindlichkeit auf das Zehnfache.

Einen Literaturüberblick über die bisher vorliegenden Untersuchungen zur Extrahierbarkeit der Erdalkalimetalle in Form der Ionenassoziate, gebildet aus den Trischinolinolaten (gearbeitet wurde mit den 5,7-Dihalogeno- und 5,7-Dinitrochinolin-8-ol-Derivaten) und verschiedenen Rhodaminfarbstoffen geben Beltjukova und Mitarbeiter [4]. Wir setzten bei unseren Untersuchungen Chinolin-8-ol, CMAB— und CMAP—Chinolin-8-ol [5], die 5,7-Dihalogenchinolin-8-ole (Chlor, Brom, Iod) sowie Rhodamin B, S und 6G [6] im Verteilungssystem Wasser/Toluen ein mit dem Ziel der Optimierung einer extraktion—spektrophotometrischen Magnesiumbestimmung besonders in bezug auf deren Sensitivität.

0003-2670/83/$03.00

Experimentelles

Gearbeitet wurde mit 0,1 M schwefelsaurer $2 \cdot 10^{-4}$ Magnesiumsulfatlösung, 0,1 M Tartratlösung, $5 \cdot 10^{-3}$ M Lösung von CMAB-, CMAP-, $1 \cdot 10^{-3}$ M 5,7-Dichlor(brom, iod)-chinolin-8-ol in Toluen, $5 \cdot 10^{-3}$ M (bzw. $2 \cdot 10^{-3}$ M) Rhodamin B (S, 6G)-Lösung.

Das Gemisch aus 1 ml Magnesiumlösung, 2 ml Tartratlösung und 5 ml Rhodaminlösung wird mit Wasser dest. auf ein Volumen von etwa 20 ml gebracht. Nach Einstellen des pH-Wertes, Überführen in einen Schütteltrichter und nach Zusatz von 20 ml toluenischer Ligandlösung wird 10 Min geschüttelt. Nach der Phasentrennung zentrifugiert man die organische Phase und photometriert gegen eine entsprechende Blindlösung bei einer Schichtdicke von 3 cm oder 1 cm.

Ergebnisse

Mit dem unsubstituierten Chinolin-8-ol und Rhodamin B wurde im Bereich $4{,}5 < \text{pH} < 13{,}0$ keine Extraktion beobachtet.

Die Spektren (Abb. 1) sind durch zwei Hauptbanden (die chinolinische um 395 nm bei weitgehend gleicher Intensität und die Rhodaminbande um 550 nm mit deutlich unterschiedlichen Intensitäten) charakterisiert. Die Substituenten beeinflussen in der Reihe Cl < Br < I die Farbintensität des Ionenassoziats. Aus den Spektren ist erkennbar, daß im System Mg/CMAP—Chinolinol/Rhodamin B kein Ionenassoziat gebildet wird (die Rhodaminbande fehlt), anders ist das bei Verwendung von CMAB—chinolinol.

Die Extraktionskurven (Abb. 2) zeigen und aus den Extraktionsparametern (Tab. 1) ist erkennbar, daß bei Anwesenheit von Rhodamin B die extraktionsphotometrischen Bedingungen für das System Mg/CMAB—chino-

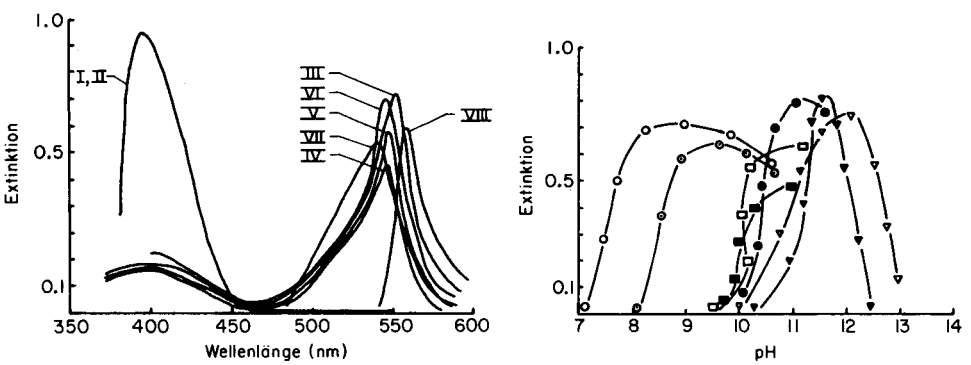

Abb. 1. Elektronenspektren der in Tab. 1 aufgeführten Spezies bei optimalen Reaktionsbedingungen (siehe Text), gemessen gegen Blindlösung. c_{Mg} = 15 nmol ml^{-1}. I—VI l = 3 cm; VII, VIII l = 1 cm.

Abb. 2. Extraktionskurven der in Tab. 1 aufgeführten Spezies, gemessen gegen Blindlösung. c_{Mg} = 15 nmol ml^{-1}. II—VI l = 3 cm; VII, VIII l = 1 cm. (▲) II; (▽) III; (■) IV; (□) V; (●) VI; (⊙) VII; (○) VIII.

TABELLE 1

Extraktionsparameter und optische Daten der extrahierten Spezies

Spezies	λ (nm)	ε (10^3 l mol^{-1} cm^{-1})	ΔpH_{max}	pK_{ex}/n
I $Mg(CMAB)_2$	394	7,3	12,8 ± 0,1	9,7
II $Mg(CMAP)_2$	392	8,0	11,8 ± 0,1	7,9
III $\{(RhB^+)[Mg(CMAB)_3^-]\}$	550	10,9	11,7 ± 0,1	8,8
IV $\{(RhB^+)[Mg(OxCl_2)_3^-]\}$	545	15,3	11,1 ± 0,1	7,2
V $\{(RhB^+)[Mg(OxBr_2)_3^-]\}$	545	21,0	10,8 ± 0,1	7,1
VI $\{(RhB^+)[Mg(OxI_2)_3^-]\}$	545	27,3	11,2 ± 0,2	7,3
VII $\{(RhS^+)[Mg(OxI_2)_3^-]\}$	540	65,0	9.5 ± 0,3	5,5
VIII $\{(Rh6G^+)[Mg(OxI_2)_3^-]\}$	560	73,0	8,8 ± 0,1	4,6

linol nur unwesentlich verbessert werden. Außerdem wird deutlich, daß die pH-Bereiche maximaler Extraktion (und damit auch die pK_{ex}/n-Werte als relative Maßzahlen für die Stabilität) durch die Art des Halogensubstituenten im Chinolin-8-ol kaum beeinflußt werden. Dagegen ist erkennbar, daß die extraktionsphotometrischen Parameter (ϵ, ΔpH_{max}, pK_{ex}/n) beim $[Mg(OxI_2)_3]^-$ durch die Art der Rhodaminkomponente im Ionenassoziat z.T. drastisch verändert werden in der Reihe $(RhB)^+ < (RhS)^+ < (Rh6G)^+$. Für eine extraktionsphotometrische Magnesiumbestimmung erscheint deshalb das Ionenassoziat $\{(Rh6G^+)[Mg(OxI_2)_3^-]\}^0$ am besten geeignet. Getestet haben wir aber die Bestimmung bei Einsatz von Rhodamin S, da sich mit Rhodamin 6G die Reproduzierbarkeit spürbar verschlechterte.

Aus dem Anstieg der linearisierten Extraktionskurven und nach der Molverhältnismethode konnten wir in jedem Fall für die extrahierte Spezies die Stöchiometrie Mg:Rh:Ox = 1:1:3 feststellen. Zur maximalen Extraktion sind wenigstens ein 20-facher Rhodamin S- und ein 50-facher 5,7-Diiodochinolin-8-ol-Überschuß erforderlich.

Mit 5,7-Dinitrochinolin-8-ol und Rhodamin S wurde unter optimalen Bedingungen für Magnesium ein Extraktionsgrad von nur 53% gefunden [4]. Wir konnten bei Verwendung von 5,7-Diiodochinolin-8-ol, Toluen und Rhodamin S nach einem Extraktionsschritt (mittels AAS) praktisch vollständige Magnesiumextraktion ($R > 99\%$) feststellen. Zusätzliche Untersuchungen ergaben bei nur einem Extraktionsschritt die Möglichkeit einer 15-fachen Anreicherung.

Testung des Grundverfahrens der Bestimmung von Magnesium mit Diiodochinolin-8-ol und Rhodamin S

Arbeitsbedingungen. In einem 100-ml Schütteltrichter gibt man zu n ml (n = 0,6; 1,2; 2,4; 3,6; 4,8; 6,0) $3{,}34 \cdot 10^{-5}$ M Magnesiumsulfatlösung, 2 ml 0,1 M Tartratlösung, ein im Vorversuch ermitteltes Volumen Natronlauge, 1 ml $5 \cdot 10^{-3}$ M Rhodamin S-lösung sowie 10 ml Glycocollpuffer pH 9,3 und füllt mit Wasser bidest. auf 20 ml auf. Dann wird mit 20 ml toluenischer

$1 \cdot 10^{-3}$ M Diiodochinolin-8-ollösung 10 Min geschüttelt. Nach der Phasentrennung wird die organische Phase zentrifugiert und sofort bei 540 nm und einer Schichtdicke von 1 cm gegen Blindlösung photometriert.

Die Auswertung der Eichung erfolgte nach Gottschalk [7]. Das ideale Lineargesetz ist streng erfüllt: Arbeitsbereich (1—10)nmol ml^{-1} Mg; Verfahrenskonstante 15,3 nmol ml^{-1}; Extinktionskoeffizient $6{,}53 \cdot 10^4$ l mol^{-1} cm^{-1}; Standardabweichung ±0,75 nmol ml^{-1}.

Nutzt man die Möglichkeit der 15-fachen Anreicherung, ist eine untere Bestimmungsgrenze von 2 ppb Magnesium (in der wäßrigen Phase) bei allerdings nur befriedigender Reproduzierbarkeit erreichbar.

Die Bestimmung wird von viel Ionen gestört, sodaß meist eine Abtrennung der Magnesiumspuren, hoch selektiv und quantitativ günstig möglich mittels CMAB—Chinolin-8-ol [8, 9] mit nachfolgender Rückextraktion in eine wäßrige Phase bei pH 8, vorangestellt werden muß.

LITERATUR

1 L. Marpurgo und R. J. P. Williams, J. Chem. Soc., Sect. A, (1966) 73.
2 Z. Marczenko, Mikrochim. Acta, II (1977) 651.
3 D. P. Shcherbov und R. N. Plotnikova, Issled. Obl. Khim. Fiz. Metodov Anal. Mineral. Rud, (1977) 39.
4 S. V. Beltjukova, I. N. Drobjazko, L. I. Kononenko und N.S. Poluektov, Ukr. Khim. Zh., 42 (1976) 83.
5 G. Röbisch und A. Rericha, Anal. Chim. Acta, im Druck.
6 Z. Holzbecher, L. Divisch, M. Kral, L. Sucha und I. Vlacil, Handbook of Organic Reagents in Inorganic Analysis, Wiley, New York, 1976.
7 G. Gottschalk, Statistik in der quantitativen Analyse, F. Enke Verlag, Stuttgart, 1962.
8 F. Umland, B. U. Poddar und K.-U. Meckenstock, Z. Anal. Chem., 185 (1962) 362.
9 G. Röbisch, Z. Chem., 11 (1971) 353.

Analytica Chimica Acta, 153 (1983) 285—290
Elsevier Science Publishers B.V., Amsterdam — Printed in The Netherlands

Short Communication

A KINETIC STUDY OF THE OXIDATION OF PHENOLS AND CHLOROPHENOLS BY METAPERIODATE

N. G. BUCKMAN, R. J. MAGEE* and J. O. HILL

Department of Inorganic and Analytical Chemistry, La Trobe University, Bundoora, Melbourne, Victoria 3083 (Australia)

(Received 4th March 1983)

Summary. The fixed-time kinetics of oxidation of phenol and di-, tri-, and tetra-chlorophenols by metaperiodate in acidic solution is assessed as a method for determination of phenols in the 50—500 mg l^{-1} concentration range in aqueous media. The effects of temperature and of acid and periodate concentration on the reaction kinetics are described.

Several procedures have been developed for the determination of phenols in water at trace concentration levels. The spectrophotometric determination of phenols with 4-aminoantipyrine derivatives is well established [1], but this method is not applicable to many *p*-substituted phenols [2]. Various chromatographic methods for the determination of phenols have also been reported, which have employed high-performance liquid chromatography [3—5] and gas chromatography [6]. Recently, a ring-oven procedure for the determination of chlorophenols has been reported in which 4-aminoantipyrine is used as the developing reagent [7]. This method has one particular advantage in that it is readily applicable to "on-site" determinations of phenols in aquatic environments.

The toxicity of phenols in the environment is of current interest. It is known that the toxicity is directly related to structure; hence in pollution studies, it is not sufficient simply to know the total phenol content of a water sample, as environmental phenol control levels are related to individual phenols. Few methods have been reported for the determination of phenols in water at environmental concentrations. A method of considerable potential in this context appears to be the spectrophotometric determination of phenols by oxidation with metaperiodate in acid solution [8, 9]. The oxidation of many aromatic systems by periodate and the kinetics of periodate oxidation of phenols catalysed by osmium(VIII) [10] and ruthenium(III) [11] in basic solution are well known. In the periodate oxidation of phenols in acidic solution, it is known that the absorbance band with λ_{max} in the region 340—300 nm relates directly to the quinonoid reaction products [8, 12, 13] and Sherman et al. [9] have proposed the measurement of absorbance in this wavelength region as the basis of an analytical procedure. However, too few phenols were investigated for a complete assessment of the procedure.

0003-2670/83/$03.00

In the present work, a spectrophotometric study was made of the kinetics of oxidation of phenol and eighteen chlorophenols and the potential application of the method to the determination of phenols in the aquatic environment is assessed.

Experimental

Absorption spectra were recorded over the 300—320 nm region with a Varian 634 spectrophotometer and standard 1-cm quartz cells and, where appropriate, were corrected for methanol absorption in the range 313—305 nm.

The following chemicals were used: anhydrous acetic acid (17.32 M; May and Baker), sodium metaperiodate (BDH; analytical-reagent grade), phenol and chlorophenols (Aldrich Chemical Co.), methanol (BDH Chemicals; redistilled, b.p. 65.5°C). All solutions were prepared with Milli-Q water. Stock phenol solutions in methanol were prepared as required at 1000 mg l^{-1} concentration. In all cases, sample solutions of fixed volume (10 ml) were employed and these solutions were subsequently heated to the desired temperature, 25, 50 or 75°C, prior to cooling in ice, for the derivation of kinetic data. A reaction period of 120 min was used throughout.

Results and discussion

Sherman et al. [9] have studied the fixed-time kinetics of various phenols, including phenol and *p*-chlorophenol, by metaperiodate in acidic solution: however, solvent effects and periodate and acid concentration effects were not studied in detail.

Solvent effects. A solvent effect study was made by comparing the absorbance of a series of blanks consisting of 0.5, 1, 2, 3, 4, 5 ml, respectively, of methanol, 0.20 M periodate (1 ml) and anhydrous acetic acid (2 ml), each solution being made up to a total volume of 10 ml with water. Over the range 305—313 nm, the maximum absorbance of these solutions varied in the ranges 0.020—0.143 (25°C), 0.035—0.245 (50°C) and 0.042—0.317 at 75° over a total time interval of 120 min. The data are summarised in Table 1.

TABLE 1

Absorbance data at 313 and 305 nm for solution blanks over the temperature range 25—75°C

Methanol (ml)	313 nm			305 nm		
	25°C	50°C	75°C	25°C	50°C	75°C
0.5	0.020	0.035	0.042	0.083	0.092	0.095
1.0	0.029	0.068	0.081	0.092	0.139	0.149
2.0	0.052	0.117	0.128	0.126	0.192	0.198
3.0	0.078	0.160	0.196	0.144	0.246	0.273
4.0	0.117	0.194	0.261	0.185	0.284	0.329
5.0	0.143	0.245	0.317	0.212	0.315	0.377

In cases where λ_{max} for the phenol oxidation reaction products is in the range coincident with that for methanol absorption, corrections to λ_{max} are necessary.

Effect of metaperiodate concentration. The effect of metaperiodate concentration on the kinetics of oxidation of phenol and chlorophenols has not been previously determined. A concentration of 300 mg l^{-1} phenol was selected for this study. A series of phenol solutions was prepared from 3 ml of a standard 1000 mg l^{-1} stock solution of the phenol in methanol, 1 ml of sodium metaperiodate solution of varying concentration (0.12—0.36 M) and 2 ml of anhydrous acetic acid; each solution was diluted to a total volume of 10 ml with water. The absorbance of these solutions was measured at 50°C with reference to a corresponding blank, after a reaction time of 120 min. Results for six phenols are shown in Fig. 1. Similar trends in the results were obtained for solutions heated at 25 and 75°C. For general analytical purposes, a 0.24 M [IO_4^-] concentration is recommended because, although greater sensitivities are associated with the higher periodate concentrations, the reaction rate is outside the range of measurement, particularly at temperatures greater than 50°C.

Effect of acid concentration. A concentration of 300 mg l^{-1} phenol was employed. A series of standard phenol solutions was prepared from 3 ml of the standard 1000 mg l^{-1} methanolic stock solution of the phenol, 1 ml of

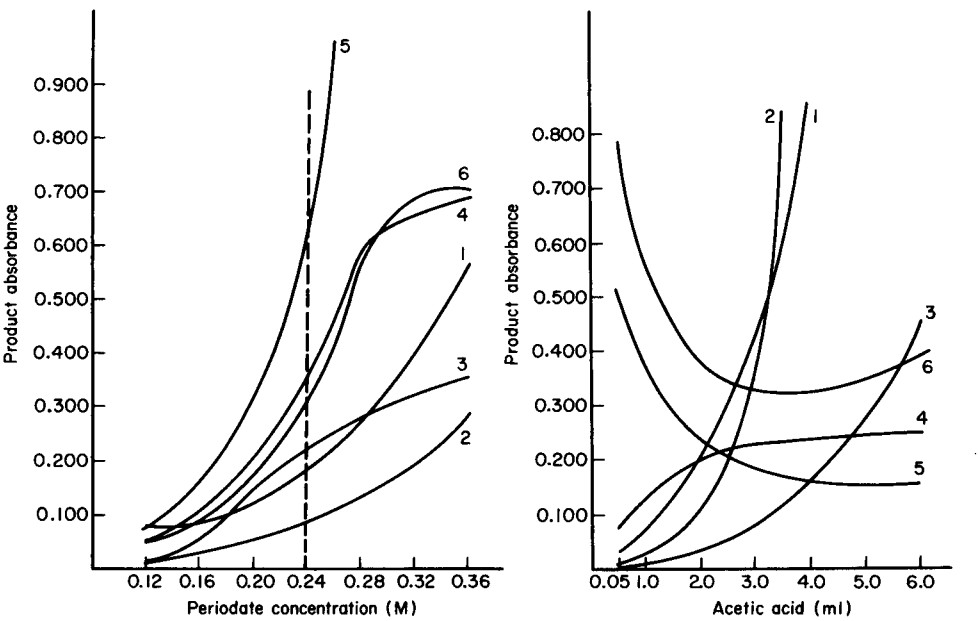

Fig. 1. Effect of periodate concentration at 50°C and 0.24 M sodium metaperiodate. (1) Phenol; (2) 2-chlorophenol; (3) 2,5-dichlorophenol; (4) 2,4,6-trichlorophenol; (5) 2,3,4,6-tetrachlorophenol; (6) pentachlorophenol.

Fig. 2. Effect of acid concentration at 50°C. (1) Phenol; (2) 2-chlorophenol; (3) 3-chlorophenol; (4) 2,5-dichlorophenol; (5) 2,4,5-trichlorophenol; (6) 2,3,4,5-tetrachlorophenol.

0.24 M sodium metaperiodate and 0.5, 1, 2, 3, 4, 5, 6 ml of anhydrous acetic acid, respectively; the solutions were diluted to final volumes of 10 ml. The absorbance of these solutions was measured at 50°C against a corresponding blank after a reaction time of 120 min. The results are shown in Table 2 and Fig. 2. It is difficult to recognise any well-defined correlation between the effect of the acid concentration and the structure of the phenol. An assessment of the overall data, however, shows that the use of 2 ml of anhydrous acetic acid (equivalent to a concentration of 3.464 M) represents a balance between a measurable reaction rate and acceptable sensitivity for all phenol types at the three temperatures studied.

Kinetic data. Standard phenol solutions were prepared, each consisting of 0.5, 1, 2, 3, 4, 5 ml of the standard 1000 mg l^{-1} methanolic stock solution of the phenol, 1 ml of 0.24 M sodium metaperiodate and 2 ml of anhydrous acetic acid diluted to a total volume of 10 ml. Three temperatures were employed (25, 50, 75°C) and a reaction time of 120 min was used throughout. Representative results for dichlorophenols are shown in Fig. 3. All kinetic data were interpreted in terms of the equation $C = (aKt_0)_x^{-1}$ [14], where C is the phenol concentration, x the absorbance, t_0 the preselected reaction time, K the analytical rate constant, and a an experimental constant.

Data for aK at the three selected temperatures are given in Table 3. Previously Sherman et al. [9] used aKt_0 as the parameter for comparison of phenols, but in the present work t_0 is constant (120 min), hence aK values were taken for comparison purposes: aKt_0 is the slope of the plots in Fig. 3.

TABLE 2

Absorbance data for phenols (300 mg l^{-1} concentration) at 50°C as a function of acid concentration

Phenol	Absorbance for different volumes (ml) of added acetic acid						
	0.5	1	2	3	4	5	6
Phenol	0.030	0.073	0.206	0.423	0.872	—	—
2-Chlorophenol	0.013	0.022	0.108	0.349	0.751	—	—
3-Chlorophenol	0.000	0.001	0.035	0.083	0.166	0.276	0.450
4-Chlorophenol	0.006	0.032	0.133	0.432	—	—	—
2,3-Dichlorophenol	0.081	0.041	0.207	0.234	0.251	0.267	0.278
2,4-Dichlorophenol	0.073	0.146	0.217	0.245	0.267	0.280	0.303
3,5-Dichlorophenol	0.040	0.075	0.124	0.150	0.163	0.176	0.182
2,5-Dichlorophenol	0.068	0.124	0.197	0.223	0.232	0.240	0.245
3,4,5-Trichlorophenol	0.512	0.476	0.236	0.184	0.162	0.149	0.161
2,3,4-Trichlorophenol	0.125	0.203	0.226	0.201	0.174	0.211	0.256
2,3,5-Trichlorophenol	0.007	0.022	0.051	0.054	0.055	0.055	0.056
2,3,6-Trichlorophenol	0.024	0.050	0.116	0.198	0.322	0.499	0.736
2,4,5-Trichlorophenol	0.521	0.439	0.339	0.309	0.298	0.316	0.320
2,4,6-Trichlorophenol	0.524	0.451	0.350	0.318	0.317	0.337	0.370
2,3,5,6-Tetrachlorophenol	0.522	0.426	0.306	0.278	0.277	0.280	0.286
2,3,4,5-Tetrachlorophenol	0.782	0.573	0.378	0.328	0.317	0.347	0.391
2,3,4,6-Tetrachlorophenol	0.614	0.604	0.606	0.605	0.604	0.610	0.605

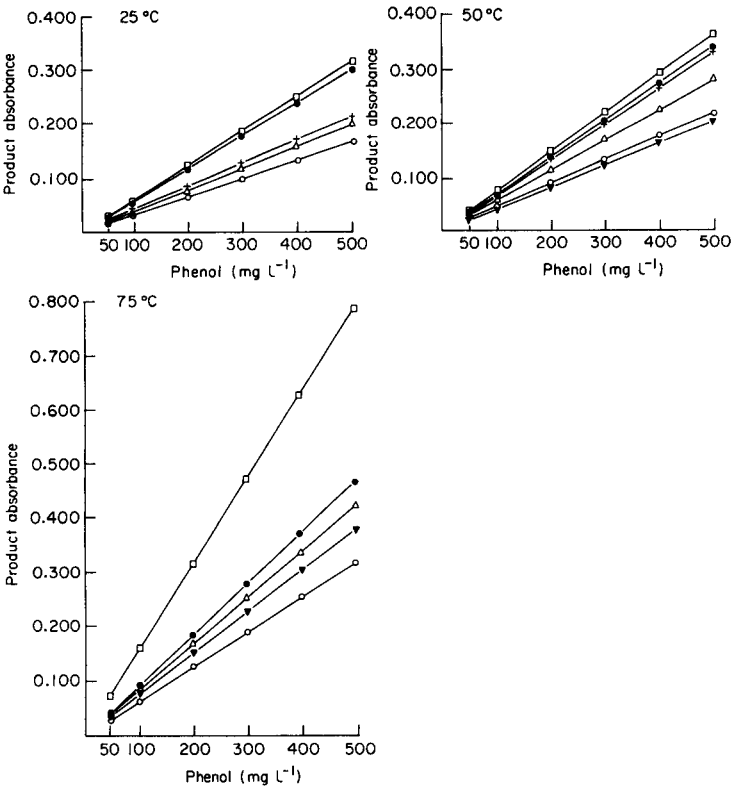

Fig. 3. Oxidation reactions for dichlorophenols at 25, 50 and 75°C. The dichlorophenols represented are: (□) 2,4-; (●) 2,3-; (△) 3,4-; (+) 2,5-; (○) 2,6-; (▼) 3,5-.

From the results shown in Fig. 3 it is clear that, for phenol and monochlorophenols, the order of reactivity at 50°C is phenol > 4-chlorophenol > 2-chlorophenol > 3-chlorophenol and for dichlorophenols the corresponding order of reactivity is 2,4-dichlorophenol > 2,3-dichlorophenol > 2,5-dichlorophenol > 3,4-dichlorophenol > 2,6-dichlorophenol > 3,5-dichlorophenol. Thus, it appears in general that the presence of *m*-substituents depresses the overall reaction rate. A similar trend is apparent for the trichlorophenol group.

From a critical assessment of the kinetic data obtained in the present study, it is apparent that as the aK values vary markedly for individual phenols at the same reaction temperature, the method may be used for the identification and determination of individual phenols in the 50—500 mg l^{-1} range. The method is also suitable for the determination of individual phenols in a multicomponent phenol system such as an industrial waste system if prior analytical [15—17] or chromatographic separations [4] of the component phenols are achieved. However, the method appears

TABLE 3

The aK values for phenols (50—500 mg l^{-1}) as a function of temperature

Phenol	aK values at different temperatures		
	25°C	50°C	75°C
Phenol	0.197	0.528	0.674
2-Chlorophenol	0.158	0.374	0.441
3-Chlorophenol	—	0.134	0.281
4-Chlorophenol	0.211	0.460	0.510
2,3-Dichlorophenol	0.811	0.923	1.260
2,6-Dichlorophenol	0.458	0.587	0.853
3,4-Dichlorophenol	0.543	0.758	1.138
2,4-Dichlorophenol	0.850	0.994	2.186
3,5-Dichlorophenol	—	0.549	1.037
2,5-Dichlorophenol	0.579	0.892	—
2,3,4-Trichlorophenol	0.992	1.235	1.562
2,4,5-Trichlorophenol	1.512	1.850	—
2,4,6-Trichlorophenol	1.288	1.946	2.261
2,3,6-Trichlorophenol	0.288	0.640	1.260
3,4,5-Trichlorophenol	1.185	1.280	1.891
2,3,5-Trichlorophenol	—	0.271	1.127
2,3,5,6-Tetrachlorophenol	1.382	1.970	1.532
2,3,4,5-Tetrachlorophenol	2.176	2.392	4.286
2,3,4,5-Tetrachlorophenol	2.639	3.891	—

to be of limited applicability to the determination of phenols in natural waters, as the lower detection limit is 50 mg l^{-1}, whereas typical phenol levels in environmental waters can be $\leqslant$0.1 mg l^{-1}. For some phenols, however, use of the appropriate conditions could well give a detection limit approaching such levels.

REFERENCES

1 M. A. Franson (Ed.), Standard Methods for Water and Wastewater, 14th edn., American Public Health Association, New York, 1976.
2 J. Farino, G. Norwitz, W. J. Boyko and P. N. Keliher, Talanta, 28 (1981) 705.
3 A. W. Wolkoff and R. H. Larose, J. Chromatogr., 99 (1974) 731.
4 K. Ogan and E. Katz, Anal. Chem., 53 (1981) 160.
5 Z. Ivanov and R. J. Magee, Microchem. J., 25 (1980) 543.
6 L. Renberg and K. Lindstrom, J. Chromatogr., 214 (1981) 327.
7 N. G. Buckman, J. O. Hill and R. J. Magee, Microchem. J., in press.
8 P. S. Radhakrishnamurti, S. C. Pati and Y. Sriramulu, Indian J. Chem., 14A (1976) 955.
9 L. R. Sherman, V. L. Trust and H. Hoang, Talanta, 28 (1981) 408.
10 S. C. Pati and Y. Sriramulu, Indian J. Chem., 16A (1978) 74.
11 S. C. Pati and Y. Sriramulu, Z. Phys. Chem., 260 (1979) 834.
12 E. Adler, G. Anderson and E. Edman, Acta Chem. Scand., B29 (1975) 909.
13 H. H. Willard and A. L. Wooten, Anal. Chem., 22 (1950) 423.
14 K. B. Yatsimirskii, Kinetic Methods of Analysis, Pergamon Press, London, 1966.
15 R. T. Coutts, E. E. Hargesheimer and F. M. Pasutto, J. Chromatogr., 179 (1979) 291.
16 V. V. Wadekar and M. M. Sharma, J. Chem. Tech. Biotechnol., 31 (1981) 279.
17 S. A. Laddha and M. M. Sharma, J. Appl. Chem. Biotechnol., 28 (1978) 69.

Analytica Chimica Acta, 153 (1983) 291—295
Elsevier Science Publishers B.V., Amsterdam — Printed in The Netherlands

Short Communication

PRECIPITATE FLOTATION OF TRACE PHOSPHATE ION IN WATERS

MAMORU AOYAMA[a], TOSHIYUKI HOBO* and SHIGETAKA SUZUKI

Department of Industrial Chemistry, Faculty of Technology, Tokyo Metropolitan University, Fukasawa 2-chome, Setagaya-ku, Tokyo 158 (Japan)

(Received 18th March 1983)

Summary. A flotation—spectrophotometric method is described for the determination of soluble inorganic phosphate in freshwaters. Phosphate (5—150 $\mu g\ l^{-1}$) in 1-l samples is coprecipitated with aluminum hydroxide at pH 8.5. The precipitate is floated with the aid of sodium oleate and nitrogen, separated, and dissolved in 1M sulfuric acid. Phosphate is determined by a conventional molybdenum blue method. Recoveries are better than 95% and the relative standard deviation is about 1%.

Flotation is well established as an effective preconcentration technique for the determination of trace species in waters [1—5]. It has been shown to be applicable to anions such as chromate, sulfide, nitrite and nitrate ions in land waters before spectrophotometric measurements [6, 7]. This communication deals with precipitation and flotation of orthophosphate before its spectrophotometric determination.

Chaine and Zeitlin [3] reported that phosphate (ca. 0.2 mg l^{-1}) in sea water could be separated by the adsorption colloid flotation method. This, however, is inadequate for the measurement of phosphate at the lower $\mu g\ l^{-1}$ level usually encountered in land waters. The precipitate flotation proposed here is suitable for the concentration of such low levels of phosphate in waters. Aluminum hydroxide serves as the carrier. The method is faster and more convenient than filtration or centrifugation. The concentrated phosphate is finally measured by using a conventional molybdenum blue method. The proposed method is applied to the determination of phosphate in tap waters and well waters.

Experimental

Apparatus. The flotation and separation system is illustrated in Fig. 1. The flotation cell is a glass cylinder (70 mm i.d., 400 mm high) fitted with a sintered glass filter (No. 4) to generate small bubbles. For the spectrophotometric measurement, a Yanaco UO-101 derivative spectrophotometer with 1-cm cells was used.

[a]Present address: Research Center, Isuzu Motors Ltd., 3-25-1 Tono-machi, Kawasaki-ku, Kawasaki 210, Japan.

0003-2670/83/$03.00

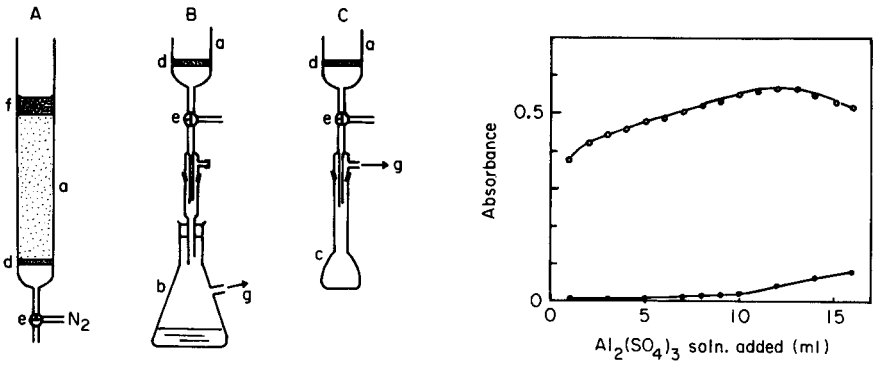

Fig. 1. Apparatus: A, flotation; B, collection and washing of precipitate; C, dissolution of precipitate. (a) Flotation cell; (b) suction bottle; (c) volumetric flask; (d) sintered-glass disk (G-4); (e) three-way cock; (f) foam layer bearing precipitates; (g) to aspirator.

Fig. 2. Effect of amount of 10% (w/v) aluminum sulfate solution on the recovery of phosphate (100 μg) from 1 l of water; (○) sample; (●) blank.

Chemicals. All chemicals were of analytical grade except sodium oleate. Water used was purified by distillation and ion exchange.

For the stock solution of phosphate (1 mg ml^{-1}), tripotassium phosphate was dissolved in water. The aluminum solution was 10% (w/v) $Al_2(SO_4)_3 \cdot 18\ H_2O$ in 0.5 M hydrochloric acid. Sodium oleate solution (1 mg ml^{-1}) was prepared in 99.5% ethanol. For the ammonium molybdate solution, 15 g of ammonium molybdate tetrahydrate was dissolved in 150 ml of water, which was mixed with 800 ml of 3.5 M sulfuric acid and diluted to 1 l with water. The tin(II) solution contained 1 g of tin(II) chloride dihydrate in 5 ml of hydrochloric acid, diluted to 50 ml with water.

Recommended procedure. Place 1 l of water sample containing 5—150 μg of phosphate in a 1-l beaker, and add 5 ml of the 10% (w/v) aluminum sulfate solution and 2 ml of the sodium oleate solution. Adjust the pH to 8.5 with aqueous ammonia solution to precipitate aluminum hydroxide, while stirring magnetically, and stir the solution further for 15 min. Transfer the contents of the beaker quantitatively to the flotation cell. Pass nitrogen at a flow rate of 50 ml min^{-1} into the flotation cell through the sintered-glass filter for 2 min to obtain complete mixing and flotation of the precipitate. Remove the solution under suction (Fig. 1B) and then add 20 ml of the ethanol to break the foam. Wash the precipitate by spraying with 50 ml of aqueous 0.1 M ammonia. Dissolve the precipitate by adding 10 ml of 1 M sulfuric acid to the cell, collecting the filtrate in a 25-ml volumetric flask (Fig. 1C). Wash the sintered disk with water. Neutralize the solution collected with 2 M sodium hydroxide and add 6 ml of the ammonium molybdate solution. While shaking, add 0.25 ml of the tin(II) chloride solution and dilute to the mark with water. Measure the absorbance at 710 nm against a blank as reference.

Results and discussion

The optimum conditions for pH, amounts of reagents, ageing of the precipitate, flow rate of nitrogen and separation time were studied. Unless indicated otherwise, 1 l of sample solution containing 100 μg of phosphate was used in the following tests.

Optimum pH for coprecipitation and flotation. Aluminum hydroxide was precipitated at different pH values in the range 4.5—10, by using aqueous ammonia solution; constant recoveries of 95% were obtained for phosphate over the pH range 6—9, which is the range for formation of amorphous aluminum hydroxide. Above pH 9.5, the recoveries of phosphate dropped very quickly. Recoveries were estimated by comparing the absorbance with that of a reference experiment in which phosphate was added to the recovered aluminum solution after flotation of a phosphate-free solution.

Amounts of aluminum and surfactant. The coprecipitation of phosphate depends on the amount of aluminum ion added to the solution. Figure 2 shows that the recoveries are poor with the addition of 1—4 ml of aluminum sulfate solution, but improve as the amount of aluminum is increased, reaching a maximum at 12 ml of aluminum solution. However, the absorbance of the blank at 710 nm also increases. Therefore, 5 ml of the 10% solution was chosen as most appropriate for routine work.

Complete flotation of the precipitate was achieved when 0.5—3.0 ml of sodium oleate solution was added; 2 ml was chosen for the 1-l samples.

Ageing time and separation time. A study of the effect of ageing time of precipitation on the phosphate recoveries showed that coprecipitation was quantitative for the range 3—30 min. In practice, the solution was stirred for 15 min after the addition of aqueous ammonia.

The flow rate of nitrogen was not critical within the range 25—100 ml min^{-1}; 50 ml min^{-1} was used for convenience. Flotation was then complete within 30 s, but 2 min was allowed for security.

Calibration graph and precision. Under the conditions of the recommended procedure, the calibration graph was linear for the phosphate concentration range 5—150 μg l^{-1}. The relative standard deviation obtained from seven replicate runs on a sample containing 100 μg l^{-1} phosphate was within 1%.

Interferences. The effects of other ions on the determination of phosphate are summarized in Table 1. As can be seen, most of the ions examined gave little or no interference on the determination of phosphate. The presence of arsenic(V) (50 μg l^{-1}) interfered, but this could be avoided by evaporating the sample with hydrobromic acid after the collection of phosphate. Therefore, this method can be applied to the determination of phosphate in fresh waters without interference from likely co-existing ions.

Application to freshwaters. The recommended method was applied to 1-l aliquots of tap and well waters, after filtration through 0.45-μm Millipore filters. Table 2 presents the results obtained by using the standard addition method.

TABLE 1

Effects of diverse ions on the determination of phosphate (50 μg) in 1 l of water

Species added	Amount (mg)	Phosphate found (μg)	Relative error (%)	Species added	Amount (mg)	Phosphate found (μg)	Relative error (%)
Na^+	1000	49.3	−1.4	NO_2^-	10	45.8	−8.4
K^+	1000	50.1	+0.2	Ni^{2+}	10	45.9	−8.2
Ca^{2+}	1000	50.6	+1.2	Co^{2+}	10	48.1	−3.8
Mg^{2+}	1000	48.3	−3.4	Cu^{2+}	1	46.8	−6.4
Cl^-	1000	49.0	−2.0	Cd^{2+}	1	49.1	−1.8
SO_4^{2-}	1000	48.9	−2.2	Mn^{2+}	1	48.0	−4.0
I^-	1000	47.9	−4.2	Fe^{2+}	1	50.0	0
NO_3^-	100	46.3	−7.4	Si(IV)	1	54.2	+8.4
ClO_4^-	100	45.8	−8.4	As(III)	0.05	47.9	−4.2
Br^-	50	45.7	−8.6	As(V)	0.05	100.8	+101.6
BO_3^{3-}	50	47.8	−4.4		0.05[a]	48.0	−4.0

[a]Treated with hydrobromic acid.

TABLE 2

Determination of soluble phosphate in natural water samples

Sample[a]	Amount of phosphate (μg)		Recovery (%)	Phosphate conc. (μg l^{-1})
	Added	Found		
Well water				
(A)	0	16		16
	20	35	95	
	30	44	93	
(B)	0	9		9
	20	29	100	
	30	38	97	
Tap water				
(A)	0	89		89
	20	110	105	
	30	121	107	
(B)	0	96		96
	20	117	105	
	30	128	107	
(C)	0	36 38[b]		36
	20	56	100	
	30	67	103	

[a]Sample volume 1000 ml. [b]Treated with hydrobromic acid.

The time required for the whole process is about 50 min for one sample. The method offers a rapid and precise means for the routine determination of phosphate in freshwaters. With suitable modification, the procedure may also be applicable to sea water.

This work was supported in part by a research grant from the Ministry of Education, Science and Culture, Japan.

REFERENCES

1 M. Hiraide, Y. Yoshida and A. Mizuike, Anal. Chim. Acta, 81 (1976) 185.
2 A. Mizuike and M. Hiraide, Pure Appl. Chem., 54 (1982) 1556.
3 F. E. Chaine and H. Zeitlin, Sep. Sci., 9 (1974) 1.
4 J. H. Tzeng and H. Zeitlin, Anal. Chim. Acta, 101 (1978) 71.
5 S. Nakashima, Analyst, 103 (1978) 1031; Bull. Chem. Soc. Jpn., 54 (1981) 291.
6 M. Aoyama, T. Hobo and S. Suzuki, Anal. Chim. Acta, 129 (1981) 237; 141 (1982) 427.
7 M. Aoyama, T. Hobo and S. Suzuki, Bunseki Kagaku, 31 (1982) E7, E99, E163.

Analytica Chimica Acta, 153 (1983) 297—300
Elsevier Science Publishers B.V., Amsterdam — Printed in The Netherlands

Short Communication

DETERMINATION OF SELENIUM IN NICKEL-BASED MATERIALS BY HYDRIDE-GENERATION ATOMIC ABSORPTION SPECTROMETRY

BERNHARD WELZ* and MARIANNE MELCHER

Department of Applied Research, Bodenseewerk Perkin-Elmer & Co. GmbH, D-7770 Überlingen (German Federal Republic)

(Received 28th March 1983)

Summary. Nickel seriously interferes with the determination of selenium by the hydride-generation technique, but is readily removed by precipitation with sodium hydroxide. After filtration and acidification of the solution, selenium can be determined down to 0.1 mg kg^{-1} in nickel-based samples.

Selenium is one of the elements that most seriously affects the mechanical properties of nickel-base alloys, even at very low concentrations. Various techniques are available for the determination of selenium at the 10 mg kg^{-1} (ppm) level, such as precipitation as the element with a carrier [1] which is collected on a membrane filter for x-ray fluorescence spectrometry. Graphite-furnace atomic absorption spectrometry has also been applied after a variety of sample preparation techniques [2]. Very few techniques are available for the determination of selenium below 1 mg kg^{-1} in nickel alloys. Graphite-furnace atomic absorption spectrometry does not provide sufficient sensitivity when the conventional solution technique is applied. Marks et al. [3] therefore utilized direct atomization of alloy chips in a graphite tube furnace to overcome this limitation, and reached a detection limit of 0.2 mg kg^{-1}. For 1-mg samples the relative standard deviation was ca. 20%.

Hydride-generation atomic absorption spectrometry should offer the best relative sensitivity for the determination of selenium. Because of the well known interferences, nothing has been reported on the analysis of nickel alloys, by this technique. In the analysis of steels, Fleming and Ide [4] found that nickel and other transition metals seriously interfered with the formation of hydrogen selenide in the absence of iron. In the presence of iron, however, they found no interference from nickel in low-alloy steels. The lowest concentration determined was 10 mg kg^{-1} (0.001%) in steel and the standard deviation was 1 mg kg^{-1} (detection limit 2 mg kg^{-1}). In earlier work [5] the present authors confirmed that up to 2% of nickel in low-alloy steels did not interfere with the determination of selenium in low-alloy steels, and as little as 1 mg kg^{-1} selenium in steel could be determined; the detection limit was 0.2 mg kg^{-1}. Higher nickel concentrations, however, caused severe

0003-2670/83/$03.00

signal suppression, even in the presence of iron, so that a direct determination of selenium in nickel alloys seemed to be impossible. This communication describes the simple precipitation of the nickel from the sample solution, thus allowing the determination of selenium in nickel down to 0.1 mg kg^{-1}.

Experimental

Apparatus. A Perkin-Elmer model 4000 atomic absorption spectrometer equipped with an electrodeless discharge lamp for selenium, operated at 6 W from an external power supply, was used for all determinations. A spectral bandpass of 2 nm was selected to isolate the 196.0-nm line, and the signals were recorded on a Perkin-Elmer model 56 recorder set at the 10 mV range. The Perkin-Elmer model MHS-20 hydride system used has been described in detail elsewhere [6]. The electrically-heated quartz tube atomizer was held at 900°C, and the time settings at the controller were 35 s for Purge I, 8 s for Reaction, and 35 s for Purge II.

Solutions. Sodium tetrahydroborate solution (3% w/v) was prepared by dissolving sodium tetrahydroborate powder (Riedel-de-Haen) in deionized water and stabilizing with 1% (w/v) sodium hydroxide solution. The solution was filtered before use and could be stored for only a few days. A standard selenium(IV) stock solution (1000 mg l^{-1}) was prepared by diluting a Titrisol solution (Merck) containing 1.000 g of selenium to 1 l with deionized water. Aliquots were diluted with 0.5 M hydrochloric acid to obtain appropriate working reference solutions. All chemicals used were of analytical-reagent grade. A nickel stock solution was prepared by dissolving 49.6 g of nickel nitrate hexahydrate in 180 ml of deionized water.

Procedures. To dissolve the nickel oxide NBS standard reference materials, 0.2—0.3 g amounts (accurately weighed) were heated to 80°C with 3 ml of 10.2 M hydrochloric acid and 2 ml of 14.2 M nitric acid in 25-ml volumetric flasks on a sand bath and left there overnight without further heating. The clear solutions were diluted to volume with deionized water.

To precipitate the nickel, 10 ml of the acidic sample solution (containing 60—70 mg Ni) was transferred to a 50-ml volumetric flask and diluted with 20 ml of deionized water. A 20-ml portion of 6% sodium hydroxide solution was added slowly with continuous shaking. After cooling, the volume was adjusted to 50 ml with deionized water, the solution was filtered through filter paper (No. 589[5] "Rotband", Schleicher and Schüll) and 40 ml of the filtrate was acidified by adding slowly 20 ml of 10.2 M hydrochloric acid. After cooling, 15 ml of this solution (corresponding to an original amount of 12—15 mg of nickel) was transferred to the reaction flask of the hydride system, and the selenium was determined as described previously [6]. Calibration solutions containing 25, 50, 100, 250, 500 and 1000 ng of selenium were carried through the same procedure to compensate for minor effects of the reagents on the selenium signal. The 15-ml portions finally analyzed contained 2, 4, 8, 20, 40 and 80 ng of selenium.

Results and discussion

In a preliminary study, the influence of nickel on the determination of selenium in different acid environments was investigated with and without the addition of iron (Fig. 1). In 0.5 M hydrochloric acid, which is typically used for hydride generation, nickel starts to interfere at concentrations above 0.25 mg l^{-1}. Above 5 mg l^{-1} there is complete signal suppression. Addition of 2 mg of iron(III) does not increase the interference-free range significantly but decreases the signal depression substantially so that about 10 mg Ni l^{-1} can be tolerated when standard additions are used. In a hydrochloric—nitric acid mixture with an addition of 2 mg of iron(III), however, the interference-free range for the determination of selenium is extended by two orders of magnitude; up to 20 mg Ni l^{-1} can be tolerated in the solution for measurement. Only a minor signal depression is found up to 100 mg l^{-1}. In addition, about 20% lower sensitivity is obtained for selenium in the more concentrated acid mixture compared to dilute hydrochloric acid. Under these conditions, selenium can be determined down to about 10 mg kg^{-1} in nickel without interference, which compares favourably with several other procedures. Lower concentrations of selenium in nickel and nickel-base alloys, however, cannot be determined in this simple way. The possibility of separating the selenium from the nickel matrix and of removing the nickel prior to the determination of selenium by hydride generation were therefore investigated. Precipitation of nickel as its hydroxide seemed to be the most promising procedure.

To test the effectiveness of this separation, 1, 5, 10, 50, 100 and 500 mg of nickel with added amounts of 10, 100 and 500 ng of selenium were taken through the precipitation procedure described in the experimental section. Under these conditions, the aliquots finally used for the determination of selenium corresponded to an original amount of up to 100 mg Ni, which is about three orders of magnitude greater than can be tolerated under optimum conditions (Fig. 1). The absorbance signals for these solutions were compared to those for reference solutions with the same amount of selenium but with no added nickel taken through the same procedure. The same sensitivity was obtained for all solutions, which shows that there is no inter-

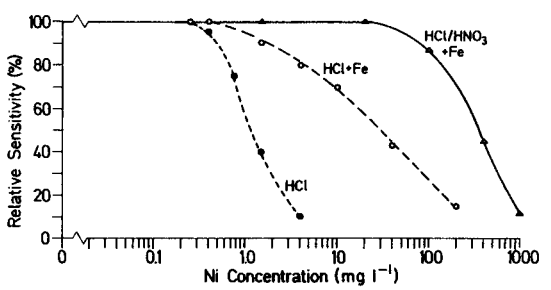

Fig. 1. Influence of nickel on the determination of selenium(IV) (100 ng) in 0.5 M HCl by hydride-generation atomic absorption spectrometry: (•) alone; (○) + 2 mg Fe(III); (△) + 2.0 M HNO_3 + 2 mg Fe(III).

TABLE 1

Determination of selenium in NBS standard reference materials Nickel Oxide

NBS No.	Selenium content (mg kg^{-1})	
	Found	Certificate
671	1.81, 1.68, 1.73	2.0 ± 0.3
672	0.37, 0.37, 0.41	0.40 ± 0.06
673	0.07, 0.09, 0.15	0.2 ± 0.1

ference from nickel on the determination of selenium even under extreme conditions. However, because of the very voluminous precipitate of nickel hydroxide, and a selenium blank corresponding to 0.03 mg kg^{-1} in the nickel nitrate used, these large amounts of nickel are not easy to handle. However, further work in that direction might be worthwhile if even lower concentrations of selenium have to be determined. For routine determinations, a practical limit of 100—150 mg of nickel is proposed for the precipitation procedure so that the aliquots used for the determination correspond to an original amount of 20—30 mg of nickel prior to precipitation. These solutions are easy to filter and there is no interference from nickel, so that selenium can be determined against reference solutions taken through the same procedure. The average recovery (and range) for 5 precipitations, each with different selenium concentrations, was 103% (94—112%) for 5 mg Ni, and 97% (93—104%) for 50 mg Ni in the original solution.

It should be possible to determine selenium routinely down to a concentration of 0.1 mg kg^{-1} in nickel and nickel-base alloys by applying the recommended procedure. Three nickel oxide standard reference materials of the National Bureau of Standards (Nos. 671, 672 and 673) with certified selenium contents between 2.0 and 0.2 mg kg^{-1} were analyzed. The results (Table 1) demonstrate the ability of the procedure accurately to determine very low selenium levels in nickel. The nickel concentration that can be tolerated is more than two orders of magnitude higher than that by the best direct method.

REFERENCES

1 G. L. Vassilaros, Talanta, 18 (1971) 1057.
2 T. R. Dulski and R. R. Bixler, Anal. Chim. Acta, 91 (1977) 199.
3 J. Y. Marks, G. G. Welcher and R. J. Spellman, Appl. Spectrosc., 31 (1977) 9.
4 H. D. Fleming and R. G. Ide, Anal. Chim. Acta, 83 (1976) 67.
5 B. Welz and M. Melcher, Spectrochim. Acta, Part B, 36 (1981) 439.
6 B. Welz and M. Melcher, Anal. Chim. Acta, 131 (1981) 17.

Analytica Chimica Acta, 153 (1983) 301—305
Elsevier Science Publishers B.V., Amsterdam — Printed in The Netherlands

Short Communication

IMPROVEMENTS IN THE DETERMINATION OF MERCURY BY COLD-VAPOR ATOMIC ABSORPTION SPECTROMETRY

O. DONARD*[a] and PH. PEDEMAY

Institut de Géologie du Bassin d'Aquitaine, 351 Cours de la Libération, 33405 Talence (France)

(Received 7th December 1982)

Summary. Several improvements to a conventional mercury analyzer system are described. The type of system, the shaking and reduction efficiency, the geometry of the absorption cell, the gas flow and the volume of the reduction vessel are modified. The detection limit is then 0.25 ng of mercury. The results emphasize the role of gas flow dynamics in the circuit.

Since the pioneering work by Hatch and Ott [1], mercury determinations by metal vapor generation have proved very successful. Improvements have been made, with collection of mercury on gold, silver or copper wool [2—5] or by the use of atomic fluorescence [6]. However, all these techniques depend on the flow dynamics of the metal vapor passing through the optical cell. In this laboratory, samples with very low mercury contents (natural background samples) or in small amounts (suspended matter, samples from ocean floors having a large amount of calcium carbonate) are often analyzed [7]. In order to improve the analytical performance of conventional systems, a careful series of improvements has been made. All parameters investigated deal mainly with the dynamics of gas flow through the system because only a small amount of mercury is effectively measured. With increase in efficiency, sensitivity is increased and the detection limit is lowered. The modifications presented here are simple, inexpensive and precise.

Experimental

Apparatus. A Perkin-Elmer model 420 S atomic absorption spectrometer fitted with a Perkin-Elmer electrodeless discharge lamp was employed. Absorbance values were recorded with a Servagor strip-chart recorder. Air filtered through a Perkin-Elmer gas filter cartridge was used as carrier gas. The air flow was controlled by a Dinal pressure gauge, a Brooks Shorate flow-meter and a stopcock. The air swept through the reduction vessel and immediately afterwards through the optical cell (see below) where the mercury absorbance was measured. Two reduction vessels (built from pyrex test tubes) were tested; they were 145 × 30 mm for 20 ml of solution and 205 ×

[a]Present address: Institut F.-A. Forel, 10 route de Suisse, Versoix (Switzerland).

0003-2670/83/$03.00

34 mm for 50 ml of solution. A two-way gas bubbler was attached to each reduction vessel; both bubbling tubes (medium porosity frit) ended 5 mm above the bottom of the reduction vessel. The reduction solution (2 ml) was manually introduced with a Cornwall syringe to the reduction vessel just before it was closed by inserting the bubbler (an automated injector will soon be adapted to avoid any mercury losses during injections). Mercury and the reduction solution were mixed in a 50-ml reduction vessel on a 50-Hz vortex mixer. All connections in the circuit were made of 5-mm diameter Versilic plastic tube.

Reagents. Mercury standards were prepared by dilution of a Merck Titrisol solution (1 g Hg l^{-1} as mercury(II) nitrate) with distilled water. Generation of mercury vapor was tested with two types of reductant solution. The first was 10% (w/v) tin(II) chloride (analytical grade, Merck) in 2 M hydrochloric acid. The second was 1% (w/v) sodium tetrahydroborate (analytical grade, Merck) in 2 M hydrochloric acid. All reagents were of mercury-free quality.

Instrumental parameters. The following parameters were used throughout the investigation: wavelength 235.7 nm, spectral bandwidth 0.7 nm, lamp power 5.5 W, cell at room temperature.

Results

Type of system. An important parameter is the type of gas circuit. Two different procedures are commonly used. In one, the mercury vapor is re-circulated through the reduction vessel and a steady-state signal is recorded. In the other, the vapor is separated from the solution and passes only once through the optical cell, giving a peak response. In the present investigation, the latter method was used because the system is easily modified and quickly purged. The absorbance measured depends on both the dead volume in the system and the shape of the absorption cell [8]; both can be optimized to increase the absorbance. Other factors such as air flow rate and shaking efficiency also modify the absorbance. The system provides a further advantage compared to the re-circulating system in that the vapour has little contact time with the system, thus minimizing mercury adsorption and variable memory effects [9]. As the vapor is swept rapidly into the cell there is no time for moisture to deposit in the absorption cell. Thus the use of magnesium perchlorate as a desiccant, which is a potential trap for mercury and may influence the precision of the measurements [10], is unnecessary.

Shaking and reduction efficiency. Obviously, greatest sensitivity is achieved by converting all mercury to the element. The reduction period can be shortened by shaking the vessel on a 50-Hz vortex mixer; this is safer than shaking by hand and gives better reproducibility. The absorbances measured for a 5 μg l^{-1} mercury solution in a 50-ml reduction vessel are identical after 10 s of vortex agitation, in agreement with the results obtained by Lawrence et al. [11]. Two sets of experiments were done on such solutions with tin(II) chloride and sodium tetrahydroborate as the reductant. In contrast to the results obtained by Rooney [12], no gain in sensitivity was achieved with

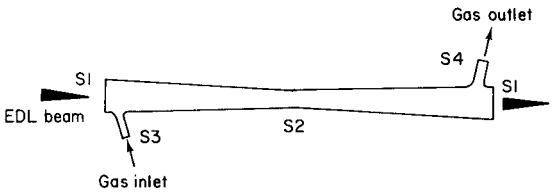

Fig. 1. Design of absorption cell. Dimensions for cells 1 and 2: S1, 15 and 18 mm diameter; S2, 7 mm diameter for both; S3, 3 mm diameter for both; S4, 5 mm diameter for both; length, 18 and 24 cm; volume, 19.5 and 35 cm^3, respectively.

the tetrahydroborate compared to tin(II). Therefore tin(II) chloride is preferred routinely because of its greater stability and lower cost. The kinetics of reduction of mercury can vary according to the sample matrix, but lengthening the agitation period to 30 s followed by 30 s standing gives no increase in absorbance.

Geometry of the absorption cell. Alteration of the shape of the absorption cell can produce a great increase in sensitivity. In the conventional cells, most of the mercury vapor does not absorb the mercury radiation because the cell diameter is generally much greater than that of the beam. Dogan and Haerdi [4] noted that elimination of the non-absorbing volume in the cell increased the sensitivity to about ten times that of a conventional cylindrical cell of the same length.

Two cells of different length but having the same shape as the beam of radiation were made from pyrex glass (Fig. 1). Their internal diameter was only slightly larger than that of the beam in order to keep the signal-to-noise ratio as small as possible. A quartz window was stuck on each end. The inlet and outlet were specially designed [13] to give a sharper peak absorbance and minimal tailing. The two cells were compared, using a 50-ml reduction vessel and 2 l min^{-1} air flow. Ten runs were made on a 5 $\mu g\ l^{-1}$ mercury solution. The results are given in Table 1. The 24-cm long cell raises the sensitivity of the method by a factor of 1.8 compared to the 18-cm long cell, in agreement with their volume ratio (35:19.5). Furthermore, the relative standard deviation is lower for cell 2 than for cell 1. Cell 2 is therefore preferred routinely.

Gas flow. Different pressures were tested on a 5 $\mu g\ l^{-1}$ mercury solution with a 50-ml reduction vessel. Pressure did not appear to affect the absorbance values, so 1 bar was used generally. Air flow rate had an influence on

TABLE 1

Cell comparison for a 5 μg Hg l^{-1} solution (10 measurements each)

	Cell 1	Cell 2
Mean absorbance	0.285	0.524
Standard deviation	0.025	0.024
Relative standard deviation (%)	8.8	4.6

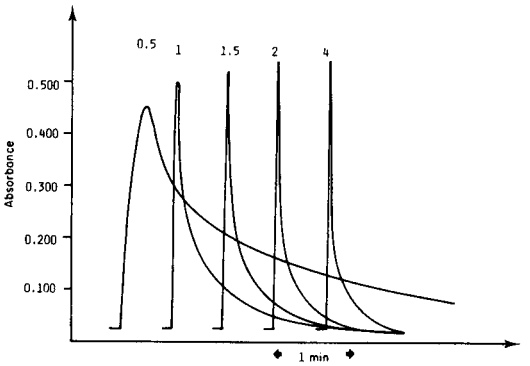

Fig. 2. Influence of air flow rate on the signal shape for a 5 μg Hg l^{-1} solution in 50-ml sample tubes. Chart speed 3 cm min^{-1}. The numbers on the peaks are the flow rates in l min^{-1}.

the absorbance from 5 μg l^{-1} solutions (Fig. 2). As expected, increasing flow rates increase the absorbance, shorten the time to maximum response, decrease tailing and improve reproducibility. The relative standard deviation (5 measurements) decreased from 2.6% at 0.5 l min^{-1} to 1.5% at 2 l min^{-1} and 1.0% at 4 l min^{-1}. An air flow rate of 2 l min^{-1} is recommended because higher flow rates deposit water in the absorption cell.

Volume of reduction vessel. According to Sighinolfi et al. [14], the absorbance will increase with decreasing volume of solution. The efficiency of two reduction vessels, containing 50 ml and 20 ml of sample solution, respectively, was studied by preparing calibration graphs in each instance. The results are summarized in Table 2. The improvement in sensitivity achieved with 50 ml of solution is only 28%, which is below the increase expected. This emphasizes the effect of increased dead volume of the reduction vessel. To obtain the highest peaks, attention should be paid to decreasing the dead volume of the circuit.

Discussion

As a result of these modifications, the recommended set-up is composed of the longer absorbance cell, with 50 ml of solution in the larger vessel, 1

TABLE 2

Comparison of calibration data for different sample volumes

Volume of solution (ml)	50	20
Air flow rate (l min^{-1})	2.0	1.0
Calibration graph slope (abs./μg l^{-1})	0.102	0.080
Correlation coefficient	1.00	1.00
Detection limit (ng Hg)[a]	0.70	0.25
R.s.d. (%)[b]	1.3	1.3

[a]Value determined from 10 successive measurements of reagent blanks and of a 0.1 μg Hg l^{-1} standard. [b]For 5 measurements of 5 μg Hg l^{-1}.

bar pressure and 2 l min^{-1} air flow. This provides a linear calibration range of 1—10 $\mu g\ l^{-1}$. The calibration graph can also be used when it is non-linear up to an absorbance of 1.5 [15], with a relative standard deviation better than 3%. The total calibration range is therefore 1—17 $\mu g\ l^{-1}$. Furthermore, the reduction vessel serves as a digestion and reduction vessel. This reduces manipulations and allows the samples to be determined immediately after wet digestion. The method has been successfully applied to the determination of mercury in sediments, suspended matters and organic tissues. The system raises the sensitivity 5 times in comparison to some commercial systems.

The authors are grateful to C. Latouche who provided all instrumental facilities and to F. Ribeyre, A. C. M. Bourg and A. Astruc for correcting the manuscript.

REFERENCES

1 W. R. Hatch and W. L. Ott, Anal. Chem., 40 (1968) 2085.
2 F. Aldrighetti, G. Carelli, A. Iannaccone, R. Labua and V. Rimatori, At. Spectrosc., 2 (1981) 13.
3 R. Dumarey, R. Heindryckx and R. Dams, Anal. Chim. Acta, 118 (1980) 381.
4 S. Dogan and W. Haerdi, Int. J. Environ. Anal. Chem., 6 (1979) 327.
5 S. Dogan and W. Haerdi, Int. J. Environ. Anal. Chem., 5 (1978) 157.
6 K. C. Thompson and R. G. Godden, Analyst, 100 (1975) 544.
7 F. Grousset and O. Donard, Deep-Sea Res., submitted.
8 G. Tuncel and Y. Ataman, At. Spectrosc., 1 (1980) 126.
9 D. C. Stuart, Anal. Chim. Acta, 101 (1978) 429.
10 A. Gardner, Anal. Chim. Acta, 119 (1980) 167.
11 K. Lawrence, M. White, J. Potts and D. Bertrand, Anal. Chem., 52 (1980) 1391.
12 R. C. Rooney, Analyst, 101 (1976) 678.
13 R. Dumarey, R. Heindryckx and R. Dams, At. Spectrosc., 2 (1981) 51.
14 G. P. Sighinolfi, C. Gordoni and A. M. Santos, Geostand. Newsl., 4 (1980) 223.
15 H. P. J. van Dalen and L. de Galan, Analyst, 106 (1981) 695.

Analytica Chimica Acta, 153 (1983) 307—311
Elsevier Science Publishers B.V., Amsterdam — Printed in The Netherlands

Short Communication

THE EFFICIENCY OF CHELATING RESINS FOR THE PRE-CONCENTRATION OF LEAD FROM TAP WATER

S. J. DE MORA and ROY M. HARRISON*

Department of Environmental Sciences, University of Lancaster, Lancaster LA1 4YQ (Gt. Britain)

(Received 5th May 1983)

Summary. The efficiency of lead recovery by two chelating resins from unmodified tap-water samples is described. Chelex-100 in the calcium form proved unsuitable for total lead determinations but polystyrene-supported poly(maleic anhydride) resin completely removed lead when used in a batch mode but not in a column mode. The eluate from this resin contained a significant proportion of lead inactive to anodic stripping voltammetry. The batch mode provides suitable pre-concentration for determination of lead in tap water by flame atomic absorption spectrometry.

The European Community directive [1] limiting the content of lead in drinking water to 50 $\mu g\ dm^{-3}$, which will become effective in July 1985, has stimulated research into the determination of total lead in tap water. Whilst methods such as atomic absorption spectrometry (a.a.s.) with electrothermal atomisation are of adequate sensitivity for the direct determination of lead in tap water, many laboratories use flame a.a.s., which requires a pre-concentration step. Recently, Rowley et al. [2] have proposed the use of a poly(maleic anhydride) chelating resin in a column method for pre-concentration of lead from unmodified tap water.

Chelating resins have been extensively used as an aid to speciation of trace metals in natural waters (see, e.g., [3, 4]). They are used in a column mode (short contact time) or batch mode (long contact time) to collect weakly complexed trace metals from water. The batch mode almost invariably allows collection of a greater fraction of a trace metal than the column mode, but the "Chelex-labile" fraction rarely approaches 100%, because of the presence of strong complexes in the water. This well-established behaviour of Chelex-100 as a collector of lead from natural waters casts some doubt upon the use of other resins, especially in a column mode, for quantitative preconcentration. Preliminary tests were made, therefore, of the efficiency of the poly(maleic anhydride) resin in the column and batch modes for removal of lead from tap water and its behaviour was compared to that of Chelex-100.

0003-2670/83/$03.00

Experimental

Apparatus. Lead was determined by a.a.s. using a Perkin-Elmer 280 spectrometer with an HGA-400 graphite furnace and an AS-40 autosampler. Background-corrected absorbances were measured at 217 nm or 283 nm and lead was quantified by standard addition. An E.G. & G. Princeton Applied Research 174A/315A polarographic system with a Model 303 static mercury drop electrode assembly was used for anodic stripping voltammetry (a.s.v.), with the following instrumental parameters: mode, differential pulse; pulse amplitude, 50 mV; stirrer speed, slow; drop size, medium; deposition for 120 s at −1.0 V (vs. Ag/AgCl); scan rate, 5 mV s^{-1}. The resins were packed in 25-cm^3 polypropylene burettes (0.8 cm i.d.) fitted with a polythene stopcock, and held in place by a polyamide screen (20-μm pore size). For filtration, polycarbonate filter units (Amicon Model 202) were used with polycarbonate filters (Nuclepore) under positive nitrogen pressure [5]. The filters and units were decontaminated with 0.05% nitric acid and pre-conditioned with 10^{-2} M calcium nitrate [3]. Standards and samples were stored in linear polyethylene bottles (Nalgene). All plastic ware was decontaminated by soaking in 10% nitric acid for 48 h followed by soaking in water for 48 h [6].

Reagents. Standard solutions were prepared by dilution of a B.D.H. standard solution containing 1 mg cm^{-3} lead as nitrate. Nitric acid was Aristar grade and water was deionized and then double-distilled in glass apparatus.

Chelex-100 (50-100 mesh; Bio-Rad Laboratories) was converted to the calcium form [7], oven-dried at 50°C for 2 h and weighed into 1-g portions. Each portion was suspended in water for 24 h and slurried into a polypropylene burette. Polystyrene-supported poly(maleic anhydride) [2, 8] was slurried into a burette and wetted with 15 cm^3 of 10% nitric acid. After a contact time of 2 min, the column was drained and washed with water until the pH of the effluent exceeded 5.0; generally 1.5—2.0 dm^3 of water was required. For use in the batch mode, the resin was transferred to a 60-cm^3 polyethylene bottle and kept suspended in a minimum volume of water.

Procedure. In the first experiments, a first-draw tap water (Bentham, N. Yorkshire) was filtered in parallel through three filters having nominal pore sizes of 12, 0.4, and 0.08 μm. (cf. the pore sizes used for speciation studies [3]). Four subsamples were then investigated, including an unfiltered aliquot (identified as NF). Total lead was determined in each fraction by a.a.s., and aliquots of 50 cm^3 were applied to both the Ca-Chelex-100 and poly(maleic anhydride) resins. Flow rates of ca. 16 cm^3 min^{-1} were maintained for both resins, giving a contact time (void volume/flow rate) of 2 s [9]. The chelated lead was eluted with 15 cm^3 of 10% nitric acid following a 2-min contact. The resin was washed with 8 cm^3 of water and the acid eluate and washings were diluted to 25 cm^3. These solutions (identified as "resin" column) were subjected to a.a.s. and a.s.v. A batch-mode extraction with each resin type was applied on the unfiltered water following column extraction. After equilibration for 48 h, the resin was slurried into a burette

and drained. The chelated lead was eluted as described above and determined. The inert metal concentration in the effluent was determined by a.a.s.

In the second set of experiments, a first-draw tap water (Wray, Lancashire) was divided into unfiltered and 0.4-μm filtered subsamples. Aliquots of 1 dm^3 were applied to the column as described by Rowley et al. [2]. The batch-mode extraction again utilized only 50 cm^3 but the water samples had not previously been column-extracted. In this experiment, total lead was measured by three techniques for each sample.

The extraction efficiency of the poly(maleic anhydride) resin for lead was investigated by using 48-h batch extractions with 50-cm^3 and 1-dm^3 aliquots of various tap-water samples. Finally, this resin was used to determine lead concentrations in waters of both high and low alkalinity.

Results and discussion

The Bentham drinking water used in the first experiments is a plumbosolvent water having a low alkalinity (18 mg dm^{-3} as $CaCO_3$) and low pH (6.58). The results in Table 1 indicate that most of the lead occurs in the smaller size fractions but a significant proportion is particulate (i.e., >0.4 μm). The Ca-Chelex-100 extraction was not 100% efficient for lead removal from any of the subsamples. This is in agreement with previous studies [4, 10]; incomplete recoveries may be due to the presence of colloidal species or to non-Chelex-labile organic complexes of lead, or both. Slow dissociation of complexes relative to the solution/resin contact time may also have an effect [9]. The polystyrene-supported poly(maleic anhydride) resin behaved in a significantly different manner. The column extraction (50 cm^3 of sample)

TABLE 1

Lead concentrations (μg dm^{-3}, a.a.s. measurements) in tap water as a function of size fraction and analytical procedure

Procedure		Size fraction (μm)			
		NF[a]	<12	<0.4	<0.08
Total		25.1	22.9	17.7	17.3
Chelex-100:	Column[b]	18.4	17.7	14.6	14.0
	Batch[b]	3.6	—[c]	—	—
	Inert	0.0	3.1	1.9	1.6
	Total	22.0	20.8	16.5	15.6
Maleic:	Column[b]	20.2	20.8	17.6	17.4
	Batch[b]	7.5	—[c]	—	—
	Inert	0.0	2.9	0.7	0.1
	Total	27.7	23.7	18.3	17.5

[a]Not filtered. [b]50 cm^3 of tap water. [c]Not tested.

gave 100% lead removal from the 0.4- and 0.08-μm filtered waters but particulate lead was not recovered from the unfiltered and 12-μm filtered samples. A batch extraction on the unfiltered sample after passage through the column chelated all the remaining lead from solution, thereby indicating its potential for total lead determinations.

The eluates from the column extractions for each resin were examined by both a.a.s. and a.s.v. In each case, the a.s.v. result was lower than the a.a.s. determination. The a.s.v. results were 90.7% ± 7.3% (one standard deviation) of the a.a.s. measurements for samples treated with Ca-Chelex-100 but only 60.6% ± 6.6% for samples treated with poly(maleic anhydride). Thus, it appears that the acid eluent must leach sequestering agents from the resin which form a.s.v.-inactive lead complexes.

Three techniques were applied to determine total lead in the Wray tap water (alkalinity 5 mg dm^{-3} as $CaCO_3$, pH 6.81). The 48-h batch extraction was 100% efficient for both unfiltered (5.0 μg Pb dm^{-3}) and 0.4-μm filtered waters (2.6 μg dm^{-3}), but column extraction of 1-dm^3 samples was only 60% and 69% effective for unfiltered and 12-μm filtered samples, respectively. Because the adsorption capacity of the resin is 0.42×10^{-3} mol Pb^{2+} g^{-1} [8], the poor recovery must result from the short contact time rather than exhaustion of the chelating capacity of the resin. To test this effect, various tap-water samples were processed by batch extractions of 50-cm^3 and 1-dm^3 aliquots. Results presented in Table 2 indicate that the lead was completely removed from the 1-dm^3 samples, giving a concentration factor of 40. Still greater concentration factors and shorter contact times may be possible.

Some tap-water samples of relatively high alkalinity were examined because such waters can attack lead. Total lead in unfiltered samples was determined by a.a.s. directly and following a 48-h batch extraction of 50 cm^3 of water. The results (Table 3) show that lead removal by the poly(maleic anhydride) resin was complete for both high and low alkalinity samples. Some apparent deterioration of the resin, as evidenced by changes in physical characteristics and poor precision of results from pre-concentration experiments, was observed after about eight repetitive uses.

TABLE 2

Comparison of batch extractions with poly(maleic anhydride) resin for 50-cm^3 and 1-dm^3 samples of three tap waters

Method	Lead (μg dm^{-3})		
	1	2	3
Total	10.0	52.5	181
50 cm^3 batch	9.9	58.9	177
1 dm^3 batch	11.0	52.0	177

TABLE 3

Total lead concentrations ($\mu g\ dm^{-3}$) in unfiltered tap waters; comparison of determinations by a.a.s. directly and after batch extraction (50 cm^3, 48 h) with poly(maleic anhydride) resin

Sample	pH	Alkalinity (mg dm^{-3} as $CaCO_3$)	Pb conc. ($\mu g\ dm^{-3}$)		Recovery (%)
			Direct	Resin	
L2	7.22	31.7	40.4	39.6	98
B6	6.75	18.4	10.0	9.9	99
NH1	7.98	119	98.8	103	104
NH2	7.44	141	28.5	28.2	99

Conclusions

While Ca-Chelex-100 is unsuitable for the preconcentration of lead from unmodified tap waters, polystyrene-supported poly(maleic anhydride) resin utilized in the batch mode but not the column mode can completely remove lead from the waters tested. Tap-water samples of high or low alkalinity can be treated, but further testing of the resin on a greater range of water types is necessary to establish general applicability. The eluates from poly(maleic anhydride) resins contain significant levels of electro-inactive lead complexes and cannot be analysed by a.s.v. without suitable sample treatment. The complexation characteristics of this novel resin indicate that it will be a valuable complement to existing physico-chemical speciation schemes.

The authors thank the S.E.R.C. for providing a research associateship to S. de M., and Dr. A. G. Rowley (Department of Chemistry, University of Edinburgh) for providing the poly(maleic anhydride) resin.

REFERENCES

1 Official Journal of the European Community, 23 (1980), No. L229/11 (80/778/EEC).
2 A. G. Rowley, I. A. Law and F. M. Husband, Anal. Chim. Acta, 143 (1982) 265.
3 D. P. H. Laxen and R. M. Harrison, Sci. Total Environ., 19 (1981) 59.
4 T. M. Florence, Anal. Chim. Acta, 141 (1982) 73.
5 S. J. de Mora and R. M. Harrison, Water Res., 17 (1983) 723.
6 D. P. H. Laxen and R. M. Harrison, Anal. Chem., 53 (1981) 345.
7 P. Figura and B. McDuffie, Anal. Chem., 49 (1977) 1950.
8 F. M. Husband and A. G. Rowley, Chem. Ind., London, (1982) 164.
9 P. Figura and B. McDuffie, Anal. Chem., 51 (1979) 120.
10 R. M. Harrison and D. P. H. Laxen, Nature, 286 (1980) 791.

Analytica Chimica Acta, 153 (1983) 313—318
Elsevier Science Publishers B.V., Amsterdam — Printed in The Netherlands

Short Communication

DIGESTION METHODS FOR DETERMINATION OF CADMIUM AND LEAD IN ORGANIC- AND SILICA-RICH SEDIMENTS

CHUNG-GIN HSU[a] and DAVID C. LOCKE*

Department of Chemistry, City University of New York, Queens College, Flushing, NY 11367 (U.S.A.)

(Received 25th January 1983)

Summary. River and deep-sea sediments are digested to clear solutions using either a simple three-step procedure in an open beaker or a closed-bomb procedure. In each, a mixture of nitric, perchloric, and hydrofluoric acids is used. All carbonaceous matter and silicates are decomposed. Cadmium and lead are quantified by flame atomic absorption spectrometry. Application of the methods to a National Bureau of Standards (NBS) sediment standard gave results in agreement with NBS values. Recoveries from spiked samples were in the range 95—103%. For various sediment samples from the Hudson River and from the North Atlantic Ocean, the relative standard deviations were less than 10%.

The cadmium and lead contents of aquatic sediments are of particular interest and importance in environmental chemistry and geochemical studies. Consequently, a wide range of methods has been applied to their determination in environmental samples. Atomic absorption spectrometry (a.a.s.) has been most extensively used. Electrothermal a.a.s. is advantageous for $\mu g\ l^{-1}$ levels of Cd and Pb in sediments [1, 2]; for higher levels, flame a.a.s. on digested samples is preferred because of better precision [3].

Because sediments often contain substantial amounts of silica and carbonaceous matter, sample pretreatment is required to liberate the metals present in bound or occluded form. Fusion techniques can introduce appreciable amounts of heavy metal impurities, as well as large quantities of salts which can interfere with a.a.s. quantitation through high background readings and spectral interferences. Although widely used for sequential stripping, extraction procedures with reagents such as EDTA, hydroxylamine/acetic acid, or dilute hydrochloric acid give low recoveries [4].

Several acid digestion procedures, in bombs and open vessels, have been described. Among the open-vessel digestion procedures for Cd and Pb in sediments, sulfuric/nitric acid mixtures are reported [1, 5] to yield low results for lead. Similarly, HCl/HNO_3 combinations gave low recoveries of cadmium [6]. Mixtures of nitric and perchloric acids are claimed [7—9] to yield high metal recoveries for sewage sludge and sediment samples, contrary to the

[a]Permanent address: Department of Chemistry, East China Normal University, 3663 Chung Shan Road (N), Shanghai, People's Republic of China.

0003-2670/83/$03.00

results reported by Agemian and Chau [4]. In all these procedures, it is necessary to filter off the residual silicic acid, which might lead to errors through loss of metals by adsorption.

Bomb digestion methods have been widely used for sediments [10, 11]; they eliminate volatilization and are generally faster. Bomb methods are, however, more restricted in temperature and may well be perceived as less safe. Agemian and Chau [10], in a thorough study of lake sediment bomb digestion, used a mixture of nitric, perchloric and hydrofluoric acids in a volume ratio of 4:1:6. They reported that clear solutions were produced and that recoveries of 20 elements were good. Lower concentrations of perchloric acid, however, reduced the oxidizing power to the point that carbonaceous residues remained. Indeed, for high silica and carbonaceous sediments, Sakata and Shimoda [11] found that bomb digestion with the acid mixture of Agemian and Chau left a black residue. Sakata and Shimoda [11], who used flameless a.a.s., suggested centrifugation of the bomb digest; with flame a.a.s., however, the presence of refractory residues could lead to clogging of the capillary tube in the nebulizer even after centrifugation, as well as to low results for metals associated chemically with the carbonaceous matter.

This communication describes a sequential open-beaker digestion procedure with nitric, perchloric and hydrofluoric acids, as well as a bomb digestion procedure with slightly different acid composition and conditions, for silica- and organic-rich sediments. Clear solutions are obtained using both procedures for all sediment samples examined; all carbonaceous matter and silicates are decomposed. The quantitation of Cd and Pb in these solutions shows both methods to be accurate and precise, and to offer satisfactory recoveries.

Experimental

Apparatus. A Perkin-Elmer Model 303 atomic absorption spectrometer was used with an air—acetylene burner and a Perkin-Elmer Model 56 strip-chart recorder. Electrodeless discharge lamps (Perkin-Elmer EDL) were used. Instrument settings were those recommended by the manufacturer. For bomb digestions, a Parr Model 4745 acid digestion bomb was used with a 25-ml teflon cup.

Reagents and materials. Deionized, glass-distilled water was used in the preparation of all solutions. The acids were Fisher ACS reagent grade. Standard metal stock solutions were prepared from certified a.a.s. solutions (Alfa Products). Standard working solutions were prepared for the beaker-digested samples by dilution with 1% (v/v) nitric acid; for the bomb-digested samples, the working standards were prepared to contain 8.0% (v/v) of concentrated nitric acid, 4.0% (v/v) of 60% perchloric acid, 8.0% (v/v) of 49% hydrofluoric acid, and 5.0% (w/v) boric acid, to match the samples. Blanks were prepared similarly. The National Bureau of Standards (NBS) River Sediment SRM-1645 was used to evaluate the accuracy and precision of the methods; it was dried in a desiccator over magnesium perchlorate before weighing.

Samples. Hudson River sediments were sampled near Kingston, New York and estuarine samples were collected near Yonkers, New York. Deep-sea

sediments were obtained from the Deep Sea Drilling Project cores of the North Atlantic Ocean. All samples were air-dried, ground in an agate mortar to 200 mesh, and dried at 110°C for 24 h.

Open-beaker digestion method. To 0.2 g or less of sediment, accurately weighed in a 100-ml teflon beaker with teflon cover, was added 5 ml of concentrated nitric acid, and the mixture was boiled gently for 30 min on a hot plate. The beaker was cooled and 2 ml of 60% perchloric acid and 5 ml of concentrated nitric acid were added. The mixture was heated on the hot plate until evaporated nearly to dryness. An additional 2 ml of 60% perchloric acid, 5 ml of concentrated nitric acid, and 5 ml of 49% hydrofluoric acid were added. The beaker was heated until the mixture was again evaporated nearly to dryness. The cover and the wall of the beaker were washed with 5 ml of water, and the solution was then heated to the evolution of dense white fumes. The beaker was cooled, and 10 ml of 5% nitric acid was added to dissolve the salts. The solution was transferred to a 50-ml volumetric flask and diluted with water washings from the digestion beaker. Samples were aspirated directly into the spectrometer in the usual fashion.

Bomb digestion, proposed method. To an accurately-weighed sediment sample (not more than 0.2 g) in the teflon cup were added 4.0 ml of concentrated nitric acid, 2.0 ml of 60% perchloric acid, and 4.0 ml of 49% hydrofluoric acid. The bomb was sealed and heated for approximately 3 h at 150°C in a drying oven. The bomb was cooled and the contents of the teflon cup were quantitatively transferred to a 125-ml polyethylene bottle containing 2.5 g of boric acid in about 15 ml of water. After shaking to dissolve salts, the solution was transferred to a 50-ml volumetric flask and diluted with water washings of the bottle. If necessary, solutions were stored in a refrigerator in 100-ml polyethylene bottles until ready for a.a.s. Samples were aspirated directly into the spectrometer in the usual fashion.

Bomb digestion, method of Agemian and Chau [10]. The above procedure was followed except that 4.0 ml of concentrated nitric acid, 1.0 ml of 60% perchloric acid, and 6.0 ml of 49% hydrofluoric acid were added to 0.1 g of sample in the teflon cup; after closure, the bomb was heated for 3.5 h at 140°C.

Results and discussion

Bomb digestion. As shown in Table 1, the Agemian and Chau digestion mixture [10] leaves a carbonaceous residue with some sediments. In the proposed method, the oxidizing power of the digestion mixture is increased by raising the proportion of perchloric acid, increasing the digestion temperature to 150°C (the manufacturer's suggested upper limit), and when necessary, lengthening the digestion time to as much as 5 h. The appearances of the digests obtained by the proposed procedure are also given in Table 1.

Boric acid is used to complex the hydrofluoric acid by formation of tetrafluoroborate which may occur in two steps [12]. The stoichiometric quantity of boric acid required for the amount of hydrofluoric acid used here is 1.5 g.

TABLE 1

Description of digested sediment solutions

Sample	Method	
	Agemian and Chau [10]	Proposed
NBS River Sediment (SRM-1645)	Yellowish-brown[a]	Green
River sediment brown-grey silt	Yellow[b]	Pale yellow
River sediment brown-grey silt	Yellow[b]	Pale yellow
Estuary sediment dark grey silt	Brownish-yellow[c]	Pale yellow
Deep-sea sediment dark grey clay	Brownish-yellow[a]	Pale yellow
Deep-sea sediment pink brown clay	Pale yellow	Nearly colorless
Deep-sea sediment grey clay	Pale yellow	Nearly colorless
Deep-sea sediment pale grey clay	Pale yellow	Nearly colorless

[a]Black residue left in bottom and on walls of cup. [b]A few black particles left in bottom of cup. [c]Black residue left in bottom of cup.

To confirm that the boric acid did not interfere with the a.a.s., 2.0, 2.4, 2.8, and 3.2 g of boric acid were added to 50-ml standard working solutions of cadmium and lead. The instrument responses to both elements in these solutions were identical to those in 1% nitric acid. However, more than 2.8 g of boric acid per 50 ml of solution does not readily dissolve. The addition of 2.5 g per 50 ml provides a 60% excess over the stoichiometric requirement but will not leave an undissolved residue.

Accuracy and precision. The accuracy of each method was tested by determination of Cd and Pb in the NBS river sediment standard. Results for eight replicate samples are given in Table 2, and are in excellent agreement with the NBS-certified values. The recoveries and precisions are entirely satisfactory. These results also indicate that none of the elements commonly accompanying Cd and Pb in sediments interfere with their determination.

To study recovery in the beaker digestion method, increments of the two analytes were added to two of the deep-sea sediment samples in the teflon beakers prior to the digestion procedure. For cadmium, 2, 4, and 6 μg of cadmium were added to 0.2 g of sample; for lead, 20, 40, and 60 μg of lead were added. The recoveries of Cd and Pb averaged 100.0% and 99.0%, respectively, with ranges of 96—102% for Cd and 95—103% for Pb.

The standard addition method gave results in good agreement with those determined by calibration plot. For samples weighing more than 1 g, however, the latter method gave slightly lower results, presumably because of some matrix effect.

TABLE 2

Quantitation of Cd and Pb in NBS River Sediment (SRM-1645)[a]

	Bomb digestion		Beaker digestion	
	Cd	Pb	Cd	Pb
Found[b] (μg/g)	10.5	718	10.1	721
RSD[c] (%)	3.7	3.9	6.1	3.6
Recovery (%)	103	101	99	101

[a]NBS values, $\mu g\ g^{-1}$: Cd, 10.2 ± 1.5; Pb, 714 ± 28. [b]Mean for 8 samples. [c]Relative standard deviation.

Seven different beaker-digested and bomb-digested samples of river and deep-sea sediments were measured by a.a.s. Cadmium values were in the range 3—10 $\mu g\ g^{-1}$ and Pb values in the range 50—327 $\mu g\ g^{-1}$. The relative differences of the results obtained by the two digestion methods are less than ±10% for both metals. The pooled standard deviations for the bomb digestion method are 0.316 and 9.48 $\mu g\ g^{-1}$ for Cd and Pb, respectively; for the beaker digestion these values are 0.447 and 14.1 $\mu g\ g^{-1}$, respectively. The relative standard deviations for the bomb method range from 3.2% to 8.1% for cadmium and 1.5% to 5.6% for lead; for the beaker digestion method, the ranges are 4.0—9.3% for cadmium and 2.6—6.3% for lead. There was no significant difference at the 95% confidence level in the precisions of the two digestion procedures.

The methods described provide accurate and precise determinations of cadmium and lead in sediments rich in silica and organic matter. The bomb digestion is more effective in oxidizing the organic matter in sediments than those procedures used previously, presumably because of the higher concentration of perchloric acid and slightly higher temperature. The beaker digestion procedure, although taking somewhat longer and involving more manipulations, should be more effective for samples containing refractory organic matter because of the sequential addition of the acids, and the higher digestion temperature with perchloric acid. The initial nitric acid digestion attacks the easily oxidized organics; the perchloric acid in the second step decomposes refractory organic matter. In the third step, the silica is dissolved by the hydrofluoric acid, and the fresh $HNO_3/HClO_4$ added with it attacks any liberated carbonaceous matter. The temperature rises in the last two steps to 200°C, the boiling point of the 78% $HClO_4/H_2O$ azeotrope [13]. Bomb methods at temperatures less than 200°C do not allow the perchloric acid to reach its maximum oxidizing strength [13], and thus are less effective in oxidizing organic matter in some sediments.

The procedures described here are safe, easily performed, and should be directly applicable to a variety of elements in sediments, sludges, and soils.

REFERENCES

1 M. J. T. Corrondo, R. Perry and J. N. Lester, Anal. Chim. Acta, 106 (1979) 309.
2 H. Gong and N. H. Suhr, Anal. Chim. Acta, 81 (1976) 297.
3 D. G. Mitchell, W. N. Mills, A. F. Ward and K. M. Aldous, Anal. Chim. Acta, 90 (1977) 275.
4 H. Agemian and A. S. Y. Chau, Analyst, 101 (1076) 761.
5 M. J. T. Corrondo, J. N. Lester and R. Perry, Talanta, 26 (1979) 929.
6 S. A. Sinex, A. Y. Cantillo and G. R. Helz, Anal. Chem., 52 (1980) 2342.
7 P. Geladi and F. Adams, Anal. Chim. Acta, 96 (1978) 229.
8 G. F. Smith, Anal. Chim. Acta, 17 (1957) 175.
9 G. K. Hoops, Geochim. Cosmochim. Acta, 28 (1964) 405.
10 H. Agemian and A. S. Y. Chau, Anal. Chim. Acta, 80 (1975) 61.
11 M. Sakata and O. Shimoda, Water Res., 16 (1982) 231.
12 B. Bernas, Anal. Chem., 40 (1968) 1682.
13 G. F. Smith, Anal. Chim. Acta, 8 (1953) 397.

Analytica Chimica Acta, 153 (1983) 319—323
Elsevier Science Publishers B.V., Amsterdam — Printed in The Netherlands

Short Communication

THE RECOVERY OF GOLD FROM ALKALINE CYANIDE MEDIA WITH A POLYURETHANE FOAM SORBENT

T. BRAUN* and A. B. FARAG[a]

Institute of Inorganic and Analytical Chemistry, L. Eötvös University, P.O. Box 123, 1443 Budapest (Hungary)

(Received 26th April 1983)

Summary. Unloaded polyether-type resilient polyurethane foams are used for the sorption and recovery of gold from ammoniacal cyanide media. The sorption capacity for gold is about 5 mg g^{-1}. Sorption with about 95% recovery is possible on successive 5-g and 2-g foam columns at flow rates of 10—20 ml min^{-1}. A pumping foam column in a syringe is also satisfactory.

The application of polyurethane foams for extraction and preconcentration of various metal ions from aqueous solution has received considerable attention in recent years [1—4]. The inselective sorption by unloaded polyurethane foams can be rendered more selective by appropriate control of the composition of the aqueous phase. In acidic aqueous chloride media, it is possible to separate and/or preconcentrate gold [5—7], gallium [8, 9], iron [9, 10], iridium [11], platinum [12], tin [13], rhodium [5], thallium [5], antimony [5] and molybdenum [5], using unloaded resilient polyurethane foams of open-cell polyether type. In acidic aqueous thiocyanate media, the sorption and separation of iron [5, 13, 14], cobalt [13—16], mercury [17], zinc [17], indium [17], rhodium [18], iridium [18] and/or palladium [19] are successful. The separation of gold from acidic aqueous thiourea [20] and neutral cyanide [21] solutions is feasible.

The application of polyurethane foams for the sorption and recovery of metal complexes in alkaline aqueous media has not been reported previously. In the present communication, the possibility of using this very cheap and readily available sorbent for the recovery of gold from ammoniacal cyanide solutions is examined. Obviously, the use of the untreated foam could be valuable in the recovery of gold from cyanide-containing industrial liquors.

Experimental

Reagents and materials. Except where otherwise specified, all chemicals used were of analytical grade. Gold chloride solution was prepared by

[a]Permanent address: Chemistry Department, Faculty of Science, Mansoura University, Mansoura, Egypt.

0003-2670/83/$03.00

dissolving the chloride salt in distilled water. Before use, the gold solution was spiked with ^{198}Au (Institute of Isotopes, Budapest).

The polyurethane foams used were of the open-cell polyether type (North Hungarian Chemical Works, Sajóbábony, Hungary; Greiner K.G.-Schaumstoffwerk, Kremsmünster, Austria). The foam materials (cubes of about 5 mm edge) were washed and dried as described previously [22].

Hydroquinone (Reanal; photographic grade) was used as supplied in the precipitation of gold, but for quantitative measurement of the recovered gold, it was necessary to recrystallize it from hot distilled water in the presence of sulphur dioxide to prevent oxidation by air.

Apparatus. Glass columns (25 mm diameter, 12 cm long) were used in the dynamic retention experiments. All-glass syringes of 200-ml capacity were used in the column pumping method. The glass columns were packed with 5 or 2 g of unloaded polyurethane foam by the vacuum method [22].

Radioactivity was measured with a NaI(Tl) well-crystal and an energy-selective counting device (type NK-107/B, Gamma, Budapest).

Measurement of isotherms. The absorption isotherms [5] of gold from ammonia solution (10% v/v) containing potassium cyanide (1% w/v) and various concentrations of gold, were measured in batchwise experiments.

Column extraction. Aliquots (100 ml) of gold in ammonia solution (10% v/v) containing potassium cyanide (1% w/v) spiked with ^{198}Au, were allowed to percolate through the foam column at a flow rate of 10—20 ml min^{-1}. From the activity measurements, the percentage extraction was calculated.

Syringe extraction [23, 24]. Sorption of gold was achieved by pressing and releasing the glass plunger of the syringe (containing 5-g or 2-g foam cylinders), with the tip of the syringe in the ammoniacal cyanide solution. The syringe was pumped about 10 times during 5 min with each solution tested.

Recovery of gold from the foam material. In these experiments, ^{198}Au was not used. After the sorption of gold on polyurethane foam, the foam material was squeezed to remove the interstitial volume of the cyanide solution. Then, the almost dry foam was either dissolved in hot aqua regia followed by evaporation three times with concentrated hydrochloric acid, or burned on a small flame followed by ignition in a muffle furnace at 700°C for about 1 h. In the latter case, the residue obtained was dissolved in a small amount of aqua regia and evaporated three times with concentrated hydrochloric acid. The gold chloride residue thus obtained was dissolved in dilute hydrochloric acid and gold was precipitated as the metal by reduction with hydroquinone [25].

Determination of gold. The recovered gold was determined either gravimetrically [25] after filtration and ignition in a weighed porcelain crucible or titrimetrically [26] after redissolution in aqua regia. The gravimetric and titrimetric methods gave the same results within the normal limits of error.

Results and discussion

Polyurethane foams have been used for the sorption of various gold complexes from different acidic media [5—7], but little has been reported on the sorption of gold—cyanide complexes. Bowen [21] used polyurethane foam to recover gold from liquid mineral wastes containing sodium cyanide in batchwise experiments. The percentage recovery of gold from the barren solution tested was found [21] to be 38%.

Gold could be recovered from alkaline cyanide media by direct evaporation of the aqueous solution followed by digestion of the residue with aqua regia. Gold chloride thus formed could be separated from the aqueous acidic solution by polyurethane foams [5—7]. Obviously, the acid treatment of the residue after evaporation is not practical, as it will produce large amounts of hydrogen cyanide. For this reason, it is advisable to extract the gold complex directly from the cyanide medium.

In preliminary experiments, polyurethane foams of the polyether and polyester type were tried for this purpose. However, the polyester type of foam was completely dissolved in the strong ammoniacal media. Two batches of polyether-type polyurethane foams (Hungarian and Austrian) were then examined. The sorption isotherms of gold from alkaline cyanide solution were measured in batchwise experiments (Fig. 1). The sorption capacities of the foams tested, as predicted from their sorption isotherms, were relatively high. As is clear from the curves in Fig. 1, the Austrian foam shows the more favourable sorption capacity. Consequently, this foam was used in further experiments.

Application of the unloaded foam material in column operation was then examined. When short foam columns (packed with 5 g of foam) were used and 100-ml aliquots of ammonia solution (10% v/v) containing 0.1 g of gold and 1 g of potassium cyanide were allowed to pass through at a flow rate of 10—20 ml min^{-1}, 90—95% of the gold was retained on the foam (measured

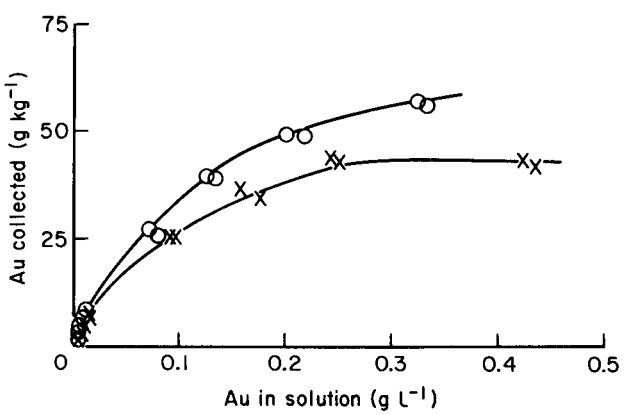

Fig. 1. Sorption isotherms for collection of gold on polyurethane foam from ammoniacal cyanide solutions: (○) Austrian foam; (X) Hungarian foam.

radiometrically). In order to improve the recovery of gold, another foam column (packed with 2 g of foam) was used. The effluent from the first column was passed directly through the second column. The total recovery of gold was then 100 ± 10%.

Owing to the simplicity and rapidity of the column pumping technique [23, 24], this method was tested with a glass syringe (200-ml capacity) packed with 5 g of unloaded polyurethane foam, as described under Experimental. About 85—90% gold was found to be absorbed on the foam after the sample solution had been pulled into and pressed out of the foam 10 times. It was found better to use the column pumping method in two steps: in the first, 5 g of foam is used and in the second, another 2 g of foam is taken. More than 95% of the gold was then retained on the foam. This method can be considered as an alternative to the normal column method, especially because it can easily be automated.

After the successful extraction of gold with polyurethane foam, the next step is to recover the gold from the foam. Water and various concentrations of mineral acids were tried, but no more than 50% of gold was leached with up to 300 ml of eluent. The gold was therefore recovered in two ways: by dissolving the foam itself in aqua regia (after squeezing it to remove the interstitial volume of cyanide solution), or by burning the foam and dissolving the residue in aqua regia. The residue obtained was then dissolved in dilute hydrochloric acid and gold was separated as the metal by reduction with hydroquinone [22]. Although both procedures gave satisfactory results, the second was preferable because a relatively large volume of aqua regia was necessary to dissolve the foam and its evaporation was time-consuming.

The recovery of gold by the polyurethane foam was tested for an industrial ammoniacal gold—cyanide waste solution and proved to be effective; more than 95% of gold was recovered with both the normal column and column pumping methods.

The use of polyurethane foams for the sorption of inorganic species from aqueous alkaline solution should extend the analytical applications of the technique and may cast light on the sorption mechanism with these foams.

REFERENCES

1 T. Braun and A. B. Farag, Talanta, 22 (1975) 699.
2 T. Braun and A. B. Farag, Anal. Chim. Acta, 99 (1978) 1.
3 G. J. Moody and J. D. R. Thomas, Analyst, 104 (1979) 1.
4 T. Braun, Fresenius Z. Anal. Chem., (1983) in press.
5 H. J. M. Bowen, J. Chem. Soc., Sect. A, (1975) 1082.
6 P. Schiller and G. B. Cook, Anal. Chim. Acta, 54 (1971) 364.
7 S. Sukiman, Radiochem. Radioanal. Lett., 18 (1974) 129.
8 H. D. Gesser and G. A. Horsfall, J. Chim. Phys., 74 (1977) 1072.
9 H. D. Gesser, E. Bock, W. G. Baldwin, A. Chow, D. W. McBride and W. Lipinski, Sep. Sci., 11 (1976) 317.
10 J. J. Oren, K. M. Gough and H. D. Gesser, Can. J. Chem., 57 (1979) 2032.
11 R. A. Moore and A. Chow, Talanta, 27 (1980) 315.

12 V. S. K. Li and A. Chow, Talanta, 28 (1981) 157.
13 T. Braun, A. B. Farag and M. P. Maloney, Anal. Chim. Acta, 93 (1977) 191.
14 T. Braun and A. B. Farag, Anal. Chim. Acta, 98 (1978) 133.
15 A. Chow, G. T. Yamashita and R. F. Hamon, Talanta, 28 (1981) 437.
16 R. F. Hamon, A. S. Khan and A. Chow, Talanta, 29 (1982) 313.
17 T. Braun and M. N. Abbas, Anal. Chim. Acta, 134 (1981) 321.
18 S. J. Al-Bazi and A. Chow, Anal. Chem., 53 (1981) 1073.
19 S. J. Al-Bazi and A. Chow, Talanta, 29 (1982) 507.
20 T. Braun and A. B. Farag, Anal. Chim. Acta, 66 (1973) 419.
21 H. J. M. Bowen, Radiochem. Radioanal. Lett., 7 (1971) 71.
22 T. Braun and A. B. Farag, Anal. Chim. Acta, 62 (1972) 476.
23 T. Braun and A. B. Farag, Anal. Chim. Acta, 65 (1973) 139.
24 T. Braun and S. Palágyi, Anal. Chem., 51 (1979) 1697.
25 A. I. Vogel, Quantitative Inorganic Analysis, 3rd edn., Longmans, London, 1961.
26 S. C. S. Rajan and N. A. Raju, Talanta, 22 (1975) 185.

Analytica Chimica Acta, 153 (1983) 325—330
Elsevier Science Publishers B.V., Amsterdam — Printed in The Netherlands

Short Communication

POTENTIAL SCANNING VOLTAMMETRIC DETECTION FOR FLOW INJECTION SYSTEMS

JOSEPH WANG* and HOWARD D. DEWALD
Department of Chemistry, New Mexico State University, Las Cruces, NM 88003 (U.S.A.)
(Received 23rd March 1983)

Summary. A flow cell with a stationary carbon disk electrode coupled with rapid differential pulse voltammetry is used. The voltammograms are recorded at a scan rate of 2 V min^{-1} during passage of the 200-μl sample plug through the detector. This detection mode allows several electroactive species to be quantified simultaneously at an injection rate of 20 samples per hour. Acetaminophen, dopamine, caffeic acid, chlorpromazine, and copper, lead, and cadmium ions are used as test species.

Flow-injection systems involve injection of a reproducible sample volume into a continuously flowing unsegmented carrier stream [1—3]. The key to successful quantitation based on flow injection is that the dispersion of the injected sample can be controlled. The use of electrochemical detection in flow injection systems is growing rapidly [4]. Most electrochemical detectors are based on amperometric operation, which has the advantage of being free of double-layer charging and surface transient background effects. Although extremely low detection limits have been achieved with some amperometric systems, such procedures do not furnish information on the analyte identity and lack any multicomponent capability.

This communication describes the use of rapid differential pulse voltammetry as a detection scheme. Various scanning potential voltammetric techniques have been introduced recently in conjunction with continuous flow systems [5, 6]; these approaches are too "slow" for incorporation with flow-injection systems. Rapid square-wave voltammetry has been applied successfully to various flow systems [7, 8], but not to flow-injection systems. The applicability of voltammetric procedures to flow-injection systems has been illustrated recently [9, 10]. In these studies anodic stripping and linear-scan voltammetric detection modes were used to monitor heavy metals and to study concentration gradients, respectively; various mercury electrodes were also used. The present study is aimed at detecting mixtures of oxidizable and reducible species utilizing carbon paste and mercury electrodes, respectively. For this purpose, differential pulse voltammetry is used to provide the current—potential information while maintaining high sensitivity. Because of the short time window available for the voltammetric measurement, fast scan rates (compared to those traditionally

0003-2670/83/$03.00

used in pulse voltammetry) are used. The characteristics and advantages of this measurement approach are described below.

Experimental

Apparatus. Carrier and sample reservoirs were 400-ml Nalgene beakers, fitted with Nalgene covers. The sample injection valve was a Rheodyne Model 7010 with a 200-μl sample loop. All connections were made with 0.5-mm i.d. teflon tubing. The length of tubing between the valve and the detector was 10 cm. Flow of the electrolyte carrier solution was maintained by gravity.

The detector design is shown in Fig. 1. The body is a 4.5 X 3 X 2-cm plexiglas block with a flow channel drilled through it. The 1.8-mm solution inlet widens to 8.3 mm to accept the working electrode, a homemade 3-mm carbon paste or glassy carbon disk. The Ag/AgCl reference electrode (Model RE-1; Bioanalytical Systems) joins the working compartment close to the face of the working electrode. The solution leaves the cell through a 2-mm channel drilled perpendicular to the working compartment, passing the carbon rod auxiliary electrode. The carbon paste was prepared by thoroughly mixing 2.5 g of graphite powder and 1.5 g of mineral oil. The paste was packed to a depth of 1.5 cm into the end of a glass tube (3-mm i.d., 6-mm o.d., 7.5-cm long). The carbon paste electrode was renewed once a week, the new surface being smoothed with a computer card. The glassy carbon electrode was polished with 0.1-μm alumina slurry before plating the mercury film. Electrical contact to the inner side of the carbon disks was made with copper wire. This cell design, with the cone-shaped working electrode compartment, was chosen to increase the dispersion, as required for potential scanning experiments. All measurements were made with a Sargent-Welch Model 4001 polarograph.

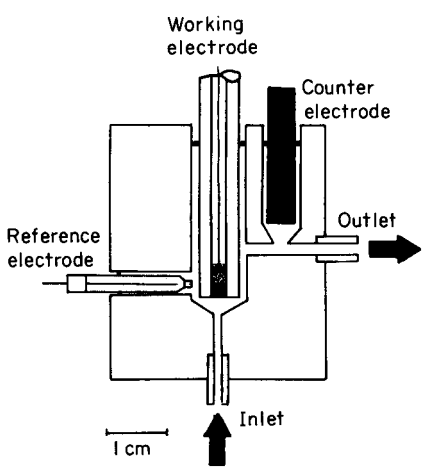

Fig. 1. Schematic diagram of the cell.

Reagents. Chemicals and reagents used have been described in detail previously [9, 11] except as noted. Millimolar stock solutions of acetaminophen, chlorpromazine, and caffeic acid (Sigma Chemical Co.) were prepared fresh each day. Aliquots of the stock solution were added to the supporting electrolyte (in the sample reservoir) to give the desired concentration.

Procedure. Blank and sample solutions were examined as follows. The valve was turned from the load position, in which the 200-μl loop had been filled by gravity flow of the sample, to the inject position. The rapid differential pulse scan was initiated 25—40 s after the injection, the time being selected to insure arrival of the sample plug at the detector and establishment of a certain concentration profile. After the scan period, the valve was turned back to the load position, the loop was refilled (usually for 2 min at 0.2 ml min^{-1}), and the procedure was repeated. A mercury film was plated onto the glassy carbon disk prior to the determination of reducible species. For this purpose a 5.0×10^{-5} M mercury(II) nitrate solution was passed through the detector at 0.20 ml min^{-1} for 20 min, with a potential of —0.8 V imposed on the working electrode. In this cathodic mode, sample and carrier solutions were purged with nitrogen before entering the system.

For amperometric detection, a preset potential was continuously applied. The loop-filling and sample-injection procedure was as above, except that the valve was turned back to the load position only after full signal decay.

Results and discussion

Manifold. To allow for scanning a voltage range of 1 V while the sample plug passes through the detector, fast scan rates are needed with relatively low flow rates and large sample volumes. Amperometric measurements were used first to examine the concentration profile in the detector. Figure 2A illustrates a characteristic current—time response for 200 μl of 2.0×10^{-4} M acetaminophen at 0.2 ml min^{-1}. The peak width indicates that the dispersed sample plug takes 90 s to pass through the detector. Based on the nature of the dispersion process and the principles of gradient techniques in flow injection [12], the individual concentration at each point of the sample zone corresponds to a specific dispersion value. Consequently, quantitative information can be obtained from a wider section of the sample peak than just the peak maxima. Therefore, voltammetric measurements at scan rates of 1—2 V min^{-1} are feasible for peak basewidths of about 60 s. With careful and reproducible timing, the entire voltammogram can be recorded while the sample zone of highest concentration is passing. The zone at which the analyte concentration ranges between 60 and 100% of the highest value (C_{max}) passes through the working electrode compartment during a 30-s period. At 1.0 ml min^{-1} the same sample zone passes through the working compartment during 15 s, while the entire sample plug passes during 60 s (not shown). Table 1 examines the effect of the time delay between the moment of injection and the initiation of the potential scan on the differ-

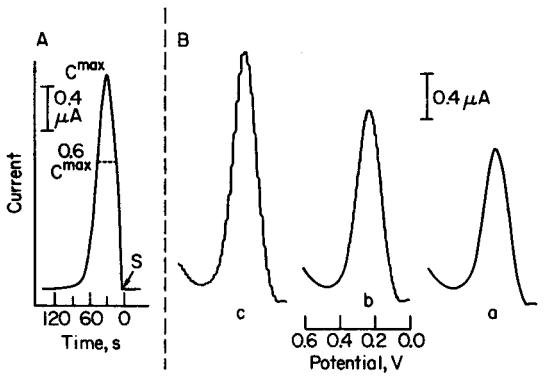

Fig. 2. Peaks for 2.0 × 10^{-4} M acetaminophen in 0.05 M phosphate buffer (pH 7.4). (A) Amperometric response at +0.6 V. (B) Differential pulse response recorded at different scan rates: (a) 0.5; (b) 1.0; (c) 2.0 V min^{-1}. Flow rate 0.2 ml min^{-1}, pulse amplitude 50 mV, repetition time 0.5 s.

ential pulse voltammetric response. The maximum peak current is obtained for a 40-s delay; the 30- and 50-s delays yield peak currents that are 85 and 93%, respectively, of the maximum peak. Overall, the differential pulse data are in good agreement with the amperometric response (Fig. 2A). A similar time delay/peak current profile was obtained in a separate experiment utilizing 2.0 × 10^{-4} M caffeic acid. For species with different redox potentials, slightly different data would be obtained because of the different timing between the start of the scan and the actual electrode reaction. The flow rate and sample volume used in this experiment allow an injection rate of twenty samples per hour. Any change in flow rate, tube diameter, length, sample size, etc. requires a reexamination of the delay time from injection to start of the scan. The degree of dispersion was estimated from dopamine measurements performed under steady-state and transient conditions. A dilution ratio of two was obtained from the ratio of the differential pulse peaks for conditions as in Fig. 2B(b) except that 5.0 × 10^{-5} M dopamine solutions were used.

Selection of scan rate. It has been shown that relatively fast differential pulse scan rates can be incorporated in solid electrode operation [13]. Figure 2B compares differential pulse voltammograms recorded at different scan rates for an acetaminophen solution flowing continuously through the cell. These data indicate that both high sensitivity and selectivity are maintained when fast scan rates are used. The change in scan rate from 0.5 to 2 V min^{-1} results in a peak-height increase of 61% while the width at half-height decreases by 7%. In a similar steady-state experiment with a 5.0 × 10^{-5} M dopamine solution, a change of scan rate from 1 to 2 V min^{-1} resulted in a 10% increase of peak height and a 11% increase in the width at half-height. Because of the speed and sensitivity of measurements at 2 V min^{-1}, this rate was used in further studies. Slower scan rates would require the use of larger sample volumes or lower flow rates.

TABLE 1

Differential pulse response for different delay times from injection to start of scan

Time delay (s)	i_p (μA)	i_p/i_{max}	Time delay (s)	i_p (μA)	i_p/i_{max}
10	0.35	0.20	50	1.68	0.93
20	0.84	0.47	60	1.35	0.75
30	1.53	0.85	75	0.90	0.50
40	1.80	1.00	90	0.57	0.31

[a] 2.0×10^{-4} M acetaminophen in 0.05 M phosphate buffer. Flow rate and differential pulse conditions as in Fig. 2B(c).

Quantitative evaluation. Differential pulse voltammograms obtained after successive injections of acetaminophen solutions of ascending concentration ($1.0—5.0 \times 10^{-4}$ M) yielded a linear calibration plot. Least-squares treatment of these data yielded the equation i (μA) = $(2.60 \pm 0.05)C$(mM) + 0.019 ± 0.016 μA with $S_{y_x} = 0.016$ μA and $r = 0.9995$ (conditions as in Fig. 2B(c)). The limit of detection of the method is similar to that of batch differential pulse voltammetry at solid electrodes (submicromolar level [14]), with slightly higher values because of the dispersion of the analyte. The precision of results was estimated by eight repeated injections of 5.0×10^{-4} M acetaminophen solution (conditions as in Fig. 3). The mean peak

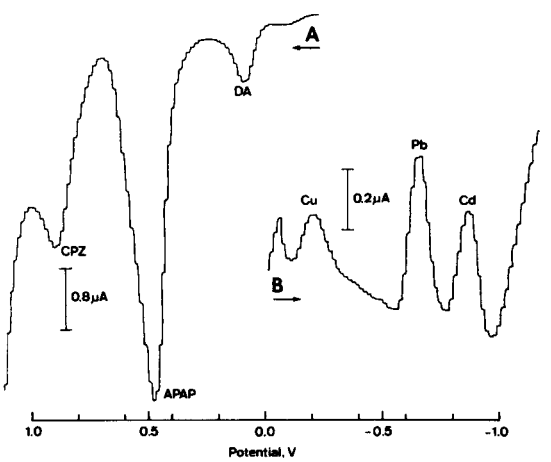

Fig. 3. Differential pulse voltammograms for the injection of sample mixtures. (A) 2.4×10^{-4} M dopamine, 9.8×10^{-5} M acetaminophen and 1.5×10^{-4} M chlorpromazine; supporting electrolyte, 0.02 M KH_2PO_4—0.08 M K_2HPO_4 acidified to pH 2 with nitric acid; carrier, 0.1 M phosphate buffer (pH 7.4). (B) 7.0×10^{-5} M Cu^{2+}, 4.3×10^{-5} M Pb^{2+} and 1.2×10^{-4} M Cd^{2+}; supporting electrolyte and carrier, 0.1 M KNO_3. Flow rate and differential pulse conditions as in Fig. 2B(c).

current found was 1.33 μA with a range 1.26—1.40 μA (n = 8) and a relative standard deviation of 4%.

Figure 3 illustrates the application of the system to the quantitation of three components in mixtures. For both oxidizable (A) and reducible (B) mixtures, well-defined and separated peaks are observed. Based on the peak potentials and peak half-widths of the sample components, it might be possible to quantify 4—5 species simultaneously within a 1—1.2 V voltage range. (For reversible systems, the differential pulse peak half-width corresponds to 90.4/n mV [14]. For simple mixtures such as antioxidants in oil, multivitamin tablets, or alloys, the simplicity of the flow-injection system makes it preferable to chromatographic systems.

This work was supported by a grant from the U.S. Department of the Interior through the New Mexico Water Resources Research Institute.

REFERENCES

1 J. Růžička and E. H. Hansen, Anal. Chim. Acta, 99 (1978) 37.
2 D. Betteridge, Anal. Chem., 50 (1978) 832A.
3 C. B. Ranger, Anal. Chem., 53 (1981) 20A.
4 E. Pungor, Z. Fehér, G. Nagy, K. Tóth, G. Horvai and M. Gratzl, Anal. Chim. Acta, 109 (1979) 1.
5 W. J. Blaedel and Z. Yim, Anal. Chem., 52 (1980) 564.
6 J. Wang and H. D. Dewald, Anal. Chim. Acta, 136 (1982) 77; 142 (1982) 239.
7 J. Wang, E. Ouziel, Ch. Yarnitzky and M. Ariel, Anal. Chim. Acta, 102 (1978) 99.
8 R. Samuelson, J. O'Dea and J. Osteryoung, Anal. Chem., 52 (1980) 2215.
9 J. Wang, H. D. Dewald and B. Greene, Anal. Chim. Acta, 146 (1983) 45.
10 J. Janata and J. Růžička, Anal. Chim. Acta, 139 (1982) 105.
11 J. Wang, Anal. Chim. Acta, 129 (1981) 253.
12 J. Růžička and E. H. Hansen, Anal. Chim. Acta, 145 (1983) 1.
13 K. Burrows and M. Hughes, Anal. Chim. Acta, 110 (1979) 255.
14 P. Soderhjelm, J. Electroanal. Chem., 71 (1976) 109.

Analytica Chimica Acta, 153 (1983) 331—335
Elsevier Science Publishers B.V., Amsterdam — Printed in The Netherlands

Short Communication

STUDY OF THE NICKEL—BROMAZEPAM COMPLEX BY DIFFERENTIAL PULSE POLAROGRAPHY AND DETERMINATION OF NICKEL

J. HERNÁNDEZ-MÉNDEZ*, C. GONZÁLEZ-PÉREZ and M. I. GONZÁLEZ-MARTÍN

Department of Analytical Chemistry, Faculty of Chemistry, University of Salamanca, Salamanca (Spain)

(Received 30th March 1983)

Summary. The nickel—bromazepam complex gives a peak at 0.8 V (vs. Ag/AgCl) which is highest at pH 4.0—6.5. The detection limit is 2.7×10^{-8} M and the calibration graph is linear up to 8×10^{-5} M nickel(II) under the recommended conditions. Cobalt, cadmium and iron(II) interfere.

A previous communication [1] described the spectrophotometric study of the complex formed by bromazepam (7-bromo-1,3-dihydro-5-(2-pyridyl)-2H-1,4-benzodiazepin-2-one, H_2Bz, with nickel(II) in acidic media at different pH values. The present work reports the differential pulse polarographic behaviour of the $Ni(Bz)_3^{2+}$ complex. Bromazepam itself has been studied by Smyth et al. [2—4], who have also made a spectrophotometric and voltammetric study of the complexation reactions of bromazepam with iron(II), copper(II) and cobalt(II) [5]. Bromazepam forms a coloured complex with iron(II) [6] which has been used for the spectrophotometric determination of iron [7] and bromazepam [8].

Experimental

Apparatus. A Metrohm Polarecord E506 was used with a polarographic stand E505, equipped with dropping mercury electrode, reference electrode (silver—silver chloride) and auxiliary electrode (platinum). The thermostat was a "Selecta".

Reagents. A 1×10^{-3} M bromazepam solution was prepared by dissolving 32.0 mg of the compound (Roche Laboratories, Madrid) in 20 ml of methanol (Panreac), and dilution to 100 ml with twice-distilled water. The solution was always freshly prepared and kept in the dark. A 1×10^{-3} M solution of nickel ($NiCl_2 \cdot 6H_2O$; Merck) was prepared from a more concentrated solution standardized gravimetrically with dimethylglyoxime.

Procedure. An aliquot containing enough nickel to give a final concentration greater than 10^{-7} M, 5 ml of 1×10^{-3} M bromazepam and 10 ml of 0.25 M acetate buffer (pH 4.7) were placed in a 25-ml volumetric flask, and made up to volume with twice-distilled water. After 15 min a sample was

0003-2670/83/$03.00

placed in the polarographic cell, nitrogen was bubbled through for 5 min and the polarogram was recorded at a pulse amplitude of −20 mV.

Results and discussion

Figure 1 shows various polarograms for nickel, bromazepam and mixtures of the two components. In pH 4.7 acetate buffer in the absence of complexing agents, nickel showed a peak close to −1.00 V. Bromazepam under the same conditions showed peaks at −0.50, −1.15 and −1.30 V. Nickel in the presence of an excess of bromazepam gave a peak at −0.80 V, the height of which increased with nickel concentration. A corresponding decrease in the height of the bromazepam peak at −0.50 V was also observed. As in the spectrophotometric study [1], the height of the complex peak increased slightly during the first 15 min after preparing the sample, after which it remained constant.

Influence of reaction parameters. The effect of pH between 2 and 9 was studied on solutions prepared according to the general procedure. The results (Fig. 2) show that the height of the peak of the complex reached a maximum at pH 4.0–6.5. The peak shape was unchanged at low pH values, but protonation of the pyridine ring took place [4], thus decreasing the concen-

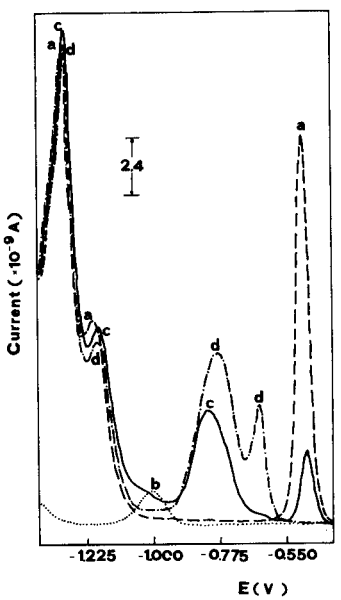

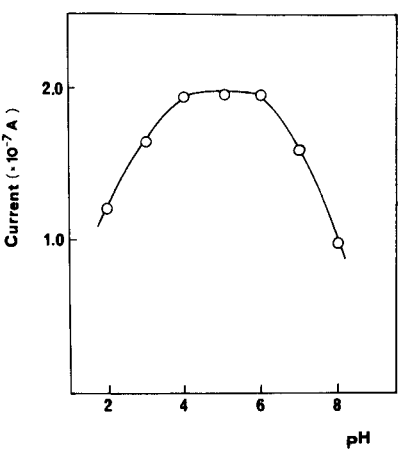

Fig. 1. Effect of nickel on the differential pulse polarogram of bromazepam in acetate buffer (pH 4.7, 0.1 M): (——, a) 6.0×10^{-5} M bromazepam; (. . . , b) 2.0×10^{-5} M Ni^{2+}; (——, c) 6.0×10^{-5} M bromazepam + 2.0×10^{-5} M Ni^{2+}; (—·—·, d) 6.0×10^{-5} M bromazepam + 8.0×10^{-5} M Ni^{2+}.

Fig. 2. Effect of pH on the peak height of the bromazepam—nickel complex at −0.80 V (1.2×10^{-5} M bromazepam + 4.0×10^{-5} M Ni^{2+}).

tration of the complex; at high pH values, the decrease in the peak height was probably due to hydrolysis of the nickel.

For a 4.0×10^{-5} M nickel solution at pH 4.7, there was a linear increase in peak height with bromazepam concentration until the bromazepam/nickel ratio reached 3, after which the peak height was constant. This confirms the spectrophotometrically determined stoichiometry of the complex [1].

Solutions containing 0.4×10^{-4} M nickel and 1.2×10^{-4} M bromazepam gave peak heights which decreased slightly (ca. 5%) on increasing the ionic strength from 0.05 M to 1.0 M in acetate buffer, possibly because of a decrease in the diffusion coefficient. For later studies, 0.1 M buffer was chosen.

Characteristics of the electrode process. The relationships between peak heights and the nickel concentration, temperature, pulse amplitude and drop time were studied, to establish the characteristics of the electrode process. A linear relationship was obtained between peak height and nickel concentration up to 0.8×10^{-4} M (Fig. 3). This plot could be used for the determination of nickel in aqueous solution, with a limit of detection (3σ) of 2.7×10^{-8} M. This value is lower than that for "free" nickel (3.6×10^{-7} M).

When the bromazepam/nickel ratio was greater than 3, a new peak close to −0.73 V (Fig. 1) appeared. The height of this peak increased with increasing nickel concentration until the bromazepam/nickel ratio reached 3:7. Its height was proportional to the nickel concentration and a temperature coefficient of 1.3% was obtained. Thus the peak current is diffusion-controlled.

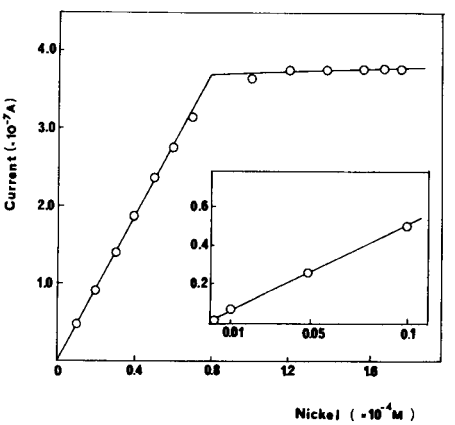

Fig. 3. Effect of nickel concentration on the peak height at −0.80 V (2.0×10^{-4} M bromazepam in acetate buffer, pH 4.7).

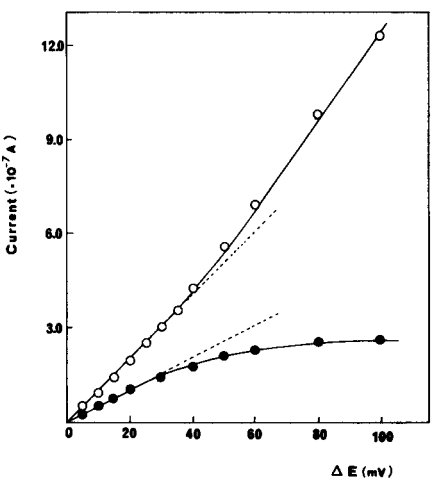

Fig. 4. Effect of pulse amplitude on peak height (1.2×10^{-4} M bromazepam + 4.0×10^{-5} M Ni^{2+} in acetate buffer, pH 4.7): (○) cathodic; (●) anodic.

The effect of temperature was studied between 8 and 60°C in a solution of 0.4×10^{-4} M nickel and 1.2×10^{-4} M bromazepam. A shift towards more negative potentials was observed and a peak height/temperature coefficient of 1.4% was obtained, in good agreement with the theoretical value for diffusion-controlled processes.

The relationship between peak height and pulse amplitude is given by $\Delta i_{max} = nFAC\ D^{1/2}\ (\sigma - 1)\ (\pi t_m)^{1/2}\ (\sigma + 1)$ where Δi_{max} is the maximum peak current, D is the diffusion coefficient, t_m is the duration of the pulse, $\sigma = \exp nF\Delta E/2RT$, ΔE is the pulse amplitude and the other symbols are conventional. When $\Delta E/2$ is less than RT/nF the previous equation reduces to $\Delta i_{max} = n^2F^2AC\Delta ED^{1/2}/4RT(\pi t_m)^{1/2}$, according to which there is a linear relationship between Δi_{max} and ΔE. The effect of pulse amplitude in the ±100 mV range is shown in Fig. 4. For values less than ±40 mV, there was a linear peak height dependence. The deviations observed for high positive pulse amplitudes are explained by the first equation, though it must be recalled that this equation is correct only when the process is reversible, which is not true in this particular case (see below). It was also observed that with increasing pulse amplitude, peak potentials shifted towards more positive values, in agreement with the expression [9], $E_{peak} = E^r_{1/2} - \Delta E/2$. The peak height varied linearly with $t^{2/3}$, where t is the drop lifetime. This agrees with the expected value for a diffusion-controlled process.

Reversibility of the polarographic process. In order to study the reversibility of the polarographic reduction, the criteria of Birke et al. [10] for simple charge-transfer processes were used. These involve the difference between cathodic and anodic peak potential $E^c_p - E^a_p$ and the anodic and cathodic peak height ratio (i^a_p/i^c_p). Table 1 shows the results obtained on application of a pulse amplitude of 20 mV to solutions containing various concentrations of nickel and bromazepam in acetate buffer at pH 4.7. From these results it may be concluded that the electrode process is quasireversible.

Polarographic determination of nickel. Nickel (1×10^{-7}—6×10^{-5} M) may be determined by differential pulse polarography as in the recommended

TABLE 1

Reversibility of the polarographic process[a]

Ni^{2+} ($\times 10^{-4}$ M)	Bromazepam ($\times 10^{-4}$ M)	E_c (V)	E_a (V)	$E_c - E_a$ (mV)	i^c_p (nA)	i^a_p (nA)	i^a_p/i^c_p
0.4	2.0	−0.814	−0.820	+6	178	119	0.66
0.4	3.0	−0.814	−0.820	+6	195	120	0.62
0.4	4.0	−0.814	−0.820	+6	195	120	0.62
0.6	2.8	−0.802	−0.811	+9	258	171	0.66
0.6	3.2	−0.802	−0.811	+9	264	174	0.66
0.6	4.0	−0.802	−0.811	+9	270	177	0.66

[a] E_c = cathodic potential; E_a = anodic potential.

procedure, using a bromazepam concentration of 2.0×10^{-4} M. Application of the method to ten solutions of 2.0×10^{-5} M nickel gave a relative standard deviation of 0.91%.

Possible interferences on the determination of nickel were studied. A 4-fold excess of bromazepam over both cations was used. Uranium(VI), Pb, Mn(II), Cu(II), Pd, Al, Tl(I), Mg, Ca, and Hg(II) did not interfere at a mole ratio to nickel of less than 10; Fe(III), V(IV) and Zn interfered at a ratio of 10, but not 1. Cobalt(II) interfered at unit ratio and Cd and Fe(II) at a 1/10 ratio.

REFERENCES

1 J. Hernández-Méndez, C. González-Pérez and M. I. González-Martín, Microchem. J., (1983) in press.
2 W. F. Smyth (Ed.), Polarography of Molecules of Biological Significance, Academic Press, London, 1979, p. 92.
3 W. F. Smyth, M. R. Smyth, J. A. Groves and S. B. Tan, Analyst, 103 (1978) 497.
4 M. R. Smyth, T. S. Beng and W. F. Smyth, Anal. Chim. Acta, 92 (1977) 129.
5 W. F. Smyth, R. Scannell, T. K. Goggin and L. Hernández-Hernández, Anal. Chim. Acta, 141 (1982) 321.
6 J. D. Sabatino, D. W. Weber, G. R. Padmanabhan and B. Z. Senkowski, Anal. Chem., 41 (1969) 905.
7 B. Flein, B. K. Weber, L. Lucas, J. K. Foreman and R. L. Searcy, Clin. Chim. Acta, 26 (1969) 77.
8 M. Fukumoto, Chem. Pharm. Bull., 28 (1980) 3678.
9 A. M. Bond, Modern Polarographic Methods in Analytical Chemistry, M. Dekker, New York, 1980, p. 249.
10 R. L. Birke, Kim Myung-Hoon and M. Strassfeld, Anal. Chem., 53 (1981) 852.

Analytica Chimica Acta, 153 (1983) 337—340
Elsevier Science Publishers B.V., Amsterdam — Printed in The Netherlands

Short Communication

AMPEROMETRIC DETERMINATION OF PHOSPHOLIPIDS IN BLOOD SERUM WITH A LECITHIN-SENSITIVE ELECTRODE IN A FLOW INJECTION SYSTEM

TOSHIO YAO*, YOSHIAKI KOBAYASHI and MINORU SATO

Department of Applied Chemistry, College of Engineering, University of Osaka Prefecture, Mozu-Umemachi, Sakai 591 (Japan)

(Received 15th April 1983)

Summary. A chemically-modified enzyme membrane electrode for phospholipids was constructed by cross-linking choline oxidase and phospholipase D with bovine serum albumin using glutaraldehyde on a platinum electrode silanized with 3-aminopropyltriethoxysilane. The hydrogen peroxide produced was measured amperometrically at 0.8 V applied. In the flow system, the peak current was linearly related to lecithin concentration in the range 20—350 mg dl^{-1}, for 10-μl injections. The sample throughput was 60 h^{-1}. The r.s.d. was <1.5%.

The determination of phospholipids in serum is important in clinical analysis and chemical [1] and enzymatic [2] determinations have been reported. Enzymatic methods involve a combination of phospholipase D and choline oxidase, and were claimed to be more selective, sensitive, precise, and simple than direct chemical methods. Karube et al. [3] developed an enzymatic method for determining lecithin which is a main serum phospholipid, utilizing phospholipase D and choline oxidase immobilized together on agarose gel as an enzyme reactor in a flow stream. In this communication, a flow-type lecithin electrode is reported. It is constructed by cross-linking both phospholipase D and choline oxidase with glutaraldehyde on a platinum electrode silanized with 3-aminopropyltriethoxysilane [4]. It provides an amperometric detector for phospholipids in blood serum.

Experimental

Reagents. Choline oxidase (EC 1.1.3.17., 12.7 IU mg^{-1}, from *Alcaligenes* sp.) and phospholipase D (EC 3.1.4.4., 59.0 IU mg^{-1}, from *Streptomyces chromofuscus*) were obtained from Toyobo Co. and Toyo Jozo Co., respectively. The bovine serum albumin (BSA) powder was 96—99% albumin (Sigma Chemical Co.; fraction V). 3-Aminopropyltriethoxysilane was obtained from Tokyo Kasei Kogyo Co. Glutaraldehyde (aqueous 20% solution), Triton X-100, choline chloride and lecithin (from egg) (all from Wako Pure Chemicals Co.) were used as received. A lecithin dispersion (1000 mg dl^{-1}) was prepared with distilled water by the method of Huang [5]. All dilutions were made in the appropriate buffers. ORTHO control human serum (Ortho Diagnostic

0003-2670/83/$03.00

Systems) was used as standard. All other chemicals were of analytical-reagent grade.

Preparation of lecithin electrode. The method was similar to that described before [4]. A platinum sheet (1 cm × 2 cm, 0.1 mm thick) was anodized, silanized and washed as before [4]. On one side of this sheet, 6-μl of aqueous 20% (w/v) BSA solution, 8 μl of 4% (w/v) choline oxidase in pH 7.5 phosphate buffer and 4 μl of aqueous 4% (v/v) glutaraldehyde were mixed and spread rapidly [6]. The membrane was allowed to form at room temperature. After 3 h, 20 μl of 4% (w/v) phospholipase D in pH 7.5 phosphate buffer and 4 μl of 4% (v/v) glutaraldehyde were added to the center of the electrode. The solutions were mixed and left open to air overnight.

The amperometric flow-cell was assembled as described previously [7].

Flow system and procedure for phospholipid determination. The flow cell was used with the continuous flow system described earlier [6, 7]. A constant potential of 0.8 V was applied. A phosphate buffer (0.1 M, pH 8.0, 0.1% Triton X-100 and 40 μM in calcium chloride) served as the carrier solution and was pumped at a constant flow rate of 1.5 ml min^{-1}. An electrolytic column packed with reticulated vitreous carbon (RVC, 100—200 mesh) [8] was positioned just before the flow-through detector to remove interfering substances such as ascorbic acid and uric acid in serum; a constant potential (1.0 V) was applied to the column with a NICHIA NP-1 potentiostat.

A 10-μl aliquot of lecithin dispersion or human serum was injected. Injected lecithin is hydrolyzed to choline at the surface layer of the immobilized enzyme electrode. The produced choline is then oxidized to betaine in the immobilized choline oxidase layer, producing hydrogen peroxide which is monitored amperometrically [3]. Lecithin was determined from the peak current by using a calibration graph prepared from the results obtained with standard lecithin dispersion.

Results and discussion

Response of the system. Typical response curves at various concentrations of lecithin under the recommended conditions are shown in Fig. 1. Figure 2 shows the effect of the carrier flow rate on the peak current and on the peak width at half-height of the signal obtained for injections of 300 mg dl^{-1} lecithin dispersion. As the flow rate increased, the peak current decreased because of incomplete conversion of lecithin to choline. However, the time required for determination became excessive at low flow rates and a flow rate of 1.5 ml min^{-1} is recommended. This provides relatively good sensitivity and reasonable sample throughput (about 60 determinations per hour).

Effects of pH and cofactor concentrations. Experiments were conducted to establish the optimum pH under these flow conditions. Phosphate and pyrophosphate buffers were tested in the carrier solution as shown in Fig. 3. Although the optimum pH of native phospholipase D is 7.0—8.0, a broad optimum pH range of 8.0—10.4 was observed after immobilization; pH 8.0 was chosen because the pH of serum is similar.

Phospholipase D requires calcium ions and Triton X-100 as cofactors in the enzymatic determination of phospholipids [2, 3]. Therefore, the effect

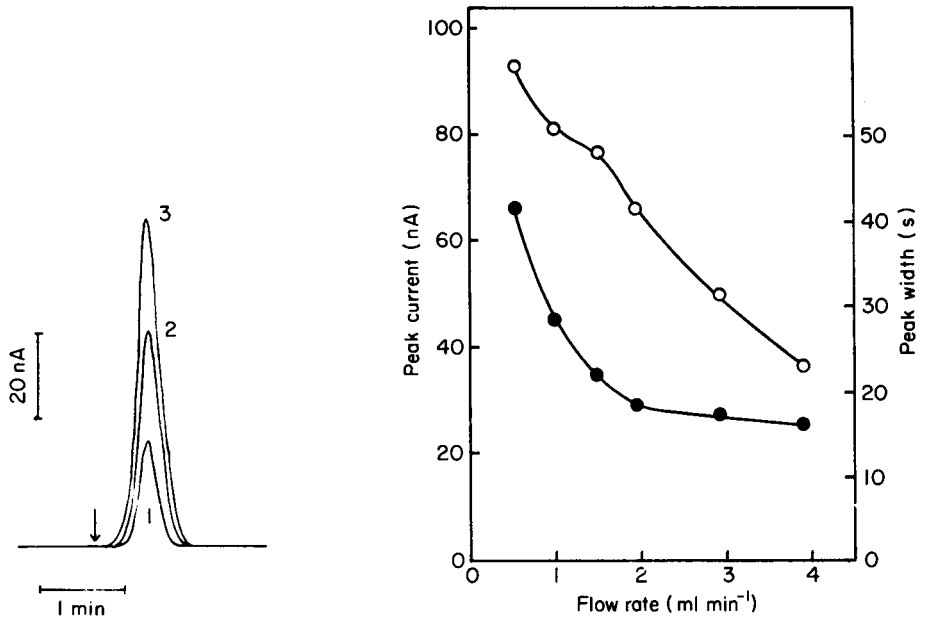

Fig. 1. Response curves for lecithin at concentrations of: (1) 100; (2) 200; (3) 300 mg dl^{-1}. Conditions as in the procedure.

Fig. 2. Effect of carrier flow rate on peak current (○) and peak width at half-height (●) for 300 mg dl^{-1} lecithin.

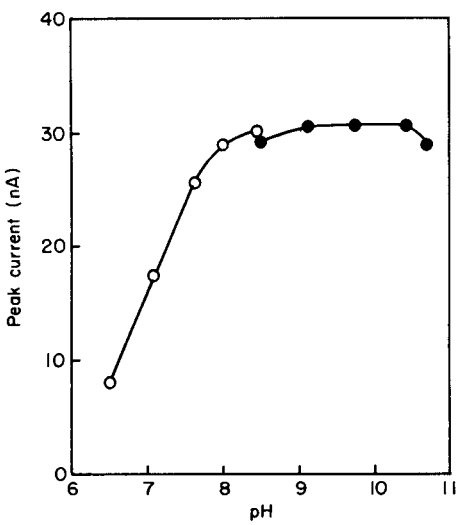

Fig. 3. Effect of pH on the peak current: (○) phosphate buffer (0.1 M); (●) pyrophosphate buffer (0.1 M). Conditions: 0.1% Triton X-100; flow rate 1.5 ml min^{-1}; 10 μl of lecithin (300 mg dl^{-1}).

of their concentrations in the carrier solution was examined. At the optimum calcium concentration (40—80 μM), the peak current was 2.7 times greater than that without calcium ion; higher calcium concentrations decreased the peak current slightly. The current increased rapidly with increasing Triton X-100 concentration in the carrier solution, becoming almost constant between 0.07 and 0.15% (v/v). Therefore, 0.1 M phosphate buffer (pH 8.0) 40 μM in calcium chloride and 0.1% in Triton X-100 is recommended as the carrier solution.

Interferences. Electroactive species such as ascorbate, urate, tyrosine, cysteine, glutathione and bilirubin are usually present in blood serum; they may diffuse through the membrane and be oxidized on the electrode at 0.8 V. Most of these substances can be eliminated electrochemically by placing a vitreous carbon column [8] just before the detector.

Calibration and reproducibility. A linear calibration graph was obtained over the lecithin concentration range 20—350 mg dl^{-1} for 10-μl injections; slope, y-intercept, and linear correlation coefficient were 0.256 nA (mg $dl^{-1})^{-1}$, 0.22 nA, and 0.9997, respectively. The normal concentration of phospholipids in human serum is 150—300 mg dl^{-1}, within this linear range. The detection limit of the present system was 8 mg dl^{-1} (S:N = 2).

Reproducibility of results was tested by repeated 10-μl injections of lecithin standard dispersions and control serum; results are shown in Table 1. The relative standard deviations were less than 1.5% for all samples. Also the average amount of phospholipids found in the control serum closely agreed with the manufacturer's data.

The electrode was used repeatedly to assess its stability with time. When not in use, the electrode was stored at 4°C in 0.1 M phosphate buffer (pH 7.5). Even after repeated use for one month, the electrode retained about 80% of its original activity.

TABLE 1

Reproducibility of measurements of lecithin dispersion and control human serum

	Lecithin dispersion (mg dl^{-1})			Control serum (mg dl^{-1})	
	100	200	300	164	190
N	10	10	10	8	8
Mean (nA)	13.0	25.8	38.7	158.8	186.0
S.d. (nA)	0.20	0.36	0.46	2.37	2.68
R.s.d. (%)	1.50	1.38	1.20	1.49	1.44

REFERENCES

1 G. R. Bartlett, J. Biol. Chem., 234 (1959) 466.
2 S. Imamura, M. Ohno and Y. Hirouchi, J. Biochem., 81 (1977) 6.
3 I. Karube, K. Hara, I. Satoh and S. Suzuki, Anal. Chim. Acta, 106 (1979) 243.
4 T. Yao, Anal. Chim. Acta, 148 (1983) 27.
5 C. H. Huang, Biochemistry, 8 (1969) 344.
6 T. Yao, Anal. Chim. Acta, 153 (1983) 169.
7 T. Yao, Anal. Chim. Acta, 153 (1983) 175.
8 T. Yao and Y. Kobayashi, Bunseki Kagaku, 32 (1983) 253.

Analytica Chimica Acta, 153 (1983) 341—345
Elsevier Science Publishers B.V., Amsterdam — Printed in The Netherlands

Short Communication

THE EQUILIBRIUM CONSTANT AND FORMAL POTENTIALS OF THE MERCURY ELECTRODE IN EQUILIBRIUM WITH MERCURY(I) AND MERCURY(II) AT UNIT IONIC STRENGTH AND 25°C

JAMES I. WATTERS* and PAULA DUNNIGAN[a]
Chemistry Department, The Ohio State University, Columbus, OH 43210 (U.S.A.)
(Received 12th October 1982)

Summary. The formal reduction potentials of the Hg(II)—Hg(I)—Hg(0) system and the equilibrium constant were evaluated in 1 M KNO_3 at 25°C. For the couple, Hg(I)/Hg(0), E_1^f = 0.7677 V; for Hg(II)/Hg(I), E_{21}^f = 0.8857 V; for Hg(II)/Hg(0), E_2^f = 0.8267 V; the equilibrium constant concentration ratio K^0 = Hg(I)/Hg(II) = 98.8.

The present communication is concerned with the evaluation of the formal potentials of the three mercury couples and the constant for the equilibrium of free mercury, mercury(I), and mercury(II) in aqueous solutions containing 1 M KNO_3 at 25°C. The evaluation of stability constants of metal complexes on the basis of the shift in the potential of a metal electrode caused by complex formation by ions of the metal requires the accurate evaluation of the formal electrode potential in a solution having a similar electrolyte composition. The cells must also have similar liquid-junction potentials and a similar reference electrode. Because this potential for the Hg(II)/Hg(0) couple was not available and because the actual electrode potential which can be measured is essentially that of the Hg(I)/Hg(0) couple, it has been common practice in the past to replace it by the standard potential at infinite dilution. For the Hg(II)/Hg(0) couple, this potential is close to 0.030 V more positive than the formal potential with the ionic strength adjusted to unity and the temperature 25°C. The latter were the conditions in a series of studies performed in this laboratory using this electrode in the indirect study of the stability of the complexes of other metal ions.

The excellent reversibility of the quiet or dropping mercury electrode in solutions containing Hg(I) and Hg(II) even in the presence of highly stable complexes or very insoluble compounds makes it an ideal indicator electrode because it undergoes very little chemical activity in aqueous solutions.

The following equations can be written for the Nernst potentials of the three electrode reactions.

[a]Present address: B. F. Goodrich Chemical Company Technical Center, Avon Lake, OH 43012, U.S.A.

$$E = E_1^0 + \tfrac{1}{2}S \log (Hg_2^{2+})/(Hg^0)^2 = E_1^f + \tfrac{1}{2}S \log [Hg_2^{2+}]/(Hg^0)^2 \quad (1)$$

$$E = E_2^0 + \tfrac{1}{2}S \log (Hg^{2+})/(Hg^0) = E_2^f + \tfrac{1}{2}S \log [Hg^{2+}]/(Hg^0) \quad (2)$$

$$E = E_{21}^0 + \tfrac{1}{2}S \log (Hg^{2+})^2/(Hg_2^{2+}) = E_{21}^f + \tfrac{1}{2}S \log [Hg^{2+}]^2/[Hg_2^{2+}] \quad (3)$$

Here the superscripts 0 and f indicate, respectively, standard reduction potentials at infinite dilution and formal reduction potentials in the presence of background electrolytes of the indicated composition. The subscripts after E indicate the oxidation state of the mercury ions involved. The symbol, S, indicates 2.303 $RT\ F^{-1}$, having the value 0.05916 V at 25°C. Brackets and parentheses indicate concentrations and activities, respectively; (Hg^0) indicates the activity of free mercury which is unity for pure mercury. This symbol for free mercury is retained in both activity and concentration studies for use in certain derivations and for applications in which the mercury is present in the form of an amalgam.

A mercury electrode must be used to measure the potentials for Eqns. (1) and (2) while an inert electrode, usually platinum, must be used to evaluate E in Eqn. (3). The standard and formal potentials, E_1^0, E_1^f, E_{21}^0 and E_{21}^f can be evaluated experimentally. Then E_2^0 can be evaluated mathematically from $E_2^0 = \frac{1}{2}(E_1^0 + E_{21}^0)$. Equating the expressions for E in Eqns. (1) and (3) leads to the following expression for solving K^0:

$$K^0 = \text{antilog}\,[(E_{21}^0 - E_1^0)/S] = (Hg_2^{2+})/[(Hg^{2+})(Hg^0)] \quad (4)$$

Equations analogous to those for E_2^0 and K^0, in terms of concentrations, yield E_2^f and K^f.

It is well known that the potential E_1^0 (Eqn. 1) obtained at a mercury electrode is established rapidly so that the probability of error is small. However, it is also known [1—3] that potential E_{21}^0 (Eqn. 3) obtained at a noble metal electrode, usually platinum, is established only slowly, requiring at least 30 min to reach equilibrium.

It is assumed here that only Hg(II) forms significant concentrations of stable complexes with hydroxide ions. In nitrate solutions, the stabilities of the Hg(I) and Hg(II) complexes are nearly equal, so that complex formation with nitrates can be neglected [1]. In all of the solutions investigated, the pH was kept at about 2 so that complex formation with hydroxide could usually be neglected. However, perchlorate ion forms a weak complex with Hg(I) but not Hg(II). The effects of these anions and correction for their effects in terms of Leden's function have been discussed by Hietanen et al. [1, 4]. Results from several earlier studies [1, 3, 5—8] were used to guide these studies.

Experimental

A solution of 0.0980 M mercury(II) was prepared by dissolving reagent-grade mercury(II) oxide in sufficient freshly boiled nitric acid to make the final solution 0.1 M in this acid. The concentration of mercury(II) ions was determined by using the mercury(II) solution to titrate weighed amounts of

previously dried, reagent-grade sodium chloride with *s*-diphenylcarbazone serving as an indicator [9]. The acid concentration in the mercury(II) solution was evaluated by titrating with previously standardized potassium hydroxide in the presence of a large excess of sodium chloride. The chloride forms a stable complex with the Hg(II) which prevents the precipitation of mercury(II) hydroxide and, as a consequence, prevents high results.

A 100-fold dilution of the standard mercury(II) solution was made with 1.0 M potassium nitrate in each of two flasks. Both solutions were deaerated by bubbling oxygen-free nitrogen through them for about 1 h. A few milliliters of free mercury was added to one solution, and the solution was vigorously shaken for 24 h before use, to insure that the mercury(II)—mercury(I) equilibrium had been attained. This equilibrated solution is designated as solution B. The original solution, containing only Hg(II), is designated as solution A. A series of solutions containing significant concentrations of both Hg(I) and Hg(II) were prepared by mixing various ratios of solutions A and B. A stream of purified nitrogen was passed through each sample solution for at least 30 min to remove any oxygen present and to stir the solution which was kept at 25°C.

Results and discussion

Attempts to measure the potential of solution B with a platinum electrode were unsuccessful because of a continuous drift in potential. Probably the poor poise of the electrode was due to the low concentration of mercury(II) present. Instead, a mercury J-shaped electrode, described by Holloway and Reilley [10], was used. The mercury electrode can replace the platinum electrode only in a solution of one particular Hg(I)/Hg(II) concentration ratio, which has the value of K^f. The mean value (E_m) obtained for several measurements of the potential of this mercury electrode is given in the first line of Table 1. Equilibrium was attained quickly with deviations no larger than ±0.0005 V. The remainder of the experiments was performed using the indicated volume ratios of solution B and A and the platinum foil electrode. Equilibrium was attained in about 30 min. The deviations in voltage were no greater than ±0.0005 V.

Sophisticated mathematical procedures could be used to treat the data independently of the value of K^f. However, because of the small equilibrium concentrations of Hg(II) present in the presence of free mercury, a fairly good first approximation of E_1^f could be made by neglecting the equilibrium concentration of Hg(II) present in solution B. This calculation yielded a preliminary value of 0.5231 V for $E_1^{f''}$, where the double primes indicate that the potential is evaluated versus the saturated calomel electrode (SCE).

A similar approximation was also valid in the volume ratio experiments because the small equilibrium concentration of Hg(II) in solution B could be neglected. These calculations yielded a preliminary value of 0.6418 V for $E_{21}^{f''}$ and a preliminary value of 101.7 for K^f. Correcting for the concentration of Hg^{2+} introduced by equilibrium with free mercury yielded: $E_1^{f''} = 0.5232 \pm$

0.0005 V, $E_{21}^{f'} = 0.6412 \pm 0.0005$ V, $E_2^{f'''} = 0.5822 \pm 0.0010$ V and $K^f = 98.8$ in the presence of 1 M KNO_3 at 25°C. These values did not change with further reiterations. Assigning a potential of 0.2445 V to the SCE as recommended by Ives and Janz [12] yields $E_1^f = 0.7677 \pm 0.0005$ V, $E_{21}^f = 0.8857 \pm 0.0005$ V, and $E_2^f = 0.8267 \pm 0.0010$ V versus the SHE, and $K^f = 98.8 \pm 1.0$, all at 25°C and at an ionic strength adjusted to unity with potassium nitrate.

Salvesen and Bjerrum [2] measured these potentials under similar conditions, including the purging with nitrogen. However, they used a normal calomel reference electrode which was separated from the half-cell being studied by a 10 M ammonium nitrate salt bridge. They measured the potentials of pairs of half-cells containing the same composition of background electrolyte to evaluate E_1^f and E_{21}^f and calculated K^f from their difference. They obtained values of K^f which varied from 94 to 120. However, their values appreciably above 106 were obtained in solutions having nitric acid concentrations much greater than 0.01 M and in the presence of more than 1×10^{-3} M Hg^{2+} and Hg_2^{2+}. Ionic strength and liquid junction effects may have been significant in these more concentrated solutions. Our calculations were limited to their solutions in which the concentrations of nitric acid was close to 0.01 M and the mercury ion concentrations were of the order of 0.001 M. These solutions having compositions comparable to ours yielded mean values for E_1^f and E_{21}^f of 0.7679 ± 0.0002 V and 0.8854 ± 0.0008 V, respectively, and 96.9 ± 1.0 for K^f at unit ionic strength and 25°C. These values are almost identical with the present values of 0.7677 V, 0.8857 V and 98.8, respectively. The value of K^f is also very close to the 96.6 obtained here by interpolation of Schwarzenbach and Anderegg's results [3]. This close agreement supports the reliability of the results obtained here. It further confirms the important experimental consideration that results obtained by using a normal calomel electrode assigned a potential of 0.2829 V and a 10 M ammonium nitrate salt bridge, as has often been done in European studies, are consistent with those obtained with a cell using a saturated calomel reference electrode, assigned a potential of 0.2445 V, and a 1 M KNO_3 salt bridge, as widely used in America. This potential of 0.2829 V was assigned to the normal calomel electrode by Britton [11] and is consistent with the best value 0.283 ± 0.001 V chosen by Ives and Janz [12].

The increasing value of K^f with increasing ionic strength indicates that the behavior of the activity coefficients of one or both of the mercury ions is anomalous and not consistent with limiting equations based on the ionic charge of the metal ions. The use of these equations and published activity coefficients accounts for the large range of published standard potentials. Consequently, the apparent formal potentials were calculated versus that of the reference electrode and these values were plotted versus the square root of the ionic strength using the data of Linhart [5], El Wakkad and Salem [6] and Popoff et al. [8]. Upon extrapolation to infinite dilution, the potential of the reference electrode approaches ideal behavior and the extent of

TABLE 1

Measured potential as a function of Hg(I)/Hg(II) concentration ratio (Various volumes, V_B, of solution B containing 9.89×10^{-4} M ($[Hg_2^{2+}] + [Hg^{2+}]$) were mixed with various volumes, V_A, of solution A containing 9.89×10^{-4} M Hg^{2+}. A mercury pool electrode was used in the first experiment and a platinum electrode was used in the remaining mixtures of solution A and B, $T = 25°C$)

Volume ratio (V_B/V_A)	Equil. conc. Hg_2^{2+} (10^{-4} M)	Equil. conc. Hg^{2+} (10^{-4} M)	E_m vs. SCE (V)	$E_{21}^{1''}$ vs. SCE (V)
5/0	9.79	0.1001	0.4342	—
4/1	7.83	2.06	0.5152	0.6411
3/2	5.87	4.02	0.5362	0.6414
2/3	3.92	5.97	0.5515	0.6414
1/4	1.96	7.93	0.5673	0.6410

complex formation with perchlorate approaches zero. In this way, we obtained the following results which are independent of any other theoretical assumptions. For the couple Hg(I)/Hg(0), $E_1^0 = 0.7952 \pm 0.0003$ V; for Hg(II)/Hg(I), $E_{21}^0 = 0.9091 \pm 0.0003$ V; for Hg(II)/Hg(I), $E_{20}^0 = 0.8522 \pm 0.0006$ V; $K^0 = 84.2 \pm 1.0$. Because these results are based on data from carefully performed classical studies which probably cannot be improved upon, they are probably as reliable as is possible.

REFERENCES

1 S. Hietanen and L. G. Sillen, Arkiv. For. Kem., 10-2 (1956) 103.
2 B. Salvesen and J. Bjerrum, Acta Chem. Scand., 16 (1962) 735.
3 G. Schwarzenbach and G. Anderegg, Helv. Chim. Acta, 37 (1954) 1289.
4 S. Hietanen and E. Hogfeldt, Chem. Scr., 10-1 (1976) 41.
5 G. A. Linhart, J. Am. Chem. Soc., 38 (1916) 2356.
6 S. E. S. El Wakkad and T. M. Salem, J. Phys. Chem., 54 (1950) 1371.
7 G. N. Lewis and M. Randall, Thermodynamics and Free Energy of Chemical Substances, McGraw-Hill, New York, 1923, pp. 382, 419.
8 S. Popoff, J. A. Riddick, V. I. Wirth and L. D. Ough, J. Am. Chem. Soc., 53 (1931) 1195.
9 I. M. Kolthoff, E. B. Sandell, E. J. Meehan and S. Bruckenstein, Quantitative Chemical Analysis, MacMillan, New York, 1969.
10 J. H. Holloway and C. N. Reilley, Anal. Chem., 32 (1960) 255.
11 H. T. S. Britton, Hydrogen Ions, 2nd edn., Chapman and Hall, London, 1956.
12 D. J. G. Ives and G. J. Janz, (Eds.), Reference Electrodes, Theory and Practice, Academic Press, London, 1961.

Analytica Chimica Acta, 153 (1983) 347—350
Elsevier Science Publishers B.V., Amsterdam — Printed in The Netherlands

Short Communication

THE DETERMINATION OF ^{14}N:^{15}N ISOTOPE RATIOS BY USING THE (3,0) AND (4,1) BANDHEADS OF THE N_2 SECOND POSITIVE SYSTEM

J. C. BURRIDGE and I. J. HEWITT

The Macaulay Institute for Soil Research, Craigiebuckler, Aberdeen AB9 2QJ (Gt. Britain)

(Received 11th April 1983)

Summary. A good linear calibration for the isotopic composition of ammonia can be obtained over the range 5—30 atom-% nitrogen-15, by using an electrodeless discharge tube excited at 2450 MHz and cooled to suppress OH emission. Reproducible relative intensities of comparable bandheads from the two transitions indicate a stable excitation temperature in the discharge tube. It is concluded that the transitions in general use, the (2,0) or (1,0), are preferable for the determination of ^{14}N:^{15}N ratios.

The (2,0) and (1,0) bandheads of the N_2 $C^3\Pi_u$—$B^3\Pi_g$ Second Positive System are generally the most useful for determining ^{14}N:^{15}N isotope ratios by optical emission spectroscopy (o.e.s.) when nitrogen-15 is used as a stable isotope tracer in biological studies [1, 2]. The possible use of the (3,0) bandhead, which has a larger isotopic wavelength shift than the (2,0) and (1,0) bandheads, has not been demonstrated by other workers, probably because in most emission sources the (3,0) bandhead is too weak and suffers considerable interference from coincident OH bands in the 281—283-nm region. The efficient suppression of these OH bands, achieved by cooling part of the discharge tube to around —60°C [3], permitted the (3,0) and adjacent (4,1) bandheads to be examined in this investigation under substantially interference-free conditions.

The large isotope shifts of the (3,0) and (4,1) bandheads produce a pattern of overlapping bands (Fig. 1). The spectrometer used had a dispersion of only 2 nm mm^{-1} so that the bandheads of $^{14}N_2$(3,0) at 281.98 nm and of $^{14}N^{15}N$(4,1) at 282.11 nm were only partly resolved, while the bandheads of $^{14}N^{15}N$(3,0) at 282.71 nm and of $^{15}N_2$(4,1) at 282.78 nm were completely unresolved. Nevertheless, it was found that the isotope ratio could be determined satisfactorily from the intensity ratio of the $^{14}N_2$(4,1) and combined $^{14}N^{15}N$(3,0) and $^{15}N_2$(4,1) bandheads.

In the many o.e.s. methods described in the literature for the ^{14}N:^{15}N isotope ratio determination, isotopically-shifted bandheads of a single transition, e.g., the (2,0), have invariably been used. The relative intensities of such closely related bandheads are very insensitive to variations of the excitation conditions in the discharge tube, arising from changes in the sample-gas

0003-2670/83/$03.00

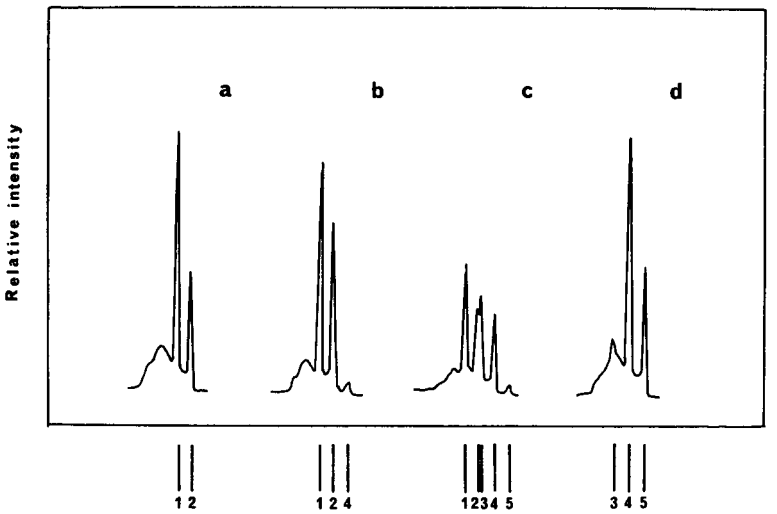

Fig. 1. Spectral pattern of (3,0) and (4,1) bands of the N_2 Second Positive System, obtained with moderate resolution and with OH bands suppressed. Atom-% nitrogen-15: (a) <0.1; (b) 5; (c) 30; (d) 97. Bandhead wavelengths (nm): (1) $^{14}N_2$ (4,1) 281.43; (2) $^{14}N_2$ (3,0) 281.98; (3) $^{14}N^{15}N$ (4,1) 282.11; (4) $^{14}N^{15}N$ (3,0) and $^{15}N_2$ (4,1) unresolved 282.8; (5) $^{15}N_2$ (3,0) 283.6.

pressure and temperature. Changes of these parameters affect the distribution of energy among the molecular states, and in consequence the relative intensity of emission from different transitions is altered. Examples of this have been cited by Tyte and Nicholls [4]. The present work demonstrates, however, that the simultaneous use of bandheads from two transitions, the (3,0) and (4,1), can provide an adequate basis for the o.e.s. determination of ^{14}N:^{15}N isotope ratios. This indicates that the emission source developed previously [3] can be readily operated with a reproducible excitation temperature.

Experimental

The N_2 spectra were emitted by electrodeless discharge tubes filled with ammonia, without any inert carrier gas, and excited in a 3/4-wave tuned cavity at 2450 MHz, as described in detail elsewhere [3]. The principal feature of the source is that the dinitrogen required for the molecular emission is formed within the discharge tube as a product of the dissociation of ammonia. Bandhead intensity ratios were determined from peak heights on pen-recorder tracings of photomultiplier output, with a simple correction for background emission. The major component of background radiation emitted by this source is a continuum derived from hydrogen, another product of the dissociated ammonia. At 280 nm, this background intensity is approximately half that of the N_2(4,1) bandhead obtained with 100 atom-% ^{14}N. It has little apparent structure and its intensity changes only slowly with wavelength. Samples containing ^{15}N in the range 0.01—97 atom-% were studied.

Theoretical

If in a population of nitrogen atoms the relative numbers of ^{14}N and ^{15}N atoms are a and b (where $a + b = 1$), the assumption of unbiased, random combinations of any two atoms to form dinitrogen leads to expected population ratios of $^{14}N_2$:$^{14}N^{15}N$:$^{15}N_2$::a^2:$2ab$:b^2. In addition to this assumption, o.e.s. methods require the further assumption that the three isotopically-different forms of dinitrogen emit similar spectra with intensities proportional to their populations. Although not rigorously exact, these approximations have proved to be adequate for determining isotope ratios. Making the further assumption that, for the source used in this investigation, there is a constant intensity ratio (k) between the $N_2(4,1)$ and $N_2(3,0)$ bands emitted by isotopically-identical dinitrogen, the six bandheads of interest have the following relative intensities: (i) $^{14}N_2(4,1)$, a^2; (ii) $^{14}N_2(3,0)$, ka^2; (iii) $^{14}N^{15}N(4,1)$, $2ab$; (iv) $^{14}N^{15}N(3,0)$, $2kab$; (v) $^{15}N_2(4,1)$, b^2; (vi) $^{15}N_2(3,0)$, kb^2. The intensity ratio R = (i)/[(iv) + (v)] was measured and the readily derived equation

$$\text{atom-\% } ^{15}N = 100/[1 + kR + (R + k^2R^2)^{1/2}] \quad (1)$$

was evaluated for given values of k and R.

Results

Spectra from samples containing 0.01 and 0.37 atom-% ^{15}N were used to determine a value for k from the intensities of the $^{14}N_2(4,1)$ and $^{14}N_2(3,0)$ bandheads. Samples having these low ^{15}N contents produce spectra with two bandheads and without complication from unresolved peaks (Fig. 1a). The combined measurements from 11 replicated spectra at each ^{15}N content gave the value 0.513 for k with a standard error of the mean ±0.002. The highest available ^{15}N content of 97 atom-% also produced a relatively simple pattern of bandheads (Fig. 1d) but the $^{15}N_2(4,1)$ peak contained a small, significant signal from the unresolved $^{14}N^{15}N(3,0)$ bandhead. These $^{15}N_2$ bandheads were, therefore, less suitable for determining k. After correction for the $^{14}N^{15}N(3,0)$ component, about 3% of the $^{15}N_2(4,1)$ intensity, a value for k was obtained which was about 0.03 greater than that from the $^{14}N_2$ bandheads, a very highly significant difference ($P < 0.001$).

Values of ^{15}N content were calculated from 10 replicate spectra by means of Eqn. (1), with k = 0.513, for standard samples having nominal contents of 5.14, 10.29, 20.22 and 30.15 atom-% ^{15}N. The mean values found were as follows (with standard error of the mean in parentheses):6.05 (±0.07), 10.90 (±0.07), 19.68 (±0.09) and 28.11 (±0.06), respectively. These values differ systematically from the nominal contents, which were based on data provided by the supplier of the isotopically-enriched materials. The nominal ^{15}N contents and the calculated ^{15}N contents were related by the linear regression equation

$$\text{Nominal \%} = 1.135 \times \text{Calculated \%} - 1.920 \quad (r^2 = 0.9996) \quad (2)$$

Equations (1) and (2) were combined and the contents of the standard samples were recalculated from the measured intensity ratios, using k =

0.513. The values found, 4.94 (±0.08), 10.46 (±0.07), 20.42 (±0.11) and 29.99 (±0.06) respectively, were in close agreement with the nominal values, which demonstrates that a good calibration can be obtained from the concurrent use of two different transitions, even when bandheads are not fully resolved.

Variations in a weak interfering band around 282—283 nm prevented the measurement of contents below 1 atom-% ^{15}N, while calibrations above 30 atom-% ^{15}N were not examined.

Discussion

The results above show that the (3,0) and (4,1) bandheads can be used for the o.e.s. determination of ^{14}N:^{15}N isotope ratios, provided that OH emission is suppressed and reproducible excitation conditions exist. However, it is clear that their lower intensity, and overlapping of the isotopically-shifted bands, make them less useful than the alternative (2,0) and (1,0) transitions at present in general use.

A satisfactory explanation for the values of the coefficients in the above regression equation has not been found. Neither the use of unresolved bands, nor the method of correcting for background emission, appears to account for them. The departure of the slope from unity suggests a variation of k with ^{15}N content, and the disagreement between the k values obtained for $^{14}N_2$ and $^{15}N_2$ supports this possibility. A fuller investigation of the effect of ^{15}N content on the relative intensities of these and other transitions is being undertaken.

The good precision of the R values indicates that the excitation source developed previously [3] can be operated with very reproducible excitation temperatures. Application of the calibration equation (Eqn. 2), a year after it was established, to a sample having a nominal content of 50.0 atom-% ^{15}N, gave its content as 50.27 (±0.11) atom-%, in good agreement with the expected value. This shows that calibration based on R values obtained with this o.e.s. method has good long-term stability.

REFERENCES

1 J. P. Leicknam, V. Middleboe and G. Proksch, Anal. Chim. Acta, 40 (1968) 487.
2 R. Fiedler and G. Proksch, Anal. Chim. Acta, 78 (1975) 1.
3 J. C. Burridge and I. J. Hewitt, Anal. Chim. Acta, 118 (1980) 11.
4 D. C. Tyte and R. W. Nicholls, Identification Atlas of Molecular Spectra 2: The $N_2 C^3\Pi_u$—$B^3\Pi_g$ Second Positive System, The University of Western Ontario, London, Ontario, Canada, 1964.

Analytica Chimica Acta, 153 (1983) 351—355
Elsevier Science Publishers B.V., Amsterdam — Printed in The Netherlands

Short Communication

ABSORPTION OF MERCURY BY SOLUTIONS CONTAINING OXIDANTS

H. MORITA, T. MITSUHASHI[a], H. SAKURAI and S. SHIMOMURA*

Faculty of Pharmaceutical Sciences, Tokushima University, 1-78 Sho-machi, Tokushima-shi 770 (Japan)

(Received 28th January 1983)

Summary. The transfer of mercury vapor into solutions containing mercury(II) ions and/or oxidants (dichromate, permanganate, cerium(IV) sulfate, silver nitrate) is investigated. The rate of absorption increases with increasing Hg^{2+} concentration and with increasing oxidation potential of dichromate solutions in sulfuric acid. A mechanism is proposed for the transfer.

Losses of mercury from dilute aqueous solutions of mercury(II) and from natural water samples have often been reported [1—8]. Adsorption of mercury on the container wall and volatilization of mercury from the solution were considered as the cause of the loss. In contrast Bothner and Robertson [9] reported the accumulation of mercury in acidified sample solutions when the solutions were stored in polyethylene bottles on a laboratory floor known to be contaminated with mercury. In the course of the present study on the loss of mercury from solutions containing oxidants, mercury was again found to accumulate in the solution. Ure [10] reported that unstoppered acidic potassium permanganate solutions readily absorb mercury from contaminated laboratory air. However, there is no detailed report on the mechanism of mercury absorption by solutions. This communication describes the transfer of mercury vapor into solutions containing mercury(II) and/or various oxidants in a closed system. A mechanism to explain the transfer is proposed.

Experimental

Apparatus. A Nippon Jarrel-Ash Model AA-8500 atomic absorption spectrometer equipped with a deuterium background corrector was used for the measurement of mercury vapor concentration at the 253.7-nm line from a mercury hollow-cathode lamp. Absorbance was recorded with a Hitachi Model 056 recorder. The closed cell (Fig. 1) was constructed from quartz tubing (i.d. 45 mm, length 100 mm) and a reaction vessel (i.d. 25 mm, height 35 mm). The quartz tube ends were ground perpendicular to the longitudinal axis, and quartz windows (i.d. 45 mm, thickness 2 mm) were fitted thereto. The burner head of the atomic absorption unit was replaced by this cell.

[a]Present address: Public Health Institute of Hyogo Prefecture, 2-1 Arata-cho, Hyogo-ku, Kobe 652, Japan.

0003-2670/83/$03.00

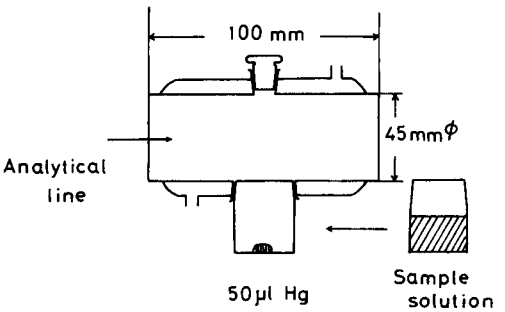

Fig. 1. Closed cell.

The redox potentials of the solutions were measured with a Hitachi-Horiba Model F-5 pH meter, with silver/silver chloride and platinum electrodes.

Reagents. Mercury was purified by distillation, and was stored in an argon atmosphere to prevent oxidation. All chemicals used were of extra-pure grade. Distilled-deionized water was used. A 0.1 M mercury(II) chloride solution was prepared by dissolving 1.357 g of the salt in 0.5 M sulfuric acid and diluting to 50 ml with this acid. Other mercury(II) chloride solutions were prepared by suitable dilution with 0.5 M sulfuric acid. Four 0.1 N oxidant solutions ($KMnO_4$, $K_2Cr_2O_7$, $Ce(SO_4)_2$ and $AgNO_3$) were prepared by dissolving appropriate amounts of the solids in 5% (v/v) nitric acid. A 0.2 N potassium dichromate solution was prepared by dissolving 2.452 g of the salt in water and diluting to 250 ml with water. Dichromate solutions (0.16 N) having various redox potentials were prepared by transfering 40 ml of the 0.2 N dichromate solution and various volumes (0—5 ml) of concentrated sulfuric acid to a 50-ml volumetric flask and diluting to the mark with water. Solutions containing potassium dichromate and mercury(II) were prepared by mixing mercury(II) chloride solution, 1 M nitric acid and 0.2 N potassium dichromate solution to give final concentrations of 0.16 N dichromate, 0.1 M nitric acid, and 0, 10^{-5}, 10^{-4} and 10^{-2} M mercury(II).

Procedure. The reaction vessel containing about 0.43 g of mercury was connected to the absorption cell until the absorbance of the volatilized mercury at 253.7 nm was constant (about 0.820). The vessel was then immediately exchanged with a reaction vessel containing 10 ml of reaction solution. The absorbance decreased by about 0.040. As the mercury vapor in the absorption cell was absorbed by the solution, the mercury vapor absorbance decreased. The decreasing absorbance was measured continuously for 1 h, without stirring the reaction solution (unless otherwise stated) at room temperature (27 ± 2° C).

Results and discussion

The gradual transfer of mercury vapor to a mercury(II) solution is illustrated in Fig. 2. The higher the concentration of mercury(II), the faster the absorption of mercury vapor. The results indicate that the mercury vapor

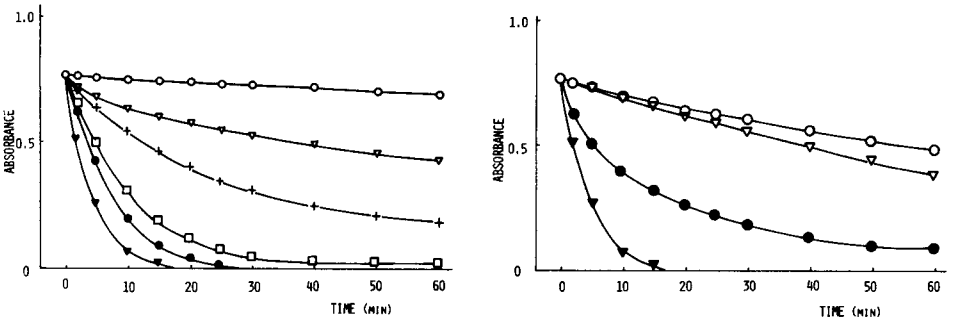

Fig. 2. Mercury transfer from the gas phase to mercury(II) chloride solutions: (○) 0 M; (▽) 10^{-5} M; (+) 10^{-4} M; (□) 10^{-3} M; (●) 10^{-2} M; (▲) 0.1 M.

Fig. 3. Mercury transfer from the gas phase to 0.1 N solutions of oxidants: (○) $K_2Cr_2O_7$; (▽) $Ce(SO_4)_2$; (●) $AgNO_3$; (▼) $KMnO_4$.

reacts with mercury(II) at the surface of the unstirred solution to form mercury(I). As the equilibrium constant [11] for the disproportionation of mercury(I) is log K = 1.94, the absorption of mercury vapor by a solution containing a large concentration of mercury(II) should be favored.

Solutions containing various oxidants also absorbed mercury vapor, as shown in Fig. 3. The rate of absorption depended on the oxidation potential and the nature of the oxidant. The dependence on oxidation potential of the dissolution of mercury vapor was studied for dichromate–sulfuric acid solutions of various potentials (Fig. 4). From the following oxidation potentials

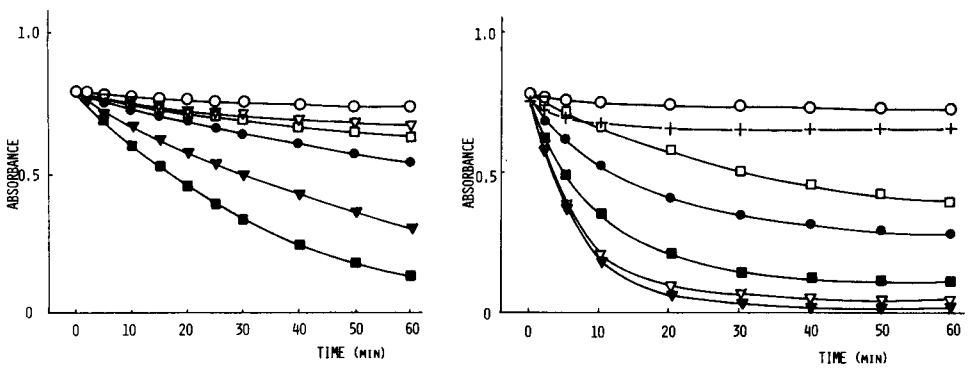

Fig. 4. Effect of oxidation potential of dichromate solutions in sulfuric acid on mercury transfer from the gas phase to solution. Initial formal potentials: (○) 0.70 V; (▽) 0.91 V; (□) 0.95 V; (●) 1.06 V; (▼) 1.11 V; (■) 1.14 V.

Fig. 5. Combined effect of dichromate and mercury(II) on mercury absorption into 0.1 M HNO_3: (+) 0.16 N dichromate; (○) 10^{-5} M $HgCl_2$; (●) 0.16 N dichromate and 10^{-5} M $HgCl_2$; (□) 10^{-4} M $HgCl_2$; (■) 0.16 N dichromate and 10^{-4} M $HgCl_2$; (▽) 10^{-2} M $HgCl_2$; (▼) 0.16 N dichromate and 10^{-2} M $HgCl_2$.

of mercury [11]:

$Hg_2^{2+} + 2e^- \rightleftharpoons 2Hg$ $E_0 = +0.7925$ V

$Hg^{2+} + 2e^- \rightleftharpoons Hg$ $E_0 = +0.850$ V

$2Hg^{2+} + 2e^- \rightleftharpoons Hg_2^{2+}$ $E_0 = +0.9075$ V

A potential of at least 0.7925 V is needed for the solution to dissolve mercury vapor. In confirmation, there was no difference between the amount of mercury vapor dissolved by a solution of initial potential 0.70 V and the amount dissolved by water. Figure 4 also shows that the rate of absorption of mercury increases with increasing potential. From these results it can be predicted that the co-existence of mercury(II) and oxidant will provide a solution that absorbs mercury vapor more rapidly than a solution containing only one of these components. As shown in Fig. 5, this prediction was confirmed experimentally. The mercury vapor dissolved slightly more slowly into a stirred potassium dichromate solution than into an unstirred solution.

From these observations, a possible mechanism for the transfer of mercury between the gas phase and solution is summarized in Fig. 6. For dissolution of mercury vapor, the reactions indicated by solid lines proceed to increase the mercury concentration of the solution. During the loss of mercury from solution, the reactions indicated by dotted lines play an important role. Toribara et al. [2] attributed the volatilization of mercury from solution to the reduction of mercury(II) to mercury(I) which then disproportionates with a resulting liberation of mercury vapor.

The above results emphasize that the presence of oxidants in solution may cause an increase of dissolved mercury concentration if the surroundings are contaminated with mercury, and that such oxidants may be added to prevent mercury loss from solutions [4, 5, 7, 10].

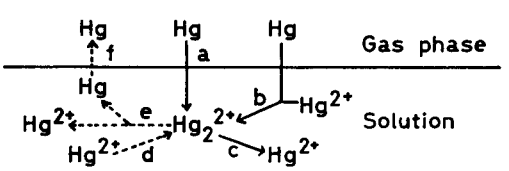

Fig. 6. Mercury transfer between gas phase and solution: (a) absorption by oxidant solution; (b) absorption by Hg(II) solution; (c) oxidation in solution; (d) reduction in solution; (e) disproportionation of Hg_2^{2+}; (f) volatilization.

REFERENCES

1 S. Shimomura, Y. Nishihara and Y. Tanase, Bunseki Kagaku, 18 (1969) 1072.
2 T. Y. Toribara, C. P. Shields and L. Koval, Talanta, 17 (1970) 1025.
3 R. M. Rosain and C. M. Wai, Anal. Chim. Acta, 65 (1973) 279.
4 C. Feldman, Anal. Chem., 46 (1974) 99.
5 J. M. Lo and C. M. Wai, Anal. Chem., 47 (1975) 1869.
6 H. V. Weiss and W. H. Shipman, Anal. Chim. Acta, 81 (1976) 211.
7 D. R. Christmann and J. D. Ingle, Jr., Anal. Chim. Acta, 86 (1976) 53.
8 K. I. Mahan and S. E. Mahan, Anal. Chem., 49 (1977) 662.
9 M. H. Bothner and D. E. Robertson, Anal. Chem., 47 (1975) 592.
10 A. M. Ure, Anal. Chim. Acta, 76 (1975) 1.
11 L. G. Sillen and A. E. Martell, Stability Constants of Metal—Ion Complexes, Spec. Publ. No. 17, Chemical Society, London, 1964, p. 21.

Analytica Chimica Acta, 153 (1983) 357
Elsevier Science Publishers B.V., Amsterdam — Printed in The Netherlands

Erratum

Janos Kristoff and George G. Guilbault, Application of Uncoated Piezoelectric Crystals for the Detection of an Organic Phosphonate.

Anal. Chim. Acta, 149 (1983) 337—341.

The following final paragraph was inadvertently omitted from this communication (p. 341):

This research was supported by the Army Research Office (Grant No. DAAG-29-77-G-0226-DR).

ANALYTICA CHIMICA ACTA, VOL. 153 (1983)

AUTHOR INDEX

(Continued from inside back cover)

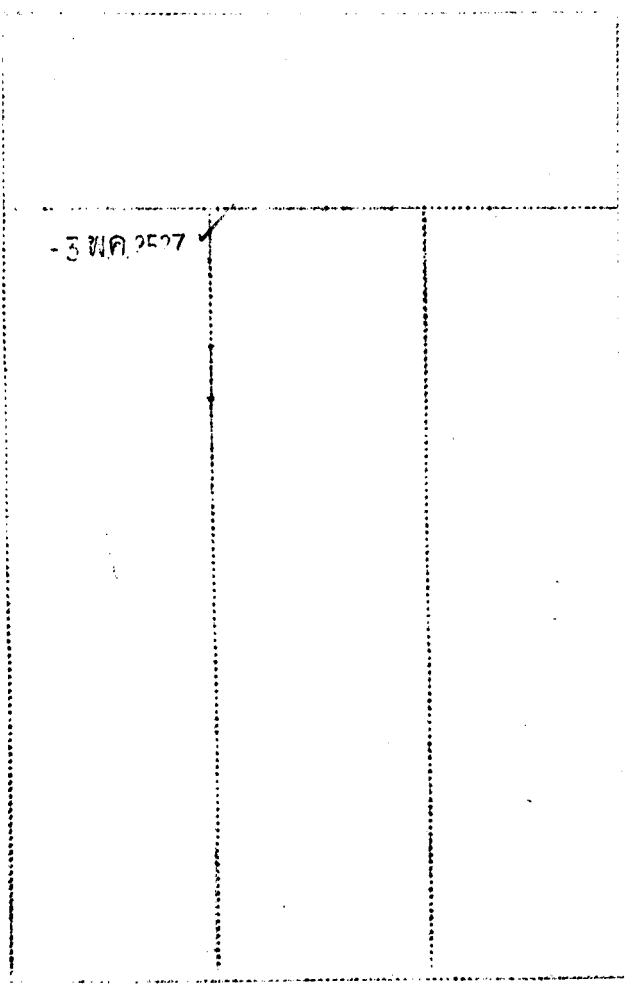

(Continued from outside back cover)

Short Communications

(Continued on page 364)

CONTENTS

(Abstracted, Indexed in: Anal. Abstr.; Biol. Abstr.; Chem. Abstr.; Curr. Contents Phys. Chem. Earth Sci.; Life Sci.; Index Med., Mass Spectrom. Bull.; Sci. Citation Index; Excerpta Med.)

(Continued on inside back cover)